FROM PLANT MERISTEM TO CROP YIELD

EDITED BY: Xigang Liu, Ram Kishor Yadav, Xia Cui and Fa Cui

PUBLISHED IN: Frontiers in Plant Science

frontiers Research Topics

ISSN 1664-8714
ISBN 978-2-88976-769-4
DOI 10.3389/978-2-88976-769-4

About Frontiers

Frontiers is more than just an open-access publisher of scholarly articles: it is a pioneering approach to the world of academia, radically improving the way scholarly research is managed. The grand vision of Frontiers is a world where all people have an equal opportunity to seek, share and generate knowledge. Frontiers provides immediate and permanent online open access to all its publications, but this alone is not enough to realize our grand goals.

Frontiers Journal Series

The Frontiers Journal Series is a multi-tier and interdisciplinary set of open-access, online journals, promising a paradigm shift from the current review, selection and dissemination processes in academic publishing. All Frontiers journals are driven by researchers for researchers; therefore, they constitute a service to the scholarly community. At the same time, the Frontiers Journal Series operates on a revolutionary invention, the tiered publishing system, initially addressing specific communities of scholars, and gradually climbing up to broader public understanding, thus serving the interests of the lay society, too.

Dedication to Quality

Each Frontiers article is a landmark of the highest quality, thanks to genuinely collaborative interactions between authors and review editors, who include some of the world's best academicians. Research must be certified by peers before entering a stream of knowledge that may eventually reach the public - and shape society; therefore, Frontiers only applies the most rigorous and unbiased reviews.
Frontiers revolutionizes research publishing by freely delivering the most outstanding research, evaluated with no bias from both the academic and social point of view. By applying the most advanced information technologies, Frontiers is catapulting scholarly publishing into a new generation.

What are Frontiers Research Topics?

Frontiers Research Topics are very popular trademarks of the Frontiers Journals Series: they are collections of at least ten articles, all centered on a particular subject. With their unique mix of varied contributions from Original Research to Review Articles, Frontiers Research Topics unify the most influential researchers, the latest key findings and historical advances in a hot research area! Find out more on how to host your own Frontiers Research Topic or contribute to one as an author by contacting the Frontiers Editorial Office: frontiersin.org/about/contact

FROM PLANT MERISTEM TO CROP YIELD

Topic Editors:
Xigang Liu, Hebei Normal University, China
Ram Kishor Yadav, Indian Institute of Science Education and Research Mohali, India
Xia Cui, Chinese Academy of Agricultural Sciences, China
Fa Cui, Ludong University, China

Citation: Liu, X., Yadav, R. K., Cui, X., Cui, F., eds. (2022). From Plant Meristem to Crop Yield. Lausanne: Frontiers Media SA. doi: 10.3389/978-2-88976-769-4

Table of Contents

frontiers in Plant Science

ORIGINAL RESEARCH
published: 27 July 2021
doi: 10.3389/fpls.2021.704958

ATBS1-INTERACTING FACTOR 2 Negatively Modulates Pollen Production and Seed Formation in *Arabidopsis*

*Yoon Kim, Sun-Ho Kim, Dong-Min Shin and Soo-Hwan Kim**

Division of Biological Science and Technology, Yonsei University, Wonju, South Korea

ATBS1-INTERACTING FACTOR 2 (AIF2) is a non-DNA-binding basic-helix-loop-helix (bHLH) transcription factor. Here, we demonstrate that AIF2 negatively modulates brassinosteroid (BR)-induced, BRASSINAZOLE RESISTANT 1 (BZR1)-mediated pollen and seed formation. *AIF2*-overexpressing *Arabidopsis* plants (AIF2ox) showed defective pollen grains and seed production while two *AIF2* knockout mutants, *aif2-1* and *aif2-1/aif4-1*, displayed opposite phenotypes. Genes encoding BZR1-regulated positive factors of seed size determination (*SHB1*, *IKU1*, *MINI3*) were suppressed in AIF2ox and genes for negative factors (*AP2* and *ARF2*) were enhanced. Surprisingly, BZR1-regulated pollen genes such as *SPL*, *MS1*, and *TDF1* were aberrantly up-regulated in AIF2ox plants. This stage-independent abnormal expression may lead to a retarded and defective progression of microsporogenesis, producing abnormal tetrad microspores and pollen grains with less-effective pollen tube germination. Auxin plays important roles in proper development of flower and seeds: genes for auxin biosynthesis such as *TCP*s and *YUCCA*s as well as for positive auxin signalling such as *ARF*s were suppressed in AIF2ox flowers. Moreover, lipid biosynthesis- and sucrose transport-related genes were repressed, resulting in impaired starch accumulation. Contrarily, sucrose and BR repressed ectopic accumulation of AIF2, thereby increasing silique length and the number of seeds. Taken together, we propose that AIF2 is negatively involved in pollen development and seed formation, and that sucrose- and BR-induced repression of AIF2 positively promotes pollen production and seed formation in *Arabidopsis*.

Keywords: auxin, ATBS1-INTERACTING FACTOR 2, BRASSINOSTEROID-INSENSITIVE 2, brassinosteroid, BRASSINAZOLE RESISTANT 1, pollen, seed

OPEN ACCESS

Edited by:
Fa Cui,
Ludong University, China

Reviewed by:
Shucai Wang,
Linyi University, China
Serena Varotto,
University of Padua, Italy

****Correspondence:***
Soo-Hwan Kim
soohwan@yonsei.ac.kr

Specialty section:
This article was submitted to Plant Physiology, a section of the journal Frontiers in Plant Science

Received: *04 May 2021*
Accepted: *02 July 2021*
Published: *27 July 2021*

Citation:
Kim Y, Kim S-H, Shin D-M and Kim S-H (2021) ATBS1-INTERACTING FACTOR 2 Negatively Modulates Pollen Production and Seed Formation in Arabidopsis. Front. Plant Sci. 12:704958. doi: 10.3389/fpls.2021.704958

INTRODUCTION

Seed development and seed size determination in plants are complicated processes controlled by diverse hormones and downstream transcription factors (Sun X. et al., 2010; Li and Li, 2016). Seeds comprise three genetically distinctive structures: the embryo giving rise to the seedling, the endosperm providing nutrients for the embryo, and the seed coat enclosing the embryo and

Abbreviations: AIF2, ATBS1-INTERACTING FACTOR 2; AIF2ox, *AIF2* over-expressing *p35S,AIF2-EGFP* transgenic plants; bHLH, basic-helix-loop-helix; BL, brassinolide; BR, brassinosteroids; DAP, days after pollination.

endosperm. The endosperm arises from the central cell and constitutes the major volume of the mature seed. In *Arabidopsis* after fertilisation, rapid proliferation and expansion of the endosperm occurs to generate a large and multinucleated cell or syncytium until the embryo reaches the heart stage and results in a large increase in seed size or volume of the seed cavity (Sun X. et al., 2010). Several factors have been shown to control seed size by regulating endosperm growth (Li and Li, 2016). Loss-of-function mutations of *HAIKU* (*IKU*) and the WRKY transcription factor *MINI-SEED 3* (*MINI3*) caused precocious cellularisation of the syncytial endosperm resulting in the reduction in endosperm size and embryo proliferation (Garcia et al., 2003; Luo et al., 2005; Wang et al., 2010). The recruitment of SHORT HYPOCOTYL UNDER BLUE1 (SHB1) by MINI3 to its own and *IKU2* promoters upregulated their expression (Zhou et al., 2009). *Arabidopsis* APETALA2 (AP2) encodes a plant transcription factor having the AP domain that is negatively involved in regulation of seed size and numbers (Ohto et al., 2009). *ap2* seeds underwent an early expanded growth period that was associated with delayed endosperm cellularisation and outgrowth of the endosperm central vacuole, resulting in an increase in embryo cell number and size, enlarged embryo sac, and large seeds with increased total protein and oil content (Jofuku et al., 2005; Ohto et al., 2009). Additionally, proteins involved in ubiquitin–proteasome pathways, G-protein signalling, mitogen-activated protein kinase signalling, and epigenetic regulation and paternal imprinting were substantially involved in the control of seed size and numbers (Sun X. et al., 2010; Li and Li, 2016; Li N. et al., 2019).

Plant hormones are closely involved in the regulation of reproduction, embryogenesis, and determination of seed size and yields. Auxin signalling was closely linked to endosperm development, embryo polarity, and patterning (Figueiredo and Köhler, 2018). Embryo sacs of plants selectively silenced for AUXIN RESPONSIVE FACTORs (ARFs) exhibited identity defects at the micropylar pole, and the pollen grains were morphologically aberrant and unviable (Liu et al., 2018). In addition, a loss-of-function mutant of *ARF2*, initially identified as *mmt* mutant, showed extra cell division in the integuments surrounding the ovule, leading to the formation of enlarged seed coats and seed size (Schruff et al., 2006). ABSCISIC ACID-INSENSITIVE5 (ABI5)-mediated abscisic acid (ABA) signalling pathways were negatively involved in the early stage of seed development by suppressing *SHB1* expression; thus, an ABA biosynthesis-deficient mutant, *aba2-1*, produced seeds with increased size, mass, and embryo cell number (Cheng et al., 2014). YODA (YDA) is a mitogen-activated protein kinase, and YDA and ETHYLENE-INSENSITIVE3 (EIN3) were integral to a sugar-mediated metabolism cascade regulating seed mass by maternally controlling embryo and seed sizes (Meng et al., 2018). Transcriptome analysis of the early stage of proliferating endosperm revealed that cytokinin signalling-related genes were significantly enriched (Day et al., 2008). Indeed, triple loss-of-function mutants of cytokinin receptors, *ahk2 ahk3 cre1*, produced enlarged but fewer seeds per silique, and this increase in seed size was correlated with an increase in the size of the mutant embryo (Riefler et al., 2006).

Brassinosteroids (BRs) are plant steroid hormones that play crucial roles in plant growth and development via extensive signal integration through direct interactions with numerous signalling pathways (Kim and Russinova, 2020). Upon binding of BRs to BRASSINOSTEROID-INSENSITIVE 1 (BRI1), the activation of BRI1 and BRI1-ASSOCIATED RECEPTOR KINASE 1 (BAK1) complex and the subsequent phosphorylation of BRASSINOSTEROID SIGNALLING KINASE (BSK) initiated a signalling cascade, relaying the membrane surface signal to the nucleus to activate the positively acting transcription factors BRASSINAZOLE RESISTANT 1/BRI1 EMS SUPPRESSOR 2 (BZR1/BES2) and BZR2/BES1 (He et al., 2005; Sun Y. et al., 2010). In the absence of BRs, their growth-promoting pathways were negatively balanced through GSK3/SHAGGY-LIKE BRASSINOSTEROID-INSENSITIVE 2 (ATSK21/BIN2)-mediated BZR1/BES1 degradation (He et al., 2002) and the antagonistic BIN2-driven increase in ATBS1-INTERACTING FACTOR 2 (AIF2) stability, an atypical non-DNA-binding bHLH transcription factor acting as a negative regulator of BR-induced growth promotion (Kim et al., 2017). Other AIF2 homologues such as AIF1, AIF3, and AIF4 were also identified with their high amino acid sequence similarity, and these AIFs were functionally redundant in inhibiting plant growth (Wang et al., 2009; Ikeda et al., 2013; Kim et al., 2017).

Environmental and endogenous stimuli affecting the timing and duration of reproductive phase can significantly impact seed yields (Shirley et al., 2019). In this regard, BRs control diverse aspects of floral organ formation, embryo and seed development, and seed size determination. For example, BSK family proteins contributed to early embryonic patterning, and *bsk1bsk2* double loss-of-function mutants exhibited reduced zygote cell growth, which resulted in a small basal cell followed by a small suspensor cell (Neu et al., 2019). Moreover, BR biosynthesis-(*cpd*) or signalling-defective (*bri1-116*, *bin2-1*) mutants had greatly reduced number of pollen grains and were defective in pollen release and exine pattern formation (Ye et al., 2010). The same study showed that BES1, a positive transcription activator for BR signalling pathways, directly bound to promoter regions of genes (*SPL*/*NZZ*, *TDF1*, *AM5*, *MS1*, and *MS2*) encoding proteins essential for anther and pollen development (Chen W. et al., 2019). BZR1 (a BES1 homologue) family transcription factors were also involved in the regulation of anther development, in a BRI1-independent manner, by upregulating *SPOROCYTELESS* (*SPL*) and its upstream activator *AGAMOUS* (*AG*) that were required for the initiation of archesporial cells (Chen L. G. et al., 2019). Furthermore, BZR1-mediated BR signalling pathways positively influenced seed numbers by regulating the expression of genes (*HLL*, *ANT*, *AP2, INO*) that were involved in development of ovule and ovule integument (Huang et al., 2013; Jia et al., 2020). BZR1 also directly bound to and activated positive regulators of seed development (*SHB1*, *MINI3*, and *IKU2*) and repressed negative regulators of seed size (*AP2* and *ARF2*) (Jiang et al., 2013). In this study, we demonstrate that AIF2 is negatively involved in pollen development and seed formation, and that sucrose- and BR-induced repression of AIF2 bHLH transcription factor positively controls pollen production and seed size/numbers in *Arabidopsis*.

MATERIALS AND METHODS

Plant Material and Growth Conditions

Wild-type *Arabidopsis thaliana* (Col-0 and WS), an *AIF2* T-DNA knockout mutant (*aif2-1*, CS811403), *aif2-1*/*aif4-1* double knockout mutant, *AIF2* overexpressing *p35S:AIF2-EGFP* transgenic plants (AIF2ox, Kim et al., 2017), a *BIN2* triple knockout mutant (*bin2*KO, *bin2bil1bil2*; Yan et al., 2009), a *BIN2* gain-of-function mutant *bin2-1* (Peng et al., 2008), *arf2-7* (Okushima et al., 2005), a *BZR1* gain-of-function mutant *bzr1-1D* (Wang et al., 2002), and a BZR1 dominant negative mutant *bzr1-1DdEAR* (Oh et al., 2014) were used for phenotype analysis and generation of transgenic plants. A native promoter-driven reporter plant, *pAIF2:AIF2-GUS*, was used to observe *AIF2* expression and localisation. Seeds were surfaced-sterilised with 95% ethanol for 10 min and cold-treated in the dark at 4°C for 72 h. These sterilised seeds were then sown in pots containing Sunshine No. 5 soil (Polysciences, United States) and grown in a growth room operating under a 16 h light (100–150 μmol m^{-2} s^{-1}) and 8 h dark cycle at 23–25℃.

Generation of Transgenic Plants With Different Mutant Backgrounds

For generation of transgenic plants ectopically expressing variants of AIF2-EGFP, cDNAs encoding either the full-length (AIF2ox) or C-terminus truncated forms of AIF2 (AIF2dC) were amplified using primers listed (**Supplementary Table 1**) and inserted upstream of the myc-tag EGFP-expressing pB7FWG2 (Karimi et al., 2002) binary vectors. Subsequently, *Agrobacterium* cultures carrying each construct were used to transform Col-0, *aif2-1*, *bzr1-1D*, *bin2-1,* and *bin2bil1bil2* genetic lines, generating plants designated as *p35S:AIF2FL-EGFP*/Col-0 (AIF2ox), *p35S::AIF2dC-EGFP*/Col-0 (AIF2dC), *p35S:AIF2FL-EGFP*/*aif2-1*(AIF2ox/*aif2-1*), *p35S:AIF2dC-EGFP*/*aif2-1*(AIF2dC/*aif2-1*), *p35S:AIF2FL-EGFP*/*bzr1-1D* (AIF2ox/*bzr1-1D*), *p35S:AIF2dC-EGFP*/*bzr1-1D* (AIF2dC/*bzr1-1D*), *p35S:AIF2FL-EGFP*/*bin2bil1bil2* (AIF2ox/*bin2bil1bil2*), and *p35S:AIF2dC-EGFP*/*bin2-1* (AIF2dC/*bin2-1*). Pollen grains of AIF2ox or *bzr1-1DdEAR* were crossed to a stigma of *arf2-7* or *aif2-1* plants to produce the AIF2ox/*arf2-7* and the *bzr1-1DdEAR*/*aif2-1* transgenic plants, respectively.

Generation of *aif2-1*/*aif4-1* Double Knockout Plants

The CRISPR-Cas9 system was used as described previously (Kim et al., 2016). Briefly, guide RNA sequences targetting the exon of *AIF4* (At1g09250) gene were designed using the guide RNA(gRNA) design tool (Concordet and Haeussler, 2018)[1] as follows: 5′-GATTGAACTCGTCTCCGGCGCGGCG-3′ and 5′-AAACCGC CGCGCCGGAGACGAGTTC-3. The complementary gRNA was then inserted into pHAtC vector, and the resulting construct was transformed into *aif2-1* to generate the *aif2-1*/*aif4-1* double knockout mutant. A deletion of guanine at base pair position 249 starting from the initiator ATG was confirmed by performing DNA sequencing for the PCR-amplified *AIF4* gene.

[1]http:crispor.tefor.net/

Total RNA Isolation and qRT-PCR Analysis

Total RNAs were extracted using a plant RNA extraction kit (Intron Biotechnology, South Korea) from flowers at different floral stages, siliques with developing seeds, or siliques isolated from *in vitro*-cultured flowers. To examine semi-quantitative RNA expression, the first-strand cDNA was synthesised using a ReverTra Ace qPCR RT Master Mix kit (Toyobo) according to the manufacturer's instructions. Quantitative real-time RT-PCR (qRT-PCR) was performed by the SYBR green method using the Applied Biosystems Step One Plus System (Applied Biosystems, United States) with appropriate primers (**Supplementary Table 2**). The conditions for PCR amplification were as follows: 1 cycle of 95℃ for 10 min; 40 cycles of 95℃ for 15 s, 60℃ for 30 s, and 72℃ for 30 s. Expression of each transcript was normalised against the amount of *UBC1* control in each sample. Three biological replicates were included in each experiment, and expression in each replicate was measured three times.

Protein Isolation and Western Blot Analysis

To examine expression of AIF2-EGFP in AIF2ox transgenic plants, total proteins were extracted from *in vitro*-cultured flowers using a homogenisation buffer (125 mM Tris-Cl, 4% sodium dodecyl sulphate, 2% β-mercaptoethanol, 1 mM phenylmethylsulfonyl, pH 7.9) and size-fractionated on 12% SDS-PAGE. Fractioned total proteins were then transferred onto a nitrocellulose membrane (Whatman, Germany) and probed against anti-GFP rabbit polyclonal antibodies (Santa Cruz Biotechnology, United States) in 5% milk/TBST (50 mM Tris-acetate, 150 mM NaCl, 0.05% Tween 20, pH 7.6). Goat anti-rabbit HRP-conjugated secondary antibody (Abcam, United Kingdom) was used to quantify the AIF2-EGFP protein. Peroxidase activity was detected using an ECL solution (Thermo Fisher Scientific Inc., United States) according to the manufacturer's instructions.

Histochemical Staining and Microscopic Observation

For pollen grain staining, anthers were removed from newly opening flowers and stained with Alexander's solution for 8 h at 50°C (Peterson et al., 2010), mPS-PI solution for 2 h at room temperature (Truernit et al., 2008), or pollen isolation solution containing 5μg/ml DAPI. Stained anthers or pollens were then observed using either a differential interference contrast (DIC)-equipped fluorescence microscope (Olympus BX60, Japan) or a Meta NLO-UV confocal laser scanning microscope (Zeiss LSM510, Germany).

To examine *in vivo* pollen tube growth, pistils were hand-pollinated with pollen grains of the same flower. The pollinated pistils were then fixed with 25% acetic

acid at different times (h) after pollination, hydrated with an ethanol series, and softened with NaOH. Pollen tubes were then stained with aniline blue following a previously reported method (Mori et al., 2006) and their growth was examined using the Zeiss confocal microscope. For *in vitro* pollen tube growth assay, pollen grains were collected from 10–20 freshly opened flowers and grown on a solid germination medium (Boavida and McCormick, 2007) for 6 h in the dark at room temperature. Pollen tubes were photographed using a camera connected to the DIC-equipped Olympus microscope and their lengths were measured using Image J.[2]

To examine AIF2 expression *in planta*, opened flowers of *pAIF2:AIF2-GUS* transgenic plants were collected and fixed in 90% acetone for 20 min on ice. Staining and detection of GUS activity were performed according to the method described by Jefferson (1987). The stained floral organs were observed under the DIC-equipped Olympus microscope.

For starch staining of developing seeds, pistils were hand-pollinated with pollen grains of the same flower. Developing siliques were then collected at different days after pollination (DAP), placed in fixing solution containing 10% acetic acid and 90% ethanol (v/v), and incubated overnight in a water bath at 60℃ followed by washing with 70% ethanol. Siliques were then stained in Lugol's iodine solution for 5 min and observed under a DIC-equipped Olympus microscope.

Seed Clearing and Imaging Analysis

For determination of embryo developmental stages, siliques were fixed overnight in solution containing 10% acetic acid and 90% ethanol (v/v) and washed twice sequentially with 90% and 70% ethanol. Siliques were then cleared overnight with chloral hydrate solution (Yadegari et al., 1994). These cleared seeds from siliques were mounted in clearing solution for observation under the Olympus microscope. Afterward, the embryo area and the rest of the integument-surrounded area were measured using Image J.

In vitro Flower Culture

Flowers in an early stage of seed development (between DAP3.5 to DAP4) were cut and immediately transferred to 30% ethanol for 3 min. These sterilised flowers were placed in half-strength solid MS media containing brassinolide (BL, 10^{-9} M) supplemented with or without 3% sucrose (w/v). These flowers were then cultured for 9 days in a growth chamber operating under a 16 h light (100–150 μmol m^{-2} s^{-1}) and 8 h dark cycle at 23–25℃. Siliques were collected from *in vitro*-cultured flowers to examine their phenotypes.

Measurement and Statistical Analysis

Over 100 siliques or flowers were collected from 30–40 plants and used for each experiment. All experiments were conducted in triplicate at a minimum, and the data were statistically analysed using the Student's *t*-test.

[2]http://rsbweb.nih.gov/ij/

RESULTS

Overexpression of AIF2 Resulted in Defective Formation of Pollen Grains and Reduced Seed Production

Previously, we demonstrated that AIF2 were negatively involved in BR-induced growth regulation (Kim et al., 2017); nonetheless, its roles in the development of other organs are unknown. As an initial step to elucidate the roles of AIF2 in pollen and seed development, we first investigated silique phenotype of AIF2ox transgenic plants (*p35S:AIF2-EGFP*/Col-0). Three independent transgenic lines (AIF2ox-1 to AIF2ox-3) differentially expressed AIF2 protein, ranged from high to low levels compared with the Col-0 plants (AIF2ox-1 to AIF2ox-3, respectively) and showed retarded growth phenotypes as previously reported (**Supplementary Figures 1A,B**; Kim et al., 2017). Interestingly, their siliques were smaller in AIF2ox plants, and their reduction in silique length at floral stage 17 was inversely correlated with the abundance of AIF2 proteins: for instance, AIF2ox-1 showed the most severely retarded silique phenotype (**Supplementary Figures 1C,D**). Hereafter, we took AIF2ox-1 line for further analysis of pollen, embryo, and seed phenotypes.

Disrupting pollen/ovule development, pollination, pollen tube growth, and fertilisation results in a reduced number of seed sets and silique size. We found that *AIF2*-overexpressing transgenic *Arabidopsis* plants produced smaller and frequently unfused siliques (**Figure 1A**, left and middle panels). Regarding unfused siliques, INDEHISCENT (IND), SPATULA (SPT), and ALCATRAZ (ALC) are bHLH transcription factors required for proper valve margin development and later differentiation of the silique dehiscence zone, allowing seed dispersal (Girin et al., 2011; Groszmann et al., 2011; Kay et al., 2013). Accordingly, we found that *IND* and *ALC* expression was down-regulated in *AIF2*-overexpressing plants, whereas it was upregulated in *aif2-1* and *aif2-1*/*aif4-1* plants (**Figure 1A**, right panel). In addition to the short and unfused silique phenotypes, the number of ovules in a silique was also greatly reduced in AIF2ox (**Figure 1B**, left and middle panels), and even the fertilised eggs of AIF2ox plants produced a higher ratio of aborted seeds (**Figure 1B**, right panel). Consequently, the number of both siliques per plant (**Figure 1C**) and seeds per silique (**Figure 1D**) in AIF2ox plants was lower than that in wild-type Col-0, resulting in a significantly reduced total seed weight or productivity in AIF2ox plants (**Figure 1E**). In contrast, *aif2-1*/*aif4-1* plants displayed opposite silique and seed phenotypes.

Arabidopsis plants are propagated through self-pollination; thus, the ratio of stamen to pistil length is important for successful pollination. We found that pistils and stamens of AIF2ox plants were shorter than those of Col-0 plants (**Figure 2A**, 1^{st} to 3^{rd} panels). Two knockout plants of *AIF2*, *aif2-1* and *aif2-1*/*aif4-1*, had longer pistils and stamen. Nonetheless, the ratio of stamen

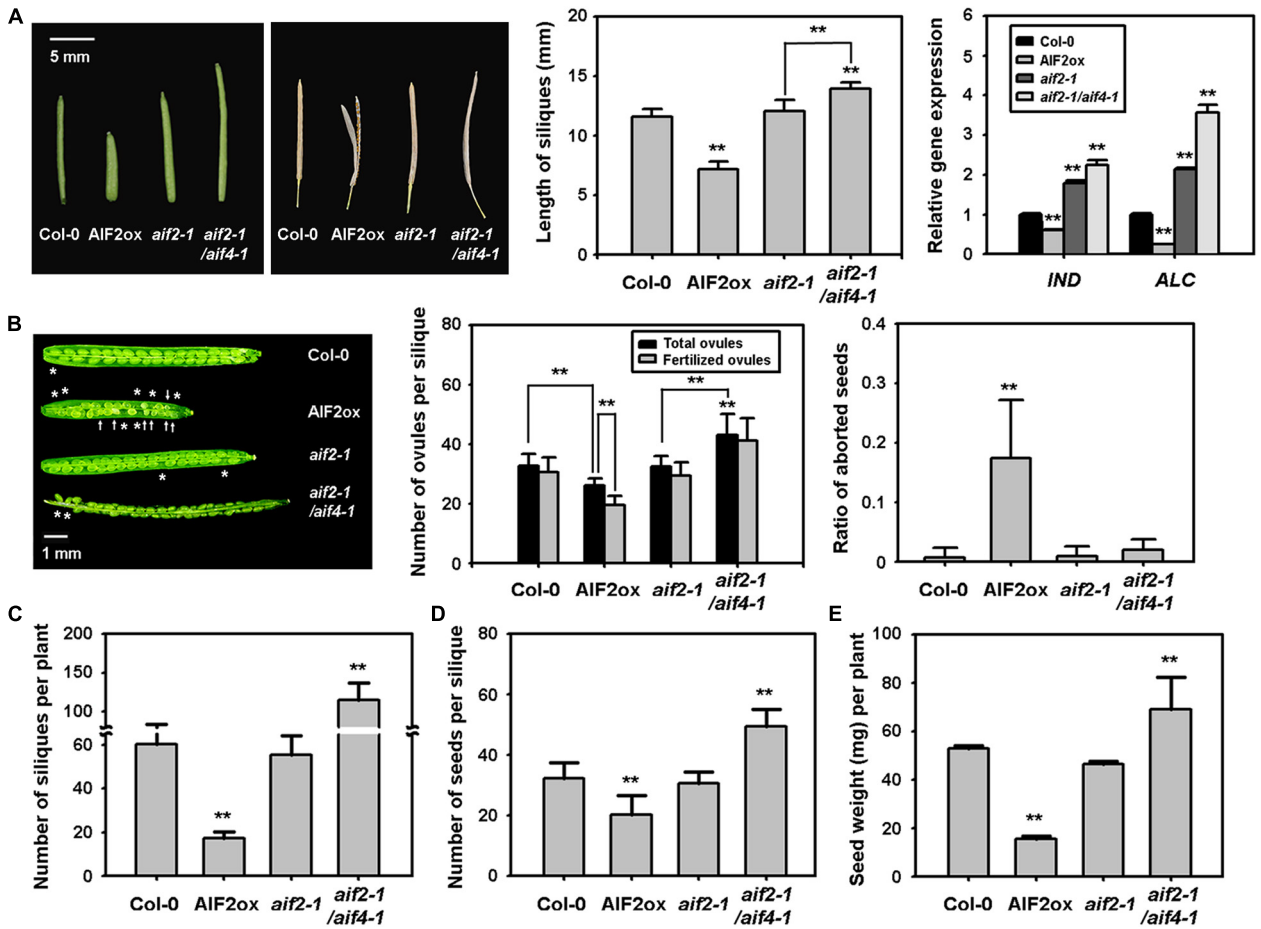

FIGURE 1 | Defective silique phenotypes of *AIF2*-overexpressing *p35S:AIF2-EGFP* transgenic plants (AIF2ox). **(A)** Silique with shorter and premature dehiscence phenotypes. The picture on the left shows representative shorter and unfused gynoecia silique phenotypes. Siliques from opened flowers were measured for their length (middle) and transcript expression of genes involved in valve margin development of the carpel (right). Relative expression of each gene is normalised as a ratio of the Col-0 plants, which was set to 1. **(B)** Reduced ovule development and aborted seeds. The picture on the left shows regions lacking ovule development (*) and aborted fertilised eggs (arrow). Total ovules presented in the middle are calculated by the sum of visibly developed ovules and invisible empty ovule area. Fertilised ovules indicate the visible ovules. The ratio of aborted seeds on the right represents the ratio of seeds with defective phenotype (such as smaller or white) to total visible seeds. **(C–E)** Number of siliques **(C)**, seeds **(D)**, and total seed weight **(E)** was measured from more than 100 siliques collected from 30–40 plants. Bar graphs represent means ± SD and statistical difference from either the Col-0 control or bracketed samples is indicated by two asterisks (**) at $P < 0.01$.

to pistil was higher in AIF2ox plants (**Figure 2A**, right panel) indicating that the reduced growth of the stamen or pistil in AIF2ox plants is unlikely to be the cause of the reduced seed production and retarded silique development.

Next, we examined pollen productivity and viability. *AIF2* was specifically expressed in unfertilised ovules and pollen grains of *pAIF2:AIF2-GUS* plants but not in the petal, sepal, stigma, and style (**Supplementary Figure 2A**). This expression pattern of *AIF2* implies that AIF2 may play a role in male- and female gametophyte development. Similarly, AIF2-EGFP proteins of AIF2ox plants were abundantly expressed in ovules and pollen grains (**Supplementary Figures 2B–D**). Interestingly, AIF2ox plants contained fewer pollen grains in the anthers, and this reduction in pollen numbers was inversely correlated with the expression levels of AIF2 proteins (**Supplementary Figure 3**). Consequently, the number of pollens harvested from all anthers from a flower was lower in AIF2ox plants, but slightly higher in *aif2-1* and *aif2-1*/*aif4-1* plants, than in Col-0 plants (**Figure 2B**). To test pollen viability, we performed *in vitro* pollen germination assay and found that the efficiency of pollen germination was dramatically reduced in AIF2ox plants (**Figure 2C**). More than 80% of pollen grains in Col-0 and the two *AIF2* knockout plants germinated successfully and initiated pollen tube growth, whereas only 9.2% of pollen germinated in AIF2ox plants. This poor germination efficiency may due to, in part, the high frequency of aborted and smaller pollens commonly observed in AIF2ox plants (**Figure 2D**).

In *Arabidopsis*, microspore mother cell (2N) undergoes a series of meiosis I and meiosis II (microsporogenesis) to produce a tetrad of microspores (N), and each microspore develops into a bicellular pollen containing a vegetative cell and a generative cell and further to tricellular mature pollen having one vegetative

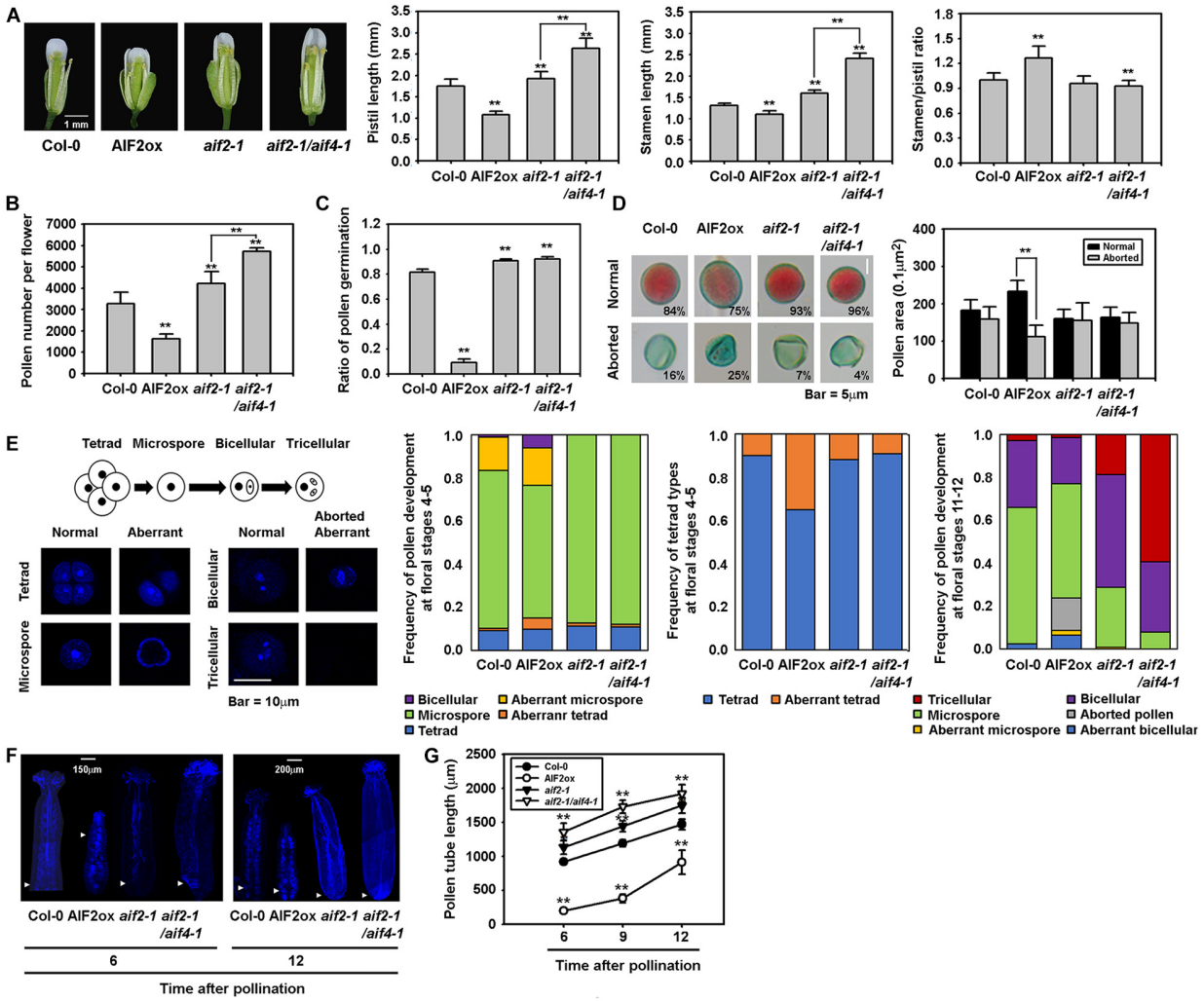

FIGURE 2 | Retarded growth of reproductive organs and degenerated pollen production and germination found in AIF2ox plants. **(A)** Flowers of Col-0, AIF2ox, *aif2-1* and *aif2-1/aif4-1* plants and the lengths of pistils, stamens, and the ratio of stamen to pistil. Number of open flowers examined >30. **(B)** Measurement of pollen numbers counted under a bright microscope without pollen staining. Number of open flowers examined >20. **(C)** *In vitro* pollen germination analysis. The efficiency of germination is represented by the ratio of germinated pollens after 6 h incubation in the germination medium. Number of pollens examined >3,000 taken from 20–25 flowers. **(D)** Frequency and size of the Alexander solution -stained viable pollens (normal) and non-stained aborted pollens. Number of pollens examined >2,000 taken from 15–20 open flowers **(E)** Defective pollen development in AIF2ox flowers. Pollens in different floral stages were stained with DAPI to reveal pollen developmental stages and pollens with intact nuclei (normal), without (aborted) or abnormal nuclei having defects in mitosis and appearance (aberrant). Number of pollens examined >1,000 taken from flowers at stage 4–5 or stage 11-12. **(F,G)** *In vivo* pollen tube growth assay. Arrowhead indicates the end of aniline blue-stained pollen tubes at 6 or 12 h after hand-pollinated self-pollination in the same flowers **(F)** and lengths of pollen tubes at different times were measured after hand-pollination **(G)**. $n > 15$ for each time point was used for analysis. Statistical difference from either the Col-0 control or bracketed samples is indicated by two asterisks (**) at $P < 0.01$.

cell and two sperm cells (microgametogenesis) (**Figure 2E**, 1st panel). We found that AIF2ox plants produced higher frequency of aberrant tetrad (36% of tetrads), a tetrad microspore having no nucleus or less microspores, in flowers of stage 4—5 (**Figure 2E**, 2nd and 3rd panel). These defects may lead an increased ratio of aborted/aberrant microspore and bicellular pollens (**Figure 2E**, 4th panel). In contrast, the ratio of normal microspore, bicellular and tricellular pollens at floral stage 11—12 was decreased. These results imply that AIF2ox plants underwent a defective microsporogenesis, thus produced less mature and viable pollens. Notably, it seemed that male gametophytogenesis progressed faster in *aif2-1* and *aif2-1*/*aif4-1* than in Col-0 plants (**Figure 2E**, 4th panel). Nonetheless, they had a similar ratio of normal microspore, bicellular and tricellular pollens in total. To further test pollen activity, we manually self-pollinated stigmas of test plants and measured the growth of pollen tubes. At 6 h after hand-pollination, the wild-type pollen tubes grew 917 μm on average, whereas those of *aif2-1* and *aif2-1*/*aif4-1* plants were longer and those of AIF2ox plants were shorter (**Figures 2F,G**). This retarded pollen growth in AIF2ox plants was also confirmed

by the fact that all AIF2ox pollen tubes germinated *in vitro* were in the range of 0 to 150 μm (average 67.2 μm), whereas those of Col-0 and *aif2-1* plants grew 240 μm and 184 μm on average, respectively (**Supplementary Figure 4**). Nonetheless, most pollen tubes of Col-0 (1,468 μm), AIF2ox (914 μm), *aif2-1*(1,746 μm), and *aif2-1*/*aif4-1*(1,920 μm) reached almost the end of the pistils at 12 h, considering the pistil lengths of Col-0 (1.74 mm), AIF2ox (1.08 mm), *aif2-1* (1.92 mm), and *aif2-1*/*aif4-1* (2.53 mm) (**Figure 2A**). These results suggest that pollen tube growth is unlikely the reason for reduced male sterility and seed productivity in the AIF2ox plants. Collectively, we demonstrated that the defective silique growth and seed production in *AIF2*-overexpressing transgenic plants were caused by the reduced amount of pollen production and less-effective pollen tube germination but not by retarded stamen/pistil growth or pollen tube elongation.

Expression Patterns of Pollen- and Auxin-Related Genes Were Significantly Modulated in AIF2-Overexpressing Plants

Timely expression of *SPL*/*NZZ*, *TDF1*, and *MS1* is essential for early microspore mother cell formation to late pollen maturation (Yang et al., 2007; Ye et al., 2010; Chen L. G. et al., 2019; Chen W. et al., 2019). We examined transcript expression of these genes in flowers at floral stages 11/12 and 15. Two mitotic divisions of microspores and tapetum degeneration occur at floral stage 11, and desiccation of pollen grains followed by anther dehiscence occurs in flowers of floral stage 12 (Kim et al., 2001). Then, the flower opens and is self-pollinated during the stages 13 to 15. As expected, in floral stage 15 of Col-0 and the two *AIF2* knockout plants, these genes were transcriptionally down-regulated compared to the transcription of these genes in stage 11 or 12 flowers (**Figures 3A–C**). Unexpectedly, we found that *SPL* and *TDF1* at stage 15 maintained a higher expression both in AIF2ox and *pAIF2:AIF2-GUS* plants. In addition, although *MS1* in floral stage 15 showed lower expression than that at stage 11/12, a relatively higher expression was maintained than that of the same floral stage in Col-0 and the two *AIF2* knockout plants.

Auxin plays important roles in the proper development of flower and seeds (Shirley et al., 2019); thus, the mutants defective in auxin biosynthetic genes, such as *YUCCA*s, show not only abnormal flowers but also defects in the embryo and endosperm of seeds (Cheng and Zhao, 2007; Figueiredo and Köhler, 2018). TEOSINTE BRANCHED 1, CYCLODEA, and PROLIFERATING CELL FACTORSs (TCPs) bind to the promoters of *YUCCAs* to promote their gene expression and directly upregulate auxin levels (Challa et al., 2016; Zhou et al., 2018). Moreover, TCP1 promotes BR biosynthesis by directly upregulating the expression of a BR-biosynthetic gene *DWARF4* (*DWF4*) (Guo et al., 2010). We found that *TCP1* and *TCP4* genes of AIF2ox or the *pAIF2:AIF2-GUS* plants were relatively down-regulated at stage 11/12 compared with those of Col-0 plants at the same stage, and they were further downregulated at stage 15 (**Figures 3D,E**). Interestingly, these two genes were greatly upregulated at stage 15 and/or stage 11/12 of *aif2-1* and *aif2-1*/*aif4-1* plants. Similarly, three auxin biosynthetic genes (*YUCCA*s) and genes for two positive regulators of auxin signalling (*ARF*s) were down-regulated at either stage 11/12 (*YUCCA1*, *YUCCA2*, and *YUCCA6*) or 15 (*YUCCA1*, *YUCCA2*, *ARF6,* and *ARF8*) of AIF2ox plants while expression of these genes in the two *AIF2* knockout plants at the same stage was relatively up-regulated compared with those of Col-0 plants (**Figures 3F–J**). Transcript expression pattern of *DWF4* was also similar to that of the *TCP1*, so that it was relatively down-regulated when *TCP1* was suppressed at stage 15 of two *AIF2*-expressing transgenic lines (**Figure 3K**). These results indicate that aberrant expressions of pollen development-, auxin-, and BR-related genes in AIF2ox plants may partially explain the observed reduction in pollen grains together with the less-effective pollen tube germination and aborted seed development.

AIF2ox Plants Differentially Regulated Transcript Expression of Seed-Forming Regulators

Previously, BZR1-mediated BR signalling pathways were shown to increase seed size by affecting the integument, endosperm, and embryo development (Jiang et al., 2013). We found that ectopic expression of *AIF2* in *aif2-1* plants results in smaller and lighter plant seeds. The seed length to width ratio in Col-0 or *aif2-1* and *aif2-1*/*aif4-1* plants was 1.8–2.2, and ectopic expression of *AIF2* in the *aif2-1* plants modified the average ratio to 1.54 (**Figure 4A**). This implies that seeds of *AIF2*-overexpressing plants were likely to be rounder rather than ellipsoidal, typical of the seeds of Col-0 and the two *AIF2* knockout plants. As for a confirmation of the AIF2 functions in seed size and weight determination, we demonstrated that expression of C-terminal deleted *AIF2* (AIF2dC, a dominant negative form of AIF2 function, Kim et al., 2020) obliterated this complementation effect. In addition, AIF2ox plants produced lighter seeds than those of Col-0, *aif2-1*, *aif2-1*/*aif4-1*, and AIF2dC-overexpressing *aif2-1* plants (**Figure 4B**). Accordingly, we found that expression of the endosperm- and embryo-forming *SHB1*, *IKU1*, and *MINI3* were greatly reduced in AIF2ox plants. In contrast, *AP2* and *ARF2*, which negatively act in seed formation, were upregulated (**Figure 4C**) in the same AIF2ox plants. ARF2 is a transcriptional repressor of auxin-regulated genes, and *arf2* loss-of-function mutations increased seed size and weight as well as showed late flowering phenotypes under long day conditions in *Arabidopsis* (Schruff et al., 2006; Choi et al., 2018). To further investigate genetically whether the increased expression of *ARF2* in the AIF2ox plants was responsible for the small-seed phenotype, we crossed pollen of AIF2ox with ovules of *arf2-7* plants and found that an ectopic expression of AIF2 did not modulate *arf2-7* seed phenotypes (**Figure 4D**). These findings suggest that AIF2 acted upstream of ARF2 in negatively regulating seed shape and weight.

Reduction in seed size often results from coordinated reduction in endosperm size, embryo proliferation, and cell elongation of the maternally derived integument. *AIF2* was predicted to be highly expressed in the seed coats, chalazal endosperm, and spotted areas of peripheral endosperms through

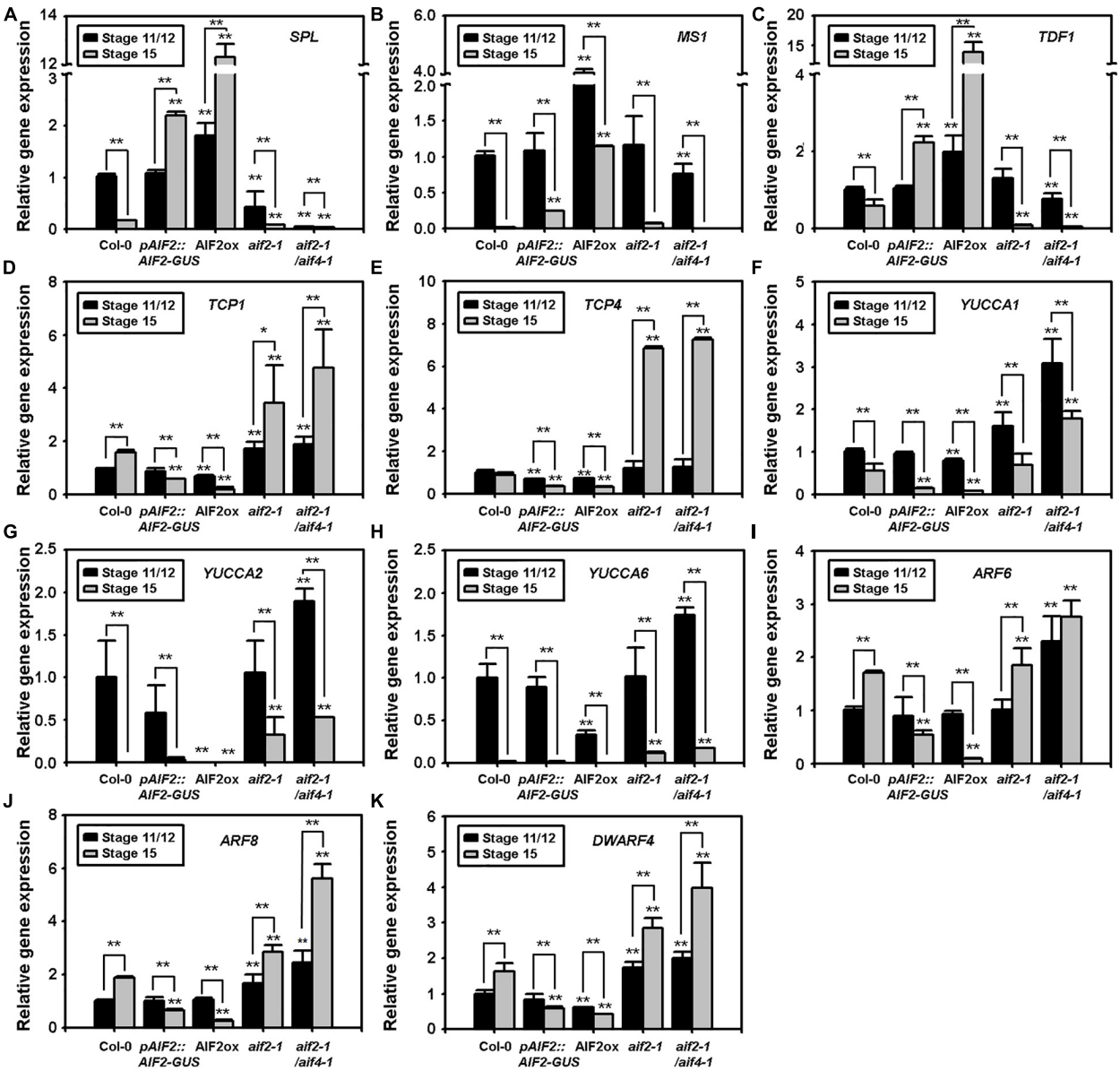

FIGURE 3 | (A–K) Transcript expressions of pollen- and seed-regulating transcription factors **(A–C)**, auxin biosynthesis **(D–H)** and signalling-related genes **(I,J)**, and a brassinosteroid biosynthesis gene, *DWF4* **(K)**. Total RNA was isolated from flowers at floral stages 11/12 or 15, and transcript expression of genes was examined using qRT-PCR. Relative expression of each gene is normalised as a ratio of the Col-0 plants at floral stage 11/12, which was set to 1. Statistical difference from the same stage of the Col-0 flowers or bracketed samples is indicated by an asterisk (*) on bars at $P < 0.05$ and two asterisks (**) at $P < 0.01$.

the pre-globular to torpedo stages (**Supplementary Figure 5**).[3] In contrast, its expression was low in the developing embryo. To evaluate the effects of AIF2 on the endosperm- and embryo-forming processes, we morphologically investigated the progression of seed development in AIF2ox plants. All Col-0 plants at DAP3 progressed to globular embryos, whereas none of the AIF2ox plants showed distinct globular embryos (**Figure 5A**). At DAP6, all Col-0 and *aif2-1* plants developed into heart stage embryos. In contrast, almost half the AIF2ox plants remained as globular stage embryos. At DAP8, more than 40% of Col-0 plants had torpedo stage embryos, which further progressed in *aif2-1* plants such that all embryos were at the torpedo stage. Again, most embryos of AIF2ox plants were still at the heart stage, and only 5% of the total embryos were at the torpedo stage at DAP8. These results imply that embryonic progression is severely delayed in *AIF2*-overexpressing plants.

After fertilisation, the embryo grows to fill the cavity at the expense of the endosperm; thus, at maturity, the seed contains only a single layer of endosperm cells in *Arabidopsis* (Olsen, 2001; Sun X. et al., 2010). We found that the embryo area was

[3]http://bar.utoronto.ca/eplant/

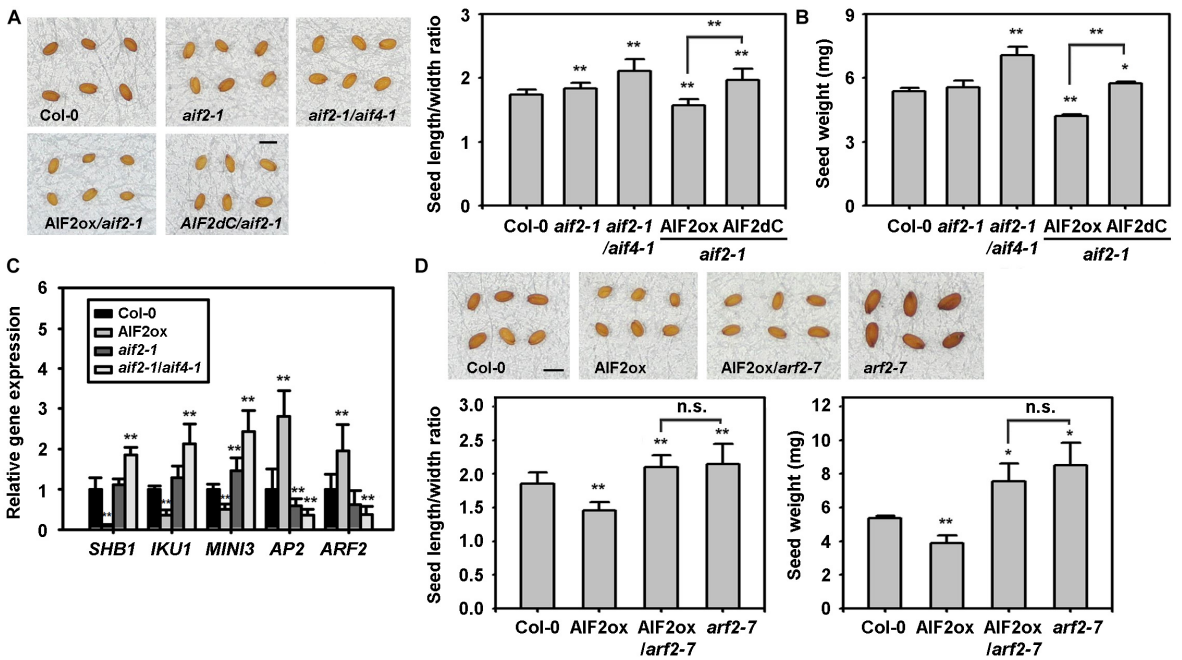

FIGURE 4 | AIF2-mediated negative regulation of seed size and weight. **(A,B)** AIF2 overexpression-led smaller and rounder (less length to width ratio) **(A)** and lighter **(B)** seeds of *aif2-1* loss-of-function plants and their reciprocal confirmation through complementation assay with a dominant negative form of AIF2, AIF2dC. **(C)** Transcript expression of seed size-related genes in siliques with developing seeds. Relative expression of each gene is normalised as a ratio of the Col-0 plants, which was set to 1. **(D)** ARF2-dependent AIF2 effects on seed size and weight. Scale bars in pictures represent 0.5 mm in length. Statistical difference from the Col-0 control is indicated by an asterisk (*) at $P < 0.05$ and two asterisks (**) at $P < 0.01$. n.s., non-significant. Number of seeds examined for measurement of length/width ratio and weight >800.

increased in Col-0 plants (**Figure 5B**). A dramatic increase in the embryo size was especially observed at DAP5 when more than 75% of embryos progressed to the heart stage from the globular stage. The embryo area of *aif2-1* at DAP7 and 8 was much larger than that of Col-0 plants, mainly because most *aif2-1* embryos were in the torpedo stage. In comparison, the average embryo area in AIF2ox plants was much smaller, mainly because of their delayed embryonic progression. For example, embryos of AIF2ox seeds were at the globular or heart stage at DAP6 when all embryos of Col-0 or *aif2-1* seeds were at the heart stage. Similarly, integument-surrounded seed area excluding the embryo area showed a size reduction in AIF2ox plants (**Figure 5C**). Collectively, our results demonstrated that *AIF2*-overexpressing transgenic plants suppressed genes encoding positive factors (*SHB1*, *IKU1*, *MINI3*) of seed size determination but promoted gene expression for negative factors (*AP2* and *ARF2*), resulting in delayed embryogenesis and seeds with smaller size.

AIF2-Regulation of Seed Shape and Weight Is Epistatic to Those by BZR1 and BIN2

Previously, we demonstrated that AIF2 was significantly suppressed by BRI1/BZR1-mediated signalling pathways, and BIN2-mediated AIF2 phosphorylation augmented the BIN2/AIF2-mediated negative circuit of BR signalling pathways in growth-promoting cellular activities (Kim et al., 2017). In this study, *BIN2* triple knockout mutant (*bin2bil1bil2*, *bin2*KO) had ellipsoidal seed shape which was almost similar to that of WS plants (insignificant increase in seed length to width ratio) (**Figure 6A**). However, constitutive expression of *AIF2* in *bin2*KO background produced rounder seeds by significantly decreasing the seed length to width ratio. In contrast, *BIN2* gain-of-function mutant (*bin2-1*) produced rounder seeds, and an ectopic expression of a C-terminal deleted *AIF2* (*bin2-1*/AIF2dC) resulted in the ellipsoidal shape owing to an increase in seed length to width ratio. Similarly, transgenic expression of *AIF2* or C-terminal-deleted *AIF2* either decreased or increased seed weights in *bin2*KO and *bin2-1*, respectively (**Figure 6B**). These results suggest that AIF2 acted downstream of BIN2 in the regulation of seed size and weight.

Deletion of ERF-associated amphiphilic repression (EAR) motif at the carboxy terminus of BZR1 abolished the abilities to regulate gene expression and cell elongation (Oh et al., 2014). We found that transgenic expression of EAR-deleted *bzr1-1D* (*bzr1-1DdEAR*) produced round and light seeds, similar to the seeds of *bzr1-1D* that ectopically expressing AIF2ox. Again, expression of *AIF2dC* in *bzr1-1D* partially negated the AIF2 effects on seed shape determination (**Figure 6C**) and even greatly increased seed weights in the same plants (**Figure 6D**). These results imply that AIF2 acted downstream of BZR1 for seed size and weight determination. Supporting this idea, the described dominant negative effects of *bzr1-1DdEAR* in seed phenotypes

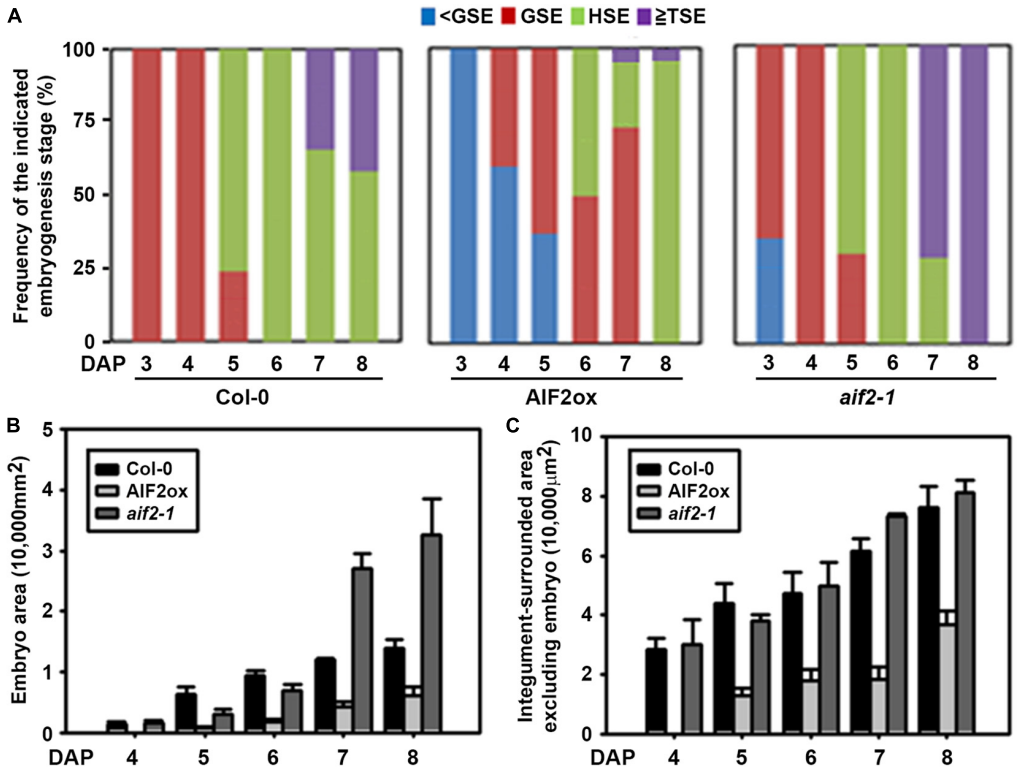

FIGURE 5 | Delayed embryogenesis and smaller embryo development in *AIF2*-overexpressing *p35S:AIF2-EGFP* (AIF2ox) transgenic plants. **(A–C)** Comparison of the frequency of developmental stages of embryos **(A)**, size of embryo area **(B)**, and the size of remaining integument-surrounded area excluding the embryo **(C)** observed at different days after hand-pollinated self-pollination (DAP). <GSE, pre-globular stage; GSE, globular stage embryo; HSE, heart stage embryo; TSE, torpedo stage embryo. Number of embryos examined for each time point >150–200.

were not functional in *aif2-1* genetic background plants. Thus, AIF2-controlled seed phenotypes acted downstream of BZR1 and BIN2, and BZR1-regulated seed shape and size were contrary to that by AIF2, whereas BIN2 functioned similar to AIF2.

Transcript Suppression of Sucrose Transporter Genes and Lipid-Biosynthetic Genes in AIF2ox Plants and Subsequent Defects in Starch and Oil Accumulation

AIF2ox plants presented in this report not only delayed embryogenesis but also generated wrinkled and shrunken seeds (**Supplementary Figure 6**). Therefore, we examined starch accumulation in developing seeds, investigated transcript expression of proteins which promote sucrose transport and lipid biosynthesis, and scrutinised the cause of AIF2ox phenotypes.

Starch is actively accumulated in the proliferating tissues, whole seed coat, ovary wall, placenta–septum region, and funiculus during early zygote and embryo development (Hedhly et al., 2016), which was also seen in the globular to torpedo stage embryos of Col-0 and *aif2-1* plants (**Figure 7A**). In contrast, starch granules in the seed coat of AIF2ox plants were relatively weakly stained with Lugol's iodine dye. Sucrose, the major transport form of carbohydrate in plants, is delivered via the phloem to the maternal seed coat and then secreted from the seed coat to the embryo through SWEET11, 12, and 15 efflux carriers (Chen et al., 2015). Compared to the transcript levels of *SWEET11*, *SWEET12*, and *SWEET15* in Col-0, the transcript levels were greatly down-regulated in siliques of AIF2ox plants but upregulated in those of *aif2-1* (except for *SWEET12*) (**Figure 7B**). We hypothesised that reduced expression of sucrose transporter genes in AIF2ox plants and the subsequent defects in starch accumulation resulted in seeds with delayed embryogenesis and wrinkled phenotype.

Developing embryos of *Arabidopsis* and oilseed rape initially accumulated mother plant-driven starch, but the starch levels were declined with increase in the rates of storage lipid and protein synthesis (Andriotis et al., 2012). Accumulation of seed oil requires the co-ordination of *de novo* fatty acid (FA) biosynthesis and triacylglycerol (TAG) assembly. It was known that FA desaturase 2/3 (FAD 2/3), acyl-CoA:lysophosphatidylcholine acyl transferases (LPCATs), acyl-CoA:diacylglycerol acyltransferase 1 (DGAT1), and phospholipid:diacylglycerol acetyltransferase 1 (PDAT1) were positively involved in the modification of FAs and subsequent assembly of FA-driven acyl-CoA into glycerol, producing TAGs (Zhang et al., 2009; Xu et al., 2012; Lou et al., 2014). We showed

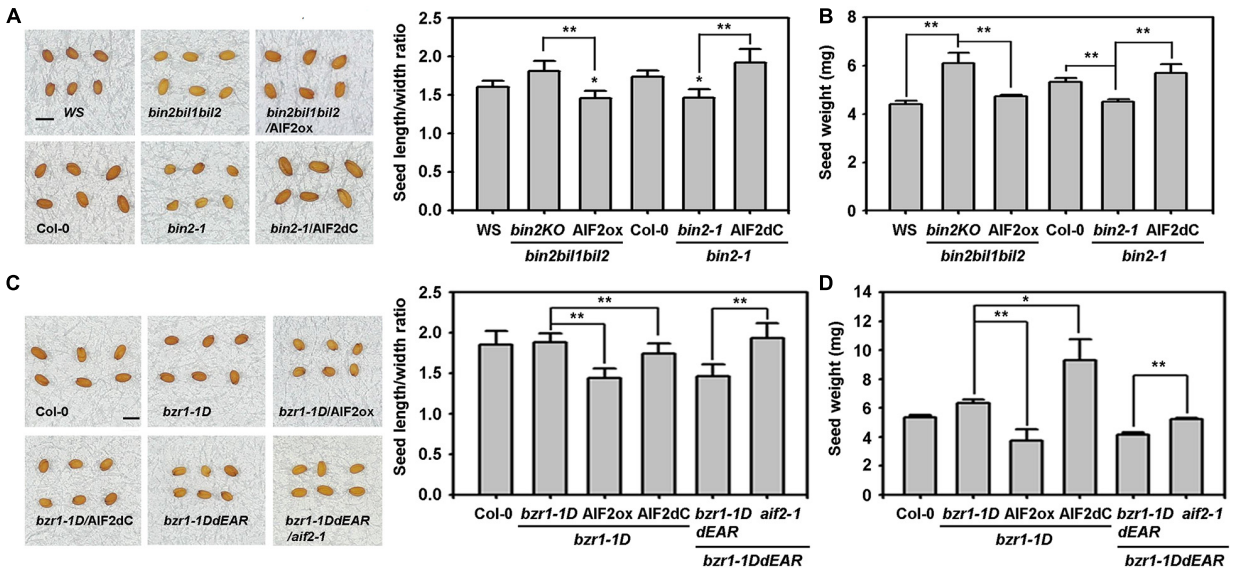

FIGURE 6 | Genetic and functional interactions of AIF2 with BIN2 and BZR1 in the regulation of seed size and weight. **(A,B)** Evaluation of genetic and functional interaction of AIF2 with BIN2 in the regulation of seed size **(A)** and seed weight **(B)**. Transgenic constructs ectopically expressing AIF2ox or AIF2dC were transformed into a BIN2 gain-of-function mutant, *bin2-1*, or a BIN2 loss-of-function mutant, *bin2bil1bil2* (*bin2*KO), and their seed phenotypes were evaluated. **(C,D)** Evaluation of genetic and functional interaction of AIF2 with BZR1 in the regulation of seed size **(C)** and seed weight **(D)**. Transgenic constructs ectopically expressing AIF2ox or AIF2dC were transformed into a BZR1 gain-of-function mutant, *bzr1-1D*, or plants constitutively expressing *bzr1-1DdEAR*, a loss-of-function form of BZR1, were crossed to *aif2-1* to examine their seed phenotypes. Statistical difference between bracketed samples is indicated by an asterisk (*) at $P < 0.05$ and two asterisks (**) at $P < 0.01$. Number of seeds examined for measurement of length/width ratio and weight >800. Scale bars in pictures represent 0.5 mm in length.

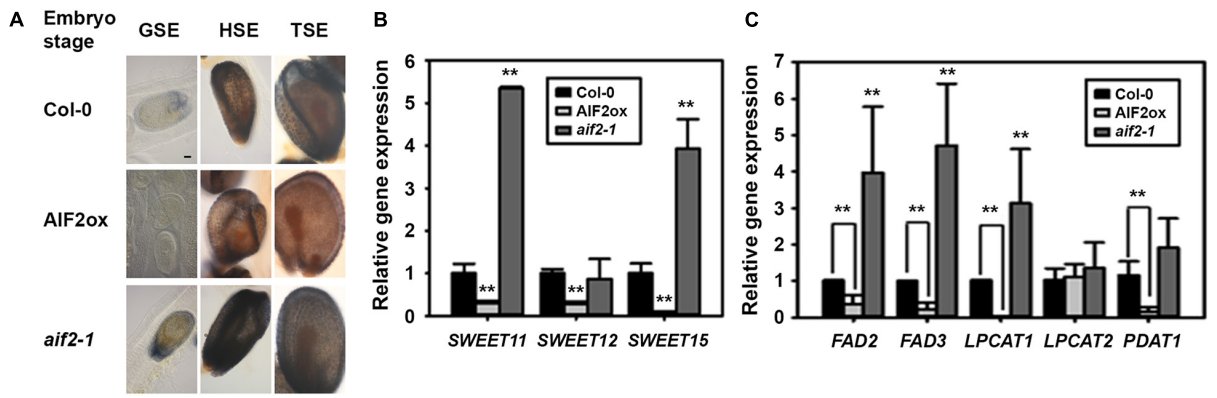

FIGURE 7 | Reduced starch and oil accumulation in seeds of *AIF2*-overexpressing *p35S:AIF2-EGFP* (AIF2ox) transgenic plants. **(A)** Photographic comparison of starch accumulation in developing seeds. Siliques were stained with Lugol's staining dye, and seeds with embryos at the same developmental stage were compared for starch accumulation. Number of seeds examined for each stage of the corresponding plants >150. Pictures show a representative image. **(B,C)** Total RNA was extracted from siliques with developing seeds, and the transcript expression for sucrose transport-related genes **(B)** and lipid biosynthesis genes **(C)** was measured using qRT-PCR. Relative expression of each gene is normalised as a ratio of the Col-0 plants, which was set to 1. Statistical difference from the Col-0 control is indicated by two asterisks (**) at $P < 0.01$.

that transcript expression of *FAD2*, *FAD3*, *LPCAT1*, and *PDAT1* was greatly suppressed in AIF2ox plants but promoted in *aif2-1* plants (**Figure 7C**). Thus, we concluded that suppressed expression of sucrose-transporting genes (*SWEET11/12/15*) and lipid-biosynthesis genes (*FAD2/3*, *LPCAT1*, and *PDAT1*) in *AIF2*-overexpressing transgenic plants resulted in reduced starch and lipid accumulation in the developing seeds resulting in shrunken and small phenotypes.

Sucrose- and BR-Induced Repression of AIF2 Positively Controlled Seed and Silique Development

Sucrose is a necessary nutrient for embryo and seed development. Developing seeds form new carbon sink, generating high sugar flow from vegetative tissues to the seeds. To further confirm sucrose- and BL-mediated

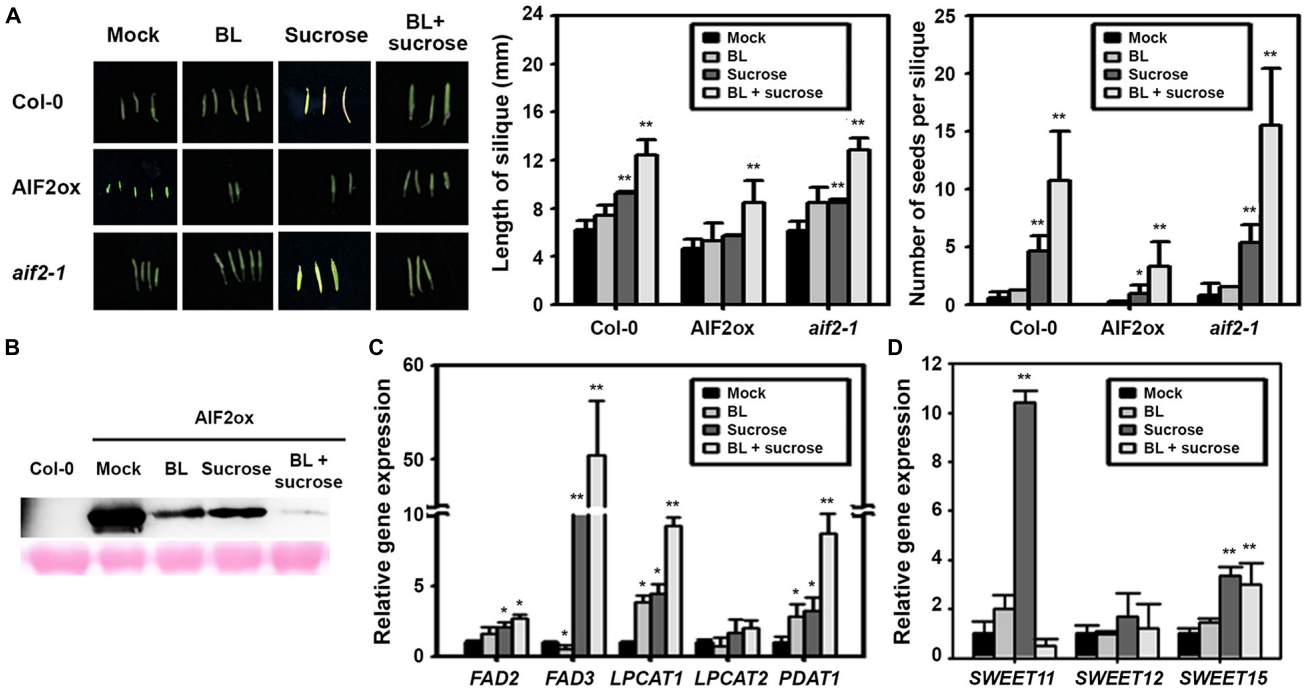

FIGURE 8 | Sucrose- and brassinosteroid-induced suppression of AIF2 stability and silique phenotypes. Flowers in between DAP3.5 to DAP4 ($n > 40$ for each experiment) were collected and cultured for 9 days in solid MS media containing brassinolide (BL, 10^{-9} M) supplemented with or without 3% sucrose (w/v). **(A)** Length and seed numbers of *in vitro*-cultured silique. **(B)** Western blot analysis of AIF2-EGFP expression in siliques of *in vitro*-cultured *p35S:AIF2-EGFP* transgenic lines (AIF2ox) **(C,D)** Total RNA was extracted from *in vitro*-cultured siliques of the AIF2ox, and the transcript expression for lipid biosynthesis genes **(C)** and sucrose transport-related genes **(D)** was measured using qRT-PCR. Relative expression of each gene is normalised as a ratio of the mock-treated plants, which was set to 1. Statistical difference from the mock-treated control is indicated by an asterisk (*) at $P < 0.05$ and two asterisks (**) at $P < 0.01$.

regulation of the AIF2ox phenotype, we examined the effects of BL and sucrose on silique phenotype and AIF2 stability in *in vitro*-cultured flowers. We found that the supply of BL did not result in an increase in silique length or seed numbers (**Figure 8A**). However, providing BL and sucrose promoted silique growth and seed production in AIF2ox, Col-0, and *aif2-1* plants, but was less effective in AIF2ox plants. Non-efficient promotion of BL itself might be attributed to the lack of nutrient supply found normally in intact plants. Such rescues of silique development were accompanied with a dramatic reduction in AIF2 stability in BL- and sucrose-treated AIF2ox plants (**Figure 8B**). BL-induced AIF2 degradation did not seem enough to cause the substantial recovery of silique growth because of the shortage in nutrients. Accordingly, supplying sucrose together with BL to the *in vitro* culture medium was the most effective in increasing transcript expression of *FAD3*, *LPCAT1*, and *PDAT1* (**Figure 8C**). Moreover, *SWEET15* was upregulated by the supplementation of BL or BL with sucrose (**Figure 8D**). Unexpectedly, *SWEET11* was highly upregulated by sucrose, and this effect was obliterated by the additional supplementation of BL. These results suggest that BR and sucrose reduced protein abundance of AIF2 transcription factor and increased starch and oil production for the successful generation of seeds.

DISCUSSION

BRs control diverse aspects of floral organ formation, seed development, and seed size determination. For example, two BR signalling activators, BES1 and its homologue BZR1, positively regulated tapetum and microspore development by directly upregulating *SPL/NZZ*, *TDF1*, and *MS1/2* (Ye et al., 2010; Chen L. G. et al., 2019; Chen W. et al., 2019). In contrast, the expression of *SPL* and *MS1* was significantly reduced in BR biosynthesis- (*cpd*) or signalling-defective (*bri1-116*, *bin2-1*) mutants producing greatly reduced number of pollen grains (Ye et al., 2010). Surprisingly, we found that *SPL* and *MS1* were highly upregulated in pollen- and seed-defective AIF2ox plants (**Figures 3A,B**). It is notable that *MS1*-overexpressing transgenic plants exhibited an excess deposition of wall materials and a loss of the regular structure of the pollen wall, eventually resulting in defective pollen development (Yang et al., 2007). MS1 protein was expressed in a developmentally regulated manner between late tetrad spore and microspore release and then broken down rapidly (Yang et al., 2007). Hence, it was suggested that MS1 breakdown was critical for the progression of pollen development, and the persistence of MS1 protein may serve to downregulate genes required for continued development of microspores. We showed that *SPL*, *MS1*, and *TDF1* in AIF2ox plants were relatively highly expressed even in flowers

of stages 11/12 and 15 (**Figures 3A–C**). Moreover, AIF2ox plants showed retarded and defective progression of microsporogenesis, producing aberrant tetrad microspores (**Figure 2E**). Thus, it is possible that the stage-independent aberrant expression of pollen-producing genes such as *SPL* and *MS1* in AIF2ox plants may act reversibly on microspore development and viability.

The auxin biosynthetic pathway is majorly regulated by catalytic activities of multiple monooxygenases encoded by the *YUCCA* genes, and TCP transcription factors can directly upregulate *YUCCA*s to increase auxin levels (Guo et al., 2010; Challa et al., 2016). Disruption of *TCP*s caused phenotypes that resemble *spl-D*, the heterozygous gain-of-function mutants of *SPL* (Wei et al., 2015). In other hand, *spl-D* mutants showed repressed expression of *YUCCA2* and *YUCCA6* and produced few and small flowers and short/wrinkled siliques with shrivelled seeds that could be partially rescued by crossing with *yuc6-D*, a dominant mutant of *YUC6* (Li et al., 2008). ARFs are a class of transcriptional modulators that regulate auxin-mediated gene expression. Likely, auxin biosynthesis-regulating genes, *Arabidopsis ARF6* and *ARF8*, through proper *microRNA167*-controlled cleavage, were critically involved in regulation of both gametophyte reproduction (Wu et al., 2006) and embryonic and seed development (Yao et al., 2019). In addition, ARF2 was negatively involved in the regulation of auxin-induced flowering time and seed size (Choi et al., 2018). Notably, similar to *aif2-1* plants, *arf2* loss-of-function mutants produced seeds with dramatically increased size and weight (Schruff et al., 2006). Based on the above studies, we suggest that ectopic expression of *SPL* in AIF2ox plants together with downregulation of *TCP*s, *YUCCA*s, and *ARF6/8* (**Figure 3**) and upregulation of *ARF2* (**Figure 4C**) may lead to the observed defective phenotypes of pollen, embryogenesis, and seeds/siliques (**Figure 9**). We demonstrated that AIF2-regulation of seed size and shape was epistatic to *bzr1-1D* and *bin2-1* genetic backgrounds (**Figure 6**). *bin2-1* exhibited reduced fertility, aborted ovules, and short siliques similar to those of AIF2ox plants, and auxin partially rescued the infertility phenotype of *bin2-1* (Li T. et al., 2019). Thus, it is probable that BIN2/AIF2 regulatory networks act via a coordinative interaction with auxin signalling pathways. In fact, rice OsSK41 (also known as OsGSK5, a BIN2 homologue) interacted with and phosphorylated OsARF4 (Hu et al., 2018). As a result, the expression of a common set of downstream genes was repressed, including some auxin-responsive genes during rice grain development; thus, the loss-of-function mutants of *OsSK41* and *OsARF4* showed increased grain length and weight. Further genetic analysis demonstrating *in vivo* functional interactions of BIN2/AIF2 and auxin signalling pathways are needed in future study.

Sucrose is delivered via the phloem to the maternal seed coat and then to the embryo through SWEET11, 12, and 15 efflux carriers (Chen et al., 2015). In addition, seeds with delayed embryogenesis and wrinkled phenotype commonly arise from defects in sucrose transport and endosperm formation (Andriotis et al., 2012; Chen et al., 2015). In this study, we further demonstrated that transcript suppression of sucrose transporter genes (*SWEET11*, *SWEET12*, and *SWEET15*) and lipid-biosynthesis genes (*FAD2*, *FAD3*, *LPCAT1*, and *PDAT1*) in *AIF2*-overexpressing plants resulted in the production of wrinkled seeds with reduced starch and oil levels (**Figure 7**). Similar to our *AIF2*-overexpressing transgenic plants, the *sweet11;12;15* triple mutant (lacking the ability to provide nutrients to the embryo and endosperm) showed delayed embryo development and reduced seed weight and lipid content, and exogenously supplied sucrose promoted embryo growth of *sweet11;12;15* mutants (Chen et al., 2015). *Arabidopsis SWEET*s such as *SWEET8* and *SWEET13* also played important roles in nurturing pollen grains; thus, mutation of these genes caused defective primexine deposition and pollen wall pattern formation resulting in male sterility (Sun et al., 2013).

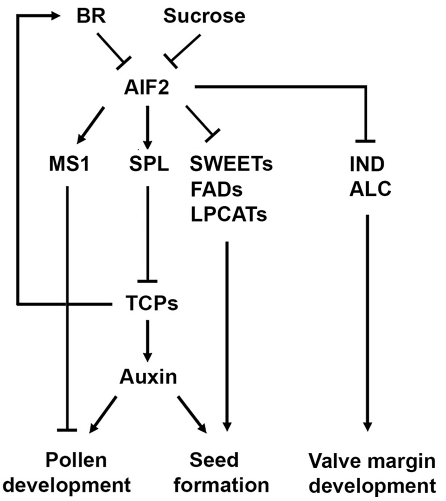

FIGURE 9 | A diagram explaining AIF2-regulated pollen development and seed formation. Stage-independent aberrant expression of pollen-producing genes such as *SPL* and *MS1* together with suppression of sucrose-transporting *SWEET*s, lipid biosynthesis-regulating *FADs*/*LPCAT*s, and valve margin-forming *IND/ALC* in AIF2ox plants may act adversely on pollen microspore development, auxin-regulated seed formation and proper silique development. Sucrose- and BR-induced repression of AIF2 bHLH transcription factor positively controls pollen development and/or seed size and numbers.

Antisense expression of *CPD*, a gene involved in BR biosynthesis, in *Arabidopsis* impaired the ability of the plant to assimilate carbohydrates, and such transgenic plants displayed a clear reduction in starch content (Schlüter et al., 2002). Moreover, increasing BR levels in rice enhanced CO_2 assimilation, favoured sucrose accumulation in the leaf, and increased assimilation of glucose to starch in the seed (Wu et al., 2008). Thus, the high expression level of *SPL* in AIF2ox plants and the subsequent reduction in *TCP1* expression followed by the decrease in BR biosynthesis resulted from a transcriptional decrease in *DWF4* may lead to attenuation of BZR1-mediated BR signalling pathways and reinforced BIN2/AIF2-mediated BR-defective signalling pathways. Supporting this idea, BR- and sucrose-regulated negative repression of AIF2 accumulation were co-related with accumulation of oil and starch and a resulting

increase in seed number and silique length (**Figure 8**). Collectively, we propose that the impaired pollen and seed phenotypes of AIF2-overexpressing transgenic plants may be, in part, owing to the reduced capacity for sugar/starch production and defects in sugar transport during gametophyte formation, embryogenesis, and seed formation.

In this study, we demonstrated that multiple genes regulating development of pollen grains, seeds, and siliques were differentially regulated in AIF2ox plants (**Figure 9**). AIF2 is a non-DNA-binding bHLH transcription factor and it regulates target gene expression by binding to other DNA-binding bHLH proteins. Previously, we showed that AIF2 interacts with INDUCER OF CBF EXPRESSION 1 (ICE1), a nuclear-localised MYC-like bHLH transcription factor, via their C-termini (Kim et al., 2020). A successful formation of the AIF2–ICE1 complex, the subsequent direct upregulation of *C-REPEAT BINDING FACTORS* (*CBF*s), and the antagonistic downregulation of *PIF4* were negatively involved in dark-triggered and BR-induced leaf senescence, thus, helping plants continue to grow and remain green for a long time (Kim et al., 2020). Many transcription factors with bHLH domain have been shown to regulate flower and seed development. For instance, SPT can heterodimerise with ALC, and these two proteins apparently undergo sub-functionalisation with SPT, being essential for earlier development of carpel margin tissues, and ALC, specialising in later dehiscence zone development (Groszmann et al., 2011). Therefore, future studies need to verify whether AIF2 interacts with other bHLH family proteins and whether this interaction and the resulting functions depend on age-specific binding partners of AIF2 during plant reproductive processes.

DATA AVAILABILITY STATEMENT

All data associated with the paper are available in this manuscript. Novel materials used and described in the paper are available for non-commercial research purposes from the corresponding author (soohwan@yonsei.ac.kr).

AUTHOR CONTRIBUTIONS

Soo-HK managed whole experimental processes and wrote this manuscript. YK performed most experiments and generated **Figures 2**, **3**, **5–9**. Sun-HK made **Figures 1** and **3**. D-MS generated the *aif2-1*/*aif4-1* double knockout plants. All authors contributed to the article and approved the submitted version.

FUNDING

This work was supported by the Basic Science Research Program through the National Research Foundation of Korea (NRF) funded by the Ministry of Education, Science, and Technology (grant numbers NRF-2019R1H1A2080044 and NRF-2020R1F1A1068793 to Soo-HK and NRF-2018R1A6A3A01013324 and NRF-2019R1C1C1006182 to YK).

SUPPLEMENTARY MATERIAL

The Supplementary Material for this article can be found online at: https://www.frontiersin.org/articles/10.3389/fpls.2021.704958/full#supplementary-material

Supplementary Figure 1 | Expression level-dependent aerial and silique phenotypes of AIF2-overexpressing independent transgenic lines (*p35S:AIF2-EGFP*/Col-0, AIF2ox).

Supplementary Figure 2 | Expression of the native promoter-driven and CaMV35S promoter-driven AIF2 protein in floral organs.

Supplementary Figure 3 | Reduced pollen production in AIF2ox plants.

Supplementary Figure 4 | Efficacy of *in vitro*-germinated pollen tube growth.

Supplementary Figure 5 | Relative expression of *AIF2* (At3g06590) in developing seeds.

Supplementary Figure 6 | Morphology of seeds stained with mPS-PI, followed by confocal microscope observation.

Supplementary Table 1 | Primers used in cDNA amplification of *AIF2*.

Supplementary Table 2 | Primers used in quantitative real time RT-PCR analysis.

REFERENCES

Andriotis, V. M. E., Pike, M. J., Schwarz, S. L., Rawsthorne, S., Wang, T. L., and Smith, A. M. (2012). Altered starch turnover in the maternal plant has major effects on *Arabidopsis* fruit growth and seed composition. *Plant Physiol.* 160, 1175–1186. doi: 10.1104/pp.112.205062

Boavida, L. C., and McCormick, S. (2007). Temperature as a determinant factor for increased and reproducible *in vitro* pollen germination in *Arabidopsis thaliana*. *Plant J.* 52, 570–582. doi: 10.1111/j.1365-313x.2007.03248.x

Challa, K. R., Aggarwal, P., and Nath, U. (2016). Activation of *YUCCA5* by the transcription factor TCP4 integrates developmental and environmental signals to promote hypocotyl elongation in *Arabidopsis*. *Plant Cell* 28, 2117–2130. doi: 10.1105/tpc.16.00360

Chen, L. G., Gao, Z., Zhao, Z., Liu, X., Li, Y., Zhang, Y., et al. (2019). BZR1 family transcription factors function redundantly and indispensably in BR signaling but exhibit BRI1-independent function in regulating anther development in *Arabidopsis*. *Mol. Plant* 12, 1408–1415. doi: 10.1016/j.molp.2019.06.006

Chen, L. Q., Lin, I. W., Qu, X. Q., Sosso, D., McFarlane, H. E., Londoño, A., et al. (2015). A cascade of sequentially expressed sucrose transporters in the seed coat and endosperm provides nutrition for the *Arabidopsis* embryo. *Plant Cell* 27, 607–619. doi: 10.1105/tpc.114.134585

Chen, W., Lv, M., Wang, Y., Wang, P. A., Cui, Y., Li, M., et al. (2019). BES1 is activated by EMS1-TPD1-SERK1/2-mediated signaling to control tapetum development in *Arabidopsis thaliana*. *Nat. Commun.* 10:4164.

Cheng, Z. J., Zhao, X. Y., Shao, X. X., Wang, F., Zhou, C., Liu, Y. G., et al. (2014). Abscisic acid regulates early seed development in *Arabidopsis* by ABI5-mediated transcription of *SHORT HYPOCOTYL UNDER BLUE1*. *Plant Cell* 26, 1053–1068. doi: 10.1105/tpc.113.121566

Cheng, Y., and Zhao, Y. (2007). A role for auxin in flower development. *J. Integr. Plant Biol.* 49, 99–104. doi: 10.1111/j.1744-7909.2006.00412.x

Choi, H. S., Seo, M., and Cho, H. T. (2018). Two TPL-binding motifs of ARF2 are involved in repression of auxin responsiveness. *Front. Plant Sci.* 9:372. doi: 10.3389/fpls.2018.00372

Concordet, J. P., and Haeussler, M. (2018). CRISPOR intuitive guide selection for CRISPR/Cas9 genome editing experiments and screens. *Nucleic Acids Res.* 46, W242–W245.

Day, R. C., Herridge, R. P., Ambrose, B. A., and Macknight, R. C. (2008). Transcriptome analysis of proliferating *Arabidopsis* endosperm reveals

biological implications for the control of syncytial division, cytokinin signaling, and gene expression regulation. *Plant Physiol.* 148, 1964–1984. doi: 10.1104/pp.108.128108

Figueiredo, D. D., and Köhler, C. (2018). Auxin: a molecular trigger of seed development. *Genes Dev.* 32, 479–490. doi: 10.1101/gad.312546.118

Garcia, D., Saingery, V., Chambrier, P., Mayer, U., Jürgens, G., and Berger, F. (2003). *Arabidopsis haiku* mutants reveal new controls of seed size by endosperm. *Plant Physiol.* 131, 1661–1670. doi: 10.1104/pp.102.018762

Girin, T., Paicu, T., Stephenson, P., Fuentes, S., Körner, E., O'Brien, M., et al. (2011). INDEHISCENT and SPATULA interact to specify carple and valve margin tissue and thus promote seed dispersal in *Arabidopsis*. *Plant Cell* 23, 3641–3653. doi: 10.1105/tpc.111.090944

Groszmann, M., Paicu, T., Alvarez, J. P., Swain, S. M., and Smyth, D. R. (2011). *SPATULA* and *ALCATRAZ*, are partially redundant, functionally diverging bHLH genes required for *Arabidopsis* gynoecium and fruit development. *Plant J.* 68, 816–829. doi: 10.1111/j.1365-313x.2011.04732.x

Guo, Z., Fujioka, S., Blancaflor, E. B., Miao, S., Gou, X., and Li, J. (2010). TCP1 modulates brassinosteroid biosynthesis by regulating the expression of the key biosynthetic gene DWARF4 in *Arabidopsis thaliana*. *Plant Cell* 22, 1161–1173. doi: 10.1105/tpc.109.069203

He, J. X., Gendron, J. M., Sun, Y., Gampala, S. S., Gendron, N., Sun, C. Q., et al. (2005). BZR1 is a transcriptional repressor with dual roles in brassinosteroid homeostasis and growth responses. *Science* 307, 1634–1638. doi: 10.1126/science.1107580

He, J. X., Gendron, J. M., Yang, Y., Li, J., and Wang, Z. Y. (2002). The GSK3-like kinase BIN2 phosphorylates and destabilizes BZR1, a positive regulator of the brassinosteroid signaling pathway in *Arabidopsis*. *Proc. Natl. Acad. Sci. U.S.A.* 99, 10185–10190. doi: 10.1073/pnas.152342599

Hedhly, A., Vogler, H., Schmid, M. W., Galliardini, V., Santelia, D., and Grossniklaus, U. (2016). Starch turnover and metabolism during flower and early embryo development. *Plant Physiol.* 172, 2388–2402. doi: 10.1104/pp.16.00916

Hu, Z., Lu, S. J., Wang, M. J., He, H., Sun, L., Wang, H., et al. (2018). A novel QTL q*TGW3* encodes the GSK3/SHAGGY-Like Kinase OsGSK5/OsSK41 that interacts with OsARF4 to negatively regulate grain size and weight in rice. *Mol. Plant* 11, 736–749. doi: 10.1016/j.molp.2018.03.005

Huang, H. Y., Jiang, W. B., Hu, Y. W., Wu, P., Zhu, J. Y., Liang, W. Q., et al. (2013). BR signal influences *Arabidopsis* ovule and seed numbers through regulating related genes expression by BZR1. *Mol. Plant* 6, 456–469. doi: 10.1093/mp/sss070

Ikeda, M., Mitsuda, N., and Takagi, O.-M. (2013). ATBS1 interacting factors negatively regulate *Arabidopsis* cell elongation in the triantagonistic bHLH system. *Plant Signal. Behav.* 8:e23448. doi: 10.4161/psb.23448

Jia, D., Chen, L. G., Yin, G., Yang, X., Gao, Z., Guo, Y., et al. (2020). Brassinosteroids regulate outer ovule integument growth in part via the control of *INNER NO OUTER* by BRASSINOZOLE-RESISTANT family transcription factors. *J. Integr. Plant Biol.* 62, 1093–1111. doi: 10.1111/jipb.12915

Jiang, W. B., Huang, H. Y., Hu, Y. W., Zhu, S. W., Wang, Z. Y., and Lin, W. H. (2013). Brassinosteroid regulates seed size and shape in *Arabidopsis*. *Plant Physiol.* 162, 1965–1977. doi: 10.1104/pp.113.217703

Jefferson, R. A. (1987). Assaying chimeric genes in plants: the GUS gene fusion system. *Plant Mol. Biol. Rep.* 5, 387–405. doi: 10.1007/bf02667740

Jofuku, K. D., Omidyar, P. K., Gee, Z., and Okamuro, J. K. (2005). Control of seed mass and seed yield by the floral homeotic gene *APETALA2*. *Proc. Natl. Acad. Sci. U.S.A.* 102, 3117–3122. doi: 10.1073/pnas.0409893102

Karimi, M., Inzé, D., and Depicker, A. (2002). GATEWAY vectors for *Agrobacterium*-mediated plant transformation. *Trends Plant Sci.* 7, 193–195. doi: 10.1016/s1360-1385(02)02251-3

Kay, P., Groszmann, M., Ross, J. J., Parish, R. W., and Swain, S. M. (2013). Modifications of a conserved regulatory network involving INDEHISCENT controls multiple aspects of reproductive tissue development in *Arabidopsis*. *New Phytol.* 197, 73–87. doi: 10.1111/j.1469-8137.2012.04373.x

Kim, E. J., and Russinova, E. (2020). Brassinosteroid signaling. *Curr. Biol.* 30, R287–R301.

Kim, H., Kim, S. T., Ryu, J., Choi, M. K., Kweon, J., Kang, B. C., et al. (2016). A simple, flexible and high-throughput cloning system for plant genome editing via CRISPR-Cas system. *J. Integr. Plant Biol.* 58, 705–712. doi: 10.1111/jipb.12474

Kim, S. Y., Hong, C. B., and Lee, I. (2001). Heat shock stress causes stage-specific male sterility in *Arabidopsis thaliana*. *J. Plant Res.* 114, 301–307. doi: 10.1007/pl00013991

Kim, Y., Park, S. U., Shin, D. M., Pham, G., Jeong, Y. S., and Kim, S. H. (2020). ATBS1-INTERACTING FACTOR 2 negatively regulates dark- and brassinosteroid-induced leaf senescence through interactions with INDUCER OF CBF EXPRESSION 1. *J. Exp. Bot.* 71, 1475–1490. doi: 10.1093/jxb/erz533

Kim, Y., Song, J. H., Park, S. U., Jeong, Y. S., and Kim, S.-H. (2017). Brassinosteroid-induced transcriptional repression and dephosphorylation-dependent protein degradation negatively regulate BIN2-interacting AIF2 (a BR Signaling-negative regulator) bHLH transcription factor. *Plant Cell Physiol.* 58, 227–239.

Li, L. C., Qin, G. J., Tsuge, T., Hou, X. H., Ding, M. Y., Aoyama, T., et al. (2008). SPOROCYTELESS modulates *YUCCA* expression to regulate the development of lateral organs in *Arabidopsis*. *New Phytol.* 179, 751–764. doi: 10.1111/j.1469-8137.2008.02514.x

Li, N., and Li, Y. (2016). Signaling pathways of seed size control in plants. *Curr. Opin. Plant Biol.* 33, 23–32. doi: 10.1016/j.pbi.2016.05.008

Li, N., Xu, R., and Li, Y. (2019). Molecular networks of seed size control in plants. *Annu. Rev. Plant Biol.* 70, 435–463. doi: 10.1146/annurev-arplant-050718-095851

Li, T., Kang, X., Wei, L., Zhang, D., and Lin, H. (2019). A gain-of-function mutation in Brassinosteroid-insensitive 2 alters *Arabidopsis* floral organ development by altering auxin levels. *Plant Cell Rep.* 39, 259–271. doi: 10.1007/s00299-019-02489-9

Liu, Z., Miao, L., Huo, R., Song, X., Johnson, C., Kong, L., et al. (2018). ARF2-*ARF4* and *ARF5* are essential for female and male gametophyte development in *Arabidopsis*. *Plant Cell Physiol.* 59, 179–189. doi: 10.1093/pcp/pcx174

Lou, Y., Schwender, J., and Shanklin, J. (2014). FAD2 and FAD3 desaturases form heterodimers that facilitate metabolic channeling *in vivo*. *J. Biochem. Chem.* 289, 17996–18007. doi: 10.1074/jbc.m114.572883

Luo, M., Dennis, E. S., Berger, F., Peacock, W. J., and Chaudhury, A. (2005). MINISEED3 (*MINI3*), a WRKY family gene, and *HAIKU2* (*IKU2*), a leucine-rich repeat (LRR) KINASE gene, are regulators of seed size in *Arabidopsis*. *Proc. Natl. Acad. Sci. U.S.A.* 102, 17531–17536. doi: 10.1073/pnas.0508418102

Meng, L. S., Xu, M. K., Wan, W., and Wang, J. Y. (2018). Integration of environmental and developmental (or metabolic) control of seed mass by sugar and ethylene metabolisms in *Arabidopsis*. *J. Agric. Food Chem.* 66, 3477–3488. doi: 10.1021/acs.jafc.7b05992

Mori, T., Kuroiwa, H., Higashiyama, T., and Kuroiwa, T. (2006). GENERATIVE CELL SPECIFIC 1 is essential for angiosperm fertilization. *Nat. Cell Biol.* 8, 64–71. doi: 10.1038/ncb1345

Neu, A., Eilbert, E., Asseck, L. Y., Slane, D., Henschen, A., Wang, K., et al. (2019). Constitutive signaling activity of a receptor-associated protein links fertilization with embryonic patterning in *Arabidopsis thaliana*. *Proc. Natl Acad. Sci. U.S.A.* 116, 5795–5804. doi: 10.1073/pnas.1815866116

Oh, E., Zhu, J. Y., Ryu, H., Hwang, I., and Wang, Z. Y. (2014). TOPLESS mediates brassinosteroid-induced transcriptional repression through interaction with BZR1. *Nat. Commun.* 5:4140.

Ohto, M. A., Floyd, S. K., Fischer, R. L., Goldberg, R. B., and Harada, J. J. (2009). Effects of APETALA2 on embryo, endosperm, and seed coat development determine seed size in *Arabidopsis*. *Sex Plant Reprod.* 22, 277–289. doi: 10.1007/s00497-009-0116-1

Okushima, Y., Mitina, I., Quach, H. L., and Theologis, A. (2005). AUXIN RESPONSE FACTOR 2 (ARF2): a pleiotropic developmental regulator. *Plant J.* 43, 29–46. doi: 10.1111/j.1365-313x.2005.02426.x

Olsen, O. A. (2001). Endosperm development: cellularization and cell fate specification. *Annu. Rev. Plant Physiol. Plant Mol. Biol.* 52, 233–267. doi: 10.1146/annurev.arplant.52.1.233

Peng, P., Yan, Z., Zhu, Y., and Li, J. (2008). Regulation of the *Arabidopsis* GSK3-like kinase BRASSINOSTEROID-INSENSITIVE 2 through proteasome-mediated protein degradation. *Mol. Plant* 2, 338–346. doi: 10.1093/mp/ssn001

Peterson, R., Slovin, J. P., and Chen, C. (2010). A simplified method for differential staining of aborted and non-aborted pollen grains. *Intl. J. Plant Biol.* 1, 66–69.

Riefler, M., Novak, O., Strnad, M., and Schmülling, T. (2006). *Arabidopsis* cytokinin mutants reveal functions in shoot growth, leaf senescence, seed size, germination, root development, and cytokinin metabolism. *Plant Cell* 18, 40–54. doi: 10.1105/tpc.105.037796

Schlüter, U., Köpke, D., Altmann, T., and Müssig, C. (2002). Analysis of carbohydrate metabolism of *CPD* antisense plants and brassinosteroid-deficient *cbb1* mutant. *Plant Cell Environ.* 25, 783–791. doi: 10.1046/j.1365-3040.2002.00860.x

Schruff, M. C., Spielman, M., Tiwari, S., Adams, S., Fenby, N., and Scott, R. J. (2006). The AUXIN RESPONSE FACTOR 2 gene of *Arabidopsis* links auxin signaling, cell division, and the size of seeds and other organs. *Development* 133, 251–261. doi: 10.1242/dev.02194

Shirley, N. J., Aubert, M. K., Wilkinson, L. G., Bird, D. C., Lora, J., Yang, X., et al. (2019). Translating auxin responses into ovules, seeds and yield: insight from *Arabidopsis* and the cereals. *J. Integr. Plant Biol.* 61, 310–336. doi: 10.1111/jipb.12747

Sun, M. X., Huang, X. Y., Yang, J., Guan, Y. F., and Yang, Z. N. (2013). *Arabidopsis* RPG1 is important for primexine deposition and functions redundantly with RPG2 for plant fertility at the late reproductive stage. *Plant Reprod.* 26, 83–91. doi: 10.1007/s00497-012-0208-1

Sun, X., Shantharaj, D., Kang, X., and Ni, M. (2010). Transcriptional and hormonal signaling control of *Arabidopsis* seed development. *Curr. Opin. Plant Biol.* 13, 611–620. doi: 10.1016/j.pbi.2010.08.009

Sun, Y., Fan, X.-Y., Cao, D. M., Tang, W., He, K., Zhu, J. Y., et al. (2010). Integration of brassinosteroid signal transduction with the transcription network for plant growth regulation in *Arabidopsis*. *Dev. Cell* 19, 765–777. doi: 10.1016/j.devcel.2010.10.010

Truernit, E., Bauby, H., Dubreucq, B., Grandjean, O., Runions, J., Barthelemy, J., et al. (2008). High-resolution whole-mount imaging of three-dimensional tissue organization and gene expression enables the study of phloem development and structure in *Arabidopsis*. *Plant Cell* 20, 1494–1503. doi: 10.1105/tpc.107.056069

Wang, A., Garcia, D., Zhang, H., Feng, K., Chaudhury, A., Berger, F., et al. (2010). The VQ motif protein IKU1 regulates endosperm growth and seed size in *Arabidopsis*. *Plant J.* 63, 670–679. doi: 10.1111/j.1365-313x.2010.04271.x

Wang, H., Zhu, Y., Fujioka, S., Asami, T., Li, J., and Li, J. (2009). Regulation of *Arabidopsis* brassinosteroid signaling by atypical basal helix-loop-helix proteins. *Plant Cell* 21, 3781–3791. doi: 10.1105/tpc.109.072504

Wang, Z.-Y., Nakano, T., Gendron, J., He, H., Chen, M., Vafeados, D., et al. (2002). Nuclear-localized BZR1 mediates brassinosteroid-induced growth and feedback suppression of brassinosteroid biosynthesis. *Dev. Cell* 2, 505–513. doi: 10.1016/s1534-5807(02)00153-3

Wei, B., Zhang, J., Pang, C., Yu, H., Guo, D., Jiang, H., et al. (2015). The molecular mechanism of SPOROCYTELESS/NOZZLE in controlling *Arabidopsis* ovule development. *Cell Res.* 25, 121–134. doi: 10.1038/cr.2014.145

Wu, C.-Y., Trieu, A., Radhakrishnan, P., Kwok, S. F., Harris, S., Wang, J., et al. (2008). Brassinosteroids regulate grain filling in rice. *Plant Cell* 20, 2130–2145. doi: 10.1105/tpc.107.055087

Wu, M.-F., Tian, Q., and Reed, J. W. (2006). *Arabidopsis* microRNA167 controls patterns of *ARF6* and *ARF8* expression, and regulates both female and male reproduction. *Development* 133, 4211–4218. doi: 10.1242/dev.02602

Xu, J., Carlsson, A. S., Francis, T., Zhang, M., Hoffman, T., Giblin, M. E., et al. (2012). Triacylglycerol synthesis by PDAT1 in the absence of DGAT1 activity is dependent on re-acylation of LPC by LPCAT2. *BMC Plant Biol.* 12:4. doi: 10.1186/1471-2229-12-4

Yadegari, R., de Paiva, G. R., Laux, T., Koltunow, A. M., Apuya, N., Zimmerman, J. L., et al. (1994). Cell differentiation and morphogenesis are uncoupled in *Arabidopsis* raspberry embryos. *Plant Cell* 6, 1713–1729. doi: 10.2307/3869903

Yan, Z., Zhao, J., Peng, P., Chihara, R. K., and Li, J. (2009). BIN2 functions redundantly with other *Arabidopsis* GSK3-like kinases to regulate brassinosteroid signaling. *Plant Physiol.* 150, 710–721. doi: 10.1104/pp.109.138099

Yang, C., Vizcay-Barrena, G., Conner, K., and Wilson, Z. A. (2007). MALE STERILITY1 is required for tapetal development and pollen wall biosynthesis. *Plant Cell* 19, 3530–3548. doi: 10.1105/tpc.107.054981

Yao, X., Chen, J., Zhou, J., Yu, H., Ge, C., Zhang, M., et al. (2019). An essential role for miRNA167 in maternal control of embryonic and seed development. *Plant Physiol.* 180, 453–464. doi: 10.1104/pp.19.00127

Ye, Q., Zhu, W., Li, L., Zhang, S., Yin, Y., Ma, H., et al. (2010). Brassinosteroids control male sterility by regulating the expression of key genes involved in *Arabidopsis* anther and pollen development. *Proc. Natl. Acad. Sci. U.S.A.* 107, 6100–6105. doi: 10.1073/pnas.0912333107

Zhang, M., Fan, J., Taylor, D. C., and Ohlrogge, J. B. (2009). *DGAT1* and *PDAT1* acyltransferases have overlapping functions in *Arabidopsis* triacylglycerol biosynthesis and are essential for normal pollen and seed development. *Plant Cell* 21, 3885–3901. doi: 10.1105/tpc.109.071795

Zhou, Y., Zhang, D., An, J., Yin, H., Fang, S., Chu, J., et al. (2018). TCP transcription factors regulate shade avoidance via directly mediating the expression of both PHYTOCHROME INTERACTING FACTORs and auxin biosynthetic genes. *Plant Physiol.* 176, 1850–1861. doi: 10.1104/pp.17.01566

Zhou, Y., Zhang, X., Kang, X., Zhao, X., Zhang, X., and Ni, M. (2009). SHORT HYPOCOTYL UNDER BLUE1 associates with *MINISEED3* and *HAIKU2* promoters *in vivo* to regulate *Arabidopsis* seed development. *Plant Cell* 21, 106–117. doi: 10.1105/tpc.108.064972

Conflict of Interest: The authors declare that the research was conducted in the absence of any commercial or financial relationships that could be construed as a potential conflict of interest.

Publisher's Note: All claims expressed in this article are solely those of the authors and do not necessarily represent those of their affiliated organizations, or those of the publisher, the editors and the reviewers. Any product that may be evaluated in this article, or claim that may be made by its manufacturer, is not guaranteed or endorsed by the publisher.

frontiers in Plant Science

ORIGINAL RESEARCH
published: 01 September 2021
doi: 10.3389/fpls.2021.705286

Transcript Profiling of MIKCc MADS-Box Genes Reveals Conserved and Novel Roles in Barley Inflorescence Development

Hendrik N. J. Kuijer[1], Neil J. Shirley[1], Shi F. Khor[1], Jin Shi[2], Julian Schwerdt[1], Dabing Zhang[1,2], Gang Li[1,3] and Rachel A. Burton[1]**

[1]School of Agriculture Food and Wine, University of Adelaide, Glen Osmond, SA, Australia, [2]Joint International Research Laboratory of Metabolic and Developmental Sciences, Shanghai Jiao Tong University-University of Adelaide Joint Centre for Agriculture and Health, School of Life Sciences and Biotechnology, Shanghai Jiao Tong University, Shanghai, China, [3]School of Life Sciences and Engineering, Southwest University of Science and Technology, Mianyang, China

OPEN ACCESS

Edited by:
Fa Cui,
Ludong University, China

Reviewed by:
Luis Morales-Quintana,
Autonomous University of Chile, Chile
Yong Jia,
Murdoch University, Australia

***Correspondence:**
Gang Li
gang.li@adelaide.edu.au
Rachel A. Burton
rachel.burton@adelaide.edu.au

Specialty section:
This article was submitted to Crop and Product Physiology, a section of the journal Frontiers in Plant Science

Received: *05 May 2021*
Accepted: *04 August 2021*
Published: *01 September 2021*

Citation:
Kuijer HNJ, Shirley NJ, Khor SF, Shi J, Schwerdt J, Zhang D, Li G and Burton RA (2021) Transcript Profiling of MIKCc MADS-Box Genes Reveals Conserved and Novel Roles in Barley Inflorescence Development. Front. Plant Sci. 12:705286. doi: 10.3389/fpls.2021.705286

MADS-box genes have a wide range of functions in plant reproductive development and grain production. The ABCDE model of floral organ development shows that MADS-box genes are central players in these events in dicotyledonous plants but the applicability of this model remains largely unknown in many grass crops. Here, we show that transcript analysis of all MIKCc MADS-box genes through barley (*Hordeum vulgare* L.) inflorescence development reveals co-expression groups that can be linked to developmental events. Thirty-four MIKCc MADS-box genes were identified in the barley genome and single-nucleotide polymorphism (SNP) scanning of 22,626 barley varieties revealed that the natural variation in the coding regions of these genes is low and the sequences have been extremely conserved during barley domestication. More detailed transcript analysis showed that MADS-box genes are generally expressed at key inflorescence developmental phases and across various floral organs in barley, as predicted by the ABCDE model. However, expression patterns of some *MADS* genes, for example *HvMADS58* (AGAMOUS subfamily) and *HvMADS34* (SEPALLATA subfamily), clearly deviate from predicted patterns. This places them outside the scope of the classical ABCDE model of floral development and demonstrates that the central tenet of antagonism between A- and C-class gene expression in the ABC model of other plants does not occur in barley. Co-expression across three correlation sets showed that specifically grouped members of the barley MIKCc MADS-box genes are likely to be involved in developmental events driving inflorescence meristem initiation, floral meristem identity and floral organ determination. Based on these observations, we propose a potential floral ABCDE working model in barley, where the classic model is generally upheld, but that also provides new insights into the role of MIKCc MADS-box genes in the developing barley inflorescence.

Keywords: barley, inflorescence, floral organs, meristems, MADS, transcript profiling, ABC model, floret

INTRODUCTION

Flowers are often composed of four different floral organs organised in concentric whorls numbered from peripheral to central position. The outer whorls are sepals and petals in many dicots, including the model plant *Arabidopsis*, and lemma/palea and lodicules in grasses, while the inner whorls contain the male reproductive organs, the stamens, in the third whorl and the female organs, the carpels, in the fourth whorl (Ciaffi et al., 2011). Genetic studies have identified a large number of regulatory genes that control the specification of these distinct floral organs in plants (Alvarez-Buylla et al., 2010). The ABCDE model, originally proposed for *Arabidopsis* and *Antirrhinum majus*, associates the developmental determination of specific flower organs with the combinatorial activity of several classes of homeotic selector genes, most of which encode MIKCc MADS domain developmental transcription factors. Those MIKCc genes that function in the ABCDE model are divided into A-, B-, C-, D- and E-classes, which correspond with the AP1, AP3/PI, AG(C), AG(D) and SEP clades, respectively. A- and E-class genes determine the first whorl organs; A-, B- and E-class genes determine the second whorl; B-, C- and E-class genes control the third whorl; and C- and E-class genes specify the fourth whorl. D- and E-class genes are involved in ovule development within the carpel. Individual genes within a class usually act redundantly with each other in some roles, so that mutation of single members often leads to a subtle, absent or incomplete phenotype (Coen and Meyerowitz, 1991; Angenent et al., 1995; Pelaz et al., 2000). Studies demonstrate the conservation of gene homologues underlying the ABCDE model across most flowering plants, with only the AG subfamily (C-class) being present in gymnosperms (Theissen et al., 2016; Chen et al., 2017), suggesting the regulatory principles of some of these clades have been conserved during flower evolution.

The MADS-box genes have been divided into two subgroups: Type I and Type II, which are present in plants, animals and fungi (Kwantes et al., 2012; Chen et al., 2017). The encoded proteins cooperatively bind to DNA at conserved CArG boxes [CC(A/T)6GG] or [C(A/T)8G] to regulate gene expression (Theissen and Saedler, 2001). In plants, Type II MADS-box genes are called MIKC type, including MIKCc and MIKC* sub-types, an acronym of the four different domains that have been identified in all genes of this type. These transcription factors contain the conserved MADS DNA-binding domain (M), Intervening domain (I), Keratin-like domain (K) and the C-terminal domain (C), while the small c stands for classic. The closest relatives are the MIKC* genes, with the α-, β- and γ-MADS box genes completing the MADS family (Kwantes et al., 2012; Smaczniak et al., 2012). Within the MIKCc family, there are more clades than just those associated with the ABCDE model, such as the SVP-like floral repressors and the SOC1-like floral promotors (Becker and Theißen, 2003). The Type I lineage contains genes with simpler gene structure and lacking a Keratin-like domain. Their function is generally not well understood yet in plants, with some exceptions (Colombo et al., 2008; Callens et al., 2018). Additionally, MADS-box genes have also been reported to play an important role in abiotic stress, thermal regulation and plastic developmental responses in plants (Castelán-Muñoz et al., 2019; Li et al., 2021).

While the MIKCc clades and their roles in inflorescence development are generally conserved, the individual genes within a class often show no direct homology between grasses and *Arabidopsis*, making them co-orthologues (Ciaffi et al., 2011). More difficult to identify in grasses is the FLC-clade, which governs vernalisation and flowering time in *Arabidopsis* (Becker and Theißen, 2003). The FLC-clade genes in grasses are truncated and therefore could only be correctly classified using synteny and phylogenetic reconstruction (Ruelens et al., 2013). Present in grasses, but not in eudicots, is the OsMADS32 class, which is loosely related to B-class genes (Ciaffi et al., 2011).

The putative 11 MIKC-type MADS-box genes from the last common ancestor of monocots and eudicots increased to at least 24 genes in the last common ancestor of rice, wheat and maize (Bremer, 2002; Ciaffi et al., 2011). During this time of duplication and diversification in the MIKC family, the complex grass inflorescence and floral structures of the Poaceae family evolved. Changes in the copy number and expression pattern of MADS-box genes are closely associated with the morphological diversification of grass inflorescences (Ciaffi et al., 2011).

Generally, the ABCDE model of floral organogenesis can be applied to grasses as well. Functional studies in rice highlight mostly the homeotic changes defined by the model for predicted A-class genes (Wu et al., 2017), B-class genes (Nagasawa et al., 2003; Yadav et al., 2007; Yao et al., 2008), C- and D-class genes (Yamaguchi et al., 2006; Dreni et al., 2011) and E-class genes (Cui et al., 2010; Gao et al., 2010; Wu et al., 2018). The expression pattern and timing of MIKCc genes in other grasses indicate this likely extends to the whole grass family (Digel et al., 2015; Harrop et al., 2016; Feng et al., 2017; Callens et al., 2018; Zhu et al., 2018; Liu et al., 2020; Schilling et al., 2020).

A major determinant of floral organogenisis in grasses outside of the MADS-box genes is the YABBY family gene *DROOPING LEAF* (*DL*) which is involved in the regulation of carpel specification in rice (Nagasawa et al., 2003; Yamaguchi et al., 2004). Expression of *DL* orthologues in the carpel of maize and wheat is required to suppress the expression of B-class genes and is thus essential for floral organ specification according to the ABCDE model. Conserved expression suggests that DL function in carpel specification is a common feature in grasses (Bommert et al., 2005). While *CRABS CLAW*, the *Arabidopsis* co-orthologue of *DL*, has a function in carpel development, there is no homeotic change to the carpel identity in its absence (Bowman and Smyth, 1999), indicating a divergence in floral organogenesis between eudicots and grasses.

Some MIKCc genes associated with the ABCDE model have adopted additional roles in grasses, like the AP1 clade gene *HvMADS14* which is a vernalisation integrator in barley (Trevaskis et al., 2007a), expression of which is important for floral transition onset. Alternatively in rice, OsMADS34 has been shown to modulate inflorescence branching (Gao et al., 2010; Kobayashi et al., 2010), which is not canonically an E-class role.

The Triticeae crop barley has a simple branchless spike-type inflorescence. During early development, the inflorescence

meristem differentiates several spikelet ridges, and each ridge develops a determinate triple spikelet meristem, which in turn gives three spikelet meristems (SM; Wang et al., 2021). Each SM produces one floral meristem, always resulting in three single-flowered spikelets per rachis node (Koppolu and Schnurbusch, 2019). Inflorescence development in barley, as well as wheat, can be divided into stages by examining the development of the inflorescence meristem and noting the emergence and shape of the floral, spikelet and floret meristems followed by the sequential initiation and growth of the floral organs (Waddington et al., 1983). These Waddington stages range from the transition of the vegetative to the reproductive meristem at W1, to pollination or anthesis at W10, and include a series of developmental and cellular events. However, the transcription and regulation of ABCDE model components in barley inflorescence development and floret formation still remain unknown. Here, we performed transcript analysis of MIKCc genes through inflorescence developmental stages and in individual floral organs by quantitative reverse transcription PCR (RT-qPCR). Our findings reveal that the ABCDE model can be mostly applied to barley, while deviations point to interesting adaptations that can reveal more about inflorescence development in grasses.

MATERIALS AND METHODS

Identification of MIKCc Genes

Barley MIKCc MADS-box genes were identified by name and BLAST searches, using rice homologues, in the HORVU data set[1] using Geneious software version 8.1.3 (Biomatters). Additional genes, and more accurate coding sequences, were found using an online tBLASTn search of transcript data at NCBI.[2] Previously identified MADS-box genes annotated as MADS-box proteins in the Uniprot database,[3] IPK Gatersleben and NCBI databases were categorised using the PlantTFDB as follow-up analysis for MIKC-type MADS-box members (Jin et al., 2014; Mascher et al., 2017; Monat et al., 2019). Where no known (complete) transcript sequences were available, the FGENESH+ protein-based gene prediction tool (Solovyev, 2007) was used to identify the most likely transcripts. Genes were named after their rice homologues, rather than the previous names used in barley, to standardise naming and make functional comparisons to other grasses easier (**Table 1**).

Phylogenetic Analysis

MIKCc MADS-box proteins from *Arabidopsis*, rice, sorghum and *Brachypodium* were collected from published data (Arora et al., 2007; Wei et al., 2014). The sequences obtained were aligned with previously identified barley MIKCc MADS-box proteins using the MUSCLE algorithm before manual inspection and minor adjustments (Edgar, 2004). The IQ-TREE web server was used to create a maximum likelihood phylogenetic tree (Trifinopoulos et al., 2016). JTT + I + G4 was selected as the best model and bootstrap was set at 1,000 replicates.

SNP Analysis

A list of barley single-nucleotide polymorphisms (SNPs) was compiled using the comprehensive SNP database, recently made accessible at IPK Gatersleben[4] and the barley pan-genome sets (Milner et al., 2019; Jayakodi et al., 2020).[5] Gene locations in the SNP-browser were found by HORVU number where available, otherwise by position on the chromosome. Exon and amino acid changes were assessed by comparison to an alignment of cDNA sequences and chromosome fragments in Geneious 8.1.3 (Biomatters Ltd). Pan-genome predicted CDS sequences were extracted and assessed by multiple alignment in EUGENE (UniPro).[6] Rice SNPs were collected using the online interface of the SNP database (Mansueto et al., 2017).[7]

Inflorescence Tissue Sampling

Hordeum vulgare L. variety Golden Promise was grown in a controlled environment room with 16 h light at 15°C day and 10°C night temperatures, at 70% humidity, in 8 cm square pots containing coco-peat standing in closed trays and watered from below every 2 days. A midday light maximum of 500 µmole photons m^{-2} s^{-1} was used. Inflorescence tissue samples were taken from the main stem and examined under a dissecting microscope. Immature spikes exactly matching the desired Waddington stage (Waddington et al., 1983) were immediately frozen in liquid nitrogen and stored at −80°C.

For the W1 stage, where the meristem height was less than 1 mm, 30 meristems were taken per sample. To capture transcript changes through pollination, one additional stage was introduced, called W10.5, which was taken 3 days after pollination. One sample represents one biological replicate, for which 25 individual meristems (IM) were collected at W1.5, 20 IM at W2, 15 IM at W2.5, 12 IM at W3.5, 10 IM at W4, 8 IM at W4.5, 6 IM at W6.5 and 5 IM at W8.5. At W9.5 and W10.5, five separate single IM were taken, and combined at a later stage, such that each final sample comes from at least five individual plants.

Additionally, floral organ samples were taken from five different plants at Waddington stage 9.5. Twelve florets were harvested for the palea/lemma, the stamens and the carpel, while 20 florets were dissected for a total of 40 lodicules.

RNA Extraction

Total RNA was extracted using the Qiagen Plant RNA Kit, Ambion Turbo RNA-free Kit and approximately 200 ng of RNA used for cDNA synthesis with Superscript III reverse transcriptase (Invitrogen) according to the manufacturer's instructions.

[1]https://webblast.ipk-gatersleben.de/barley_ibsc/downloads/
[2]https://blast.ncbi.nlm.nih.gov/Blast.cgi
[3]https://www.uniprot.org/
[4]https://bridge.ipk-gatersleben.de/#snpbrowser, accessed April 2019.
[5]https://barley-pangenome.ipk-gatersleben.de/, accessed February 2021.
[6]http://ugene.net/
[7]http://snp-seek.irri.org/_snp.zul, accessed June 2019.

TABLE 1 | The MIKCc MADS-box protein family in barley compared to rice.

	Arabidopsis	*Oryza* name	*Oryza* ID	Barley ID Morex1	Alt sequence	Barley ID Morex2	Legacy barley names
A-class	AP1, CAL, FUL	MADS14	Os03g0752800	HORVU5Hr1G095630.3		HORVU.MOREX.r2.5HG0424650.1	BM5, VRN1
				HORVU1Hr1G047550.1		HORVU.MOREX.r2.1HG0039100.1	'HvAP1b'
		MADS15	OS07G0108900	HORVU2Hr1G063800.7	AK249833.1	HORVU.MOREX.r2.2HG0129220.1	BM8
		MADS18	OS07G0605200	*HORVU0Hr1G003020.3	AK361227.1	HORVU.MOREX.r2.2HG0105150.1	BM3
		MADS20	OS12G0501700	No equivalent			
B-class	PI	MADS2	OS01G0883100	HORVU3Hr1G091000.8		HORVU.MOREX.r2.3HG0256620.1	
		MADS4	OS05G0423400	HORVU1Hr1G063620.2		HORVU.MOREX.r2.1HG0051900.1	
	AP3	MADS16	OS06G0712700	*HORVU7Hr1G091210.4	AK373398.1	HORVU.MOREX.r2.7HG0598100.1	
C-class	AG, SHP1/2, STK	MADS3	OS01G0201700	HORVU3Hr1G026650.1		HORVU.MOREX.r2.3HG0202320.1	HvAG1
		MADS58	OS05G0203800	HORVU1Hr1G029220.1		HORVU.MOREX.r2.1HG0024570.1	HvAG2
D-class		MADS13	OS12G0207000	HORVU1Hr1G023620.1		HORVU.MOREX.r2.1HG0019750.1	
		MADS21	OS01G0886200	HORVU1Hr1G064150.2		HORVU.MOREX.r2.1HG0052300.1	
E-class	SEP1/2/4	MADS1	OS03G0215400	HORVU4Hr1G067680.2		HORVU.MOREX.r2.4HG0329790.1	HvMADS7
		MADS5	OS06G0162800	HORVU7Hr1G025700.6		HORVU.MOREX.r2.7HG0543420.1	
		MADS34	OS03G0753100	HORVU5Hr1G095710.1		HORVU.MOREX.r2.5HG0424690.1	
	SEP3	MADS7	OS08G0531700	HORVU7Hr1G054220.1		HORVU.MOREX.r2.7HG0567840.1	
		MADS8	OS09G0507200	HORVU5Hr1G076400.1		HORVU.MOREX.r2.5HG0409590.1	M9
AGL6	AGL6/13	MADS6	OS02G0682200	HORVU6Hr1G066140.9		HORVU.MOREX.r2.6HG0500990.1	AGL6
		MADS17	OS04G0580700	No equivalent			
	FCL1/2, AGL27/31	No equivalent in rice/barley					
	AGL14/19/42, SOC1	MADS50	OS03G0122600	No horvu number	AK368348.1	HORVU.MOREX.r2.4HG0343680.1	SOC1-1
		MADS56	OS10G0536100	*HORVU1Hr1G051660.8	JN673265	*HORVU.MOREX.r2.1HG0042540.1	SOC1-L
	AGL24, SVP(AGL22)	MADS22	OS02G0761000	HORVU6Hr1G077300.1		HORVU.MOREX.r2.6HG0511230.1	BM10
		MADS55	OS06G0217300	*HORVU7Hr1G036130.1	AK356695.1	HORVU.MOREX.r2.7HG0551090.1	VRT2
		MADS47	OS03G0186600	HORVU4Hr1G077850.3		HORVU.MOREX.r2.4HG0338120.1	BM1

(Continued)

TABLE 1 | Continued

	Arabidopsis	*Oryza* name	*Oryza* ID	Barley ID Morex1	Alt sequence	Barley ID Morex2	Legacy barley names
	AGL12	MADS26	OS08G0112700	HORVU7Hr1G076310.14	AK370468.1	HORVU.MOREX.r2.7HG0585040.1	
		MADS33	OS12G0206800	No horvu number	AK250031.1	HORVU.MOREX.r2.2HG0140850.1	
	AGL16/17/44/21	MADS23	OS08G0431900	HORVU1Hr1G008290.1		HORVU.MOREX.r2.1HG0006360.1	
				HORVU1HR1G008300.3		HORVU.MOREX.r2.1HG0006350.1	M23b
		MADS25	OS04G0304400	M25a HORVU5Hr1G000480.1		HORVU.MOREX.r2.5HG0349390.1	
				M25b HORVU5Hr1G000370.3		*HORVU.MOREX.r2.5HG0349480.1	
				M25c HORVU7Hr1G023940.2		HORVU.MOREX.r2.7HG0541840.1	
				M25d HORVU7Hr1G024000.1		HORVU.MOREX.r2.7HG0541900.1	
		MADS27	OS02G0579600	HORVU2Hr1G080490.1		HORVU.MOREX.r2.2HG0143360.1	
		MADS57	OS02G0731200	*HORVU6Hr1G073040.13	AK363243.1	HORVU.MOREX.r2.6HG0507700.1	
B-sister	ABS	MADS29	OS02G0170300	HORVU6Hr1G032220.8		HORVU.MOREX.r2.6HG0473980.1	
		MADS30	OS06G0667200	HORVU7Hr1G108280.4	AK375718	HORVU.MOREX.r2.7HG0611760.1	
		MADS31	OS04G0614100	HORVU2Hr1G098930.2		*HORVU.MOREX.r2.2HG0158040.1	
	No At equivalent	MADS32	OS01G0726400	HORVU3Hr1G068900.3		*HORVU.MOREX.r2.3HG0237490.1	

*The Arabidopsis co-orthologues are given per protein class where available, as the relation within classes is generally not homologous.*An incomplete sequence or protein model.*

Real-Time RT-qPCR and Co-expression Analysis

Primers were designed across the stop codon of each gene, forward in the gene and reverse in the 3′UTR (**Supplementary Table 2**). This is not only to avoid problems with sequence similarity between closely related genes, but also because the RNA in this position is less likely to be degraded.

RT-qPCR was performed as described by Burton et al. (2008). The quantity of the cDNA was assessed with four standard genes (*HvGAP*, *HvCyclophilin*, *HvTubulin* and *HvHSP70*) and normalised by relative threshold cycle value over the time course and floral organ samples individually using the average expression of the best matching three standard genes (*HvGAP* was excluded). All RT-qPCR was performed on three independent technical repeats with similar results. Transcript correlation analysis of the normalised expression values was done using the Pearson correlation function in MeV4.9.[8] Hierarchical clustering analysis was performed using pheatmap package in R.[9]

RNA *In situ* Hybridisation

Meristems were obtained as described, placed into FAA fixative solution (3.7% formaldehyde, 50% ethanol and 5% acetic acid) and vacuum infiltrated. Samples were dehydrated in an ethanol series which was subsequently swapped for D-lemonene (HistoChoice, Sigma), and finally paraffin wax (Paramat pastillated, Gurr) at 60°C. Embedded samples were cut into 6–8 µm sections on a Leica RM2265 microtome and placed on lysine coated slides.

Dioxigenin labelled probes were made, in sense and antisense configuration, using the DIG labelling kit (Roche Diagnostics), following the manufacturer's instructions. Primers used to generate the probes are listed in **Supplementary Table 3**.

Slides were dewaxed in D-lemonene and rehydrated in an ethanol series (2× 100%, 95% ethanol and 85 and 75% ethanol with 0.85% NaCl). The following steps were performed with an InsituPro robot (Invatis): Finalise rehydration, proteinase K digestion and re-dehydration. Re-dehydration was finalised with a reverse of the rehydration steps above, and the slides dried at 37°C. The following steps were also performed with the InsituPro robot: hybridisation, stringent washes, RNAse digestion, immunolabelling (AntiDIG-APconjugate, Roche) and washing. Substrate (NBT/BCIP, Roche) was added according to the manufacturer's instructions and incubated overnight in the dark. Slides were fixed with ImmunoHistoMount (Sigma-Aldrich) and observed with a Nikon Ni-E optical microscope. Pictures were processed for colour, brightness and contrast in GIMP2.10.2 (www.gimp.org).

Available Public Expression Data Analysis

Transcript data for barley early inflorescence development by RNA-seq were collected from supplemental data set 3 (Digel et al., 2015), selecting only the introgression line (S42-IL017) inflorescence samples grown in long day conditions.

Transcript data for rice early inflorescence meristem types were collected from supplemental data S1 (Harrop et al., 2016), selecting the MADS-box genes by name search.

Transcript data for wheat inflorescence development were collected from **Supplementary Table 4** 'List of wheat homologues similar to rice MADS-box genes' (Feng et al., 2017).

RESULTS

Identification and Phylogenetic Analysis of MIKCc MADS-Box Genes in the Barley Genome

The recent barley genome assembly contains 32 MIKCc MADS-box genes annotated as expressed sequences and a pseudogene strongly resembling *HvMADS14* with 97% identity, but only covering the latter 67% (Mascher et al., 2017; Monat et al., 2019). Through comparison with homologous genes from rice, and a tBLASTn search for available transcript sequences of barley, two genes labelled as *HvMADS27* (HORVU1Hr1G008290.1 and HORVU1HR1G008300.3) were found to be more closely related to *OsMADS23*, while another two genes, *HvMADS50* and *HvMADS33*, were identified as transcript sequences for barley, although not present in the MOREX v1 genome assembly. Additionally, a more accurate exon sequence was found for nine MIKCc genes through comparison with available transcripts for *HvMADS16*, *HvMADS18*, *HvMADS55*, *HvMADS56* and *HvMADS57*, and by analysing the genomic region with FGENESH, guided by the *OsMADS25* sequence, for *HvMADS25a*/*b*/*c*/*d*. This brings the total to 34 MIKCc MADS-box genes and one pseudogene in barley (**Table 1**).

There is a barley homologue for 31 of the 33 complete MIKCc genes in rice; missing homologues are the SQUA/AP1 gene *OsMADS20* and the AGL6-like gene *OsMADS17*. There is only one copy of *OsMADS25* in rice, but four in barley, here designated *HvMADS25a*, *HvMADS25b*, *HvMADS25c* and *HvMADS25d*. Apart from these exceptions, each barley MIKCc gene has a clear orthologue in rice. Phylogenetic analysis of encoded proteins showed that A-, B-, C-, D- and E-class proteins are conserved between rice and barley, and also with *Brachypodium* and sorghum, but show a divergence with eudicot *Arabidopsis* (**Figure 1**; **Table 1**). The FLC-like MIKCc proteins, involved in flowering time and vernalisation in *Arabidopsis* (Becker and Theißen, 2003), have truncated homologues in grasses. In barley, these homologues are *ODDSOC1* and *ODDSOC2*, which are missing the C-terminal domain and part of the keratin-like domain and fail to group with the MIKCc proteins in a phylogenetic tree based on sequence similarity alone (Ruelens et al., 2013). Conversely, the MADS32 clade has no orthologous gene group in *Arabidopsis*, or likely in any eudicot (**Figure 1**). Thus the overall phylogenetic analysis showed that most barley MIKCc MADS-box proteins have a close evolutionary relationship with their orthologues in rice, *Brachypodium* and sorghum, but not *Arabidopsis* (**Figure 1**).

The coding region of MIKCc MADS-box genes shows some expected conservation of intron-exon patterns within the different

[8]http://mev.tm4.org
[9]https://github.com/raivokolde/pheatmap

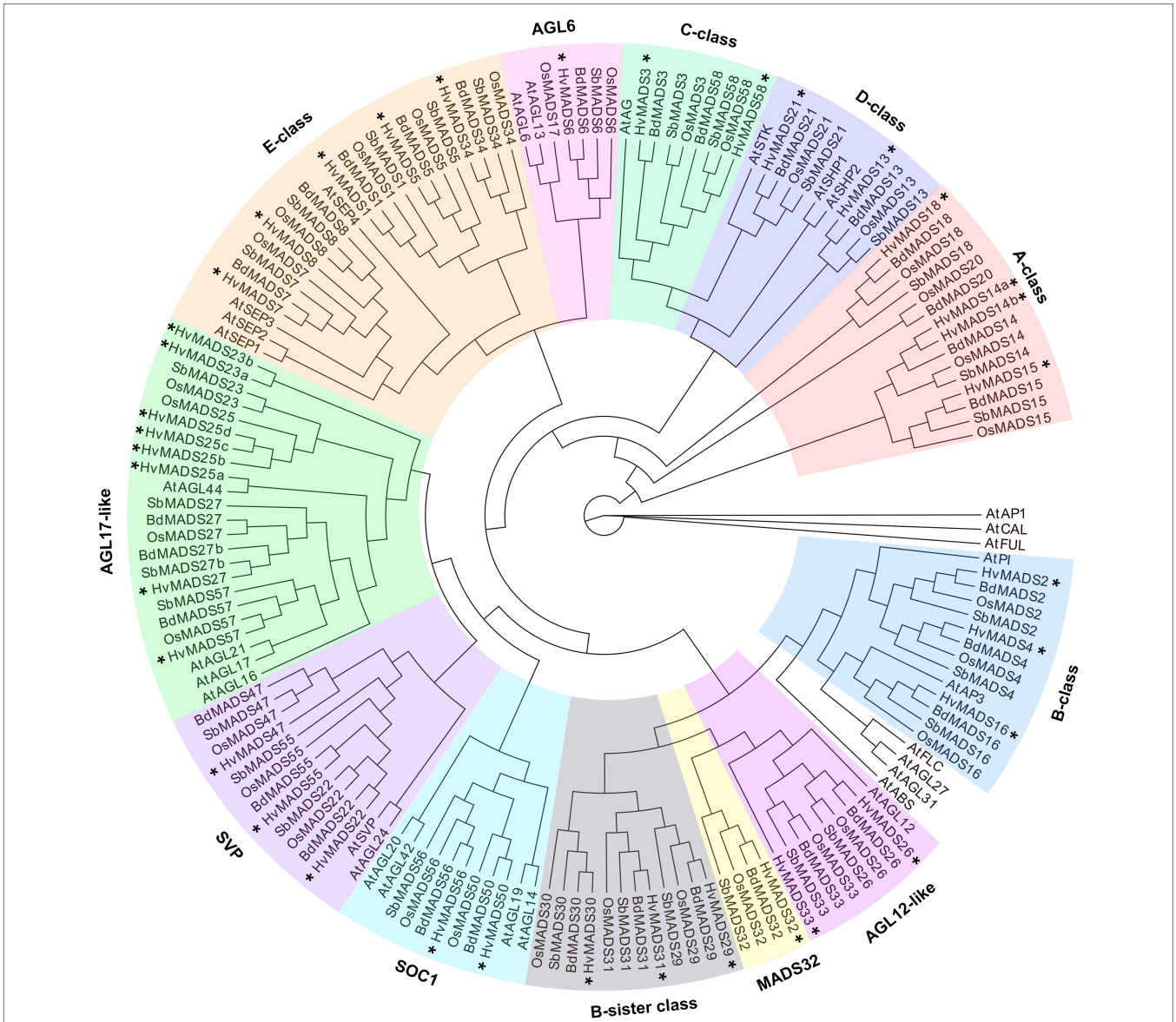

FIGURE 1 | Phylogenetic analysis of all MIKCc-type MADS-box proteins (except for the truncated FLC-like proteins) in barley compared to the homologues in rice, *Brachypodium*, sorghum and *Arabidopsis*. The classes within the family are delimited by coloured boxes. SOC1, SUPRESSOR OF CONSTANS1-like proteins; SVP, SVP/VRT-like proteins. Stars (*) indicate the MADS-box homologues of barley.

classes of closely related genes. Most exon patterns are long-short-short-medium-short-short-long, whereas intron length, and therefore gene length, varies more widely (**Supplementary Figure 1**). Some of the *HvMADS25* paralogous genes have big introns (a) 0.5 kbp, (b) 6 kbp, (c) 10 kbp and (d) 15 kbp.

Low Occurrence of Single-Nucleotide Polymorphisms Shows High Conservation of MIKCc Genes' Coding Region

To reveal the natural variation within the MIKCc MADS-box gene family during barley domestication, a comprehensive search for SNPs was performed in a database from exome sequencing of 22,626 barley cultivars, landraces and wild relatives that was recently made accessible at IPK Gatersleben, and from the barley pan-genome database that have been sequenced in 20 cultivars (Milner et al., 2019; Jayakodi et al., 2020).

The result shows that only 14 of the 34 MIKCc MADS-box genes contain any SNPs in the varieties sampled in the SNP-browser. Within these 14 genes, only half exhibit amino acid changes (**Supplementary Table 1**), although never in the first 110 amino acids, a region that contains the MADS domain and the Intervening domain. Remarkably, all but one of the 20 SNPs associated with *HvMADS2* occur between *HvMADS2* and its neighbouring gene HORVU.MOREX.r2.3HG0256630.1,

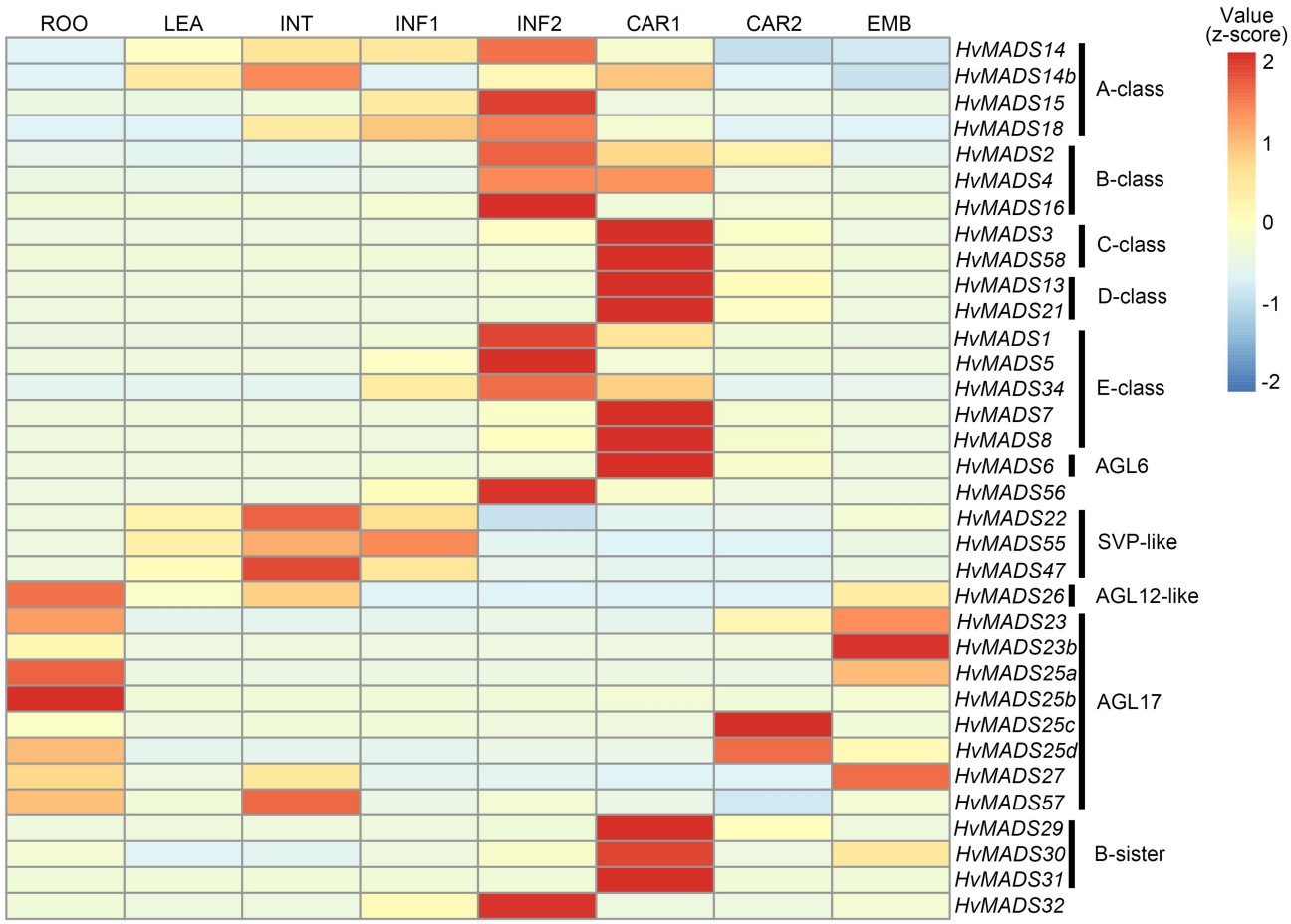

FIGURE 2 | Hierarchical clustering analysis of MIKCc genes' global transcript in different barley tissues. RPKM (Reads Per Kilobase Million) is normalised using a pheatmap package in R. ROO, roots 17 days after planting (DAP); LEA, leaves 17 DAP; INT, third internode 42 DAP; INF1, developing inflorescence 5 mm (about 30 DAP); INF2, developing inflorescence 10–15 mm (about 50 DAP); CAR1, developing grain 5 days after anthesis (DAA); CAR2, developing grain 15 DAA; and EMB, embryo 4 days after germination. Raw data from Mayer et al. (2012).

suggesting active variation of the transcriptional interaction between these two genes. In the promoter region of *HvMADS22*, within 1 kb of the start of the coding region, there are 12 SNPs of varying rarity. Three of these, 529572337T, 529572349T and 529572362A, commonly occur together and correspond to *Hybernum viborg*, a winter barley grown in many parts of the world (**Supplementary Table 1**). The results from pan-genome database show a different distribution of SNPs, but the amount is equally low in most of the clades. The more recently duplicated genes in the *AGL17* clade (e.g., *HvMADS25*) have more abundant SNPs, as do *HvMADS30* and *HvMADS50* to a lesser extent. Apart from four amino acid indels among all MIKCc encoded proteins and a deletion of the last six amino acids of HvMADS16, no other variety in the coding sequence was detected across the pan-genome (**Supplementary Table 1**).

The lack of both natural and selected variation in these genes suggests a high rate of conservation and therefore importance for fitness and domestication. In rice, there are significantly more SNPs that change an amino acid, although many occur at a very low frequency (**Supplementary Table 1**; Mansueto et al., 2017).[7] These findings demonstrate that MIKCc MADS-box genes are not only conserved among grass species, but also show very few SNPs and other sequence variety between the coding sequence in both wild and domesticated barley.

Global MIKCc Transcripts Are Concentrated in the Inflorescence and Caryopsis

The ABCDE-class MIKCc genes in barley, according to the transcript data accompanying the HORVU database (Mayer et al., 2012), are predominantly expressed in the developing inflorescence at 0.5 and 1.5 cm (INF1 and INF2) and in developing seed (CAR1 and CAR2; **Figure 2**).

Transcript in other barley tissues, such as leaf and root, is seen for the SVP-like genes *HvMADS22/47/55*. AGL17-like genes *HvMADS23a/b*, *HvMADS25a/b/c/d* and *HvMADS27* are expressed mostly in the root and during late seed development; however, their overall transcript level is low (RPKM 10 or

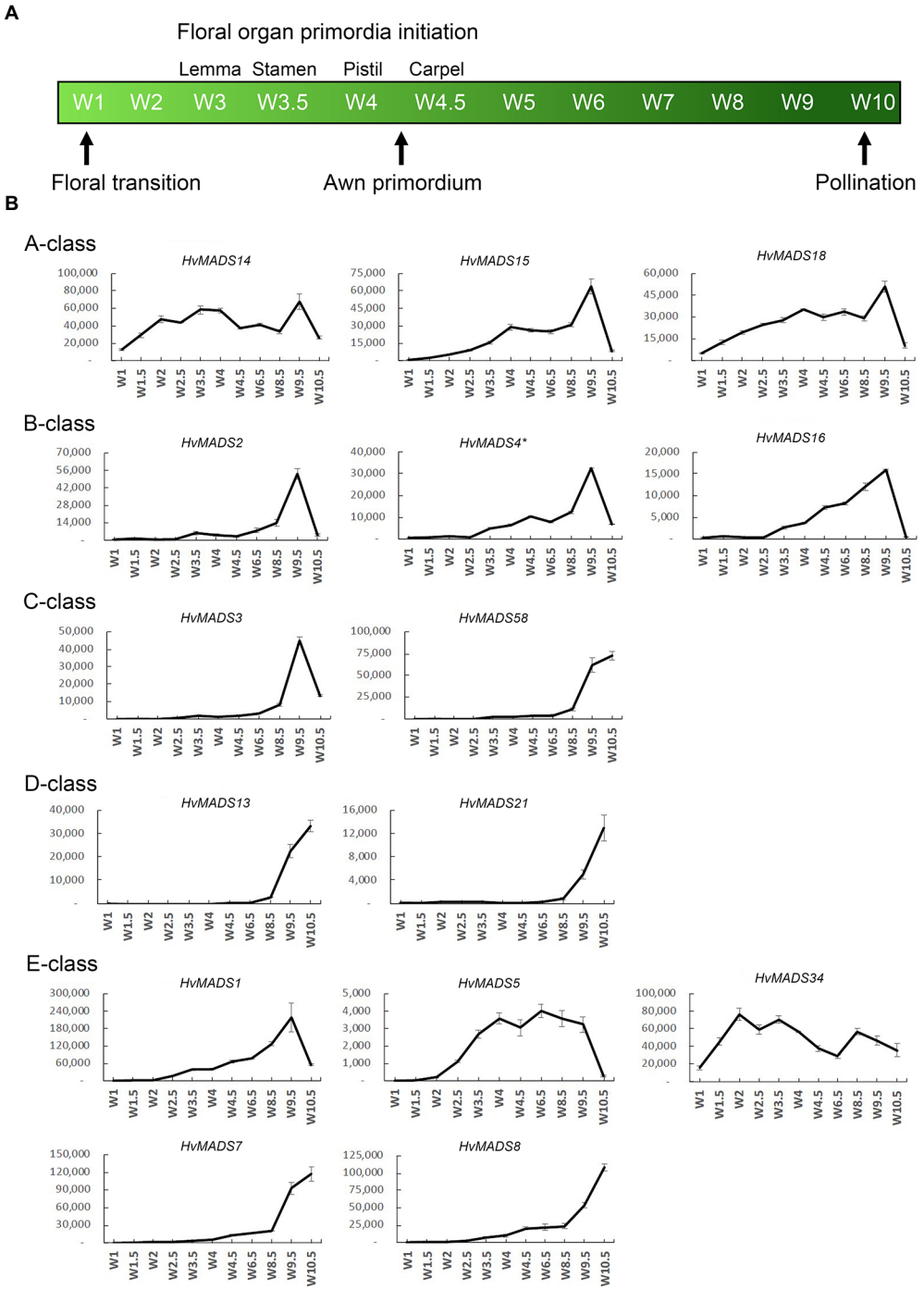

FIGURE 3 | (A) Waddington stages for barley and their relation to major developmental steps. **(B)** Transcript profiles of AP1, AP3/PI, AG(C), AG(D) and SEP MIKCc MADS-box genes in the shoot apex through inflorescence development as measured by the Waddington stage in Golden Promise. Error bars represent one standard deviation, based on technical replicates. A-class: The predicted A-class function in the outer floral organs predicts that transcript starts after W3, where the lemma primordium is first formed. However, expression of all three AP1 genes increases earlier, at the floral transition W1. AP3/PI: The expression of predicted B-class genes starts to increase at W3.5, where the stamen primordia are formed, and peaks right before pollination. AG(C): *HvMADS3* and *HvMADS58* both start expression around W3.5 when the stamen primordia appear, however *HvMADS3* peaks before pollination and declines quickly afterwards, while HvMADS58 maintains peak expression through to W10. AG(D): *HvMADS13* and *HvMADS21* both start significant expression only after W6.5, well after the pistil primordium is formed, which first appears at W4. Their peak expression is after pollination. E-class: There is a clear difference between the LOFSEP genes *HvMADS1*, *HvMADS5* and *HvMADS34* that express earlier and sharply drop at pollination (W10) and *HvMADS7* and *HvMADS8* expression, which starts later around W3.5 and continues to rise through pollination.

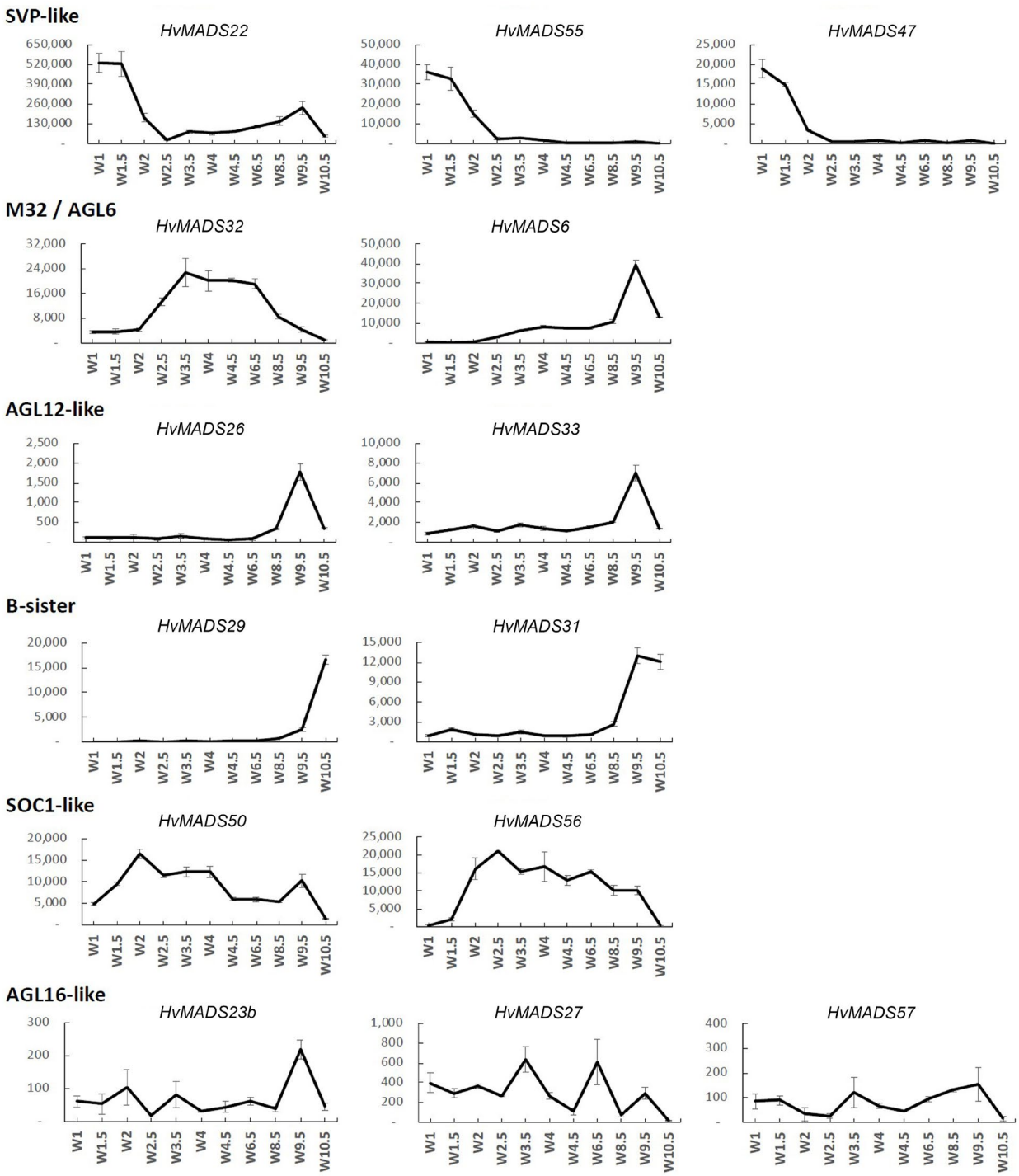

FIGURE 4 | Transcript profile of the non-ABCDE MIKCc MADS-box genes through inflorescence development by Waddington stage in Golden Promise. Error bars represent one standard deviation, based on technical replicates.

less), suggesting they may not be functional, or they are only expressed under stress conditions, like some AGL17-like genes in wheat (Schilling et al., 2020). *HvMADS57* has RPKMs of 25 and 35 in root and internode, respectively, which indicates it is the most likely among the AGL17-like genes to be functional. *OsMADS57* has been shown to function in cold tolerance in rice, directly targeting *OsWRKY94* and *OsD14* (Guo et al., 2013; Chen et al., 2018b).

Overall, among the 34 MIKCc MADS-box genes, most of them (20) are expressed in the developing inflorescence

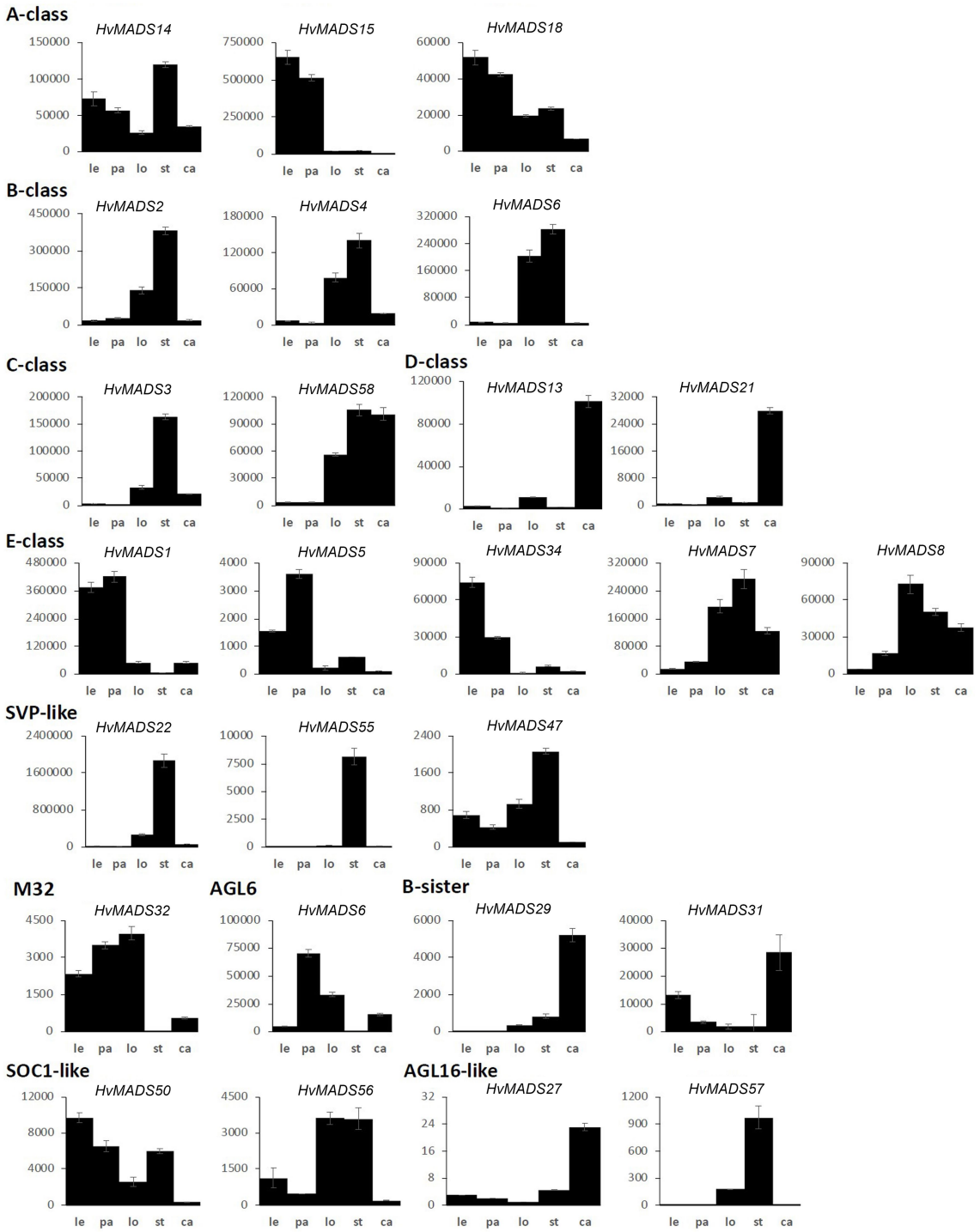

FIGURE 5 | MIKCc MADS-box gene expression in floral organs at Waddington stage 9.5. Error bars represent one standard deviation, based on technical replicates. Le, lemma; pa, palea; lo, lodicules; st, stamens; and ca, carpel.

and, similar to homologues in related species, are probably involved in meristem transitions and floral organ development (Arora et al., 2007; Paollacci et al., 2007; Wei et al., 2014). However, to gain any insight into transcript similarities and differences of the MIKCc genes in barley inflorescence development, and to what extent the ABCDE model is likely conserved, a higher resolution transcript profile from floral transition to pollination and a complete set of floral organ transcript data would be required.

Transcript Profiles of MIKCc Genes in Inflorescence Development and Floral Organs

The transcript profiles of MIKCc genes through barley inflorescence development (**Figures 3, 4**) can be related to developmental events by Waddington stage (**Figure 3A**). Combined with transcript data in the floral organs at Waddington stage W9.5 (**Figure 5** and **Supplementary Figure 4**), a comparison to established ABCDE models in other species can be made.

AP1 (A-Class)

Canonical A-class function in the outer floral organs would predict expression starting after the lemma primordium is first formed, at W3. However, expression of all three A-class genes increases before this, at the floral transition W1, indicating a role in earlier inflorescence development. *HvMADS14* transcript is already present at W1, peaks at W3.5, declines into W4.5 and peaks again at W9.5, right before pollination. The early expression of *HvMADS18*, along with the decline at W4.5, is less pronounced than for *HvMADS14*, but still recognisable (**Figure 3B**). *HvMADS15* transcript is closer to the expected profile of an A-class function gene, and transcript is indeed confined to the lemma and palea. While *HvMADS14* and *HvMADS18* are also expressed in the lemma and palea, their transcript is not confined there and *HvMADS14* is surprisingly more strongly expressed in the stamens than in the first whorl, indicating that the barley AP1 clade genes may have an additional function diverging from the classical ABCDE model (**Figure 5** and **Supplementary Figure 4**).

AP3/PI (B-Class)

B-class gene transcripts start to increase at W3.5, where the stamen primordia are formed, and peak right before pollination (**Figure 3B**). Transcript is confined to the lodicules and stamens, exactly following the ABCDE model, indicating B-class function is likely to be completely conserved in barley (**Figure 5** and **Supplementary Figure 4**).

AG (C-Class)

HvMADS3 and *HvMADS58* both start expression around W3.5 when stamen primordia appear, in accordance with the ABCDE model. However, where *HvMADS3* peaks before pollination and declines quickly afterwards, *HvMADS58* maintains peak expression through W10, indicating subfunctionalisation of the two genes, where *HvMADS58* is responsible for the C-class function in the carpel (**Figures 3, 5**). Both C-class genes also show some expression in the lodicules, which does not fit with the ABCDE model (**Figure 5** and **Supplementary Figure 4**).

AG (D-Class)

HvMADS13 and *HvMADS21* both start significant expression only after W6.5, well after the pistil primordium is first formed at W4. Peak transcript is after pollination and confined to the fruit, indicating that their canonical role in ovule development and into fruit development is likely to be conserved in barley (**Figure 3B**).

SEP (E-Class)

There is a clear difference between the 'LOFSEP' genes *HvMADS1*, *HvMADS5* and *HvMADS34* that express earlier and sharply drop at pollination (W10) and *HvMADS7* and *HvMADS8* expression, which starts later around W3.5 and continues to rise through pollination (**Figures 3A**,**B**). Floral organ transcripts show a division along the same line, where the LOFSEP genes are mostly confined to the lemma and palea, whereas *HvMADS7* and *HvMADS8* are expressed in the lodicules, stamens and carpel (**Figure 5** and **Supplementary Figure 4**). Therefore, the LOFSEP genes probably perform the E-class function in the lemma and palea, while *HvMADS7* and *HvMADS8* fulfil the E-class function in the other floral organs. In contrast to all other E-class genes, *HvMADS34* is expressed at W1 and peaks at W2, similar to *HvMADS14*, hinting at a function in early inflorescence development.

SVP-Like

The three SVP-like genes, *HvMADS22*, *HvMADS47* and *HvMADS55*, are highly expressed at the start of the floral transition and quickly decline to insignificant expression at W2.5, which indicates a role at this early stage. *HvMADS22* has a surprising resurgence in expression to a new maximum at W9.5, exclusively in the stamens, indicating possible neofunctionalisation (**Figures 4, 5** and **Supplementary Figure 4**).

MADS6

HvMADS6, closely related to the E-class genes, has an expression profile similar to *HvMADS1* (**Figure 4**), but contrastingly is not expressed in the lemma, but rather in the lodicules (**Figure 5** and **Supplementary Figure 4**). *HvMADS1* and *HvMADS6* may be partially redundant in E-class function, but not in the lemma and lodicules.

MADS32

HvMADS32 has no direct equivalent in *Arabidopsis*, and no assigned function in the original ABCDE model. The *HvMADS32* transcript appears before initiation of the floral organs and uniquely declines after W6.5, unlike any other MIKCc gene (**Figure 4**). Floral organ expression is concentrated in the lemma, palea and lodicules (**Figure 5** and **Supplementary Figure 4**).

B-Sister

HvMADS29 and *HvMADS31* are expressed late in inflorescence development, mostly after W8.5, and are strongly expressed after pollination (**Figure 4**). Combined with a nearly exclusive expression in the carpel, they are likely to be involved in ovule and seed development (**Figure 5** and **Supplementary Figure 4**).

SOC1-Like

HvMADS50 and *HvMADS56* expression starts early, with a peak at W2 and W2.5, much like *HvMADS14* and *HvMADS34*. Late expression is weaker, but only disappears after pollination (**Figures 4, 5** and **Supplementary Figure 4**).

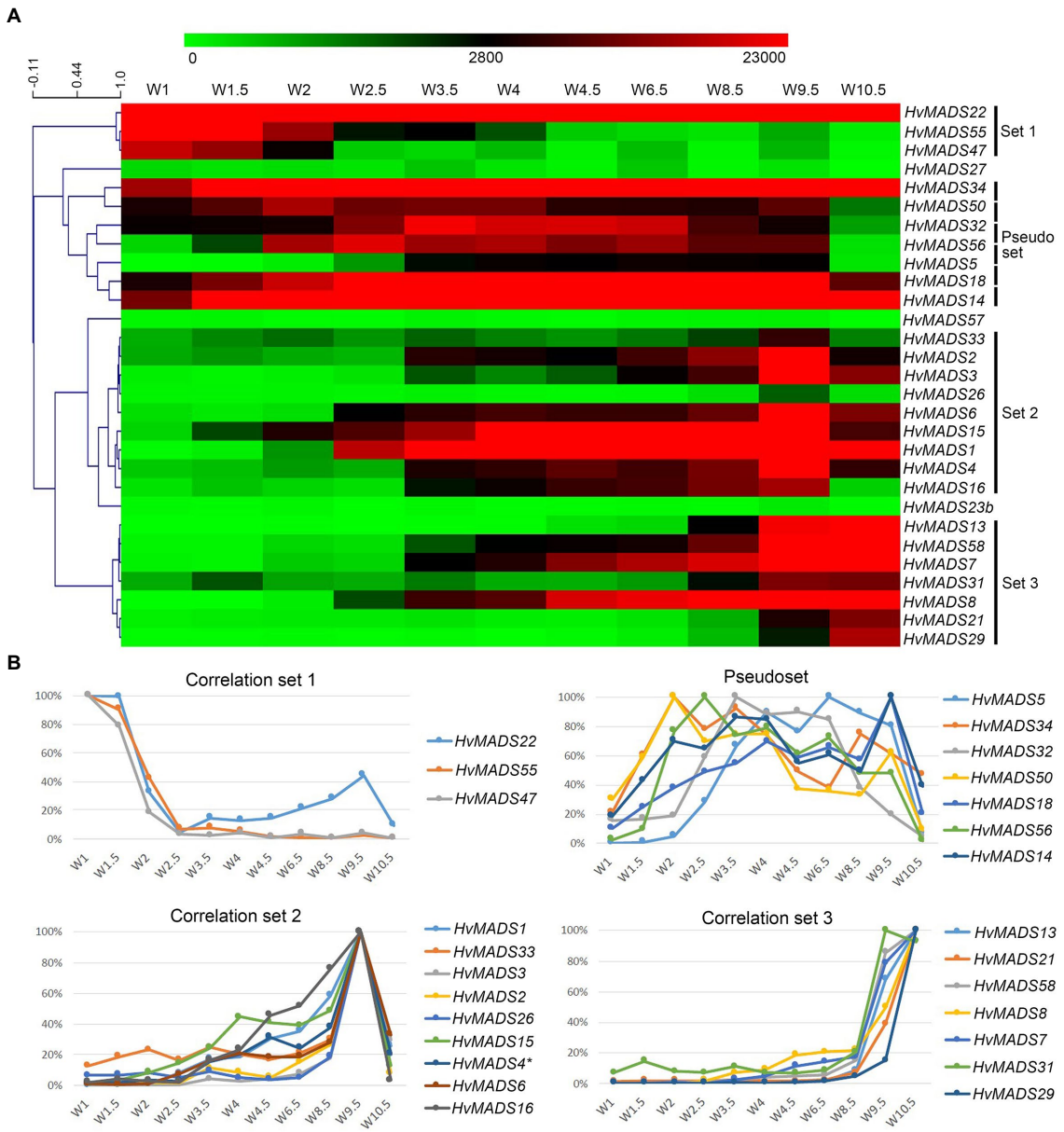

FIGURE 6 | Transcript profiles of MIKCc MADS-box genes can be grouped into correlation sets. **(A)** Pearson correlation of time course expression reveals three sets and a pseudoset. Expression is represented on a logarithmic colour scale, where the maximum value is capped to provide the best visual contrast in the data set spanning orders of magnitude. Correlation tree and scale bar are presented on the left side. **(B)** Relative expression profiles through inflorescence development of the MADS-box genes within each correlation set.

MIKCc Genes With Low Transcript in the Inflorescence

There was no significant transcript detected for several AGL17-like genes, including *HvMADS23a* and all four *HvMADS25* co-orthologues during the stages of inflorescence development examined here. Global expression analyses indicated that these transcripts are more prevalent in embryo, leaf and root tissue (**Figure 2**). Of the AGL17-like genes that did have measurable transcript, namely, *HvMADS23b*, *HvMADS27* and *HvMADS57*, low abundance and erratic profiles preclude any meaningful speculation on their function (**Figure 4**). The *HvMADS14b* pseudogene did seem to be expressed based on primer pair tests at various temperatures, but could never be sufficiently separated from the very similar and much more abundant *HvMADS14* transcript to provide a clear expression profile (data not shown). The final missing profile is that of *HvMADS30*, a B-sister gene, for which no expression was detected.

Co-expression Profiles Reveal a Novel Regulatory Network Among MADs-Box Genes in Barley Developing Inflorescences

To quantify co-expression of MIKCc MADS-box genes, which indicates possible functional connections, a correlation analysis was performed. Correlation analysis of the transcript profiles generated by RT-qPCR of all MIKCc MADS-box genes reveals three sets, here defined as members having a correlation coefficient of over 0.9 with at least two other members, and a less cohesive pseudoset (**Figures 6A**,**B**; **Supplementary Table 4**). A cluster analysis of the data showed a similar result of grouping (**Supplementary Figure 5**). Correlation set 1 is expressed mostly at W1 and W1.5, during the floral transition, and quickly disappears after this stage (**Figure 6**). In contrast, the pseudoset is spread out over the whole time course, but has some members with high transcript levels between W1.5 and W3.5 where none of the other sets show strong expression. This is the window for spikelet- and floret meristem initiation and development and then follows correlation set 2, which starts at W3 and stops after W9.5, where most floral organs develop. Finally, correlation set 3 shows transcript the latest and generally has maximum expression at W10.5, after pollination. *HvMADS23B*, *HvMADS27* and *HvMADS57* did not group into any set (**Figure 6**).

Set 1: Floral Transition

This contains three SVP-like genes, *HvMADS22*, *HvMADS47* and *HvMADS55*. Expression starts high at W1 and quickly declines to a minimum at W2.5. Remarkably, the expression of *HvMADS22* is upregulated again after W2.5 and peaks at W9.5 (**Figures 4, 6**). As the members of this set are already a class within the MIKCc genes, it is likely that they redundantly repress further inflorescence development.

Pseudoset: Expressed During Development of the Spikelet- and Floret Meristem

Expression of genes in the pseudoset is not as closely correlated as members of the other sets, but a general pattern can still be distinguished. Transcript mostly rises between the floral transition (W1) and emergence of the floral organs (W3–W4), and for some genes, the maximum expression is also in this early time-frame (**Figure 6B**). The SEP clade genes in the pseudoset are LOFSEP genes *HvMADS5* and *HvMADS34*. *HvMADS34* really stands out from the other E-class genes due to the very early high level of expression peaking at W2. *SUPPRESSOR OF OVEREXPRESSION OF CONSTANS* (*SOC1*)-like genes *HvMADS50* and *HvMADS56* are both expressed early in barley inflorescence development with a maximum at W2 and W2.5, respectively, and show a steep decline after W4. Early expression of pseudoset members indicates a function in floral development prior to the formation of the floral organs, such as a role in the spikelet- or floret meristem. Correlation of *HvMADS14*, *HvMADS34* and *HvMADS50* early expression suggests the possibility of related functions (**Figure 7A**).

Set 2: Lemma, Palea, Lodicule and Stamen Development

Correlation set 2 is not as uniform as sets 1 and 3. Transcripts in general appear around W3–W3.5, increase to a maximum right before anthesis at W9.5 and quickly diminish immediately after pollination at W10.5 (**Figure 6B**).

All three AP1 clade genes are strongly expressed in the lemma and palea, although the expression of *HvMADS14* and

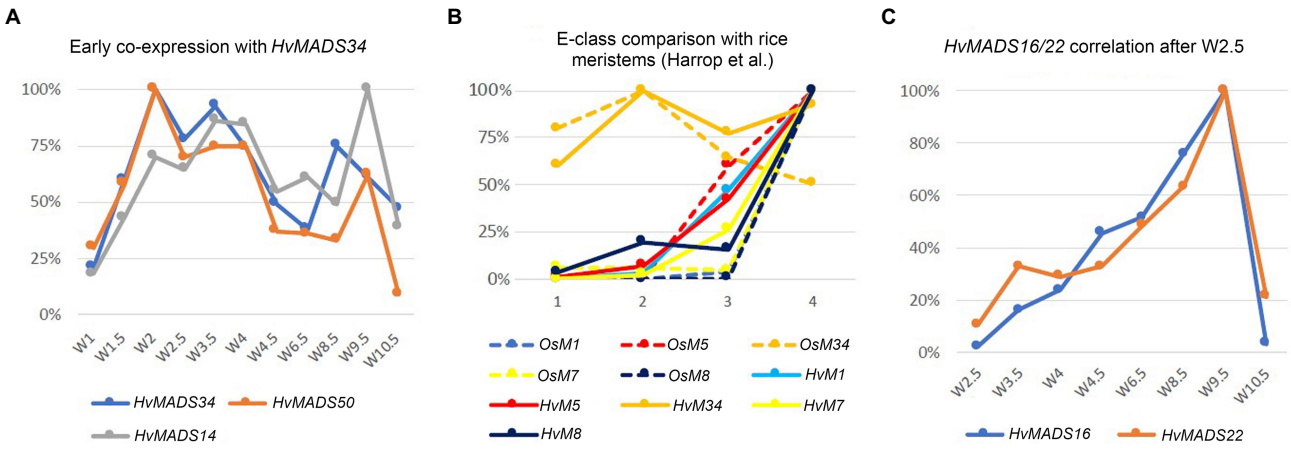

FIGURE 7 | Co-expression within barley or with equivalent stages in rice can suggest related functions. **(A)** Early co-expression of *HvMADS34* with *HvMADS14* (A-class) and *HvMADS50* (SOC1-like). **(B)** Comparison of early E-class gene expression in barley and rice. Analysis of the differential gene expression in the inflorescence meristem types of rice using laser microdissection followed by RNA sequencing (dashed lines) from the supplemental data of Harrop et al. (2016). While directly comparing the results of their work with expression in the early stages of the whole barley inflorescence meristem is a false equivalency, it can still provide some insights. The best matching Waddington stages W1.5–W3.5 expression data are shown (solid lines; this paper). On the *x*-axis, 1 is inflorescence meristem/W1.5, 2 is branch meristem/W2, 3 is elongated branch meristem/W2.5 and 4 is spikelet meristem/W3.5. **(C)** Correlation of the relative expression of *HvMADS22* and *HvMADS16* between W2.5 and W10.5.

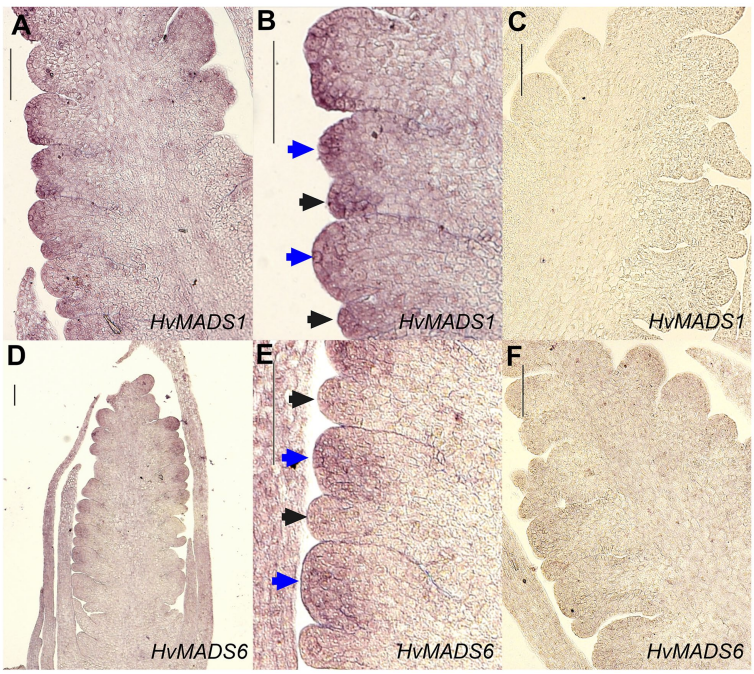

FIGURE 8 | *In situ* hybridisation of *HvMADS1* and *HvMADS6* probes to sections of the barley inflorescence at W3. *HvMADS1* is expressed in the floret meristem (blue arrowheads) and the lemma primordium (black arrowheads; **A,B**), but *HvMADS6* is more strongly expressed in the floret meristem **(D,E)**. **(C, F)** are the sense probe controls. Scale bars: 100 μm.

HvMADS18 starts significantly earlier. The LOFSEP subclade, *HvMADS1*, *HvMADS5* and *HvMADS34*, are strongly expressed in the lemma and palea, but hardly at all in the lodicule, stamen and carpel (**Figure 5**). Of these, only *HvMADS1* appears in correlation set 2. The strongest difference in expression between the lemma and palea is for *HvMADS6*, which is expressed in the palea, but at very low levels in the lemma (**Figures 5, 8**). In general, this indicates A- and E-class genes are expressed in the first whorl, which is consistent with the ABCDE model in other plants.

Lodicule expression is shown for the AP1 clade genes *HvMADS14* and *HvMADS18*, all three B-class and both C-class genes *HvMADS3* and *HvMADS58* plus strongly for the SEP3 subclade of the E-class genes, *HvMADS7* and *HvMADS8*. In this tissue, the *HvMADS32* transcript profile in the pseudoset is not similar to that of set 2 members, with the most notable difference being an early sharp decline after W6.5. *HvMADS6* is also expressed in the lodicules. Canonically, the second whorl has A-, B- and E-class gene expression so the C-class transcript in barley lodicules is unexpected, and clashes strongly with the ABCDE model.

The AP1 clade genes *HvMADS14* and *HvMADS18* are both expressed in the stamens, and for *HvMADS14*, this is the highest expression seen in any floral organ. All three B-class genes and both C-class genes, *HvMADS3* and *HvMADS58* plus the E-class genes *HvMADS7* and *HvMADS8* are expressed here too, while the LOFSEP genes are only marginally expressed. Surprisingly, the highest expressed MIKCc gene in the stamens is *HvMADS22*, an SVP-like gene from correlation set 1. Ignoring the *HvMADS22* expression before W2.5, the profile thereafter is very similar to that of correlation set 2, for *HvMADS16* in particular (**Figure 7C**). The expected B-, C- and E-class expression for the third whorl is present in barley stamens, but the addition of A-class expression and *HvMADS22* is unexpected.

Set 3: Carpel and Ovule Development

Correlation set 3 contains the canonical members of a carpel and an ovule quartet: C-, D- and E-class genes. Additionally, the expression of set 3 genes peaks past pollination at W10.5. *HvMADS58*, an AG clade (C-class) gene that is part of correlation set 3, shows strong expression in the carpel, while the other AG (C-class) gene *HvMADS3*, a member of set 2, is only marginally expressed (**Figure 5**). The expression of D-class genes *HvMADS13* and *HvMADS21* starts late, even compared to other set 3 members, after W6.5, and is found almost exclusively in the carpel tissue. *HvMADS7* and *HvMADS8* are expressed late in floret development, and the final two genes in correlation set 3 are the B-sister genes *HvMADS29* and *HvMADS31*.

MADS2 and *MADS4* Are Covered by Neighbouring Kinase Transcripts

The *HvMADS4* (*HORVU1Hr1G063620*) genomic sequence is completely covered by the transcript of the neighbouring gene on the opposite DNA strand, *HORVU1Hr1G063610*, a serine/threonine protein kinase. As a result, any primer pair that targets *HvMADS4* will also amplify this protein kinase transcript.

To circumvent this problem, we designed a primer pair at the end of the *HvMADS4* transcript, with an alternative reverse primer just outside of the *HvMADS4* transcript. Subtracting the signal of the latter pair from the former provides a more accurate representation of the expression level of *HvMADS4* only, which is designated *HvMADS4** here.

A similar problem occurs with *HvMADS2* where the genomic span of the gene is also transcribed from the opposite direction, encoding a neighbouring kinase, *HORVU3Hr1G090990*. In this case however, the kinase expression was so low compared to the *HvMADS2* expression that trying to subtract it did not increase accuracy significantly.

DISCUSSION

In this study, we revealed that the MIKCc MADS-box genes in barley are highly conserved and that their expression can be grouped in correlated sets that are linked to developmental events in the spike, spikelet and floret. This suggests that floral organogenesis is regulated by the ABCDE model in barley. Phylogeny shows that the MIKCc MADS-box family in barley is highly conserved, and SNP data confirm that natural variations of MIKCc MADS-box genes do not occur frequently during barley domestication. The consistency in the number of genes in each class and the mostly one to one matching homology of MIKCc genes between barley, rice, sorghum and *Brachypodium* (**Figure 1**; Arora et al., 2007; Wei et al., 2014) suggests that the determination of floral organs, a process dominated by the MIKCc family, is probably conserved as well. In the genome of bread wheat, 195 MIKCc MADS-box genes have been identified (Schilling et al., 2020). This high number is not only due to hexaploidy and subsequent frequent retention of MIKCc genes, but also due to recent duplication events, theorised to help wheat adapt to diverse growth conditions. The redundancy and neofunctionalisation have led to much more frequent and severe changes in nucleotide sequences of MIKCc genes in wheat. Nevertheless, retention of functional homologues of each rice MIKCc gene suggests the conservation of their role in the inflorescence development of wheat (Schilling et al., 2020). This is also reflected in the similar floral organ development pathway seen among grasses. The ABCDE model has been extrapolated to rice, maize and wheat previously (Ciaffi et al., 2011), and the morphological and genetic conservation suggests that it may apply to barley as well. While the barley MIKCc genes are highly conserved, variation in their expression profiles can provide an insight into the robustness of the ABCDE model in barley.

Grouping MIKCc MADS-box genes using a temporal expression profile in the developing inflorescence and floral organs has its drawbacks. Many shoot apical meristem samples contain spikelets and florets at multiple stages, with younger meristems near the top (**Supplementary Figure 3**). Additionally, many of the ABCDE proteins are predicted to participate in multiple floral quartets, or even have roles before the floral organs are initiated, like some A-class and E-class genes, which also complicates deconvoluting transcript profiles. However, these expression profiles can still be divided into four distinct groups mathematically (**Figures 6A**,**B**; **Supplementary Figure 5**). The profile of each gene, combined with expression data from individual floral organs, gives a clear indication of whether each gene conforms to their expected role within the ABCDE model, as found for homologues in rice, wheat and other plant species. Nonconforming transcript profiles are also highlighted which may hint at subfunctionalisation, neofunctionalisation or new interactions that warrant further investigation. Our data showed that most barley MIKCc MADS-box genes are expressed at the specific developmental stage and in the predicted floral organs during barley inflorescence development. However, there are several strong deviations in the expression patterns of some genes expected to have an ABCDE-class function, indicating neofunctionalisation.

SVP-Like MIKCc Genes Likely Act as Floral Inhibitors

The high start and quick decline of *HvMADS22*, *HvMADS47* and *HvMADS55* expression is in accordance with previous RNA sequencing of barley early inflorescence meristems (Digel et al., 2015; **Supplementary Figure 2A**) and is similar to RT-qPCR results reported by (Trevaskis et al., 2007b). In rice, the same pattern can be observed through the progression of meristem types, where *OsMADS22* and *OsMADS55* expression is high in the inflorescence meristem, lower in the branch meristem and at a minimum in the spikelet meristem (Harrop et al., 2016). In the inflorescence of *Setaria viridis*, a member of the Panicoideae (e.g. maize and sorghum) again the same decline in early inflorescence development is observed (Zhu et al., 2018). This conserved expression pattern likely indicates a conserved function of the SVP clade in grasses. In barley, the expression of *HvMADS22* peaks again at W9.5, but this re-emergence later in floret development is mirrored only in wheat (Feng et al., 2017; **Supplementary Figure 2B**). *HvMADS22* (*BM10*) and *HvMADS47* (*BM1*) act as floral inhibitors and can cause partial or full floral reversion when ectopically expressed (Trevaskis et al., 2007b). The expression profiles of *HvMADS22*, *HvMADS47* and *HvMADS55* fit the function as floral inhibitors well, except for the resurgence of *HvMADS22* expression.

APETALA and *LOFSEP* Transcripts Dominate in the Lemma and Palea

The ABCDE model states the first floral whorl is defined by A- and E-class genes (Theissen and Saedler, 2001). However, whether the palea and lemma are true first whorl floral organs in grasses is still debated (Ciaffi et al., 2011). *HvMADS14*, *HvMADS15*, and *HvMADS18* are all strongly expressed in the lemma and palea, similar to observations in *Brachypodium* (Wei et al., 2014) and wheat (Paollacci et al., 2007), giving each APETALA gene the potential to fill the A-class role. Since *HvMADS7* and *HvMADS8* are not expressed in the lemma and palea, the E-class role is likely performed by the *LOFSEP* genes, also seen in *Brachypodium* (except for the *MADS7* homologue being expressed in the palea; Wei et al., 2014)

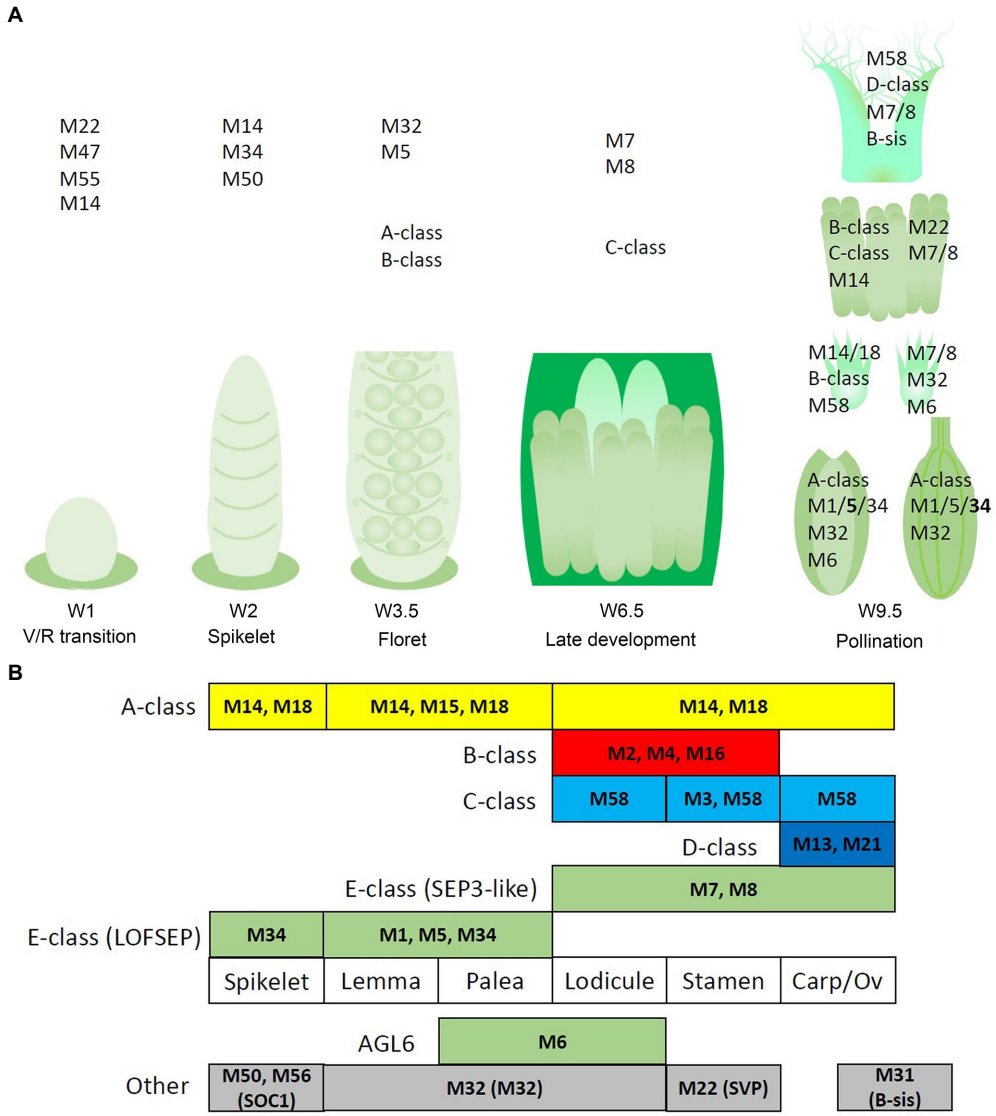

FIGURE 9 | Potential regulatory networks of MIKCc MADS-box genes in barley inflorescence and floral development. In this figure, 'MADS' is abbreviated as 'M'. **(A)** Prominent expression of the MIKCc MADS-box genes through developmental stages and the floral organs of barley. **(B)** Schematic of an adapted ABCDE model for barley floral development. Canonical ABCDE genes are depicted above the floral organs where they are expressed, while additional expressed MIKCc genes are shown below. Transcript before the start of floral organ primordia initiation is given in the leftmost column, tentatively labelled 'spikelet'.

and in wheat (Paollacci et al., 2007). The quadruple knockdown of *OsMADS1/5/7/8* (leaving *OsMADS34* as the only remaining E-class gene) transforms all floral organs in the rice floret into leaf-like structures, except for the lemma (Cui et al., 2010). As *HvMADS34* is more strongly expressed in the lemma in barley, this may be the only floral organ where HvMADS34 acts in an E-class role. Accumulation of barley *HvMADS1* mRNA also showed a high level in lemma (**Figures 8A–C**). Expression of *HvMADS32*, the only member of a MIKCc class unique to monocots, in the lemma and palea makes it likely to be a member of the lemma and palea floral quartet, although its unique expression profile does not match the other likely members of the quartet. Additionally, the *MADS32* homologue in *Brachypodium* shows only weak expression in the palea and not the lemma (Wei et al., 2014). The strongest difference in expression between the lemma and palea is for *HvMADS6*, which is weakly expressed in the lemma (**Figures 8D–F**). Even though *HvMADS6* does not belong to the SEPALLATA clade, it has been reported to fulfil an E-class function in plants (reviewed by Dreni and Zhang, 2016).

The lemma and palea floral quartets in barley are probably composed of APETALA and LOFSEP proteins, in accordance with predictions from the ABCDE model (**Figure 9**). In the palea, *HvMADS6* may play an E-class role in the floral quartet, possibly resulting in the morphological differences between the lemma and palea in barley.

Lodicules Contain Predicted AP1, AP3/PI and SEP Transcript but Surprising AG (C-Class) Expression

The second whorl is canonically determined by a floral quartet consisting of one A-class, two B-class and one E-class protein. Unlike the APETALA gene *MADS15* in rice and wheat (Kyozuka et al., 2000; Paollacci et al., 2007), the barley orthologue, *HvMADS15*, is not expressed in the lodicules. All three B-class genes are expressed in the barley lodicules, in accordance with the ABCDE model and this expression is neatly matched in *Brachypodium* and wheat (Paollacci et al., 2007; Wei et al., 2014). The conservation of this B-class function and mechanism in grasses is shown by the homeotic conversion of lodicules into whorl 1-like bracts in mutants of AP3/DEF subclade members *OsMADS16*/*SUPERWOMAN1* in rice (Nagasawa et al., 2003) and *SILKY* in maize (Ambrose et al., 2000). The role of *OsMADS2* and *OsMADS4* as redundant PI/GLO seems clear from the spw1-like phenotype (homeotic conversion of stamens to carpels) of the double knockout line (Yao et al., 2008; Ciaffi et al., 2011). Moreover, the strong expression of E-class genes *HvMADS7*, *HvMADS8* and AGL6-like gene *HvMADS6* in the lodicules makes them the likely candidates for the E-class role in the lodicule-defining floral quartet in barley, which is consistent with rice homologues and maize *MADS6* homologue *ZAG3* (Thompson et al., 2009). Furthermore, the osmads7/8 double mutant shows aberrant lodicules (Cui et al., 2010), indicating that the LOFSEP (E-class) genes do not redundantly cover this function. Additionally, *HvMADS32* is strongly expressed in the lodicules, but its transcript profile in the pseudoset is not similar to that of other potential members of the lodicule quartet, most notably its early sharp decline after W6.5. However, in rice, the *osmads32* mutants do show some homeotic conversion of the lodicules (Sang et al., 2012), and a disrupted protein interaction with *OsMADS2* and *OsMADS4* is likely to be responsible for at least part of the *OsMADS32* function (Wang et al., 2015). Therefore, *HvMADS32* could have a function in lodicule determination and potentially be part of a lodicule quartet, but only in the early stages (Thompson et al., 2009).

Surprisingly, both barley C-class genes *HvMADS3* and *HvMADS58* are expressed in the lodicules, similar to homologues of wheat TaAG-1 and TaAG-2 and *Brachypodium BdMADS18*, but not with maize orthologues (*ZAG1*, *ZmM2*, and *ZmM23*; Mena et al., 1996; Paollacci et al., 2007; Wei et al., 2014). One of the central regulatory mechanisms in the ABCDE model is the antagonistic role of A- and C-class genes. In rice, the C-class genes have a role in suppressing additional lodicule formation (Yamaguchi et al., 2006). The separation of expression domains of the A-class and C-class genes, by mutual negative regulation, is one of the core tenets of the ABC model as originally devised in *Arabidopsis*. Here, we show that in barley, APETALA clade genes are expressed in the inner floral organs, and AGAMOUS clade transcripts show up in the second whorl floral organs, the lodicules.

Stamens Contain Transcripts of Both Predicted and Unexpected Members

The A-class genes *HvMADS14* and *HvMADS18* are both expressed in the stamens, where for *HvMADS14*, it is the highest expression in any floral organ. Similarly, the wheat homologue *TaAP1-1* is expressed in all floral organs, and in *Brachypodium*, the *AP1* gene *BdMADS3* is also expressed in the stamens (Paollacci et al., 2007). In rice, *OsMADS14* and *OsMADS18* are expressed in the stamens, but *OsMADS14* is the main actor in stamen identity (Wu et al., 2017). All three B-class genes are expressed as expected, which is similar to rice, where a knockdown of the rice B-class gene *OsMADS16* or both *OsMADS2* and *OsMADS4* results in homeotic conversion of the stamens into carpel-like organs (Yao et al., 2008). C-class genes, *HvMADS3* and *HvMADS58*, are strongly expressed here, similar to their counterparts in rice. Rice *OsMADS3* plays a crucial role in stamen identity (Yamaguchi et al., 2006), but the relative importance of C-class genes in barley will have to be investigated further. Furthermore, transcripts of E-class genes *HvMADS7* and *HvMADS8* are present, where the LOFSEP genes are only marginally expressed. The homologous genes in wheat, *TaSEP4* and *TaSEP3*, are also predominantly expressed in the inner floral organs (Paollacci et al., 2007). In rice, *OsMADS7/8* double knockdown plants the stamens were affected, but not completely abolished as in the *OsMADS1/5/7/8* quadruple knockdown lines, so *OsMADS7* and *OsMADS8* have a primary E-class function, but not an exclusive one (Cui et al., 2010). Surprisingly, the most highly expressed MIKCc gene in the stamens is HvMADS22, an SVP-like gene, which normally functions as a floral repressor and in *Brachypodium* the *HvMADS22* homologue *BdMADS30* is also strongly expressed (Wei et al., 2014). Investigating expression and phenotypic differences correlated with the SNPs variations may provide insight in the *HvMADS22* role.

In summary, the canonical members of the third whorl floral quartet are expressed in barley stamens: *HvMADS16* (AP3/DEF B-class), *HvMADS2* or *HvMADS4* (PI/GLO B-class), *HvMADS3* or *HvMADS58* (C-class) and HvMADS7 or HvMADS8 (E-class). However, the APETALA clade genes *HvMADS14* and *HvMADS18*, and an SVP-like gene, *HvMADS22*, also show significant expression (**Figure 9A**). While the expression profiles for *HvMADS14* and *HvMADS18* do not reveal meaningful co-expression, *HvMADS22* expression after W2.5 is very similar to other probable stamen quartet members (**Figure 7C**), suggesting the unlikely neofunctionalisation of a floral repressor in this organ.

AG, *SEP*, and B-Sister Genes Are Expressed in the Carpel and Ovule

Carpel fate is induced by a quartet of two C- and two E-class genes, while the ovule quartet contains one C-, two D- and one E-class gene (Theissen et al., 2016). Floral meristem determinacy (FMD) is likely to be regulated by the remnant of the floret meristem, located within the carpel samples.

Strong carpel expression of the AG (C-class) gene *HvMADS58*, in contrast to marginal *HvMADS3* (**Figure 3B**) expression, is

a sign of subfunctionalisation among the *AG* genes where the C-class role in carpel development is fulfilled primarily by *HvMADS58*. The wheat homologue of *HvMADS3*, *TaAG-2*, is also predominantly expressed in the stamens, compared to the carpel (Paollacci et al., 2007). An osmads58 mutant in rice develops abnormal carpels, while osmads3 carpels develop almost completely normally, showing that *OsMADS58* is the primary C-class gene for carpel development (Yamaguchi et al., 2006). The late expression of D-class genes *HvMADS13* and *HvMADS21* is found almost exclusively in the carpel samples (collected at W9.5), which is consistent with a potential role in ovule development. *HvMADS7* and *HvMADS8*, E-class genes of the SEP3 sub-clade, are expressed late in floret development, as in wheat (Feng et al., 2017) and potentially fulfil the E-class role for the inner floral organs. For *HvMADS8* (*BM9*), this boundary at the lodicule has also been shown by *in situ* hybridisation; however, it also shows *HvMADS1* (*BM7*) expression in the developing ovule (Schmitz et al., 2000). While *HvMADS1* is expressed in the carpel at W9.5, most of it disappears after pollination. This leads to the conclusion that HvMADS7 and HvMADS8 are likely part of the carpel and ovule quartets, and *HvMADS1* may have a function during ovule development or FMD. The final two genes in correlation set 3 are the B-sister genes *HvMADS29* and *HvMADS31*. *AtABS*, a B-sister gene in *Arabidopsis*, has been linked to endothelium development and interaction with *AtSEP3*, and D-class genes suggest they may function in an additional floral quartet (Kaufmann et al., 2005). No expression of the B-sister gene *HvMADS30* was detected. *OsMADS30* is not a suitable guide for the function of its homologue in barley because the rice gene has a recent insertion and an altered expression pattern compared to related grass species (Schilling et al., 2015). However, it was recently revealed that MADS30-like gene expression is induced by biotic stress in wheat (Schilling et al., 2020), suggesting that a similar mechanism in barley may be why no *HvMADS30* expression was identified. Short genes can be expressed more rapidly than long genes and can be associated with fast dividing cells, particularly in zygotic tissue (Heyn et al., 2015). B-sister genes have short introns (**Supplementary Figure 1**), and their expression is associated with tissues of the ovule and developing grain. Long genes take longer to express, causing a so-called 'intron delay' that can be of regulatory significance. Additionally, longer genes with sizable introns are often more highly expressed (Heyn et al., 2015). However, there does not seem to be any clear correlation between intron size and frequency of expression for MIKCc genes in barley.

To summarise, the canonical MIKCc members of the fourth whorl quartet are present in the barley carpel: C-class gene *HvMADS58* and E-class genes *HvMADS7* and *HvMADS8*. The ovule quartet is also represented in the carpel samples: *HvMADS58* as the C-class gene, both D-class genes (*HvMADS13* and *HvMADS21*) and two E-class genes: *HvMADS7* and *HvMADS8* (**Figures 9A**,**B**). The additional expression of B-sister genes in this correlation set may imply a redundant function in the carpel or the ovule-determining quartet; however, it is more likely to be related to a function in the endothelium and other ovule and early seed roles. The B-sister proteins in eudicots have been shown to interact with C-, D- and E-class proteins, and the mutant has defects in the endothelium (de Folter et al., 2006).

MIKCc Gene Expression Implies a Role in Inflorescence-, Spikelet- and Floret Meristems

MIKCc genes play an important role in grass inflorescence architecture and spikelet differentiation (Digel et al., 2015; Liu et al., 2015; Li et al., 2021; Wang et al., 2021). In our study, SVP-like genes, *HvMADS22*, *HvMADS47* and *HvMADS55*, and one A-class gene *HvMADS14* (*VRN1*), and E-class gene *HvMADS34*, show a high transcription level at the early inflorescence development stage before spikelet differentiation, suggesting a role for these genes in inflorescence meristem maintenance and spikelet meristem identity. *APETALA1* genes in barley are likely to perform A-class functions in floral organ determination (see below); however, *HvMADS14* (*VRN1*) has an additional role in the vernalisation response and probably in establishing and maintaining inflorescence meristem identity in barley (Trevaskis et al., 2007a). The early expression of *HvMADS18*, along with the decline at W4.5, is less pronounced than for *HvMADS14*, but still recognisable, indicating a potentially weaker redundant role in establishing and maintaining inflorescence meristem identity. *HvMADS15* is part of correlation set 2 and is therefore more likely to perform an A-class function exclusively. A similar divide is present in wheat, where *MADS14* and *MADS18* co-homologues have reduced expression after W4, while *MADS15* co-homologues do not (Feng et al., 2017).

Mutants in rice show that E-class *OsMADS34* gene is involved in inflorescence branching (Gao et al., 2010; Kobayashi et al., 2010), and unsurprisingly, *OsMADS34* is highly expressed in the inflorescence branch meristem of rice (Harrop et al., 2016). However, mutation of barley *HvMADS34* does not show the change of inflorescence architecture (Li et al., 2021). When comparing E-class gene expression in the early inflorescence meristem between barley and rice, the early peak of *HvMADS34* expression is conserved (**Figures 7A**,**B**). No other E-class gene (nor *HvMADS6*) could provide redundancy for a potential *HvMADS34* function around stage W2, because their expression starts later in inflorescence development. We can only speculate that the early *HvMADS34* expression is merely a vestigial remnant from the ancestral inflorescence, which did have a branched morphology (Remizowa et al., 2013). Recently, barley E-class MADS-box protein, HvMADS1, has been reported to be responsible for maintaining an unbranched spike architecture at high temperatures; the *hvmads1* mutant shows the changed inflorescence meristem determinacy at warm temperature conditions, forming a branched inflorescence-like structure (Li et al., 2021). Thus, the *Triticeae* spikes merely suppress inflorescence branching is given credence by the branching phenotype of the *com2* (*COMPOSITUM2*) and *com1/bdi1* (*COMPOSITUM1/BRANCHED AND INDETERMINATE SPIKELET 1*) mutants in barley and the tetraploid 'miracle wheat' (Poursarebani et al., 2015, 2020; Shang et al., 2020) and in the loss-of-function of barley *HvMADS1* mutant under

high ambient temperature (Li et al., 2021) which show that most of the components for a branching inflorescence are still present in some *Triticeae*.

The loosely correlated genes in the pseudoset display early expression in the window between floral transition and the start of floral organ formation, when the spikelet and floret meristems are formed. The sudden downturn in transcript between W4 and W4.5 that many members of the pseudoset have in common (**Figure 6B**) coincides with the end of formation of new spikelet meristems at the awn primordium stage (Alqudah and Schnurbusch, 2014). This indicates that members of this pseudoset could be involved in inflorescence meristem determination, including the inflorescence-, spikelet- and floret meristems.

Adapting the ABCDE Model for Barley

Overall, the ABCDE model for grasses still follows the same basic structure as the model from *Arabidopsis*, the addition of DELLA notwithstanding (Ciaffi et al., 2011). The results presented here show that this generally holds true for MIKCc gene expression in barley as well, although there are some deviations. The ABCDE proteins are known to initiate floral organ fate, as shown by mutants with homeotic changes. However, their role is not limited to just the initial direction of floral organ primordia. ABCDE proteins have been shown to bind in an organ specific way to promoter regions of genes involved in growth and differentiation of floral organ tissues, up to *SPOROCYTELESS*, a master regulator of gametogenesis in *Arabidopsis* (Chen et al., 2018a). The rising expression levels of most ABCDE-class genes throughout floret development indicate this continuous affirmation of organ identity by floral quartets may be present in barley as well. These persistent roles make floral organ sample collection at W9.5 a reasonable predictor of floral organ fate determining ABCDE-class genes. However, when looking at the MIKCc genes outside the ABCDE-functions, the most strongly expressed genes are *HvMADS22* in the stamens, usually classified as a floral repressor, and *HvMADS32*, which may be crucial for the discrete border between the outer and inner floral organs (**Figure 9B**). Some basal angiosperms have a more gradual transition between their floral organs, which does not fit with the ABCDE model, which results in discrete floral whorls. This is accompanied by a more gradual change in gene expression in these taxa and is captured in the 'fading borders' model (Buzgo et al., 2004; Soltis et al., 2007). This states that the gradually rising expression of, for example, C-class genes, and the slowly fading expression of A-class genes, results in intermediate floral organs with some characteristics from the adjacent organs. This may be the ancestral angiosperm ABC model, where only later more stringent restrictions on the expression evolved to separate the second and third whorls, resulting in the A–C antagonism in the ABCDE model for eudicots, and perhaps a different solution evolved in grasses, involving *HvMADS32*.

Because MIKCc proteins function in floral quartets, the next step to gain more insight into the potentially changed roles of these genes should be protein interaction studies. So far, when discussing the ABCDE model, the floral organs have often been considered indivisible units that either gain the correct identity or are homeotically converted. In the barley stamens, 10 different MIKCc genes from five classes are strongly expressed (**Figure 9B**), which are unlikely to form just one floral quartet. There may be variants of the stamen quartet that help define specific tissues within the stamens or even complete quartets. Alternatively, some of these MIKCc genes may have a function in stamens independent of a floral quartet structure. A somewhat similar tissue-specific expression of MIKCc genes has been shown in the ovule of rice (Kubo et al., 2013).

Altogether, these findings show that while the general setup of flowering is conserved, there are many interesting deviations in barley, and likely other grasses, that merit further research into what they mean for both the evolution of flowering in grasses and the potential adaptability of the inflorescence for crop yield breeding.

DATA AVAILABILITY STATEMENT

The original contributions presented in the study are included in the article/**Supplementary Material**; further inquiries can be directed to the corresponding authors.

AUTHOR CONTRIBUTIONS

Study was conceived by HK and DZ. Experiments were done by HK, NS, and SK. Bioinformatics were done by HK, JSh, and JSc. Data analysis was done by HK, NS, and GL. Manuscript was written by HK, GL, and RB. Supervision and funding by RB and DZ. All authors contributed to the article and approved the submitted version.

FUNDING

HK was supported by a University of Adelaide Beacon postgraduate scholarship, and the work was completed as part of the Australian Research Council Discovery Project (grant no. DP170103267 and DP170103352) and the Science and Research grant of Southwest University of Science and Technology (grant no. 19zx7146).

ACKNOWLEDGMENTS

We would like to thank Dr. Xiuyuan Yang, Dr. Gwen Mayo and Adelaide Microscopy for help with the *in situ* experiment; Laura Wilkinson for the *HvMADS13* primers; and Cindy Callens for the *HvMADS29* primers.

SUPPLEMENTARY MATERIAL

The Supplementary Material for this article can be found online at: https://www.frontiersin.org/articles/10.3389/fpls.2021.705286/full#supplementary-material

REFERENCES

Alqudah, A. M., and Schnurbusch, T. (2014). Awn primordium to tipping is the most decisive developmental phase for spikelet survival in barley. *Funct. Plant Biol.* 41:424. doi: 10.1071/FP13248

Alvarez-Buylla, E. R., Benítez, M., Corvera-Poiré, A., Chaos Cador, A., de Folter, S., Gamboa de Buen, A., et al. (2010). Flower development. *Arabidopsis Book* 8:e0127. doi: 10.1199/tab.0127

Ambrose, B. A., Lerner, D. R., Ciceri, P., Padilla, C. M., Yanofsky, M. F., and Schmidt, R. J. (2000). Molecular and genetic analyses of the silky1 gene reveal conservation in floral organ specification between eudicots and monocots. *Mol. Cell* 5, 569–579. doi: 10.1016/S1097-2765(00)80450-5

Angenent, G. C., Franken, J., Busscher, M., Vandijken, A., Vanwent, J. L., Dons, H. J. M., et al. (1995). A novel class of mads box genes is involved in ovule development in petunia. *Plant Cell* 7, 1569–1582. doi: 10.1105/tpc.7.10.1569

Arora, R., Agarwal, P., Ray, S., Singh, A. K., Singh, V. P., Tyagi, A. K., et al. (2007). MADS-box gene family in rice: genome-wide identification, organization and expression profiling during reproductive development and stress. *BMC Genomics* 8:242. doi: 10.1186/1471-2164-8-242

Becker, A., and Theißen, G. (2003). The major clades of MADS-box genes and their role in the development and evolution of flowering plants. *Mol. Phylogenet. Evol.* 29, 464–489. doi: 10.1016/s1055-7903(03)00207-0

Bommert, P., Satoh-Nagasawa, N., Jackson, D., and Hirano, H.-Y. (2005). Genetics and evolution of inflorescence and flower development in grasses. *Plant Cell Physiol.* 46, 69–78. doi: 10.1093/pcp/pci504

Bowman, J. L., and Smyth, D. R. (1999). CRABS CLAW, a gene that regulates carpel and nectary development in *Arabidopsis*, encodes a novel protein with zinc finger and helix-loop-helix domains. *Development* 126, 2387–2396. doi: 10.1242/dev.126.11.2387

Bremer, K. (2002). Gondwanan evolution of the grass alliance of families (Poales). *Evolution* 56, 1374–1387. doi: 10.1111/j.0014-3820.2002.tb01451.x

Burton, R. A., Jobling, S. A., Harvey, A. J., Shirley, N. J., Mather, D. E., Bacic, A., et al. (2008). The genetics and transcriptional profiles of the cellulose synthase-like HvCslF gene family in barley. *Plant Physiol.* 146, 1821–1833. doi: 10.1104/pp.107.114694

Buzgo, M., Soltis, D. E., Soltis, P. S., and Ma, H. (2004). Towards a comprehensive integration of morphological and genetic studies of floral development. *Trends Plant Sci.* 9, 164–173. doi: 10.1016/j.tplants.2004.02.003

Callens, C., Tucker, M. R., Zhang, D., and Wilson, Z. A. (2018). Dissecting the role of MADS-box genes in monocot floral development and diversity. *J. Exp. Bot.* 69, 2435–2459. doi: 10.1093/jxb/ery086

Castelán-Muñoz, N., Herrera, J., Cajero-Sánchez, W., Arrizubieta, M., Trejo, C., García-Ponce, B., et al. (2019). MADS-box genes are key components of genetic regulatory networks involved in abiotic stress and plastic developmental responses in plants. *Front. Plant Sci.* 10:853. doi: 10.3389/fpls.2019.00853

Chen, D., Yan, W., Fu, L. Y., and Kaufmann, K. (2018a). Architecture of gene regulatory networks controlling flower development in *Arabidopsis thaliana*. *Nat. Commun.* 9:4534. doi: 10.1038/s41467-018-07850-2

Chen, F., Zhang, X., Liu, X., and Zhang, L. (2017). Evolutionary analysis of MIKCc-type MADS-box genes in gymnosperms and angiosperms. *Front. Plant Sci.* 8:895. doi: 10.3389/fpls.2017.02248

Chen, L., Zhao, Y., Xu, S., Zhang, Z., Xu, Y., Zhang, J., et al. (2018b). OsMADS57 together with OsTB1 coordinates transcription of its target *OsWRKY94* and *D14* to switch its organogenesis to defense for cold adaptation in rice. *New Phytol.* 218, 219–231. doi: 10.1111/nph.14977

Ciaffi, M., Paolacci, A. R., Tanzarella, O. A., and Porceddu, E. (2011). Molecular aspects of flower development in grasses. *Sex. Plant Reprod.* 24, 247–282. doi: 10.1007/s00497-011-0175-y

Coen, E. S., and Meyerowitz, E. M. (1991). The war of the whorls – genetic interactions controlling flower development. *Nature* 353, 31–37. doi: 10.1038/353031a0

Colombo, M., Masiero, S., Vanzulli, S., Lardelli, P., Kater, M. M., and Colombo, L. (2008). AGL23, a type I MADS-box gene that controls female gametophyte and embryo development in *Arabidopsis*. *Plant J.* 54, 1037–1048. doi: 10.1111/j.1365-313X.2008.03485.x

Cui, R., Han, J., Zhao, S., Su, K., Wu, F., Du, X., et al. (2010). Functional conservation and diversification of class E floral homeotic genes in rice (*Oryza sativa*). *Plant J.* 61, 767–781. doi: 10.1111/j.1365-313X.2009.04101.x

de Folter, S., Shchennikova, A. V., Franken, J., Busscher, M., Baskar, R., Grossniklaus, U., et al. (2006). A B-sister MADS-box gene involved in ovule and seed development in petunia and *Arabidopsis*. *Plant J.* 47, 934–946. doi: 10.1111/j.1365-313X.2006.02846.x

Digel, B., Pankin, A., and von Korff, M. (2015). Global transcriptome profiling of developing leaf and shoot apices reveals distinct genetic and environmental control of floral transition and inflorescence development in barley. *Plant Cell* 27, 2318–2334. doi: 10.1105/tpc.15.00203

Dreni, L., Pilatone, A., Yun, D., Erreni, S., Pajoro, A., Caporali, E., et al. (2011). Functional analysis of all AGAMOUS subfamily members in rice reveals their roles in reproductive organ identity determination and meristem determinacy. *Plant Cell* 23, 2850–2863. doi: 10.1105/tpc.111.087007

Dreni, L., and Zhang, D. (2016). Flower development: the evolutionary history and functions of the AGL6 subfamily MADS-box genes. *J. Exp. Bot.* 67, 1625–1638. doi: 10.1093/jxb/erw046

Edgar, R. C. (2004). MUSCLE: multiple sequence alignment with high accuracy and high throughput. *Nucleic Acids Res.* 32, 1792–1797. doi: 10.1093/nar/gkh340

Feng, N., Song, G., Guan, J., Chen, K., Jia, M., Huang, D., et al. (2017). Transcriptome profiling of wheat inflorescence development from spikelet initiation to floral patterning identified stage-specific regulatory genes. *Plant Physiol.* 174, 1779–1794. doi: 10.1104/pp.17.00310

Gao, X., Liang, W., Yin, C., Ji, S., Wang, H., Su, X., et al. (2010). The SEPALLATA-like gene OsMADS34 is required for rice inflorescence and spikelet development. *Plant Physiol.* 153, 728–740. doi: 10.1104/pp.110.156711

Guo, S., Xu, Y., Liu, H., Mao, Z., Zhang, C., Ma, Y., et al. (2013). The interaction between OsMADS57 and OsTB1 modulates rice tillering via DWARF14. *Nat. Commun.* 4:1566. doi: 10.1038/ncomms2542

Harrop, T. W., Ud Din, I., Gregis, V., Osnato, M., Jouannic, S., Adam, H., et al. (2016). Gene expression profiling of reproductive meristem types in early rice inflorescences by laser microdissection. *Plant J.* 86, 75–88. doi: 10.1111/tpj.13147

Heyn P, Kalinka AT, Tomancak, P, Neugebauer, KM. (2015). Introns and gene expression: cellular constraints, transcriptional regulation, and evolutionary consequences. *Bioessays* 37, 148–154. doi: 10.1002/bies.201400138

Jayakodi, M., Padmarasu, S., Haberer, G., Bonthala, V. S., Gundlach, H., Monat, C., et al. (2020). The barley pan-genome reveals the hidden legacy of mutation breeding. *Nature* 588, 284–289. doi: 10.1038/s41586-020-2947-8

Jin, J., Zhang, H., Kong, L., Gao, G., and Luo, J. (2014). PlantTFDB 3.0: a portal for the functional and evolutionary study of plant transcription factors. *Nucleic Acids Res.* 42, D1182–D1187. doi: 10.1093/nar/gkt1016

Kaufmann, K., Anfang, N., Saedler, H., and Theissen, G. (2005). Mutant analysis, protein-protein interactions and subcellular localization of the *Arabidopsis* B-sister (ABS) protein. *Mol. Gen. Genomics.* 274, 103–118. doi: 10.1007/s00438-005-0010-y

Kobayashi, K., Maekawa, M., Miyao, A., Hirochika, H., and Kyozuka, J. (2010). PANICLE PHYTOMER2 (PAP2), encoding a SEPALLATA subfamily MADS-box protein, positively controls spikelet meristem identity in rice. *Plant Cell Physiol.* 51, 47–57. doi: 10.1093/pcp/pcp166

Koppolu, R., and Schnurbusch, T. (2019). Developmental pathways for shaping spike inflorescence architecture in barley and wheat. *J. Integr. Plant Biol.* 61, 278–295. doi: 10.1111/jipb.12771

Kubo, T., Fujita, M., Takahashi, H., Nakazono, M., Tsutsumi, N., and Kurata, N. (2013). Transcriptome analysis of developing ovules in rice isolated by laser microdissection. *Plant Cell Physiol.* 54, 750–765. doi: 10.1093/pcp/pct029

Kwantes, M., Liebsch, D., and Verelst, W. (2012). How MIKC* MADS-Box genes originated and evidence for their conserved function throughout the evolution of vascular plant gametophytes. *Mol. Biol. Evol.* 29, 293–302. doi: 10.1093/molbev/msr200

Kyozuka, J., Kobayashi, T., Morita, M., and Shimamoto, K. (2000). Spatially and temporally regulated expression of rice MADS box genes with similarity to *Arabidopsis* class A, B and C genes. *Plant Cell Physiol.* 41, 710–718. doi: 10.1093/pcp/41.6.710

Li, G., Kuijer, H. N. J., Yang, X., Liu, H., Shen, C., Shi, J., et al. (2021). MADS1 maintains barley spike morphology at high ambient temperatures. *Nat. Plants*. doi: 10.1038/s41477-021-00957-3

Liu, H., Li, G., Yang, X., Kuijer, H. N. J., Liang, W., and Zhang, D. (2020). Transcriptome profiling reveals phase-specific gene expression in the developing barley inflorescence. *Crop J.* 8, 71–86. doi: 10.1016/j.cj.2019.04.005

Mansueto, L., Fuentes, R. R., Borja, F. N., Detras, J., Abriol-Santos, J. M., Chebotarov, D., et al. (2017). Rice SNP-seek database update: new SNPs,

indels, and queries. *Nucleic Acids Res.* 45, D1075–D1081. doi: 10.1093/nar/gkw1135

Mascher, M., Gundlach, H., Himmelbach, A., Beier, S., Twardziok, S. O., Wicker, T., et al. (2017). A chromosome conformation capture ordered sequence of the barley genome. *Nature* 544, 427–433. doi: 10.1038/nature22043

Mayer, K. F. X., Waugh, R., Langridge, P., Close, T. J., Wise, R. P., Graner, A., et al. (2012). A physical, genetic and functional sequence assembly of the barley genome. *Nature* 491, 711–716. doi: 10.1038/nature11543

Mena, M., Ambrose, B. A., Meeley, R. B., Briggs, S. P., Yanofsky, M. F., and Schmidt, R. J. (1996). Diversification of C-function activity in maize flower development. *Science* 274, 1537–1540. doi: 10.1126/science.274.5292.1537

Milner, S. G., Jost, M., Taketa, S., Mazón, E. R., Himmelbach, A., Oppermann, M., et al. (2019). Genebank genomics highlights the diversity of a global barley collection. *Nat. Genet.* 51, 319–326. doi: 10.1038/s41588-018-0266-x

Monat, C., Padmarasu, S., Lux, T., Wicker, T., Gundlach, H., Himmelbach, A., et al. (2019). TRITEX: chromosome-scale sequence assembly of Triticeae genomes with open-source tools. *Genome Biol.* 20:284. doi: 10.1186/s13059-019-1899-5

Nagasawa, N., Miyoshi, M., Sano, Y., Satoh, H., Hirano, H., Sakai, H., et al. (2003). SUPERWOMAN1 and DROOPING LEAF genes control floral organ identity in rice. *Development* 130, 705–718. doi: 10.1242/dev.00294

Paollacci, A. R., Tanzarella, O. A., Porceddu, E., Varotto, S., and Ciaffi, M. (2007). Molecular and phylogenetic analysis of MADS-box genes of MIKC type and chromosome location of SEP-like genes in wheat (*Triticum aestivum* L.). *Mol. Gen. Genomics.* 278, 689–708. doi: 10.1007/s00438-007-0285-2

Pelaz, S., Ditta, G. S., Baumann, E., Wisman, E., and Yanofsky, M. F. (2000). B and C floral organ identity functions require SEPALLATA MADS-box genes. *Nature* 405, 200–203. doi: 10.1038/35012103

Poursarebani, N., Seidensticker, T., Koppolu, R., Trautewig, C., Gawronski, P., Bini, F., et al. (2015). The genetic basis of composite spike form in barley and "miracle-wheat". *Genetics* 201, 155–165. doi: 10.1534/genetics.115.176628

Poursarebani, N., Trautewig, C., Melzer, M., Nussbaumer, T., Lundqvist, U., Rutten, T., et al. (2020). COMPOSITUM 1 contributes to the architectural simplification of barley inflorescence via meristem identity signals. *Nat. Commun.* 11:5138. doi: 10.1038/s41467-020-18890-y

Remizowa, M. V., Rudall, P. J., Choob, V. V., and Sokoloff, D. D. (2013). Racemose inflorescences of monocots: structural and morphogenetic interaction at the flower/inflorescence level. *Ann. Bot.* 112, 1553–1566. doi: 10.1093/aob/mcs246

Ruelens, P., de Maagd, R. A., Proost, S., Theißen, G., Geuten, K., and Kaufmann, K. (2013). FLOWERING LOCUS C in monocots and the tandem origin of angiosperm-specific MADS-box genes. *Nat. Commun.* 4:2280. doi: 10.1038/ncomms3280

Sang, X. C., Li, Y. F., Luo, Z. K., Ren, D. Y., Fang, L. K., Wang, N., et al. (2012). Chimeric floral Organs1, encoding a monocot-specific MADS box protein, regulates floral organ identity in rice. *Plant Physiol.* 160, 788–807. doi: 10.1104/pp.112.200980

Schilling, S., Gramzow, L., Lobbes, D., Kirbis, A., Weilandt, L., Hoffmeier, A., et al. (2015). Non-canonical structure, function and phylogeny of the B-sister MADS-box gene OsMADS30 of rice (*Oryza sativa*). *Plant J.* 84, 1059–1072. doi: 10.1111/tpj.13055

Schilling, S., Kennedy, A., Pan, S., Jermiin, L. S., and Melzer, R. (2020). Genome-wide analysis of MIKC-type MADS-box genes in wheat: pervasive duplications, functional conservation and putative neofunctionalization. *New Phytol.* 225, 511–529. doi: 10.1111/nph.16122

Schmitz, J., Franzen, R., Ngyuen, T. H., Garcia-Maroto, F., Pozzi, C., Salamini, F., et al. (2000). Cloning, mapping and expression analysis of barley MADS-box genes. *Plant Mol. Biol.* 42, 899–913. doi: 10.1023/A:1006425619953

Shang, Y., Yuan, L., Di, Z., Jia, Y., Zhang, Z., Li, S., et al. (2020). A CYC/TB1-type TCP transcription factor controls spikelet meristem identity in barley. *J. Exp. Bot.* 71–22, 7118–7131. doi: 10.1093/jxb/eraa416

Smaczniak, C., Immink, R. G. H., Angenent, G. C., and Kaufmann, K. (2012). Developmental and evolutionary diversity of plant MADS-domain factors: insights from recent studies. *Development* 139, 3081–3098. doi: 10.1242/dev.074674

Soltis, D. E., Chanderbali, A. S., Kim, S., Buzgo, M., and Soltis, P. S. (2007). The ABC model and its applicability to basal angiosperms. *Ann. Bot.* 100, 155–163. doi: 10.1093/aob/mcm117

Solovyev, V. (2007). "Statistical approaches in eukaryotic gene prediction," in *Handbook of Statistical Genetics. 3rd Edn.* eds. D. J. Balding, M. Bishop, and C. Cannings (Wiley-Interscience), 1616.

Theissen, G., Melzer, R., and Rumpler, F. (2016). MADS-domain transcription factors and the floral quartet model of flower development: linking plant development and evolution. *Development* 143, 3259–3271. doi: 10.1242/dev.134080

Theissen, G., and Saedler, H. (2001). Floral quartets. *Nature* 409, 469–471. doi: 10.1038/35054172

Thompson, B. E., Bartling, L., Whipple, C., Hall, D. H., Sakai, H., Schmidt, R., et al. (2009). Bearded-ear encodes a MADS box transcription factor critical for maize floral development. *Plant Cell* 21, 2578–2590. doi: 10.1105/tpc.109.067751

Trevaskis, B., Hemming, M. N., Dennis, E. S., and Peacock, W. J. (2007a). The molecular basis of vernalization-induced flowering in cereals. *Trends Plant Sci.* 12, 352–357. doi: 10.1016/j.tplants.2007.06.010

Trevaskis, B., Tadege, M., Hemming, M. N., Peacock, W. J., Dennis, E. S., and Sheldon, C. (2007b). Short vegetative phase-like MADS-box genes inhibit floral meristem identity in barley. *Plant Physiol.* 143, 225–235. doi: 10.1104/pp.106.090860

Trifinopoulos, J., Nguyen, L. T., von Haeseler, A., and Minh, B. Q. (2016). W-IQ-TREE: a fast online phylogenetic tool for maximum likelihood analysis. *Nucleic Acids Res.* 44, W232–W235. doi: 10.1093/nar/gkw256

Waddington, S. R., Cartwright, P. M., and Wall, P. C. (1983). A quantitative scale of spike initial and pistil development in barley and wheat. *Ann. Bot.* 51, 119–130. doi: 10.1093/oxfordjournals.aob.a086434

Wang, C., Yang, X., and Li, G. (2021). Molecular insights into inflorescence meristem specification for yield potential in cereal crops. *Int. J. Mol. Sci.* 22:3508. doi: 10.3390/ijms22147719

Wang, H. H., Zhang, L., Cai, Q., Hu, Y., Jin, Z. M., Zhao, X. X., et al. (2015). OsMADS32 interacts with PI-like proteins and regulates rice flower development. *J. Integr. Plant Biol.* 57, 504–513. doi: 10.1111/jipb.12248

Wei, B., Zhang, R. Z., Guo, J. J., Liu, D. M., Li, A. L., Fan, R. C., et al. (2014). Genome-wide analysis of the MADS-box gene family in *Brachypodium distachyon*. *PLoS One* 9:e84781. doi: 10.1371/journal.pone.0116239

Wu, D., Liang, W., Zhu, W., Chen, M., Ferrandiz, C., Burton, R. A., et al. (2018). Loss of LOFSEP transcription factor function converts spikelet to leaf-like structures in rice. *Plant Physiol.* 176, 1646–1664. doi: 10.1104/pp.17.00704

Wu, F., Shi, X., Lin, X., Liu, Y., Chong, K., Theissen, G., et al. (2017). The ABCs of flower development: mutational analysis of AP1/FUL-like genes in rice provides evidence for a homeotic (A)-function in grasses. *Plant J.* 89, 310–324. doi: 10.1111/tpj.13386

Yadav, S. R., Prasad, K., and Vijayraghavan, U. (2007). Divergent regulatory OsMADS2 functions control size, shape and differentiation of the highly derived rice floret second-whorl organ. *Genetics* 176, 283–294. doi: 10.1534/genetics.107.071746

Yamaguchi, T., Lee, D. Y., Miyao, A., Hirochika, H., An, G., and Hirano, H. Y. (2006). Functional diversification of the two C-class MADS box genes OSMADS3 and OSMADS58 in *Oryza sativa*. *Plant Cell* 18, 15–28. doi: 10.1105/tpc.105.037200

Yamaguchi, T., Nagasawa, N., Kawasaki, S., Matsuoka, M., Nagato, Y., and Hirano, H. Y. (2004). The YABBY gene DROOPING LEAF regulates carpel specification and midrib development in *Oryza sativa*. *Plant Cell* 16, 500–509. doi: 10.1105/tpc.018044

Yao, S. G., Ohmori, S., Kimizu, M., and Yoshida, H. (2008). Unequal genetic redundancy of rice PISTILLATA orthologs, OsMADS2 and OsMADS4, in lodicule and stamen development. *Plant Cell Physiol.* 49, 853–857. doi: 10.1093/pcp/pcn050

Zhu, C., Yang, J., Box, M. S., Kellogg, E. A., and Eveland, A. L. (2018). A dynamic co-expression map of early inflorescence development in *Setaria*

viridis provides a resource for gene discovery and comparative genomics. *Front. Plant Sci.* 9:1309. doi: 10.3389/fpls.2018.01309

Conflict of Interest: The authors declare that the research was conducted in the absence of any commercial or financial relationships that could be construed as a potential conflict of interest.

Publisher's Note: All claims expressed in this article are solely those of the authors and do not necessarily represent those of their affiliated organizations, or those of the publisher, the editors and the reviewers. Any product that may be evaluated in this article, or claim that may be made by its manufacturer, is not guaranteed or endorsed by the publisher.

frontiers in Plant Science

ORIGINAL RESEARCH
published: 05 October 2021
doi: 10.3389/fpls.2021.743838

Genome-Wide Association Mapping Identifies Novel Panicle Morphology Loci and Candidate Genes in Sorghum

Lihua Wang[1†], Hari D. Upadhyaya[2†], Jian Zheng[1], Yanlong Liu[1], Shailesh Kumar Singh[2], C. L. L. Gowda[2], Rajendra Kumar[3], Yongqun Zhu[4], Yi-Hong Wang[5] and Jieqin Li[1*]*

[1] College of Agriculture, Anhui Science and Technology University, Chuzhou, China, [2] Gene Bank, International Crops Research Institute for the Semi-Arid Tropics (ICRISAT), Patancheruvu, India, [3] Division of Genetics, ICAR-Indian Agricultural Research Institute, New Delhi, India, [4] Institute of Agricultural Resources and Environment, Sichuan Academy of Agricultural Sciences (SAAS), Chengdu, China, [5] Department of Biology, University of Louisiana at Lafayette, Lafayette, LA, United States

OPEN ACCESS

Edited by:
Fa Cui,
Ludong University, China

Reviewed by:
Yanan Guan,
Shandong Academy of Agricultural Sciences, China
Xiaochun Lu,
Sichuan Academy of Agricultural Sciences, China

***Correspondence:**
Yi-Hong Wang
yihong.wang@louisiana.edu
Jieqin Li
lijq@ahstu.edu.cn

[†]These authors have contributed equally to this work

Specialty section:
This article was submitted to Crop and Product Physiology, a section of the journal Frontiers in Plant Science

Received: *19 July 2021*
Accepted: *06 September 2021*
Published: *05 October 2021*

Citation:
Wang L, Upadhyaya HD, Zheng J, Liu Y, Singh SK, Gowda CLL, Kumar R, Zhu Y, Wang Y-H and Li J (2021) Genome-Wide Association Mapping Identifies Novel Panicle Morphology Loci and Candidate Genes in Sorghum. Front. Plant Sci. 12:743838. doi: 10.3389/fpls.2021.743838

Panicle morphology is an important trait in racial classification and can determine grain yield and other agronomic traits in sorghum. In this study, we performed association mapping of panicle length, panicle width, panicle compactness, and peduncle recurving in the sorghum mini core panel measured in multiple environments with 6,094,317 single nucleotide polymorphism (SNP) markers. We mapped one locus each on chromosomes 7 and 9 to recurving peduncles and eight loci for panicle length, panicle width, and panicle compactness. Because panicle length was positively correlated with panicle width, all loci for panicle length and width were colocalized. Among the eight loci, two each were on chromosomes 1, 2, and 6, and one each on chromosomes 8 and 10. The two loci on chromosome 2, i.e., *Pm 2-1* and *Pm 2-2*, were detected in 7 and 5 out of 11 testing environments, respectively. *Pm 2-2* colocalized with panicle compactness. Candidate genes were identified from both loci. The rice *Erect Panicle2* (*EP2*) ortholog was among the candidate genes in *Pm 2-2*. *EP2* regulates panicle erectness and panicle length in rice and encodes a novel plant-specific protein with unknown functions. The results of this study may facilitate the molecular identification of panicle morphology-related genes and the enhancement of yield and adaptation in sorghum.

Keywords: sorghum, panicle morphology, association mapping, mini core, candidate genes

INTRODUCTION

The sorghum inflorescence consists of a single panicle with many racemes and is an important determinant of grain yield (Hmon et al., 2013). Sorghum panicles are more extensively branched than maize and rice (Vollbrecht et al., 2005; Brown et al., 2006) and vary significantly in number, length, and angle of primary branches as well as the three-dimensional shape, size, and distribution of the seed (Li et al., 2020), especially compared to other major cultivated cereal crops (Brown et al., 2006). Therefore, sorghum is an excellent model for studying panicle morphology in panicle-bearing grasses. Sorghum panicles may be compact or open up to 50 cm long and 30 cm wide (Doggett, 1988),

and their morphology depends on the number and length of panicle branches and the number of aborted spikelets (Brown et al., 2006). The panicle morphology is an important criterion for the racial classification of sorghum. The compact panicle is typical of domesticated sorghum, especially elite high-yielding modern commercial varieties (Kimber, 2000; Brown et al., 2006; Dillon et al., 2007; OGTR, 2017), whereas undomesticated species are more likely to have open panicles (Harlan and de Wet, 1972). Plants with open or loose panicles are more likely to be small-seeded, reducing grain yield (Desmae et al., 2016). However, compact panicles are also more prone to infection/infestation by grain mold (Sharma et al., 2010), webworm [*Celama sorghiella* (Riley)] (Hobbs et al., 1979), head bug (*Calocoris angustatus* Leth.), and head caterpillar (*Helicoverpa armigera* Hb.) (Sharma et al., 1994). As a result, race guinea with loose panicles is more common in wet environments to prevent grain molding, and race durra with compact panicles is more common in dry environments (Harlan and de Wet, 1972; Doggett, 1988; Ayana and Bekele, 1998).

Despite its importance in yield and adaptation, the genetic control of panicle morphology is not fully understood. Approximately 300 panicle morphology-related quantitative trait loci (QTLs) have been cataloged by Mace et al. (2019) from previous studies. More recently, Girma et al. (2019) identified 15 regions across the sorghum genome associated with panicle compactness and shape, and Faye et al. (2019) identified 13 panicle compactness loci that colocalize with *a priori* candidate genes. Olatoye et al. (2020) also found a significant enrichment of QTL colocalized with grass panicle-related genes such as maize *Ramosa2* and rice *Aberrant Panicle Organization1* (*APO1*) and *TAWAWA1*, but many QTLs did not colocalize with panicle gene orthologs (Olatoye et al., 2020). They suggested that global panicle diversity in sorghum is largely controlled by oligogenic, epistatic, and pleiotropic variations in ancestral regulatory networks. Zhou et al. (2019) detected 35 unique SNPs associated with variation in panicle architecture using a semiautomated phenotyping pipeline called Toolkit for Inflorescence Measurement (TIM). They also found colocalization with previously mapped panicle-related loci and identified nine candidate genes.

The objective of this study was to identify QTL related to panicle morphology and recurving of peduncles and determine the candidate genes that regulate panicle morphology in sorghum using a genome-wide association study (GWAS) with phenotyping data on sorghum panicle length and width in 11 environments at International Crops Research Institute for the Semi-Arid Tropics (ICRISAT), India, panicle compactness in two environments in China, and 6,094,317 single nucleotide polymorphism (SNP) markers in the sorghum mini core (MC) collection panel (Upadhyaya et al., 2009).

MATERIALS AND METHODS

A total of 242 accessions of sorghum MC (Upadhyaya et al., 2009) were phenotyped in rainy and post-rainy seasons with or without irrigation at ICRISAT, Patancheru, India. The plants were grown in an alpha design with three replicates. Each single-row plot was 4 m long with a row spacing of 75 cm and plant spacing within a row of 10 cm. Ammonium phosphate (150 kg/ha) was applied before planting, and 100 kg/ha of urea was applied as a top dressing 3 weeks after planting. For the post-rainy season with irrigation, field plots were irrigated five times at equal intervals, each with 7 cm of water. Panicle length and width were measured in centimeters according to the International Board for Plant Genetic Resources IBPGR/ICRISAT (1993).

The MC panel was also grown in Tengqiao, Hainan, China (18°24′ N, 109°45′ E) in 2017 and 2020. All experiments used a completely randomized block design with three replicates. Before harvest, panicle pictures were taken and panicle compactness, length/width, and peduncle recurving were scored according to IBPGR/ICRISAT (1993). When panicles were scored as 1 = loose, 2 = semi-compact/semi-loose, and 3 = compact (Mohammed et al., 2015), the original IBPGR/ICRISAT codes of 1, 2, 3, 4, and 11 were converted to 1; 6 and 7 to 2; and 8, 9, 10, and 13 to 3. The coefficient of variation (CV) was calculated as the ratio between SD and mean. The broad-sense heritability was calculated using the R lme4 package.

The genome resequencing of 242 MC accessions and SNP development was performed as follows. The reference genome was the sorghum BTx623 (Paterson et al., 2009) version 3.1.1 (https://phytozome-next.jgi.doe.gov/info/Sbicolor_v3_1_1), which was also used to identify candidate genes. Sequencing reads were mapped to the reference genome using BWA-MEM version 0.7.17 (Li, 2013) and sorted by SAMtools version 1.10 (Li et al., 2009). Duplicate reads were removed using Picard version 2.0.1 (http://broadinstitute.github.io/picard/). The SAMtools flagstat was used to calculate the mapping percentage. Sequence variation detection and SNP calling were performed using the GATK version 4.17 function HaplotypeCaller and SelectVariants (McKenna et al., 2010). SNPs were called with parameters "QD < 2.0, MQ < 40.0, FS > 60, SOR > 3.0, MQRankSum < −12.5, ReadPosRankSum < −8.0." SNPs were filtered with VCFtools version 1.16 (Li, 2013) using the parameters "max-missing 0.1, maf 0.05, maxDP 50, and minDP 10." Only SNPs on chr1–chr10 were used. This produced 6,094,317 SNPs for the GWAS analysis. Population structure was analyzed using Admixture version 1.3 (Alexander et al., 2015). The number of clusters (k) in MC was set to 2–15. Admixture version 1.3 was run for each *k*-value, using 489,339 SNPs (**Supplementary Figure 1**). The optimal *k* was determined to be 10, as the CV (i.e., cross-validation) error was the lowest at $k = 10$. This *k*-value was used to generate the Q matrix used in the GWAS, as described below.

The GWAS and linkage disequilibrium (LD) analysis were performed using the 6,094,317 SNPs after filtering based on the criteria of minor allele frequency of >0.05 and missing data rate of 10% or less in the population. The kinship matrix (K) was generated using EMMAX (Kang et al., 2010), and the GWAS was performed using EMMAX with Q matrix. The modified Bonferroni correction was used to determine the genome-wide significance thresholds of the GWAS, based on a nominal level of $\alpha = 0.05$, corresponding to a raw *P*-value of 8.2×10^{-9} or a –log10(*P*)-value of 8.08. Candidate genes were identified using

FIGURE 1 | Panicle morphology of the five major races in the association mapping panel (Upadhyaya et al., 2009). IS 7250 has loose panicles, and IS 4631, IS 4092, and IS 12937 have compact panicles, whereas IS 608 has semi-compact panicles.

the reference sequence *Sorghum bicolor* version 3.1.1, curated at Phytozome (Goodstein et al., 2012) 13 (https://phytozome-next.jgi.doe.gov/).

RESULTS

Phenotyping

Panicle length and width were found to be correlated with Pearson's correlation coefficients ranging from 0.56 to 0.70 (significant at $P < 0.001$). **Figure 1** shows variations in panicle morphology of the five primary sorghum races in the association mapping panel (Upadhyaya et al., 2009) from a field evaluation in Hainan in 2020. Based on the panicle compactness data from the Hainan 2020 environment, 64% of the MC accessions had compact panicles, 14% had semi-compact panicles, and 22% had loose panicles. In the 11 ICRISAT testing environments (**Supplementary Table 1**), panicle width was more variable across the environments than panicle length as measured by the coefficient of variation (CV). The CV for panicle length ranged from 0.27 to 0.39, with a mean of 0.33, while that for panicle width ranged from 0.21 to 0.61, with a mean of 0.48 (**Table 1**; refer to **Supplementary Table 2** for variance). In contrast, irrigation in Environments 3 and 5 did affect panicle length and width compared to no irrigation in Environments 4 and 6 but not consistently. By comparing Environments 3 to 5, irrigation did not significantly affect the panicle length ($P = 0.17$) but decreased the panicle width by 1.42 cm on average ($P = 0.0034$). Between Environments 4 and 6, irrigation increased the panicle length by 1.9 cm on average ($P = 0.0030$) but decreased the panicle width by 1.85 cm on average ($P = 0.000012$). When panicle compactness was scored only as compact, semi-compact, and loose, panicle length and width were negatively correlated with panicle compactness with $r = -0.40$ and -0.27, respectively, in Environment 1 at ICRISAT, and both were significant at $P < 0.001$ (i.e., panicle compactness was only measured in Environment 1 at ICRISAT). Similarly, in the 2020 Hainan dataset, panicle length and width were negatively correlated with panicle compactness with $r = -0.42$, and -0.47, respectively, and both were also significant at $P < 0.001$. These results indicate that loose panicles tend to be longer and wider, and compact panicles are shorter and narrower. Using 100 seed weight data obtained from the studies by Upadhyaya et al. (unpublished) and Li et al. (unpublished), we found that seed weight was positively correlated with panicle compactness both at ICRISAT ($r = 0.33$; significant at $P < 0.001$) and Hainan ($r = 0.31$; significant at $P < 0.001$), indicating that loose panicles often carry smaller seeds and that compact panicles carry larger seeds. This may have contributed to the positive correlation between panicle compactness and seed weight per panicle ($r = 0.23$; significant at $P < 0.01$). Since the untransformed data were used in this study, heritability may not be as accurately estimated (Fusi et al., 2014), and small-effect QTLs may not be identified by GWAS (Goh and Yap, 2009). Nevertheless, variance, broad-sense heritability, and the Shapiro–Wilk normality test are presented in **Supplementary Table 2**.

Genome-Wide Association Study

For a trait to be mapped, the association had to be strong in multiple environments with multiple SNPs and reached the Bonferroni correction P-value of 8.2×10^{-9} or a $-\log(P)$ of 8.08, in at least two environments, except for recurving peduncles, which was evaluated only in one environment. Using these criteria, we identified 11 QTLs: one on chromosome 4 for panicle length/width ratio, two for peduncle recurving with one each on chromosomes 7 and 9, eight for panicle length and width, and one compactness colocalized with panicle length and width on chromosome 2 (**Table 2**; representing SNPs from each locus are presented in **Supplementary Table 3**). For the eight-panicle length and width QTLs, two were on chromosomes 1, 2, and 6, and one each was located on chromosomes 8 and 10 (**Figure 2**,

TABLE 1 | Coefficient of variation (CV) for panicle length and width in the 11 testing environments.

Environment	1	2	3	4	5	6	7	8	9	10	11
Panicle length	0.27	0.27	0.33	0.32	0.39	0.35	0.29	0.29	0.36	0.37	0.39
Panicle width	0.21	0.34	0.55	0.51	0.61	0.53	0.49	0.39	0.5	0.53	0.6

TABLE 2 | Panicle morphology-related quantitative trait loci (QTLs) mapped in multiple environments.

QTL	Trait*	Chromosome: position (bp)	Gene in or near QTL	No. of environment QTL detected	Colocalization with other QTL	References**
Pm 1-1	PL, PW	1: 10423724–10464740	Sobic.001G132600	1 (PL), 4 (PW)		
Pm 1-2	PL, PW	1: 59803397–59808620	Sobic.001G311050	5 (PW)	*QPLEN1.7*	Hmon et al., 2013
Pm 2-1	PL, PW	2: 71879000–71902200	See **Table 3**	7 (PL), 5 (PW)		
Pm 2-2	PL, PW, PC	2: 73190000–73247000	See **Table 3**	7 (PL), 5 (PW), 1 (PC)		
Pm 4-1	PL/PW ratio	4: 8275699–8300275	Sobic.004G095300	2, 10, 11		
Pm 6-1	PL, PW	6: 32406706–32416278		1 (PL), 3 (PW)	*QPLEN6.6*	Reddy et al., 2013
Pm 6-2	PL, PW	6: 48330285–48349357	Sobic.006G115600	5 (PL), 3 (PW)	*QPLEN6.12*	Zou et al., 2012
Pr 7-1	PR	7: 8189476–8208789	Sobic.007G072600, Sobic.007G072800, Sobic.007G072901	1 (PR)		
Pm 8-1	PL, PW	8: 53337842–53434526	Promoter of Sobic.008G120200	3 (PL), 5 (PW)	*QPWTH8.1*	Zhou et al., 2019
Pr 9-1	PR	9: 4118798–4127062		1 (PR)		
Pm 10-1	PL, PW	10: 13724096–13790887		3 (PL), 2 (PW)	*QPTYP10.1*	Hmon et al., 2013

*PL, panicle length; PW, panicle width; PC, panicle compactness; PR, peduncle recurving.
**From the data cataloged by Mace et al. (2019).

Table 2, **Supplementary Figures 2–9**). Associations with *P*-values lower than the Bonferroni threshold were not observed in environments with a CV lower than the average, 0.33 and 0.48 for panicle length and width, respectively, except for panicle width in Environment 8 (**Figure 2**, **Table 1**, **Supplementary Figures 2–9**). *Pm 2-1* and *Pm 2-2* were both detected in the greatest number of environments with low *P*-values (**Figure 2**); *Pr 7-1* and *Pr 9-1* were associated with peduncle recurving with the lowest *P*-values (**Supplementary Figure 9**). We focused on these loci to identify candidate genes.

Candidate Panicle Morphology Genes

To identify candidate panicle morphology-related genes, we examined genomic regions covered by each QTL in the *Sorghum bicolor* version 3.1.1 genome at Phytozome (Goodstein et al., 2012) 13 (https://phytozome-next.jgi.doe.gov/info/Sbicolor_v3_1_1). For the two peduncle QTLs, there were no protein-coding genes in the *Pr 9-1* locus (**Table 2**). However, *Pr 9-1* was 748 bp from the 5′ end of the Sobic.009G043600 coding region and 48 bp from the 5′ end of the Sobic.009G043500 coding region. Sobic.009G043600 encodes glutathione S-transferase 4, and Sobic.009G043500 encodes sulfite oxidase. There were three large genes (i.e., Sobic.007G072600, Sobic.007G072800, and Sobic.007G072901) and one small gene (i.e., Sobic.007G072700) in the *Pr 7-1* locus. Sobic.007G072600, Sobic.007G072800, and Sobic.007G072901 all encode F-box proteins. Sobic.007G072700 encodes an unknown protein specific to sorghum-based on a BLAST search.

We examined *Pm 2-1* and *Pm 2-2* loci in more detail. The genomic regions of the two loci are displayed in **Figure 3** for panicle length and width from two testing environments and compactness from one. *Pm 2-1* included four genes, and *Pm 2-2* included six genes (**Figure 3**, **Table 3**). Each of the four genes (i.e., Sobic.002G355700, Sobic.002G355800, Sobic.002G355900, and Sobic.002G356000) in *Pm 2-1* resided in an LD block, except Sobic.002G355900, but in *Pm 2-2*, only Sobic.002G374400 was inside an LD block (**Figure 3**). Functional studies are necessary to identify the genes underlying each locus.

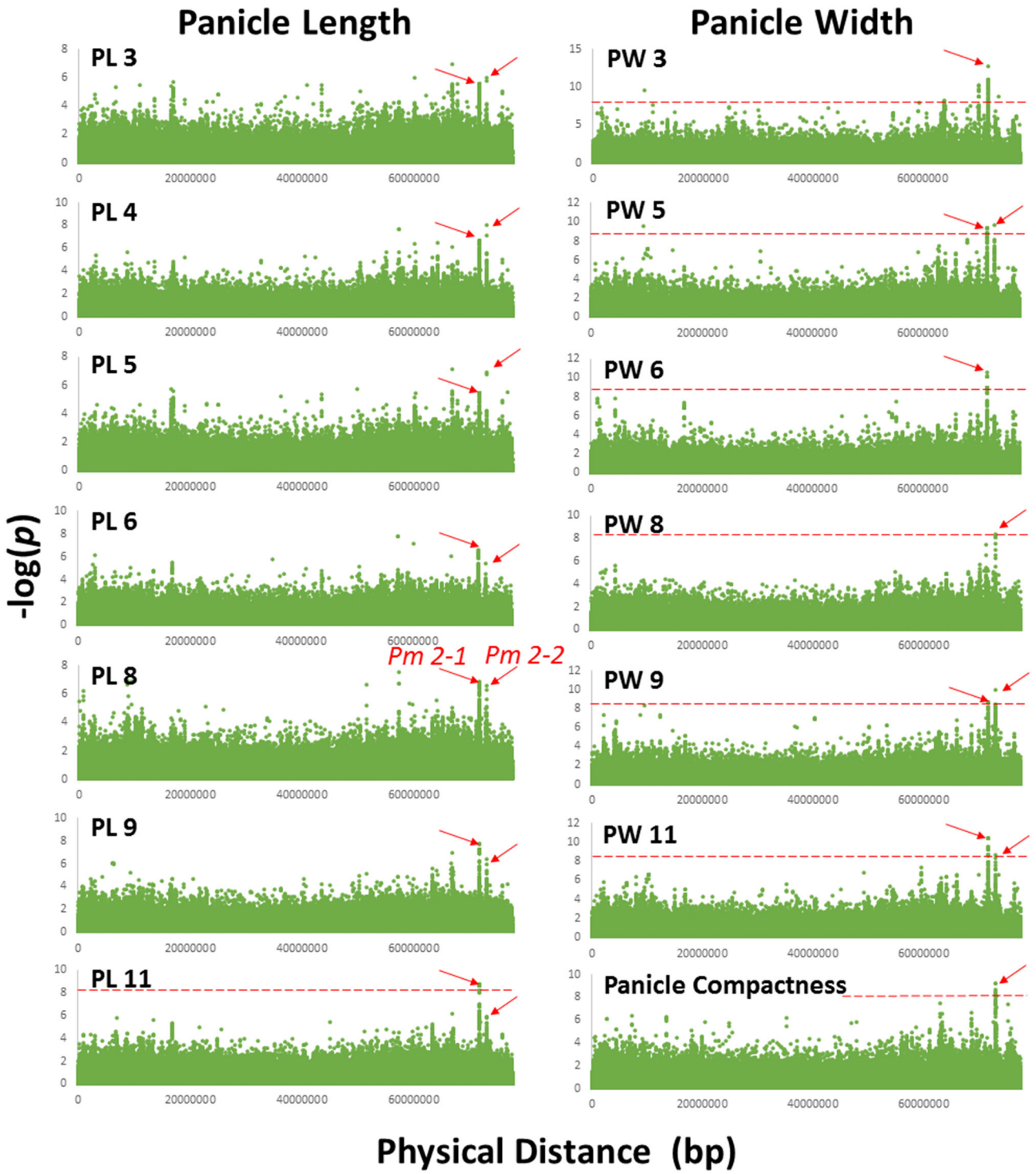

FIGURE 2 | Manhattan plot of chromosome 2 showing *Pm 2-1* and *Pm 2-2* associated with panicle length and width in 7 and 6 out of 11 environments, respectively. Association with panicle compactness was identified in a separate environment. PL 3, 4, 5, 6, 8, 9, and 11 and PW 3, 5, 6, 8, 9, and 11 were the environments in which panicle length and width QTLs *Pm 2-1* and *Pm 2-2* were detected. The red dashed horizontal lines indicate the Bonferroni threshold *P*-value.

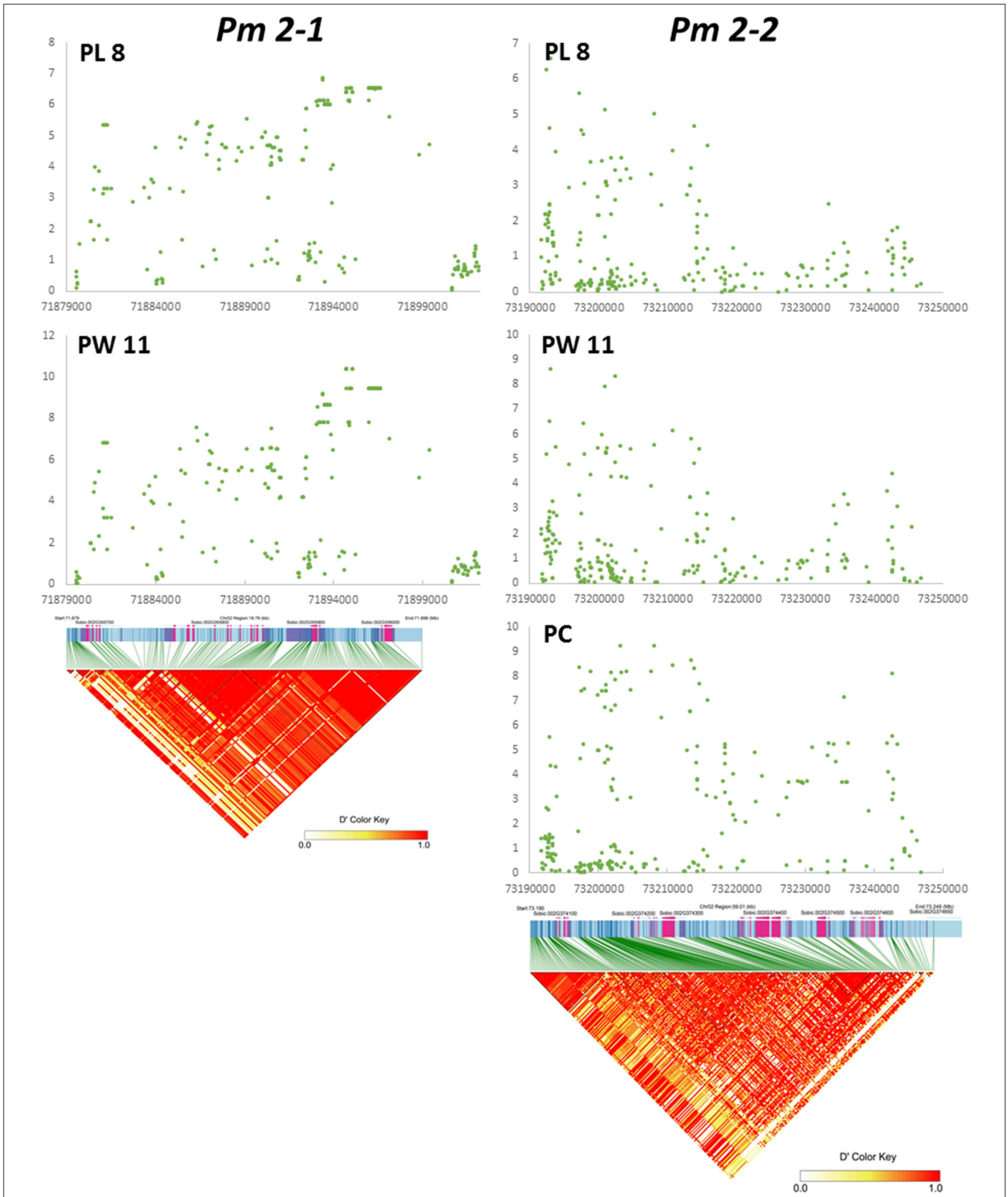

FIGURE 3 | Detailed map of *Pm 2-1* and *Pm 2-2* loci. *X* and *Y* axes represent –log(*P*) and physical distance in bp, respectively. At the bottom of *Pm 2-1* and *Pm 2-2*, the panels are linkage disequilibrium (LD) plots aligned to the respective locus map.

TABLE 3 | Sorghum panicle morphology candidate genes in *Pm 2-1* and *Pm 2-2*.

Sorghum gene ID	Annotation
Pm 2-1	
Sobic.002G355700	Histone H3
Sobic.002G355800	Ca^{2+}-binding protein
Sobic.002G355900	Lipid transfer protein
Sobic.002G356000	Lipid transfer protein
Pm 2-2	
Sobic.002G374100	Jasmonate ZIM domain-containing TIFY 10b
Sobic.002G374200	DNA-directed RNA polymerase
Sobic.002G374300	FAR1 transcription factor
Sobic.002G374400	*Erect panicle2* protein
Sobic.002G374500	Unknown protein
Sobic.002G374600	Beta-ketoacyl-ACP synthase

DISCUSSION

Our goal was to map major QTLs that are stable across environments and identify genes that can be used to improve economically important traits in sorghum and other species. In this study, we mapped nine panicle morphology QTLs, such as *Pm 2-1* and *Pm 2-2*, and two peduncle recurving QTLs, such as *Pr 7-1* and *Pr 9-1*. Neither *Pm 2-1*, *Pm 2-2*, *Pr 7-1*, and *Pr 9-1* were previously identified by other groups (Faye et al., 2019; Girma et al., 2019; Zhou et al., 2019; Olatoye et al., 2020), nor they were identified in 22 studies cataloged by Mace et al. (2019). The *Pr 7-1*, *Pm 2-1*, and *Pm 2-2* loci contained four, four, and six genes, respectively. The RNAseq data available at Phytozome (McCormick et al., 2018) may provide insight into their functions. In addition, LD can be used to identify candidate genes mapped by GWAS (Sulem et al., 2008). For the three genes in *Pr 7-1*, the highest expression of Sobic.007G072600 and Sobic.007G072901 was in both the peduncle and the panicle at the floral initiation stage, while the highest expression of Sobic.007G072800 was in the leaf sheath. Sobic.007G072700 was not expressed in the peduncles. Both Sobic.007G072600 and Sobic.007G072901 are good candidates in determining which gene in this locus causes recurving peduncles. Among the four genes in *Pm 2-1*, Sobic.002G355700 and Sobic.002G356000 were not expressed in peduncles and Sobic.002G355900 was almost exclusively expressed in dry seeds. The remaining Sobic.002G355800 was highly expressed in leaf sheaths, panicles, shoots, and stems, with slightly lower expression in peduncles, and resides inside an LD block (**Figure 3**). Therefore, Sobic.002G355800 is a candidate gene for the *Pm 2-1* locus. In the *Pm 2-2* locus, Sobic.002G374100 is co-expressed with genes in an anthesis stage-specific co-expression subnetwork with very low expression in peduncles; Sobic.002G374500 is not expressed in panicles or peduncles, and the highest expression of Sobic.002G374600 is in leaves and shoots. The remaining three genes (Sobic.002G374200, Sobic.002G374300, and Sobic.002G374400) were highly expressed in the panicles and peduncles. However, Sobic.002G374400 shares 66% identity and 77% similarity with *Erect Panicle2* (*EP2*) in indica rice and is the only gene inside an LD block (**Figure 3**). *EP2* regulates panicle erectness, panicle length, and grain size in rice (Zhu et al., 2010). The *EP2* mutants have shorter panicle length, more vascular bundles, and a thicker stem than that of wild-type plants, creating an erect panicle phenotype. *EP2* encodes a novel plant-specific protein localized to the endoplasmic reticulum with unknown function (Zhu et al., 2010) and is a candidate for the *Pm 2-2* locus. This is possible because panicle morphology regulation in both sorghum and rice may have similar mechanisms (Chen et al., 2015).

Previous studies have identified genes related to panicle/tassel morphology in the grasses. In maize, mutations in *Ramosa* produce a maize tassel resembling a loose sorghum panicle (Vollbrecht et al., 2005). *Ramosa1* transcription factor regulates long inflorescence branch architecture similarly in maize and sorghum but is absent in rice and heterochronically expressed in sorghum (Vollbrecht et al., 2005). Several panicle morphology-related genes have been identified in rice. A rice ncl-1, HT2A, and lin-41 (NHL)-domain-containing protein encoded by *FUWA* produces a more compact and erect panicle when the gene is mutated, and the mutant can be rescued by orthologs from sorghum and maize, indicating that the regulation of panicle morphology by this gene is evolutionarily conserved in rice, sorghum, and maize (Chen et al., 2015). The *OsLG1* gene product also regulates rice panicle compactness; its overexpression converts compact panicles to loose panicles. OsLG1 is an squamosa promoter-binding (SBP)-domain transcription factor that controls the development of rice ligules. The association analysis found that an SNP in the *OsLG1* regulatory region led to a compact panicle architecture in cultivated rice during rice domestication (Zhu et al., 2013). Another rice panicle morphology gene, *APO1*, encodes an F-box protein. The overexpression of *APO1* increases panicle branches and spikelets (Ikeda et al., 2007), whereas *APO1* mutation reduces the number of secondary branches by >90% and the total number of flowers by >70% (Ikeda et al., 2005). The abovementioned studies of *Ramosa* in maize and *FUWA* in rice, as well as the fact that the bulk of maize tassel and sorghum panicle developmental activities are shared (Leiboff and Hake, 2019), demonstrate similarities and differences in inflorescence development in maize, rice, and sorghum. Further studies are required to confirm whether the candidate genes identified in this study play a role in panicle morphology in sorghum and their possible effects on yield and related traits.

DATA AVAILABILITY STATEMENT

The datasets presented in this study can be found in online repositories. The names of the repository/repositories and accession number(s) can be found in the article/**Supplementary Material**.

AUTHOR CONTRIBUTIONS

HU, SS, CG, and RK phenotyped panicle length and width in the 11 environments at ICRISAT. LW, JZ, YL, and YZ

performed phenotyping in Hainan 2017 and 2020. Y-HW scored panicle compactness in Hainan 2017 and 2020, as well as peduncle recurving in Hainan 2020 and wrote the manuscript. JL performed GWAS/LD analysis and normality test and calculated variance and broad-sense heritability. JL and Y-HW analyzed the GWAS results. All authors have read and approved the manuscript for publication.

FUNDING

This study was supported by the National Natural Science Foundation of China (31971993), the Anhui Provincial Natural Science Fund (2008085MC73), the Anhui Provincial Key R&D Programs (202004b11020003), and the Key Project of Natural Science Research of the Anhui Provincial Education Department (KJ2019A0811).

SUPPLEMENTARY MATERIAL

The Supplementary Material for this article can be found online at: https://www.frontiersin.org/articles/10.3389/fpls.2021.743838/full#supplementary-material

Supplementary Figure 1 | Distribution of 489,339 SNPs used in population structure analysis.

Supplementary Figure 2 | Manhattan plot of chromosome 1 showing *Pm* 1-1 associated with panicle length (PL) and panicle width (PW) (red arrow). Numbers after PL or PW indicate different testing environments. Red dashed line indicates Bonferroni threshold *P*-value.

Supplementary Figure 3 | Manhattan plot of chromosome 1 showing *Pm 1-2* associated with panicle length (PL) and panicle width (PW) (red arrow). Numbers after PL or PW indicate different testing environments. Red dashed line indicates Bonferroni threshold *P*-value.

Supplementary Figure 4 | Manhattan plot of chromosome 4 showing *Pm 4-1* associated with panicle length and width ratio (red arrow). Numbers after LW indicate different testing environments. Red dashed line indicates Bonferroni threshold *P*-value.

Supplementary Figure 5 | Manhattan plot of chromosome 6 showing Pm 6-i associated with panicle length (PL) and panicle width (PW) (red arrow). Numbers after PL or PW indicate different testing environments. Red dashed line indicates Bonferroni threshold *P*-value.

Supplementary Figure 6 | Manhattan plot of chromosome 6 showing *Pm 6-2* associated with panicle length (PL) and panicle width (PW) (red arrow). Numbers after PL or PW indicate different testing environments. Red dashed line indicates Bonferroni threshold *P*-value.

Supplementary Figure 7 | Manhattan plot of chromosome 8 showing *Pm 8-1* associated with panicle length (PL) and panicle width (PW) (red arrow). Numbers after PL or PW indicate different testing environments. Red dashed line indicates Bonferroni threshold *P*-value.

Supplementary Figure 8 | Manhattan plot of chromosome 10 showing *Pm 10-1* associated with panicle length (PL) and panicle width (PW) (red arrow). Numbers after PL or PW indicate different testing environments. Red dashed line indicates Bonferroni threshold *P*-value.

Supplementary Figure 9 | Manhattan plot of chromosome 7 showing *Pr 7-1* (top) and 9 showing *Pr 9-1* (bottom) associated with peduncle recurving (red arrow). Red dashed line indicates Bonferroni threshold *P*-value.

Supplementary Table 1 | Environment and traits evaluated in this study. *PRi-postrainy season with irrigation; PR-postrainy season; R-rainy season. **PC, panicle compactness; PL, panicle length; PR, peduncle recurving; PW, panicle width.

Supplementary Table 2 | Variance, heritability and normality for panicle length and width in the 11 testing environments.

Supplementary Table 3 | SNPs associated with panicle morphological traits in sorghum.

REFERENCES

Alexander, D. H., Shringarpure, S. S., Novembre, J., and Lange, K. (2015). *Admixture 1.3 Software Manual*. Los Angeles, CA: UCLA Human Genetics Software Distribution.

Ayana, A., and Bekele, E. (1998). Geographical patterns of morphological variation in sorghum [*Sorghum bicolor* (L.) Moench] germplasm from ethiopia and eritrea: qualitative characters. *Hereditas* 129, 195–205. doi: 10.1111/j.1601-5223.1998.t01-1-00195.x

Brown, P. J., Klein, P. E., Bortiri, E., Acharya, C. B., Rooney, W. L., and Kresovich, S. (2006). Inheritance of inflorescence architecture in sorghum. *Theor. Appl. Genet.* 113, 931–942. doi: 10.1007/s00122-006-0352-9

Chen, J., Gao, H., Zheng, X. M., Jin, M., Weng, J. F., Ma, J., et al. (2015). An evolutionarily conserved gene, *FUWA*, plays a role in determining panicle architecture, grain shape and grain weight in rice. *Plant J.* 83, 427–438. doi: 10.1111/tpj.12895

Desmae, H., Jordan, D. R., and Godwin, I. D. (2016). Geographic patterns of phenotypic diversity in sorghum [*Sorghum bicolor* (L.) Moench] landraces from North Eastern Ethiopia. *Afr. J. Agri. Res.* 11, 3111–3122. doi: 10.5897/AJAR2016.11121

Dillon, S. L., Shapter, F. M., Henry, R. J., Cordeiro, G., Izquierdo, L., and Lee, L. S. (2007). Domestication to crop improvement: genetic resources for *Sorghum* and *Saccharum* (Andropogoneae). *Ann. Bot.* 100, 975–989. doi: 10.1093/aob/mcm192

Doggett, H. (1988). *Sorghum, 2nd Edn*. Harlow: Longmans Scientific and Technical.

Faye, J. M., Maina, F., Hu, Z., Fonceka, D., Cisse, N., and Morris, G. P. (2019). Genomic signatures of adaptation to sahelian and soudanian climates in sorghum landraces of Senegal. *Ecol. Evol.* 9, 6038–6051. doi: 10.1002/ece3.5187

Fusi, N., Lippert, C., Lawrence, N. D., and Stegle, O. (2014). Warped linear mixed models for the genetic analysis of transformed phenotypes. *Nat. Commun.* 5:4890. doi: 10.1038/ncomms5890

Girma, G., Nida, H., Seyoum, A., Mekonen, M., Nega, A., Lule, D., et al. (2019). A large-scale genome-wide association analyses of ethiopian sorghum landrace collection reveal loci associated with important traits. *Front. Plant Sci.* 10:691. doi: 10.3389/fpls.2019.00691

Goh, L., and Yap, V. B. (2009). Effects of normalization on quantitative traits in association test. *BMC Bioinform.* 10:415. doi: 10.1186/1471-2105-10-415

Goodstein, D. M., Shu, S., Howson, R., Neupane, R., Hayes, R. D., Fazo, J., et al. (2012). Phytozome: a comparative platform for green plant genomics. *Nucleic Acids Res.* 40, D1178–D1186. doi: 10.1093/nar/gkr944

Harlan, J. R., and de Wet, J. M. (1972). A simplified classification of cultivated sorghum 1. *Crop Sci.* 12, 172–176. doi: 10.2135/cropsci1972.0011183X001200020005x

Hmon, K. P., Shehzad, T., and Okuno, K. (2013). Variation in inflorescence architecture associated with yield components in a sorghum germplasm. *Plant Genet. Resour.* 11, 258–265. doi: 10.1017/S1479262113000154

Hobbs, J. R., Teetes, G. L., Johnson, J. W., and Wuensche, A. L. (1979). Management tactics for the sorghum webworm in sorghum. *J. Econ. Entomol.* 72, 362–366. doi: 10.1093/jee,/72.3.362

IBPGR/ICRISAT (1993). *Descriptors for Sorghum [Sorghum bicolor (L.) Moench]*. Rome; Patancheru: International Board for Plant Genetic Resources; International Crops Research Institute for the Semi-Arid Tropics.

Ikeda, K., Ito, M., Nagasawa, N., Kyozuka, J., and Nagato, Y. (2007). Rice *ABERRANT PANICLE ORGANIZATION 1*, encoding an F-box protein, regulates meristem fate. *Plant J.* 51, 1030–1040. doi: 10.1111/j.1365-313X.2007.03200.x

Ikeda, K., Nagasawa, N., and Nagato, Y. (2005). *ABERRANT PANICLE ORGANIZATION 1* temporally regulates meristem identity in rice. *Dev. Biol.* 282, 349–360. doi: 10.1016/j.ydbio.2005.03.016

Kang, H. M., Sul, J. H., Service, S. K., Zaitlen, N. A., Kong, S. Y., Freimer, N. B., et al. (2010). Variance component model to account for sample structure in genome-wide association studies. *Nat. Genet*. 42, 348–354. doi: 10.1038/ng.548

Kimber, C. T. (2000). "Chapter 1.1: origin of domesticated sorghum and its early diffusion to India and China," in *Sorghum: Origin, history, technology and production,* eds C. W. Smith, and R. A. Frederiksen (New York, NY: John Wiley and Sons, Inc), 3–98.

Leiboff, S., and Hake, S. (2019). Reconstructing the transcriptional ontogeny of maize and sorghum supports an inverse hourglass model of inflorescence development. *Curr. Biol*. 29, 3410–3419. doi: 10.1016/j.cub.2019.08.044

Li, H. (2013). Aligning sequence reads, clone sequences and assembly contigs with BWA-MEM. *arXiv preprint* arXiv:1303.3997.

Li, H., Handsaker, B., Wysoker, A., Fennell, T., Ruan, J., Homer, N., et al. (2009). The sequence alignment/map format and SAMtools. *Bioinformatics* 25, 2078–2079. doi: 10.1093/bioinformatics/btp352

Li, M., Shao, M. R., Zeng, D., Ju, T., Kellogg, E. A., and Topp, C. N. (2020). Comprehensive 3D phenotyping reveals continuous morphological variation across genetically diverse sorghum inflorescences. *New Phytol*. 226, 1873–1885. doi: 10.1111/nph.16533

Mace, E., Innes, D., Hunt, C., Wang, X., Tao, Y., Baxter, J., et al. (2019). The Sorghum QTL Atlas: a powerful tool for trait dissection, comparative genomics and crop improvement. *Theor. Appl. Genet*. 132, 751–766. doi: 10.1007/s00122-018-3212-5

McCormick, R. F., Truong, S. K., Sreedasyam, A., Jenkins, J., Shu, S., Sims, D., et al. (2018). The *Sorghum bicolor* reference genome: improved assembly, gene annotations, a transcriptome atlas, and signatures of genome organization. *Plant J*. 93, 338–354. doi: 10.1111/tpj.13781

McKenna, A., Hanna, M., Banks, E., Sivachenko, A., Cibulskis, K., Kernytsky, A., et al. (2010). The genome analysis toolkit: a MapReduce framework for analyzing next-generation DNA sequencing data. *Genome Res*. 20, 1297–1303. doi: 10.1101/gr.107524.110

Mohammed, R., Are, A. K., Bhavanasi, R., Munghate, R. S., Kavi Kishor, P. B., and Sharma, H. C. (2015). Quantitative genetic analysis of agronomic and morphological traits in sorghum, *Sorghum bicolor*. *Front. Plant Sci*. 6:945. doi: 10.3389/fpls.2015.00945

OGTR (2017). *The Biology of Sorghum bicolor (L.) Moench subsp. bicolor (Sorghum)*. Australian Government Office of the Gene Technology Regulator. Available online at: http://www.ogtr.gov.au/internet/ogtr/publishing.nsf/Content/5DCF28AD2F3779C4CA257D4E001819B9/\protect\T1\textdollarFile/Sorghum%20Biology%20Version%201.1%20July%202017.pdf

Olatoye, M. O., Marla, S. R., Hu, Z., Bouchet, S., Perumal, R., and Morris, G. P. (2020). Dissecting adaptive traits with nested association mapping: genetic architecture of inflorescence morphology in sorghum. *G3 Genes Genomes Genet.* 10, 1785–1796. doi: 10.1534/g3.119.400658

Paterson, A. H., Bowers, J. E., Bruggmann, R., Dubchak, I., Grimwood, J., Gundlach, H., et al. (2009). The Sorghum bicolor genome and the diversification of grasses. *Nature* 457, 551–556. doi: 10.1038/nature07723

Reddy, R. N., Madhusudhana, R., Mohan, S. M., Chakravarthi, D. V., Mehtre, S. P., Seetharama, N., et al. (2013). Mapping QTLfor grain yield and other agronomic traits in post-rainy sorghum [*Sorghum bicolor* (L.) Moench]. *Theor. Appl. Genet*. 126, 1921–1939. doi: 10.1007/s00122-013-2107-8

Sharma, H. C., Lopez, V. F., and Vidyasagar, P. (1994). Influence of panicle compactness and host plant resistance in sequential plantings on population increase of panicle-feeding insects in *Sorghum bicolor* (L.) Moench. *Int. J. Pest Manage.* 40, 216–221. doi: 10.1080/09670879409371885

Sharma, R., Rao, V. P., Upadhyaya, H. D., Reddy, V. G., and Thakur, R. P. (2010). Resistance to grain mold and downy mildew in a mini-core collection of sorghum germplasm. *Plant Dis*. 94, 439–444. doi: 10.1094/PDIS-94-4-0439

Sulem, P., Gudbjartsson, D. F., Stacey, S. N., Helgason, A., Rafnar, T., Jakobsdottir, M., et al. (2008). Two newly identified genetic determinants of pigmentation in Europeans. *Nat. Genet*. 40, 835–837. doi: 10.1038/ng.160

Upadhyaya, H. D., Pundir, R. P., Dwivedi, S. L., Gowda, C. L., Reddy, V. G., and Singh, S. (2009). Developing a mini core collection of sorghum for diversified utilization of germplasm. *Crop Sci*. 49, 1769–1780. doi: 10.2135/cropsci2009.01.0014

Vollbrecht, E., Springer, P. S., Goh, L., Buckler, I. V. E. S., and Martienssen, R. (2005). Architecture of floral branch systems in maize and related grasses. *Nature* 436, 1119–1126. doi: 10.1038/nature03892

Zhou, Y., Srinivasan, S., Mirnezami, S. V., Kusmec, A., Fu, Q., Attigala, L., et al. (2019). Semiautomated feature extraction from RGB images for sorghum panicle architecture GWAS. *Plant Physiol*. 179, 24–37. doi: 10.1104/pp.18.00974

Zhu, K., Tang, D., Yan, C., Chi, Z., Yu, H., Chen, J., et al. (2010). *ERECT PANICLE2* encodes a novel protein that regulates panicle erectness in *indica* rice. *Genetics* 184, 343–350. doi: 10.1534/genetics.109.112045

Zhu, Z., Tan, L., Fu, Y., Liu, F., Cai, H., Xie, D., et al. (2013). Genetic control of inflorescence architecture during rice domestication. *Nat. Commun*. 4:2220. doi: 10.1038/ncomms3200

Zou, G., Zhai, G., Feng, Q., Yan, S., Wang, A., Zhao, Q., et al. (2012). Identification of QTLs for eight agronomically important traits using an ultra-high-density map based on SNPs generated from high-throughput sequencing in sorghum under contrasting photoperiods. *J. Exp. Bot.* 63, 5451–5462. doi: 10.1093/jxb/ers205

Conflict of Interest: The authors declare that the research was conducted in the absence of any commercial or financial relationships that could be construed as a potential conflict of interest.

Publisher's Note: All claims expressed in this article are solely those of the authors and do not necessarily represent those of their affiliated organizations, or those of the publisher, the editors and the reviewers. Any product that may be evaluated in this article, or claim that may be made by its manufacturer, is not guaranteed or endorsed by the publisher.

frontiers in Plant Science

ORIGINAL RESEARCH
published: 16 December 2021
doi: 10.3389/fpls.2021.796397

Spike Density Quantitative Trait Loci Detection and Analysis in Tetraploid and Hexaploid Wheat Recombinant Inbred Line Populations

Jianing You[1†], Hang Liu[1†], Surong Wang[1], Wei Luo[1], Lulu Gou[1], Huaping Tang[1], Yang Mu[1], Mei Deng[1], Qiantao Jiang[1], Guoyue Chen[1], Pengfei Qi[1], Yuanying Peng[1], Liwei Tang[2], Ahsan Habib[3], Yuming Wei[1], Youliang Zheng[1], Xiujin Lan[1] and Jian Ma[1]**

[1] Triticeae Research Institute, Sichuan Agricultural University, Chengdu, China, [2] Panzhihua Academy of Agricultural and Forestry Sciences, Panzhihua, China, [3] Biotechnology and Genetic Engineering Discipline, Khulna University, Khulna, Bangladesh

OPEN ACCESS

Edited by:
Fa Cui,
Ludong University, China

Reviewed by:
Xiaoli Fan,
Chengdu Institute of Biology, Chinese Academy of Sciences (CAS), China
Jianhui Wu,
Northwest A&F University, China

***Correspondence:**
Xiujin Lan
lanxiujin@163.com
Jian Ma
jianma@sicau.edu.cn

† These authors have contributed equally to this work

Specialty section:
This article was submitted to Crop and Product Physiology, a section of the journal Frontiers in Plant Science

Received: *16 October 2021*
Accepted: *26 November 2021*
Published: *16 December 2021*

Citation:
You J, Liu H, Wang S, Luo W, Gou L, Tang H, Mu Y, Deng M, Jiang Q, Chen G, Qi P, Peng Y, Tang L, Habib A, Wei Y, Zheng Y, Lan X and Ma J (2021) Spike Density Quantitative Trait Loci Detection and Analysis in Tetraploid and Hexaploid Wheat Recombinant Inbred Line Populations. Front. Plant Sci. 12:796397. doi: 10.3389/fpls.2021.796397

Spike density (SD) is an agronomically important character in wheat. In addition, an optimized spike structure is a key basis for high yields. Identification of quantitative trait loci (QTL) for SD has provided a genetic basis for constructing ideal spike morphologies in wheat. In this study, two recombinant inbred line (RIL) populations (tetraploid RIL AM and hexaploid RIL 20828/SY95-71 (2SY)) previously genotyped using the wheat55K SNP array were used to identify SD QTL. A total of 18 QTL were detected, and three were major and one was stably expressed (*QSd.sau-2SY-7A.2, QSd.sau-AM-5A.2*, *QSd.sau-AM-7B*, and *QSd.sau-2SY-2D*). They can explain up to 23.14, 19.97, 12.00, and 9.44% of phenotypic variation, respectively. QTL × environment and epistatic interactions for SD were further analyzed. In addition, pyramiding analysis further revealed that there were additive effects between *QSd.sau-2SY-2D* and *QSd.sau-2SY-7A.2* in 2SY, and *QSd.sau-AM-5A.2* and *QSd.sau-AM-7B* in AM. Pearson's correlation between SD and other agronomic traits, and effects of major or stable QTL on yield related traits indicated SD significantly impacted spike length (SL), spikelet number per spike (SNS) and kernel length (KL). Several genes related to spike development within the physical intervals of major or stable QTL were predicted and discussed. Collectively, our research identified QTL with potential applications for modern wheat breeding and broadening the genetic basis of SD.

Keywords: spike density, quantitative trait loci, wheat, wheat55K SNP array, pyramiding analysis

INTRODUCTION

As one of the most important food crops in the world, the yield of common wheat (*Triticum aestivum* L.) should be increased to meet the growing demand for food for human beings (Zhou et al., 2017; Xu et al., 2018). The spike is an important part of the wheat plant. Cultivating wheat varieties with longer spike length (SL) and higher spike density (SD) could increase yield (Faris et al., 2014; Li et al., 2016). Thus, as a spike trait controlled by genes and influenced by the environment (Ma et al., 2007), identification of quantitative trait loci (QTL) associated with SD has importantly theoretical value for breeding high-yield wheat varieties.

Q, *Compactum* (*C*), and *Sphaerococcum* (*S1*) are three well-known genes related to spike development in common wheat (Fellers et al., 2003). The *Q* gene, located on the long arm of chromosome 5A, not only plays a role in spike morphogenesis, but also has pleiotropic effects on seed threshability, spike emergence time, and plant height (PH) (Faris and Gill, 2002; Fellers et al., 2003; Simons et al., 2006; Xu et al., 2018). The *C* gene, located on chromosomes 2D near the centromere, is involved in regulating SD, grain shape, and grain number per spike (Johnson et al., 2008). The *S1* gene on chromosome 3D defines grain shape and SD in wheat (Prabhakararao, 1977). However, *C* or *S* genes do not exist in tetraploid cultivars or varieties since they do not possess D-genome chromosomes. Thus, variation in spike morphology of tetraploid wheat may be caused by genes other than *Q*, *C*, or *S* or by alleles of these three genes on homologous chromosomes (Faris et al., 2014; Zhou et al., 2017). Therefore, it is necessary to excavate more QTL or genes associated with SD in tetraploid wheat.

Previous studies have reported that dwarf genes were involved in the regulation of wheat spike development. For example, *Rht-9* and *Rht-12* are gibberellin-sensitive genes, and they can affect heading date (Ellis et al., 2005); *Rht-8* was close to the marker *Xgwm261* (Korzun et al., 1998), while a QTL for SD was also reported to be tightly linked to this marker (Heidari et al., 2011; Zhao et al., 2013), indicating that dwarf genes may have some intrinsic interaction with SD. Additionally, photoperiod (*Ppd*), vernalization (*Vrn*) as well as earliness *per se* (*Eps*) genes also have certain effects on spike development (Alvarez et al., 2016; Guedira et al., 2016).

In order to further excavate major loci associated with spike development among modern wheat varieties, scholars worldwide have identified a large number of QTL for spike traits (Jantasuriyarat et al., 2004; Kumar et al., 2007; Ma et al., 2007; Cui et al., 2012; Zhai et al., 2016; Tao et al., 2019; Kuang et al., 2020; Li et al., 2021). For example, Ma et al. (2007) analyzed five spike traits in a recombinant inbred line (RIL) population and an immortalized F_2 population. They found QTL controlling SD were distributed on chromosomes 1A, 4A, 5A, 5B, 2D, and 7D, and single QTL was able to explain 7.9–36.3% of phenotypic variation. Based on the genetic map constructed using the wheat55K SNP array, Liu et al. (2019) detected 24 SD QTL. Three of them were major QTL being located on chromosomes 2D, 4B, and 5B, and stably expressed in various environments, indicating that high-density genetic mapping is a critical approach to QTL mapping. Although loci associated with spike development in common wheat have been extensively studied, there have been few studies on identification of loci in tetraploid wheat (*Triticum turgidum* L.). There are still many loci that could be mined and utilized from such germplasm resources.

In the present study, two RIL populations previously genotyped using the wheat55K SNP array were used to identify SD QTL in combination with the phenotypic data from multiple environments. The correlations between SD and other agronomic traits were analyzed. Major SD QTL were identified. Pyramiding analysis for these major QTL was performed. In addition, candidate genes for QTL were also predicted.

MATERIALS AND METHODS

Plant Materials

Three RIL populations of wheat were used in the study: hexaploid population 20828/SY95-71 (2SY, 128 F_7 RILs including parents) (Liu et al., 2020), hexaploid population 20828/Chuanmai60 (2CM, 207 $F_{2:3}$ lines) (Ma et al., 2019b), and tetraploid population Ailanmai (AL)/LM001 (AM, 121 F_8 RILs including parents) (Mo et al., 2021).

The wheat line 20828 is highly resistant to stripe rust disease (Ma et al., 2019b), and has a short spike extension length (Li et al., 2020), a large uppermost-internode diameter (Liu et al., 2021), and multiple spikelets per spike (Ding et al., 2021). SY95-71 is a stable line with a well-developed root system (Zheng et al., 2019) and a relatively high number of tillers (Liu et al., 2020). Chuanmai60 is a commercial cultivar. AL is a unique germplasm resource from China, and has characteristics of dwarf plants and multiple florets (Liu et al., 1999). As a wild emmer wheat line, LM001 exhibits fewer kernels per spikelet, non-free threshability and long awns (Mo et al., 2021). The 2SY and AM populations were used for QTL identification, and the 2CM population was used for verification of major QTL identified in the 2SY population.

Phenotypic Evaluation

Three populations and their parental lines were evaluated at Wenjiang (WJ, 103° 51′ E, 30° 43′ N), Chongzhou (CZ, 103° 38′ E, 30° 32′ N), Ya'an (YA, 103° 0′ E, 29° 58′ N) in China, and Khulna (KB, 89° 34′ E, 22° 49′ N) in Bangladesh during 2017–2021.

The 2SY population was planted in seven environments, encoded as 2017WJ, 2018WJ, 2017CZ, 2018CZ, 2017YA, 2018YA, and 2018KB, respectively, based on the year and location. The AM population was planted in eight environments: 2017CZ, 2018CZ, 2019CZ, 2020CZ, 2021CZ, 2020WJ, 2021WJ, and 2020YA. The validation population 2CM was planted in 2018CZ. The RILs and their parents were planted in a single row for each environment. Each line consisted of 15 seeds evenly planted in a single 1.5-m row with 0.3 m between rows. Field management was conducted in accordance with the general practice of wheat production.

In the study, three individual plants with consistent growth of each line were selected to measure agronomic traits in the 2SY population and five individual plants with consistent growth of each line were selected to measure agronomic traits in the AM population. The phenotypic data of agronomic traits used in this experiment have been measured in previous studies, including spikelet number per spike (SNS), SL, PH, anthesis date (AD), productive tiller number (PTN), thousand kernel weight (TKW), kernel length (KL), kernel number per spike (KNS), kernel number per spikelet (KNL), and kernel width (KW). The agronomic traits of the 2SY populations were measured by Liu et al. (2020) (PH, AD, TKW, PTN, SNS), Ding et al. (2021) (SNS), Li et al. (2020) (SL), and Qu et al. (2021) (KL, KW). The phenotype values for SNS in 2018KB were determined by Ding et al. (2021), and the SNS data across remainder environments

was determined by Liu et al. (2020). The agronomic traits of the AM population were measured by Mo et al. (2021) (PH, AD, TKW, SL, SNS, PTN, KNL and KNS) and Zhou et al. (2021) (KL, KW). The phenotypic data of SL and SNS in the 2CM population were measured by Ma et al. (2019a). Furthermore, SD was obtained by dividing SNS by SL. The detailed information of agronomic traits in different environments are presented in **Supplementary Table 1**.

Data Analysis

The best linear unbiased prediction (BLUP) of agronomic traits and the broad-sense heritability (H^2) of SD were calculated using SAS version 9.1 (SAS Institute, Cary, NC, United States). Based on phenotypic data and BLUP values, IBM SPSS 27 (IBM SPSS, Armonk, NY, United States) was used for Pearson's correlation analysis to assess the relationships between SD and agronomic traits. Significant differences were evaluated using Student's *t*-test. Origin 2018[1] was used to describe the frequency distribution for phenotypic data from the two populations.

Quantitative Trait Loci Mapping

Two genetic linkage maps constructed based on the wheat55K SNP array were used in the present study. The genetic map of the 2SY population covered a total genetic distance of 4,273.03 cM containing 2529 bin markers, and the mean interval between markers was 1.69 cM (Liu et al., 2020). In the AM population, the genetic distance for linkage maps was 2411.8 cM containing 1150 bin markers, and the mean interval between markers was 2.10 cM (Mo et al., 2021).

Individual environment QTL detection was performed using the biparental populations (BIP) module with inclusive composite interval mapping (ICIM) in IciMaing4.1. To improve the reliability of QTL results, the step was set to 1 cM, the PIN value was 0.001, and the logarithm of odds (LOD) score threshold was set to 3. Then, the multi-environment trials (MET-ADD) model in IciMapping4.1 was used to analyze the interaction between QTL and environment (Step = 1 cM, PIN = 0.001, and LOD = 7), and the epistatic effects between QTL were analyzed by multi-environmental trials (MET-EPI) in IciMapping4.1. In this study, QTL identified in two or more environments were treated as stable, and those explained more than 10% of phenotypic variation explained (PVE) were considered major loci. QTL were named according to the Catalogue of Gene Symbols for Wheat (McIntosh et al., 2013), where "sau" represents "Sichuan Agricultural University", 2SY and AM represent population names.

Physical Intervals of the Quantitative Trait Loci and Comparison With Previously Reported Quantitative Trait Loci

Sequences of flanking markers for a given QTL were blasted against the genomes of "Chinese spring" (CS; v2.1) (Zhu et al., 2021), wild emmer (Zavitan; v2.0) (Zhu et al., 2019), and *Aegilops tauschii* (Aet; v4.0) (Luo et al., 2017) to determine the corresponding physical intervals. QTL were determined to check if they were novel loci or not by comparing their physical locations with those of reported ones. Furthermore, candidate genes with functional annotations were obtained from the Triticeae Multi-omics Center[2] and UniProt[3].

[1]https://www.originlab.com/

RESULTS

Phenotype Analysis

Significant differences between the parents of the 2SY and AM populations were observed in several environments (**Figure 1**). The phenotypic values of 2SY and AM RIL populations and their corresponding parents were statistically analyzed under multiple environments and based on BLUP datasets (**Table 1**).

In the 2SY RILs, variance analysis results showed that the SD of SY95-71 was significantly higher than that of 20828 in 2017WJ, 2018WJ, and 2018KB ($P < 0.05$), SD showed prominent variation, varying between 1.34 and 4.14. AL SD was significantly higher than LM001 in 2020WJ and 2021WJ environments ($P < 0.05$), while there was no significant difference in other environments. And a SD range from 1.65 to 3.85 was observed in AM RILs. The frequency distribution presented an approximately normal distribution and was bidirectionally transgressive in two RIL populations (**Figure 2**). The H^2 in

[2]http://202.194.139.32/

[3]http://www.uniprot.org/

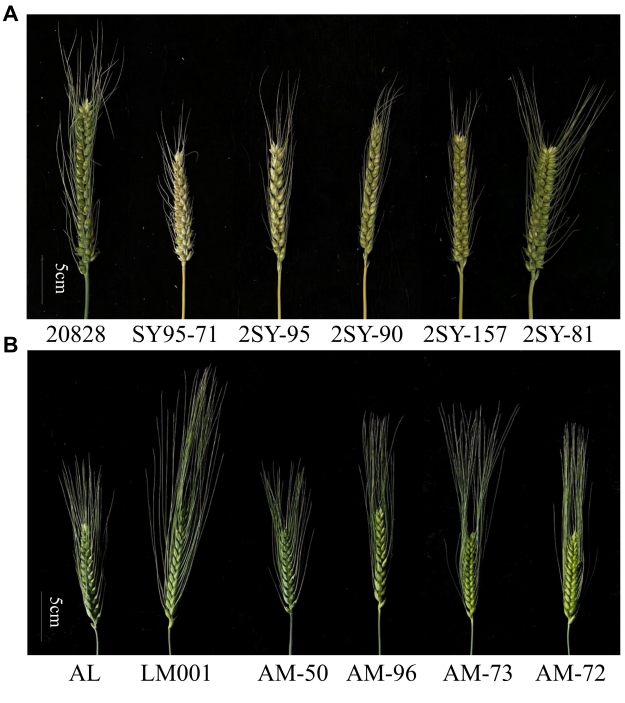

FIGURE 1 | Spike morphology of 20828, SY95-71, and four selected lines **(A)** and AL, LM001 and four selected lines **(B)** (scale bar = 5 cm).

TABLE 1 | Phenotypic evaluation of spike density (SD) for the parents and two recombinant inbred lines (RIL) populations in different environments.

Population	Environment	Mean of female parent (20828 or Ailanmai)	Mean of male parent (SY95-71 or LM001)	Min–Max	Mean	STD	*Skew*	*Kurt*	H^2
2SY	2017WJ	1.71**	2.04	1.34–2.84	1.86	0.27	1.31	2.85	
	2017CZ	1.75	1.94	1.34–3.19	1.84	0.30	0.98	1.12	
	2017YA	2.06	2.24	1.58–3.35	2.19	0.35	1.19	3.10	
	2018WJ	2.05*	2.26	1.48–3.33	2.10	0.33	0.87	0.84	
	2018CZ	2.13	2.30	1.60–3.25	2.17	0.32	0.96	1.55	
	2018YA	2.49	2.66	1.57–3.55	2.38	0.39	0.84	0.48	
	2018KB	2.08**	2.74	1.35–4.14	2.41	0.58	0.65	0.57	
	BLUP	1.95	2.30	1.70–2.80	2.14	0.21	0.82	0.90	0.67
AM	2017CZ	2.06	2.02	1.66–2.73	2.08	0.20	0.62	0.87	
	2018CZ	2.40	2.44	1.88–3.03	2.29	0.21	0.57	0.95	
	2019CZ	2.30	2.09	1.65–2.67	2.09	0.20	0.58	0.37	
	2020CZ	2.61	2.65	2.04–3.48	2.50	0.25	0.79	1.69	
	2020WJ	2.55*	2.06	1.72–3.31	2.27	0.25	0.63	1.23	
	2020YA	2.41	2.41	1.84–3.85	2.70	0.38	0.56	0.57	
	2021CZ	2.30	2.12	1.90–3.13	2.30	0.21	0.84	1.21	
	2021WJ	2.29*	2.09	1.68–2.71	2.20	0.20	0.54	0.06	
	BLUP	2.01	2.87	2.01–2.87	2.31	0.15	0.64	1.03	0.69

2SY, 20828/SY95-71; AM, AL/LM001; WJ, Wenjiang; CZ, Chongzhou; YA, Ya'an; KB, Khulna, in Bangladesh; BLUP, best linear unbiased prediction environments; STD, standard deviation; Skew, skewness; Kurt, kurtosis; H^2, the broad-sense heritability.
** Significance level at $P < 0.05$; ** Significance level at $P < 0.01$.*

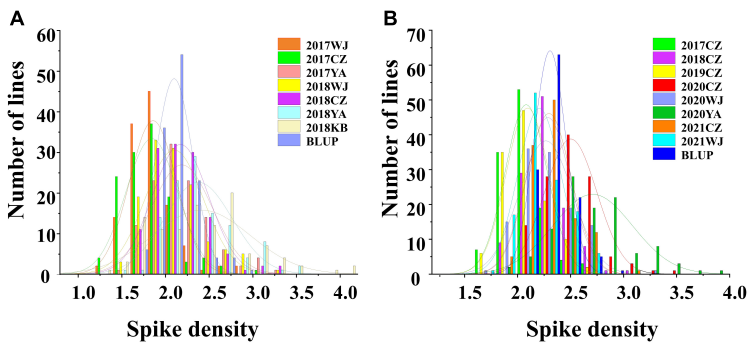

FIGURE 2 | The phenotype and frequency distribution of spike density (SD) in the 2SY population **(A)** and AM population **(B)** under different environments.

the 2SY and AM populations were 0.67 and 0.69, respectively. Moreover, significant correlations for SD among different environments in the 2SY and AM populations were detected (**Supplementary Table 2**). The SD phenotypes in the 2SY population exhibited significant correlations in all environments except 2018KB ($0.48 \leq r \leq 0.79$). The values of SD in the AM population were significantly correlated among all environments ($0.24 \leq r \leq 0.61$).

Correlations Between Spike Density and Other Agronomic Traits

Correlation analysis between SD and other agronomic traits was conducted based on BLUP values (**Table 2**). In the 2SY and AM populations, SD was negatively correlated with KL and SL, but positively correlated with SNS ($P < 0.01$). Moreover, TKW was significantly and negatively correlated with SD in the 2SY population ($P < 0.01$).

Quantitative Trait Loci Mapping of Spike Density and Prediction of Candidate Genes

In total, 18 QTL for SD were identified in the two RIL populations by single-environment analysis, and they were distributed on

TABLE 2 | Correlation analysis between SD and other agronomic traits in two recombinant inbred lines (RIL) populations.

Traits	PH	AD	SL	SNS	TKW	PTN	KL	KW
2SY-SD	−0.07	−0.04	−0.60**	0.43**	−0.35**	−0.03	−0.41**	−0.12
AM-SD	−0.02	0.13	−0.45**	0.32**	0.15	0.03	−0.24**	−0.16

2SY, 20828/SY95-71; AM, AL/LM001; SD spike density; PH, plant height; AD, anthesis date; SL, spike length; SNS, spikelet number per spike; TKW, thousand kernel weight; PTN, productive tiller number; KL, kernels length; KW, kernels width.
*** Significance level at $P < 0.01$.*

chromosomes 1B, 2A, 2D, 3A, 3B, 4A, 4B, 5A, 5B, 6D, 7A, and 7B. A single QTL was able to explain 4.16–23.14% of the phenotypic variation (**Table 3**). Three QTL were regarded as major (including *QSd.sau-2SY-7A.2, QSd.sau-AM-5A.2*, and *QSd.sau-AM-7B*) and one can be stably expressed in multiple environments (*QSd.sau-2SY-2D*). Due to the stability of the *QSd.sau-2SY-2D*, it was further analyzed together with the major ones in the present study. In the 2SY population, *QSd.sau-2SY-2D* was stably expressed in three environments and the BLUP dataset, and it was mapped to the interval *AX-111093303*∼*AX-109338052*, and explained 4.45–9.44% of the phenotypic variance. The positive allele at this locus was from SY95-71. The stably expressed locus *QSd.sau-2SY-2D* was physically located at 602.76–610.04 Mb on 2D of the CS genome and 598.14–604.92 Mb on 2D of the *A. tauschii* genome, respectively (**Figure 3A**). According to the flanking markers of *QSd.sau-2SY-2D*, 2SY RILs could be divided into two groups (with or without the positive allele of *QSd.sau-2SY-2D*). The phenotypic values for SD carrying positive alleles were significantly higher than those with negative ones ($P < 0.05$) (**Figure 4A**).

QSd.sau-2SY-7A.2 was identified under five environments as well as in the BLUP dataset, and its positive allele was from 20828. This QTL was able to explain 10.56–23.44% of the phenotypic variance, and its LOD value ranged from 5.32 to 10.12. *AX-110518554* and *AX-110094527* were its flanking markers and it was located at 678.47–682.29 and 682.56–686.58 Mb on chromosome 7A of the CS and *A. tauschii* genome, respectively (**Figure 3B**). We further divided the 2SY population into two groups, one with alleles from SY95-71 and one with alleles from 20828. Lines with 20828 alleles had larger SD values than those with SY95-71 alleles in all environments except 2018KB ($P < 0.01$) (**Figure 4B**).

In the AM population, *QSd.sau-AM-5A.2* was identified in a 0.85 cM region between markers *AX-110035703* and *AX-111076855* under three environments and the BLUP dataset. It explained 12.29–19.97% of phenotypic variance, and its LOD value was up to 48.58. Then, this locus was anchored at 618.87–621.62 and 684.82–687.74 Mb on chromosome 5A of the CS and wild emmer reference genome, respectively (**Figure 3C**).

QSd.sau-AM-7B, with a LOD value ranging between 4.07 and 4.57, was detected in two environments, and it accounted for 11.06–12.00% of the phenotypic variance. The positive alleles of *QSd.sau-AM-5A.2* and *QSd.sau-AM-7B* were both contributed by LM001. The AM population was grouped and compared

TABLE 3 | Quantitative trait loci (QTL) for spikelet density (SD) in two recombinant inbred lines (RIL) populations under different environments.

Populations	QTL	Environments	Position (cM)	Left marker	Right marker	LOD	PVE (%)	Add
2SY	*QSd.sau-2SY-2A*	2018WJ	41.97–43.47	*AX-109397555*	*AX-111595047*	3.11	9.16	0.11
	QSd.sau-2SY-2D	2017CZ	71.71–72.68	*AX-111093303*	*AX-109338052*	3.21	9.14	−0.09
		2018CZ	71.71–72.68	*AX-111093303*	*AX-109338052*	4.81	4.45	−0.10
		2018YA	71.71–72.68	*AX-111093303*	*AX-109338052*	3.78	9.44	−0.13
		BLUP	71.71–72.68	*AX-111093303*	*AX-109338052*	3.36	7.33	−0.06
	QSd.sau-2SY-4A	2018CZ	81.51–82.33	*AX-111045592*	*AX-108734258*	12.63	14.19	−0.17
	QSd.sau-2SY-4B	2017WJ	39.27–44.89	*AX-110033929*	*AX-108935259*	3.50	7.79	−0.08
	QSd.sau-2SY-5A	2018CZ	56.91–57.64	*AX-109362376*	*AX-108878364*	4.38	4.16	−0.09
	QSd.sau-2SY-6D	2018CZ	169.59–170.43	*AX-110412658*	*AX-109195537*	5.95	5.90	−0.11
	QSd.sau-2SY-7A.1	2017CZ	77.29–86.69	*AX-111511322*	*AX-110483331*	4.58	14.93	0.11
	QSd.sau-2SY-7A.2	2017WJ	101.73–103.88	*AX-110518554*	*AX-110442528*	5.32	12.51	0.10
		2017YA	103.88–106.49	*AX-110442528*	*AX-110094527*	8.09	21.10	0.18
		2018WJ	101.73–103.88	*AX-110518554*	*AX-110442528*	7.58	16.69	0.15
		2018CZ	101.73–103.88	*AX-110518554*	*AX-110442528*	10.12	10.56	0.15
		2018YA	101.73–103.88	*AX-110518554*	*AX-110442528*	8.30	23.14	0.21
		BLUP	100.63–101.73	*AX-108735843*	*AX-110518554*	9.60	23.44	0.11
	QSd.sau-2SY-7A.3	2018WJ	202.86–204.53	*AX-109947373*	*AX-111044435*	3.66	7.44	−0.10
AM	*QSd.sau-AM-3A*	2020CZ	51.33–53.05	*AX-109316902*	*AX-110445703*	3.28	7.29	0.08
	QSd.sau-AM-5A.1	2019CZ	156.06–162.34	*AX-110021952*	*AX-110503841*	4.81	16.77	−0.08
	QSd.sau-AM-5A.2	2018CZ	165.75–166.60	*AX-110035703*	*AX-111076855*	6.25	19.97	−0.09
		2020YA	165.75–166.60	*AX-110035703*	*AX-111076855*	3.02	12.29	−0.13
		BLUP	165.75–166.60	*AX-110035703*	*AX-111076855*	48.58	15.11	−0.29
	QSd.sau-AM-7A.1	2021WJ	76.99–85.22	*AX-111699124*	*AX-108740541*	3.16	9.89	0.06
	QSd.sau-AM-7A.2	2020CZ	162.62–107.05	*AX-109860028*	*AX-109624261*	3.82	8.59	0.08
	QSd.sau-AM-1B	2018CZ	24.81–27.15	*AX-110430183*	*AX-110539078*	3.60	10.86	0.07
	QSd.sau-AM-3B	2021CZ	48.34–49.69	*AX-109393346*	*AX-110548993*	4.51	13.47	0.08
	QSd.sau-AM-5B	2021WJ	40.88–41.31	*AX-109330727*	*AX-111107210*	6.14	20.23	0.09
	QSd.sau-AM-7B	2020CZ	154.97–157.71	*AX-110936825*	*AX-109955661*	4.57	11.06	−0.10
		2021CZ	154.97–157.71	*AX-110936825*	*AX-109955661*	4.07	12.00	−0.07

PVE, phenotype variance explained; LOD, logarithm of odds; Add, additive effect of a QTL; BLUP, phenotype values based on the best linear unbiased prediction.

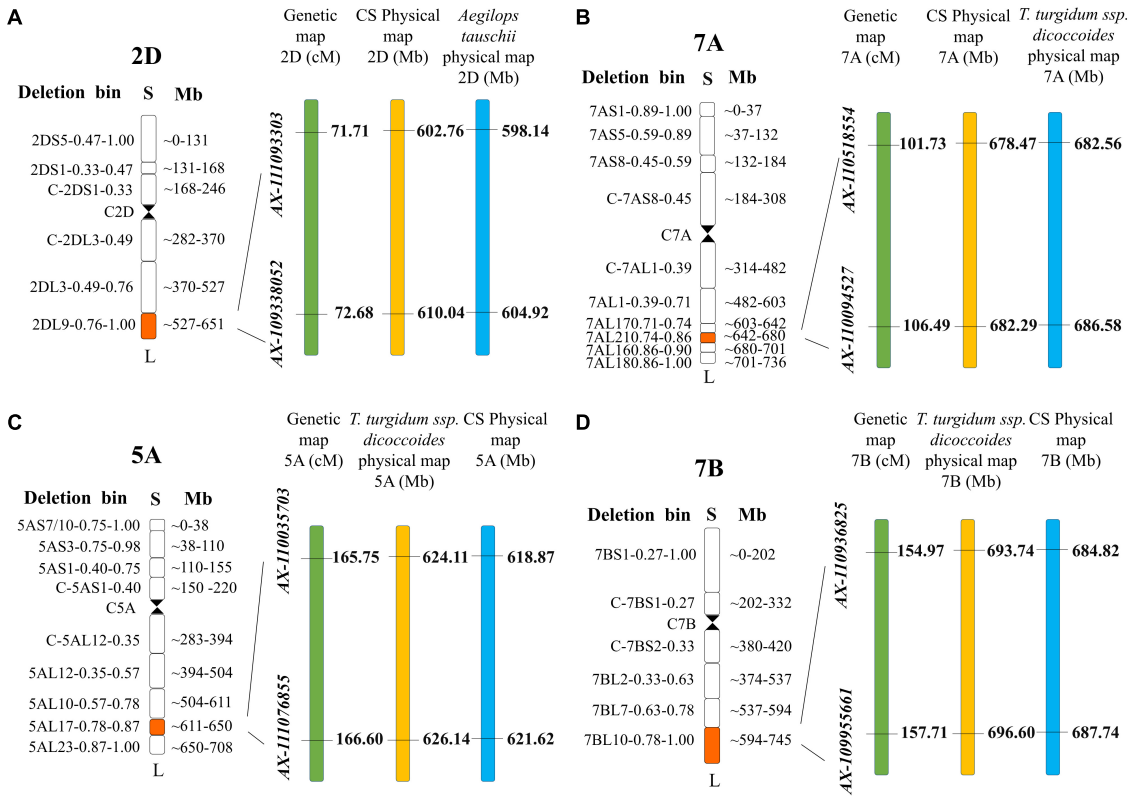

FIGURE 3 | The maps of major QTL. **(A)** QSd.sau-2SY-2D; **(B)** QSd.sau-2SY-7A.2; **(C)** QSd.sau-AM-5A; **(D)** QSd.sau-AM-7B.

using the flanking markers of these two QTL (**Figures 4C,D**). Compared to the RILs with alleles from AL, those with LM001 alleles showed a significant increase in SD across multiple environments. Moreover, the physical position of *QSd.sau-AM-7B* was at 684.82–687.74 and 693.74–696.60 Mb on 7B of the CS and wild emmer reference genome, respectively (**Figure 3D**). Further, candidate genes were analyzed in the regions with these major and stable QTL. Based on the reference genome of CS v2.1 and *A. tauschii*, 47 orthologs in the interval of *QSd.sau-2SY-2D* were obtained (**Supplementary Table 3a**). In addition, based on the genome of wild emmer and CS v2.1, there were 30, 27 and 25 orthologs obtained for *QSd.sau-2SY-7A.2*, *QSd.sau-AM-5A.2*, and *QSd.sau-AM-7B*, respectively (**Supplementary Tables 3b–d**).

Quantitative Trait Loci × Environment and Epistatic Interactions for Spike Density

There were 5 and 11 QTL for SD identified by QTL and environment interaction analysis in the two RIL populations (**Supplementary Table 4**), respectively. Four of them (*QSd.sau-2SY-7A.2, QSd.sau-AM-5A.2, QSd.sau-AM-7B,* and *QSd.sau-2SY-2D*) were identical to the three major and one stable QTL which were detected by single-environment analysis, suggesting they are stably expressed loci. In addition, ten pairs of QTL were detected by epistatic interaction analysis in two populations. However, all of them were identified in only a single environment and there were no interactions between QTL identified by single-environment analysis (**Supplementary Table 5**).

Quantitative Trait Loci Validation

As *QSd.sau-2SY-7A.2* identified in the present study and *QSns.sau-2SY-7A* for SNS reported by Ding et al. (2021) correspond to the same interval, they may be regulated by the same locus. The SNS QTL has been verified in the 2CM population. Therefore, the phenotypic value of SD was calculated and verified in the present study based on the SNS and SL data from the 2CM population.

Student's *t*-test was performed to compare phenotypes of lines homozygous for the alleles from 20828 with those from CM60. There were significant differences in phenotypic values between the two genotypes ($P < 0.05$) (**Figure 5**). The SD values of the lines homozygous for the allele from 20828 were obviously higher than those without the corresponding alleles. These results indicated that *QSd.sau-2SY-7A.2* should be a reliable and major SD locus.

Effects of Major Quantitative Trait Loci on Spike Density in the 2SY and AM Populations

The interactions between *QSd.sau-2SY-2D* and *QSd.sau-2SY-7A.2* and between *QSd.sau-AM-5A.2* and *QSd.sau-AM-7B* were further analyzed, respectively.

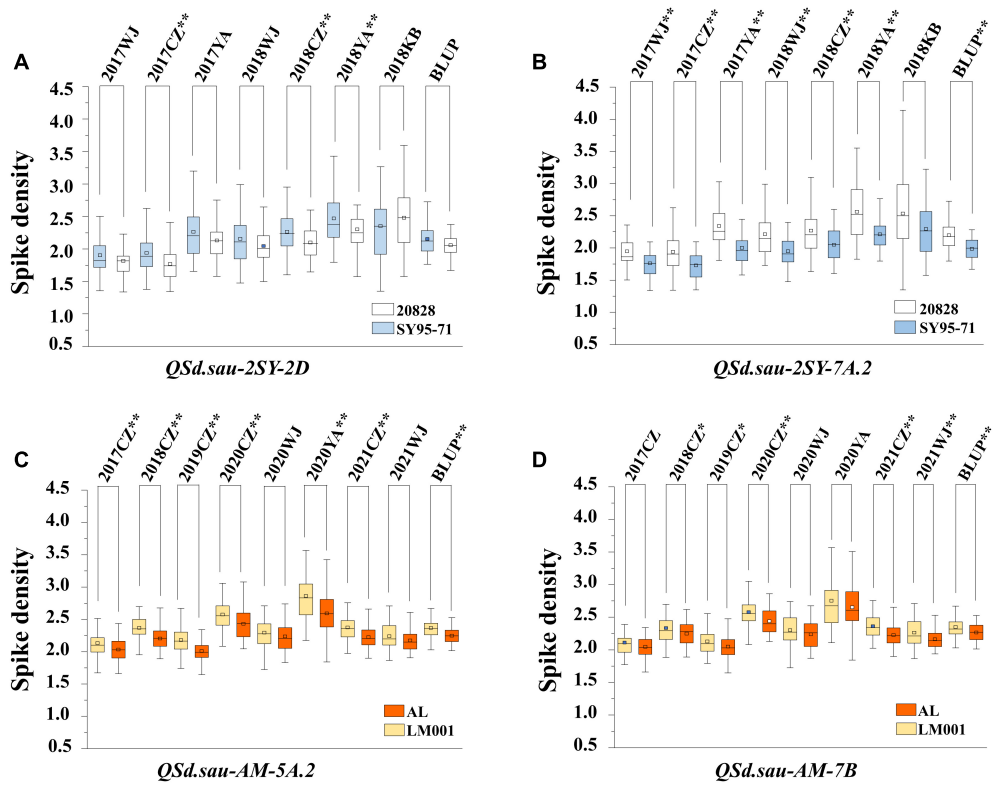

FIGURE 4 | The effect of major QTL *QSd.sau-2SY-2D* **(A)**, *QSd.sau-2SY-7A.2* **(B)**, *QSd.sau-AM-5A.2* **(C)**, and *QSd.sau-7B* **(D)**. 20828 and SY95-71 indicate the phenotypes of the 2SY population with and without positive alleles of the corresponding QTL, respectively; AL and LM001 indicate the phenotypes of the AM population with and without positive alleles of the corresponding QTL, respectively. * Significance level at $P < 0.05$; ** Significance level at $P < 0.01$.

Based on their flanking markers, the two populations were divided into four groups. In the 2SY population, compared to lines without any positive alleles of *QSd.sau-2SY-2D* or *QSd.sau-2SY-7A.2,* the SD of lines containing both the positive alleles of these two QTL was significantly increased by 20.53%.

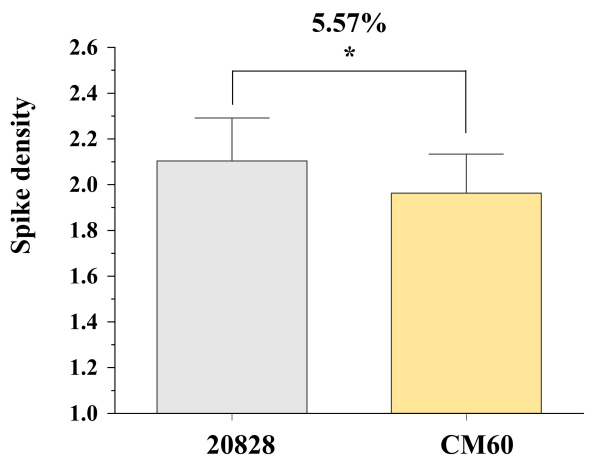

FIGURE 5 | Effects of *QSd.sau-2SY-7A.2* in 20828 × CM60 (2CM) population. * Significance level at $P < 0.05$.

When the positive allele from *QSd.sau-2SY-2D* or *QSd.sau-2SY-7A.2* was expressed alone, SD increased by 1.63 and 8.39%, respectively (**Figure 6A**). In the AM population, *QSd.sau-AM-5A.2* and *QSd.sau-AM-7B* have a strong association with SD. Lines with a combination of positive alleles from *QSd.sau-AM-5A.2* and *QSd.sau-AM-7B* significantly increased SD by 7.97%, compared to those without any of the positive alleles. However, SD can only increase by 3.88 or 1.81% when the positive allele from *QSd.sau-AM-5A.2* or *QSd.sau-AM-7B* was present alone, respectively (**Figure 6B**).

Effects of Major and Stable Quantitative Trait Loci on Yield-Related Traits

We further performed analysis of the effects of major and stable QTL for SD on other yield-related traits. In the 2SY population, as shown in **Figure 7A**, significant differences for SL, SNS, and AD existed among the different lines carrying various alleles. Specifically, SL of 22 lines possessing a combination of positive alleles from *QSd.sau-2SY-2D* and *QSd.sau-2SY-7A.2* were significantly lower ($P < 0.01$, 10.6%) than those carrying the positive allele from *QSd.sau-2SY-7A.2* only and those without *QSd.sau-2SY-2D* or *QSd.sau-2SY-7A.2*. Moreover, highly significant difference ($P < 0.01$) was detected between the lines carrying increased alleles from *QSd.sau-2SY-2D* and *QSd.sau-2SY-7A.2*. Compared with those without positive alleles

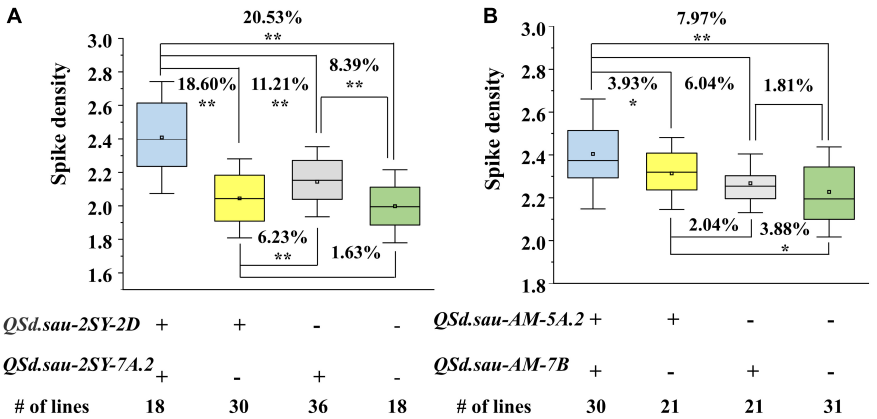

FIGURE 6 | The aggregation effect of the major QTL for spike density (SD) in two RIL populations. **(A)** Effect of *QSd.sau-2SY-2D* and *QSd.sau-2SY-7A.2* for SD in the 2SY population; **(B)** Effect of *QSd.sau-AM-5A.2* and *QSd.sau-AM-7B* for SD in the AM population; + and − represent lines with and without the positive alleles of the corresponding QTL based on the flanking marker of the corresponding QTL, respectively; **Significant at $P < 0.01$, *Significant at $P < 0.05$.

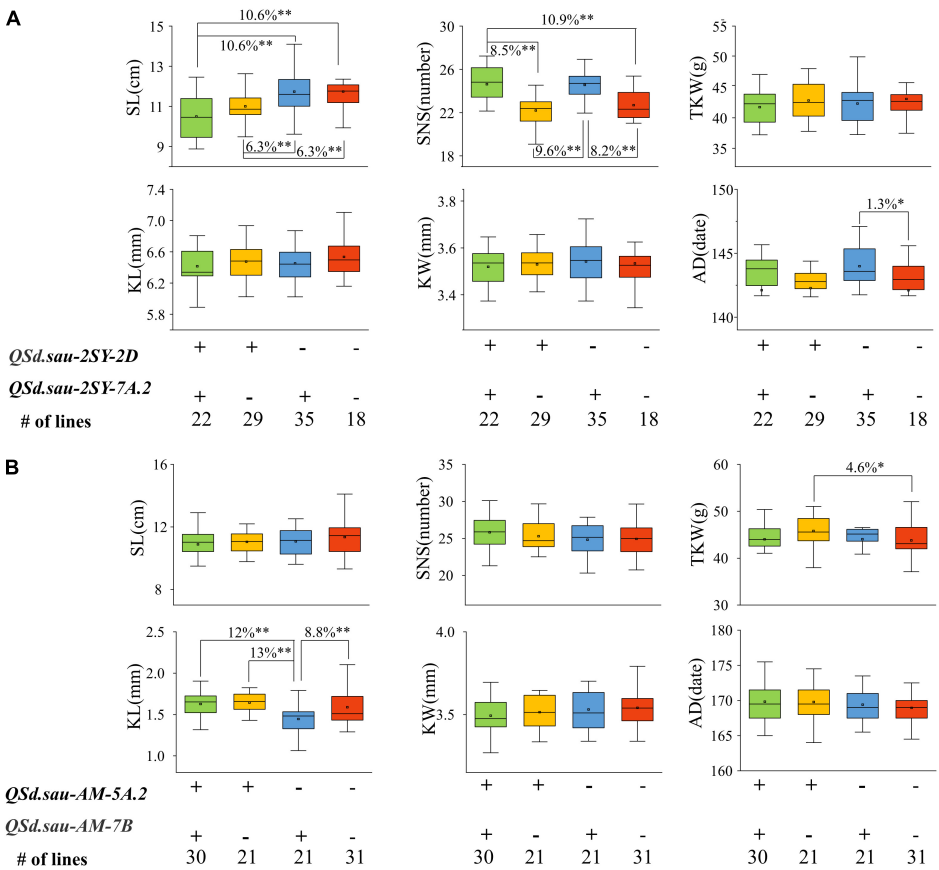

FIGURE 7 | The effects of major quantitative trait loci (QTL) on yield-related traits in the 20828/SY95-71 (2SY) population **(A)** and AL /LM001 (AM) population **(B)**. SL, spike length; SNS, spikelet number per spike; TKW, thousand kernel weight; KL, kernels length; KW, kernels width; AD, anthesis date; + and − represent lines with and without the positive alleles of the target QTL based on the flanking markers the corresponding QTL, respectively. *Significance level at $P < 0.05$; **Significance level at $P < 0.01$.

from *QSd.sau-2SY-2D* or *QSd.sau-2SY-7A.2*, lines possessing that from *QSd.sau-2SY-2D* extremely and significantly ($P < 0.01$) reduced SL by 6.3%. For SNS, the phenotypic values of lines with a combination of *QSd.sau-2SY-2D* and *QSd.sau-2SY-7A.2* increased alleles were extremely and significantly higher than those with *QSd.sau-2SY-2D* increased allele or those without

QSd.sau-2SY-2D or *QSd.sau-2SY-7A.2*, respectively. SNS of 29 lines possessing increased alleles from *QSd.sau-2SY-2D* was extremely and significantly ($P < 0.01$, 9.6%) lower than that of 35 lines from *QSd.sau-2SY-7A.2*. Additionally, compared with those without increased alleles from *QSd.sau-2SY-2D* or *QSd.sau-2SY-7A.2*, lines possessing alleles from *QSd.sau-2SY-7A.2* extremely and significantly ($P < 0.01$) increased SNS by 8.2%. In terms of AD, significant differences in phenotypic values were found only in lines carrying increased alleles from *QSd.sau-2SY-7A.2* and those none carrying *QSd.sau-2SY-7A.2* or *QSd.sau-2SY-2D* increased alleles.

In the AM population, for KL, compared with the lines with increased allele from *QSd.sau-AM-7B*, those from a combination of *QSd.sau-AM-5A.2* and *QSd.sau-AM-7B* extremely and significantly ($P < 0.01$) increased KL up to 12% (**Figure 7B**). Furthermore, the phenotype value of lines harboring *QSd.sau-AM-5A.2* increased alleles was significantly higher than those containing *QSd.sau-AM-7B* with difference being up to 13% ($P < 0.01$). The KL of 31 lines with positive allele from *QSd.sau-AM-7B* was significantly higher than those possessing the negative one. For TKW, compared with those without increased alleles from *QSd.sau-AM-5A.2* or *QSd.sau-AM-7B*, lines carrying alleles from *QSd.sau-AM-5A.2* extremely and significantly increased ($P < 0.01$, 8.2%). In addition to the significant differences described above, no differences were detected among lines with or without different positive alleles of the target QTL based on the flanking markers of the corresponding QTL. The above results indicated that QTL controlling SD significantly impacted SL, SNS, KL, AD, and TGW.

DISCUSSION

The Possibility of Detection of Quantitative Trait Loci for Spike Density in the Mapping Populations Where No Significant Differences Are Present Between Their Parents

Based on the phenotypic analysis for 2SY and AM populations, there were no significant differences for SD between parents in multiple environments. Similarly, SNS between the parental lines exhibited no difference as well in AM population (Mo et al., 2021). However, we observed an approximately normal distribution and transgressive segregation in the two RIL populations, which conforms to the characteristics of quantitative traits. Above all, 18 QTL for SD were identified in this study and some of these major or stably expressed QTL have been proved to be reliable given their co-localization with other loci previously reported.

In fact, this phenomenon exists in many QTL mapping studies (Zhou et al., 2017; Liu et al., 2019). Previous studies have shown that the phenotype of a trait is usually established by an interaction of several genes (Liu et al., 2019), such as reciprocal inhibition between genes causing the lack of a corresponding phenotype for these genes. However, through hybridization between two given genotypes, genetic recombination makes it possible for an offspring to carry a locus independent of other inhibited loci, and thus the corresponding phenotype can be expressed. Therefore, even if the parental phenotypes are not significantly different, it is possible to identify major QTL for a given traits in a RIL population.

Major Quantitative Trait Loci for Spike Density

In this study, four QTL *QSd.sau-2SY-2D.3*, *QSd.sau-2SY-7A*, *QSd.sau-AM-5A.2,* and *QSd.sau-AM-7B* were identified on chromosomes 2D, 5A, 7A, and 7B, and they showed high PVE and were expressed in multiple environments. According to genomes of CS, wild emmer, and *A. tauschii*, these QTL were anchored in the corresponding reference genome intervals, respectively (**Figure 3**).

Many QTL controlling SD have been identified by genetic analysis. To further determine whether these QTL in this study are novel loci, we obtained the physical locations of previously reported QTL and genes associated with SD (**Supplementary Table 6**).

In the CS genome, the *QSd.sicau-2D.3* identified by Liu et al. (2019) overlapped with *QSd.sau-2SY-2D* between 605.12 and 609.88 Mb on chromosome 2DL (**Figure 3A**); *qSc-7A* (Fan et al., 2019), explaining 4.87–17.22% of variation in SD, was located between 679.70 and 679.92 Mb, and *QSd.sau-2SY-7A.2* was mapped to between 678.47 and 682.29 Mb (**Figure 3B**), indicating that they may be allelic variants. In addition, comparing with the physical maps of QTL for other yield-related traits such as SNS (Ding et al., 2021), KL, KW, kernel thickness (KT), TKW, kernel length–width ratio (LWR), and kernel size (KS) (Qu et al., 2021), none of the physical regions of QTL for SD in the present study overlapped with these yield-related loci.

QSd.sau-AM-5A.2 and *QSd.sau-AM-7B* were identified in the AM population. Specifically, *QSd.sau-AM-5A.2*, located between 618.87 and 621.62 Mb (**Figure 3C**), was determined to be distinct from *Q* (651.82 Mb) and *Vrn-A1* (589.27 Mb). There were no overlapping regions with other QTL or genes for SD reported on 5AL comparing with the previous studies (**Supplementary Table 6**). We also performed QTL analysis for KNS and KNL in the AM population (**Supplementary Table 7**), and results indicated that two minor QTL *QKns.sau-AM-5A* and *QKnl.sau-AM-5A* were both located in the physical interval 619.18–622.72 and 613.60–617.54 Mb on wild emmer and CS genome, respectively. These two loci were close to the interval of *QSd.sau-AM-5A.2*, suggesting they may be controlled by a pleiotropic locus.

QSd.sau-AM-7B, located between 684.82 and 687.74 Mb (**Figure 3D**), was determined to be close to *Sd.sicau-7B.1* (688.53–689.86 Mb) (Liu et al., 2019), suggesting they may be allelic. Thus, comparisons showed that *QSd.sau-AM-5A.2* may be a novel and major QTL controlling SD.

Comparison of *QSd.sau-AM-5A.2* to Other Loci for Spike Length and Spikelet Number Per Spike

Spike density and spike length as well as SNS are tightly correlated traits and many QTL for SNS and SL also have pleiotropic effects on SD, and co-location of QTL related to these

three traits has been reported in many studies. For example, QTL conferring SNS, SL, KNS, and TKW were co-located at *Xgwm126 – Xgwm291* (672.92–700.49 Mb; Wang et al., 2011); *QHd.sau-5A*, *QAn.sau-5A*, *QPht.sau-5A*, *QSl.sau-5A1,* and *QSd.sau-5A1* were co-located at *wPt-9094–wPt-9513* (435.00–536.98 Mb; Luo et al., 2016). Compared with kernel size-related QTL in the AM population, no QTL for such as KL and KW were detected on chromosome 5A (Zhou et al., 2021). Additionally, *QSd.sau-AM-5A.2* (624.11–626.14 Mb on wild emmer genome) in the present study and *QSns.sau-AM-5A* (557.72–571.41 Mb; Mo et al., 2021) are not co-located in the same region. A great deal of QTL or genes related to yield traits existed on chromosome 5A. To identify whether *QSd.sau-AM-5A.2* is co-located with QTL or genes for SNS or SL reported previously, based on the comparison of QTL for SNS on chromosome 5A with previous studies (Mo et al., 2021), we reviewed the recently published articles related to SL and SNS (**Supplementary Table 8**). Results showed that many SL or SNS related loci located on chromosome 5AL, but most of the reported QTL or genes were at least tens of Mb away from *QSd.sau-AM-5A.2* detected in this study, such as *QSl.cib-5A* (516.60–521.27 Mb; Ji et al., 2021), *QTgw.cau.5A_140-142* (698.00–705.40 Mb) and *QSsi.cau.5A_91* (586.61–589.22 Mb; Wang et al., 2021), *QSl.wa-5AL.e1*/*QSl.wa-5AL.e2*/*QSns.wa-5AL.e1*/*QSns.wa-5AL.e2*/*QSns.wa-5AL.e3*/ *QGns.wa-5AL.e2*/*QTgw.wa-5AL.e2*/*QTgw.wa-5AL.e3* (672.92–700.49 Mb; Wang et al., 2011). However, Cui et al. (2012) reported that a major locus *QSl.WY.5A.1* for SL was marked with *Xcfa2163.2* and *Xcwm216*, and this locus was tightly closed to *QSd.sau-AM-5A.2* in the physical interval (**Supplementary Table 8**), indicating pleiotropic effects might exist between them.

Pyramiding Analysis of Major Quantitative Trait Loci for Spike Density

Previous studies have found that integrating multiple favorable QTL into the same genetic background can significantly optimize plant traits (Fan et al., 2019; Li et al., 2021). This pyramiding effect of multiple loci is an effective means for the improvement of modern wheat varieties.

In the present study, three major QTL and one stable QTL were detected in the two mapping populations. The pyramiding effect analysis was used to further verify the role of those QTL and analyze the relationships among them. The lines carrying a combination of positive alleles of two given QTL showed significantly greater SD than those from other lines. This indicated an additive effect between these two QTL increasing SD. Through the accumulation of elite genes, an improved SD phenotype can be constructed.

Phenotypic Correlations Between Spike Density and Other Agronomically Important Traits

Spike density, obtained by dividing SNS by SL, is an important factor in cultivating high-yield wheat. Therefore, theoretically, SD should be positively correlated with SNS and negatively correlated with SL. In the present study, the Pearson's correlation analysis showed that SD was indeed negatively correlated with KL and SL and positively correlated with SNS. Moreover, the correlation between SD with TKW was positive in the 2SY population.

Most of the loci controlling spike traits of wheat were observed to be closely linked in previous studies. Major loci for SNS and SD in wheat identified by Fan et al. (2019) were clustered within the same confidence interval on chromosome 7AL. Similarly, Zhai et al. (2016) detected multiple spike QTL in two winter variety populations, among which QTL associated with SD and SL were included in the two genomic regions on chromosomes 2D and 5A, respectively. These studies revealed the potential for pleiotropism of corresponding traits and also revealed the genetic correlations among SD, SL, and SNS. In addition, higher SD may result in shorter kernels and smaller TKW, being consistent with the study reported by Qu et al. (2021). Thus, it is essential to determine relationships among different characters to accelerate breeding process.

Analysis of Candidate Genes

Candidate genes were analyzed in the regions with major and stable QTL. Further analysis indicated that some genes are related to the regulation of plant growth, and they may affect the formation of the spike in wheat.

For example, *TraesCS2D03G1128600* encodes an AP2-like transcription factor that plays a crucial role in flower development. Previous studies have reported that AP2 was involved in growth and development of the floral organs and seed development (Kunst et al., 1989; Schultz and Haughn, 1993; Okamuro et al., 1997). In the physical interval of *QSd.sau-2SY-7A.2*, we found that *TraesCS7A03G1166400* encoding the UNUSUAL FLORAL ORGANS (UFO) protein was involved in floral meristem development and was a key regulatory factor in floral bud differentiation (Levin and Meyerowitz, 1995). *Traescs7A03G1173200* encodes a receptor-like protein kinase that regulates the expression of floral meristem formation factors and promotes cell proliferation to control flower development and organ growth in *Arabidopsis thaliana* (Shpak et al., 2004).

The candidate gene *TRIDC5AG062530* on chromosome 5A controls flowering time by encoding a FRIGIDA-like protein, leading to a late flowering phenotype in plants (Yang et al., 2012). *TRIDC7BG064700*, a candidate gene for *QSd.sau-AM-7B*, encodes a DA2 protein. Xia et al. (2013) found that DA2 can regulate seed size by restricting cell proliferation in the integument.

Furthermore, it is noteworthy that five genes identified in this study (*TraesCS7A03G1167800, TraesCS7A03G1169000, TraesCS7A03G1169300, TRIDC5AG062440,* and *TRIDC5AG062450*) encode cortical cell-delineating proteins. Previous research has revealed that cortical cell-delineating proteins affect plant morphological development by regulating cell division and expansion (Fu et al., 2009). Therefore, these candidate genes may be of vital significance for understanding the genetic mechanism of spike development in wheat. They may also provide clues for further fine mapping of major QTL.

CONCLUSION

In this study, three major QTL and a stable one, located on chromosomes 5A, 7A, 7B, and 2D, were identified in two independent wheat RIL populations. Based on genetic analysis, *QSd.sau-2SY-2D, QSd.sau-2SY-7A.2*, and *QSd.sau-AM-7B* were found to overlap with reported SD loci. However, *QSd.sau-AM-5A.2* identified in the tetraploid wheat RIL population may be a new QTL. Furthermore, the correlations between SD and other agronomic traits, and the candidate genes related to spike development in the corresponding loci were analyzed and discussed, laying a foundation for subsequent fine mapping.

DATA AVAILABILITY STATEMENT

The original contributions presented in the study are included in the article/**Supplementary Material**, further inquiries can be directed to the corresponding authors.

AUTHOR CONTRIBUTIONS

JY and HL performed the entire study and drafted this manuscript. SW did phenotype measurement and data analysis. WL and LG did field work and data analysis. QJ, GC, PQ, and YP helped with data collection and analysis. HT, YM, and MD helped with field work and phenotype measurement. LT, AH, YW, and YZ discussed results. XL guided the study and revised the manuscript. JM designed the experiments, guided the entire study, participated in data analysis, wrote, and extensively revised this manuscript. All authors participated in the research and approved the final manuscript.

FUNDING

This work was supported by the National Natural Science Foundation of China (31971937 and 31970243), the Applied Basic Research Programs of Science and Technology Department of Sichuan Province (2021YJ0503), and the International Science and Technology Cooperation and Exchanges Program of Science and Technology Department of Sichuan Province (22GJHZ0244 and 2021YFH0083). The funders did not participate in the study design, data analysis, or preparation of the manuscript.

ACKNOWLEDGMENTS

We thank the referees for critical reading and revising this manuscript. We also thank MogoEdit company for language editing.

SUPPLEMENTARY MATERIAL

The Supplementary Material for this article can be found online at: https://www.frontiersin.org/articles/10.3389/fpls.2021.796397/full#supplementary-material

REFERENCES

Alvarez, M. A., Tranquilli, G., Lewis, S., Kippes, N., and Dubcovsky, J. (2016). Genetic and physical mapping of the earliness per se locus *Eps-A* ^{m} *1* in Triticum monococcum identifies *EARLY FLOWERING 3 (ELF3)* as a candidate gene. *Funct. Integr. Genomics* 16, 365–382. doi: 10.1007/s10142-016-0490-3

Cui, F., Ding, A., Li, J., Zhao, C., Wang, L., Wang, X., et al. (2012). QTL detection of seven spike-related traits and their genetic correlations in wheat using two related RIL populations. *Euphytica* 186, 177–192. doi: 10.1007/s10681-011-0550-7

Ding, P., Mo, Z., Tang, H., Mu, Y., Deng, M., Jiang, Q., et al. (2021). A major and stable QTL for wheat spikelet number per spike was validated in different genetic backgrounds. *J. Integr. Agricult.* 20, 2–13. doi: 10.1016/S2095-3119(20)63602-4

Ellis, M. H., Rebetzke, G. J., Azanza, F., Richards, R. A., and Spielmeyer, W. (2005). Molecular mapping of gibberellin-responsive dwarfing genes in bread wheat. *Theor. Appl. Genet.* 111, 423–430. doi: 10.1007/s00122-005-2008-6

Fan, X., Cui, F., Ji, J., Zhang, W., Zhao, X., Liu, J., et al. (2019). Dissection of Pleiotropic QTL Regions Controlling Wheat Spike Characteristics Under Different Nitrogen Treatments Using Traditional and Conditional QTL Mapping. *Front. Plant Sci.* 10, 1–13. doi: 10.3389/fpls.2019.00187

Faris, J. D., and Gill, B. S. (2002). Genomic targeting and high-resolution mapping of the domestication gene *Q* in wheat. *Genome* 45, 706–718. doi: 10.1139/g02-036

Faris, J. D., Zhang, Z., Garvin, D. F., and Xu, S. S. (2014). Molecular and comparative mapping of genes governing spike compactness from wild emmer wheat. *Mole. Genet. Genom.* 289, 641–651. doi: 10.1007/s00438-014-0836-2

Fellers, J. P., Gill, B. S., Fellers, J. P., Brooks, S. A., Gill, B. S., and Faris, J. D. (2003). A bacterial artificial chromosome contig spanning the major domestication locus *Q* in wheat and identification of a candidate gene. *Genetics* 164, 311–321. doi: 10.1023/A:1022937713781

Fu, Y., Xu, T., Zhu, L., Wen, M., and Yang, Z. (2009). A ROP GTPase Signaling Pathway Controls Cortical Microtubule Ordering and Cell Expansion in *Arabidopsis*. *Curr. Biol.* 19, 1827–1832. doi: 10.1016/j.cub.2009.08.052

Guedira, M., Xiong, M., Hao, Y. F., Johnson, J., Harrison, S., Marshall, D., et al. (2016). Heading Date QTL in Winter Wheat (*Triticum aestivum* L.) Coincide with Major Developmental Genes *VERNALIZATION1* and *PHOTOPERIOD1*. *PLoS One* 11, 1–21. doi: 10.1371/journal.pone.0154242

Heidari, B., Sayed-Tabatabaei, B. E., Saeidi, G., Kearsey, M., and Suenaga, K. (2011). Mapping QTL for grain yield, yield components, and spike features in a doubled haploid population of bread wheat. *Genome* 54, 517–527. doi: 10.1139/g11-017

Jantasuriyarat, C., Vales, M. I., Watson, C. J. W., and Riera-Lizarazu, O. (2004). Identification and mapping of genetic loci affecting the free-threshing habit and spike compactness in wheat (*Triticum aestivum* L.). *Theoret. Appl. Genet.* 108, 261–273. doi: 10.1007/s00122-003-1432-8

Ji, G., Xu, Z., Fan, X., Zhou, Q., Yu, Q., Liu, X., et al. (2021). Identification of a major and stable QTL on chromosome 5A confers spike length in wheat (*Triticum aestivum L.*). *Mol. Breed.* 41:56. doi: 10.1007/s11032-021-01249-6

Johnson, E. B., Nalam, V. J., Zemetra, R. S., and Riera-Lizarazu, O. (2008). Mapping the compactum locus in wheat (*Triticum aestivum* L.) and its relationship to other spike morphology genes of the Triticeae. *Euphytica* 163, 193–201. doi: 10.1007/s10681-007-9628-7

Korzun, V., Röder, M. S., Ganal, M. W., Worland, A. J., and Law, C. N. (1998). Genetic analysis of the dwarfing gene (*Rht8*) in wheat. Part I. Molecular mapping of Rht8 on the short arm of chromosome 2D of bread wheat (*Triticum aestivum* L.). *Theoret. Appl. Genet.* 96, 1104–1109. doi: 10.1007/s001220050845

Kuang, C., Zhao, X., Yang, K., Zhang, Z., Ding, L., Pu, Z., et al. (2020). Mapping and characterization of major QTL for spike traits in common wheat. *Physiol. Mole. Biol. Plants* 26, 1295–1307. doi: 10.1007/s12298-020-00823-0

Kumar, N., Kulwal, P. L., Balyan, H. S., and Gupta, P. K. (2007). QTL mapping for yield and yield contributing traits in two mapping populations of bread wheat. *Mole. Breed.* 19, 163–177. doi: 10.1007/s11032-006-9056-8

Kunst, L., Klenz, J. E., Martinez-Zapater, J., and Haughn, G. W. (1989). AP2 Gene Determines the Identity of Perianth Organs in Flowers of *Arabidopsis thaliana*. *Plant Cell* 1, 1195–1208. doi: 10.2307/3868917

Levin, J. Z., and Meyerowitz, E. M. (1995). *UFO*: an Arabidopsis gene involved in both floral meristem and floral organ development. *Plant Cell* 7, 529–548. doi: 10.1105/tpc.7.5.529

Li, C., Bai, G., Carver, B. F., Chao, S., and Wang, Z. (2016). Mapping quantitative trait loci for plant adaptation and morphology traits in wheat using single nucleotide polymorphisms. *Euphytica* 208, 299–312. doi: 10.1007/s10681-015-1594-x

Li, C., Tang, H., Luo, W., Zhang, X., Mu, Y., Deng, M., et al. (2020). A novel, validated, and plant height-independent QTL for spike extension length is associated with yield-related traits in wheat. *Theoret. Appl. Genet.* 133, 3381–3393. doi: 10.1007/s00122-020-03675-0

Li, T., Deng, G., Su, Y., Yang, Z., Tang, Y., Wang, J., et al. (2021). Identification and validation of two major QTLs for spike compactness and length in bread wheat (*Triticum aestivum* L.) showing pleiotropic effects on yield-related traits. *Theor. Appl. Genet.* 2013, 1–17. doi: 10.1007/s00122-021-03918-8

Liu, D., Yen, C., Yang, J., Zheng, Y., and Lan, X. (1999). The chromosomal locations of high crossability genes in tetraploid wheat *Triticum turgidum* L. cv. Ailanmai native to Sichuan, China. *Euphytica* 108, 79–82. doi: 10.1023/A:1003691925501

Liu, H., Ma, J., Tu, Y., Zhu, J., Ding, P., Liu, J., et al. (2019). Several stably expressed QTL for spike density of common wheat (*Triticum aestivum*) in multiple environments. *Plant Breed.* 139, 284–294. doi: 10.1111/pbr.12782

Liu, H., Tang, H.-P., Luo, W., Mu, Y., Jiang, Q.-T., Liu, Y.-X., et al. (2021). Genetic dissection of wheat uppermost-internode diameter and its association with agronomic traits in five recombinant inbred line populations at various field environments. *J. Integr. Agricult.* 20, 2849–2861. doi: 10.1016/S2095-3119(20)63412-8

Liu, J., Tang, H., Qu, X., Liu, H., Li, C., Tu, Y., et al. (2020). A novel, major, and validated QTL for the effective tiller number located on chromosome arm 1BL in bread wheat. *Plant Mole. Biol.* 104, 173–185. doi: 10.1007/s11103-020-01035-6

Luo, M., Gu, Y. Q., Puiu, D., Wang, H., Twardziok, S. O., Deal, K. R., et al. (2017). Genome sequence of the progenitor of the wheat D genome *Aegilops tauschii*. *Nature* 551, 498–502. doi: 10.1038/nature24486

Luo, W., Ma, J., Zhou, X., Sun, M., Kong, X., Wei, Y., et al. (2016). Identification of Quantitative Trait Loci Controlling Agronomic Traits Indicates Breeding Potential of Tibetan Semiwild Wheat (*Triticum aestivum* ssp. *tibetanum*). *Crop Sci.* 56, 2410–2420. doi: 10.2135/cropsci2015.11.0700

Ma, J., Qin, N., Cai, B., Chen, G., Ding, P., Zhang, H., et al. (2019b). Identification and validation of a novel major QTL for all-stage stripe rust resistance on 1BL in the winter wheat line 20828. *Theor. Appl. Genet.* 132, 1363–1373. doi: 10.1007/s00122-019-03283-7

Ma, J., Ding, P., Liu, J., Li, T., Zou, Y., Habib, A., et al. (2019a). Identification and validation of a major and stably expressed QTL for spikelet number per spike in bread wheat. *Theor. Appl. Genet.* 132, 3155–3167. doi: 10.1007/s00122-019-03415-z

Ma, Z., Zhao, D., Zhang, C., Zhang, Z., Xue, S., Lin, F., et al. (2007). Molecular genetic analysis of five spike-related traits in wheat using RIL and immortalized F_2 populations. *Mol. Genet. Genomics* 277, 31–42. doi: 10.1007/s00438-006-0166-0

McIntosh, R. A., Yamazaki, Y., Dubcovsky, J., Rogers, W., Morris, C., Appels, R., et al. (2013). "Catalogue of gene symbols for wheat," in *Proceedings of the 12th International Wheat Genetics Symposium*, 8–13 September 2013, Yokohama.

Mo, Z., Zhu, J., Wei, J., Zhou, J., Xu, Q., Tang, H., et al. (2021). The 55K SNP-Based Exploration of QTLs for Spikelet Number Per Spike in a Tetraploid Wheat (T*riticum turgidum* L.) Population: Chinese Landrace "Ailanmai" × Wild Emmer. *Front. Plant Sci.* 12, 1–14. doi: 10.3389/fpls.2021.732837

Okamuro, J. K., Szeto, W., and Jofuku, L. (1997). Photo and hormonal control of meristem identity in the Arabidopsis flower mutants apetala2 and apetala1. *Plant Cell* 9, 37–47. doi: 10.2307/3870369

Prabhakararao, M. V. (1977). Mapping of the sphaerococcum gene '*S*' on chromosome 3D of wheat. *Cereal Res. Comm.* 5, 15–17.

Qu, X., Liu, J., Xie, X., Xu, Q., Tang, H., Mu, Y., et al. (2021). Genetic Mapping and Validation of Loci for Kernel-Related Traits in Wheat (*Triticum aestivum* L.). *Front. Plant Sci.* 12, 1–17. doi: 10.3389/fpls.2021.667493

Schultz, E. A., and Haughn, G. W. (1993). Genetic analysis of the floral initiation process (FLIP) in Arabidopsis. *Development* 119, 745–765. doi: 10.1002/cyto.990140816

Shpak, E. D., Berthiaume, C. T., Hill, E. J., and Torii, K. U. (2004). Synergistic interaction of three ERECTA-family receptor-like kinases controls Arabidopsis organ growth and flower development by promoting cell proliferation. *Development* 131, 1491–1501. doi: 10.1242/dev.01028

Simons, K. J., Fellers, J. P., Trick, H. N., Zhang, Z., Tai, Y.-S., Gill, B. S., et al. (2006). Molecular Characterization of the Major Wheat Domestication Gene *Q*. *Genetics* 172, 547–555. doi: 10.1534/genetics.105.044727

Tao, Y., Yi, X., Lin, Y., Wang, Z., Wu, F., Jiang, X., et al. (2019). Quantitative trait locus mapping for panicle exsertion length in common wheat using two related recombinant inbred line populations. *Euphytica* 215, 104–117. doi: 10.1007/s10681-019-2433-2

Wang, J., Liu, W., Wang, H., Li, L., Wu, J., Yang, X., et al. (2011). QTL mapping of yield-related traits in the wheat germplasm 3228. *Euphytica* 177, 277–292. doi: 10.1007/s10681-010-0267-z

Wang, X., Guan, P., Xin, M., Yongfa, W., Chen, X., Zhao, A., et al. (2021). Genome-wide association study identifies QTL for thousand grain weight in winter wheat under normal- and late-sown stressed environments. *Theor. Appl. Genet.* 134, 143–157. doi: 10.1007/s00122-020-03687-w

Xia, T., Li, N., Dumenil, J., Li, J., Kamenski, A., Bevan, M. W., et al. (2013). The ubiquitin receptor DA1 interacts with the E3 ubiquitin ligase DA2 to regulate seed and organ size in Arabidopsis. *Plant Cell* 25, 3347–3359. doi: 10.1105/tpc.113.115063

Xu, B. J., Chen, Q., Zheng, T., Jiang, Y. F., Qiao, Y. Y., Guo, Z. R., et al. (2018). An Overexpressed *Q* Allele Leads to Increased Spike Density and Improved Processing Quality in Common Wheat *(Triticum aestivum). G3 Genes Genomes Genetics* 8, 771–778. doi: 10.1534/g3.117.300562

Yang, Q., Kang, J., Zhang, T., and Sun, Y. (2012). Expression of the alfalfa *FRIGIDA*-Like Gene, *MsFRI-L* delays flowering time in transgenic Arabidopsis thaliana. *Mole. Biol. Rep.* 40, 2083–2090. doi: 10.1007/s11033-012-2266-8

Zhai, H., Feng, Z., Li, J., Liu, X., Xiao, S., Ni, Z., et al. (2016). QTL Analysis of Spike Morphological Traits and Plant Height in Winter Wheat (*Triticum aestivum* L.) Using a High-Density SNP and SSR-Based Linkage Map. *Front. Plant Sci.* 7, 1–14. doi: 10.3389/fpls.2016.01617

Zhao, C., Cui, F., Fan, Z., Li, J., Ding, A., and Wang, H. (2013). Genetic analysis of important loci in the winter wheat backbone parent Aimengniu-V. *Austr. J. Crop Sci.* 7, 182–188.

Zheng, X., Wen, X., Qiao, L., Zhao, J., Zhang, X., Li, X., et al. (2019). A novel QTL *QTrl.saw-2D.2* associated with the total root length identified by linkage and association analyses in wheat (*Triticum aestivum* L.). *Planta* 250, 129–143. doi: 10.1007/s00425-019-03154-x

Zhou, J., Li, C., You, J., Tang, H., Mu, Y., Jiang, Q., et al. (2021). Genetic identification and characterization of chromosomal regions for kernel length and width increase from tetraploid wheat. *BMC Genomics* 22, 1–12. doi: 10.1186/s12864-021-08024-z

Zhou, Y., Conway, B., Miller, D., Marshall, D., Cooper, A., Murphy, P., et al. (2017). Quantitative Trait Loci Mapping for Spike Characteristics in Hexaploid Wheat. *Plant Genome* 10, 1–15. doi: 10.3835/plantgenome2016.10.0101

Zhu, T., Wang, L., Rimbert, H., Rodriguez, J. C., Deal, K. R., De Oliveira, R., et al. (2021). Optical maps refine the bread wheat *Triticum aestivum* cv. Chinese Spring genome assembly. *Plant J.* 107, 303–314. doi: 10.1111/tpj.15289

Zhu, T., Wang, L., Rodriguez, J., Deal, K., Avni, R., Distelfeld, A., et al. (2019). Improved Genome Sequence of Wild Emmer Wheat Zavitan with the Aid of Optical Maps. *G3-Genes Genomes Genetics* 9, 619–624. doi: 10.1534/g3.118.200902

Conflict of Interest: The authors declare that the research was conducted in the absence of any commercial or financial relationships that could be construed as a potential conflict of interest.

Publisher's Note: All claims expressed in this article are solely those of the authors and do not necessarily represent those of their affiliated organizations, or those of the publisher, the editors and the reviewers. Any product that may be evaluated in this article, or claim that may be made by its manufacturer, is not guaranteed or endorsed by the publisher.

frontiers in Plant Science

REVIEW
published: 20 December 2021
doi: 10.3389/fpls.2021.800332

HAM Gene Family and Shoot Meristem Development

Yuan Geng[1,2] *and Yun Zhou*[1,2]*

[1]*Department of Botany and Plant Pathology, Purdue University, West Lafayette, IN, United States,* [2]*Purdue Center for Plant Biology, Purdue University, West Lafayette, IN, United States*

Land plants develop highly diversified shoot architectures, all of which are derived from the pluripotent stem cells in shoot apical meristems (SAMs). As sustainable resources for continuous organ formation in the aboveground tissues, SAMs play an important role in determining plant yield and biomass production. In this review, we summarize recent advances in understanding one group of key regulators – the HAIRY MERISTEM (HAM) family GRAS domain proteins – in shoot meristems. We highlight the functions of HAM family members in dictating shoot stem cell initiation and proliferation, the signaling cascade that shapes HAM expression domains in shoot meristems, and the conservation and diversification of HAM family members in land plants. We also discuss future directions that potentially lead to a more comprehensive view of the *HAM* gene family and stem cell homeostasis in land plants.

Keywords: shoot meristems, stem cells, land plants, HAM, GRAS proteins, microRNAs

OPEN ACCESS

Edited by:
Xigang Liu,
Hebei Normal University, China

Reviewed by:
Bo Sun,
Nanjing University, China
Sascha Biedermann,
University of Freiburg, Germany

***Correspondence:**
Yun Zhou
zhouyun@purdue.edu

Specialty section:
This article was submitted to Plant Physiology, a section of the journal Frontiers in Plant Science

Received: *22 October 2021*
Accepted: *19 November 2021*
Published: *20 December 2021*

Citation:
Geng Y and Zhou Y (2021) HAM Gene Family and Shoot Meristem Development. Front. Plant Sci. 12:800332. doi: 10.3389/fpls.2021.800332

HAM KEEPS SHOOT STEM CELLS UNDIFFERENTIATED

Land plants develop diversified shoot architectures, which are determined and sustained by pluripotent stem cells in shoot apical meristems (SAMs). In seed plants, the multicellular SAMs are organized into distinct cell layers and zones (Foster, 1938; Satina et al., 1940; Meyerowitz, 1997). In the model species Arabidopsis and many other flowering plants, SAMs consist of three clonally distinct cell layers: the epidermal layer (L1), the sub-epidermal layer (L2), and the corpus (L3) (**Figure 1**). In addition, SAMs can be divided into different functional zones, including the central zone (CZ) where the self-renewing stem cells reside, the peripheral zone (PZ) where organ initiation takes place, and the rib meristem (RM) where the differentiated cells help specify the overlaying stem cells (Meyerowitz, 1997). Over more than 20 years of studies, multiple key regulatory pathways, such as the WUSCHEL-CLAVATA loop, KNOX/SHOOTMERISTEMLESS pathway, ERECTA family receptors, Class III HD-ZIP transcription factors, and the cytokinin and auxin signaling, have been identified and well characterized in Arabidopsis SAMs (Sablowski, 2007; Barton, 2010; Su et al., 2011; Shpak, 2013; Gaillochet and Lohmann, 2015; Somssich et al., 2016; Fletcher, 2018; Kieber and Schaller, 2018; Shi and Vernoux, 2021; Willoughby and Nimchuk, 2021). In this review, we focus on the function and regulation of one group of conserved stem cell regulators, the HAIRY MERISTEM (HAM) family GRAS (GAI, RGA, and SCR) domain proteins, in shoot meristems.

The *HAIRY MERISTEM* (*HAM*) gene was firstly identified and characterized in Petunia, and it was named after the phenotype of its loss-of-function mutant, the ectopic formation of differentiated hairs (trichomes) at the surface of shoot apices (Stuurman et al., 2002).

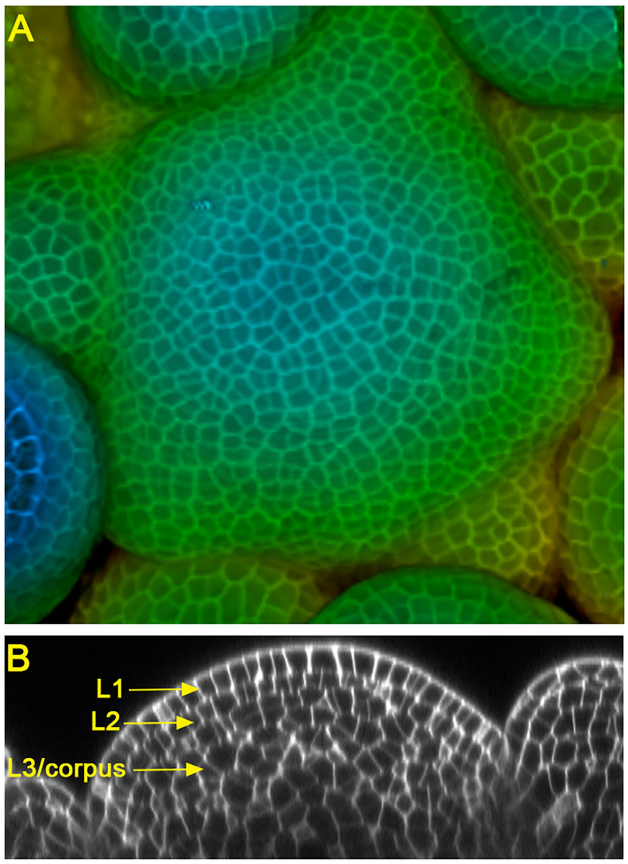

FIGURE 1 | Confocal images of Arabidopsis inflorescence shoot apical meristems (SAMs). **(A)** The 3D projection view of an Arabidopsis SAM, with the depth color coding. Blue represents the top surface layer and red represents the deepest layer. **(B)** The orthogonal view of an Arabidopsis SAM, showing three clonally distinct cell layers: the epidermal layer (L1), sub-epidermal layer (L2), and corpus (L3).

The *HAM* loss-of-function in Petunia also shows early termination of SAMs, arrested axillary shoot development, and reduced number of carpels and stamens (Stuurman et al., 2002), suggesting the key role of HAM in maintaining shoot meristems undifferentiated in Petunia. In the model species Arabidopsis, four HAM homologs (HAM1-HAM4) are classified into two different groups, based on the phylogenetic analyses (Engstrom et al., 2011; Geng et al., 2021b). HAM1, HAM2, and HAM3, which are also named as LOST MERISTEM1 (LOM1), LOM2, and LOM3, respectively (Schulze et al., 2010), belong to the Type II group (Engstrom et al., 2011; Geng et al., 2021b). These Type II members (*HAM1-3*) are expressed in Arabidopsis shoot meristems, root meristems, and vascular tissues (Schulze et al., 2010; Engstrom et al., 2011; Zhou et al., 2015). HAM4, the only member of the Type I group in Arabidopsis (Engstrom et al., 2011; Geng et al., 2021b), is specifically expressed in the provascular and vascular tissues (Zhou et al., 2015), sharing redundant function with HAM1-3 during shoot and root development (Engstrom et al., 2011; Zhou et al., 2015).

The Type II HAM members (HAM1, HAM2, and HAM3) play both overlapping and distinct roles in control of Arabidopsis SAMs. The single loss-of-function mutant of each Type II member does not result in any obvious defects in Arabidopsis shoot meristem development (Schulze et al., 2010; Engstrom et al., 2011). By contrast, the *ham1ham2ham3* (*ham123*) triple loss-of-function mutant or the *ham1ham2* (*ham12*) double mutant showed delayed inflorescence initiation, early termination of shoot meristems, disorganized meristem structure and morphology, and reduced axillary shoot branches (Schulze et al., 2010; Wang et al., 2010; Engstrom et al., 2011; Han et al., 2020a), demonstrating essential and redundant roles of Type II members in meristem initiation and maintenance in Arabidopsis. A recent study further shows that HAM1 and HAM2, both of which are expressed in the L3 layer, are required for maintaining SAMs undifferentiated and driving *de novo* formation of new axillary stem cell niches (Han et al., 2020a). HAM3, the other member of the Type II group, plays a minor role in shoot stem cell maintenance but likely contributes to other aspects of shoot development (Han et al., 2020a).

HAM SUSTAINS THE WUSCHEL-CLAVATA REGULATORY LOOP

In Arabidopsis, the homeobox domain transcription factor WUSCHEL (WUS) and the secreted peptide CLAVATA3 (CLV3) form a negative feedback loop to keep a constant population of stem cells in SAMs (Schoof et al., 2000; Somssich et al., 2016; Fletcher, 2018; **Figure 2A**). The *WUS* transcripts are restricted into the organizing center (OC) in deep cell layers (Mayer et al., 1998) and WUS proteins move into stem cells in the central zone to activate *CLV3* expression (Schoof et al., 2000; Yadav et al., 2011; Daum et al., 2014). On the contrary, the CLV3 peptide, secreted from stem cells, activates the CLV receptor signaling pathways and confines *WUS* transcripts to the OC to avoid overproliferation of stem cells (Schoof et al., 2000). The ability of WUS to directly activate its own inhibitor *CLV3* brings a potential risk to shut down itself and the feedback loop; therefore, the precise spatial–temporal regulations of *WUS* and *CLV3* are required for stem cell maintenance.

Several studies demonstrated that Type II HAM members play essential roles in initiating and maintaining the WUS-CLV3 feedback loop, and further sustaining shoot stem cell homeostasis in Arabidopsis (Schulze et al., 2010; Zhou et al., 2015, 2018; Gruel et al., 2018; Han et al., 2020a; Geng et al., 2021b), which also has been summarized in the reviews (Biedermann and Laux, 2018; Han et al., 2020b). Through the screening of an Arabidopsis transcription factor library, Type II HAM proteins are identified as the WUS interacting partners (Zhou et al., 2015). Among them, both *HAM1* and *HAM2* are co-expressed with *WUS* in the L3 layer. HAM1/2 act as WUS transcriptional cofactors to regulate the downstream targets and drive proliferation of shoot stem cells (Zhou et al., 2015). In addition, the expression patterns of HAM1/2 and *CLV3* are largely complementary in Arabidopsis SAMs (Zhou et al., 2018). *CLV3* is highly expressed in the L1 and L2 layers of the central zone, where HAM1 and HAM2 are absent or barely detectable (Zhou et al., 2018; Han et al., 2020a). These results lead to a

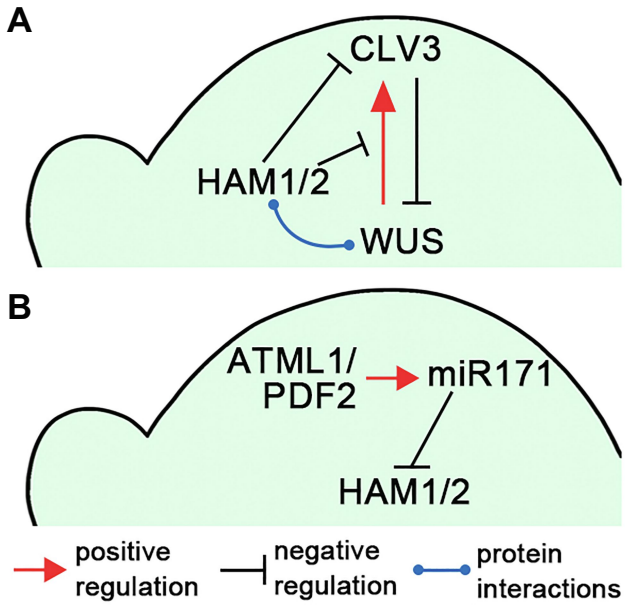

FIGURE 2 | Illustrations of the HAM regulatory circuits in SAMs. **(A)** A diagram illustrates that HAM1/2 sustain the WUS-CLV3 feedback loop in Arabidopsis SAMs. **(B)** A diagram illustrates the L1(ATML1/PDF2)-miR171-HAM signaling cascade, which shapes HAM1/2 expression patterns in Arabidopsis SAMs. The positive and negative regulations and protein–protein interactions are indicated in **(A,B)**.

hypothesis that HAM1/2 together with WUS determine the *CLV3* expression pattern and confine the *CLV3* domain to the stem cells in the outer layers of SAMs (Zhou et al., 2018; Han et al., 2020b; **Figure 2A**). Specifically, WUS protein activates *CLV3* in the central zone where HAM1/2 proteins are absent, and HAM1/2 keep *CLV3* off in the rib meristem, preventing WUS-dependent activation of *CLV3* and/or repressing *CLV3* transcription (Zhou et al., 2018). This working model has been supported by (Zhou et al., 2018; Han et al., 2020a; Geng et al., 2021b) and aligns with (Brand et al., 2000, 2002; Schoof et al., 2000; Graf et al., 2010; Schulze et al., 2010) a number of experimental results. It is also shown plausible by several independent computational simulations (Gruel et al., 2018; Zhou et al., 2018; Liu et al., 2020). In addition, through confocal imaging of HAM translational reporters and genetic complementation analyses, recent work shows that both HAM1 and HAM2 proteins, which show highly comparable expression patterns in the L3 layer of SAMs, are necessary and sufficient for determining the *CLV3* pattern (Han et al., 2020a). HAM3, which is only expressed in the boundary between the meristem and primordia and at a few cells of the peripheral zone, is dispensable in shaping the *CLV3* domain (Han et al., 2020a). In contrast, when HAM3 is expressed in the rib meristem under the control of the *HAM2* promoter, it rescues the ectopic expression of *CLV3* in the *ham123* triple mutant (Han et al., 2020a), suggesting HAM3 protein maintains the function interchangeable with that of HAM1 and HAM2.

During the *de novo* formation of shoot stem cell niches, the expression patterns of HAM1/2 are dynamically regulated, which drive the switch of the *CLV3* expression domain from the basal to apical region of developing axillary meristems over time (Zhou et al., 2018). In contrast, the expression of *CLV3* is restricted to the basal part of developing axillary meristems in the *ham123* mutant, consistent with the mutant defects in axillary bud initiation (Schulze et al., 2010; Wang et al., 2010; Engstrom et al., 2011; Zhou et al., 2018).

A SIGNALING CASCADE SHAPES HAM PATTERNS IN ARABIDOPSIS SHOOT MERISTEMS

In Arabidopsis, a small group of micro RNAs – the microRNA171 (miR171) – function as the negative regulator of Type II HAM members (Llave et al., 2002; Rhoades et al., 2002; Schulze et al., 2010; Wang et al., 2010; Engstrom et al., 2011; Han et al., 2020c). miR171 specifically recognizes and binds to Arabidopsis *HAM1, HAM2*, and *HAM3*, mediating the cleavage of their transcripts (Llave et al., 2002; Rhoades et al., 2002). Consistently, *MIR171* overexpression leads to ectopic expression of *CLV3* in the rib meristem and reduced shoot branching, which mimic the phenotype of the *ham123* mutant (Schulze et al., 2010; Wang et al., 2010; Zhou et al., 2018; Han et al., 2020a).

The epidermis-derived miR171 defines the apical-basal concentration gradient of HAM1/2 in Arabidopsis SAMs and axillary meristems (Takanashi et al., 2018; Han et al., 2020c). Four *MIR171* family genes (*MIR171A*, *MIR171B*, *MIR171C*, and *MIR170*) are identified in Arabidopsis, all producing miR171 precursors and contributing to the total level of mature miR171 (Llave et al., 2002; Rhoades et al., 2002). All these *MIR171/170* genes are directly activated by the homeodomain transcription factor ARABIDOPSIS THALIANA MERISTEM LAYER 1 (ATML1) and its close homolog PROTODERMAL FACTOR 2 (PDF2) in the L1 layer (Han et al., 2020c). Once synthesized in the epidermis, mature miR171 moves downwards within limited distance and it mediates the cleavage of the transcripts of *HAM1-3* in the apical region of SAMs (Han et al., 2020c). Based on these results, a L1(ATML1/PDF2)-miR171-HAM signaling cascade has been proposed, which initiates and then maintains the apical-basal concentration gradient of Type II HAM proteins in Arabidopsis shoot meristems (Han et al., 2020c; **Figure 2B**). The essential function of the L1-miR171-HAM signaling cascade is simulated by a computational model and further validated by *in vivo* experimentations including the time-lapse live imaging upon the transient activation of ATML1 in the SAMs (Han et al., 2020c).

EVOLUTION OF *HAM* GENE FAMILY IN LAND PLANTS

The phylogenetic analysis suggested that the *HAM* gene family emerged during the divergence of land plant lineages (Geng et al., 2021b). In non-flowering plants including bryophytes, lycophytes, ferns, and gymnosperms, *HAM* members are maintained with a low copy number (Engstrom et al., 2011; Geng et al., 2021b).

By contrast, the *HAM* gene family likely duplicated in a common ancestor of flowering plants, expanding to two diversified groups (Type I and Type II) as mentioned above, in flowering plants (Geng et al., 2021b). Type II HAM members are widely present in flowering plants, whereas Type I HAM members were independently lost in the species from different orders (including Poales and Asparagales) in monocots (Geng et al., 2021b).

HAM family members from several flowering plants share similar functions in maintaining indeterminacy of SAMs and promoting *de novo* formation of axillary meristems (Stuurman et al., 2002; Schulze et al., 2010; Wang et al., 2010; Engstrom et al., 2011; David-Schwartz et al., 2013; Zhou et al., 2015, 2018; Hendelman et al., 2016). For example, the *ham* loss-of-function mutant in pepper (*Capsicum annuum*) shows the shoot meristem defect (David-Schwartz et al., 2013) comparable to that characterized in the Petunia *ham* mutant and in the Arabidopsis *ham123* mutant (Stuurman et al., 2002; Schulze et al., 2010; Engstrom et al., 2011). Several HAM homologs, including AmHAM1 (the Type I) and AmHAM2 (the Type II) from *Amborella trichopoda* (the species as a sister group to all other flowering plants), one Type II HAM from a monocot (rice), and two Type II HAM members from eudicots (soybean and pepper), are able to replace the role of Arabidopsis Type II HAM members in Arabidopsis shoot meristems (Geng et al., 2021b), demonstrating the conserved function of HAM family members in flowering plants.

The results from cross-species complementation assays also indicate the conserved biochemical function between the non-flowering HAM proteins and the Type II HAM proteins from flowering plants, in regulating meristem development (Geng et al., 2021b). When different non-flowering *HAM* members (including *PpHAM* from the bryophyte *Physcomitrium* (*Physcomitrella*) *patens*, *SmHAM* from the lycophyte *Selaginella moellendorffii*, *CrHAM* from the fern *Ceratopteris richardii*, and *LkHAM* from the gymnosperm *Larix kaempferi*) are expressed under the control of the Arabidopsis *HAM2* promoter, they replace the function of Type II members (*HAM1*, *HAM2*, and *HAM3*) in regulating the *CLV3* expression domain, maintaining established SAMs, and promoting the initiation of new stem cell niches in Arabidopsis *ham123* mutants (Geng et al., 2021b). Consistently, the function of *PpGRAS12*/*PpHAM* was also characterized in the moss *Physcomitrium* (*Physcomitrella*) *patens* (Beheshti et al., 2021). Overexpression of *PpGRAS12* leads to formation of supernumerary apical meristems on each gametophore, suggesting a positive role of *PpGRAS12*/*PpHAM* in control of stem cell population at the gametophyte stage (Beheshti et al., 2021). Taken together, all the current results lead to a hypothesis that regulation of stem cell homeostasis is an ancestral and conserved trait of the *HAM* gene family, which deserves more functional studies of *HAM* homologs in land plants, especially in seed-free plants. Recent advances in the genomic and transcriptomic resources (Marchant et al., 2019; Geng et al., 2021a), established transformation system (Plackett et al., 2014) and quantitative confocal imaging platform (Wu et al., 2021) in seed-free vascular plants, such as in *Ceratopteris richardii*, will facilitate us to test this hypothesis and further understand meristem evolution in land plants.

CONSERVATION AND DIVERSIFICATION OF THE *MIR171-HAM* REGULATION IN LAND PLANTS

The phylogenetic analysis and sequence alignment demonstrate that the 21-nt miR171 binding site (5′-GATATTGGCGCGGC TCAATCA-3′) is highly conserved within the coding sequences of the non-flowering *HAM* members and the majority of Type II *HAM* members in flowering plants (Engstrom et al., 2011; Geng et al., 2021b). The negative regulation of Type II *HAM* members by miR171 seems to be conserved in flowering plants as well. For example, transcripts of two *HAM* family genes (*SlHAM1* and *SlHAM2*) in tomato (*Solanum lycopersicum*) and four *HAM* homologs in rice (*Oryza sativa*) are also specifically targeted and cleaved by miR171 (Fan et al., 2015; Hendelman et al., 2016). Overexpression of *MIR171* genes in tomato and rice results in reduced expression of these *HAM* homologs and the disruption of meristem development (Fan et al., 2015; Hendelman et al., 2016).

Furthermore, when the non-flowering HAM members (such as *PpHAM*, *SmHAM*, *CrHAM*, and *LkHAM*) and several Type II HAM members from flowering plants (including *Amborella*, the monocot rice, and the dicot soybean and pepper) are expressed under the control of Arabidopsis *HAM2* promoter, these HAM reporters showed the concentration gradient from low to high along the apical-basal axis of Arabidopsis SAMs (Geng and Zhou, 2021; Geng et al., 2021b). These expression patterns are largely comparable to that of the miR171-sensitive *HAM2* translational reporter (Han et al., 2020a; Geng et al., 2021b); however, they are different from that of the miR171-insenstive *HAM2* transcriptional reporter, which shows high expression in all the cells from different layers in Arabidopsis SAMs (Han et al., 2020a). These findings suggest a conserved role of the miR171 binding sites in the non-flowering HAM members and in the majority of Type II HAM members from flowering plants.

Different from the Type II, Type I *HAM* genes show different extents of diversification in the miR171 binding site (Engstrom et al., 2011; Geng et al., 2021b). Based on the sequence alignment (Geng et al., 2021b), only a few Type I *HAM* members (such as *AmHAM1* from *Amborella trichopoda* and the *HAM* homologs from *Nelumbo nucifera* and *Vitis vinifera*) maintain the conserved miR171 binding site, and many others from a considerable number of flowering plants lost the conservation of the miR171 binding site. For example, *HAM4* (the Arabidopsis Type I *HAM*) contains six nucleotides different from the conserved miR171 binding sequence and is unlikely targeted by miR171 (Engstrom et al., 2011; Geng et al., 2021b).

FUTURE PERSPECTIVES

Over the last several years, significant progress has been made in understanding the functions of Type II HAM members in shoot meristems and their interaction with the WUS-CLV3 loop, the regulatory mechanism by which Type II HAM proteins are excluded from stem cells in Arabidopsis SAMs, and evolution of different groups of HAM members in land plants. In the

future, several important questions are still remaining to be explored. For example, in Arabidopsis SAMs, in contrast to *WUS* and *CLV3* that are specifically expressed in a few cells, HAM1 and HAM2 proteins are expressed in a broader domain (Zhou et al., 2015, 2018; Han et al., 2020a). It will be interesting to explore whether the Type II HAM members also integrate additional and multiple regulatory pathways in control of shoot stem cells. In addition, the L1-miR171-HAM signaling cascade plays a crucial role during the initiation and maintenance of Arabidopsis shoot meristems (Han et al., 2020c). It will be worth determining whether this signaling cascade also functions in other meristematic tissues in Arabidopsis and whether this regulatory mechanism is conserved across flowering plants or even in non-flowering plants. Furthermore, the function of Type I HAM members is not completely understood yet. Determining whether and how this group of HAM members have been recruited into various developmental processes and undergone neofunctionalization in land plants will be an essential question in the future.

AUTHOR CONTRIBUTIONS

All authors listed have made a substantial, direct and intellectual contribution to the work, and approved it for publication.

FUNDING

This work was supported by the Purdue start-up package and National Science Foundation IOS-1931114 (to YZ), and the Purdue Center for Plant Biology Graduate Student Fellowship and Ross-Lynn Graduate Research Scholarship (to YG).

ACKNOWLEDGMENTS

We apologize to the colleagues whose work was not cited in this review due to the space limitation.

REFERENCES

Barton, M. K. (2010). Twenty years on: the inner workings of the shoot apical meristem, a developmental dynamo. *Dev. Biol.* 341, 95–113. doi: 10.1016/j.ydbio.2009.11.029

Beheshti, H., Strotbek, C., Arif, M.A., Klingl, A., Top, O., and Frank, W. (2021). *PpGRAS12* acts as a positive regulator of meristem formation in *Physcomitrium patens*. *Plant Mol. Biol.* doi: 10.1007/s11103-021-01125-z, [Epub ahead of print].

Biedermann, S., and Laux, T. (2018). Plant development: adding HAM to stem cell control. *Curr. Biol.* 28, R1261–R1263. doi: 10.1016/j.cub.2018.09.039

Brand, U., Fletcher, J. C., Hobe, M., Meyerowitz, E. M., and Simon, R. (2000). Dependence of stem cell fate in *Arabidopsis* on a feedback loop regulated by CLV3 activity. *Science* 289, 617–619. doi: 10.1126/science.289.5479.617

Brand, U., Grünewald, M., Hobe, M., and Simon, R. (2002). Regulation of CLV3 expression by two homeobox genes in *Arabidopsis*. *Plant Physiol.* 129, 565–575. doi: 10.1104/pp.001867

Daum, G., Medzihradszky, A., Suzaki, T., and Lohmann, J. U. (2014). A mechanistic framework for noncell autonomous stem cell induction in *Arabidopsis*. *Proc. Natl. Acad. Sci. U. S. A.* 111, 14619–14624. doi: 10.1073/pnas.1406446111

David-Schwartz, R., Borovsky, Y., Zemach, H., and Paran, I. (2013). CaHAM is autoregulated and regulates CaSTM expression and is required for shoot apical meristem organization in pepper. *Plant Sci.* 203-204, 8–16. doi: 10.1016/j.plantsci.2012.12.011

Engstrom, E. M., Andersen, C. M., Gumulak-Smith, J., Hu, J., Orlova, E., Sozzani, R., et al. (2011). Arabidopsis homologs of the Petunia *HAIRY MERISTEM* gene are required for maintenance of shoot and root indeterminacy. *Plant Physiol.* 155, 735–750. doi: 10.1104/pp.110.168757

Fan, T., Li, X., Yang, W., Xia, K., Ouyang, J., and Zhang, M. (2015). Rice Osa-miR171c mediates phase change from vegetative to reproductive development and shoot apical meristem maintenance by repressing four OsHAM transcription factors. *PLoS One* 10:e0125833. doi: 10.1371/journal.pone.0125833

Fletcher, J. C. (2018). The CLV-WUS stem cell signaling pathway: a roadmap to crop yield optimization. *Plants* 7:87. doi: 10.3390/plants7040087

Foster, A. S. (1938). Structure and growth of the shoot apex in *Ginkgo Biloba*. *Bull. Torrey. Bot. Club* 65, 531–556. doi: 10.2307/2480793

Gaillochet, C., and Lohmann, J. U. (2015). The never-ending story: from pluripotency to plant developmental plasticity. *Development* 142, 2237–2249. doi: 10.1242/dev.117614

Geng, Y., Cai, C., Mcadam, S. A. M., Banks, J. A., Wisecaver, J. H., and Zhou, Y. (2021a). A de novo transcriptome assembly of *Ceratopteris richardii* provides insights into the evolutionary dynamics of complex gene families in land plants. *Genome Biol. Evol.* 13:evab042. doi: 10.1093/gbe/evab042

Geng, Y., Guo, L., Han, H., Liu, X., Ann Banks, J., Wisecaver, J. H., et al. (2021b). Conservation and diversification of *HAIRY MERISTEM* gene family in land plants. *Plant J.* 106, 366–378. doi: 10.1111/tpj.15169

Geng, Y., and Zhou, Y. (2021). N-terminal region is required for functions of the HAM family member. *Plant Signal. Behav.* 16:1940001. doi: 10.1080/15592324.2021.1940001

Graf, P., Dolzblasz, A., Würschum, T., Lenhard, M., Pfreundt, U., and Laux, T. (2010). *MGOUN1* encodes an *Arabidopsis* type IB DNA topoisomerase required in stem cell regulation and to maintain developmentally regulated gene silencing. *Plant Cell* 22, 716–728. doi: 10.1105/tpc.109.068296

Gruel, J., Deichmann, J., Landrein, B., Hitchcock, T., and Jönsson, H. (2018). The interaction of transcription factors controls the spatial layout of plant aerial stem cell niches. *NPJ Syst. Biol. Appl.* 4:36. doi: 10.1038/s41540-018-0072-1

Han, H., Geng, Y., Guo, L., Yan, A., Meyerowitz, E. M., Liu, X., et al. (2020a). The overlapping and distinct roles of HAM family genes in *Arabidopsis* shoot meristems. *Front. Plant Sci.* 11:541968. doi: 10.3389/fpls.2020.541968

Han, H., Liu, X., and Zhou, Y. (2020b). Transcriptional circuits in control of shoot stem cell homeostasis. *Curr. Opin. Plant Biol.* 53, 50–56. doi: 10.1016/j.pbi.2019.10.004

Han, H., Yan, A., Li, L., Zhu, Y., Feng, B., Liu, X., et al. (2020c). A signal cascade originated from epidermis defines apical-basal patterning of *Arabidopsis* shoot apical meristems. *Nat. Commun.* 11:1214. doi: 10.1038/s41467-020-14989-4

Hendelman, A., Kravchik, M., Stav, R., Frank, W., and Arazi, T. (2016). Tomato *HAIRY MERISTEM* genes are involved in meristem maintenance and compound leaf morphogenesis. *J. Exp. Bot.* 67, 6187–6200. doi: 10.1093/jxb/erw388

Kieber, J. J., and Schaller, G. E. (2018). Cytokinin signaling in plant development. *Development* 145:dev149344. doi: 10.1242/dev.149344

Liu, Z., Shpak, E. D., and Hong, T. (2020). A mathematical model for understanding synergistic regulations and paradoxical feedbacks in the shoot apical meristem. *Comput. Struct. Biotechnol. J.* 18, 3877–3889. doi: 10.1016/j.csbj.2020.11.017

Llave, C., Xie, Z., Kasschau, K. D., and Carrington, J. C. (2002). Cleavage of *scarecrow-like* mRNA targets directed by a class of *Arabidopsis* miRNA. *Science* 297, 2053–2056. doi: 10.1126/science.1076311

Marchant, D. B., Sessa, E. B., Wolf, P. G., Heo, K., Barbazuk, W. B., Soltis, P. S., et al. (2019). The C-Fern (*Ceratopteris richardii*) genome: insights into plant genome evolution with the first partial homosporous fern genome assembly. *Sci. Rep.* 9:18181. doi: 10.1038/s41598-019-53968-8

Mayer, K. F. X., Schoof, H., Haecker, A., Lenhard, M., Jürgens, G., and Laux, T. (1998). Role of *WUSCHEL* in regulating stem cell fate in the *Arabidopsis* shoot meristem. *Cell* 95, 805–815. doi: 10.1016/S0092-8674(00)81703-1

Meyerowitz, E. M. (1997). Genetic control of cell division patterns in developing plants. *Cell* 88, 299–308. doi: 10.1016/S0092-8674(00)81868-1

Plackett, A. R. G., Huang, L., Sanders, H. L., and Langdale, J. A. (2014). High-efficiency stable transformation of the model fern species *Ceratopteris*

richardii via microparticle bombardment. *Plant Physiol.* 165, 3–14. doi: 10.1104/pp.113.231357

Rhoades, M. W., Reinhart, B. J., Lim, L. P., Burge, C. B., Bartel, B., and Bartel, D. P. (2002). Prediction of plant microRNA targets. *Cell* 110, 513–520. doi: 10.1016/S0092-8674(02)00863-2

Sablowski, R. (2007). The dynamic plant stem cell niches. *Curr. Opin. Plant Biol.* 10, 639–644. doi: 10.1016/j.pbi.2007.07.001

Satina, S., Blakeslee, A. F., and Avery, A. G. (1940). Demonstration of the three germ layers in the shoot apex of *Datura* by means of induced polyploidy in periclinal chimeras. *Am. J. Bot.* 27, 895–905. doi: 10.1002/j.1537-2197.1940.tb13952.x

Schoof, H., Lenhard, M., Haecker, A., Mayer, K. F. X., Jürgens, G., and Laux, T. (2000). The stem cell population of *Arabidopsis* shoot meristems is maintained by a regulatory loop between the *CLAVATA* and *WUSCHEL* genes. *Cell* 100, 635–644. doi: 10.1016/S0092-8674(00)80700-X

Schulze, S., Schäfer, B. N., Parizotto, E. A., Voinnet, O., and Theres, K. (2010). *LOST MERISTEMS* genes regulate cell differentiation of central zone descendants in *Arabidopsis* shoot meristems. *Plant J.* 64, 668–678. doi: 10.1111/j.1365-313X.2010.04359.x

Shi, B., and Vernoux, T. (2021). Hormonal control of cell identity and growth in the shoot apical meristem. *Curr. Opin. Plant Biol.* 65:102111. doi: 10.1016/j.pbi.2021.102111

Shpak, E. D. (2013). Diverse roles of *ERECTA* family genes in plant development. *J. Integr. Plant Biol.* 55, 1238–1250. doi: 10.1111/jipb.12108

Somssich, M., Je, B. I., Simon, R., and Jackson, D. (2016). CLAVATA-WUSCHEL signaling in the shoot meristem. *Development* 143, 3238–3248. doi: 10.1242/dev.133645

Stuurman, J., Jäggi, F., and Kuhlemeier, C. (2002). Shoot meristem maintenance is controlled by a GRAS-gene mediated signal from differentiating cells. *Genes Dev.* 16, 2213–2218. doi: 10.1101/gad.230702

Su, Y.-H., Liu, Y.-B., and Zhang, X.-S. (2011). Auxin–cytokinin interaction regulates meristem development. *Mol. Plant* 4, 616–625. doi: 10.1093/mp/ssr007

Takanashi, H., Sumiyoshi, H., Mogi, M., Hayashi, Y., Ohnishi, T., and Tsutsumi, N. (2018). miRNAs control HAM1 functions at the single-cell-layer level and are essential for normal embryogenesis in *Arabidopsis*. *Plant Mol. Biol.* 96, 627–640. doi: 10.1007/s11103-018-0719-8

Wang, L., Mai, Y. X., Zhang, Y. C., Luo, Q., and Yang, H. Q. (2010). MicroRNA171c-targeted *SCL6-II*, *SCL6-III*, and *SCL6-IV* genes regulate shoot branching in *Arabidopsis*. *Mol. Plant* 3, 794–806. doi: 10.1093/mp/ssq042

Willoughby, A. C., and Nimchuk, Z. L. (2021). WOX going on: CLE peptides in plant development. *Curr. Opin. Plant Biol.* 63:102056. doi: 10.1016/j.pbi.2021.102056

Wu, X., Yan, A., Mcadam, S. A. M., Banks, J. A., Zhang, S., and Zhou, Y. (2021). Timing of meristem initiation and maintenance determines the morphology of fern gametophytes. *J. Exp. Bot.* 72, 6990–7001. doi: 10.1093/jxb/erab307

Yadav, R. K., Perales, M., Gruel, J., Girke, T., Jonsson, H., and Reddy, G. V. (2011). WUSCHEL protein movement mediates stem cell homeostasis in the *Arabidopsis* shoot apex. *Genes Dev.* 25, 2025–2030. doi: 10.1101/gad.17258511

Zhou, Y., Liu, X., Engstrom, E. M., Nimchuk, Z. L., Pruneda-Paz, J. L., Tarr, P. T., et al. (2015). Control of plant stem cell function by conserved interacting transcriptional regulators. *Nature* 517, 377–380. doi: 10.1038/nature13853

Zhou, Y., Yan, A., Han, H., Li, T., Geng, Y., Liu, X., et al. (2018). HAIRY MERISTEM with WUSCHEL confines CLAVATA3 expression to the outer apical meristem layers. *Science* 361, 502–506. doi: 10.1126/science.aar8638

Conflict of Interest: The authors declare that the research was conducted in the absence of any commercial or financial relationships that could be construed as a potential conflict of interest.

Publisher's Note: All claims expressed in this article are solely those of the authors and do not necessarily represent those of their affiliated organizations, or those of the publisher, the editors and the reviewers. Any product that may be evaluated in this article, or claim that may be made by its manufacturer, is not guaranteed or endorsed by the publisher.

frontiers in Plant Science

ORIGINAL RESEARCH
published: 05 January 2022
doi: 10.3389/fpls.2021.808136

Analysis of Genetic Regions Related to Field Grain Number per Spike From Chinese Wheat Founder Parent Linfen 5064

Ling Qiao[1,2†], Hanlin Li[1,2†], Jie Wang[2], Jiajia Zhao[2], Xingwei Zheng[2], Bangbang Wu[2], Weijun Du[1], Juanling Wang[1*] and Jun Zheng[2*]*

[1] College of Agronomy, State Key Laboratory of Sustainable Dryland Agriculture (in Preparation), Shanxi Agricultural University, Jinzhong, China, [2] Institute of Wheat Research, Shanxi Agricultural University, Linfen, China

OPEN ACCESS

Edited by:
Xia Cui,
Insititute of Vegetables and Flowers, Chinese Academy of Agricultural Sciences (CAAS), China

Reviewed by:
Yongzhen Wu,
Ludong University, China
Jianhui Wu,
Northwest A&F University, China

***Correspondence:**
Weijun Du
duweijun68@126.com
Juanling Wang
13994267508@163.com
Jun Zheng
sxnkyzj@126.com

† These authors have contributed equally to this work

Specialty section:
This article was submitted to Crop and Product Physiology, a section of the journal Frontiers in Plant Science

Received: *03 November 2021*
Accepted: *29 November 2021*
Published: *05 January 2022*

Citation:
Qiao L, Li H, Wang J, Zhao J, Zheng X, Wu B, Du W, Wang J and Zheng J (2022) Analysis of Genetic Regions Related to Field Grain Number per Spike From Chinese Wheat Founder Parent Linfen 5064. Front. Plant Sci. 12:808136. doi: 10.3389/fpls.2021.808136

Wheat founder parents have been important in the development of new wheat cultivars. Understanding the effects of specific genome regions on yield-related traits in founder variety derivatives can enable more efficient use of these genetic resources through molecular breeding. In this study, the genetic regions related to field grain number per spike (GNS) from the founder parent Linfen 5064 were analyzed using a doubled haploid (DH) population developed from a cross between Linfen 5064 and Nongda 3338. Quantitative trait loci (QTL) for five spike-related traits over nine experimental locations/years were identified, namely, total spikelet number per spike (TSS), base sterile spikelet number per spike (BSSS), top sterile spikelet number per spike (TSSS), fertile spikelet number per spike (FSS), and GNS. A total of 13 stable QTL explaining 3.91–19.51% of the phenotypic variation were found. The effect of six of these QTL, *Qtss.saw-2B.1*, *Qtss.saw-2B.2*, *Qtss.saw-3B*, *Qfss.saw-2B.2*, *Qbsss.saw-5A.1*, and *Qgns.saw-1A*, were verified by another DH population (Linfen 5064/Jinmai 47), which showed extreme significance ($P < 0.05$) in more than three environments. No homologs of reported grain number-related from grass species were found in the physical regions of *Qtss.saw-2B.1* and *Qtss.saw-3B*, that indicating both of them are novel QTL, or possess novel-related genes. The positive alleles of *Qtss.saw-2B.2* from Linfen 5064 have the larger effect on TSS (3.30%, 0.62) and have 66.89% in Chinese cultivars under long-term artificial selection. This study revealed three key regions for GNS in Linfen 5064 and provides insights into molecular marker-assisted breeding.

Keywords: founder parent, Linfen 5064, wheat, grain number per spike, quantitative trait locus

INTRODUCTION

Founder parents are not only successful cultivars that are cultivated in large areas but are also used extensively as parents in breeding programs. These valuable genetic resources are crucial to Chinese wheat breeding programs (Zhuang, 2003). Analyzing the genetic diversity of founder parents and the genetic basis of their widespread success can provide a foundation for more efficient use of these germplasm resources.

A Chinese wheat founder parent named Linfen 5064 is the pedigree of more than 80 high-quality strong gluten cultivars in China. Linfen 5064 has the strong-gluten trait, a high grain number per spike (GNS), and excellent agronomic traits (Qiao et al., 2018). Linfen 5064 and cultivars derived from it not only have high yields but have also been used as the main parents for improving wheat quality in Chinese breeding programs. The use of Linfen 5064 as the founder parent addressed three difficult points in the breeding for strong-gluten wheat (Qiao et al., 2018). The first difficultly is that quality is negatively correlated with GNS and thousand kernel weight (TKW). Chinese wheat cultivars with premium grain quality, such as Xinong 20, Fengdecun 5, Shiluan 02-1 and Jimai 20, usually have lower GNS and lower yields. The GNS of Linfen 5064 and cultivars and lines derived from it have higher yields than other high-quality cultivars. The second difficult point is that dwarfism is associated with late maturity. Linfen 5064 does not show this association as it matures early and is a semi-dwarf height of about 75 cm. Finally, Linfen 5064 overcomes the need to have the glutenin subunit combination 5 + 10 for good quality, since it lacks these subunits yet still has good quality. Therefore, the utilization of valuable traits of Linfen 5064, and the successful future breeding program of Wheat, it is essential to explore and analyze their genetic base.

In most wheat cultivars, a spike usually generates more than 10–20 spikelets, and each spikelet can differentiate into 9–10 florets (Cui et al., 2008). The differentiation of bract and floret primordia determines the number of spikelets and initial florets. During floret development, 60–80% of the initial florets either abort or otherwise lose fertility (Guo et al., 2015). The number of surviving florets which can eventually develop into grains determines the number of grains per spike (Zhang et al., 2021). GNS shows high heritability (Isham et al., 2021). Increasing GNS is an important way to increase grain yield. GNS can be divided into total spikelet number per spike (TSS), fertile spikelet number per spike (FSS), base sterile spikelet number per spike (BSSS), top sterile spikelet number per spike (TSSS), and grains per spikelet. The heritability of TSS was higher (Isham et al., 2021), but the number of grains per spikelet and spikelet propagation ability were greatly affected by the environment. The map-based cloning of common wheat genes lags that of other crops because of wheat's large genome size. Consequently, most studies focus on the quantitative trait loci (QTL) level of analysis, especially genes/QTL that control yield traits.

Hundreds of QTL for GNS have been found to be distributed across the 21 wheat chromosomes (Börner et al., 2002; Huang et al., 2006; Narasimhamoorthy et al., 2006; Li et al., 2007; Ma et al., 2007; Wu et al., 2012; Jia et al., 2013; Zhang et al., 2016; Cui et al., 2017; Guan et al., 2018; Keeble-Gagnere et al., 2018; Onyemaobi et al., 2018; Su et al., 2018; Deng et al., 2019; Fan et al., 2019; Liu et al., 2019; Yao et al., 2019). Some genes related to GNS had been reported, such as homology-based cloned genes *TaTAR2.1-3A* (Shao et al., 2017), *TaCWI-4A* (Jiang et al., 2015), *TaMOC1-7A* (Zhang et al., 2015), *TaSnRK2.9-5A* (Rehman et al., 2019), *TaAPO-A1* (Muqaddasi et al., 2019), *TaGW8-B1* (Yan et al., 2019), *TaPHR3-A1* (Zheng et al., 2020), the *Q* gene (Chuck et al., 1998; Debernardi et al., 2017; Xie et al., 2018), and genes *GNI-A1* (Sakuma et al., 2019) and *WFZP* identified *via* map-based cloning (Du et al., 2021). Genes for other traits of agronomic importance, such as flowering time (FT) and plant height (PH), can have significant effects on grain yield (Cuthbert et al., 2008; Zhou et al., 2017; Guan et al., 2018). *Ppd-1* participates in the regulation of flower spike development in wheat, which affects the number of spikes and seed setting (Boden et al., 2015).

Although many QTL/genes associated with GNS have been reported in wheat, the major and stable QTL identified under multiple environments are still limited. In addition, the biparents used for mapping were mostly accessions aim at certain traits rather than founder cultivars, the use of QTL identified need long-term backcross process which is time-consuming and low efficiency. We especially used founder parent and core cultivars in breeding as biparents for mapping, the loci obtained and markers developed are easily used in breeding, also provide evidence on utilization of the derivatives. Two doubled haploid (DH) populations (Linfen 5064 × Nongda 3338 and Linfen 5064 × Jinmai 47) were analyzed for five GNS-related traits over the nine experimental locations/years to (1) identify and validate major, stable QTL for GNS that can be used for molecular marker-assisted breeding and (2) identify genetic regions associated with GNS of Linfen 5064, elucidate the genetic mechanism of GNS in the founder parent, and discover favorable allele variations.

MATERIALS AND METHODS

Plant Materials

A total of two DH populations were used, 192 lines from the cross Linfen 5064 × Nongda 3338 (LN) and 194 lines from the cross Linfen 5064 × Jinmai 47 (LJ). Linfen 5064 is a Chinese wheat founder parent with strong gluten, a high GNS, and an excellent array of other characteristics (Qiao et al., 2018). Nongda 3338, developed by China Agricultural University, is a "core parental" breeding line for the North China Winter Wheat Breeding Program with high general combining ability and the dwarfing genes *Rht-B1b* and *Rht-D1b* (Kabir et al., 2015). Jinmai 47 has the advantages of drought tolerance, stable yield, and a high utilization rate of water and fertilizer (Song et al., 2017). The phenotypic difference between the two cultivars and Linfen 5064 was significant and there was obvious trait separation in the population. LN was used for QTL analysis and LJ was used to validate the effects of putative QTL identified in LN.

Field Evaluation

The two DH populations were planted as a single replication in three locations in 2018–2019, 2019–2020, and 2020–2021. Locations were in the Yaodu district in Shanxi province of China, at Linfen (36°08′N, 111°52′E, altitude 450 m) (19 YD, 20 YD, and 21 YD), Hancun (36°25′N, 111°67′E, altitude 450 m) (19 HC, 20 HC, and 21 HC), and Yuncheng (35°15′ N, 110°98′ W, altitude 369 m) (19 YC, 20YC, and 21 YC). The seed was sown in two 1.5 m rows per line spaced 0.3 m apart at 21 seeds per row. Field management practices were those commonly used in wheat production in the region.

TABLE 1 | Phenotypic variation and distribution of five spike-related traits in parents and the doubled haploid (Linfen 5064 × Nongda 3338) in nine field trials.

Traits	Environment	LF 5064	ND 3338	MIN	MAX	Mean	SD	H^2
TSS	19HC	16.47	16.82	13.20	21.60	17.09	1.56	0.90
	20HC	18.12	18.36	15.50	23.20	18.31	1.30	
	21HC	17.07	17.12	13.60	20.80	17.31	1.17	
	19YD	19.13*	21.07*	17.40	23.40	20.34	1.08	
	20YD	20.13	20.87	17.60	25.80	20.31	1.07	
	21YD	19.00**	20.60**	17.40	25.40	20.12	1.20	
	19YC	19.27**	21.65**	16.20	26.00	20.58	1.34	
	20YC	20.60	21.00	16.67	24.20	20.73	1.17	
	21YC	18.80*	20.73*	17.40	24.20	20.16	1.12	
	BLUP	18.83	19.74	17.80	23.12	19.44	0.85	
FSS	19HC	15.72	14.82	12.80	20.30	16.32	1.55	0.89
	20HC	17.12	16.83	14.00	23.20	17.28	1.31	
	21HC	16.60	16.99	12.20	20.20	16.99	1.17	
	19YD	17.20	16.54	9.60	20.20	17.39	1.43	
	20YD	19.40	19.13	16.20	24.40	18.85	1.16	
	21YD	17.73	18.33	15.20	22.80	18.39	1.32	
	19YC	17.87	19.23	13.80	22.20	18.29	1.35	
	20YC	18.53	17.40	14.67	22.00	18.26	1.25	
	21YC	16.40	17.13	13.60	21.80	17.54	1.41	
	BLUP	17.63	18.01	15.13	20.75	17.70	0.78	
TSSS	19HC	0.00	1.27	0.00	2.00	0.23	0.36	0.78
	20HC	0.44*	1.53*	0.00	4.60	0.44	0.55	
	21HC	0.13	0.00	0.00	2.20	0.09	0.24	
	19YD	0.13**	1.40**	0.00	4.40	0.81	0.95	
	20YD	0.20	0.53	0.00	2.00	0.28	0.39	
	21YD	0.33	0.33	0.00	4.00	0.51	0.63	
	19YC	0.20	1.83	0.00	3.80	0.78	0.75	
	20YC	0.67	2.27	0.00	4.40	0.76	0.73	
	21YC	0.20	1.53	0.00	6.40	0.85	1.02	
	BLUP	0.32	1.05	0.13	2.15	0.53	0.32	
BSSS	19HC	0.75	0.73	0.00	2.00	0.53	0.47	0.92
	20HC	0.56	0.00	0.00	2.00	0.59	0.50	
	21HC	0.33	0.13	0.00	1.40	0.22	0.29	
	19YD	1.80	3.13	0.60	4.40	2.14	0.81	
	20YD	0.53	1.20	0.00	2.80	1.18	0.56	
	21YD	0.93	1.93	0.00	3.00	1.21	0.58	
	19YC	1.20	0.58	0.00	3.20	1.51	0.57	
	20YC	1.40	1.33	0.20	3.60	1.71	0.63	
	21YC	2.20	2.07	0.00	3.60	1.78	0.67	
	BLUP	1.09	1.23	0.46	2.08	1.21	0.32	
GNS	19HC	53.80*	40.84*	26.00	66.80	47.51	7.34	0.81
	20HC	56.78	47.33	22.80	68.80	47.84	7.36	
	21HC	52.20	45.33	29.20	70.60	52.92	6.54	
	19YD	42.27	34.60	13.20	104.20	37.17	8.20	
	20YD	52.80	47.20	31.20	65.20	44.76	5.94	
	21YD	51.93	37.47	25.00	74.20	45.84	7.63	
	19YC	49.87	45.47	20.80	68.00	44.37	7.73	
	20YC	50.03	37.27	17.20	58.80	42.32	7.60	
	21YC	46.27	33.67	13.50	70.60	42.78	8.67	
	BLUP	49.64	42.69	32.39	54.31	45.04	3.87	

H^2, broad-sense heritability; BLUP, best linear unbiased prediction.
**Significant at $p < 0.05$; **significant at $p < 0.01$.*

Phenotypic Evaluation and Data Analysis

Ten days before harvest, data of five spike traits, TSS, BSSS, TSSS, FSS, and GNS, were collected by randomly choosing 10 plants in each line. FSS = TSS-BSSS-TSSS. The best linear unbiased prediction (BLUP) of target traits in different environments (Smith et al., 1998) and the broad-sense heritability (H^2) were obtained using SAS (SAS Institute, Cary, NC, USA; https://www.sas.com). The SPSS18.0 software (SPSS, Chicago, Illinois, USA; http://en.wikipedia.org/wiki/SPSS) was used to perform Student's *t*-test ($p < 0.05$) and correlation analysis of phenotype values in different environments.

Genetic Map Construction and Linkage Analysis

The two DH and parental lines were genotyped with a 15 K single-nucleotide polymorphism (SNP) panel developed based on 20 resequencing datasets, 1,520 genotyping datasets collected globally from multiple platforms, and publicly released resequencing and exon capture data. These datasets were developed and optimized using GenoBait technology to finally yield 14,868 mSNP regions for use in this study.

The genetic map of LN was constructed using IciMapping 4.1 (Meng et al., 2015) and JoinMap 4.0. Markers were binned if the correlation coefficient between them was 1 using the BIN function in IciMapping 4.1 according to the method reported by Winfield et al. (2016). WinQTLCart version 2.5 (Wang et al., 2012) for composite interval mapping was used to detect QTL. The minimal logarithm of odds (LOD) score to accept the presence of a QTL was set at 2.5. QTL was considered major when more than 10% of the phenotypic variation was explained in at least one environment and it was detected in at least three environments, including the BLUP dataset. QTL either <1 cM apart or sharing common flanking markers were treated as a single locus.

Validation for the Major QTL Identified

Peak SNPs for stable QTL identified in the LN population were genotyped in the LJ population. The differences in spike-related traits between both groups in the LJ population were analyzed with a *t*-test in SAS V8.0.

Genes Identified in the Major QTL

Genes within the target region of major QTL were obtained using the genome browser (JBrowse) on the WheatOmics-bata website http://wheatomics.sdau.edu.cn/ (Ma et al., 2021). Functional annotation and enrichment analysis of genes in these regions were done using the gene ontology (GO) database and the R package cluster Profiler. Analysis of orthologs between wheat and rice used the Triticeae-Gene Tribe website (http://wheat.cau.edu.cn/TGT/). The expVIP public database (http://www.wheat-expression.com/) was used to search for the expression data of genes in 16 tissues and organs, perform log2 conversion processing, and analyze the expression patterns of genes.

The R software package LD heatmap of major QTL was used to draw the linkage disequilibrium heatmap according to the resequencing data in 145 landmark cultivars that were downloaded from http://wheat.cau.edu.cn/WheatUnion/ (Hao et al., 2020).

TABLE 2 | Coefficients of pairwise Pearson correlations among five spike-related traits in the DH population Linfen 5064 × Nongda 3338.

	TSS	FSS	TSSS	BSSS
FSS	0.815**			
TSSS	0.271**	−0.207**		
BSSS	0.328**	−0.073	0.067	
GNS	0.336**	0.630**	−0.437**	−0.162*

*Significance level: ** and * indicate p < 0.01 and 0.05, respectively.*

RESULTS

Phenotypic Variation and Correlations of Five Traits in Nine Environments

Linfen 5064 had lower values for TSS and TSSS, and a higher value of GNS than Nongda 3338 (**Table 1**). The spike traits of the DH population showed continuous variation, suggesting multigene genetic control. The estimated H^2 of five traits ranged from 0.78 to 0.92, indicating that these traits were significantly affected by genetic factors (**Table 1**). The Pearson correlation coefficients among different environments were significant ($P < 0.05$, **Supplementary Table S1**). Better among-environment correlations were observed for TSS than for FSS, TSSS, BSSS, and GNS.

Phenotypic correlations among spike traits were evaluated using the BLUP dataset (**Table 2**). GNS significantly and positively correlated with FSS and TSS. GNS and FSS significantly and negatively correlated with BSSS and TSSS ($p < 0.01$, **Table 2**). The order of correlation coefficient with GNS were FSS (0.630) > TSSS (−0.437) > TSS (0.336) > BSSS (−0.162). These results showed that FSS and TSSS exerted great influence on GNS.

Linkage Map Construction

In total, 841 SNP markers were used for constructing the LN genetic map. The map had 21 linkage groups, a total length of 3045.86 cM, and an average interval distance of 3.62 cM. The D genome had the lowest marker coverage, especially for chromosomes 5D and 6D. The maps of the A, B, and D genomes had, respectively, lengths of 1324.20, 1322.53, and 399.14 cM and densities of 3.99, 3.28, and 3.77 cM/marker (**Supplementary Table S2**).

QTL for Spikelet Number per Spike

A total of 64 QTL for TSS, FSS, TSSS, and BSSS were detected on 18 chromosomes (**Supplementary Table S3**) with 13 stable QTL identified (**Table 3**). QTL were found on all chromosomes except 1D, 6D, and 7D (**Supplementary Table S3**). The QTL explained 3.91–19.51% of the phenotypic variation in different environments. Linfen 5064 alleles contributed 30 of the 64 QTL, and Nongda 3338 contributed 34 alleles. Nine stable QTL, *Qtss.saw-2B.1*, *Qtss.saw-2B.2*, *Qtss.saw-3B*, *Qtss.saw-4A.1*, *Qtss.saw-5A.1*, *Qtss.saw-5D*, *Qfss.saw-2B.2*, *Qbsss.saw-2B.2*, and

TABLE 3 | Stable quantitative trait loci (QTL) detected for total spikelet number per spike (TSS), base sterile spikelet number per spike (BSSS), fertile spikelet number per spike (FSS), and grain number per spike (GNS) in the Linfen 5064 × Nongda 3338-derived doubled haploid population.

Traits	QTL	Trial	Chr.	Peak marker	Left marker	Right marker	Genetic distance (cM)	LOD	R^2 (%)	Add
TSS	*Qtss.saw-2B.1*	20YC	2B	*2B_712761198*	*2B_712761198*	*2B_690211134*	188.803-191.932	5.75	11.75	0.41
		20HC	2B	*2B_690211134*	*2B_712761198*	*2B_690211134*	188.803–191.932	4.49	8.69	0.39
		20YD	2B	*2B_690211134*	*2B_712761198*	*2B_690211134*	188.803–191.932	3.00	5.32	0.26
		21YD	2B	*2B_690211134*	*2B_712761198*	*2B_690211134*	188.803–191.932	2.76	4.59	0.27
	Qtss.saw−2B.2	19YD	2B	*2B_76515060*	*2B_76515060*	*2B_54768734*	278.205–296.593	3.60	5.96	0.27
		20YD	2B	*2B_58866091*	*2B_76515060*	*2B_54768734*	278.205–296.593	6.97	12.99	0.40
		21YD	2B	*2B_58866091*	*2B_76515060*	*2B_54768734*	278.205–296.593	6.60	12.52	0.43
		19YC	2B	*2B_58866091*	*2B_76515060*	*2B_54768734*	278.205–296.593	7.53	13.89	0.51
		20YC	2B	*2B_54768734*	*2B_76515060*	*2B_54768734*	278.205–296.593	4.99	10.66	0.39
		21YC	2B	*2B_58866091*	*2B_76515060*	*2B_54768734*	278.205–296.593	7.33	12.02	0.41
		19HC	2B	*2B_54768734*	*2B_76515060*	*2B_54768734*	278.205–296.593	5.76	13.17	0.59
		20HC	2B	*2B_54768734*	*2B_76515060*	*2B_54768734*	278.205–296.593	2.64	5.81	0.32
		21HC	2B	*2B_53026013*	*2B_76515060*	*2B_54768734*	278.205–296.593	5.20	9.55	0.37
		BLUP	2B	*2B_54768734*	*2B_76515060*	*2B_54768734*	278.205–296.593	8.73	18.45	0.37
	Qtss.saw-3B	19YC	3B	*3B_586733548*	*3B_586733548*	*3B_592271369*	39.632–42.79	3.46	6.07	0.34
		21YC	3B	*3B_586733548*	*3B_586733548*	*3B_592271369*	39.632–42.79	2.72	4.74	0.25
		BLUP	3B	*3B_586733548*	*3B_586733548*	*3B_592271369*	39.632–42.79	3.41	5.42	0.20
	Qtss.saw-4A.1	19HC	4A	*4A_119796282*	*4A_466206488*	*4A_200909913*	42.02–43.583	5.51	9.52	0.50
		21HC	4A	*4A_200909913*	*4A_444151741*	*4A_290138679*	42.541–44.625	3.95	7.27	0.51
		21YD	4A	*4A_444151741*	*4A_466206488*	*4A_200909913*	42.02–43.583	6.50	11.90	0.33
		BLUP	4A	*4A_444151741*	*4A_466206488*	*4A_200909913*	42.02–43.583	4.26	6.34	0.23
	Qtss.saw−5A.1	21HC	5A	*5A_455140212*	*5A_456278473*	*5A_455140212*	182.321–184.952	3.03	5.42	−0.27
		20YC	5A	*5A_455140212*	*5A_456278473*	*5A_455140212*	182.321–184.952	2.93	5.47	−0.28
		21YC	5A	*5A_455140212*	*5A_456278473*	*5A_455140212*	182.321–184.952	3.41	6.71	−0.29
		BLUP	5A	*5A_455140212*	*5A_456278473*	*5A_455140212*	182.321–184.952	2.58	3.91	−0.17
	Qtss.saw-5D	19YD	5D	*5D_147564473*	*5D_314429199*	*5D_147564473*	5.748–12.53	7.10	12.77	−0.39
		20YD	5D	*5D_147564473*	*5D_314429199*	*5D_147564473*	5.748–12.53	4.10	7.12	−0.29
		BLUP	5D	*5D_147564473*	*5D_314429199*	*5D_147564473*	5.748–12.53	4.82	7.96	−0.24
FSS	*Qfss.saw-2B.2*	19YD	2B	*2B_76515060*	*2B_76515060*	*2B_54768734*	278.205–296.593	3.08	8.26	0.46
		20YD	2B	*2B_76515060*	*2B_76515060*	*2B_54768734*	278.205–296.593	6.60	15.65	0.47
		19YC	2B	*2B_76515060*	*2B_76515060*	*2B_54768734*	278.205–296.593	7.06	13.69	0.50
		21YC	2B	*2B_76515060*	*2B_76515060*	*2B_54768734*	278.205–296.593	3.47	6.29	0.36
		19HC	2B	*2B_76515060*	*2B_76515060*	*2B_54768734*	278.205–296.593	3.81	8.44	0.47
		BLUP	2B	*2B_76515060*	*2B_76515060*	*2B_54768734*	278.205–296.593	6.93	17.70	0.39
BSSS	*Qbsss.saw−2B.2*	19YD	2B	*2B_76515060*	*2B_76515060*	*2B_54768734*	278.205–296.593	11.02	19.51	0.37
		20YC	2B	*2B_76515060*	*2B_76515060*	*2B_54768734*	278.205–296.593	3.30	6.80	0.18
		19HC	2B	*2B_60980426*	*2B_76515060*	*2B_54768734*	278.205–296.593	3.49	6.84	0.13
		20HC	2B	*2B_60980426*	*2B_76515060*	*2B_54768734*	278.205–296.593	2.87	4.86	0.11
		BLUP	2B	*2B_76515060*	*2B_76515060*	*2B_54768734*	278.205–296.593	6.96	11.12	0.11
	Qbsss.saw−5A.1	19HC	5A	*5A_682703894*	*5A_682703894*	*5A_684699297*	0–6.813	3.15	6.46	−0.12
		20HC	5A	*5A_682703894*	*5A_682703894*	*5A_684699297*	0–6.813	3.98	7.37	−0.14
		19YC	5A	*5A_684699297*	*5A_682703894*	*5A_684699297*	0–6.813	3.79	8.64	−0.17
		BLUP	5A	*5A_682703894*	*5A_682703894*	*5A_684699297*	0–6.813	5.35	8.68	−0.10
GNS	*Qgns.saw−5B.2*	19YD	5B	*5B_603868252*	*5B_610798888*	*5B_654359522*	275.112–310.501	3.73	5.34	−2.06
		21YC	5B	*5B_654359522*	*5B_610798888*	*5B_654359522*	275.112–310.501	3.30	7.20	−2.41
		BLUP	5B	*5B_603868252*	*5B_610798888*	*5B_654359522*	275.112–310.501	4.31	8.21	−1.17
	Qgns.saw-7A.1	19YD	7A	*7A_658134960*	*7A_657918003*	*7A_658134960*	112.675–113.208	2.78	4.55	1.79
		19YC	7A	*7A_657918003*	*7A_657918003*	*7A_675589691*	112.675–113.208	2.83	5.42	1.86
		20YC	7A	*7A_657918003*	*7A_657918003*	*7A_675589691*	112.675–136.68	3.25	6.80	1.99

(Continued)

TABLE 3 | Continued

Traits	QTL	Trial	Chr.	Peak marker	Left marker	Right marker	Genetic distance (cM)	LOD	R^2 (%)	Add
		21HC	7A	*7A_657918003*	*7A_657918003*	*7A_675589691*	112.675–136.68	5.19	9.94	2.13
		BLUP	7A	*7A_658134960*	*7A_657918003*	*7A_658134960*	112.675–113.208	4.06	9.44	1.20
	Qgns.saw-4D	21YC	4D	*4D_15772687*	*4D_15772687*	*4D_48697668*	0–7.629	4.27	7.66	−2.46
		20YC	4D	*4D_48697668*	*4D_15772687*	*4D_48697668*	0–7.629	3.43	6.71	−2.02
		19HC	4D	*4D_193777167*	*4D_15772687*	*4D_48697668*	0–7.629	5.63	10.80	−2.44
	Qgns.saw-1A	21YD	1A	*1A_567714120*	*1A_567714120*	*1A_568327780*	0–1.46	3.72	6.60	−2.03
		21HC	1A	1A_568327780	1A_567714120	1A_568327780	0–1.46	5.79	11.16	−0.92
		21YC	1A	1A_568327780	1A_567714120	1A_568327780	0–1.46	2.56	4.47	−2.25
		BLUP	1A	1A_567714120	1A_567714120	1A_568327780	0–1.46	2.75	5.25	−1.88

Qbsss.saw-5A.1 were detected in more than three environments and with BLUP values. Except for *Qtss.saw-3B*, *Qtss.saw-5A.1*, and *Qbsss.saw-5A.1*, the other six QTL explained more than 10% of the phenotypic variance and thus can be considered major stable QTL. The additive effect showed that the alleles of *Qtss.saw-5A.1* and *Qtss.saw-5D* that increased TSS in grain were from Nongda 3338. The six stable QTL *Qtss.saw-2B.1*, *Qtss.saw-2B.2*, *Qtss.saw-3B*, *Qtss.saw-4A.1*, *Qfss.saw-2B.2*, and *Qbsss.saw-2B.2* carried positive alleles from Linfen 5064. *Qtss.saw-2B.2*, *Qfss.saw-2B.2*, and *Qbsss.saw-2B.2* were co-located in the *2B_54768734-2B_76515060* interval.

QTL for Grain Number per Spike

For GNS, 16 QTL were detected and these QTL explained 4.18–15.83% of the phenotypic variance (**Supplementary Table S3**). Four stable QTL, *Qgns.saw-5B.2*, *Qgns.saw-7A.1*, *Qgns.saw-4D*, and *Qgns.saw-1A*, explaining 4.47–11.16% of the phenotypic variance were identified in more than three environments and with BLUP values (**Table 3**). The additive effect of *Qgns.saw-7A.1* was from Linfen 5064 indicating that Linfen 5064 contributed the allele for increased GNS. No stable QTL clusters for GNS and spikelet number per spike were detected on the same chromosome, indicating that the QTL of GNS were most likely independent of spikelet number per spike and therefore have great potential in wheat breeding.

QTL Validation

To further validate the stable QTL, the peak SNPs for each were used to evaluate their effects on corresponding traits in the LJ population. The peak markers for *Qtss.saw-4A.1*, *Qtss.saw-5A.1*, and *Qgns.saw-4D* were not polymorphic between the LJ parents, and thus could not be evaluated. The remaining 10 QTL were evaluated. The effect of *Qtss.saw-5D*, *Qgns.saw-5B.2*, *Qgns.saw-7A.1*, and *Qbsss.saw-2B.2* did not differ significantly between the two groups in the LJ population (**Figure 1**). The effect of other six QTL, *Qtss.saw-2B.1*, *Qtss.saw-2B.2*, *Qfss.saw-2B.2, Qtss.saw-3B*, *Qbsss.saw-5A.1*, and *Qgns.saw-1A*, were highly significant ($P < 0.05$) in more than three environments. According to marker profiles of *Qtss.saw-2B.1*, *Qtss.saw-2B.2*, and *Qtss.saw-3B*, lines with homozygous alleles from Linfen 5064 had significantly higher ($P < 0.05$) values for TSS than those from Nongda 3338 and the difference ranged from 1.14 to 3.65%. The *Qtss.saw-2B.2* lines homozygous for the Linfen 5064 alleles had significantly higher phenotypic values than those with the Jinmai 47 alleles irrespective of QTL region, with differences in TSS ranging from 1.29 to 3.21%. Lines with the positive allele from *Qfss.saw-2B.2* had significantly greater FSS ranging from 0.88 to 3.38%, corresponding to 0.15–0.62 more spikelets than the lines with the alternate allele.

Analyses of Additive Effects of the Major QTL

In the LN population, we detected six stable QTL for TSS (*Qtss.saw-2B.1*, *Qtss.saw-2B.2*, *Qtss.saw-3B*, *Qtss.saw-4A.1*, *Qtss.saw-5A.1*, and *Qtss.saw-5D*), *two* stable QTL for BSSS (*Qbsss.saw-2B.2* and *Qbsss.saw-5A.1*), and four stable QTL for GNS (*Qgns.saw-5B.2*, *Qgns.saw-7A.1*, *Qgns.saw-4D*, and *Qgns.saw-1A*) (**Table 3**). The additive effects of these QTL on corresponding traits were analyzed based on linked markers. The average corresponding trait values increased as the number of positive alleles increased (**Figures 2A–C**). Lines with favorable alleles at all the six QTL regions had an average TSS increase of 2.25 vs. those possessing contrasting alleles (**Supplementary Table S4**, **Figure 2A**). Lines with both the positive alleles had significantly increased values for BSSS (**Figure 2B**). The combination of positive alleles from *Qgns.saw-5B.2*, *Qgns.saw-7A.1*, *Qgns.saw-4D*, and *Qgns.saw-1A* had the largest effect on GNS (**Supplementary Table S4**, **Figure 2C**).

Qtss.saw-2B.1, *Qtss.saw-2B.2*, and *Qtss.saw-3B* were validated in the LJ population, and the positive alleles of three QTL were derived from Linfen 5064, the additive effects on each corresponding trait were analyzed based on linked markers (**Supplementary Table S5**, **Figure 2D**). The combination of positive alleles from *Qtss.saw-2B.1*, *Qtss.saw-2B.2*, and *Qtss.saw-3B* (7.33%, 1.38) had the largest effect on TSS. Compared with lines lacking positive alleles for increased TSS, the positive allele from *Qtss.saw-2B.2* significantly increased TSS by 3.30%, which was higher than that for the other single positive alleles of *Qtss.saw-2B.1* (1.92%, 0.36) and *Qtss.saw-3B* (2.45%, 0.46). DH lines with both *Qtss.saw-2B.1* and *Qtss.saw-3B* positive alleles significantly increased TSS (2.56%, 0.48) less than that of DH lines with single positive alleles of *Qtss.saw-2B.2* (3.30%, 0.62). These results indicated that the positive allele of *Qtss.saw-2B.2* from Linfen 5064 has a larger effect on TSS.

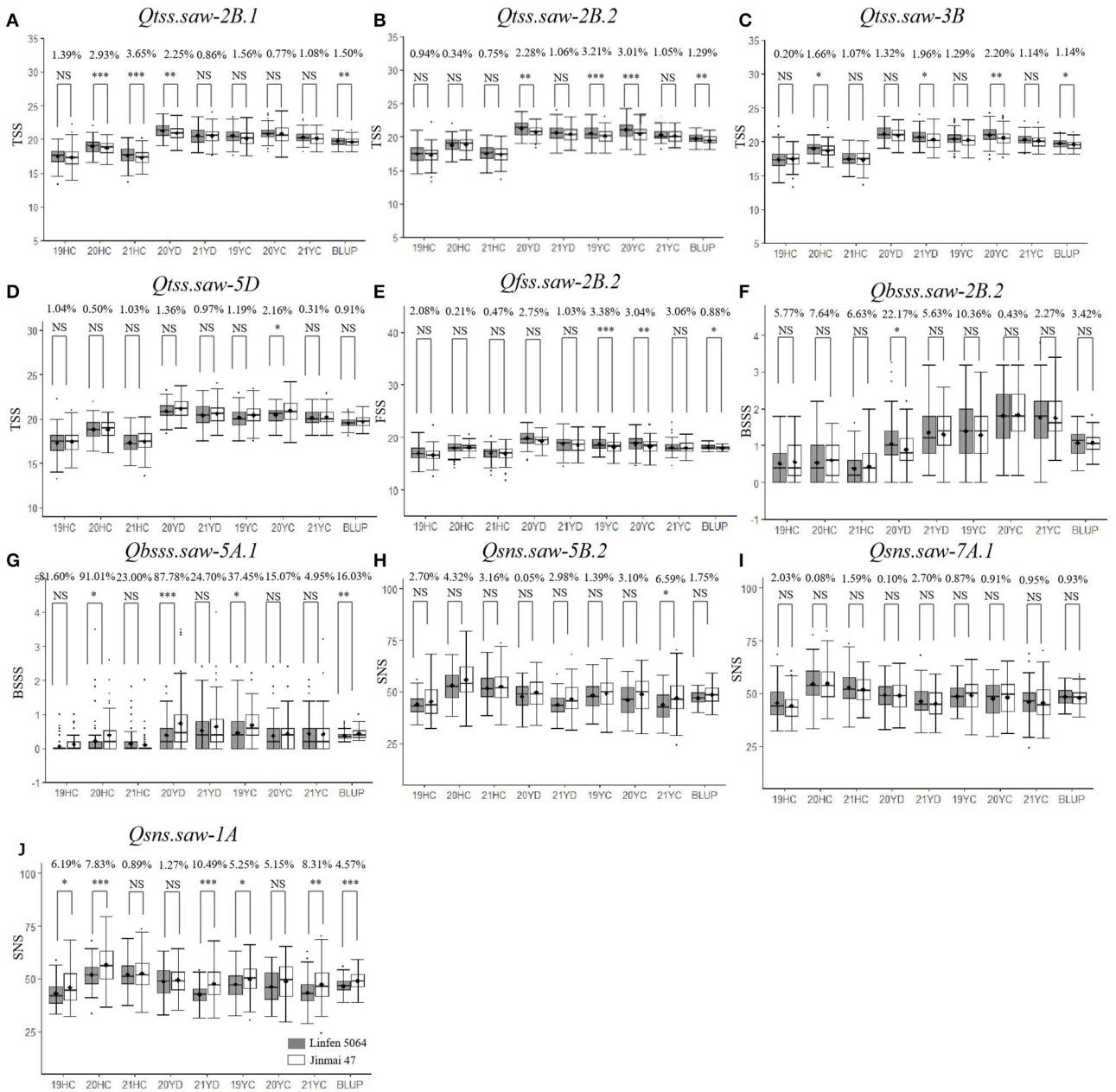

FIGURE 1 | Validation of 10 stable quantitative trait loci (QTL) in LJ population. Effects of **(A)** Qtss.saw-2B.1, **(B)** Qtss.saw-2B.2, **(C)** Qtss.saw-3B, **(D)** Qtss.saw-5D, **(E)** on total spikelet number per spike (TSS) and effects of Qfss.saw-2B.2, **(F)** on fertile spikelet number per spike (FSS) and effects of Qbsss.saw-2B.2, **(G)** Qbsss.saw-5A.1, **(H)** on base sterile spikelet number per spike (BSSS) and effects of Qsns.saw-5B.2, **(I)** Qsns.saw-7A.1, **(J)** and Qsns.saw-1A on grain number per spike (GNS). *, **, *** and NS represent $P < 0.05$, $P < 0.01$, $P < 0.001$ and no significant difference,respectively.

Distribution of Linfen 5064 Favorable Alleles Across Cultivars

The three stable QTL *Qtss.saw-2B.1*, *Qtss.saw-2B.2*, and *Qtss.saw-3B* were detected in more than three environments and were validated in the LJ population. The additive effects of these QTL were from Linfen 5064. Based on the resequencing of 145 wheat cultivars, linkage disequilibrium analysis was performed to assess variation sites within three target QTL regions (**Figure 3**). *Qtss.saw-2B.1*, *Qtss.saw-2B.2*, and *Qtss.saw-3B* had high recombination rates corresponding to recombination hotspot areas. Therefore, for three QTL the distribution of favorable alleles from Linfen 5064 was analyzed in 145 landmark cultivars (**Table 4**). The favorable alleles of Linfen 5064 for *Qtss.saw-2B.2* had a lower proportion in the Chinese landraces

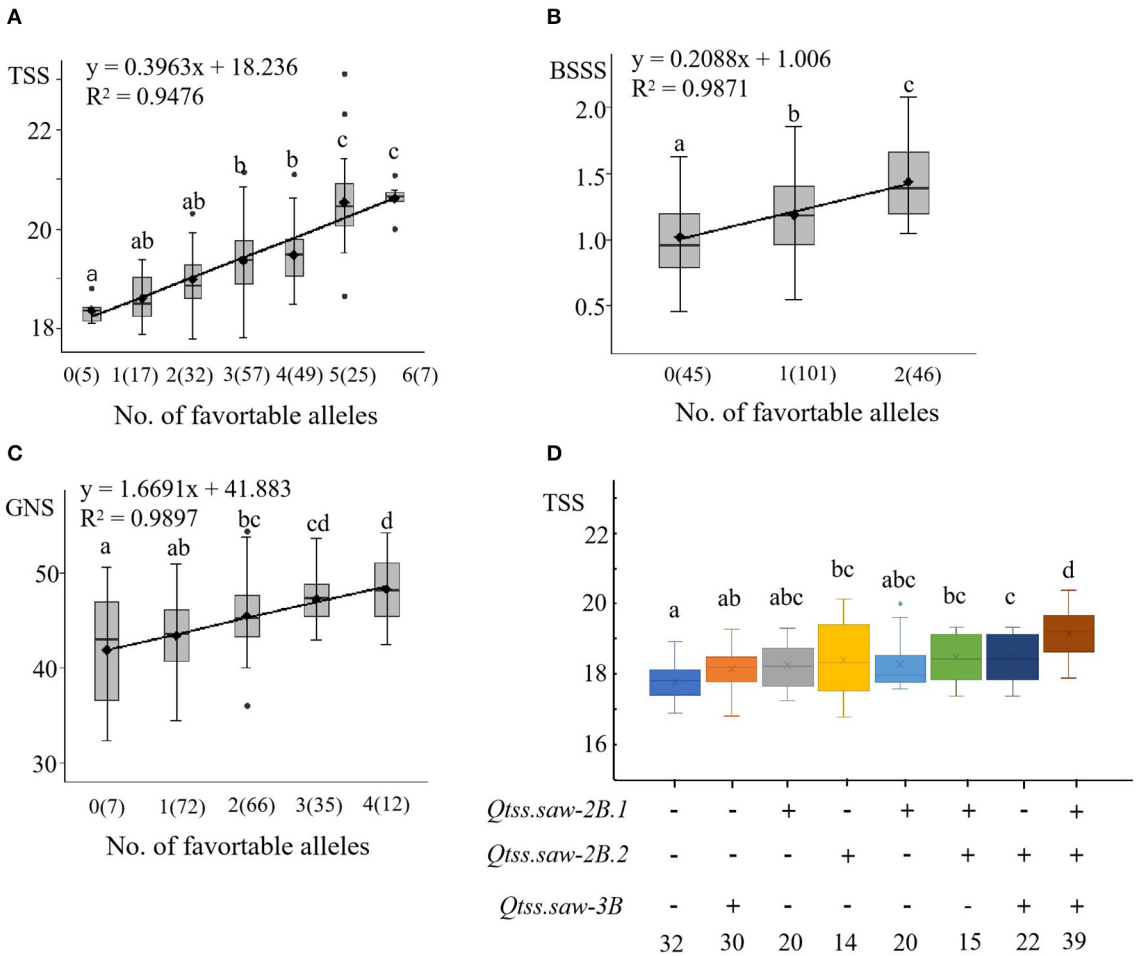

FIGURE 2 | Linear regressions between the number of TSS, BSSS, and GNS **(A–C)** and additive effects of the QTL for TSS **(D)** in the LN population. The numbers of lines carrying the corresponding number of favorable alleles are shown in brackets. The letter above the bars indicated comparisons result at the significant level 0.05, respectively. Plus and minus represent lines with and without the positive alleles of the target QTL based on the flanking markers and the corresponding QTL.

(CL) (44%) and introduced modern cultivars (IMC) (45%), but a higher proportion in the modern Chinese cultivars (MCC) (77%). Therefore, the favorable alleles of Linfen 5064 at the *Qtss.saw-2B.2* locus were selected because of their value in breeding new Chinese cultivars. *Qtss.saw-2B.1* and *Qtss.saw-3B* with the positive Linfen 5064 alleles were less frequent in Chinese landmark cultivars (29.66 and 15.86%, respectively), indicating that *Qtss.saw-3B* landmark alleles tended to be replaced during breeding by the Linfen 5064 alleles.

Genes Identified in the Major QTL

A series of orthologous GNS-related genes have been cloned in rice (Huang et al., 2009; Kyoko et al., 2009; Qiao et al., 2011; Gao et al., 2016) and wheat (Jiang et al., 2015; Zhang et al., 2015; Shao et al., 2017; Muqaddasi et al., 2019; Rehman et al., 2019), these genes always showed conserved functions across grass species (Valluru et al., 2014). Based on the result of local-blast browse through the IWGSC reference sequence, no homologs of the above genes were found in the physical regions of 690.21–712.76 Mb on 2BL and 586.73–592.27 Mb on 3BL in wheat. It indicated that there might be novel genes related to GNS among the two QTL, thus, these QTL were chosen for further analysis. *Qtss.saw-2B.1* was in the interval 690.21–712.76 Mb on 2BL and where 260 genes have been found in the variety Chinese Spring (CS) (**Supplementary Table S6**). Gene annotation, expression pattern, and orthologous gene analysis indicate that three genes are likely involved in spike development (**Supplementary Table S6**, **Supplementary Figure S1**). The function of *TraesCS2B02G500100*, *TraesCS2B02G500200*, and *TraesCS2B02G500300* are annotated as a series of molecular signals generated by the binding of the plant hormone abscisic acid to a receptor and ending with modulation of a cellular process. *Qtss.saw-3B* has 20 genes in CS and 13 common predicated genes between CS and rice (**Supplementary Table S7**). The genes were not preferentially expressed in spike and grain (**Supplementary Figure S2**).

TABLE 4 | The proportion of the Linfen 5064 favorable alleles detected in 145 cultivars *Qtss.saw-2B.1*, *Qtss.saw-2B.2*, and *Qtss.saw-3B*.

QTL	Parent	Allele	CL (%)	IMC (%)	MC (%)	Cultivars (%)
Qtss.saw-2B.1	Linfen 5064	A	20.00	20.00	34.00	29.66
		G	76.00	35.00	43.00	47.59
Qtss.saw-2B.2	Linfen 5064	A	44.00	45.00	77.00	66.90
		C	36.00	50.00	18.00	25.52
Qtss.saw-3B	Linfen 5064	C	8.00	10.00	19.00	15.86
		T	92.00	90.00	81.00	84.14

CL, Chinese landraces, IMC, introduced modern cultivars; MCC, modern Chinese cultivars.

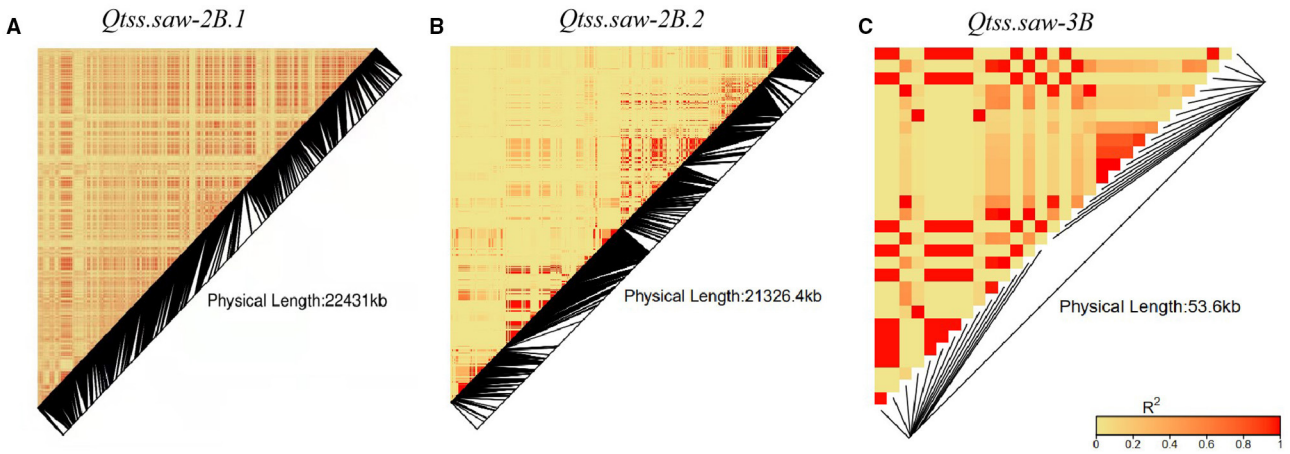

FIGURE 3 | Linkage disequilibrium heatmap of three target QTL regions **(A)** Qtss.saw-2B.1, **(B)** Qtss.saw-2B.2, and **(C)** Qtss.saw-3B.

DISCUSSION

Linfen 5064 Possess Favorable Key Genomic Regions

Analyzing founder parents at the whole genome level and studying the genome regions of the founder parents of high value is important for wheat breeding, especially molecular marker-assisted breeding. As a founder parent, Linfen 5064 has greatly contributed to wheat breeding in China. The high-quality characteristics of Linfen 5064 are derived from the spring wheat SARICF74 introduced from the Centro Internacional de Mejoramiento de Maizy Trigo (CIMMYT). Linfen 5064 was selected from a cross of SARICF74 and Linfen 5694 for early maturity and good agronomic traits. In this study, two DH populations were constructed with Linfen 5064 as the female parent and with Nongda 3338 and Jinmai 47 as male parents. A total of 13 stable QTL were identified through the investigation of spike traits in three field locations over 3 years. Seven stable QTL carried positive alleles from Linfen 5064. For spikelet number per spike, the additive effect of *Qtss.saw-2B.1*, *Qtss.saw-2B.2*, *Qtss.saw-3B*, *Qtss.saw-4A.1*, *Qfss.saw-2B.2*, and *Qbsss.saw-2B.2* were from Linfen 5064. And except for *Qtss.saw-4A.1 and Qbsss.saw-2B.2*, other QTL were validated in the LJ population. The QTL *Qtss.saw-2B.2*, *Qfss.saw-2B.2*, and *Qbsss.saw-2B.2* were located in the same region. Therefore, *Qtss.saw-2B.1*, *Qtss.saw-2B.2*, and *Qtss.saw-3B* were the most important regions of Linfen 5064 controlling spikelet number per spike. Lines with the positive allele from *Qtss.saw-2B.2* significantly increased TSS by 3.30%, which is higher than other single positive alleles of either *Qtss.saw-2B.1* (1.92%) or *Qtss.saw-3B* (2.45%). The region *Qtss.saw-2B.2* from Linfen 5064 had the larger effect on TSS and was present in 66.89% of Chinese landmark cultivars tested. For GNS, the only positive effect from a Linfen 5064 allele was from *Qgns.saw-7A.1*. The positive effects of *Qgns.saw-5B.2*, *Qgns.saw-4D*, and *Qgns.saw-1A* alleles were from Nongda 3338. The effect of *Qgns.saw-1A* was validated in the LJ population. These results indicate that this allele was unfavorable, but through breeding, improvement was made for the trait in Linfen 5064 presumably from contributions from other loci. This study examined the QTL of Linfen 5064 for GNS and analyzed the characteristics of genetic effects of related regions. These results further clarify the genetic contribution and intrinsic value of Linfen 5064 to GNS and provide a reference for future founder parent utilization and molecular breeding.

Qtss.saw-2B.1 and *Qtss.saw-3B* Are Novel Loci for Wheat Spike-Related Traits

To compare the intervals of the 13 QTL detected with those identified previously, we physically mapped these QTL on target chromosomes in CS. The QTL *Qtss.saw-5D* for TSS is physically located between 147.56 and 314.43 Mb on 5D (**Table 3**). It overlapped with a major QTL *QSN.caas-5DL* found in wheat

by Li et al. (2018). *Qgns.saw-7A.1* was located between 657.92 and 675.59 Mb on chromosome 7AL (**Table 3**). This region has QTL-rich clusters for wheat yield component traits. *QSn-7A.2* (Fan et al., 2019), *Qmt.tamu.7A.1* (Assanga et al., 2017), *QTgw.cau-7A.4* (Guan et al., 2018), and *Qkns.caas-7AL* (Li et al., 2018) overlap with *Qgns.saw-7A.1*. Likewise, *TaAPO-A1* is in this cluster, namely, *Qkns.caas-7AL*, *QGne.nfcri-7A*, and *QGns.cau-7A.5* for Kernel number per spike, so it probably is the candidate gene of these QTL (Cao et al., 2020). *TaAPO-A1* is orthologous to *APO1*, a rice gene that positively controls spikelet number on panicles (Muqaddasi et al., 2019). *Qgns.saw-4D* was located within 15.77–48.70 Mb on chromosome 4DS (**Table 3**). Comparative analysis revealed that this locus overlaps *TB-D1* (Dixon et al., 2018), *Rht-D1* (Peng et al., 1999), *QTKW-4D-AN* (Mohler et al., 2016), *QGn.nau-4D* (Jia et al., 2013), *QTgw-4D*, and *QGns-4D* (Liu et al., 2014), suggesting this region is a QTL-rich cluster for wheat yield component traits. *Qtss.saw-2B.2*, *Qfss.saw-2B.2*, and *Qbsss.saw-2B.2* were co-located in the interval of *2B_54768734-2B_76515060* and physically mapped to 54.77–76.52 Mb on 2BS. This region has the *Ppd-B1* gene which is a key component in the photoperiod regulatory flowering pathway (Beales et al., 2007; Nishida et al., 2013) and is associated with flag leaf size and grain yield (Kirby, 1992; Snape et al., 2001; Foulkes et al., 2004). No stable QTL have been reported previously overlapped with the other stable QTL from this study, *Qtss.saw-2B.1*, *Qtss.saw-3B*, *Qtss.saw-5A*, and *Qgns.saw-5B.2*. Both *Qtss.saw-2B.1* and *Qtss.saw-3B* had significant effects on TSS and GNS that were detected in the validation population. Therefore, *Qtss.saw-2B.1* and *Qtss.saw-3B* are likely novel loci for TSS. Therefore, spikelet development of wheat is a complex process, which is regulated by different types of genes. With the development of biotechnology, combining multiple technologies to analyze the development of GNS will help clarify the formation mechanism of GNS.

New Genes Were Identified in the Interval of the Stable QTL to Control Spike-Related Traits

Genes related to spike traits can be divided into two categories. The first category is flowering time (FT) genes which have significant effects on grain yield, namely, *Vrn1*, *Vrn2*/*ZCCT1*, *Vrn3*, and *Ppd-D1* (Cuthbert et al., 2008; Zhou et al., 2017; Guan et al., 2018). Other genes were mainly involved in spike differentiation which influenced the number of grains per spike by regulating the rate and direction of differentiation. For example, *aberrant panicle organization 1 (APO1)* controls cell proliferation of the rice meristem, leading to the reduction of the primary and secondary branches of the panicle, thereby affecting panicle development (Kyoko et al., 2009). In addition, some genes can control panicle morphogenesis by regulating hormone and protein expression during rice growth (Huang et al., 2009; Qiao et al., 2011; Gao et al., 2016). *BG1* regulates auxin transport and increases biomass, grain number per spike, and grain size to increase yield (Liu et al., 2015). In this study, we find three new genes for controlling spike-related traits. *TraesCS2B02G500100*, *TraesCS2B02G500200*, and *TraesCS2B02G500300* and involved the phytohormone regulatory and ubiquitin proteasoma. In the next step, we will fine-mapping these QTL which will help explain the formation and development of GNS in wheat and develop linked molecular markers for use by breeders.

DATA AVAILABILITY STATEMENT

The datasets presented in this study can be found in online repositories. The names of the repository/repositories and accession number(s) can be found in the article/**Supplementary Material**.

AUTHOR CONTRIBUTIONS

JZhe, WD, JuW, and LQ designed the experiment and developed the original manuscript. LQ, HL, JZha, XZ, JiW, and BW performed the field experiments. LQ, HL, XZ, WD, and JZhe performed the phenotypic data analysis and the QTL detection. WD, JuW, and JZhe revised the manuscript. All authors approved the submitted version of the manuscript.

FUNDING

This study was supported by the State Key Laboratory of Integrative Sustainable Dryland Agriculture (in preparation), the Shanxi Agricultural University (No. 202105D121008-2-1), the Shanxi Scholarship Council of China (2020-159), the Shanxi Province Research Program (20210302124505), and the Agricultural Science Research of Shanxi Academy of Agricultural Sciences (YCX2020YQ47, YCX2020YQ34, and YZGC013).

ACKNOWLEDGMENTS

We are grateful to Professor Jian Gu, Food Crops Research Institute, Yunnan Academy of Agricultural Sciences, for providing help in developing DH populations. We also thank Professor Jianli Chen of the University of Idaho for critical advice on the design of these experiments.

SUPPLEMENTARY MATERIAL

The Supplementary Material for this article can be found online at: https://www.frontiersin.org/articles/10.3389/fpls.2021.808136/full#supplementary-material

REFERENCES

Assanga, S. O., Fuentealba, M., Zhang, G. R., Tan, C., Dhakal, S., Rudd, J. C., et al. (2017). Mapping of quantitative trait loci for grain yield and its components in a US popular winter wheat TAM 111 using 90K SNPs. *PLoS ONE* 12:e189669. doi: 10.1371/journal.pone.0189669

Beales, J., Turner, A., Griffiths, S., Snape, J. W., and Laurie, D. A. (2007). A *pseudo-response regulator* is misexpressed in the photoperiod insensitive *Ppd-D1a*

mutant of wheat (*Triticum aestivum* L.). *Theor. Appl. Genet.* 115, 721–733. doi: 10.1007/s00122-007-0603-4

Boden, S. A., Cavanagh, C., Cullis, B. R., Ramm, K., Greenwood, J. L., Finnegan, E. J., et al. (2015). *Ppd-1* is a key regulator of inflorescence architecture and paired spikelet development in wheat. *Nat Plants.* 1:14016. doi: 10.1038/nplants.2014.16

Börner, A., Schumann, E., Fürste, A., Cöster, H., Leithold, B., Röder, M., et al. (2002). Mapping of quantitative trait locus determining agronomic important characters in hexaploid wheat (*Triticum aestivum* L.). *Theor. Appl. Genet.* 105, 921–936. doi: 10.1007/s00122-002-0994-1

Cao,. S. H., Xu, D. A., Hanif, M., Xia, X. C., and He, Z. H. (2020). Genetic architecture underpinning yield component traits in wheat. *Theor. Appl. Genet*. 133, 1811–1823. doi: 10.1007/s00122-020-03562-8

Chuck, G., Meeley, R. B., and Hake, S. (1998). The control of maize spikelet meristem fate by the *APETALA2*-like gene indeterminate spikelet1. *Gene Dev*. 12, 1145–1154. doi: 10.1101/gad.12.8.1145

Cui, F., Zhang, N., Fan, X. L., Zhang, W., Chun, H. Z., Li, J. Y., et al. (2017). Utilization of a Wheat660K SNP array-derived high-density genetic map for high-resolution mapping of a major QTL for kernel number. *Sci. Rep.* 7:3788. doi: 10.1038/s41598-017-04028-6

Cui, J. M., Guo, T. C., Zhu, Y., j., Wang, C. Y., and Ma, X. M. (2008). *Spike of Wheat*. Beijing: Agriculture Press, 18–33.

Cuthbert, J. L., Somers, D. J., Brûlé-Babel, A. L., Brown, P. D., and Crow, G. H. (2008). Molecular mapping of quantitative trait loci for yield and yield components in spring wheat (*Triticum aestivum* L.). *Theor. Appl. Genet*. 117, 595–608. doi: 10.1007/s00122-008-0804-5

Debernardi, J. M., Lin, H., Chuck, G., Faris, J. D., and Dubcovsky, J. (2017). micro-RNA172 plays a crucial role in wheat spike morphogenesis and grain threshability. *Development* 144, 1966–1975. doi: 10.1242/dev.146399

Deng, M., Wu, F. K., Zhou, W. L., Li, J., Shi, H. R., Wang, Z. Q., et al. (2019). Mapping of QTL for total spikelet number per spike on chromosome 2D in wheat using a high-density genetic map. *Genet. Mol. Biol*. 42, 603–610. doi: 10.1590/1678-4685-gmb-2018-0122

Dixon, L. E., Greenwood, J. R., Bencivenga, S., Zhang, P., Cockram, J., Mellers, G., et al. (2018). *TEOSINTE BRANCHED1* regulates inflorescence architecture and development in bread wheat (*Triticum aestivum* L.). *Plant Cell*. 30, 563–581. doi: 10.1105/tpc.17.00961

Du, D. J., Zhang, D. X., Yuan, J., Feng, M., Li, Z. J., Wang, Z. H., et al. (2021). *FRIZZY PANICLE* defines a regulatory hub for simultaneously controlling spikelet formation and awn elongation in bread wheat. *New Phytol*. 231, 814–833. doi: 10.1111/nph.17388

Fan, X. L., Cui, F., Ji, J., Zhang, W., Zhao, X. Q., Liu, J. J., et al. (2019). Dissection of pleiotropic QTL regions controlling wheat spike characteristics under different nitrogen treatments using traditional and conditional QTL mapping. *Front. Plant Sci*. 10:187. doi: 10.3389/fpls.2019.00187

Foulkes, M. J., Sylvester-Bradley, R., Worland, A. J., and Snape, J. W. (2004). Effects of a photoperiod-response gene *Ppd-D1* on yield potential and drought resistance in UK winter wheat. *Euphytica* 135, 63–73. doi: 10.1023/B:EUPH.0000009542.06773.13

Gao, S. P., Fang, J., Xu, F., Wang, W., and Chu, C. C. (2016). Rice HOX12 regulates panicle exsertion by directly modulating the expression of *ELONGATED UPPERMOST INTERNODE1*, *Plant Cell* 28, 680–695. doi: 10.1105/tpc.15.01021

Guan, P. F., Lu, L. H., Jia, L. J., Kabir, M. R., Zhang, J. B., Lan, T. Y., et al. (2018). Global QTL analysis identifies genomic regions on Chromosomes 4A and 4B harboring stable loci for yield-related traits across different environments in wheat (*Triticum aestivum* L.). *Front. Plant Sci*. 9:529. doi: 10.3389/fpls.2018.00529

Guo, J., Zhang, Y., Shi, W. P., Zhang, B. Q., Xu, Y. H., et al. (2015). Association analysis of grain-setting rates in apical and basal spikelets in bread wheat (*Triticum aestivum* L.). *Front. Plant Sci*. 6:1029. doi: 10.3389/fpls.2015.01029

Hao, C. Y., Jiao, C. Z., Hou, J., Li, T., Liu, H. X., Wang, Y. Q., et al. (2020). Resequencing of 145 landmark cultivars reveals asymmetric sub-genome selection and strong founder genotype effects on wheat breeding in China. *Mol. Plant*. 13, 1733–1751. doi: 10.1016/j.molp.2020.09.001

Huang, X. Q., Cloutier, S., Lycar, L., Radovanovic, N., Humphreys, D. G., Noll, J. S., et al. (2006). Molecular detection of QTL for agronomic and quality traits in a doubled haploid population derived from two Canadian wheats (*Triticum aestivum* L.). *Theor. Appl. Genet*. 113, 753–766. doi: 10.1007/s00122-006-0346-7

Huang, X. Z., Qian, Q., Liu, Z. B., Sun, H. Y., He, S. Y., Luo, D., et al. (2009). Natural variation at the *DEP1* locus enhances grain yield in rice. *Nat. Genet*. 41, 494–497. doi: 10.1038/ng.352

Isham, K., Wang, R., Zhao, W. D., Wheeler, J., Klassen, N., Akhunov, E., et al. (2021). QTL mapping for grain yield and three yield components in a population derived from two high-yielding spring wheat cultivars. *Theor. Appl. Genet*. 134, 2079–2095. doi: 10.1007/s00122-021-03806-1

Jia, H. Y., Wan, H. S., Yang, S. H., Zhang, Z. Z., Kong, Z. X., X, S. L., et al. (2013). Genetic dissection of yield-related traits in a recombinant inbred line population created using a key breeding parent in China's wheat breeding. *Theor. Appl. Genet*. 126, 2123–2139. doi: 10.1007/s00122-013-2123-8

Jiang, Y. M., Jiang, Q. Y., Hao, C. Y., Hou, J., Wang, L. F., Zhang, H. N., et al. (2015). A yield-associated gene *TaCWI*, in wheat: its function, selection and evolution in global breeding revealed by haplotype analysis. *Theor. Appl. Genet*. 128, 131–143. doi: 10.1007/s00122-014-2417-5

Kabir, M. R., Liu, G., Guan, P. F., Wang, F., Khan, A. A., Ni, Z. F., et al. (2015). Mapping QTL associated with root traits using two different populations in wheat (*Triticum aestivum* L.). *Euphytica* 206, 175–190. doi: 10.1007/s10681-015-1495-z

Keeble-Gagnere, G., Rigault, P., Tibbits, J., Pasam, R., Hayden, M., Forrest, K., et al. (2018). Optical and physical mapping with local finishing enables megabase-scale resolution of agronomically important regions in the wheat genome. *Genome Biol*. 19:112. doi: 10.1186/s13059-018-1475-4

Kirby, E. J. M. (1992). A field study of the number of main shoot leaves in wheat in relation to vernalization and photoperiod. *J. Agric. Sci*. 118, 271–278. doi: 10.1017/S0021859600070635

Kyoko, I. K., Naoko, Y., Tetsuo, O., Shigeru, I., Yasuo, N., Masahiko, M., et al. (2009). Expression Level of *ABERRANT PANICLE ORGANIZATION1* determines rice inflorescence form through control of cell proliferation in the meristem. *Plant Physiol*. 150, 736–747. doi: 10.1104/pp.109.136739

Li, F., Wen, W., He, Z., Liu, J., Jin, H., Cao, S., et al. (2018). Genome-wide linkage mapping of yield-related traits in three Chinese bread wheat populations using high-density SNP markers. *Theor. Appl. Genet.* 131, 1903–1924. doi: 10.1007/s00122-018-3122-6

Li, S. S., Jia, J. Z., Wei, X. Y., Zhang, X. C., Li, L. Z., Chen, H. M., et al. (2007). A intervarietal genetic map and QTL analysis for yield traits in wheat. *Mol. Breed.* 20, 167–178. doi: 10.1007/s11032-007-9080-3

Liu, G., Jia, L. J., Lu, L. H., Qin, D. D., Zhang, J. P., Guan, P. F., et al. (2014). Mapping QTL of yield-related traits using RIL population derived from common wheat and Tibetan semi-wild wheat. *Theor. Appl. Genet*. 127, 2415–2432. doi: 10.1007/s00122-014-2387-7

Liu, J., Wu, B. H., Singh, R. P., and Velu, G. (2019). QTL mapping for micronutrients concentration and yield component traits in a hexaploid wheat mapping population. *J. Cereal Sci*. 88, 57–64. doi: 10.1016/j.jcs.2019.05.008

Liu, L. C., Tong, H. N., Xiao, Y. H., Che, R. H., Xu, F., Hu, B., et al. (2015). Activation of *Big Grain1* significantly improves grain size by regulating auxin transport in rice. *Proc. Natl. Acad. Sci. U.S.A*. 112, 11102–11107. doi: 10.1073/pnas.1512748112

Ma, S. W., Wang, M., Wu, J. H., Guo, W. L., Chen, Y. M., Li, G. W., et al. (2021). WheatOmics: a platform combining multiple omics data to accelerate functional genomics studies in wheat. *Mol. Plant.* 14, 1965–1968. doi: 10.1016/j.molp.2021.10.006

Ma, Z. Q., Zhao, D. M., Zhang, C. Q., Zheng, Z. Z., Shu, L. X., Feng, L., et al. (2007). Molecular genetic analysis of five spike-related traits in wheat using RIL and immortalized F_2 populations. *Mol. Gen. Genomics* 277, 31–42. doi: 10.1007/s00438-006-0166-0

Meng, L., Li, H. H., Zhang, L. Y., and Wang, J. K. (2015). QTL IciMapping: integrated software for genetic linkage map construction and quantitative trait locus mapping in biparental populations. *Crop J.* 3, 269–283. doi: 10.1016/j.cj.2015.01.001

Mohler, V., Albrecht, T., Castell, A., Diethelm, M., Schweizer, G., and Hartl, L. (2016). Considering causal genes in the genetic dissection of kernel traits in common wheat. *J. Appl. Genet*. 57, 467–476. doi: 10.1007/s13353-016-0349-2

Muqaddasi, Q. H., Brassac, J., Koppolu, R., Plieske, J., Ganal, M. W., and Röder, M. S. (2019). *TaAPO-A1*, an ortholog of rice *ABERRANT PANICLE*

ORGANIZATION 1, is associated with total spikelet number per spike in elite hexaploid winter wheat varieties (*Triticum aestivum* L.). *Sci. Rep.* 9:13853. doi: 10.1038/s41598-019-50331-9

Narasimhamoorthy, B., Gill, B. S., Fritz, A. K., Nelson, J. C., and Broen-Guedira, G. L. (2006). Advanced backcross QTL analysis of a hard winter wheat × synthetic wheat population. *Theor. Appl. Genet.* 112, 787–796. doi: 10.1007/s00122-005-0159-0

Nishida, H., Yoshida, T., Kawakami, K., Fujita, M., Long, B., Akashi, Y., et al. (2013). Structural variation in the 5' upstream region of photoperiod-insensitive alleles *Ppd-A1a* and *Ppd-B1a* identified in hexaploid wheat (*Triticum aestivum* L.), and their effect on heading time. *Mol. Breed.* 31, 27–37. doi: 10.1007/s11032-012-9765-0

Onyemaobi, I., Ayalew, H., Liu, H., Siddique, K. H. M., and Yan, G. J. (2018). Identification and validation of a major chromosome region for high grain number per spike under meiotic stage water stress in wheat (*Triticum aestivum* L.). *PLoS ONE* 13:e194075. doi: 10.1371/journal.pone.0194075

Peng, J., Richards, D. E., Hartley, N. M., Murphy, G. P., Devos, K. M., Flintham, J. E., et al. (1999). 'Green revolution' genes encode mutant gibberellin response modulators. *Nature* 400, 256–261. doi: 10.1038/22307

Qiao, L., Liu, C., Zheng, X. W., Zhao, J. J., Shang, B. H., Ma, X. F., et al. (2018). Genetic analysis of haplotype-blocks from wheat founder parent Linfen 5064. *Acta. Agron. Sin.* 44, 931–937. doi: 10.3724/SP.J.1006.2018.00931

Qiao, Y. L., Piao, R., Shi, J., Lee, S. I., Jiang, W., Kim, B. K., et al. (2011). Fine mapping and candidate gene analysis of *dense and erect panicle 3*, *DEP3* which confers high grain yield in rice (*Oryza sativa* L.). *Theor Appl Genet.* 122, 1439–1449. doi: 10.1007/s00122-011-1543-6

Rehman, S. U., Wang, J. Y., Chang, X. P., Zhang, X. Y., Mao, X. G., et al. (2019). A wheat protein kinase gene *TaSnRK2.9-5A* associated with yield contributing traits. *Theor. Appl. Genet.* 132, 907–919. doi: 10.1007/s00122-018-3247-7

Sakuma, S., Golan, G., Guo, Z. F., Ogawa, T., Tagiri, A., Sugimoto, K., et al. (2019). Unleashing floret fertility in wheat through the mutation of a homeobox gene. *Proc. Natl. Acad. Sci. U.S.A.* 116, 5182–5187. doi: 10.1073/pnas.1815465116

Shao, A., Ma, W. Y., Zhao, X. Q., Hu, M. Y., He, X., Teng, W., et al. (2017). The auxin biosynthetic *TRYPTOPHAN AMINOTRANSFERASE RELATED TaTAR2.1-3A* increases grain yield of wheat. *Plant Physiol.* 174, 2274–2288. doi: 10.1104/pp.17.00094

Smith, S. E., Kuehl, R. O., Ray, I. M., Hui, R., and Soleri, D. (1998). Evaluation of simple methods for estimating broad-sense heritability in stands of randomly planted genotypes. *Crop Sci.* 38, 1125–1129. doi: 10.2135/cropsci1998.0011183X003800050003x

Snape, J. W., Butterworth, K., Whitechurch, E., and Worland, A. J. (2001). Waiting for fine times: genetics of flowering time in wheat. *Euphytica.* 119, 185–190. doi: 10.1023/A:1017594422176

Song, Q. H., Liu, C. Y., Bachir, D. G., Chen, L., and Hu, Y. G. (2017). Drought resistance of new synthetic hexaploid wheat accessions evaluated by multiple traits and antioxidant enzyme activity. *Field Crops Res.* 210, 91–103. doi: 10.1016/j.fcr.2017.05.028

Su, Q. N., Zhang, X. L., Zhang, W., Zhang, N., Song, L. Q., Liu, L., et al. (2018). QTL detection for kernel size and weight in bread wheat (*Triticum aestivum* L.) using a high-density SNP and SSR-based linkage map. *Front. Plant Sci.* 9:1484. doi: 10.3389/fpls.2018.01484

Valluru, R., Reynolds, M. P., and Salse, J. (2014). Genetic and molecular bases of yield-associated traits: a translational biology approach between rice and wheat. *Theor. Appl. Genet.* 127, 1463–1489. doi: 10.1007/s00122-014-2332-9

Wang, S., Basten, C., and Zeng, Z. (2012). *Windows QTL Cartographer 2.5*. Raleigh: Department of Statistics, North Carolina State University.

Winfield, M. O., Allen, A. M., Burridge, A. J., Barker, G. L. A., Benbow, H. R., Wilkinson, P. A., et al. (2016). High-density SNP genotyping array for hexaploid wheat and its secondary and tertiary gene pool. *Plant Biotechnol. J.* 14, 1195–1206. doi: 10.1111/pbi.12485

Wu, X. S., Chang, X. P., and Jing, R. L. (2012). Genetic insight into yield-associated traits of wheat grown in multiple rain-fed environments. *PLoS ONE* 7:e31249. doi: 10.1371/journal.pone.0031249

Xie, Q., Li, N., Yang, Y., Lv, Y. L., Yao, H. N., Wei, R., et al. (2018). Pleiotropic effects of the wheat domestication gene *Q* on yield and grain morphology. *Planta* 247, 1089–1098. doi: 10.1007/s00425-018-2847-4

Yan, X. F., Zhao, L., Ren, Y., Dong, Z. Z., Cui, D. Q., and Chen, F. (2019). Genome-wide association study revealed that the *TaGW8* gene was associated with kernel size in Chinese bread wheat. *Sci. Rep.* 9:2702. doi: 10.1038/s41598-019-38570-2

Yao, H. N., Xie, Q., Xue, S. L., Luo, J., Lu, J. K., Kong, Z. X., et al. (2019). *HL2* on chromosome 7D of wheat (*Triticum aestivum* L.) regulates both head length and spikelet number. *Theor. Appl. Genet.* 132, 1789–1797. doi: 10.1007/s00122-019-03315-2

Zhang, B., Liu, X., Xu, W. N., Chang, J. Z., Li, A., Mao, X. G., et al. (2015). Novel function of a putative *MOC1* ortholog associated with spikelet number per spike in common wheat. *Sci. Rep.* 5:12211. doi: 10.1038/srep12211

Zhang, H., Chen, J. S., Li, R. Y., Mao, X. G., Li, A., Wang, J. Y., et al. (2016). Conditional QTL mapping of three yield components in common wheat (*Triticum aestivum* L.). *Crop J.* 4, 220–228. doi: 10.1016/j.cj.2016.01.007

Zhang, Z., Li, J., Hu, N., Li, W., Qin, W., Li, J., et al. (2021). Spike growth affects spike fertility through the number of florets with green anthers before floret abortion in wheat. *Field Crop. Res.* 260:108007. doi: 10.1016/j.fcr.2020.108007

Zheng, X. W., Liu,. C., Qiao, L., Zhao, J. J., Han, R., Wang, X. L., et al. (2020). The MYB transcription factor TaPHR3-A1 is involved in phosphate signaling and governs yield-related traits in bread wheat. *J. Exp. Bot.* 71, 5808–5822. doi: 10.1093/jxb/eraa355

Zhou,. Y. P., Conway, B., Miller, D., Marshall, D., Cooper, A., Murphy, P., et al. (2017). Quantitative trait loci mapping for spike characteristics in hexaploid wheat. *Plant Genome.* 10, 1–15. doi: 10.3835/plantgenome2016.10.0101

Zhuang, Q. S. (2003). *Chinese Wheat Improvement and Pedigree Analysis*. Beijing: China Agricultural Press.

Conflict of Interest: The authors declare that the research was conducted in the absence of any commercial or financial relationships that could be construed as a potential conflict of interest.

Publisher's Note: All claims expressed in this article are solely those of the authors and do not necessarily represent those of their affiliated organizations, or those of the publisher, the editors and the reviewers. Any product that may be evaluated in this article, or claim that may be made by its manufacturer, is not guaranteed or endorsed by the publisher.

frontiers in Plant Science

ORIGINAL RESEARCH
published: 21 January 2022
doi: 10.3389/fpls.2021.805879

Histone Acetyltransferase SlGCN5 Regulates Shoot Meristem and Flower Development in *Solanum lycopersicum*

*Amangul Hawar, Shiqi Xiong, Zhen Yang and Bo Sun**

State Key Laboratory of Pharmaceutical Biotechnology, School of Life Sciences, Nanjing University, Nanjing, China

The histone acetyltransferase (HAT) general control non-repressed protein 5 (GCN5) plays important roles in plant development *via* epigenetic regulation of its target genes. However, the role of GCN5 in tomato, especially in the regulation of tomato shoot meristem and flower development, has not been well-understood. In this study, we found that silencing of *Solanum lycopersicum GCN5* (*SlGCN5*, *Solyc10g045400.1.1*) by virus-induced gene silencing (VIGS) and RNA interference (RNAi) resulted in the loss of shoot apical dominance, reduced shoot apical meristem (SAM) size, and dwarf and bushy plant phenotype. Besides, we occasionally observed extra carpelloid stamens and carpels fused with stamens at the late stages of flower development. Through gene expression analysis, we noticed that SlGCN5 could enhance *SlWUS* transcript levels in both SAM and floral meristem (FM). Similar to the known function of GCN5 in *Arabidopsis*, we demonstrated that SlGCN5 may form a HAT unit with *S. lycopersicum* alteration/deficiency in activation 2a (SlADA2a) and SlADA2b proteins in tomato. Therefore, our results provide insights in the SlGCN5-mediated regulation of SAM maintenance and floral development in tomato.

Keywords: tomato, SAM, *SlGCN5*, *SlWUS*, *SlADA2*

OPEN ACCESS

Edited by:
Xigang Liu,
Hebei Normal University, China

Reviewed by:
Weibing Yang,
Institute of Plant Physiology and Ecology, Shanghai Institutes for Biological Sciences, Chinese Academy of Sciences (CAS), China
Yun Zhou,
Purdue University, United States

***Correspondence:**
Bo Sun
sunbo@nju.edu.cn

Specialty section:
This article was submitted to Crop and Product Physiology, a section of the journal Frontiers in Plant Science

Received: *31 October 2021*
Accepted: *21 December 2021*
Published: *21 January 2022*

Citation:
Hawar A, Xiong S, Yang Z and Sun B (2022) Histone Acetyltransferase SlGCN5 Regulates Shoot Meristem and Flower Development in Solanum lycopersicum. Front. Plant Sci. 12:805879. doi: 10.3389/fpls.2021.805879

INTRODUCTION

Plants have a unique ability to give rise to new organs continuously due to the indeterminate production of undifferentiated stem cells located in specific regions of meristems. The shoot apical meristem (SAM) gives rise to the aerial organs, and the maintenance of SAM is key for the development of plants and adaptation to the changes of external environment (Pfeiffer et al., 2017). Unlike *Arabidopsis*, tomato is a typical sympodial plant. After the formation of 8–10 leaves, tomato SAM terminated and transforms into inflorescence meristem (IM) and sympodial meristem (SYM), which are formed at the leaf axils beneath the IM to sustain continuous growth. Thereafter, IM transforms to floral meristem (FM) and initiates a second IM in the meantime (Schmitz and Theres, 1999; Périlleux et al., 2014). Tomato FMs generate four whorls of floral organs, namely, sepals, petals, stamens, and carpels, sequentially in concentric whorls (Sekhar and Sawhney, 1984).

In *Arabidopsis*, the maintenance of the stem cell pool in the SAM is regulated by *CLAVATA-WUSCHEL* (*CLV-WUS*) feedback loop (Schoof et al., 2000). In this feedback loop, WUS could directly induce stem cell identity and the expression of the stem cell marker gene *CLV3* (Yadav et al., 2011; Daum et al., 2014). The *CLV* genes including *CLV1* and *CLV3* repress *WUS* through signaling cascades (Shang et al., 2019; Han et al., 2020), therefore coordinating and balancing stem cell proliferation with differentiation. The *CLV-WUS* feedback loop appears to be highly conserved

across different plant species (Somssich et al., 2016). In tomato, the mutation of *SlCLV3* promotes stem cell overproliferation and results in extra floral organs and bigger fruits (Rodríguez-Leal et al., 2017). In *SlWUS* RNA interference (RNAi) lines, plants have reduced flower size and fruit locule numbers (Li et al., 2017). Changes in tomato meristem size have also been observed in *fasciated* (*fas*) and *locule number* (*lc*) mutants, both of which have misexpression of *SlWUS* and *SlCLV3*, respectively (Muños et al., 2011; Xu et al., 2015; Chu et al., 2019).

In various plant species, studies have discovered that the *CLV-WUS* regulatory loop could be modified by many additional factors, which can contribute to plant growth and productivity (Galli and Gallavotti, 2016). Among these factors, histone modifications including acetylation or methylation on several lysine residues of H3 are important for gene expression during plant development (Servet et al., 2010). Histone acetyltransferases (HATs) can catalyze acetylation of specific lysine residues on histone N-tails and leads to transcriptional regulation (Bannister and Kouzarides, 2011). It has been reported that in most cases, GCN5 acts as the catalytic core of the HAT complex, which also include vital adaptor proteins ADA2a and ADA2b (Shahbazian and Grunstein, 2007). GCN5 acetylates lysine 14 of histone H3 (H3K14ac) and influences H3K9ac and H3K27ac levels in promoter region of its targets (Benhamed et al., 2006; Servet et al., 2010; Ruggieri et al., 2020). In contrast, ADA2 proteins could help increase the HAT activity of GCN5 (Mao et al., 2006).

In *Arabidopsis*, both GCN5 and ADA2b are required for many developmental processes such as shoot apical dominance, root meristem activity, leaf development, IM or FM function, and flower fertility (Bertrand et al., 2003; Vlachonasios et al., 2003; Cohen et al., 2009; Kornet and Scheres, 2009; Anzola et al., 2010; Servet et al., 2010). In poplar trees, ABRE-motif binding protein PtrAREB1-2 binds to *PtrNAC* genes, recruits the HAT unit ADA2b-GCN5 by forming a AREB1-ADA2b-GCN5 protein complexes, and results in increased H3K9 acetylation levels on *PtrNAC* genes (Li et al., 2019). In rice, the homeodomain protein OsWOX11 recruits a HAT complex containing OsGCN5 to establish the programs of cell proliferation in crown root meristem (Zhou et al., 2017). One study implies that the SAGA (Spt-Ada-GCN5 acetyltransferase) complex is an evolutionarily conserved complex that has a critical role in various developmental processes (Spedale et al., 2012).

In this work, we identified *SlGCN5*, *SlADA2a,* and *SlADA2b* in tomato and found that SlGCN5 can form a HAT unit with SlADA2a and SlADA2b and influences H3K9ac, H3K14ac, and H3ac at the genomic level. Silencing of *SlGCN5* resulted in dwarf plant phenotype, reduced SAM size, carpelloid stamens, and fusion of carpels with stamens in flowers. Furthermore, we proposed that SlGCN5 could enhance *SlWUS* expression, thereby maintaining stem cell homeostasis in tomato.

MATERIALS AND METHODS

Plant Materials and Growth Conditions

Arabidopsis plants and wild-type (WT) tomato (*Solanum lycopersicum*) plants of Micro-Tom (MT) and transgenic *Arabidopsis* and tomato lines were grown in the greenhouse, under long-day condition (16-h light/8-h dark). For transformation, tomato cotyledons were cultivated *in vitro* in MS medium in a growth chamber (Panasonic, MLR-352H-PC) at 22°C/20°C under16-h light and 8-h dark conditions.

Construction of TRV-*SlGCN5* and RNAi Vectors and Tomato Transformation

The tobacco rattle virus (TRV)-based vectors, i.e., pTRV1 and pTRV2, were used for virus-induced gene silencing (VIGS). To construct a pTRV2-*SlGCN5* vector, according to the website[1], a 400-bp DNA fragment of the *SlGCN5* CDS was amplified from tomato cDNA using primers in **Supplementary Table 1**. The constructs were introduced into *Agrobacterium tumefaciens* GV301. Then, VIGS assays were carried out as previously described (Fu et al., 2005).

To generate amiRNA for silencing *SlGCN5*, the amiRNAs (21-nt) were designed by using the web MicroRNA Designer (WMD3[2]). Pre-amiRNA was assembled by several rounds of PCR using primers listed in **Supplementary Table 1**. The final PCR fragments were driven under 35S promoters in pCHF3 vector. After *SlGCN5*-RNAi construct is transformed into *Agrobacterium* GV3101, the *Agrobacterium*-mediated transformation of tomato cotyledons was performed as described (Cortina and Culiáñez-Macià, 2004; Tripodi, 2020).

Phylogenetic Analysis

For phylogenetic analysis, the coding sequences of *ADA2* orthologs were retrieved from JGI Genome Portal and Resources for Plant Comparative Genomics[3] by BLAST using *AtADA2a* coding sequence as a query with default parameters. The phylogenetic tree of ADA2 orthologs in dicots was constructed by W-IQ-TREE (Nguyen et al., 2015), which identified the best evolutionary model as the general time reversible model (GTR + F + I + G4). The non-parametric UltraFast Bootstrap (UFBoot) method (Minh et al., 2013) was used to calculate the node support, and 1,000 bootstrap pseudo replicates were performed with bootstrap values indicated in branches.

Subcellular Localization Analysis

DNA fragment of *SlGCN5* was amplified by PCR (primers are listed in **Supplementary Table 1**) and inserted into pGreenII vector to generate the SlGCN5-GFP (green fluorescent protein) fusion protein. Then, pGreenII vector-based 35S:SlGCN5-GFP and the control vector pGreenII-based 35S:GFP were transformed into *A. tumefaciens* strain GV3101 and injected into 4-week-old tobacco leaves. GFP fluorescence was observed using Olympus (BX53) microscope after 72 h of infiltration.

RNA Extraction and Expression Analyses

RNA extraction and quantitative real-time (qRT)-PCR analysis were carried out as described previously (Sun et al., 2019).

[1]https://solgenomics.net

[2]http://wmd3.weigelworld.org./cgi-bin/webapp.cgi

[3]https://phytozome-next.jgi.doe.gov/

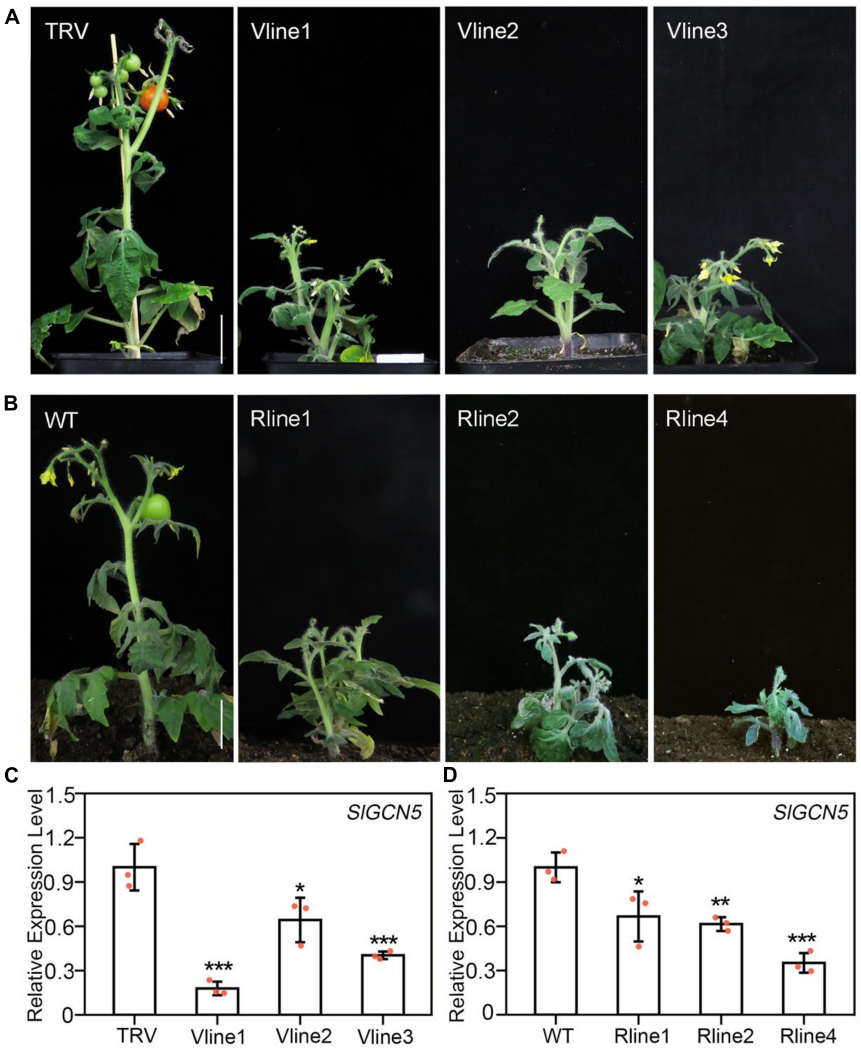

FIGURE 1 | Silencing of *SlGCN5* affects plant development. **(A)** Phenotype of three independent TRV-*SlGCN5* lines of Micro-Tom tomato. V lines represent *SlGCN5-VIGS* lines. **(B)** Phenotype of three independent *SlGCN5-RNAi* lines. **(C)** qRT-PCR analysis of *SlGCN5* transcripts in TRV control and TRV-*SlGCN5* plants. **(D)** Transcript levels of *SlGCN5* in *SlGCN5-RNAi* lines relative to wild type (WT). Error bars represent SD of three biological replicates. Asterisks indicate significant differences (*$p < 0.05$, **$p < 0.01$, and ***$p < 0.001$). Scale bars = 3 cm.

ACTIN2 and *SlACTIN2* were served as the internal control in *Arabidopsis* and tomato, respectively. The sequences of all primers are listed in **Supplementary Table 1**.

In situ Hybridization

RNA *in situ* hybridization was performed as described previously (Sun et al., 2019). Briefly, *SlGCN5* (*Solyc10g045400.1.1*) and *SlWUS* (*Solyc02g083950*) probes were synthesized from cDNA by using the primers listed in **Supplementary Table 1**, and the PCR products were cloned into pGEM-T Easy vector (TIANGEN, VT307). After linearization, the DIG RNA labeling kit (Roche, 11175025910) was used for *in vitro* transcription of probes. The experiments were performed twice using two different batches of plants. Photographs were taken by using an Olympus BX53 microscope.

Yeast Two-Hybrid Assay

To obtain yeast two-hybrid vectors, the full-length *SlGCN5* was cloned into pGADT7 (Clontech). The full-length *SlADA2a* and *SlADA2b* were individually cloned into pGBKT7 (Clontech). The yeast two-hybrid assay was performed using the Yeastmaker Yeast Transformation System 2 (Clontech, T2001) according to the instruction of the manufacturer. Primer sequences are provided in **Supplementary Table 1**.

Bimolecular Fluorescence Complementation Assay

For bimolecular fluorescence complementation (BiFC) assay, SlGCN5 and SlADA2 were tagged with the C-terminal part of YFP (YFPC) and the N-terminal part of YFP (YFPN), respectively, as previously described (Kudla and Bock, 2016).

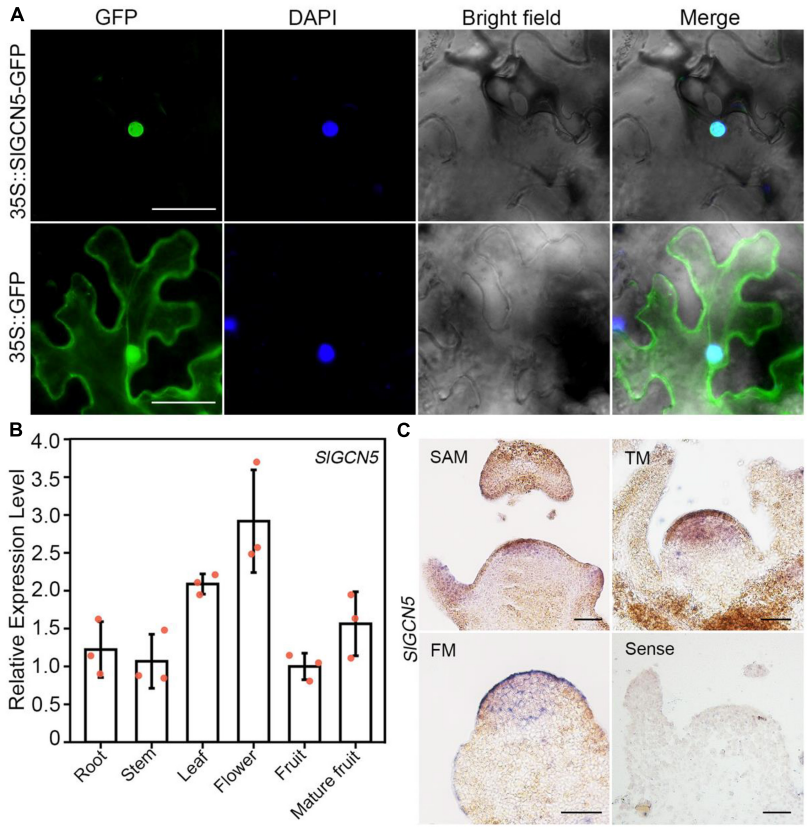

FIGURE 2 | Subcellular localization and gene expression pattern of *SlGCN5*. **(A)** Subcellular localization of SlGCN5 in nuclei. 35S:SlGCN5-GFP represents SlGCN5-GFP fusion protein. 35S:GFP represents the control. Scale bars = 20 μm. **(B)** qRT-PCR analysis of *SlGCN5* in different tomato organs. *SlACTIN* served as the internal control. Error bars represent SD of three biological replicates. **(C)** *In situ* hybridization of *SlGCN5* in SAM, floral transition meristem (TM), and FM, respectively. Scale bars = 50 μm.

Cloning primers are listed in **Supplementary Table 1**. After vectors were transformed into *Agrobacterium*, the *Agrobacterium* carrying different vectors were co-infiltrated into tobacco (*Nicotiana benthamiana*) leaves of 4-week-old plants as described previously (Sparkes et al., 2006). The infected tobacco leaves were cultured for 72 h before observation. Notably, 5 μg/ml DAPI was used to visualize the nuclei. The fluorescence was observed by using Olympus (BX53) microscope.

Statistical Analysis

The statistical analysis was conducted using two-tailed *t*-test. The statistically significant differences are indicated by $^{*}p < 0.05$, $^{**}p < 0.01$, or $^{***}p < 0.001$.

RESULTS

Silencing of *SlGCN5* Affects Tomato Plant Development

GCN5 was reported to participate in many biological processes in *Arabidopsis*, especially in plant development (Vlachonasios et al., 2003). In this study, we aimed to investigate the function of GCN5 in tomato development. For this purpose, we first searched for putative homologs of *AtGCN5* in tomato genome sequence, and only one homologous gene with three isoforms was identified (**Supplementary Figure 1**). Among these three isoforms, we chose the one with the highest expression level in tomato inflorescences and the highest protein similarity with AtGCN5 for further study. To explore the effect of *SlGCN5* silencing, tomato seedlings in two-cotyledon stage were infected with *Agrobacterium* carrying the TRV-based VIGS of *SlGCN5* vector. TRV-*SlGCN5* plants exhibited predominantly developmental defects, including reduced plant height, loss of shoot apical dominance, altered pattern of axillary shoot development, shortened internode, late flowering, and male sterility (**Figure 1A**), suggesting that SlGCN5 is required in various tomato plant developmental processes. To verify the phenotype of TRV-*SlGCN5*, we created *SlGCN5-RNAi* plants and found all three of the *SlGCN5-RNAi* lines exhibited similar phenotype with TRV-*SlGCN5* plants (**Figure 1B**).

Results of qRT-PCR showed that *SlGCN5* transcription level in the TRV-*SlGCN5*-infected plants was significantly lower than plants infected with TRV control (**Figure 1C**), confirming that the abnormal phenotypes are caused by *SlGCN5* gene silencing. Similarly, the expression level of *SlGCN5* was significantly reduced in the RNAi lines compared with WT plants (**Figure 1D**).

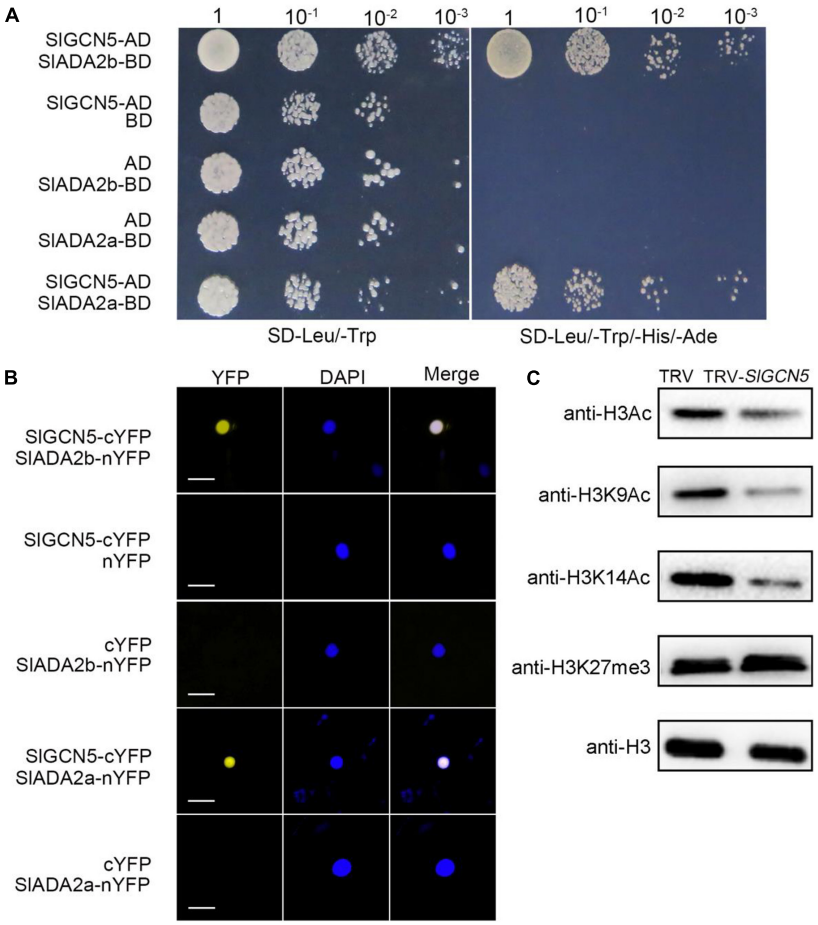

FIGURE 3 | SlGCN5 functions as a histone H3 acetyltransferase. **(A)** Yeast two-hybrid assays of SlGCN5, SlADA2a, and SlADA2b. Full-length cDNAs of *SlGCN5*, *SlADA2a,* and *SlADA2b* were cloned into AD (the prey plasmid pGADT7) and BD (the bait plasmid pGBKT7), respectively. Yeast cells transformed with the indicated plasmids were grown on medium lacking leucine and tryptophan (SD/-Leu/-Trp) and selective medium lacking leucine, tryptophan, histidine, and adenine (SD/-Leu/-Trp/-His/-Ade). **(B)** Bimolecular fluorescent complementation analysis in tobacco leaves. Merge refers to merged images for yellow fluorescent protein (YFP) and DAPI fluorescence. SlGCN5 and SlADA2a/b were fused to cCFP and nYFP, respectively. Scale bars = 20 μm. **(C)** Histone acetyltransferase activity of SlGCN5 determined by *in vivo* histone acetyltransferase assay. Histone acetylation levels were detected by immunoblotting with antibodies of the indicated histone acetylation marks in TRV and TRV-*SlGCN5* plants. Anti-H3 antibody was used as loading control.

Due to the similar phenotypes of *SlGCN5-RNA*i and TRV-*SlGCN5* plants, we used TRV-*SlGCN5* plants for subsequent functional studies in tomato plant development.

SlGCN5 Is Located in the Nucleus and Highly Expresses in Tomato Early Floral Bud

To investigate the expression pattern of *SlGCN5*, we first analyzed subcellular localization of SlGCN5 protein. Results showed that SlGCN5-GFP fusion protein driven by constitutive cauliflower mosaic virus 35S promoter exclusively localized in the nucleus (**Figure 2A**), suggesting that SlGCN5 may have a putative role in histone modification. During tomato plant development, *SlGCN5* transcripts expressed widely in roots, stems, leaves, flowers, and fruits (**Figure 2B**). Our *in situ* hybridization assays revealed that *SlGCN5* is strongly expressed in the upper cell layers of SAM. Meanwhile, *SlGCN5* was expressed throughout the entire floral transition meristem and FM of WT plants, which may overlap with the expression domain of *SlWUS* (**Figure 2C**), hinting at a potential role for SlGCN5 in regulation of meristematic activities.

SlGCN5 Catalyzes Histone Acetylation

The SAGA (Spt-Ada-Gcn5 acetyltransferase) complex is highly conserved for active regulation of gene transcription in yeast and plants (Carrozza et al., 2003; Vlachonasios et al., 2003; Zhou et al., 2017; Li et al., 2019). We also identified ADA2a- and ADA2b-like proteins in tomato (**Supplementary Figure 2**) and named them as SlADA2a and SlADA2b, respectively, which have the highest homology with AtADA2a and AtADA2b in *Arabidopsis*. SlADA2a and SlADA2b have 3 and 2 isoforms respectively. According to the transcript analysis results in tomato inflorescences, XP_004243566 and XP_004239816 were selected as representatives of *SlADA2a* and *SlADA2b* for further study (**Supplementary Figure 3**). To confirm the interactions

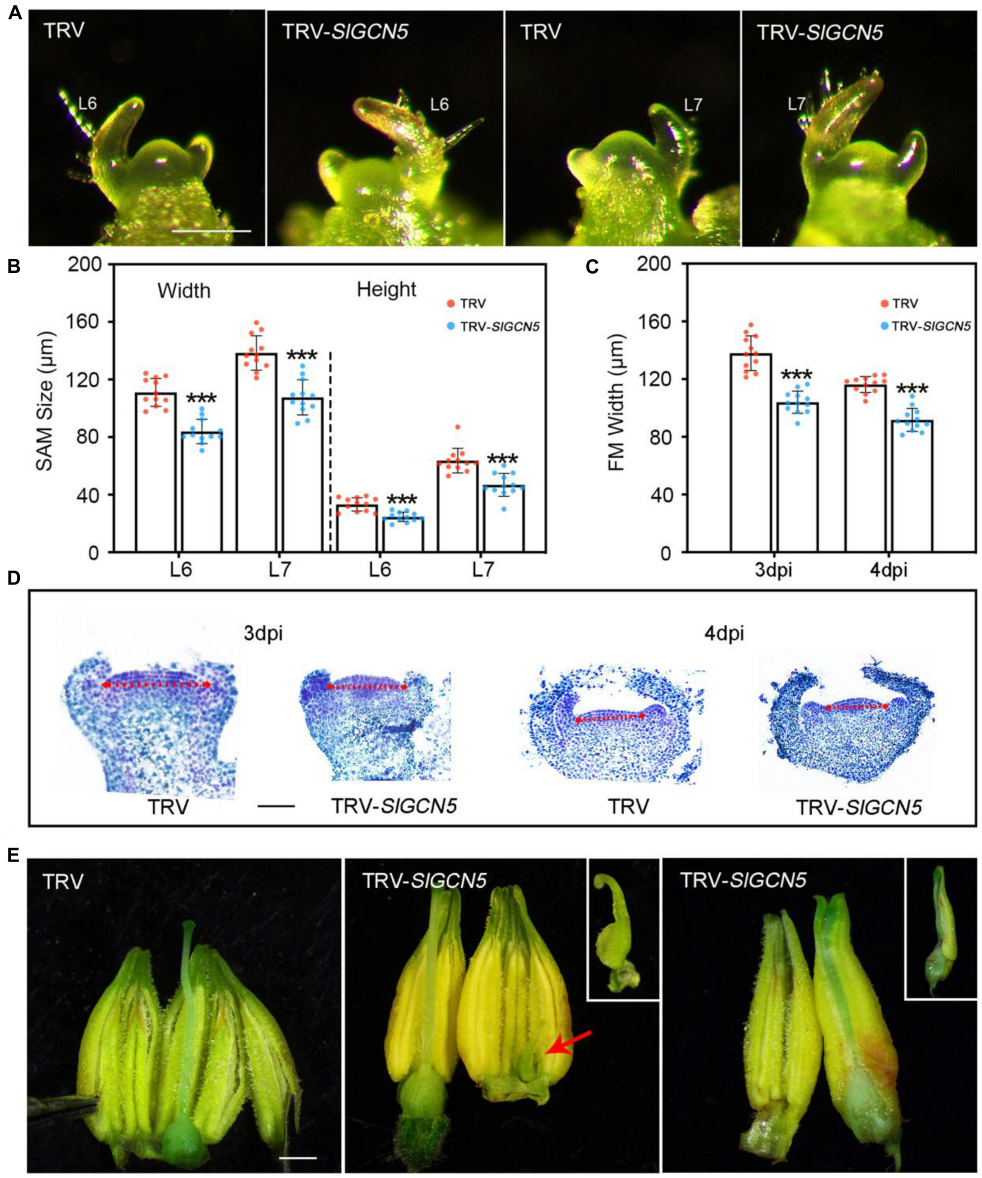

FIGURE 4 | SAM and floral phenotype of silenced-*SlGCN5* plants. **(A)** Images of the SAMs from TRV control and TRV-*SlGCN5* plants. L6 and L7 indicate Leaf 6 and Leaf 7, respectively. Scale bars = 200 μm. **(B)** SAM size from TRV control and TRV-*SlGCN5* plants. Error bar indicates SD of 12 biological replicates. **(C)** FM size from TRV control and TRV-*SlGCN5* plants at 3 and 4 dpi (days post floral initiation). Error bar indicates SD of 12 biological replicates. **(D)** Longitudinal sections of floral meristem of TRV control and TRV-*SlGCN5* plants. The red dash arrow marks the width of each floral meristem. Scale bars = 50 μm. **(E)** Flowers of TRV and TRV-*SlGCN5*. Scale bars = 1 mm. Asterisks indicate significant differences between TRV control and *TRV-SlGCN5* (***$p < 0.001$).

between SlADA2a with SlGCN5 and SlADA2b with SlGCN5, we cloned the full-length cDNAs of SlADA2a, SlADA2b, and SlGCN5 and performed yeast two-hybrid assays. The results showed that SlGCN5 can interact with both SlADA2a and SlADA2b in yeast cells (**Figure 3A**). To verify the yeast two-hybrid results, we performed BiFC analysis in tobacco (*Nicotiana tabacum*) leaves. SlGCN5 was fused to the C-terminus of YFP and named as SlGCN5-cYFP. SlADA2a or SlADA2b was fused to the N-terminus of YFP and named as SlADA2a-nYFP or SlADA2b-nYFP, respectively. We noticed interactions between SlGCN5 and SlADA2a, as well as SlGCN5 and SlADA2b in the nucleus, both of which gave clear signals (**Figure 3B**). These results suggest that SlGCN5 can interact with both SlADA2a and SlADA2b and that the three proteins may form a protein complex.

To test the HAT activity of SlGCN5 *in vivo*, we compared histone acetylation levels in TRV-*SlGCN5* plants with TRV control plants by immunoblotting, using anti-H3K9Ac, anti-H3K14Ac, anti-H3Ac, and anti-H3K27me3 antibodies. Our results revealed that obvious reduction of H3ac, H3K9ac, and H3K14ac levels in TRV-*SlGCN5* compared with

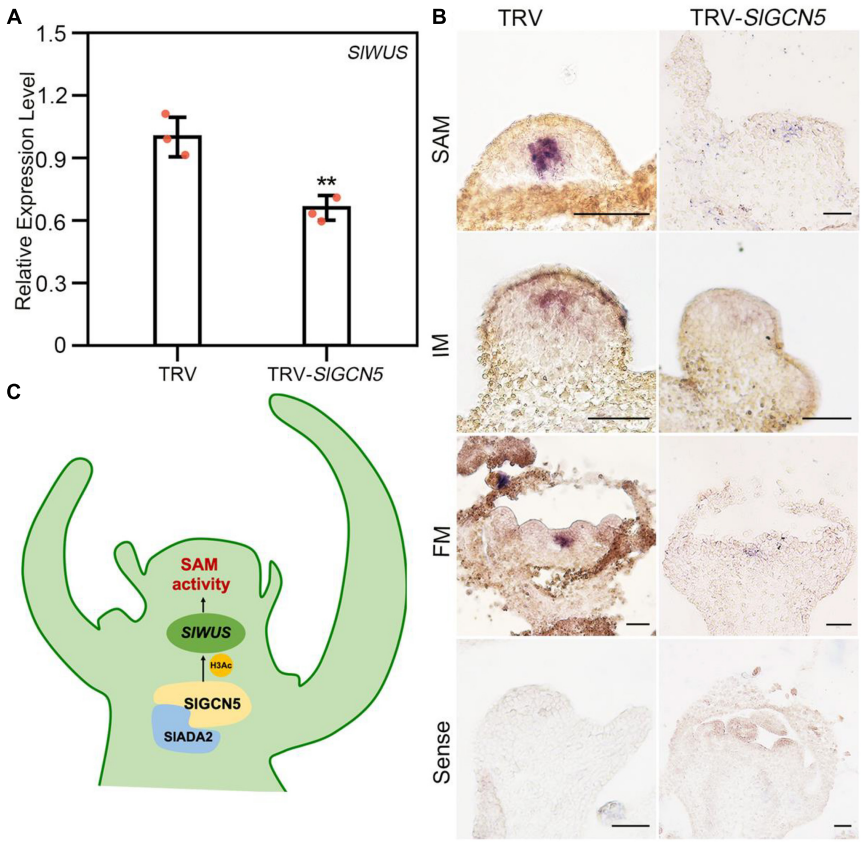

FIGURE 5 | SlGCN5 positively regulates *SlWUS* in tomato. **(A)** qRT-PCR analysis of *SlWUS* expression level in SAM. The error bar represents SD of three biological replicates. The asterisks indicate significant differences between TRV and TRV-*SlGCN5* (**$p < 0.01$). **(B)** Expression of *SlWUS* mRNA in TRV control and TRV-*SlGCN5* plants by *in situ* hybridization. Scale bars = 50 μm. **(C)** Model: SlGCN5 together with SlADA2a and SlADA2b could form HAT complex, which positively regulate *SlWUS* to ensure the proper development of SAM.

the TRV control plants (**Figure 3C**), suggesting that SlGCN5 can catalyze acetylation on histone H3, specifically at H3K9 and H3K14 residues. These results are consistent with the known function of AtGCN5, which was reported to catalyze H3K14ac, and additional histone residues, including H3K9, H3K18, H3K27, and H3K36, and other histones such as H4 and H2B in *Arabidopsis* (Kuo et al., 1996; Grant et al., 1997; Morris et al., 2007). To confirm the role of *SlGCN5* in plant development, we generated transgenic *Arabidopsis* plants by transforming the null-mutant *gcn5-7* with *35S:SlGCN5-GFP*. *35S:SlGCN5-GFP gcn5-7* plants have noticeable gene and protein expressions of SlGCN5, which are examined by qRT-PCR and Western blot (**Supplementary Figure 4A**). Furthermore, *35S:SlGCN5-GFP gcn5-7* plants show almost fully rescued phenotype compared with *gcn5-7* (**Supplementary Figure 4B**), indicating that SlGCN5 functions similarly as AtGCN5.

SlGCN5 Regulates Tomato Shoot Meristem and Flower Development

SlGCN5-silenced plants exhibited reduced plant height. Thus, we measured SAM size in TRV-*SlGCN5* and TRV control plants and observed reduced SAM size in TRV-*SlGCN5* at different developmental stages compared with TRV control plants (**Figures 4A,B**). We also observed reduced FM width but relatively unchanged FM height (**Supplementary Figure 5**) in TRV-*SlGCN5* young floral buds prior to the emergence of the carpel primordia (**Figures 4C,D**). Although FM size in TRV-*SlGCN5* is reduced, floral organ number remains largely unaffected. However, in TRV-*SlGCN5* flowers, we occasionally noticed some carpelloid stamens and carpels fused with stamens [2/15 (13.3%) independent transgenic lines show abnormal flowers] (**Figure 4E**). These results implied that silencing of *SlGCN5* resulted in reduced SAM and FM sizes in tomato and may also influence reproductive floral organ development.

SlGCN5 Positively Regulates *SlWUS* Expression

The reduced SAM and FM size leads us to examine expression changes of *SlWUS* in TRV-*SlGCN5* plants. Expression analysis by qRT-PCR revealed that *SlWUS* transcript level was significantly reduced in TRV-*SlGCN5* meristems (**Figure 5A**). To validate the qRT-PCR results, expression pattern of *SlWUS* was examined by *in situ* hybridization assays. We noticed obviously reduced expression of *SlWUS* mRNA in TRV-*SlGCN5* SAMs and FMs

(**Figure 5B**) compared with TRV control plants. These results suggested that SlGCN5 may positively regulate *SlWUS* expression in tomato shoot meristem and FM. Furthermore, we observed remarkable decrease in the transcript level of *SlCLV1* and *SlCLV3*, the other two key factors in *CLV-WUS* feedback loop, in TRV-*SlGCN5* meristems by qRT-PCR analysis (**Supplementary Figure 6**). These results indicate that SlGCN5 may potentially regulate multiple genes in meristem development of tomato.

DISCUSSION

Histone lysine acetylation is an essential chromatin modification for epigenetic regulation of gene expression in plant development and plant response to environmental stress. AtGCN5 was identified as the first transcription-linked HAT (Brownell et al., 1996), with specificity for histone H3K14ac (Kuo et al., 1996). In addition, GCN5 could also acetylate histone lysine residues such as H3K9, H3K18, H3K23, H3K27, and H3K36 and other histones such as H4 and H2B (Grant et al., 1997; Morris et al., 2007). The SAGA complex is an evolutionarily conserved HAT complex (Spedale et al., 2012), which catalyzes histone acetylation for modulating gene expression and participates in various developmental processes in eukaryotes. In this study, we showed that SlGCN5 can acetylate histones H3K9 and H3K14 at the genomic level in tomato, and SlGCN5 also interacts with SlADA2a and SlADA2b to form HAT unit.

Shoot apical meristem is an organized structure and responds to different development signals. The stem cell pool is maintained within the central zone of the SAM (Fletcher, 2018). Compromised SAM activity leads to premature plant growth stagnation before forming full organs (Laux et al., 1996; Kieffer et al., 2006), whereas plants with overproliferated stem cells in SAM can produce many extra organs (Clark et al., 1993; Taguchi-Shiobara et al., 2001; Yuste-Lisbona et al., 2020). Therefore, the maintenance of SAM homeostasis is key for plant development. It is well-understood that conserved *CLV-WUS* feedback signaling is important for the maintenance of SAM activity (Somssich et al., 2016), but it is not well-known how this feedback loop is modified in various plant species. In this study, we characterized the function of SlGCN5 and studied its role in SAM maintenance. Our data indicate that *SlGCN5* is important to maintain SAM activity in tomato. Weakened SlGCN5 activity affects SAM development and resulted in reduced SAM and FM size (**Figure 4**). Consistent with the phenotype, we also observed reduced *SlWUS* expression (**Figure 5B**) in SAM and FM in the plants with compromised *SlGCN5* activity. However, we did not observe obvious changes in floral organ numbers. Instead, we occasionally observed some carpelloid stamens and carpels fused with stamens (**Figure 4E**). These phenotypes resemble the *S. lycopersicum GT11 (SlGT11)* mutant, in which the function of floral B-class genes was affected (Yang et al., 2020). Therefore, we suspect that the transformation of floral homeotic genes may also exist in TRV-*SlGCN5* plants and that *SlGCN5* could participate in the maintenance of floral organ identity.

Modulation of *CLV-WUS* pathway is one important approach to increase crop yield (Fletcher, 2018). In tomato, several transcription factors that could influence the *CLV-WUS* loop also have been discovered. DEFECTIVE TOMATO MERISTEM (DTM) forms a negative feedback loop with the class III homeodomain-leucine zipper (HD-ZIP III) transcription factors to confine *SlCLV3* and *SlWUS* expression to specific domains in the shoot meristem of tomato (Xu et al., 2019). APETALA2/ethylene responsive factor (AP2/ERF) superfamily transcription factor excessive number of floral organs (ENO) regulates *SlWUS* expression to restrict stem cell proliferation, thereby maintaining floral stem cell homeostasis (Yuste-Lisbona et al., 2020). In addition to transcription factors, *SlWUS* expression can also be regulated by chromatin remodeling factors such as histone deacetylase 19 in tomato (Bollier et al., 2018).

In this study, we identified and investigated the function of *SlGCN5* in tomato meristem development and found that SlGCN5 acts as an acetyltransferase to activate the expression of *SlWUS*, thus maintaining SAM activity (**Figure 5C**). We also noticed SlGCN5 may play a role in floral organ development. These findings could potentially shed light on genetic enhancement of tomato plants.

DATA AVAILABILITY STATEMENT

The original contributions presented in the study are included in the article/**Supplementary Material**, further inquiries can be directed to the corresponding author/s.

AUTHOR CONTRIBUTIONS

BS conceived and designed research, wrote the manuscript, and revised the manuscript. AH and SX conducted experiments. ZY performed data analysis. All authors have read and approved the manuscript.

FUNDING

This work was supported by the Fundamental Research Funds for the Central Universities (0208/14380167) to BS.

ACKNOWLEDGMENTS

We would like to thank Zhuqing Shao (Nanjing University) for providing tomato seeds and Bote Luo from Xiaofeng Wang lab (Northwest A&F University) for providing pTRV1 and pTRV2 vectors.

SUPPLEMENTARY MATERIAL

The Supplementary Material for this article can be found online at: https://www.frontiersin.org/articles/10.3389/fpls.2021.805879/full#supplementary-material

REFERENCES

Anzola, J. M., Sieberer, T., Ortbauer, M., Butt, H., Korbei, B., Weinhofer, I., et al. (2010). putative arabidopsis transcriptional adaptor protein (PROPORZ1) is required to modulate histone acetylation in response to auxin. *Proc. Natl. Acad. Sci. U.S.A.* 107, 10308–10313. doi: 10.1073/pnas.0913918107

Bannister, A. J., and Kouzarides, T. (2011). Regulation of chromatin by histone modifications. *Cell Res.* 21, 381–395. doi: 10.1038/cr.2011.22

Benhamed, M., Bertrand, C., Servet, C., and Zhou, D.-X. (2006). Arabidopsis GCN5, HD1, and TAF1/HAF2 interact to regulate histone acetylation required for light-responsive gene expression. *Plant Cell* 18, 2893–2903. doi: 10.1105/tpc.106.043489

Bertrand, C., Bergounioux, C., Domenichini, S., Delarue, M., and Zhou, D.-X. (2003). Arabidopsis histone acetyltransferase AtGCN5 regulates the floral meristem activity through the WUSCHEL/AGAMOUS pathway. *J. Biol. Chem.* 278, 28246–28251. doi: 10.1074/jbc.M302787200

Bollier, N., Sicard, A., Leblond, J., Latrasse, D., Gonzalez, N., Gevaudant, F., et al. (2018). At-MINI ZINC FINGER2 and Sl-INHIBITOR OF MERISTEM ACTIVITY, a conserved missing link in the regulation of floral meristem termination in *Arabidopsis* and tomato. *Plant Cell* 30, 83–100. doi: 10.1105/tpc.17.00653

Brownell, J. E., Zhou, J., Ranalli, T., Kobayashi, R., Edmondson, D. G., Roth, S. Y., et al. (1996). Tetrahymena histone acetyltransferase A: a homolog to Yeast Gcn5p linking histone acetylation to gene activation. *Cell* 84, 843–851. doi: 10.1016/S0092-8674(00)81063-6

Carrozza, M. J., Utley, R. T., Workman, J. L., and Côté, J. (2003). The diverse functions of histone acetyltransferase complexes. *Trends Genet.* 19, 321–329. doi: 10.1016/S0168-9525(03)00115-X

Chu, Y. H., Jang, J. C., Huang, Z., and van der Knaap, E. (2019). Tomato locule number and fruit size controlled by natural alleles of lc and fas. *Plant Direct* 3:e00142. doi: 10.1002/pld3.142

Clark, S. E., Running, M. P., and Meyerowitz, E. M. (1993). Clavata1, a regulator of meristem and flower development in *Arabidopsis*. *Development* 119, 397–418.

Cohen, R., Schocken, J., Kaldis, A., Vlachonasios, K. E., Hark, A. T., and McCain, E. R. (2009). The histone acetyltransferase GCN5 affects the inflorescence meristem and stamen development in *Arabidopsis*. *Planta* 230, 1207–1221. doi: 10.1007/s00425-009-1012-5

Cortina, C., and Culiáñez-Macià, F. A. (2004). Tomato transformation and transgenic plant production. *Plant Cell Tissue Organ Cult.* 76, 269–275. doi: 10.1023/B:TICU.0000009249.14051.77

Daum, G., Medzihradszky, A., Suzaki, T., and Lohmann, J. U. (2014). A mechanistic framework for noncell autonomous stem cell induction in *Arabidopsis*. *Proc. Natl. Acad. Sci. U.S.A.* 111:14619.

Fletcher, J. C. (2018). The CLV-WUS stem cell signaling pathway: a roadmap to crop yield optimization. *Plants* 7:87. doi: 10.3390/plants7040087

Fu, D.-Q., Zhu, B.-Z., Zhu, H.-L., Jiang, W.-B., and Luo, Y.-B. (2005). Virus-induced gene silencing in tomato fruit: VIGS in tomato fruit. *Plant J.* 43, 299–308. doi: 10.1111/j.1365-313X.2005.02441.x

Galli, M., and Gallavotti, A. (2016). Expanding the regulatory network for meristem size in plants. *Trends Genet.* 32, 372–383. doi: 10.1016/j.tig.2016.04.001

Grant, P. A., Duggan, L., Cote, J., Roberts, S. M., Brownell, J. E., Candau, R., et al. (1997). Yeast Gcn5 functions in two multisubunit complexes to acetylate nucleosomal histones: characterization of an Ada complex and the SAGA (Spt/Ada) complex. *Genes Dev.* 11, 1640–1650. doi: 10.1101/gad.11.13.1640

Han, H., Liu, X., and Zhou, Y. (2020). Transcriptional circuits in control of shoot stem cell homeostasis. *Curr. Opin. Plant Biol.* 53, 50–56.

Kieffer, M., Stern, Y., Cook, H., Clerici, E., Maulbetsch, C., Laux, T., et al. (2006). Analysis of the transcription factor WUSCHEL and its functional homologue in antirrhinum reveals a potential mechanism for their roles in meristem maintenance. *Plant Cell* 18, 560–573. doi: 10.1105/tpc.105.039107

Kornet, N., and Scheres, B. (2009). Members of the GCN5 histone acetyltransferase complex regulate PLETHORA-mediated root stem cell niche maintenance and transit amplifying cell proliferation in *Arabidopsis*. *Plant Cell* 21, 1070–1079. doi: 10.1105/tpc.108.065300

Kudla, J., and Bock, R. (2016). Lighting the way to protein-protein interactions: recommendations on best practices for bimolecular fluorescence complementation analyses[OPEN]. *Plant Cell* 28, 1002–1008. doi: 10.1105/tpc.16.00043

Kuo, M.-H., Brownell, J. E., Sobel, R. E., Ranalli, T. A., Cook, R. G., Edmondson, D. G., et al. (1996). Transcription-linked acetylation by Gcn5p of histones H3 and H4 at specific lysines. *Nature* 383, 269–272. doi: 10.1038/383269a0

Laux, T., Mayer, K. F. X., Berger, J., and Jurgens, G. (1996). The WUSCHEL gene is required for shoot and floral meristem integrity in *Arabidopsis*. *Development* 122, 87–96.

Li, H., Qi, M., Sun, M., Liu, Y., Liu, Y., Xu, T., et al. (2017). Tomato Transcription factor SlWUS plays an important role in tomato flower and locule development. *Front. Plant Sci.* 8:457. doi: 10.3389/fpls.2017.00457

Li, S., Lin, Y.-C. J., Wang, P., Zhang, B., Li, M., Chen, S., et al. (2019). The AREB1 transcription factor influences histone acetylation to regulate drought responses and tolerance in populus trichocarpa. *Plant Cell* 31, 663–686. doi: 10.1105/tpc.18.00437

Mao, Y., Pavangadkar, K. A., Thomashow, M. F., and Triezenberg, S. J. (2006). Physical and functional interactions of Arabidopsis ADA2 transcriptional coactivator proteins with the acetyltransferase GCN5 and with the cold-induced transcription factor CBF1. *Biochim. Biophys. Acta* 1759, 69–79.

Minh, B. Q., Nguyen, M. A., and von Haeseler, A. (2013). Ultrafast approximation for phylogenetic bootstrap. *Mol. Biol. Evol.* 30, 1188–1195. doi: 10.1093/molbev/mst024

Morris, S. A., Rao, B., Garcia, B. A., Hake, S. B., Diaz, R. L., Shabanowitz, J., et al. (2007). Identification of histone H3 lysine 36 acetylation as a highly conserved histone modification. *J. Biol. Chem.* 282, 7632–7640. doi: 10.1074/jbc.M607909200

Muños, S., Ranc, N., Botton, E., Bérard, A., Rolland, S., Duffé, P., et al. (2011). Increase in tomato locule number is controlled by two single-nucleotide polymorphisms located near WUSCHEL1[C][W]. *Plant Physiol.* 156, 2244–2254. doi: 10.1104/pp.111.173997

Nguyen, L.-T., Schmidt, H. A., von Haeseler, A., and Minh, B. Q. (2015). IQ-TREE: a fast and effective stochastic algorithm for estimating maximum-likelihood phylogenies. *Mol. Biol. Evol.* 32, 268–274. doi: 10.1093/molbev/msu300

Périlleux, C., Lobet, G., and Tocquin, P. (2014). Inflorescence development in tomato: gene functions within a zigzag model. *Front. Plant Sci.* 5:121. doi: 10.3389/fpls.2014.00121

Pfeiffer, A., Wenzl, C., and Lohmann, J. U. (2017). Beyond flexibility: controlling stem cells in an ever changing environment. *Curr. Opin. Plant Biol.* 35, 117–123. doi: 10.1016/j.pbi.2016.11.014

Rodríguez-Leal, D., Lemmon, Z. H., Man, J., Bartlett, M. E., and Lippman, Z. B. (2017). Engineering quantitative trait variation for crop improvement by genome editing. *Cell* 171, 470–480.e8. doi: 10.1016/j.cell.2017.08.030

Ruggieri, V., Alexiou, K., Morata, J., Argyris, J., and Benhamed, M. (2020). GCN5 modulates salicylic acid homeostasis by regulating H3K14ac levels at the 5′ and 3′ ends of its target genes. *Nucleic Acids Res.* 48, 5953–5966.

Schmitz, G., and Theres, K. (1999). Genetic control of branching in *Arabidopsis* and tomato. *Curr. Opin. Plant Biol.* 2, 51–55. doi: 10.1016/S1369-5266(99)80010-7

Schoof, H., Lenhard, M., Haecker, A., Mayer, K. F. X., Jürgens, G., and Laux, T. (2000). The stem cell population of arabidopsis shoot meristems is maintained by a regulatory loop between the CLAVATA and WUSCHEL genes. *Cell* 100, 635–644. doi: 10.1016/S0092-8674(00)80700-X

Sekhar, K., and Sawhney, V. K. (1984). A scanning electron microscope study of the development and surface features of floral organs of tomato (*Lycopersicon esculentum*). *Can. J. Bot.* 62, 2403–2413.

Servet, C., Conde e Silva, N., and Zhou, D.-X. (2010). Histone acetyltransferase AtGCN5/HAG1 is a versatile regulator of developmental and inducible gene expression in *Arabidopsis*. *Mol. Plant* 3, 670–677. doi: 10.1093/mp/ssq018

Shahbazian, M. D., and Grunstein, M. (2007). Functions of site-specific histone acetylation and deacetylation. *Annu. Rev. Biochem.* 76, 75–100. doi: 10.1146/annurev.biochem.76.052705.162114

Shang, E., Ito, T., and Sun, B. (2019). Control of floral stem cell activity in Arabidopsis. *Plant Signal. Behav.* 14:1659706. doi: 10.1080/15592324.2019.1659706

Somssich, M., Je, B. I., Simon, R., and Jackson, D. (2016). CLAVATA-WUSCHEL signaling in the shoot meristem. *Development* 143, 3238–3248. doi: 10.1242/dev.133645

Sparkes, I. A., Runions, J., Kearns, A., and Hawes, C. (2006). Rapid, transient expression of fluorescent fusion proteins in tobacco plants and generation of stably transformed plants. *Nat. Protoc.* 1, 2019–2025. doi: 10.1038/nprot.2006.286

Spedale, G., Timmers, H. T. M., and Pijnappel, W. W. M. P. (2012). ATAC-king the complexity of SAGA during evolution. *Genes Dev.* 26, 527–541. doi: 10.1101/gad.184705.111

Sun, B., Zhou, Y., Cai, J., Shang, E., Yamaguchi, N., Xiao, J., et al. (2019). Integration of transcriptional repression and polycomb-mediated silencing of WUSCHEL in floral meristems. *Plant Cell* 31, 1488–1505. doi: 10.1105/tpc.18.00450

Taguchi-Shiobara, F., Yuan, Z., Hake, S., and Jackson, D. (2001). The fasciated ear2 gene encodes a leucine-rich repeat receptor-like protein that regulates shoot meristem proliferation in maize. *Genes Dev* 15, 2755–2766. doi: 10.1101/gad.208501

Tripodi, P. (2020). *Crop Breeding: Genetic Improvement Methods. Methods in Molecular Biology*. New York, NY: Humana.

Vlachonasios, K. E., Thomashow, M. F., and Triezenberg, S. J. (2003). Disruption mutations of ADA2b and GCN5 transcriptional adaptor genes dramatically affect arabidopsis growth, development, and gene expression. *Plant Cell* 15, 626–638. doi: 10.1105/tpc.007922

Xu, C., Liberatore, K. L., MacAlister, C. A., Huang, Z., Chu, Y.-H., Jiang, K., et al. (2015). A cascade of arabinosyltransferases controls shoot meristem size in tomato. *Nat. Genet.* 47, 784–792. doi: 10.1038/ng.3309

Xu, Q., Li, R., Weng, L., Sun, Y., Li, M., and Xiao, H. (2019). Domain-specific expression of meristematic genes is defined by the LITTLE ZIPPER protein DTM in tomato. *Commun. Biol.* 2:134. doi: 10.1038/s42003-019-0368-8

Yadav, R. K., Perales, M., Gruel, J., Girke, T., Jnsson, H., and Reddy, G. V. (2011). WUSCHEL protein movement mediates stem cell homeostasis in the *Arabidopsis* shoot apex. *Genes Dev.* 25, 2025–2030.

Yang, L., Qi, S., Touqeer, A., Li, H., Zhang, X., Liu, X., et al. (2020). SlGT11 controls floral organ patterning and floral determinacy in tomato. *BMC Plant Biol.* 20:562. doi: 10.1186/s12870-020-02760-2

Yuste-Lisbona, F. J., Fernández-Lozano, A., Pineda, B., Bretones, S., Ortíz-Atienza, A., García-Sogo, B., et al. (2020). ENO regulates tomato fruit size through the floral meristem development network. *Proc. Natl. Acad. Sci. U.S.A.* 117, 8187–8195. doi: 10.1073/pnas.1913688117

Zhou, S., Jiang, W., Long, F., Cheng, S., Yang, W., Zhao, Y., et al. (2017). Rice homeodomain protein WOX11 recruits a histone acetyltransferase complex to establish programs of cell proliferation of crown root meristem. *Plant Cell* 29, 1088–1104. doi: 10.1105/tpc.16.00908

Conflict of Interest: The authors declare that the research was conducted in the absence of any commercial or financial relationships that could be construed as a potential conflict of interest.

Publisher's Note: All claims expressed in this article are solely those of the authors and do not necessarily represent those of their affiliated organizations, or those of the publisher, the editors and the reviewers. Any product that may be evaluated in this article, or claim that may be made by its manufacturer, is not guaranteed or endorsed by the publisher.

frontiers in Plant Science

ORIGINAL RESEARCH
published: 26 January 2022
doi: 10.3389/fpls.2021.806295

Genome-Wide Association Study of Grain Number in Common Wheat From Shanxi Under Different Water Regimes

Xingwei Zheng[1†], Ling Qiao[1†], Ye Liu[2], Naicui Wei[2], Jiajia Zhao[1], Bangbang Wu[1], Bin Yang[1], Juanling Wang[1] and Jun Zheng[1]**

[1] State Key Laboratory of Sustainable Dryland Agriculture, Institute of Wheat Research, Shanxi Agricultural University, Linfen, China, [2] College of Life Science, Shanxi University, Taiyuan, China

Water availability is a crucial environmental factor on grain number in wheat, which is one of the important yield-related traits. In this study, a diverse panel of 282 wheat accessions were phenotyped for grain number per spike (GNS), spikelet number (SN), basal sterile spikelet number (BSSN), and apical sterile spikelet number (ASSN) under different water regimes across two growing seasons. Correlation analysis showed that GNS is significantly correlated with both SN and BSSN under two water regimes. A total of 9,793 single nucleotide polymorphism (SNP) markers from the 15 K wheat array were employed for genome-wide association study (GWAS). A total of 77 significant marker-trait associations (MTAs) for investigated traits as well as 8 MTAs for drought tolerance coefficient (DTC) were identified using the mixed linear model. Favored alleles for breeding were inferred according to their estimated effects on GNS, based on the mean difference of varieties. Frequency changes in favored alleles associated with GNS in modern varieties indicate there is still considerable genetic potential for their use as markers for genome selection of GNS in wheat breeding.

Keywords: water regime, Shanxi wheat, GNS, GWAS, DTC

OPEN ACCESS

Edited by:
Fa Cui,
Ludong University, China

Reviewed by:
Shuaifeng Geng,
Institute of Crop Sciences, Chinese Academy of Agricultural Sciences, China
Mingming Xin,
China Agricultural University, China

***Correspondence:**
Juanling Wang
13994267508@163.com
Jun Zheng
sxnkyzj@126.com

[†] These authors have contributed equally to this work

Specialty section:
This article was submitted to Plant Physiology, a section of the journal Frontiers in Plant Science

Received: *31 October 2021*
Accepted: *08 December 2021*
Published: *26 January 2022*

Citation:
Zheng X, Qiao L, Liu Y, Wei N, Zhao J, Wu B, Yang B, Wang J and Zheng J (2022) Genome-Wide Association Study of Grain Number in Common Wheat From Shanxi Under Different Water Regimes. Front. Plant Sci. 12:806295. doi: 10.3389/fpls.2021.806295

INTRODUCTION

Wheat (*Triticum aestivum* L.) is one of the most important crops globally, mainly grown in semiarid and arid regions of the world (Khan et al., 2019). To keep pace with the expanding global population, wheat yield is projected to increase 60% by 2050 (Ray et al., 2013; Cao et al., 2020), whereas wheat production will inevitably be affected by abiotic stresses, such as drought stress. As reported, significant wheat yield losses of 40% in less-developed irrigated growing areas occurred (Joshi et al., 2007). Therefore, it is imperative to scale up wheat yield under water deficit conditions, thus ensuring food security.

Wheat yield is determined by three factors, namely, spike number per unit area, grain number per spike (GNS), and thousand grain weight (TGW), which are important grain yield components (Shi et al., 2017). Recent studies have suggested that wheat grain yield is affected more by variation in GNS than by variation in grain size (Feng et al., 2018; Sakuma et al., 2019). GNS in wheat is determined by spikelet number and spikelet fertility, in addition to grain number per spikelet. Among these traits, spikelet number had higher heritability, whereas fertile spikelet number (SN) and grain number per spikelet were manipulatable with different environments. Molecular biology

and genomics have become the key tools to understand the basis of GNS formation and deploying those genes for yield improvement (Cao et al., 2020). For example, the GNS-related genes in cereals, especially in rice, have a series of homologs that have been isolated from wheat by homology-based cloning, including *TaTEF* (Zheng et al., 2014), *FZP* (Dobrovolskaya et al., 2015), *TaTOC1* (Zhao et al., 2016), *TaSPL20*, and *TaSPL21* (Zhang et al., 2017). At the present, there are fewer genes related to the regulation of GNS in map-based cloning. For example, the floret fertility-regulated gene *GNI-A1* (Sakuma et al., 2019), triple-spikelet gene *WFZP* (Du et al., 2021), and aberrant panicle organization 1 gene *APO1* (Kuzay et al., 2019) were shown to be involved in regulating the formation of GNS in wheat. Accordingly, the identification of novel genetic loci controlling GNS is significant for broadening the genetic variation in molecularly designed wheat breeding.

Among the three main yield components in wheat, GNS is more affected by drought stress during the productive period than TGW (Fischer, 2008, 2011). Water deficiency directly affects both the vegetative and reproductive growth stages, ultimately reducing fertility parameters, grain yield components, and thus final yield (Ahmed et al., 2021; Jallouli et al., 2021). It seems likely that improvements in grain yield may derive from improvements in grain number, particularly under water stress conditions (Li et al., 2019; Sun et al., 2019; Zhang et al., 2020). Therefore, dissecting the genetic basis of grain number and its responses to water deficit is indispensable for the improvement of wheat.

To date, most of the reported quantitative trait loci (QTLs) controlling GNS and spikelet infertility were identified under high-yield potential conditions (Miura et al., 1992; Li et al., 2007; Ma et al., 2007; Jia et al., 2013; Zhai et al., 2016; Zhang H. et al., 2016; Cui et al., 2017; Deng et al., 2017). Relatively few studies have examined the consistency of QTLs under varying environmental stress conditions (Bilgrami et al., 2020). Therefore, it is essential to identify stable genetic loci for better agronomic performance, which can be selected for producing stable, high-yielding genotypes under diverse environments. The lack of major, stable genetic loci across multiple environments as well as the low-marker densities restricts the utilization efficiency for both marker-assisted selection and gene isolation (Ma et al., 2019). Despite this, most of the QTLs have been identified using biparental or multi-parental populations. The genetic variation of the population has been so far limited only to the genomes of the parents (Bilgrami et al., 2020). Based on the high-density single nucleotide polymorphisms (SNPs), genome-wide association study (GWAS) has been identified as an effective tool for discovering QTLs and genes associated with target traits in various crops such as wheat (Wang et al., 2014; Juliana et al., 2019). Shi et al. (2017) detected 62 significantly associated signals for kernel number per spike at 47 SNP loci on 19 chromosomes through GWAS. However, research to identify major stable loci of yield-related traits in wheat under water-stress conditions has been conducted using GWAS has been limited.

Shanxi Province in China is situated in a semiarid region, with an annual rainfall between 400 and 650 mm. Dryland occupies 70% of the wheat planting area. Shanxi has a long history of wheat planting and has always been famous for its drought resistance and stable yield varieties of wheat. Varieties such as Jinmai 33, Chang 6878, and Jinmai 47 were widely cultivated in dryland areas. The descendants of these excellent accessions are the main varieties currently spreading in China, thus making it a representative to study the genetic evolution of wheat GNS in semiarid areas and the effects of water regimes on GNS with Shanxi wheat varieties. In this study, 15 K SNP array markers were used to identify the population structure of the Shanxi wheat panel and genome-wide MTAs of wheat GNS, SN, BSSN, and ASSN under different water regimes. This association analysis provides useful information for marker-assisted selection in breeding wheat for increasing yield.

MATERIALS AND METHODS

Plant Material

A total of 282 hexaploid wheat collections in Shanxi Province of China were used in this experiment (**Supplementary Table 1**). These genotypes differ by their origin and planting model, including 127 irrigated wheat cultivars, 115 dryland cultivars, and 40 landraces. These landrace samples are Chinese wheat mini core collection from Shanxi (Hao et al., 2011).

Field Experiment

This study examined the results under two irrigation regimes at the experimental station of Linfen in Shanxi Province, China, located at 36°48′ N and 111°30′ E. The study was conducted over 2 consecutive years (2019–2020, 2020–2021). The monthly rainfall rates and average temperature during the two trial years are presented in **Supplementary Figure 1**. The rainfall amount during the months of October–May in 2019–2020 was 201 mm and in 2020–2021 was 111 mm. The regimes were conducted as irrigation: once (I1) at the overwintering stage and three times (I3) at overwintering, jointing, and booting stage. The wheat genotypes were assessed in controlled field conditions using a randomized complete block design with three replications. Each plot represented one experimental unit: a single-row plot of 1.5 m in length containing 21 seeds evenly distributed with 0.30 m spacing between rows. The field trial area was leveled before seeding to ensure that all plants would be under the same water level.

Trait Phenotyping and Data Analysis

Ten representative primary tillers from the center of each row were collected to investigate the following traits: total SN per spike, the GNS, the basal sterile spikelet number (BSSN), and the apical sterile spikelet number (ASSN). After harvest, thousand grain weight (TGW) was measured. The drought tolerance coefficient (DTC) of GNS, SN, and TGW values was calculated using the formula I1/I3, while for BSSN and ASSN, it was calculated using I3/I1.

To eliminate environmental effects, the best linear unbiased prediction (BLUP) values across two repetitions were conducted using *R*. The H^2 value was calculated using the formula $H^2 = VG/(VG + VE/r)$, where *VG* is the genotypic variance, *VE* is the environment variance, and *r* is the number of replications

TABLE 1 | Analysis of variance in SN, GNS, BSSN, ASSN, and TGW of wheat under different irrigation conditions (I1 and I3) during the 2019–2020 and 2020–2021 growing seasons.

Traits	Water regimes	Descriptive statistics		Variance parameters			
		Mean	Range	G	G × E	E	H^2 (%)
GNS	I1	41.12	22.50–68.00	18.16	49.15	32.68	87.76
(number)	I3	52.07	28.00–88.60	**	***	***	
SN	I1	21.50	16.80–26.20	42.94	56.08	0.98	82.40
(number)	I3	21.66	16.75–25.80	***	***		
BSSN	I1	2.00	0.00–7.60	33.19	49.25	17.57	68.18
(number)	I3	1.86	0.00–5.80	***	***		
ASSN	I1	0.63	0.00–4.20	8.455	72.28	19.274	26.46
(number)	I3	0.52	0.00–3.00		***	**	
TGW	I1	37.13	21.50–54.95	46.83	21.15	32.03	95.06
(g)	I3	39.93	17.00–57.75	***		**	

Data were presented as the mean.
*** and *** represent significance level of $P < 0.01$ and $P < 0.001$.*
GNS, the grain number per spike; SN, total spikelet number per spike; BSSN, the basal sterile spikelet number; ASSN, the top sterile spikelet number; TGW, thousand-grain weight; I1, irrigation once at overwintering stage; I3, irrigation three times at overwintering, jointing, and booting stage.

TABLE 2 | Correlation analysis of different traits for 282 common wheat accessions under the I1 and I3 treatments.

	SN	GNS	BSSN	ASSN	TGW
SN		0.429**	0.194**	0.162**	0.083
GNS	0.302**		−0.509**	−0.022	0.245
BSSN	0.241**	−0.340**		0.091	−0.339**
ASSN	0.181**	−0.263**	0.169**		−0.005
TGW	0.105	0.076	−0.215**	−0.070	

*The lower left triangular matrix represents I1; the upper right triangular matrix represents I3. **Indicates significant differences at $P < 0.01$.*

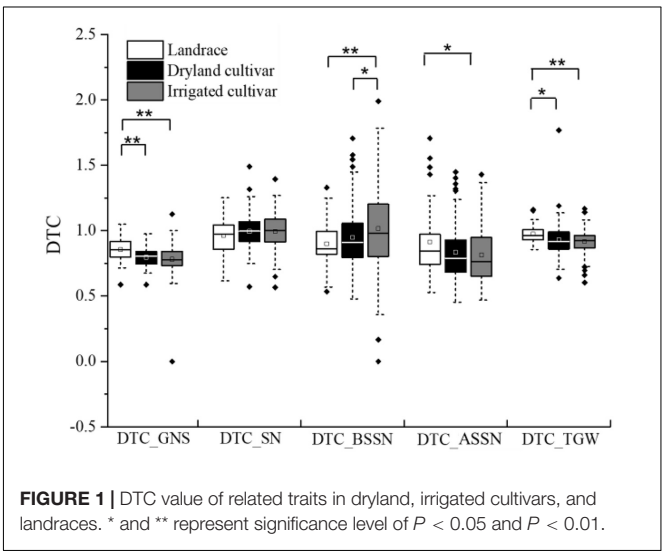

FIGURE 1 | DTC value of related traits in dryland, irrigated cultivars, and landraces. * and ** represent significance level of $P < 0.05$ and $P < 0.01$.

(Lin et al., 2020). Correlation analyses were performed using SPSS 20 (IBM SPSS Statistics; IBM Corp., Armonk, NY, United States).

Single Nucleotide Polymorphism Genotyping

For the genotyping assay, approximately 1.0 g of a young leaf was collected from each wheat genotype before they reached the elongation stage. Genomic DNA was extracted using the cetyl trimethyl ammonium bromide (CTAB) method and stored at − 80°C until use. DNA dissolved in TE buffer was sent to MOL-BREEDING company (Shijiazhuang, China) for high-throughput genotyping using a set of GenoBaits Wheat 20995 (10111mSNP) panels. After filtering out markers with minimum allele frequency (MAF) <0.05 and markers with >10% missing data, as well as >20% heterozygosity (Jung et al., 2021), a total of 9,793 high-quality SNPs were included in the following population structure and GWAS analyses.

Genome-Wide Association Analysis

TASSEL 5.0 was used to examine the associations between SNPs and phenotypic variations (Bradbury et al., 2007). SNPs-trait association was tested using the mixed linear model (MLM). A threshold P-value of < 0.001 or $-\log_{10}(P\text{-value}) < 3$ was used as the screening criterion (Guan et al., 2019). The linkage disequilibrium (LD) of each single SNP marker was extended on each chromosome. The extended region where the LD between nearby SNPs and the peak SNP decayed to $r^2 = 0.2$ was defined as the local LD-based QTL interval (Zhang X. H. et al., 2016). Therefore, significant SNPs were selected with a physical distance ≤ LD-based interval and referred to as a conservative QTL.

RESULTS

Phenotype Assessments

The phenotypes of 282 wheat accessions were characterized during two crop seasons (2019–2021) in I1 and I3 environments. Descriptive statistics data and frequency distribution of the genotypes for the investigated traits in I1 and I3 environments

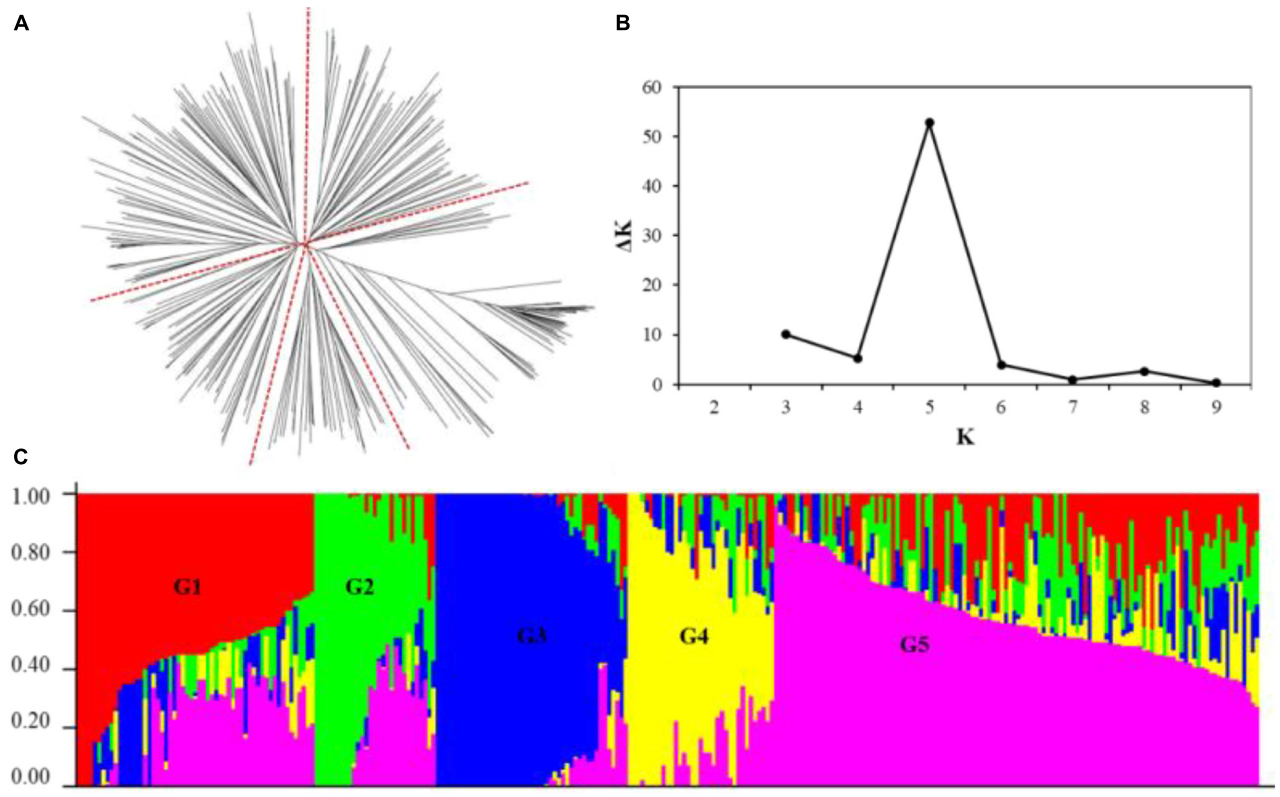

FIGURE 2 | Population structure of the 282 wheat accessions using 9,793 single nucleotide polymorphism (SNP) markers across the whole genome. **(A)** Neighbor-joining tree of the 282 accessions; **(B)** a number of subpopulations estimated by ΔK at a range of K values; and **(C)** population structure inference of the 282 wheat genotypes based on the SNP marker, using STRUCTURE version 2.3.4.

based on the average data over years are presented in **Table 1** and **Supplementary Figure 2**, respectively. There was a significant genetic variation among accessions for all the traits in the two water conditions, the water treatments had highly significant effects on GNS and ASSN ($p < 0.001$; **Table 1** and **Supplementary Figure 2**). In the I3 condition, averaged over 2 years, GNS of the wheat genotypes varied from 28.00 to 88.60, generated 16.75–25.80 SN, 0–5.80 BSSN, 0–3 ASSN, and weighted 17.00–57.75 g TGW. After water regimes were changed to I1, the genotypes varied in GNS from 22.50 to 68.00, generated 16.80–26.20 SN, 0–7.6 BSSN, 0–4.2 ASSN, and weighted 21.50–54.95 g TGW. Compared with the I1 treatment, under the I3 condition, the mean value for GNS was significantly increased by 26.63%, and SN and TGW were both slightly increased to 0.74 and 7.54%, respectively. The highest heritability was observed for TGW, GNS, and SN with values of H^2 = 95.06, H^2 = 87.76, and H^2 = 82.40 (**Table 1**). Compared with I1, BSSN and ASSN were decreased by 7.53 and 21.15%, respectively.

For the three different types, compared with I1, under the I3 irrigation regime, the highest increase in the mean value of GNS happened in irrigated varieties (29.85%) than in dryland ones (25.33%) and landraces (20.44%). Among the irrigated varieties, Taimai 101, Xiangmai 23, and Yunhei 161 were most sensitive to water supply, with an increase in GNS by 89.53, 84.23, and 73.57%, respectively. Otherwise, the most insensitive ones were Ziyou 5, Yunyin 1, and Tai 615, and their GNS were increased by 3.01, 3.37, and 3.40%. SN did not change much under two conditions, namely, irrigated varieties and dryland varieties, and landraces were increased by 0.38, 0.95, and 1.24% in I3, respectively. The TGW of irrigated varieties increased the most, 14.30%, that of dryland varieties increased by 6.89%, and that of landrace varieties increased by 3.84%. In the I3 condition, the ASSN decreased by 32.42% in irrigated varieties, more than in dryland (22.93%) and landraces (− 6.46%), whereas the BSSN were less decreased in irrigated varieties (1.26%) than in dryland varieties (10.71%) and landraces (12.17%).

Correlation Between Traits Under Two Water Regimes

Pearson's coefficient of correlation between traits was calculated based on the data averaged across 2 years under the two irrigation conditions (**Table 2**). GNS was significantly positively correlated with SN under both I1 and I3 conditions but was significantly negatively correlated with BSSN under the two irrigation regimes. GNS was also significantly negatively correlated with ASSN under I1. In addition, TGW was slightly positively correlated with GNS but significantly negatively correlated with BSSN under both conditions. Importantly, compared with the I1 treatment, the correlation between GNS and SN, as well as GNS and BSSN, were

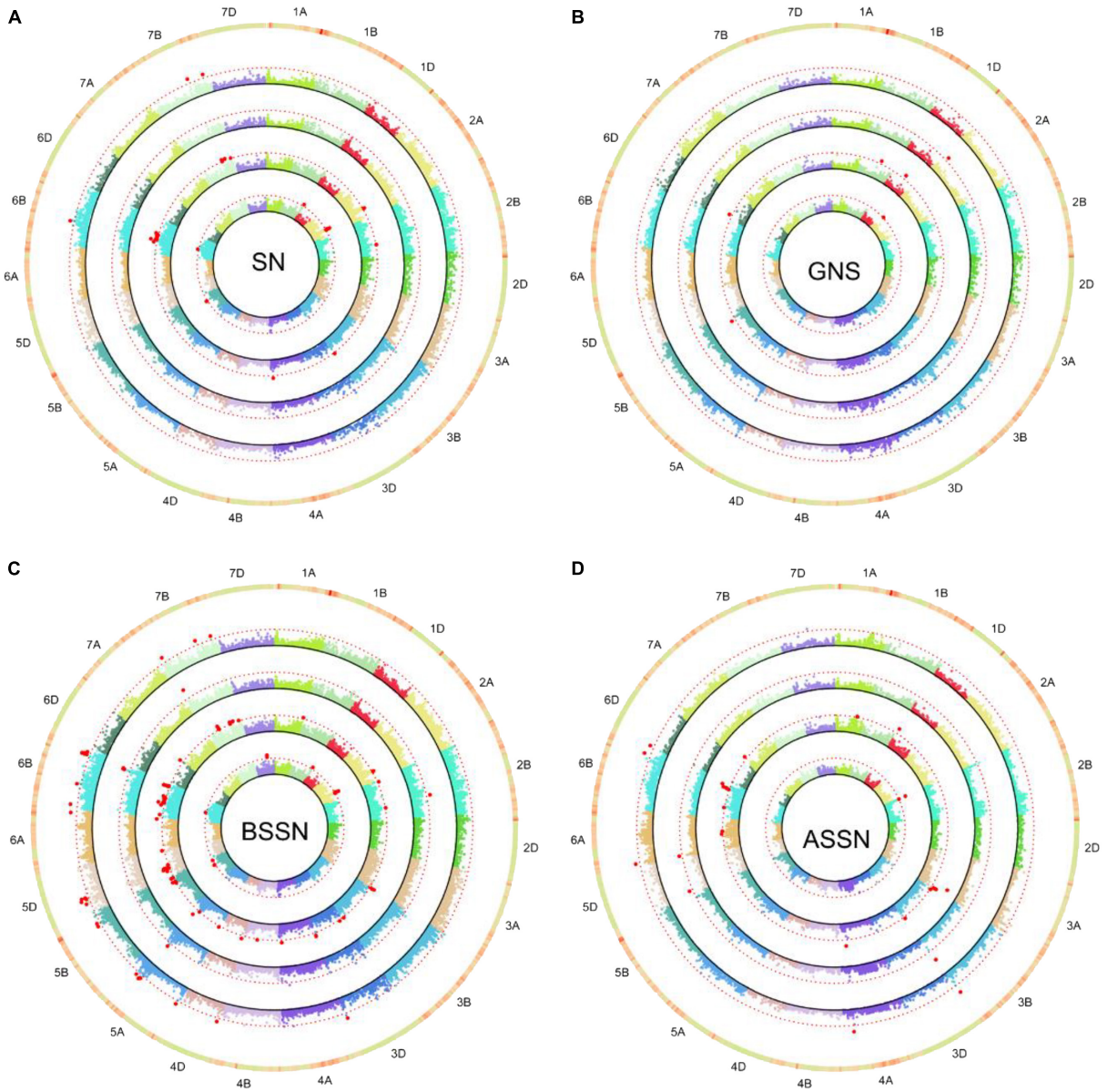

FIGURE 3 | Circular-Manhattan plots for SNP significantly associated with SN **(A)**, grain number per spike (GNS, **B**), the basal sterile spikelet number (BSSN, **C**), and the top sterile spikelet number (ASSN, **D**) under two water regimes identified by genome-wide association study based on the mixed linear model (MLM). Circles from inner to outer represents I1-BLUP, I3-BLUP, BLUP-ALL, and DTC_{trait}, respectively. The dashed red line represents the threshold $-\log_{10}$ (*P*-value) value of 3.0. SNPs markers that met this significant level are highlighted with red dots.

closer in the I3 treatment, while the correlation between GNS and ASSN was decreased. Results also showed that under both conditions, the correlation coefficients between GNS and both SN and BSSN were highest, while the correlation coefficients between GNS and TGW were lower.

The Effect of Water Regimes Evaluated by Drought Tolerance Coefficient Value

The DTC value for each trait was used to evaluate the influence caused by the different water regimes. DTC_{TGW} and DTC_{SN} of most accessions were close to 1 (**Figure 1**), indicating that these traits of corresponding wheat type were less influenced by water supply. The mean values of DTC_{GNS} in dryland cultivars and irrigated cultivars were 0.81 and 0.79, respectively, and DTC_{GNS} values in landraces were larger than in modern cultivars. The mean value of DTC_{BSSN} and DTC_{ASSN} was less than 1, indicating that the BSSN and ASSN were decreased in the I3 treatment. DTC_{ASSN} was lower than DTC_{BSSN}, indicating that compared with BSSN, ASSN was more influenced by water conditions, especially in modern cultivars. Under the two environments, both DTC_{ASSN} and DTC_{BSSN} of this

TABLE 3 | List of significant ($p < 0.001$) marker-DTC$_{trait}$ associations detected by GWAS using the MLM model.

Trait	Marker	Chr	Position (Mb)	*F* value	*p*-value	$-\log_{10} p$	R^2 (%)
DTC_{GNS}	*2A_82034103*	2A	82.03	7.31874	8.05E-04	3.09	4.64
DTC_{SN}	*1B_668028290*	1B	66.80	7.93578	4.50E-04	3.35	5.83
DTC_{SN}	*2A_567774459*	2A	547.34-578.37	8.98284	1.68E-04	3.78	6.52
DTC_{SN}	*5B_448275690*	5B	447.78-448.28	7.61609	6.07E-04	3.22	5.53
DTC_{SN}	*6B_283377788*	6B	283.38	7.50109	6.77E-04	3.17	5.44
DTC_{BSSN}	*5B_603760636*	5B	603.76	7.15395	9.41E-04	3.03	5.32
DTC_{BSSN}	*7D_412588658*	7D	408.467-412.59	8.52763	2.57E-04	3.59	6.35
DTC_{ASSN}	*2B_3313327*	2B	3.31-5.67	10.30421	4.90E-05	4.31	7.42

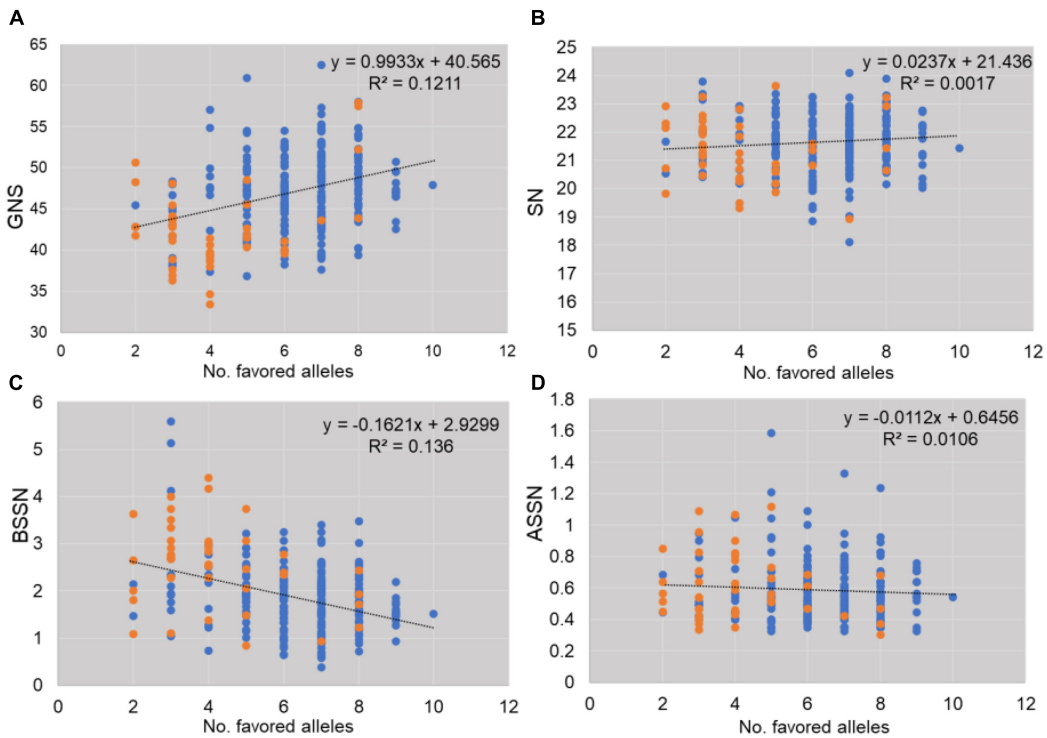

FIGURE 4 | Effects of favorable alleles estimated for traits studied (**A**: GNS, **B**: SN, **C**: BSSN, **D**: ASSN). Blue spots indicate modern varieties and orange spots indicate landraces.

panel showed a larger variation range than DTC_{GNS}, DTC_{SN}, and DTC_{TGW}.

Association Analysis Between Phenotypes and Single Nucleotide Polymorphism Markers

Two methods were used to analyze the population structure of wheat genotypes from Shanxi. According to the phylogenetic tree constructed using the neighbor-joining method based on Nei's standard genetic distance, the 282 genotypes were partitioned into five principal groups (**Figure 2A**). When the number of subpopulations (*K*s) was plotted against the ΔK calculated using software STRUCTURE version 2.3.4, the highest ΔK was observed at $K = 5$ (**Figures 2B,C**), which, following the results obtained using the phylogenetic tree, confirmed that the 282 accessions could be divided into five subgroups. The largest group (G5) consists of 115 genotypes, and the other four groups (G1–G4) consist of 57, 30, 45, and 35 genotypes, respectively. Most genotypes belonging to G2 and G4 were modern cultivars developed after 2000. Landraces were grouped into G3. The early-year cultivars, as well as the well-known drought-tolerant wheat accessions such as Jinmai 47 and Chang 6878, were clustered in G1.

The MLM model was used to make association analyses between phenotype traits and SNP markers. GWAS was conducted on four datasets: BLUP-I1, BLUP-I3, BLUP-ALL, and DTC. Significant MTAs [$-\log_{10}$ (*p*-value) ≥ 3.0] were identified for the traits in the two water regimes examined. In total, 77 MTAs distributed on 20 chromosomes (except 2D) were identified. Among them, 18, 39, and 20 were on genomes A, B, and D. The phenotypic variation explanation rate (R^2) ranged

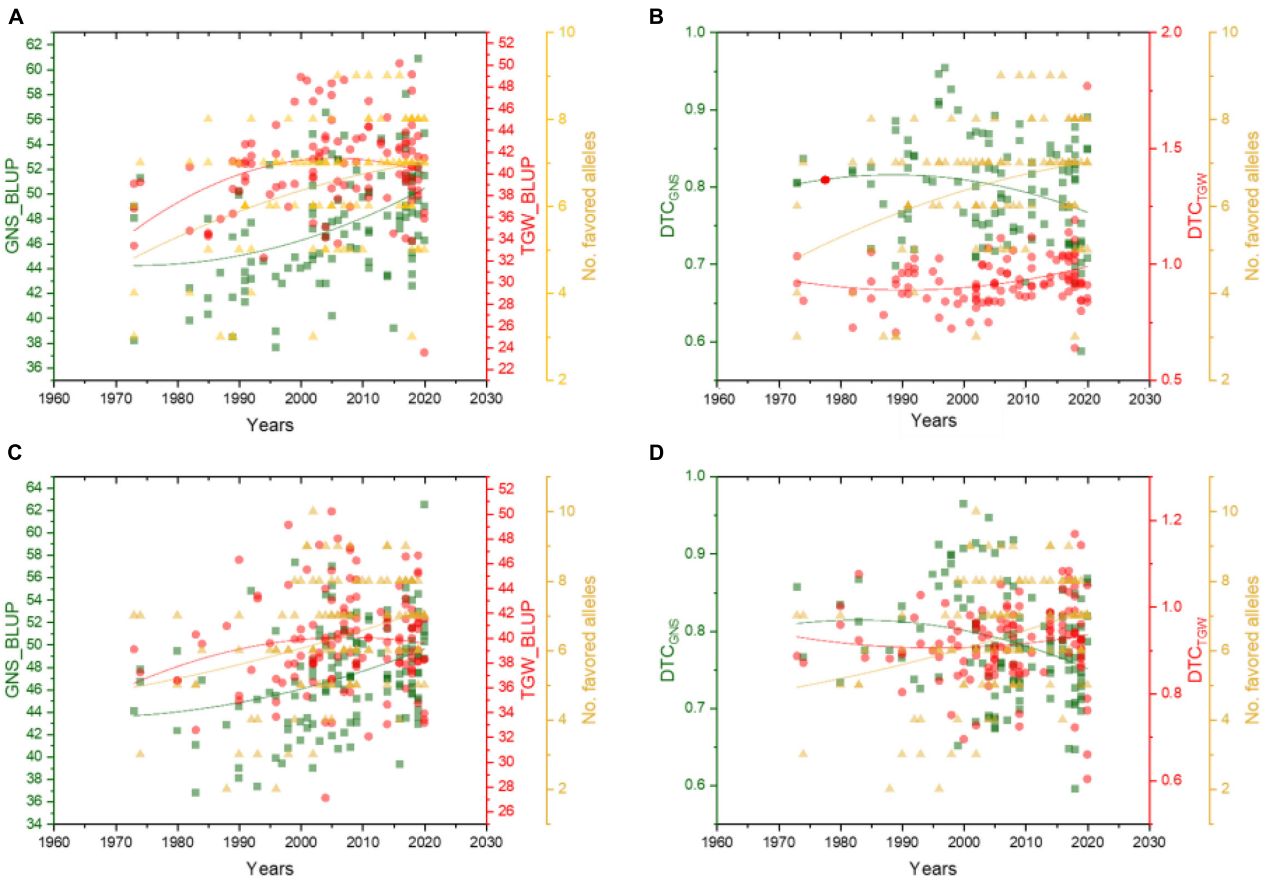

FIGURE 5 | Effect of favorable alleles on GNS, TGW, and their DTC values in dryland **(A,B)** and irrigated wheat **(C,D)** over the years. The red dots represent TGW_BLUP **(A,C)** and DTC_{TGW} **(B,D)**, green squares represent GNS_BLUP **(A,C)** and DTC_{GNS} **(B,D)**, yellow triangles represent the number of favored alleles.

from 4.62 to 11.19% (**Supplementary Table 2**). There were 48 and 21 SNPs examined under I1 and I3, respectively. Among them, five SNPs were significantly associated with the same trait under both water regimes. Meanwhile, five SNPs showed significant associations with two or more traits (**Supplementary Table 2**).

For GNS, nine MTAs were identified on 1B, 1D, 2A, 2B, 3B, 5A, 5B, and 6D. Among these, 4 SNPs under the I1 condition and 4 SNPs under the I3 condition were associated with GNS, respectively. The trait SN was found to be associated with twelve SNPs/genomic regions in I1 and two SNPs in I3. The BSSN trait was associated with the largest number of SNPs: 41 markers/regions were identified in I1 and I3. Twelve markers were found associated with ASSN in the I1 condition and five in the I3 condition. Under both I1 and I3 treatments, four SNPs including *5D_156778694*, *5D_184179300*, *6B_52209942*, and *6B_619721911* were identified for BSSN as well as *3B_806263030* for ASSN (**Supplementary Table 2** and **Figure 3**). *3B_806263030* was associated with not only SN (I1_BLUP and BLUP_ALL) but also ASSN (I1_BLUP, I3_BLUP, and BLUP_ALL). *5A_30786531* was significantly associated with GNS (I3_BLUP) and BSSN (I1_BLUP and BLUP_ALL). *6B_623314284* was significantly associated with ASSN (I1_BLUP and BLUP_ALL) and BSSN (I1_BLUP, I3_BLUP, and BLUP_ALL). *3D_68039763* and *7B_650666608* were significantly associated with both SN and BSSN traits. *5A_575163867* associated with BSSN (575.2 Mb) was colocated with QTLs *qSN5A.3*, *qSL5A.1*, *qGN5A.3*, and *qGS5A.2* (574.6–575.4 Mb) (Pang et al., 2020).

For the DTC values of each trait, eight SNPs/genetic regions were identified in DTC_{GNS} (1), DTC_{SN} (4), DTC_{BSSN} (2), and DTC_{ASSN} (1) (**Table 3** and **Figure 3**). Four of them were significantly associated with both trait and its corresponding DTC value, including *2A_82034103* (GNS_I3_BLUP and DTC_{GNS}), *2A_567774459* (SN_I1_BLUP and DTC_{SN}), *2B_3313327* (ASSN_I3_BLUP and DTC_{ASSN}), and *6B_283377788* (SN_I1_BLUP, SN_BLUP_ALL, and DTC_{SN}).

The Distribution of Favored Alleles at Associated Loci

The effect of favored alleles was estimated for GNS investigated in this study (**Supplementary Table 3** and **Figure 4**). Higher allelic effects were found in GNS and BSSN compared with SN and ASSN. Accessions with favorable alleles of locus $2B\_26062934_{TT}$, $6B\_52209942_{GG}$, and $6B\_283377788_{GG}$ showed more GNS (increased by 1.09–2.03 with I1 and by 3.29–4.21 with I3; **Supplementary Table 3**). Genotypes (serial number 74,

89, 150, 151, 180, 259, 269, and 271; **Supplementary Table 1**) with nine favorable alleles exhibited the considerably higher GNS (40.86–46.76 under I1 and 52.53–70.93 under I3), meanwhile, all these genotypes were found belonging to G5 group in **Figure 2C**. In addition, the proportion of favored allele for each locus was different, which indicated that these important loci had experienced different degrees of selection during wheat breeding. For example, the proportions of favored alleles for loci *6B_52209942* and *6D_83175038* were 81.91 and 92.20%, respectively, whereas the proportion for locus *2B_132280332* was only 17.73%, which implied that *2B_132280332* had not experienced strong selection. **Figure 4** shows that the frequency of favored alleles was much lower in landraces than in modern varieties, which reflected a positive selection of the favorable alleles during the breeding process.

We also analyzed the changing trends of GNS and TGW, as well as the DTC value, of these two traits in dryland and irrigated wheat varieties over the years. Results showed that the GNS of both dryland and irrigated wheat was increased along with the increasing frequency of favored alleles, and the TGW also improved together with GNS over the years (**Figures 5A,C**). For the dryland varieties, the DTC_{TGW} showed a slight increase over the years; however, the DTC_{GNS} showed a decrease in recent years (**Figure 5B**), which indicated that the dryland varieties bred in recent years could maintain grain weight if there is not enough water. However, its potential in improving GNS is dependent on sufficient water, which also showed a trend in the present dryland wheat cultivars breeding. **Figure 5D** shows that, compared with dryland accessions, the irrigated ones exhibited higher DTC_{TGW}, indicating that irrigated cultivars were less sensitive in TGW when encountering water deficiency.

DISCUSSION

A wheat spike normally produces up to 180 floret primordia; however, during development, more than 70% of the florets abort (Guo et al., 2015, 2016). A number of studies showed that the final formation of GNS is determined by the floret initiation and abortion periods (Zhang et al., 2021). Hence, a crucial way to improve grain number is by generating more floret primordia or decreasing floret mortality. The development of young panicles at the jointing stage encounters the differentiation of pistil and stamens to the initial stage of connectivum formation. The water supply at the booting stage is of great significance to the floret development and accumulation of dry matter. This is consistent with the emphasis on irrigation at the jointing and booting stage in wheat production (Cui et al., 2008).

Due to nutritional competition, the increase in spikelet and grain number of a panicle is often accompanied by a decrease in TGW. In this study, there is no significant correlation between SN and TGW or GN and TGW under the I1 and I3 environments (**Table 2**). Studies have shown that the trade-off between grain number and grain size depends on the growth environment and genotype (Hoang et al., 2019). In the analysis of Shanxi wheat in this study, the GNS and TGW showed a synergistic increase (**Figure 5**). The GNS and SN showed a low heritability relative to the TGW (**Table 1**), especially for dryland varieties. The GNS and SN of irrigated wheat showed a strong sensitivity to different water environments. When the water is insufficient, the SN and TGW of dryland wheat do not change so much, while the GNS decreases significantly. This indicates that water affects the firmness of dryland wheat spikelets, thus reducing wheat yield. Therefore, in dryland wheat breeding, we should not blindly select large spikes. For the improvement of fertile spikelets, the yield is increased by increasing the number of grains per spike. The GNS and TGW of irrigated wheat have the lowest response to the water environments and show strong genetic plasticity. Therefore, it is feasible to increase the yield of irrigated wheat by selecting accessions with large spikes and more grains.

Irrigation conditions can also affect the increase in GNS of favored alleles. In **Supplementary Table 3**, we can find that GNS showed a higher increase in favored alleles under the I3 condition than I1 condition. The impact of the environment on the effect of different haplotypes on grain yield was also observed in the previous reports. For instance, in *SNS_7AL* QTL, the increase in total grain yield in haplotype 2 relative to haplotype 1 was higher in the irrigated treatments than in drought treatments (Kuzay et al., 2019; Voss-Fels et al., 2019). This may be explained by the source-sink changing trends during breeding history. The wheat varieties were changed from weak source and sink strength to considerably weaker source strength and stronger sink. Under the I3 conditions, sufficient water supply promotes the source strength (such as developed leaves) to assimilate enough carbon, which makes the increase in grain yield in cultivars with favored alleles higher (Rodrigues et al., 2019).

As Li et al. (2021) reported in wheat salt tolerance research, two strategies were used to dissect the basis of stress tolerance: one is to identify loci associated with stress tolerance by comparing the different associated markers identified between stress and normal conditions (Hoang et al., 2019; Pradhan et al., 2019; Lin et al., 2020; Ahmed et al., 2021) and the other is to identify associated loci with stress-tolerant indices of investigated traits (Hu et al., 2021; Jeong et al., 2021; Li et al., 2021). In this study, we used these two strategies to identify the GNS-associated markers under water stress. Our results showed that several SNPs for the DTC of related traits were co-localized with SNPs identified under the I1 treatment. For instance, *2A_82034103* for DTC_{GNS}, *2A_567774459* for DTC_{SN}, *2B_3313327* for DTC_{ASSN}, these markers were significantly associated with traits under the I1 condition but cannot be examined under the I3 condition (**Supplementary Table 2**).

DATA AVAILABILITY STATEMENT

The original contributions presented in the study are included in the article/**Supplementary Material**, further inquiries can be directed to the corresponding authors.

AUTHOR CONTRIBUTIONS

XZ and LQ drafted and revised the manuscript and contributed to data analysis. YL, NW, JJZ, and BW performed the phenotypic

evaluation and helped with data analysis. JJZ, BY, and JZ helped to draft the manuscript. JZ and JW designed and coordinated the study and revised the manuscript. All authors have read and approved the final manuscript for publication.

FUNDING

This study was supported by the Research Program Sponsored by the State Key Laboratory of Sustainable Dryland Agriculture (in preparation), Shanxi Agricultural University (No. 202002-1), Shanxi Scholarship Council of China (2020-159), and Research Program of Shanxi Agricultural University (YZGC013, YBSJJ2006, and YCX2020YQ34).

SUPPLEMENTARY MATERIAL

The Supplementary Material for this article can be found online at: https://www.frontiersin.org/articles/10.3389/fpls.2021.806295/full#supplementary-material

REFERENCES

Ahmed, H. G. M., Iqbal, M. N., Iqbal, M. A., Zeng, Y., Ullah, A., Iqbal, M., et al. (2021). Genome-wide association mapping for stomata and yield indices in bread wheat under water limited conditions. *Agronomy* 11:1646. doi: 10.3390/agronomy11081646

Bilgrami, S. S., Ramandi, H. D., Shariati, V., Razavi, K., Tavakol, E., Fakheri, B. A., et al. (2020). Detection of genomic regions associated with tiller number in Iranian bread wheat under different water regimes using genome-wide association study. *Sci. Rep.* 10:14034. doi: 10.1038/s41598-020-69442-9

Bradbury, P. J., Zhang, Z., Kroon, D. E., Casstevens, T. M., Ramdoss, Y., and Buckler, E. S. (2007). TASSEL: software for association mapping of complex traits in diverse samples. *Bioinformatics* 23, 2633–2635. doi: 10.1093/bioinformatics/btm308

Cao, S., Xu, D., Hanif, M., Xia, X., and He, Z. (2020). Genetic architecture underpinning yield component traits in wheat. *Theor. Appl. Genet.* 133, 1811–1823. doi: 10.1007/s00122-020-03562-8

Cui, F., Zhang, N., Fan, X. L., Zhang, W., Zhao, C. H., Yang, L. J., et al. (2017). Utilization of a Wheat660K SNP array-derived high-density genetic map for high-resolution mapping of a major QTL for kernel number. *Sci. Rep.* 7:3788. doi: 10.1038/s41598-017-04028-6

Cui, J. M., Guo, T. C., Zhu, Y. J., Wang, C. Y., and Ma, X. M. (2008). *Spike of Wheat*. Beijing: China Agriculture Press, 6.

Deng, Z. Y., Cui, Y., Han, Q. D., Fang, W. D., Li, J. F., and Tian, J. C. (2017). Discovery of consistent QTLs of wheat spike-related traits under nitrogen treatment at different development stages. *Front. Plant Sci.* 8:2120. doi: 10.3389/fpls.2017.02120

Dobrovolskaya, O., Pont, C., Sibout, R., Martinek, P., Badaeva, E., Murat, F., et al. (2015). Frizzy panicle drives supernumerary spikelets in bread wheat. *Plant Physiol.* 167, 189–199. doi: 10.1104/pp.114.250043

Du, D., Zhang, D., Yuan, J., Feng, M., Li, Z., Wang, Z., et al. (2021). Frizzy panicle defines a regulatory hub for simultaneously controlling spikelet formation and awn elongation in bread wheat. *New Phytol.* 231, 814–833. doi: 10.1111/nph.17388

Feng, F., Han, Y., Wang, S., Yin, S., Peng, Z., Zhou, M., et al. (2018). The effect of grain position on genetic improvement of grain number and thousand grain weight in winter wheat in North China. *Front. Plant Sci.* 7:129. doi: 10.3389/fpls.2018.00129

Fischer, R. A. (2008). The importance of grain or kernel number in wheat: a reply to Sinclair and Jamieson. *Field Crops Res.* 105, 15–21. doi: 10.1016/j.fcr.2007.04.002

Fischer, R. A. (2011). Wheat physiology: a review of recent developments. *Crop Pasture Sci.* 62, 95–114. doi: 10.1071/CP10344

Guan, M., Huang, X., Xiao, Z., Jia, L., Wang, S., Zhu, M., et al. (2019). Association mapping analysis of fatty acid content in different ecotypic rapeseed using mrMLM. *Front. Plant Sci.* 9:1872. doi: 10.3389/fpls.2018.01872

Guo, J., Zhang, Y., Shi, W., Zhang, B., Zhang, J., Xu, Y., et al. (2015). Association analysis of grain-setting rates in apical and basal spikelets in bread wheat (*Triticum aestivum* L.). *Front. Plant Sci.* 6:1029. doi: 10.3389/fpls.2015.01029

Guo, Z., Slafer, G. A., and Schnurbusch, T. (2016). Genotypic variation in spike fertility traits and ovary size as determinants of floret and grain survival rate in wheat. *J. Exp. Bot.* 67, 4221–4230. doi: 10.1093/jxb/erw200

Hao, C. Y., Wang, L. F., Ge, H. M., Dong, Y. C., and Zhang, X. Y. (2011). Genetic diversity and linkage disequilibrium in Chinese bread wheat (*Triticum aestivum* L.) revealed by SSR markers. *PloS One* 6:e17279. doi: 10.1371/journal.pone.0017279

Hoang, G. T., Dinh, L. V., Nguyen, T. T., Nhung, K. T., Floran, G., Chung, D. M., et al. (2019). Genome-wide association study of a panel of Vietnamese rice landraces reveals new qtls for tolerance to water deficit during the vegetative phase. *Rice* 12:4. doi: 10.1186/s12284-018-0258-6

Hu, P., Zheng, Q., Luo, Q., Teng, W., Li, H., Li, B., et al. (2021). Genome-wide association study of yield and related traits in common wheat under salt-stress conditions. *BMC Plant Biol.* 21:27. doi: 10.1186/s12870-020-02799-1

Jallouli, S., Chamekh, Z., Ayadi, S., Zouari, L., Chabchoub, H., Hammami, Z., et al. (2021). Changes in yield and yield stability of durum wheat genotypes (*Triticum turgidum* ssp. *Durum*) under different environments and water regimes. *Cereal Res. Commun.* doi: 10.1007/s42976-021-00197-3

Jeong, B. Y., Lee, Y., Kwon, Y., Kim, J. H., Ham, T. H., Kwon, S. W., et al. (2021). Genome-wide association study reveals the genetic basis of chilling tolerance in rice at the reproductive stage. *Plants* 10:1722. doi: 10.3390/plants10081722

Jia, H. Y., Wan, H. S., Yang, S. H., Zhang, Z. Z., Kong, Z. X., Xue, S. L., et al. (2013). Genetic dissection of yield-related traits in a recombinant inbred line population created using a key breeding parent in China's wheat breeding. *Theor. Appl. Genet.* 126, 2123–2139. doi: 10.1007/s00122-013-2123-8

Joshi, A. K., Mishra, B., Chatrath, R., Ferrara, G. O., and Singh, R. P. (2007). Wheat improvement in India: present status, emerging challenges and future prospects. *Euphytica* 157, 431–446. doi: 10.1007/s10681-007-9385-7

Juliana, P., Poland, J., Huerta-Espino, J., Shrestha, S., Crossa, J., Crespo-Herrera, L., et al. (2019). Improving grain yield, stress resilience and quality of bread wheat using large-scale genomics. *Nat. Genet.* 51, 1530–1539. doi: 10.1038/s41588-019-0496-6

Jung, W. J., Lee, Y. J., Kang, C., and Seo, Y. W. (2021). Identification of genetic loci associated with major agronomic traits of wheat (*Triticum aestivum* L.) based on genome-wide association analysis. *BMC Plant Biol.* 21:418. doi: 10.1186/s12870-021-03180-6

Khan, S., Anwar, S., Yu, S., Sun, M., Yang, Z. P., and Gao, Z. Q. (2019). Development of drought-tolerant transgenic wheat. Achievements and Limitations. *Int. J. Mol. Sci.* 20:3350. doi: 10.3390/ijms20133350

Kuzay, S., Xu, Y., Zhang, J., Katz, A., Pearce, S., Su, Z., et al. (2019). Identification of a candidate gene for a QTL for spikelet number per spike on wheat chromosome arm 7AL by high-resolution genetic mapping. *Theor. Appl. Genet.* 132, 2689–2705. doi: 10.1007/s00122-019-03382-5

Li, J., Zhang, Z., Liu, Y., Yao, C., Song, W., Xu, X., et al. (2019). Effects of micro-sprinkling with different irrigation amount on grain yield and water use efficiency of winter wheat in the North China Plain. *Agric. Water Manage* 224:105736. doi: 10.1016/j.agwat.2019.105736

Li, L., Peng, Z., Mao, X., Wang, J., and Jing, R. (2021). Genetic insights into natural variation underlying salt tolerance in wheat. *J. Exp. Bot.* 72, 1135–1150. doi: 10.1093/jxb/eraa500

Li, S. S., Jia, J. Z., Wei, X. Y., Zhang, X. Y., Li, L. Z., Chen, H. C., et al. (2007). A intervarietal genetic map and QTL analysis for yield traits in wheat. *Mol. Breeding* 20, 167–178. doi: 10.1007/s11032-007-9080-3

Lin, Y., Chen, G. D., Hu, H. Y., Yang, X. L., Zhang, Z. L., Jiang, X. J., et al. (2020). Phenotypic and genetic variation in phosphorus-deficiency-tolerance traits in

Chinese wheat landraces. *BMC Plant Biol.* 20:330. doi: 10.1186/s12870-020-02492-3

Ma, J., Ding, P. Y., Liu, J. J., Li, T., Zou, Y. Y., Habib, A., et al. (2019). Identification and validation of a major and stably expressed QTL for spikelet number per spike in bread wheat. *Theor. Appl. Genet.* 132, 3155–3167. doi: 10.1007/s00122-019-03415-z

Ma, Z., Zhao, D., Zhang, C., Zhang, Z., Xue, S., Lin, F., et al. (2007). Molecular genetic analysis of five spike-related traits in wheat using RIL and immortalized F_2 populations. *Mol. Genet. Genomics*. 277, 31–42. doi: 10.1007/s00438-006-0166-0

Miura, H., Parker, B. B., and Snape, J. W. (1992). The location of major genes and associated quantitative trait loci on chromosome arm 5BL of wheat. *Theor. Appl. Genet*. 85, 197–204. doi: 10.1007/BF00222860

Pang, Y. L., Liu, C. X., Wang, D. F., Amand, P. S., Bernardo, A., Li, W. H., et al. (2020). High-resolution genome-wide association study identifies genomic regions and candidate genes for important agronomic traits in wheat. *Mol. Plant*. 13, 1311–1327. doi: 10.1016/j.molp.2020.07.008

Pradhan, S., Babar, M. A., Robbins, K., Bai, G., Mason, R. E., Khan, J., et al. (2019). Understanding the genetic basis of spike fertility to improve grain number, harvest index, and grain yield in wheat under high temperature stress environments. *Front. Plant Sci*. 29:1481. doi: 10.3389/fpls.2019.01481

Ray, D. K., Mueller, N. D., West, P. C., and Foley, J. A. (2013). Yield trends are insufficient to double global crop production by 2050. *PLoS One* 8:e66428. doi: 10.1371/journal.pone.0066428

Rodrigues, J., Inzé, D., Nelissen, H., and Saibo, N. J. M. (2019). Source-sink regulation in crops under water deficit. *Trends Plant Sci.* 24, 652–663. doi: 10.1016/j.tplants.2019.04.005

Sakuma, S., Golan, G., Guo, Z., Ogawa, T., Tagiri, A., Sugimoto, K., et al. (2019). Unleashing floret fertility in wheat through the mutation of a homeobox gene. *Proc. Natl. Acad. Sci. U.S.A.* 116, 5182–5187. doi: 10.1073/pnas.1815465116

Shi, W. P., Hao, C. Y., Zhang, Y., Cheng, J. Y., Zhang, Z., Liu, J., et al. (2017). A combined association mapping and linkage analysis of kernel number per spike in common wheat (*Triticum aestivum* L.). *Front. Plant Sci.* 8:1412. doi: 10.3389/fpls.2017.01412

Sun, Z., Zhang, Y., Zhang, Z., Gao, Y., Yang, Y., Han, M., et al. (2019). Significance of disposable presowing irrigation in wheat in increasing water use efficiency and maintaining high yield under winter wheat-summer maize rotation in the North China Plain. *Agric. Water Manag.* 225:105766. doi: 10.1016/j.agwat.2019.105766

Voss-Fels, K. P., Keeble-Gagnère, G., Hickey, L. T., Tibbits, J., Nagornyy, S., Hayden, M. J., et al. (2019). High-resolution mapping of rachis nodes per rachis, a critical determinant of grain yield components in wheat. *Theor. Appl. Genet.* 132, 2707–2719. doi: 10.1007/s00122-019-03383-4

Wang, S. C., Wong, D., Forrest, K., Allen, A., Chao, S. M., Huang, B. E., et al. (2014). Characterization of polyploid wheat genomic diversity using a high-density 90000 single nucleotide polymorphism array. *Plant Biotechnol.* 12, 787–796. doi: 10.1111/pbi.12183

Zhai, H., Feng, Z., Li, J., Liu, X., Xiao, S., Ni, Z., et al. (2016). QTL analysis of spike morphological traits and plant height in winter wheat (*Triticum aestivum* L.) using a high-density SNP and SSR-based linkage map. *Front. Plant Sci.* 7:1617. doi: 10.3389/fpls.2016.01617

Zhang, B., Xu, W., Liu, X., Mao, X., Li, A., Wang, J., et al. (2017). Functional conservation and divergence among homoeologs of TaSPL20 and TaSPL21, two SBP-Box genes governing yield-related traits in hexaploid wheat. *Plant Physiol.* 174, 1177–1191. doi: 10.1104/pp.17.00113

Zhang, H., Chen, J. S., Li, R. Y., Deng, Z. Y., Zhang, K. P., Liu, B., et al. (2016). Conditional QTL mapping of three yield components in common wheat (*Triticum aestivum* L.). *Crop J.* 4, 220–228. doi: 10.1016/j.cj.2016.01.007

Zhang, X. H., Warburton, M. L., Setter, T., Liu, H. J., Xue, Y. D., Yang, N., et al. (2016). Genome-wide association studies of drought-related metabolic changes in maize using an enlarged SNP panel. *Theor. Appl. Genet*. 129, 1449–1463. doi: 10.1007/s00122-016-2716-0

Zhang, Z., Huang, J., Gao, Y. M., Liu, Y., Li, J. P., Zhou, X. N., et al. (2020). Suppressed ABA signal transduction in the spike promotes sucrose use in the stem and reduces grain number in wheat under water stress. *J. Exp. Bot* 71, 7241–7256. doi: 10.1093/jxb/eraa380

Zhang, Z., Li, J., Hu, N., Li, W., Qin, W., Li, J., et al. (2021). Spike growth affects spike fertility through the number of florets with green anthers before floret abortion in wheat. *Field Crops Res.* 260:108007. doi: 10.1016/j.fcr.2020.108007

Zhao, X. Y., Hong, P., Wu, J. Y., Chen, X. B., Ye, X. G., Pan, Y. Y., et al. (2016). The tae-miR408-mediated control of *TaTOC1* genes transcription is required for the regulation of heading time in wheat. *Plant Physiol.* 170, 1578–1594. doi: 10.1104/pp.15.01216

Zheng, J., Liu, H., Wang, Y. Q., Wang, L. F., Chang, X. P., Jing, R. L., et al. (2014). *TEF-7A*, a transcript elongation factor gene, influences yield-related traits in bread wheat (*Triticum aestivum* L.). *J. Exp. Bot*. 65, 5351–5365. doi: 10.1093/jxb/eru3060

Conflict of Interest: The authors declare that the research was conducted in the absence of any commercial or financial relationships that could be construed as a potential conflict of interest.

Publisher's Note: All claims expressed in this article are solely those of the authors and do not necessarily represent those of their affiliated organizations, or those of the publisher, the editors and the reviewers. Any product that may be evaluated in this article, or claim that may be made by its manufacturer, is not guaranteed or endorsed by the publisher.

frontiers in Plant Science

PERSPECTIVE
published: 08 February 2022
doi: 10.3389/fpls.2022.798502

Reflections on the Triptych of Meristems That Build Flowering Branches in Tomato

Claire Périlleux and Samuel Huerga-Fernández*

Laboratory of Plant Physiology, Research Unit InBioS—PhytoSYSTEMS, Institute of Botany B22 Sart Tilman, University of Liège, Liège, Belgium

Branching is an important component determining crop yield. In tomato, the sympodial pattern of shoot and inflorescence branching is initiated at floral transition and involves the precise regulation of three very close meristems: (i) the shoot apical meristem (SAM) that undergoes the first transition to flower meristem (FM) fate, (ii) the inflorescence sympodial meristem (SIM) that emerges on its flank and remains transiently indeterminate to continue flower initiation, and (iii) the shoot sympodial meristem (SYM), which is initiated at the axil of the youngest leaf primordium and takes over shoot growth before forming itself the next inflorescence. The proper fate of each type of meristems involves the spatiotemporal regulation of FM genes, since they all eventually terminate in a flower, but also the transient repression of other fates since conversions are observed in different mutants. In this paper, we summarize the current knowledge about the genetic determinants of meristem fate in tomato and share the reflections that led us to identify sepal and flower abscission zone initiation as a critical stage of FM development that affects the branching of the inflorescence.

Keywords: tomato, flowering, branching, *Solanum lycopersicum*, sympodial, inflorescence

OPEN ACCESS

Edited by:
Xia Cui,
Insititute of Vegetables and Flowers, Chinese Academy of Agricultural Sciences (CAAS), China

Reviewed by:
Yuyang Zhang,
Huazhong Agricultural University, China
Ren Li,
Insititute of Vegetables and Flowers, Chinese Academy of Agricultural Sciences (CAAS), China

****Correspondence:***
Claire Périlleux
cperilleux@uliege.be

Specialty section:
This article was submitted to Plant Development and EvoDevo, a section of the journal Frontiers in Plant Science

Received: *20 October 2021*
Accepted: *14 January 2022*
Published: *08 February 2022*

Citation:
Périlleux C and Huerga-Fernández S (2022) Reflections on the Triptych of Meristems That Build Flowering Branches in Tomato. Front. Plant Sci. 13:798502. doi: 10.3389/fpls.2022.798502

INTRODUCTION

Branching patterns of shoots and inflorescences have important impacts on the yield of agricultural plants. They do not only determine the potential number of fruits or seeds, but also the timing at which they develop and the staggering of the harvest period. In the monopodial pattern, the axes of growth continue from single apical meristems: the primary shoot apical meristem (SAM) initiates leaves on its flanks and axillary meristems (AXM), laid down at the axil of each leaf, can be activated to produce a branch that extends laterally. In the sympodial pattern, the axes of growth result from the functioning of successive meristems that are activated when the preceding one undergoes differentiation.

In tomato, shoot growth is monopodial during vegetative development, and AXM initiation is delayed in respect to formation of the subtending leaf primordium. However, once the SAM undergoes floral transition, AXM are formed slightly later than the supporting leaf primordia and the growth pattern shifts to sympodial. The outgrowth of the uppermost AXM, called the shoot sympodial meristem (SYM), displaces laterally the nascent inflorescence being formed by the SAM, and continues the main shoot axis. The SYM produces few leaves before it undergoes floral transition at its turn, and is relayed by a second order SYM. This iterative pattern elaborates an infinite shoot made by the addition of the initial segment formed by the SAM and sympodial

segments made by the SYM. The inflorescences are constructed using a similar sympodial pattern (**Figure 1A**): once the SAM (or the SYM in sympodial segments) transitions into the first flower meristem (FM), a sympodial inflorescence meristem (SIM) emerges on its side, and itself maturates toward FM fate while a second order SIM is initiated, and so on. The inflorescences are thus formed by the addition of the first flower formed by the SAM (or the SYM) and one-flowered sympodial segments made by successive SIMs. Each new SIM develops perpendicular to the one formed previously, resulting in the typical zigzag shape of tomato inflorescences.

Floral transition in tomato thus marks the switch of the SAM from a monopodial "shoot branching" program to a sympodial "shoot and inflorescence" patterning. One key trigger of this switch is the systemic protein SINGLE FLOWER TRUSS (SFT) that is synthesized in mature leaves, and travels toward the apical bud via phloem cells (Lifschitz et al., 2006). *SFT* is an ortholog of *FLOWERING LOCUS T* (*FT*) in Arabidopsis (Molinero-Rosales et al., 2004; Lifschitz et al., 2006) and its loss-of-function in tomato delays flowering, reduces the inflorescences to one or a few flowers and suppresses sympodial growth (Molinero-Rosales et al., 2004; Lifschitz and Eshed, 2006). This indicates that multiflowered inflorescences and regular sympodial segments of tomato plants are formed in the presence of florigen only. The three meristems that start the sympodial pattern—the SAM and the laterals SYM and SIM—are in very close vicinity, and hence branching and meristem fate regulatory networks can be expected to be tightly interconnected. Genetic determinants of these processes have been identified from forward genetic studies. **Figure 1B** summarizes the phenotypes of the mutants

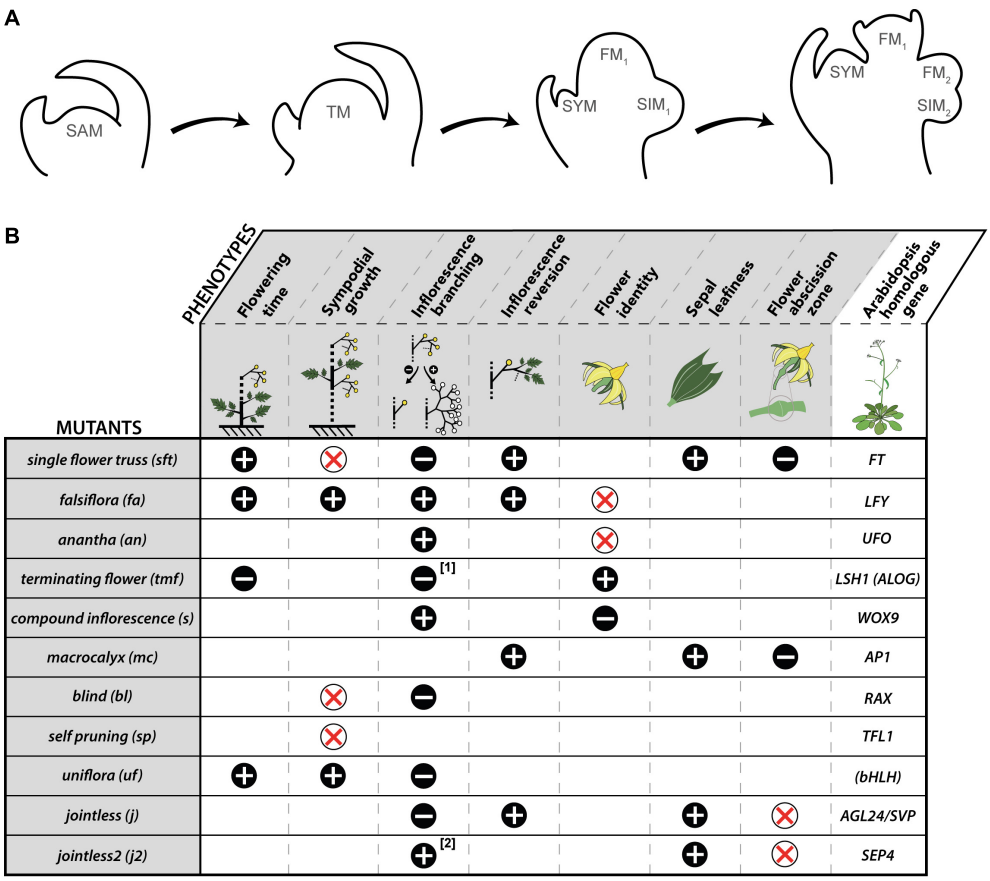

FIGURE 1 | Inflorescence formation in tomato and phenotypic traits of mutants showing flowering time, sympodial growth, or inflorescence abnormalities. **(A)** Steps of inflorescence formation: (1) pre-transition vegetative shoot apical meristem (SAM); (2) transitional meristem (TM); (3) start of inflorescence branching: the first flower meristem (FM_1) is developing while a sympodial inflorescence meristem (SIM_1) appears laterally; the vegetative meristem at the axil of the youngest leaf is the shoot sympodial meristem (SYM) that takes over shoot growth; (4) the first flower is reaching the sepal initiation stage, while SIM_1 has formed the second flower meristem (FM_2) and the second SIM (SIM_2). **(B)** Phenotypic traits of tomato mutants. "+" means that the phenotypic trait is increased; "–" means that the phenotypic trait is decreased, "x" means that the phenotypic trait is suppressed. The mutants are listed in their order of appearance in the text where relevant references can be found. [1] *tmf* mutation affects the first inflorescence only; [2] *j2* mutation mostly affects inflorescence branching when a second mutation called *enhancer of jointless 2* (*ej2*) in another *SEP4* homolog is also present. Arabidopsis gene abbreviations: *AGL24/SVP*, *AGAMOUS LIKE 24/SHORT VEGETATIVE PHASE*; *ALOG*, *Arabidopsis LSH1 Oryza G1; AP1, APETALA1*; *bHLH*, *basic Helix-Loop-Helix; FT*, *FLOWERING LOCUS T*; *LFY*, *LEAFY*; *LSH1*, *LIGHT-DEPENDENT SHORT HYPOCOTYL 1*; *RAX*, *REGULATORS OF AXILLARY MERISTEMS*; *SEP4*: *SEPALLATA 4; TFL1*, *TERMINAL FLOWER1*; *UFO*, *UNUSUAL FLORAL ORGANS*; *WOX9*; *WUSCHEL-RELATED HOMEOBOX 9*. Names in brackets refer to gene families.

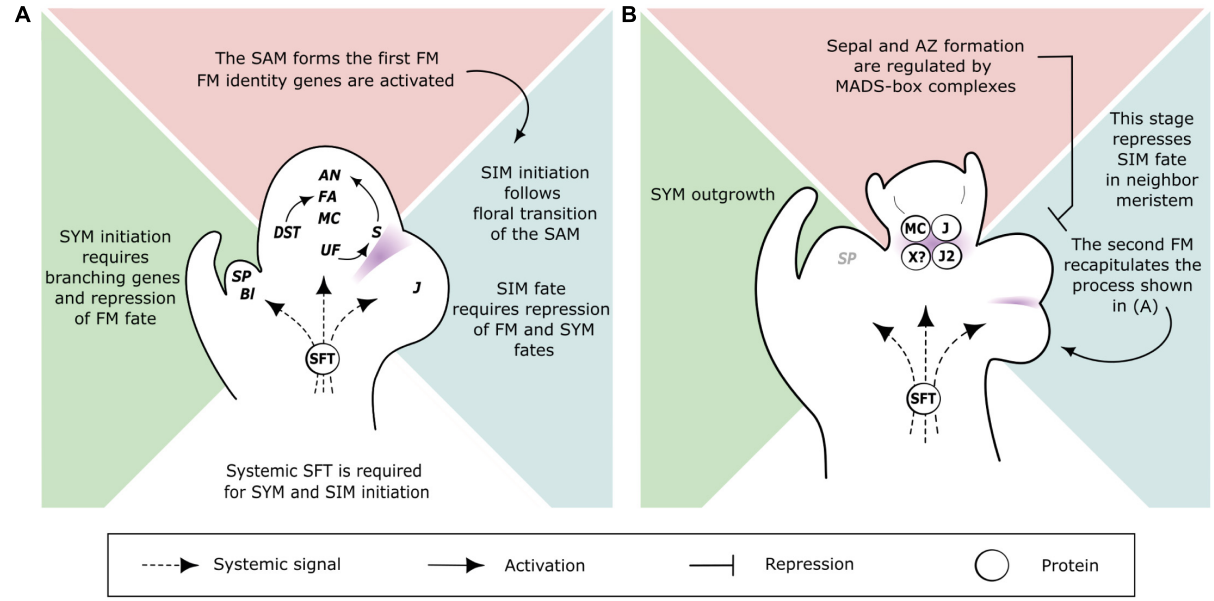

FIGURE 2 | Proposed models of genetic and spatiotemporal regulation of meristem fate and branching in the inflorescence of tomato. **(A)** Triptych of meristems developing side-by-side at the start of inflorescence branching (stage 3 of **Figure 1A**). Central panel (pink): the SAM. A set of genes are activated early during floral transition of the SAM, including *UF*, *S*, and the FM identity genes *MC*, *FA* and *AN*. Arrows show known activation cascades. Right panel (blue): the SIM. A lateral SIM emerges after the floral transition of the SAM and requires transient repression of FM and SYM fates. The *J* gene is involved in this transient state. Left panel (green): the SYM. The branching gene *BI* is required for SYM initiation and the vegetative phase of the SYM is due to the expression of *SP*, which antagonizes florigen SFT. The systemic SFT protein is required for floral transition of the SAM, initiation of the SIM and sympodial growth of the shoot continued by the SYM. **(B)** Critical stage in flower development regulating inflorescence branching (stage 4 of **Figure 1A**). Central panel (pink): the first FM. The initiation of sepals and pedicel abscission zone is regulated by MADS-box proteins, including MC, J, J2, and a putative target of SFT (X?), which are represented as a simplified and hypothetical tetramer complex. At that stage, the FM is a non-permissive environment for initiation of a lateral SIM on its flank. Right panel (blue): the first SIM has formed the second FM and the second SIM. These meristems recapitulate the processes shown in **A**). Left panel (green): SYM outgrowth correlates with downregulation of *SP*, which allows floral transition of the sympodial shoot segment. Gene/protein abbreviations: *AN*, *ANANTHA*; *BI*, *BLIND*; *DST*, *DELAYED SYMPODIAL TRANSITION*; *FA*, *FALSIFLORA*; *J*, *JOINTLESS*; *J2*, *JOINTLESS2*; *MC*, *MACROCALYX*; *S*, *COMPOUND INFLORESCENCE*; *SFT*, *SINGLE FLOWER TRUSS*; *SP*, *SELF PRUNING*; *UF*, *UNIFLORA*. Meristem annotations: FM, flower meristem; SAM, shoot apical meristem; SIM, sympodial inflorescence meristem; SYM, sympodial shoot meristem. In **(A,B)** purple areas indicate expression domains of boundary genes.

that are mentioned in this paper as a basis of our reflections, and **Figure 2** shows our current understanding of the spatiotemporal regulation of the triptych of meristems that shape the tomato plant at flowering.

CENTRAL PANEL: THE SHOOT APICAL MERISTEM

The environmental and/or endogenous signals that activate SFT synthesis are not elucidated. The SAM of the modern tomato cultivars undergoes floral transition after the production of 6–12 leaves, depending mainly on the genetic background (Samach and Lotan, 2007; Quinet and Kinet, 2007). These cultivars have lost their photoperiodic requirement due to mutations in the *SFT* paralogs *SELF PRUNING 5G* (*SP5G*), which normally plays a flower-repressing role in long days, and *FLOWERING LOCUS LIKE1* (*FTL1*), which plays a flower-activating role in short days (Soyk et al., 2017b; Song et al., 2020). Both genes act upstream of *SFT* expression whereas in photoperiod-insensitive cultivars, *SFT* might be upregulated in a leaf age-dependent pathway (Shalit et al., 2009).

Another pathway regulating floral transition of tomato is the activation of *FALSIFLORA* (*FA*), the ortholog of *LEAFY* (*LFY*) (Molinero-Rosales et al., 1999), in the SAM. The independence of the *SFT* and *FA* pathways was shown at the genetic level by the additive—very late or never-flowering—phenotype of double *sft fa* mutants (Molinero-Rosales et al., 2004) and, at the molecular level, by the identification of distinct triggers and targets of *SFT* and *FA* (Meir et al., 2021). A gene acting upstream of *FA* was recently identified as *DELAYED SYMPODIAL TERMINATION* (*DST*), which is surprisingly not expressed in the SAM itself but in the emerging leaf primordia (Meir et al., 2021). The early sign of the transition from vegetative growth to flowering is the enlargement and doming of the SAM (Tal et al., 2017), which is accompanied by a vast transcriptomic reprogramming (Meir et al., 2021). Surprisingly, these early changes occur even in the absence of functional *SFT* or *DST*, indicating that an intrinsic floral transition transcriptional switch is initiated independently.

In addition of delaying floral transition, the lack of *FA* function impairs the development of the SAM, which cannot reach the FM state and, instead, produces proliferating SIMs or meristems that even revert to leaf initiation (Molinero-Rosales et al., 1999). Proliferating SIMs and lack of flowers are

also observed in mutants of the *ANANTHA* (*AN*) gene, which is orthologous to the *LFY* co-regulator *UNUSUAL FLORAL ORGANS* (*UFO*) in Arabidopsis (Allen and Sussex, 1996; Lippman et al., 2008). *FA* and *AN* are thus both established as FM identity genes. In the vegetative SAM, expression of *FA* and *AN* is repressed by TERMINATING FLOWER (TMF) (MacAlister et al., 2012), whose activity was recently shown to be redox-regulated (Huang et al., 2021). After floral transition, the *COMPOUND INFLORESCENCE* (*S*) gene, which encodes a protein of the WUSCHEL-RELATED HOMEOBOX (WOX) family, is transiently activated and acts upstream of *AN* (Park et al., 2012). The study of allelic variation in *S/WOX9* showed its correlation with the branching of the inflorescence (Lippman et al., 2008; Park et al., 2012; Hendelman et al., 2021). In low expression *s* mutants, the delay in *AN* expression caused by the slower maturation of FM leads to the initiation of more SIMs and excessive branching, indicating that developmental kinetics is key in regulating inflorescence complexity (Park et al., 2012). In *tmf* mutant, early activation of *FA* and *AN* accelerates the conversion of the SAM into a FM and reduces the inflorescence to a single flower (MacAlister et al., 2012). These observations suggest that the FM fate progresses in a "developmental window" during which SIM initiation on its flank is first stimulated, but at a certain stage the FM becomes a non-permissive environment for lateral SIM initiation (Périlleux et al., 2014). Beside meristem maturation, the size of the SAM is also critical for the branching of the inflorescence, since mutations in the CLAVATA (CLV) pathway genes, *SlCLV3*, *FASCIATED AND BRANCHED* (*FAB*) and *FASCIATED INFLORESCENCES* (*FIN*) that cause enlarged SAM also produce extra flowers (Xu et al., 2015).

Once the FM fate is acquired, floral organ identity genes are induced. According to the paradigm of the ABC model of flower morphogenesis, A-class genes play a dual role: they are required for normal sepal and petal development in whorls 1 and 2 and antagonize the expression of C-function genes that are consequently restricted to whorls 3 and 4 (Coen and Meyerowitz, 1991). Conservation of this model was, however, questioned because, in most species except Arabidopsis and its close relatives, mutations of A-class genes do not cause homeotic conversion of sepals and petals, indicating that other factors repress the C-function (Litt and Irish, 2003; Causier et al., 2010; Litt and Kramer, 2010; Morel et al., 2017). Moreover, mutations affecting sepal identity also affect FM identity in all species tested, indicating that completion of the FM fate might be the primary function of A-class genes and sepals might be the default organ of that stage. This is consistent with the phenotype of tomato plants mutated in the *MACROCALYX* (*MC*) gene, the ortholog of *APETALA1* (*AP1*) in Arabidopsis, which produce flowers with correctly positioned but abnormally large and leaf-like sepals (Vrebalov et al., 2002; Yuste-Lisbona et al., 2016). A function of *MC* in FM identity is also suggested by its early upregulation in the transitional SAM (Meir et al., 2021). Homologs of the other A-function gene of Arabidopsis, *APETALA2* (*AP2*), are similarly not associated with mutant defects in both sepals and petals. The *AP2* family comprises 5 members in tomato (Karlova et al., 2011). One of them (*AP2c*) was found to be more highly expressed in pre-transition SAM and to decrease at floral transition (Meir et al., 2021), whereas RNAi-mediated down-regulation of several other members produces enlarged and fused sepals (Karlova et al., 2011).

SIDE PANEL 1: THE SHOOT SYMPODIAL MERISTEM

The first SYM is usually the meristem at the axil of the last leaf initiated before the floral transition of the SAM (**Figure 1A**). Its identity is different from other AXM in that the SYM takes a pole position to continue the growth of the primary stem whereas AXM grow laterally. Genes regulating shoot branching in tomato were isolated from mutants lacking AXM. In *lateral suppressor* (*ls*) mutants, formation of AXM is almost completely blocked during vegetative development but the side shoots in the two leaf axils preceding an inflorescence, and hence the SYM, are usually formed and branching of the inflorescence is only slightly reduced (Schumacher et al., 1999). By contrast, the *blind* (*bl*) mutants lack both AXM and SYM lateral meristems, indicating that during reproductive development the initiation of lateral meristems in close proximity to the SAM requires *Bl* but not *Ls* function (Schmitz et al., 2002).

The SYM forms a small number of vegetative phytomers (usually three) before its own floral transition, whereas AXM produce as many leaves as the primary shoot before flowering. In wild type plants, the delay of the floral transition of the SYM compared with the SAM is due to the expression of the *SELF PRUNING* gene (*SP*), which exerts an antagonistic role to *SFT* and is orthologous to *TERMINAL FLOWER 1* in Arabidopsis (Pnueli et al., 1998). The function of *SP* in balancing florigen is very strong as plants overexpressing *SFT* show a dramatic acceleration of floral transition of the SAM but maintain a typical robust regularity of 3-leaf sympodial segments (Shalit et al., 2009).

As opposed to *tfl1* in Arabidopsis, *sp* mutation does neither alter flowering time nor the architecture of the inflorescence in tomato (Pnueli et al., 1998). Mutation in *SP* shortens the sympodial segments up to the termination of the plant by a terminal inflorescence; this growth habit has been exploited for breeding of determinate varieties that are grown for mechanical harvest of trusses and fruit processing (Bergougnoux, 2014). Interestingly, a gene dosage effect of *SFT* can be observed in *sp* mutants, whose determinacy is delayed in heterozygous *sft*/ + plants, leading to yield increase (Jiang et al., 2013).

The early outgrowth of the SYM reflects that apical dominance is weakened when the SAM undergoes floral transition. In many plants, the SAM exerts an auxin-mediated dominance over the AXM and axillary bud outgrowth can be triggered by the influx of promoting signals among which sugars and cytokinins play major roles (Wang et al., 2019). In AXM, these signals inhibit a repressor of axillary bud outgrowth, *BRANCHED1* (*BRC1*), but none of the two *BRC1*-like genes in tomato—*BRC1a* and *BRC1b*—were found to be expressed in the SYM, suggesting that they do no control SYM outgrowth (Martin-Trillo et al., 2011). By contrast, the expression of *SP* is downregulated upon the activation of SYM outgrowth (**Figure 2B**; Thouet et al., 2008) and it was reported

that *SP* alters polar auxin transport as well as auxin responses (Silva et al., 2018). Although the floral transition of the SYM is thought to recapitulate the processes described in the SAM, some regulators are different. For instance, *TMF* acts in the SAM only (MacAlister et al., 2012) whereas related genes act in the SYM (Huang et al., 2018). One can speculate that downregulation of *SP* is a prerequisite for the activation of the FM identity genes in the SYM, like *TFL1* represses *LFY* and *AP1* in Arabidopsis (Ratcliffe et al., 1999; Périlleux et al., 2019).

SIDE PANEL 2: THE INFLORESCENCE SYMPODIAL MERISTEM

Tomato mutants lacking SIM initiation produce isolated flowers instead of inflorescences (**Figure 1B**). As mentioned above, this can be due to the precocious activation of *FA* and *AN* in the SAM, as observed in *tmf* mutants (MacAlister et al., 2012). However, several mutants whose inflorescences are reduced to a single flower are late flowering, like *sft*, indicating that the ability to initiate a SIM is linked with the event of floral transition of the SAM (Molinero-Rosales et al., 2004; Lifschitz et al., 2006).

A very robust single flower phenotype gave its name to the *uniflora* (*uf*) mutant (Dielen et al., 1998), which was described as late flowering (Dielen et al., 2004), although new alleles produced by CRISPR-Cas9 editing show milder phenotypes (Meir et al., 2021). *UF* encodes a bHLH transcription factor that was recently shown to control the earliest transcriptional changes occurring in the SAM at floral transition, including the up-regulation of the "maturation gene" *S* (Meir et al., 2021). These changes occur even in the absence of SFT, and the *uf* and *sft* phenotype are strongly additive, indicating that *UF* function is independent of *SFT*. The initiation of additional leaves in the *uf* mutant was found to follow the enlargement and doming of the SAM, which is a hallmark of floral transition, suggesting that *UF* represses leaf initiation rather than controlling flowering time *per se*.

The nature of the SIM is only transient in that it requires to refrain premature maturation toward FM fate and to prevent return to vegetative functioning (**Figure 1B**). This dual function was attributed to *JOINTLESS* (*J*), a MADS-box gene of the *SHORT VEGETATIVE PHASE (SVP)/AGAMOUS-LIKE24* clade (Mao et al., 2000), since the inflorescences of *j* mutants return to leaf initiation after the production of few flowers (Mao et al., 2000; Szymkowiak and Irish, 2006; Thouet et al., 2012). Genetic analyses revealed that the resurgence of vegetative growth in *j* mutants was due to the fact that a lateral meristem initiated in the iterative process of sympodial construction of the inflorescence takes a SYM rather than a SIM identity, since the occurrence of this reverted meristem requires *Bl* and *SP* functions (Szymkowiak and Irish, 2006).

The reversion of the SIM to SYM is also observed in *mc* mutants, indicating that a mutation affecting FM and sepal identity somehow affects the identity of the neighbor SIM (Vrebalov et al., 2002; Yuste-Lisbona et al., 2016). The *j* and *mc* mutations are additive in respect to the reversion of the inflorescence to leaf initiation, which, in the double *j mc* mutant, occurs after the initiation of a single flower (Yuste-Lisbona et al., 2016). This is also the case in *j sft* (Thouet et al., 2012) and *mc sft* (Yuste-Lisbona et al., 2016) double mutants, indicating that *J*, *MC,* and *SFT* participate in a common network regulating SIM identity.

NOT BY COINCIDENCE: SIM IDENTITY, ABSCISSION ZONE FORMATION AND SEPAL INITIATION

The primary phenotype for which mutation of the *J* gene was studied is not the leafy inflorescences but the lack of flower pedicel abscission zone (AZ) (Butler, 1936). This jointless trait has been selected in breeding programs because it offers the advantage of keeping the flower pedicel and the calyx attached to the rest of the inflorescence, so that fruits can be harvested without any green tissues (Bergougnoux, 2014). However, because of the undesired accompanying phenotype of floral reversion in *j* mutants, it is another jointless mutation, called *j2*, which was used for agronomical purposes (Soyk et al., 2017a). The underlying gene, formerly named *SlMBP21*, encodes a MADS-box gene of the *SEPALLATA4* (*SEP4*) clade (Gomez-Roldan et al., 2017; Soyk et al., 2017a).

Tomato has four *SEP4* genes and combining their mutation revealed their redundant functions in inflorescence branching. The *enhancer of j2* (*ej2*) mutation was in fact discovered because the double *j2 ej2* mutants show excessive branching of the inflorescence, similar to *s* mutants, while the *ej2* single mutants only show elongated sepals (Soyk et al., 2017a). The combination with a third mutation in the *LONG INFLORESCENCE* (*LIN*) gene still increases inflorescence complexity, as the triple *j2 ej2 lin* mutants show *an*-like inflorescences with overproliferated SIMs and no flowers (Soyk et al., 2017a). These results suggest that despite having, apparently, distinct roles in FM development, such as the formation of the flower AZ and the development of the sepals, these *SEP4* genes have overlapping roles in inflorescence branching. An alternative interpretation is that the phenotypic traits affected in the single and multiple mutants are developmentally linked, and thus share regulatory features. This interpretation is supported by the fact that the other mutation suppressing the flower AZ, i.e., the mutation in the *SVP/AGL24*-like gene *J*, also impacts inflorescence branching. In this case, however, the *j* mutation acts as a suppressor of branching, since it was found to be epistatic to the extremely branched *s* mutant (Thouet et al., 2012).

The flower AZ contains a group of small cells that lack large vacuoles and are arrested in an undifferentiated, meristematic fate until an abscission signal is provided. It is initiated at the sepal stage of FM development (Tabuchi, 1999), when an "activation of basal cells" has been reported (Fleming and Kuhlemeler, 1994). Singularly, the sepals of tomato flowers appear sequentially, and the first one has significantly grown when the last one is initiated (Sawhney and Greyson, 1972). Consistent with a link between sepals and formation of the flower AZ, the *mc* mutant exhibits abnormal AZ (Shalit et al., 2009; Yuste-Lisbona et al., 2016). At the mechanistic level, binary physical interaction between MC, J and J2 proteins was shown, and it was then postulated that

a MADS-box protein complex including these partners is the master regulator of AZ formation (**Figure 2B**; Nakano et al., 2012; Liu et al., 2014). This hypothesis was much inspired by the floral quartet model, according to which MADS-box proteins interact in tetrameric complexes, but it cannot be excluded at this stage that MC, J, and J2 act in different complexes and timeframes. Their interaction with several other MADS-box proteins was found *in vitro* (Leseberg et al., 2008; Zhang et al., 2018), but functional validation of higher-order complexes *in vivo* and identification of their target genes are still missing. Additional actors remain to be identified, especially among the meristem genes that are activated downstream of *SFT*. Indeed the formation of the AZ is also tied with the intensity of flowering since systemic florigen SFT protein can rescue the lack of AZ in the *mc sft* mutants (Shalit et al., 2009), suggesting that *MC* function is shared with a target of SFT.

Transcriptomic analyses of the flower pedicel AZ revealed the expression of the shoot branching genes *Bl* and *Ls* (Nakano et al., 2013; Wang et al., 2013), together with other genes involved in meristem functioning, such as *GOBLET* (*GOB*) and a tomato *WUSCHEL* homolog (*LeWUS*). Importantly, *Bl*, *Ls*, and *GOB* are known as "boundary genes" since they are expressed at the boundary between the SAM and leaf primordia, in a zone where AXM are initiated (Busch et al., 2011). Expression of *Bl* was also observed at the boundary between FM and SIM (Busch, 2009), raising the question of a functional link between the early separation of meristems in the inflorescence and the isolation of flowers by their AZ. The inflorescence of *bl* mutants is strongly reduced, consisting of one or a few flowers that are usually fused (Schmitz et al., 2002). This phenotype suggests that proper separation of the first FM and SIM is important for the specification of the SIM and its indeterminate state.

In conclusion, our reflections on the triptych of meristems regulating sympodial branching in tomato led us to highlight the initiation of sepals and the flower AZ as a critical step of FM maturation that affects SIM identity and branching of the inflorescence (**Figure 2B**). This checkpoint might occur well before any visible sign of differentiation since sepal identity genes such as *MC* also affect FM identity. An obvious deriving question is whether the "demarcation" created by the sepal whorl and the AZ actually affects the mobility of a signal that coordinates FM and lateral SIM development and what would be the nature of this signal. Our reflections also highlighted the critical roles of branching/boundary genes, especially *Bl* that appears as a hub involved in SYM identity, separation of FM and SIM, and AZ formation. Understanding how flower development and boundaries establishment are intertwined will provide new perspective for manipulating inflorescence complexity in tomato.

DATA AVAILABILITY STATEMENT

The original contributions presented in the study are included in the article/supplementary material, further inquiries can be directed to the corresponding author/s.

AUTHOR CONTRIBUTIONS

CP and SH-F discussed the ideas and wrote the manuscript. Both authors approved the submitted version.

FUNDING

SH-F was grateful to F.N.R.S.-F.R.I.A. for the award of a Ph.D. fellowship (FC21283).

ACKNOWLEDGMENTS

We thank the members of the Plant Physiology Lab for their critical and fruitful discussions, and are very grateful to Frédéric Bouché for designing **Figure 1** layout.

REFERENCES

Allen, K. D., and Sussex, I. M. (1996). Falsiflora and anantha control early stages of floral meristem development in tomato (*Lycopersicon esculentum* Mill). *Planta* 200, 254–264.

Bergougnoux, V. (2014). The history of tomato: from domestication to biopharming. *Biotechnol. Adv.* 32, 170–189. doi: 10.1016/j.biotechadv.2013.11.003

Busch, B. L. (2009). *Genetic and Molecular Analysis of Sympodial Plant Architecture in Tomato*. PhD thesis. Cologne, Germany: University of Cologne.

Busch, B. L., Schmitz, G., Rossmann, S., Piron, F., Ding, J., Bendahmane, A., et al. (2011). Shoot branching and leaf dissection in tomato are regulated by homologous gene modules. *Plant Cell* 23, 3595–3609. doi: 10.1105/tpc.111.087981

Butler, L. (1936). Inherited characters in the tomato. II. jointless pedicel. *J. Hered.* 27, 25–26.

Causier, B., Schwarz-Sommer, Z., and Davies, B. (2010). Floral organ identity: 20 years of ABCs. *Semin. Cell Dev. Biol.* 21, 73–79. doi: 10.1016/j.semcdb.2009.10.005

Coen, E. S., and Meyerowitz, E. M. (1991). The war of the whorls: genetic interactions controlling flower development. *Nature* 353, 31–37. doi: 10.1038/353031a0

Dielen, V., Marc, D., and Kinet, J. M. (1998). Flowering in the uniflora mutant of tomato (*Lycopersicon esculentum* Mill.): description of the reproductive structure and manipulation of flowering time. *Plant Growth Reg.* 25, 149–157.

Dielen, V., Quinet, M., Chao, J., Batoko, H., Havelange, A., and Kinet, J. M. (2004). UNIFLORA, a pivotal gene that regulates floral transition and meristem identity in tomato (*Lycopersicon esculentum*). *New Phytol.* 161, 393–400. doi: 10.1046/j.1469-8137.2003.00937.x

Fleming, A. J., and Kuhlemeler, C. (1994). Activation of basal cells of the apical meristem during sepal formation in tomato. *Plant Cell* 6, 789–798. doi: 10.1105/tpc.6.6.789

Gomez-Roldan, M. V. G., Perilleux, C., Morin, H., Huerga-Fernandez, S., Latrasse, D., Benhamed, M., et al. (2017). Natural and induced loss of function mutations in SlMBP21 MADS-box gene led to jointless-2 phenotype in tomato. *Sci. Rep.* 7: 4402. doi: 10.1038/s41598-017-04556-1

Hendelman, A., Zebell, S., Rodriguez-Leal, D., Dukler, N., Robitaille, G., Wu, X., et al. (2021). Conserved pleiotropy of an ancient plant homeobox gene

uncovered by cis-regulatory dissection. *Cell* 184, 1724–1739. doi: 10.1016/j.cell.2021.02.001

Huang, X., Chen, S., Li, W., Tang, L., Zhang, Y., Yang, N., et al. (2021). ROS regulated reversible protein phase separation synchronizes plant flowering. *Nat. Chem. Biol.* 17, 549–557. doi: 10.1038/s41589-021-00739-0

Huang, X., Tang, L., Yu, Y., Dalrymple, J., Lippman, Z. B., and Xu, C. (2018). Control of flowering and inflorescence architecture in tomato by synergistic interactions between ALOG transcription factors. *J. Genet. Genomics* 45, 557–560. doi: 10.1016/j.jgg.2018.03.008

Jiang, K., Liberatore, K. L., Park, S. J., Alvarez, J. P., and Lippman, Z. B. (2013). Tomato yield heterosis is triggered by a dosage sensitivity of the florigen pathway that fine-tunes shoot architecture. *PLoS Genet.* 9:e1004043. doi: 10.1371/journal.pgen.1004043

Karlova, R., Rosin, F. M., Busscher-Lange, J., Parapunova, V., Do, P. T., Fernie, A. R., et al. (2011). Transcriptome and metabolite profiling show that APETALA2a is a major regulator of tomato fruit ripening. *Plant Cell* 23, 923–941. doi: 10.1105/tpc.110.081273

Leseberg, C. H., Eissler, C. L., Wang, X., Johns, M. A., Duvall, M. R., and Mao, L. (2008). Interaction study of MADS-domain proteins in tomato. *J. Exp. Bot.* 59, 2253–2265. doi: 10.1093/jxb/ern094

Lifschitz, E., and Eshed, Y. (2006). Universal florigenic signals triggered by FT homologues regulate growth and flowering cycles in perennial day-neutral tomato. *J. Exp. Bot.* 57, 3405–3414. doi: 10.1093/jxb/erl106

Lifschitz, E., Eviatar, T., Rozman, A., Shalit, A., Goldshmidt, A., Amsellem, Z., et al. (2006). The tomato FT ortholog triggers systemic signals that regulate growth and flowering and substitute for diverse environmental stimuli. *Proc. Natl. Acad. Sci. U.S.A.* 103, 6398–6403. doi: 10.1073/pnas.0601620103

Lippman, Z. B., Cohen, O., Alvarez, J. P., Abu-Abied, M., Pekker, I., Paran, I., et al. (2008). The making of a compound inflorescence in tomato and related nightshades. *PLoS Biol.* 6:e288. doi: 10.1371/journal.pbio.0060288

Litt, A., and Irish, V. F. (2003). Duplication and diversification in the APETALA1/FRUITFULL floral homeotic gene lineage: implications for the evolution of floral development. *Genetics* 165, 821–833. doi: 10.1093/genetics/165.2.821

Litt, A., and Kramer, E. M. (2010). The ABC model and the diversification of floral organ identity. *Semin. Cell Dev. Biol.* 21, 129–137. doi: 10.1016/j.semcdb.2009.11.019

Liu, D., Wang, D., Qin, Z., Zhang, D., Yin, L., Wu, L., et al. (2014). The SEPALLATA MADS-box protein SLMBP21 forms protein complexes with JOINTLESS and MACROCALYX as a transcription activator for development of the tomato flower abscission zone. *Plant J.* 77, 284–296. doi: 10.1111/tpj.12387

MacAlister, C. A., Park, S. J., Jiang, K., Marcel, F., Bendahmane, A., Izkovich, Y., et al. (2012). Synchronization of the flowering transition by the tomato terminating flower gene. *Nat. Genet.* 44, 1393–1398. doi: 10.1038/ng.2465

Mao, L., Begum, D., Chuang, H. W., Budiman, M. A., Szymkowiak, E. J., Irish, E. E., et al. (2000). Jointless is a MADS-box gene controlling tomato flower abscission zone development. *Nature* 406, 910–913. doi: 10.1038/35022611

Martin-Trillo, M., Grandio, E. G., Serra, F., Marcel, F., Rodriguez-Buey, M. L., Schmitz, G., et al. (2011). Role of tomato branched1-like genes in the control of shoot branching. *Plant J.* 67, 701–714. doi: 10.1111/j.1365-313X.2011.04629.x

Meir, Z., Aviezer, I., Chongloi, G. L., Ben-Kiki, O., Bronstein, R., Mukamel, Z., et al. (2021). Dissection of floral transition by single-meristem transcriptomes at high temporal resolution. *Nat. Plants* 7, 800–813. doi: 10.1038/s41477-021-00936-8

Molinero-Rosales, N., Jamilena, M., Zurita, S., Gomez, P., Capel, J., and Lozano, R. (1999). Falsiflora, the tomato orthologue of Floricaula and Leafy, controls flowering time and floral meristem identity. *Plant J.* 20, 685–693. doi: 10.1046/j.1365-313x.1999.00641.x

Molinero-Rosales, N., Latorre, A., Jamilena, M., and Lozano, R. (2004). SINGLE FLOWER TRUSS regulates the transition and maintenance of flowering in tomato. *Planta* 218, 427–434. doi: 10.1007/s00425-003-1109-1

Morel, P., Heijmans, K., Rozier, F., Zethof, J., Chamot, S., Bento, S. R., et al. (2017). Divergence of the floral a-function between an Asterid and a Rosid Species. *Plant Cell* 29, 1605–1621. doi: 10.1105/tpc.17.00098

Nakano, T., Fujisawa, M., Shima, Y., and Ito, Y. (2013). Expression profiling of tomato pre-abscission pedicels provides insights into abscission zone properties including competence to respond to abscission signals. *BMC Plant Biol.* 13:40. doi: 10.1186/1471-2229-13-40

Nakano, T., Kimbara, J., Fujisawa, M., Kitagawa, M., Ihashi, N., Maeda, H., et al. (2012). MACROCALYX and JOINTLESS interact in the transcriptional regulation of tomato fruit abscission zone development. *Plant Physiol.* 158, 439–450. doi: 10.1104/pp.111.183731

Park, S. J., Jiang, K., Schatz, M. C., and Lippman, Z. B. (2012). Rate of meristem maturation determines inflorescence architecture in tomato. *Proc. Natl. Acad. Sci. U.S.A.* 109, 639–644. doi: 10.1073/pnas.1114963109

Périlleux, C., Bouché, F., Randoux, M., and Orman-Ligeza, B. (2019). Turning meristems into fortresses. *Trends Plant Sci.* 24, 431–442. doi: 10.1016/j.tplants.2019.02.004

Périlleux, C., Lobet, G., and Tocquin, P. (2014). Inflorescence development in tomato: gene functions within a zigzag model. *Front. Plant Sci.* 5:121. doi: 10.3389/fpls.2014.00121

Pnueli, L., Carmel-Goren, L., Hareven, D., Gutfinger, T., Alvarez, J., Ganal, M., et al. (1998). The self-pruning gene of tomato regulates vegetative to reproductive switching of sympodial meristems and is the ortholog of CEN and TFL1. *Development* 125, 1979–1989. doi: 10.1242/dev.125.11.1979

Quinet, M., and Kinet, J.-M. (2007). Transition to flowering and morphogenesis of reproductive structures in tomato. *Int. J. Plant Dev. Biol.* 1, 64–74. doi: 10.1093/jxb/erj117

Ratcliffe, O. J., Bradley, D. J., and Coen, E. S. (1999). Separation of shoot and floral identity in Arabidopsis. *Development* 126, 1109–1120. doi: 10.1242/dev.126.6.1109

Samach, A., and Lotan, H. (2007). The transition of flowering in tomato. *Plant Biotech.* 24, 71–82.

Sawhney, V. K., and Greyson, R. I. (1972). On the initiation of the inflorescence and floral organs in tomato (*Lycopersicon esculentum*). *Can. J. Bot.* 50, 1493–1495.

Schmitz, G., Tillmann, E., Carriero, F., Fiore, C., Cellini, F., and Theres, K. (2002). The tomato Blind gene encodes a MYB transcription factor that controls the formation of lateral meristems. *Proc. Natl. Acad. Sci. U.S.A.* 99, 1064–1069. doi: 10.1073/pnas.022516199

Schumacher, K., Schmitt, T., Rossberg, M., Schmitz, G., and Theres, K. (1999). The Lateral suppressor (Ls) gene of tomato encodes a new member of the VHIID protein family. *Proc. Natl. Acad. Sci. U.S.A.* 96, 290–295. doi: 10.1073/pnas.96.1.290

Shalit, A., Rozman, A., Goldshmidt, A., Alvarez, J. P., Bowman, J. L., Eshed, Y., et al. (2009). The flowering hormone florigen functions as a general systemic regulator of growth and termination. *Proc. Natl. Acad. Sci. U.S.A.* 106, 8392–8397. doi: 10.1073/pnas.0810810106

Silva, W. B., Vicente, M. H., Robledo, J. M., Reartes, D. S., Ferrari, R. C., Bianchetti, R., et al. (2018). SELF-PRUNING acts synergistically with DIAGEOTROPICA to guide auxin responses and proper growth form. *Plant Physiol.* 176, 2904–2916. doi: 10.1104/pp.18.00038

Song, J., Zhang, S., Wang, X., Sun, S., Liu, Z., Wang, K., et al. (2020). Variations in both FTL1 and SP5G, two tomato FT paralogs, control day-neutral flowering. *Mol. Plant* 13, 939–942. doi: 10.1016/j.molp.2020.05.004

Soyk, S., Muller, N. A., Park, S. J., Schmalenbach, I., Jiang, K., Hayama, R., et al. (2017b). Variation in the flowering gene Self Pruning 5G promotes day-neutrality and early yield in tomato. *Nat. Genet.* 49, 162–168. doi: 10.1038/ng.3733

Soyk, S., Lemmon, Z. H., Oved, M., Fisher, J., Liberatore, K. L., Park, S. J., et al. (2017a). Bypassing negative epistasis on yield in tomato imposed by a domestication gene. *Cell* 169, 1142–1155. doi: 10.1016/j.cell.2017.04.032

Szymkowiak, E. J., and Irish, E. E. (2006). Jointless suppresses sympodial identity in inflorescence meristems of tomato. *Planta* 223, 646–658. doi: 10.1007/s00425-005-0115-x

Tabuchi, T. (1999). Comparison on the development of abscission zones in the pedicels between two tomato cultivars. *J. Japan. Soc. Hortic. Sci.* 68, 993–999. doi: 10.2503/jjshs.68.993

Tal, L., Friedlander, G., Gilboa, N. S., Unger, T., Gilad, S., and Eshed, Y. (2017). Coordination of meristem doming and the floral transition by late termination, a kelch repeat protein. *Plant Cell* 29, 681–696. doi: 10.1105/tpc.17.00030

Thouet, J., Quinet, M., Lutts, S., Kinet, J. M., and Perilleux, C. (2012). Repression of floral meristem fate is crucial in shaping tomato inflorescence. *PLoS One* 7:e31096. doi: 10.1371/journal.pone.0031096

Thouet, J., Quinet, M., Ormenese, S., Kinet, J. M., and Perilleux, C. (2008). Revisiting the involvement of Self-Pruning in the sympodial growth of tomato. *Plant Physiol.* 148, 61–64. doi: 10.1104/pp.108.124164

Vrebalov, J., Ruezinsky, D., Padmanabhan, V., White, R., Medrano, D., Drake, R., et al. (2002). A MADS-box gene necessary for fruit ripening at the tomato ripening-inhibitor (rin) locus. *Science* 296, 343–346.

Wang, M., Le Moigne, M. A., Bertheloot, J., Crespel, L., Perez-Garcia, M. D., Oge, L., et al. (2019). BRANCHED1: a key hub of shoot branching. *Front. Plant Sci.* 10:76. doi: 10.3389/fpls.2019.00076

Wang, X., Liu, D., Li, A., Sun, X., Zhang, R., Wu, L., et al. (2013). Transcriptome analysis of tomato flower pedicel tissues reveals abscission zone-specific modulation of key meristem activity genes. *PLoS One* 8:e55238. doi: 10.1371/journal.pone.0055238

Xu, C., Liberatore, K. L., MacAlister, C. A., Huang, Z., Chu, Y. H., Jiang, K., et al. (2015). A cascade of arabinosyltransferases controls shoot meristem size in tomato. *Nat. Genet.* 47, 784–792. doi: 10.1038/ng.3309

Yuste-Lisbona, F. J., Quinet, M., Fernandez-Lozano, A., Pineda, B., Moreno, V., Angosto, T., et al. (2016). Characterization of vegetative inflorescence (mc-vin) mutant provides new insight into the role of MACROCALYX in regulating inflorescence development of tomato. *Sci. Rep.* 6:18796. doi: 10.1038/srep18796

Zhang, Z., Coenen, H., Ruelens, P., Hazarika, R. R., Al Hindi, T., Oguis, G. K., et al. (2018). Resurrected protein interaction networks reveal the innovation potential of ancient whole-genome duplication. *Plant Cell* 30, 2741–2760. doi: 10.1105/tpc.18.00409

Conflict of Interest: The authors declare that the research was conducted in the absence of any commercial or financial relationships that could be construed as a potential conflict of interest.

Publisher's Note: All claims expressed in this article are solely those of the authors and do not necessarily represent those of their affiliated organizations, or those of the publisher, the editors and the reviewers. Any product that may be evaluated in this article, or claim that may be made by its manufacturer, is not guaranteed or endorsed by the publisher.

frontiers in Plant Science

REVIEW
published: 18 February 2022
doi: 10.3389/fpls.2022.824240

microRNAs and Their Roles in Plant Development

*Qingkun Dong[1], Binbin Hu[1,2] and Cui Zhang[1,2]**

[1]Key Laboratory of Plant Molecular Physiology, CAS Center for Excellence in Molecular Plant Sciences, Institute of Botany, Chinese Academy of Sciences, Beijing, China, [2]College of Life Sciences, University of Chinese Academy of Sciences, Beijing, China

Small RNAs are short non-coding RNAs with a length ranging between 20 and 24 nucleotides. Of these, microRNAs (miRNAs) play a distinct role in plant development. miRNAs control target gene expression at the post-transcriptional level, either through direct cleavage or inhibition of translation. miRNAs participate in nearly all the developmental processes in plants, such as juvenile-to-adult transition, shoot apical meristem development, leaf morphogenesis, floral organ formation, and flowering time determination. This review summarizes the research progress in miRNA-mediated gene regulation and its role in plant development, to provide the basis for further in-depth exploration regarding the function of miRNAs and the elucidation of the molecular mechanism underlying the interaction of miRNAs and other pathways.

Keywords: microRNA, plant development, microRNA movement, hormone, crop yield

OPEN ACCESS

Edited by:
Xigang Liu,
Hebei Normal University, China

Reviewed by:
Guodong Ren,
Fudan University, China
Stephen Jackson,
University of Warwick, United Kingdom

****Correspondence:***
Cui Zhang
cuizhang@ibcas.ac.cn

Specialty section:
This article was submitted to Plant Physiology, a section of the journal Frontiers in Plant Science

Received: *29 November 2021*
Accepted: *27 January 2022*
Published: *18 February 2022*

Citation:
Dong Q, Hu B and Zhang C (2022) microRNAs and Their Roles in Plant Development. Front. Plant Sci. 13:824240. doi: 10.3389/fpls.2022.824240

INTRODUCTION

RNA is one of the four major macromolecules of life and is essential in the regulation and expression of genes. RNA can be divided into two groups: coding and non-coding RNAs. In plants, 24 nt small interfering RNAs (siRNA) and 21 nt microRNAs (miRNA) have the highest expression abundance of small non-coding RNAs. siRNAs were first discovered in plants and are involved in the transcriptional gene silencing and post-transcriptional gene silencing (PTGS) pathway in plants (Hamilton and Baulcombe, 1999; Sijen et al., 2001; Pal-Bhadra et al., 2002) and RNA interfering pathway in animals (Elbashir et al., 2001).

miRNAs were first identified from nematodes (*Caenorhabditis elegans*) by Victor Ambros lab in collaboration with Gary Ruvkun lab, who confirmed that a miRNA (Lin-4) has a role in regulating the temporal developmental of nematode larvae (Lee et al., 1993; Wightman et al., 1993; Fire et al., 1998; Stricklin et al., 2005). Since then, miRNAs have been reported in *Drosophila*, nematodes, mammals, and plants. In plants, 22 nt miRNA is able to cut the target mRNA and the cleavage product can be further processed by RNA-DEPENDENT RNA POLYMERASE 6 (RDR6) and DICER-LIKE 4 to produce secondary 21 nt siRNA. In addition, the symmetric miRNA/miRNA* can be processed by DCL2 and generate secondary 22 nt miRNAs. These siRNAs are called phased siRNAs (PhasiRNAs) because they are the endogenous plant siRNAs with phase arrangement structure characteristics (Borges and Martienssen, 2015). PhasiRNA can be divided into cis-acting siRNA and trans-acting siRNA (ta-siRNA; Chen et al., 2010; Zhai et al., 2011; Arikit et al., 2014; Deng et al., 2018).

miRNAs are demonstrated to be vital in plant development. They are usually transcribed by RNA Polymerase II (Pol II) into pri-miRNAs. These pri-miRNAs are cleaved by a class of RNase-III nucleases called Dicer-like proteins, after which they combine with ARGONAUTE

(AGO) family proteins to form the RNA-induced silencing complexes (RISCs). RISCs are then involved in the expression and regulation of target genes (Song et al., 2019). miRNAs act in the regulation of meristem characteristics, leaf polarity, flowering patterns. etc. Mutations in miRNA transcription or processing complexes usually have multiple effects on plant from and function, indicating that miRNAs are important to coordinate plant development. For example, the roles of HD-ZIP III-miR165/166 pathway are important in the development of vascular, meristem, and leaf polarity, and the roles of miR156/miR172 are important in flowering time and flower pattern (D'Ario et al., 2017; Ramachandran et al., 2017; Du et al., 2020; Ma et al., 2020; Lian et al., 2021; Yadav et al., 2021). During plant development, endogenous miRNAs play an important role in gene regulation by targeting related target genes. Several miRNAs function through interactions with hormones. Many components in hormone signaling are targets of miRNAs, and the interactions of these components and the miRNAs enable plants to regulate their growth, development, and differentiation rapidly and effectively. This signaling is done by selecting miRNAs as intermediates to control hormone responses or, conversely, by using hormones to regulate specific miRNA levels (Jodder, 2020; Li et al., 2020; Yu and Wang, 2020). There is evidence indicating that miRNAs can diffuse in tissues as inhibitor signals, so they play an elaborate role in tissue differentiation (Chen and Rechavi, 2021). Here we will summarize the role of miRNAs in the aspects of biogenesis, action mechanism, function in specific tissues, interaction with hormones, and movement to understand how they regulate plant development. miRNAs and their targets involved in plant development are listed in **Table 1**.

BIOSYNTHESIS AND ACTION MECHANISM OF miRNAs IN PLANTS

Most of miRNAs are a kind of conserved endogenous small RNA, which plays an important regulatory role after eukaryotic gene transcription (Rodriguez et al., 2010). Most metazoan miRNA genes exist in thousands of introns or exons, whereas plant miRNA genes exist between genes. In addition to this, the secondary structures and lengths of miRNA are greatly different among plant species (Voinnet, 2009). Animal miRNAs exist in clusters along the genome, and they can be co-transcribed in the form of poly-cistrons (Ha and Kim, 2014). In contrast, plant miRNA genes are rarely arranged in series (Kim, 2005; Zhang et al., 2008). Like protein-coding genes, miRNAs start by being transcribed in the nucleus by Pol II to form pri-miRNAs, which range in length from several hundred to several thousand nucleotides and have a 5′ cap and a 3′ poly-A tail (Jones-Rhoades and Bartel, 2004; Lee et al., 2004; Jones-Rhoades et al., 2006). Under the action of DCL1, pri-miRNAs are cleaved into pre-miRNAs, which are ~70 nt – 350 nt. These pre-miRNAs are further formed by the interaction of the DCL1 enzyme, RNA-binding protein HYL1 (Hyponastic Leaves 1), and C2H2 zinc finger protein SE (Serrate) on pre-miRNA (Kurihara and Watanabe, 2004; Jones-Rhoades et al., 2006) into mature miRNAs. The mature miRNAs have 2 bases protruding at the 3′ end (miRNA double-stranded complex). This miRNA complex is methylated at the 2′-OH position of its 3′ end under the action of HUAENHANCER1 protein to prevent degradation (Li et al., 2005). Most of the methylated miRNA complexes are transported into the cytoplasm with the help of plant homolog of exportin-5, HASTY (HST; Park et al., 2005; Brioudes et al., 2021). The RNA-induced RISC, generated by miRNA, is eventually produced in the cytoplasm (Park et al., 2005; Jones-Rhoades et al., 2006). Recent studies showed that RISC can be assembled in the nucleus and exported to the cytosol by EXPO1 (Bologna et al., 2018), and HST also regulates pri-miRNA transcription and processing (Cambiagno et al., 2021). In the RISC complex, the AGO protein is the most important structural protein. It contains four domains: the N-terminal domain (N), the PIWI/Argonaute/Zwille (PAZ) domain, the MID domain, and the P-element-induced wimpy tested (PIWI) domain. The PAZ domain can bind to RNA and the PIWI domain with RNase H activity. 10 different types of AGO proteins have been found in *Arabidopsis thaliana*; most of them contain catalytic reaction residues. Of these different AGO proteins, ARGONAUTE1 (AGO1; Baumberger and Baulcombe, 2005; Qi et al., 2005), AGO2 (Carbonell et al., 2012), AGO4 (Qi et al., 2006), AGO7 (Montgomery et al., 2008), and AGO10 (Ji et al., 2011; Zhu et al., 2011) have been demonstrated in the gene silencing pathway of target RNAs. AGO1 protein is involved in PTGS as the main component of RISC that binds to a short guide RNA such as miRNA or siRNA. AGO4 and AGO6 are mainly involved in the repeat-associated siRNA pathway, and AGO7 plays a role in the formation of ta-siRNA (Vaucheret, 2008; Duan et al., 2015; Singh et al., 2015; Fang and Qi, 2016).

Studies have shown that mature miRNAs inhibit the translation of target genes, regulate the expression of plant genes by complementary pairing with coding region, some binding to 3′UTR and 5′UTR of the target mRNA, or regulate the expression of genes by cutting target gene mRNA at the post-transcriptional level. This inhibition by mature miRNAs alters the morphogenesis of plant organs, growth, development, hormone secretion, signal transduction, and the ability of plants to respond to external stress and environmental factors (Liu et al., 2009a; Yokotani et al., 2009; Naqvi et al., 2012). miRNA in plants is highly complementary to its target mRNA, so its main mode of action is cleavage. The translation inhibition pathways in plants have only been found in recent years. The cleavage and inhibition mechanisms are mostly coordinated depending on the complementarity between miRNAs and their targets (Brodersen et al., 2008; Yu et al., 2017; O'Brien et al., 2018).

THE FUNCTION OF miRNAs IN PLANT GROWTH AND DEVELOPMENT

The regulation of plant growth and development is very precise and is influenced by both internal genetic information and the external environmental factors. Normal expression of miRNAs is necessary for the growth and development of plants. Previous studies have shown that miRNA widely regulates plant growth and development.

TABLE 1 | miRNAs, the targets, and their roles in plant development.

miRNA	Target	Target function	Species	References
miR156	SPL family	Plastochron length, promoting flowering; Leaf development, root development, secondary metabolism and abiotic stress; tillering and corn development in *Zea mays*	*Arabidopsis* and *Zea mays*	Aukerman and Sakai, 2003; Chuck et al., 2007a, 2010; Wang et al., 2008; Xu et al., 2016b; Dai et al., 2018
miR159	GAMYB or GAMYB-like gene	Male reproductive development, seed development, vegetative tissues and reproductive development	*Arabidopsis*	Allen et al., 2007; Millar et al., 2019
miR160	ARFs	Embryo, leaf and root development, hypocotyl elongation	*Arabidopsis*, Medicago truncatula and *Zea mays*	Bustos-Sanmamed et al., 2013; Lopez-Ruiz et al., 2019; Yang et al., 2019; Dai et al., 2021
miR164	NAC family	Meristem boundary identity, Auxiliary meristem formation, leaf and flower development, lateral root initiation	*Arabidopsis*, *Zea mays* and *Oryza*	Li et al., 2003; Laufs et al., 2004; Hibara et al., 2006; Raman et al., 2008; Zheng et al., 2019; Wang et al., 2021b
miR165/166	HD-ZIP III	Maintaining meristematic cells, adaxial identity of leaves, lateral root growth, and procambium identity	*Arabidopsis*	Williams et al., 2005; Jia et al., 2015; Merelo et al., 2016; Yan et al., 2016
miR167	ARFs	Development of male organ、 roots、 stems、 leaves and flowers, flowering time, embryonic development, seed development and stress response, defense against pathogens	*Arabidopsis* and *Oryza*	Wu et al., 2006; Liu et al., 2012; Yao et al., 2019; Caruana et al., 2020
miR169	CBF and NF-YA family	Enhancer of C homeotic gene transcription and root architecture	*Arabidopsis*, *Antirrhinum majus* and *Zea mays*	Cartolano et al., 2007; Sorin et al., 2014; Xu et al., 2014; Xing et al., 2021
miR171	SCL	Chlorophyll biosynthesis, phase transitions and floral meristem determinacy	*Arabidopsis*，barley	Curaba et al., 2013; Ma et al., 2014; Li et al., 2021
miR172	AP2 family	Represses flowering, flower meristem identity and patterning; vegetative phase change, carpel and stamen development; flower opening, tuberization and *salt tolerance*	*Arabidopsis*, *Z. mays*, *Oryza,H. vulgare*, and *S. tuberosum*	Chuck et al., 2007b; Martin et al., 2009; Wu et al., 2009; Nair et al., 2010; Wollmann et al., 2010; Zhu and Helliwell, 2011; Cheng et al., 2021a; Lian et al., 2021; Werner et al., 2021
miR319	TCP family	Leaf development and senescence, organ curvature, and hormone biosynthesis and signaling.	*Arabidopsis* and *Solanum lycopersicum*	Ori et al., 2007; Schommer et al., 2014; Koyama et al., 2017; Bresso et al., 2018
miR390	TAS3	ta-siRNA biogenesis for ARF repression and indirect miR165/166 regulation，lateral root growth，leaf patterning	*Arabidopsis*	Fahlgren et al., 2006; Marin et al., 2010; Endo et al., 2013; Dastidar et al., 2019
miR393	TIR1 and AFB	Auxin homeostasis, lateral root growth, leaf shape/number	*Arabidopsis* and *Oryza*	Parry et al., 2009; Chen et al., 2011; Windels and Vazquez, 2011; Lu et al., 2018; Wang et al., 2018
miR394	LCR	Meristematic identity suppression *via* WUS downregulation, leaf inclination and architecture,	*Arabidopsis*	Baumann, 2013; Knauer et al., 2013; Qu et al., 2019
miR396	GRF	Cell proliferation in leaves, disease-resistance, somatic embryogenesis, grain size and panicle branching	*Arabidopsis*, *Medicago*, and *Oryza*	Debernardi et al., 2012; Bazin et al., 2013; Liu et al., 2014a; Chandran et al., 2018; Szczygiel-Sommer and Gaj, 2019; Liebsch and Palatnik, 2020; Zhang et al., 2020
mir397	OsLAC	Grain yield, panicle branches	*Oryza*	Zhang et al., 2013
miR824	AGL16	Stomatal patterning	*Arabidopsis*	Bergmann and Sack, 2007
miR828 and miR858	MYBs	Fiber development, anthocyanin, and flavonol accumulation	Cotton, grapes	Guan et al., 2014; Tirumalai et al., 2019
miR847	IAA28	Lateral root formation	*Arabidopsis*	Wang and Guo, 2015
miR857	LACCASE7	Secondary growth	*Arabidopsis*	Abdel-Ghany and Pilon, 2008; Zhao et al., 2015
TAS3	ARF3/4 and (only in mosses) AP2-like	Vasculature development, Leaf polarity / phase transition	All land plants	Fahlgren et al., 2006; Jing et al., 2017

The Role of miRNAs in the Shoot Meristem

Unlike animals, plants can continuously produce new organs throughout their life cycle. Their apical meristem forms in embryo and has a group of stem cells with multidirectional differentiation potential and the ability to self-replicate. During the development of a plant, the shoot apical meristem (SAM) plays a central role in the formation and development of its aboveground organs. The STM (shoot meristemless)-WUS (Wuschel)-CLV (Clavata) pathway plays a key role in the maintenance of meristem activity (Schoof et al., 2000; Gaillochet and Lohmann, 2015; Somssich et al., 2016). To some extent, the same mechanisms are also demonstrated in flower meristems.

miRNA plays a central role in the regulation of gene expression networks, orchestrating the establishment and the maintenance

of the SAM by targeting and regulating multiple genes in the STM-WUS-CLV signaling pathway (**Figure 1**). miR394 is generated in the L1 layer on the surface of the SAM and diffuses down to the Organizing Center (OC; **Figure 1**). In the OC, expression of Leaf Curling Responsiveness (*LCR*) is inhibited (Knauer et al., 2013) and directly results in the downregulation of *WUS*, a SAM-specific gene (Song et al., 2012). Although the concentration of miR394 in the L1 layer is higher than that in the OC layer, the inhibitory effect of miR394 on LCR only occurs in OC, implying that an exact concentration of miR394 is of great importance to its function in *A. thaliana* (Knauer et al., 2013). Meanwhile, there are diversified functions for stem cell regulation mediated by miR394-LCR (Kumar et al., 2019). AGO10 can specifically bind to miR165/166 and ultimately promote the expression of *HD-ZIP III*. *HD-ZIP III* is an important transcription factor family that regulates SAM in *A. thaliana* and is a target of miR165/166. When miR166/165 does not bind to AGO10 or the *AGO10* gene is knocked out, the meristematic tissue of plants is destroyed. AGO1 antagonizes AGO10 in the binding of miR166/165. When miR166/165 binds to AGO1, plants will decrease the expression of the *HD-ZIP III* genes and terminate SAM development. Recent studies indicate that the interaction between AGO10 and miR165/166 depends solely on the structure of miR165/166 and is independent of the catalytic activity of AGO10 (Zhu et al., 2011).

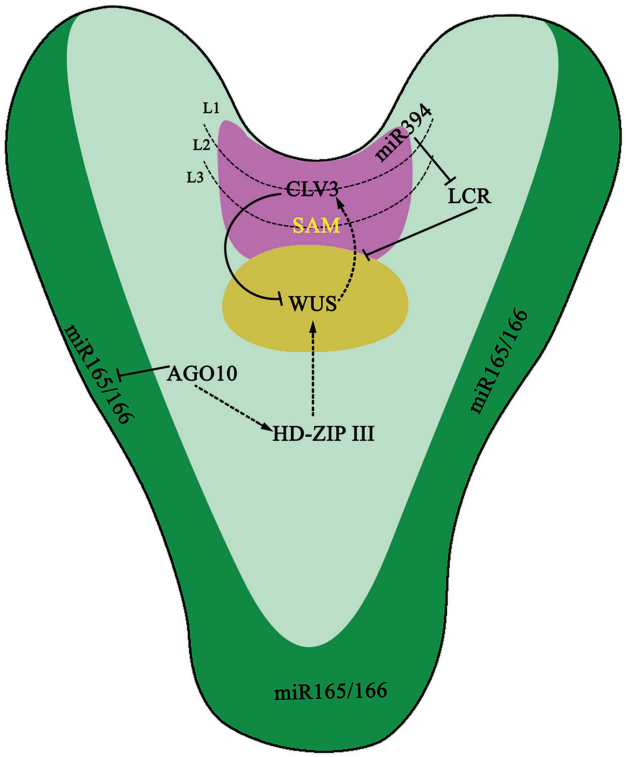

FIGURE 1 | The function of miRNAs in embryo. miR394 expresses in the L1 layer of shoot apical meristem (SAM) and then moves to L3 layer to target *Leaf Curling Responsiveness* (*LCR*) gene. LCR further regulates CLAVATA-WUSCHEL (CLV-WUS) negative feedback loop for proper SAM development and specification. ARGONAUTE10 (AGO10) specifically sequesters miR166/165 to upregulate Class III homeodomain leucine zipper transcription factors (HD-ZIP III TFs) to maintain SAM development. The dotted arrows represent a proposed positive regulation, whereas lines with perpendicular end bars indicate negative regulation.

The Role of miRNAs in Leaf Development

Leaf development includes the differentiation of leaf primordium from the SAM and the subsequent development of leaf blades. In these processes, various regulatory factors are involved. Organogenesis in the SAM is determined by the distribution and polar transport of auxin (Veit, 2009). The target genes of miR160, namely *ARF10*, *ARF16*, and *ARF17* in the auxin response factors (ARF) family affect leaf development by regulating auxin response. Mutants *arf10* and *arf17* of *A. thaliana* which are resistant to miR160 cleavage, have an abnormal number of cotyledons, and the edge of the leaves was serrated and curled upward (Liu et al., 2007). At the same time, leaf genesis is regulated by several transcription factors, such as the expression of *MYB DOMAIN PROTEIN* (*MYB*) transcription factor, in leaf primordium. These specific ASYMMETRIC LEAVES1/ROUGH SHEATH2/PHANTASTICA gene families can be used as a transcription suppressor to turn off the meristematic specific gene *KNOX1* to promote growth and differentiation (Hay et al., 2004; Piazza et al., 2005). In the process of establishing dorsal–ventral polarity in plant leaves, expression of *HD-ZIP III* and the MYB protein ASYMMETRIC LEAVES1 are the determinants of the ventral axis, while expression of *KANADI* (*KAN*), *ARF3*, and *ARF4* determine the fate of the dorsal axis. The *YABBY* gene acts downstream of the *KAN* gene in *A. thaliana* and is a decisive gene for leaf dorsal development. The function of *HD-ZIP III* genes in leaf polarization is relatively clear (**Figure 2**). The expression of *HD-ZIP III* was maintained only on the adaxial side, as members of *HD-ZIP III* family, are inhibited by miR165/166 on the abaxial side (Zhong and Ye, 2004). AGO1 is necessary for targeting miR165/166 to *HD-ZIP III* transcripts in leaves and is required for miR165/166 to regulate and restrict *PHBOLUSA* (*PHB*) to the adaxial side (Kidner and Martienssen, 2004). Like AGO1, the localization of AGO10 on the adaxial side of the leaf is necessary to inhibit the acellular autonomous miR165/166 activity and maintain the accumulation of *HD-ZIP III* mRNA in this region (Liu et al., 2009c).

At the same time, miR390 and its effector AGO7 are required to be involved in leaf polarization (**Figure 2**). TAS3 ta-siRNA determines the adaxial side by inhibiting the expression of *ARF3* and *ARF4* on the abaxial side of leaves (Chitwood et al., 2009). In *Zea maize* and *A. thaliana*, the ventral ta-siARF pathway interacts with the dorsal regulatory factors to some extent. Additionally, the ta-siARF pathway is also required to inhibit the expression of miR165/miR166, which allows for the proliferation of HD-ZIP III. Interference with ta-siARF pathway in maize will obviously affect leaf polarity. Wang et al. reported that miR396 also participated in leaf polarity formation by regulating the proliferation of leaf cells by targeting growth-regulating factors (GRFs), thus affecting the formation of dorsal–ventral axis polarity in leaves (Wang et al., 2011).

miRNAs also regulate leaf size and structure. The balance between miR396 and GRFs ultimately controls the number of cells in leaves and regulates the size of the meristem (Kim et al., 2003; Liu et al., 2009b; Rodriguez et al., 2010; Wang et al., 2011; Baucher et al., 2013; Debernardi et al., 2014). In addition, miR396 can also regulate leaf size through targeting *basic Helix–Loop–Helix 74* (Debernardi et al., 2012) and *CUC2*, which is necessary for the formation of the organ primordial boundary. miR319 regulates the growth and development of *A. thaliana* leaves by degrading the mRNA of the *TCP-like* transcription factor family which can regulate *CUC2* (Palatnik et al., 2007). In addition, *CUC2* expression is also regulated by the repressor miR164 (Koyama et al., 2010). The CUC2-miR164 system plays a key role in the evolution of composite leaves (Blein et al., 2008).

Meanwhile, miR319-TCP4 controls leaf senescence (Sun et al., 2017). The sequences of miR159 and miR319 are very similar, and the leaves of the miR159a miR159b double mutant are curled upward, indicating that miR159 also works on leaf development (Allen et al., 2007). miR393 and its target genes *TRANSPORT INHIBITOR RESPONSE 1* and *AUXIN SIGNALING F-BOX PROTEIN 1/2/3* can affect the shape and size of leaves by regulating the auxin response (Chen et al., 2011).

Stomata are special structures in the plant epidermis. miR824 and its target gene *Agamous Like 16* (*AGL16*) are involved in stomatal development. Overexpression of miR824 led to a decrease in stomatal density, similar to *agl16* mutant plants. However, when the regulation of miR824 on *AGL16* is destroyed, stomatal density will increase (Kutter et al., 2007). In maize, an increase of *GLl5* (*Glossyl5*) activity can increase the number of young leaves and delay the reproductive development. miRl72 can also promote the transformation from young leaves to mature leaves of maize through the negative regulation of *GLl5* mRNAs (Lauter et al., 2005). In tomato (*Solanum lycopersicum*), the *LANCEOLATE* gene encodes a *TCP* transcription factor. Its mutation or downregulation can cause compound leaves of plants to become single leaves. miR319 can target the *LANCEOLATE* (*LA*) gene and cause the formation of single leaves from multiple leaflets (Ori et al., 2007). Yanai et al. found that miR319 in tomato affects the differentiation and leaf shape by inhibiting the expression of the *SlGA20 oxidase1* gene, which is an enzyme involved in the GA synthesis pathway (Yanai et al., 2011). miR396 of the legume *Medicago truncatula* negatively regulates the expression of not only six *MtGRF* genes but also two *bHLH79*-like target genes and thus influences root growth and mycorrhizal associations (Bazin et al., 2013).

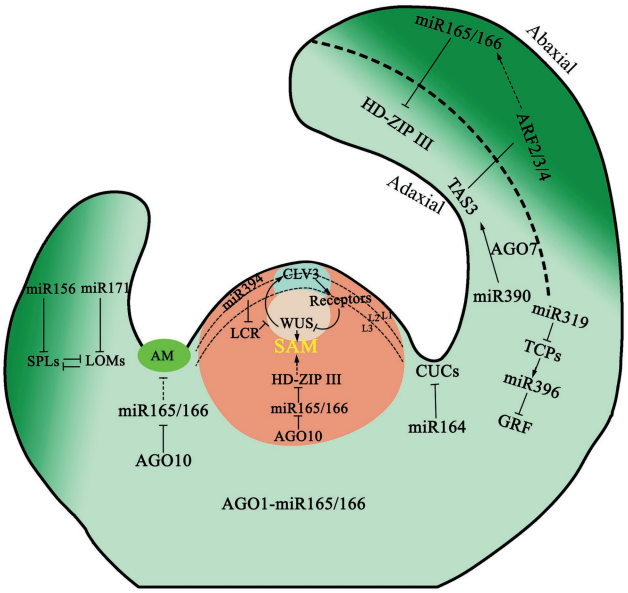

FIGURE 2 | Model for the role of miRNAs in shoot apex. miR394 synthesized at the protoderm represses *LCR* in subtending cells, which leads to the activation of the WUSCHEL (WUS) transcription factor to maintain stem cell identity and *CLAVATA3 (CLV3) peptide* expression. ARGONAUTE10 (AGO10) specifically sequesters miR165/166 and antagonizes its activity in the meristematic cells, thus regulating SAM and AM development. ARGONAUTE1 (AGO1) is expressed ubiquitously in the apex, recruit miR165/166 to form RNA-induced silencing complex (RISC). The adaxial and abaxial domains of leaves are established during leaf primordia emergence. HD-ZIP III transcription factors are restricted to the adaxial side by the action of miR165/166. In turn, AUXIN RESPONSE FACTOR 2/3/4 are restricted to the abaxial side by the action of TAS3 ta-siRNA. Two NAC-domain transcription factors are post-transcriptionally regulated by miR164 in embryonic meristem initiation, boundary size control, and cotyledon establishment. miR319 and miR396 target several *TEOSINTE BRANCHED1/CYCLOIDEA/PROLIFERATING CELL FACTOR* (*TCP*) and *Growth-Regulating Factor* (*GRF*) genes, respectively, and act coordinately to control leaf cell proliferation and differentiation. miR156 and miR171 synergistically regulate trichome initiation by targeting *SQUAMOSA PROMOTER BINDING PROTEIN-LIKE* (*SPL*) and *LOST MERISTEMS* (*LOM*), respectively. Arrows indicate positive regulation, whereas the dotted lines with perpendicular end bars represents a hypothesized negative regulation.

The Role of miRNAs in Vascular Development

Vascular plants use xylem to transport water and nutrients absorbed by roots upward and the phloem to transport the carbohydrate assimilated by leaves downward. The vascular bundle consists of three neatly arranged tissues: xylem, procambium/cambium, and phloem (**Figure 3**). In *A. thaliana*, the *HD-ZIP III* gene family is strongly expressed in vascular bundles of roots, stems, and leaves. Overexpression of miR165 in *A. thaliana* can reduce the transcription level of all members of the *HD-ZIP III* family, thus regulating the polar differentiation of vascular tissue cells and affecting plant morphogenesis (Zhong and Ye, 1999; Kang and Dengler, 2002; Zhou et al., 2007; Muraro et al., 2014; Du and Wang, 2015; Jia et al., 2015). It was reported that miR166 controls the development of vascular cells and phloem cells by regulating the Homeobox 15 protein (*ATHB15*) in *A. thaliana* (Kim et al., 2005). In almost all plant species, it is found that the target site of miR165/166 in class *HD-ZIP III* genes is highly conserved suggesting that this module is necessary in plant development and evolution (Floyd and Bowman, 2004).

Some miRNAs are also related to cell wall synthesis and fiber development in plants (Kim, 2005). It has been reported that a new miRNA (miR857), is decisive in the formation of secondary walls of vascular in a copper ion-dependent manner.

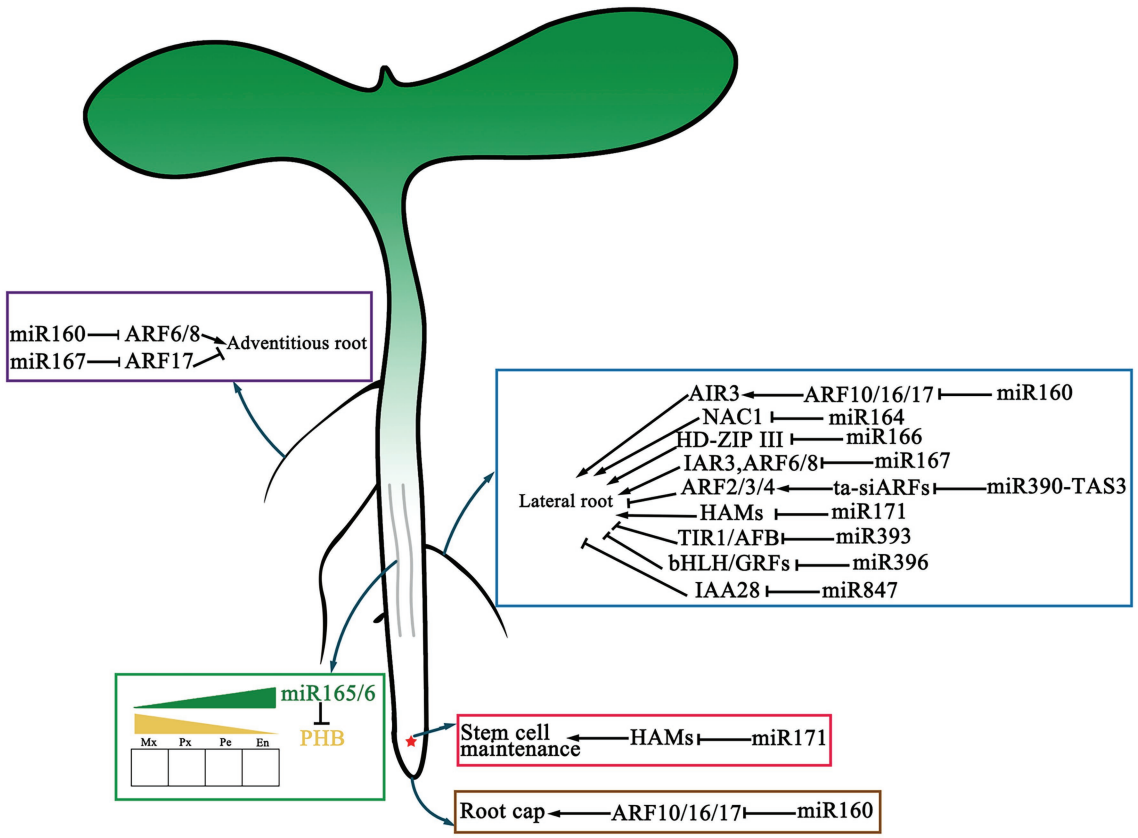

FIGURE 3 | The function of miRNAs in the development of vascular and root. microRNAs are involved in vascular and root development. All of the mRNAs with verified functions in main root, lateral root, adventitious root development as well as their respective main targets are represented. The red asterisk represents the quiescent center (QC). The solid gray line in the middle of the main root represents the vascular tissue.

miR857 regulates the expression of the putative laccase *LACCASE7*, a member of laccase family of genes, at transcriptional level and affects lignin content (Zhao et al., 2015). A recent study highlighted that some components related to leaf polarity and vascular development, such as miR390, TAS3, and ARF, are conserved across all terrestrial plants. For example, in liverworts, TAS3 ta-siRNA targets ARF as it does in angiosperms (Xia et al., 2017). In *Nicotiana tabacum*, the semi-dominant *phv* (*phavoluta*) mutant without miRl65 regulation has abnormal radial growth of stem and leaf vascular systems, and the vascular tissue of stem nodes is discontinuous, showing that miRl65 controls the growth of vascular cambium suggesting that the function of miR165/166 in vascular development is also conserved in plants (Yu et al., 2005).

The Role of miRNAs in Flower Development

Flower development is divided into three stages: flowering induction, flowering initiation, and floral organ development. It is a very complicated process involving multiple genes and is also an important event in development of higher plants. Many studies have shown that miRNA plays an important role in flowering.

In *A. thaliana*, the vegetative phase transition is promoted by a group of plant-specific transcription factors (SBP/SPL proteins). Their expression is inhibited by miR156 and miR157 in the juvenile developmental stage. When the level of miR156/miR157 decreases, the abundance of SBP/SPL proteins increases and the plant changes from vegetative phase to reproductive phase (Xu et al., 2016a; He et al., 2018; Fouracre et al., 2021). miR156 is the main regulatory gene for plant growth cycle transformation, which affects plant phase transformation by targeting *SPL* (*Squamosa Promoter binding protein-Like*) transcription factors (He et al., 2018; **Figure 4**). Overexpression of miR156 and subsequent downregulation of *SPL3/5* resulted in delayed flowering period of *A. thaliana*; downregulation of *SPL9* and *SPL15* resulted in shortened leaf plastochrons, slower growth, and extremely abundant leaves of *A. thaliana* (Schwab et al., 2005; Wu and Poethig, 2006; Xu et al., 2016b; Zhang et al., 2019). The role of miR156 and SPLs in flower development was also reported in rice (Xie et al., 2006). Studies have shown that the fine negative regulation of miR156 on *SPL3* ultimately affects the flowering phase transition process of *A. thaliana* by changing the expression of the *FT* gene in *A. thaliana* leaves leading to delayed flowering (Kim et al., 2012). Similar to the function of juvenile hormones in insects, high concentrations of miR156 keeps plants in the juvenile developmental stage. As development progresses, the amount of miR156 decreases gradually, which promotes the

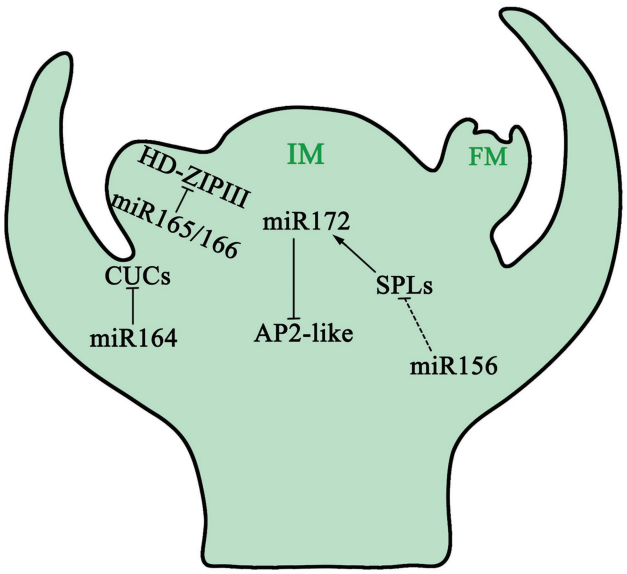

FIGURE 4 | The function of miRNAs in inflorescence meristem. As plants change growing phases from juveniles to adults, downregulation of miR156 dampens the inhibition of *SPL* expression, which in turn promotes miR172 transcription. miR172 triggers the development of inflorescence meristem by reducing the mRNA level of *AP2-like* genes. Spatiotemporal functions of miR165/166 and their targets *HD-ZIP III* genes, together with miR164, restrict the functions of *CUCs* in specific regions of the boundary to maintain the inflorescence meristem. miR156 decreases during IM development, whereas miR172 increases. IM: Inflorescence Meristem; FM: Floral Meristem.

juvenile-to-adult transition. Further studies showed that the decrease of miR156 content was not related to the absolute age (i.e., absolute time) of plants, but associated with the physiological age of plants (Cheng et al., 2021b).

miR172 is similar to miR156: namely, both are involved in controlling flowering time and the formation of floral organs by degrading and inhibiting target mRNA (Jung et al., 2007). miR172 regulates the transformation of plant development from the juvenile to flowering stage by regulating AP2-like genes including *SM-LIKE 2*, *SCHNARCHZAPFEN*, and *TARGET OF EARLY ACTIVATION TAGGED 1/2/3*. miR172 regulates plant flowering time, flower organ determination, flower morphogenesis, and plant development by controlling *AP2* transcription factors (Aukerman and Sakai, 2003). Overexpression of miR172 in *A. thaliana* will promote early flowering, while overexpression of *AP2* genes will delay flowering.

In addition, miR156 and miR172 interact together in some parts of the plant growth cycle that are regulated by miRNA. miR156 inhibited the expression of the *SPL* family, while some SPLs promoted the expression of miR172. Previous studies have shown that the miR156-SPL-miR172 pathway in *A. thaliana* is the decisive factor in controlling the juvenile-to-adult transition. The miR156-SPL-miR172 pathway can be divided into two modules: the leaf module and the apical meristem module, both of which have different combinations of SPL and miR172 encoding gene modules. In leaves, the SPL9-miR172b/c modules regulate flowering time by regulating the expression of the *FT* gene; while in apical meristem, the SPL15-miR172d modulus promotes flowering by activating the expression of *MADS-box* genes. In addition, the expression of the *MIR172* gene can be regulated by ambient temperature and photoperiod, and different *MIR172* genes have different response patterns (Lian et al., 2021).

Other miRNAs, such as miR159 and miR319, also function in flowering development. Their target genes are *MYB* and *TCP* (*TCP FAMILY TRANSCRIPTION FACTOR*) transcription factors, respectively. Overexpression of miR159 and miR319 will cause floral development disorders, such as delayed flowering (Palatnik et al., 2007). miR159 can regulate the expression of *MYB33* and *MYB65*, and a loss-of-function miR159 displays strong pleiotropic defects, stunted growth, curled leaves, defective sepals, petals, and anthers in *A. thaliana* (Achard et al., 2004; Millar and Gubler, 2005; Tsuji et al., 2006; Yu et al., 2012). At the same time, miR159 can prevent the over-activation of miR156, thus regulating the phase transition of *A. thaliana* in vegetative developmental period (Guo et al., 2017). *MYB33*, the target of miR159, promotes the transcription of *ABA INSENSITIVE 5* (*ABI5*) by binding directly to its promoter, then *ABI5* plays a role in the upstream of miR156 and regulates the juvenile-to-adult transition in *Arabidopsis* by affecting the gene expression in the miR156-SPL pathway (Guo et al., 2021).

In *A. thaliana*, miR164 regulates the number of petals and the differentiation of floral organ marginal cells and apical meristem cells by increasing the accumulation of CUC transcription factors in the boundary. Meanwhile, overexpression of miR164 leads to sepal fusion and reduction of petal number, suggesting that miR164 is related to the activity of flower meristem and the specific boundary division of the meristem region (Laufs et al., 2004; Jung et al., 2009).

miR165/166 also regulates flower morphogenesis. miR166/165 gene showed tissue-specific expression patterns in different flower organs. miR166a was mainly expressed in stamens, while miR166b was highly expressed in ovule and stigma. miR166d and miR165a were highly expressed in ovule. In contrast, miR166g had a broad expression in the stigma, stamen, and receptacle, but not in the ovule (Jung and Park, 2007). In terms of meristem activity regulation, miR165/166 is closely related to meristem formation in floral organs (Zhang et al., 2007). In the *Arabidopsis* mutants with miR165/166 overexpression, the flower structure was seriously damaged. For example, when miR166 is overproduced in *mum enhancer 1* and *jabba* mutants, and the pistil population is very small and the number of carpels is also reduced.

The significant increase of miR396 expression can cause the bending of the stigma in flowers, which demonstrated that miR396 also participates in the regulation of flower development. In *A. thaliana*, excessive production of miR167 displays floral defects resulting to that filaments were abnormally short, anthers could not properly release pollen, and pollen grains did not germinate (Ru et al., 2006). *ARF6* and *ARF8*, the target genes of miR167, play a meaningful role in the regulation of pistil and stamen population. miR167 also controls the fertility of male and female flowers of *A. thaliana* (Wu et al., 2006).

In addition to regulating reproductive organ morphology in the model organism *A. thaliana,* miRNAs have also been shown to regulate these organs in other plants. Tomato miR156b performs a key role in controlling flower and fruit morphology by regulating meristem activity and the initial stage of fruit development. Also, in tomato, overexpression of *A, thaliana* miR167a causes the downregulation of *ARF6* and *ARF8*, resulting in serious disorders in floral organ development and female gamete fertility (Liu et al., 2014b). In *Petunia* and *Antirrhinum* species, researchers found that miR169 can partially replace AP2, which results from the fact miR169 can regulate transcription factor *NF-YA*, thus affecting the development of flower organs (Chen, 2004; Cartolano et al., 2007; Zhao et al., 2009; Waheed and Zeng, 2020).

miRNAs also regulate flower and seed production in monocots. In rice, Zhu et al. found that overexpression of miR172 can cause spikelet deletion, floral organ development malformation, and fertility reduction (Zhu et al., 2009). OsmiR397 is a miRNA that is expressed at a high level in the young panicles and grains of rice, which increases grain yield by downregulating its target gene *OsLAC*. Overexpression of OsmiR397 can increase grain size and promote panicle branching (Zhang et al., 2013). In maize, Chuck et al. showed that miRNA-targeting SBP-box transcription factor *tasselsheath4* plays a critical role in the development of maize bracts and the establishment of meristem boundaries in inflorescences (Chuck et al., 2010, 2014) auxin.

Other Processes Involving miRNAs

miRNA also plays an essential regulatory role in other developmental processes. In *A. thaliana*, auxin response factors *ARF10*, *ARF16*, and *ARF17* are targeted by miR160. Studies have shown that miR160 plays a very important role in the negative regulation of *ARF10* to promote seed germination (Liu et al., 2007). Llave et al. found that during *Arabidopsis* root growth, root cap cell formation is related to miR160, which controls stem cell differentiation at the end of the root meristematic region and determines root growth direction by regulating the expression of *ARF10* (**Figure 3**; Llave et al., 2002).

In addition, miR164 and miR390 greatly influence the development of plant root organs, including root cap formation, lateral root development, and adventitious root formation (Yoon et al., 2010). The process of lateral root growth of *A. thaliana* is regulated by miR164. Guo et al. found that miR164 can mediate *NAC1* expression after being induced by auxin, thus affecting auxin transmission and regulating lateral root growth (**Figure 3**; Guo et al., 2005).

miR165/166 is related to the formation of xylem and cell arrangement in plants. The regulation of miRNA on plant tissue development is a complex molecular process (**Figure 3**; Carlsbecker et al., 2010). The same miRNA may have the multiple functions in different tissues. For example, miR165/miR166 is also related to leaf polarization in addition to xylem and cell arrangement as mentioned in a previous section (Tatematsu et al., 2015; Manuela and Xu, 2020).

Furthermore, miRNA is involved in regulating plant morphological structure and yield, which is important in crop plants. In soybean, the miR156-SPL gene module plays a key role in regulating the morphological structure and yield of soybean. In transgenic soybean overexpressing miR156b, axillary bud formation and branching are regulated by reducing the expression amount of *SPL9d* (Wang and Wang, 2015). In rice, inhibiting the expression of miR1432 or overexpressing *OsACOT* (*Acyl-CoA Thioesterase*) can cause the grain weight to be significantly boosted by increasing the grain filling rate, which can improve crop yield (Zhao et al., 2019). Genetic analysis shows that *OsSPL7* is the target of miR156f, which regulates plant morphological structure, namely tillering and height of rice (Dai et al., 2018). At the same time, *OsSPL7* directly binds to the *OsGH3.8* promoter to regulate its transcription, indicating that the miR156f-OsSPL7-OsGH3.8 is the complete regulatory pathway for these traits in rice.

miRNA is widely connected to plant diseases and environmental stress responses. Virus infections can greatly influence plant morphology and productivity. More and more evidence has shown that miRNA is related to virus-mediated diseases and virus-induced gene silencing (Chapman et al., 2004). More than 30 RNA silencing suppressors, also known as pathogenic factors, have been identified from plant viruses, including p19, p21, p25, and p69. Pathogenic factors can usually hinder the formation of siRNA, affect the stability of siRNA, or interfere with the combination of siRNA and RISC complexes, and can also lead to the generation of other diseases in plants and cause developmental malformation. Excessive HC-Pro protease (helper-component proteinase) in plants will reduce miR171 level and produce developmental deletion plants associated with miR171 which included branching defects, an increased number of short vegetative phytomers and late flowering. Through the overexpression of the *Hc-Pro* gene in *A. thaliana*, it was found that most miR171 target mRNAs are increased which results in virus-mediated diseases in plants (Kasschau et al., 2003).

Under abiotic stress, plants can directly synthesize some miRNAs and induce low or excessive expression of other miRNAs. These miRNAs act on transcription factors related to stress resistance, *Plant Growth Regulator 9* response protein genes, stress tolerance protein genes, and other target genes, which enables plants to quickly respond to environmental changes. In plants, miRNA responding to stress was first found in *A. thaliana* (Jones-Rhoades and Bartel, 2004). The expression of miR393 in *A. thaliana* was significantly upregulated after low temperature, drought, salt, or hormone (ABA) treatment. However, no responses to drought or NaCl were observed when miR310 and miR319 were upregulated after low-temperature stress indicating that these two miRNAs only function in low-temperature response. miR389a was downregulated after the above stress was induced (Sunkar and Zhu, 2004). miR393, miR397, miR402 (Sunkar and Zhu, 2004), miR165/miR166, miR169, and miR172 (Zhou et al., 2008) were all found to be induced by low temperature to enhance the plant resistance. In *A. thaliana*, the expression level of miR395 increased in the absence of sulfate, while the expression level of miR399 was upregulated, and the mRNA level of its target gene *PHO2/UBC24* (*PHOSPHATE 2*) was lower

(Chiou et al., 2006). miR169 is downregulated in a drought environment. Compared to wild-type plants, plants overexpressing miR169a or plants with *Nuclear transcription factor Y subunit A-5* deletion of miR169's target gene are more likely to lose leaf water and are more sensitive to drought (Li et al., 2008). In *grapevine*, miR398 participates in plant biotic stress, heavy metals, high salt, drought, ultraviolet radiation, and other abiotic stresses through the targeted regulation of two superoxide dismutases, *COPPER/ZINC SUPEROXIDE DISMUTASE 1/2* (Leng et al., 2017).

As mentioned above, studies in *Arabidopsis thaliana* and other plants have showed that miRNAs participate in many biological processes. Compared with the plant-wide action of hormones, miRNAs are crucial in precise regulation of gene expression in a tissue-specific pattern. How the plants integrate miRNAs fine regulation into hormonal system pathway to modulate tissue formation deserves more attention. Study the role and mechanism of miRNA movement between cells and tissues are vital to understand miRNA function.

THE INTERACTION BETWEEN miRNAs AND PLANT HORMONES

Plant hormones are important regulatory factors synthesized in plants. They regulate plant growth, development, and differentiation either individually or together. Plant hormones mainly include auxin (AUX), cytokinin (CK), abscisic acid (ABA), gibberellic acid (GA), ethylene (ET), brassinosteroid (BR), and jasmonic acid (JA). As signaling molecules regulating plant growth and development, these hormones have absolutely necessary function in controlling development timing, metabolism, and stress response through the whole plant growth cycle. Specific stages of development often involve the participation of multiple hormones; this enables plant cells to respond adaptively to development signals and changes in their internal and external environment (Li et al., 2020). miRNAs coordinate with hormones by negatively regulating target genes in hormonal pathways. It was found that in the seedlings, the overall miRNA accumulation level decreased after *HYL1* mutation, which displayed a variety of developmental defect phenotypes and abnormal sensitivity to ABA, AUX, and CK, indicating that miRNA is related to the signal responses of these hormones (Han et al., 2004). Many miRNA gene promoters contain hormone response elements as well as cis-elements response to stresses, indicating that the regulation of miRNA gene transcription may be a way of hormone and stress response (Ding et al., 2013).

miRNAs regulate auxin receptors and several transcription factors in plants. In *Arabidopsis*, when the expression of miR160 was silenced, the expression levels of *ARF16* and *ARF17* genes increased, which led to abnormal germ development, cotyledon shape defect, slow inflorescence development, stamen reduction, root shortening, and other adverse developmental symptoms. However, overexpression of miR160 in *Arabidopsis* inhibited the development of root cap and increased the number of lateral roots (**Figure 3**; Mallory et al., 2005; Wang et al., 2005). These results indicate that precise accumulation of miR160 is crucial to auxin-related plant development. miR167 and ARF6/8 co-regulate adventitious root formation (Gutierrez et al., 2009). miR847 targets and silences IAA28, the AUX/IAA inhibitory protein, to activate the auxin signaling pathway. The ubiquitination-mediated degradation of the IAA28 protein combined with miR847/IAA28 mRNA regulatory module to achieve the rapid disinhibition of the auxin signaling pathway (Wang and Guo, 2015). At the same time, miR165/166 directly targets *PHB*, an activator of *ARF5*, and then triggers the expression of miR390, which directly lead to the accumulation of ta-siRNAs (tasiR-ARF3/4; Marin et al., 2010; Muller et al., 2016; Dastidar et al., 2019). In addition, the miR165/166-tasiR-ARFs module also establishes the paraxial/distal polarity of the blade.

miR159 and miR319 inhibit the expression of *SHOOT-MERISTEMLESS* and *BREVIPEDICELLUS*, and then enhance the expression of *IPT* (*ISOPENTENYL TRANSFERASE*) and promote the biosynthesis of CK in SAM (Rubio-Somoza and Weigel, 2013; Scofield et al., 2014). At the cytokinin signal transduction level, the miR156-SPL9 complex modulates cytokinin-related plant regeneration by inhibiting the *B-type ARR genes9* [*type B Arabidopsis Response Regulators* (*ARRs*)], which are transcription factors that act as positive regulators in the two-component cytokinin signaling pathway (Zhang et al., 2015).

miRNAs also affect the biosynthesis and signal transduction of cytokinin through auxin, and then continue to maintain the dynamic balance between auxin and cytokinin, such as miR160 and miR165/6 (Dello et al., 2012; Liu et al., 2016). Another signaling molecule, gibberellin, can regulate the levels of various miRNAs through DELLA (aspartic acid–glutamic acid–leucine–leucine–alanine) protein and its interacting proteins, such as IDD2 (indeterminate (ID)-domain 2), PHYTOCHROME-INTERACTING FACTOR 4, or SCARECROW-LIKE (SCL; Han et al., 2014; Fan et al., 2018). Conversely, miRNAs can directly regulate GA biosynthesis and signal transduction through different complexes such as miR156-SPL, miR171-SCL, and miR159-GAMYB(L)s modules (Yu et al., 2012; Ma et al., 2014; Sun et al., 2018; Millar et al., 2019). Brassinosteroids (BR) negatively regulate miRNA-mediated translation inhibition of target genes by interfering with the distribution and localization pattern of AGO1, the miRNA effector protein, in the endoplasmic reticulum (Wang et al., 2021d).

miRNAs can regulate seed germination and leaf senescence by affecting the levels of ABA and ethylene. ABA, the signaling hormone, and SnRK2 (SNF1-related protein kinase 2) protein kinase, the core component of the osmotic stress response pathway, can regulate miRNA synthesis (Yan et al., 2017). At the same time, the ABA and ethylene signaling pathway can cause feedback on the level of sRNA by affecting the core protein in sRNA synthesis pathway, such as CBP20 (CAP-BINDING PROTEIN 20; Kim et al., 2008; Li et al., 2012, 2013; Zhang et al., 2016). Therefore, miRNAs coordinate with hormone responses in many ways and play an important role in plant development.

ROLE OF SMALL RNA MOVEMENT IN PLANT DEVELOPMENT

Plant small RNAs can spread silencing signals by moving in plants to participate in plant development regulation and respond to environmental stresses. Usually, mobile small RNAs generate sharply defined domains of target gene expression through an intrinsic and direct threshold-based readouts of their mobility gradients to drive developmental patterning (Skopelitis et al., 2017). There are two main types of small RNA movement in plants: one is short-distance (cell-to-cell) movement between neighboring cells, the other is long-distance (such as shoot to root or root to shoot) movement in plants. Currently, there is a hypothesis that 21 nt-siRNA are mainly involved in short-distance transport and 23\u201324 nt small RNAs are mainly involved in long-distance transport. The mechanisms of these two types of small RNA movement may be different (Tamiru et al., 2018), and will be explored in the following sections.

Short-Distance Movement

The short-distance movement of plant small RNAs is was thought to be mainly conferred *via* plasmodesmata between adjacent cells (Vaten et al., 2011). However, using a type of miR-GFP sensor system, it has been found that small RNAs are an independent mobile unit, and their mechanisms of movement between cells are different from that of proteins (Skopelitis et al., 2018). Some small RNAs have been discovered that can move in short distances of up to ten files of cells. For example, mature miR165/166 can move from the endoderm of the root to the vasculature, thereby forming a gradient-like distribution of miR165/166 to regulate the expression pattern of its target gene *PHB* and finally complete the establishment of proto- and metaxylem (Carlsbecker et al., 2010). In leaves, miR165/166 can be moved from the abaxial surface to the adaxial side, also forming a gradient to regulate the expression pattern of *HD-ZIP III* genes and ultimately form leaf polarity. In the SAM, miR394 moves to the cells in the L2 and L3 layers to repress its target gene *LCR* as a mobile signal produced by L1 layer cell. Repression of *LCR* signal in the underneath stem cells is used to maintain stem cell pluripotency by influencing the WUS-CLV loop (Knauer et al., 2013). In addition to miRNAs, PhasiRNAs have also been found to be able to move from cell to cell. For example, tasiR-ARF is produced from long non-coding RNAs transcribed at the TAS3 loci by the processing of the miR390-AGO7 complex on the adaxial side of leaves (Allen et al., 2005; Endo et al., 2013). These tasiR-ARFs can move to the abaxial side of leaves and form a gradient of to inhibit the expression of *ARF3* on adaxial side. Inhibition of *ARF3* expression ensures the establishment of leaf polarity patterns (Chitwood et al., 2009). Recent experiments show that processed tasiR-ARFs in the apical epidermal cells can move to hypodermal cells in the nucellar region to repress *ARF3* expression and suppress ectopic megaspore mother cell (MMC) fate (Su et al., 2020).

Long-Distance Movement

The long-distance movement of plant small RNA is mainly mediated through the phloem following source–sink relationships (Melnyk et al., 2011; Tamiru et al., 2018). In line with this, miRNAs have been found in the phloem saps of multiple plants (Tamiru et al., 2018). For example, miR172 was found in the vascular bundles of potatoes, indicating that miR172 might be mobile or that it regulates long-distance signals to induce tuberization(Marin et al., 2010). In *Brassica napus*, using small RNA sequencing, it was discovered that levels of miR395, miR398, and miR399 in the phloem are strongly increased in response to sulphate, copper, or phosphate starvation, respectively (Buhtz et al., 2008).

In *Arabidopsis*, miR399 moves from shoot to root to inhibit the expression of its target gene *PHO2* in response to phosphate homeostasis (Lin et al., 2008; Pant et al., 2008). During phosphate starvation, miR827 and miR2112a can also move from shoot to root (Huen et al., 2017). miR2112 can move from shoot to root to inhibit the expression of symbiosis suppressor TOO MUCH LOVE, thereby controlling rhizobial infection (Tsikou et al., 2018).

FUTURE PERSPECTIVES

Understanding the elaborate regulation of plant development by miRNAs is crucial for crop breeding. Knocking out dominant genes in development often causes lethality in plants, while miRNAs can safely modify gene expression to some extent and improve plant development. In rice, the number of branches (including tiller and inflorescence branches) determines grain yield. It was found that the genes regulating rice tillering and panicle branching consisted of miR156/miR529/SPL and miR172/AP2 modules. The *SPL* gene negatively controls tillering, but positively regulates the transformation of inflorescence meristem and spikelet. Changes in *SPL* expression will reduce panicle branching (Wang and Wang, 2015). In the regulation of seed size and grain yield, OsmiR397 can increase grain size, promote panicle branching, and increase grain yield by downregulating its target gene *OsLAC* (Zhang et al., 2013). miR1432-OsACOT modules are involved in fatty acid metabolism and plant hormone biosynthesis, and crucial for rice (Zhao et al., 2019). miR319s negatively affects tiller number and grain yield by targeting *OsTCP21* and *OsGAmyb* (Wang et al., 2021c). Changes of "miR168-AGO1" regulatory pathway influence several "miRNA-target gene" loops, which regulate the immunity and growth of rice, respectively. Among these, the "miR535-SPL14" loop regulates the yield and immunity of rice, the "miR164-NAC11" loop regulates the growth period and immunity of rice, and miR1320 regulates the immunity of rice (Wang et al., 2021a). In maize, *TASSELSEED4* encodes miR172 to control sex determination and meristem cell fate by targeting *IDS1* (*Indeterminate Spikelet1*). Moreover, miR156a-l acts on several SPL genes during the transition from young to mature ear, and indirectly activates miR172 through *SPLs* (Lauter et al., 2005; Chuck et al., 2007b; Salvi et al., 2007). In agriculture, epigenetic variations account for a great proportion for change

in crop yield. SNPs located in non-coding regions are paid more and more attention by breeders in population genetic analysis and traditional hybrid breeding. New strategies such as Short Tandem Target Mimic (STTM), a specific miRNA targeting method which is effective in blocking small RNA functions in plants (Tang et al., 2012), are adapted and utilized in generating transgenic crops. As *MIR* genes are usually short, EMS mutation and T-DNA inserted mutation are difficult to achieve ideal mutants for *MIR* genes. However, the advances of genome editing technologies make modification of miRNA expression to increase crop yield become easier.

Modes of miRNA function need to be further explored. miRNAs also act as environmental response factors, endowing plants with corresponding phenotypes and promoting plant evolution and adaptation. For example, the essential role of HD-ZIP III-miR165/166 signaling pathway in meristematic tissues and the dual regulatory role of miR156/miR172 in flower determination are conserved in plant kingdom. The function of miRNAs and their specific mechanisms need to be further studied. It is still not clearly understood how miRNAs specifically regulate a biological process in certain temporal and spatial patterns. Many miRNA gene promoters contain plant hormones and cis-elements of stress response, indicating that regulation of miRNA gene transcription may be a way to respond to plant hormone and stresses. The expression of *AGO10* is precisely regulated by auxin, brassinolide, and light to initiate axillary meristem in certain leaf axils. This provides a way to modify gene expression in a tissue-specific pattern and potentiate modulation of organ development at certain stages.

Recently, great importance has been attached to small RNA movement between cells, tissues as well as organisms by plant researchers. Much effort is made to uncover the role and mechanism of small RNA movement. So far, it is evidenced that miRNA can move to form gradient distribution between different tissues. After biogenesis, miRNA is protected from degradation and is transported to destination cells. It is noteworthy that miRNA needs to reach a certain threshold level before it can function in a non-cellular autonomous way. How intermediate steps influence miRNA movement and its non-cellular autonomous function need more studies. To understand and prime plants for abiotic stresses, it is also worth further studies to elaborate the correlation between hormone concentration and miRNA movement.

In addition, biotic and abiotic stresses can induce plants to produce new sRNA. For example, *A. thaliana* can produce a large number of 22 nt siRNAs dependent on DCL2 and RDR6 under stresses such as nitrogen deficiency. However, it is still a puzzle as to why only a small number of gene loci in *A. thaliana* can produce 22 nt siRNAs. Meanwhile, there is also a big gap in knowledge of the synthesis of 22 nt siRNAs to their biological function. More evidence is needed to verify whether 22 nt siRNAs can also regulate target genes in distal organs due to the cellular non-autonomy of sRNA. Therefore, the improvement of sequencing technology and miRNA research methods are highly recommended here. With the help of various single-cell omics and nanopore sequencing, more miRNAs, their action mechanisms, and their regulatory pathways will be discovered in model plants, which will provide important theoretical basis for understanding how miRNA regulates plant growth and development and can then be applied to agriculturally important plants.

AUTHOR CONTRIBUTIONS

QD, BH, and CZ wrote the article. All authors read and approved the manuscript.

FUNDING

Research in the Zhang lab is supported by the Strategic Priority Research Program of the Chinese Academy of Sciences, Grant Nos. XDA26030200 and XDA24010106-2 to CZ.

REFERENCES

Abdel-Ghany, S. E., and Pilon, M. (2008). MicroRNA-mediated systemic down-regulation of copper protein expression in response to low copper availability in Arabidopsis. *J. Biol. Chem.* 283, 15932–15945. doi: 10.1074/jbc.M801406200

Achard, P., Herr, A., Baulcombe, D. C., and Harberd, N. P. (2004). Modulation of floral development by a gibberellin-regulated microRNA. *Development* 131, 3357–3365. doi: 10.1242/dev.01206

Allen, R. S., Li, J., Stahle, M. I., Dubroue, A., and Gubler, F. (2007). Genetic analysis reveals functional redundancy and the major target genes of the Arabidopsis miR159 family. *Proc. Natl. Acad. Sci. U. S. A.* 104, 16371–16376. doi: 10.1073/pnas.0707653104

Allen, E., Xie, Z., Gustafson, A. M., and Carrington, J. C. (2005). MicroRNA-directed phasing during trans-acting siRNA biogenesis in plants. *Cell* 121, 207–221. doi: 10.1016/j.cell.2005.04.004

Arikit, S., Xia, R., Kakrana, A., Huang, K., and Zhai, J. (2014). An atlas of soybean small RNAs identifies phased siRNAs from hundreds of coding genes. *Plant Cell* 26, 4584–4601. doi: 10.1105/tpc.114.131847

Aukerman, M. J., and Sakai, H. (2003). Regulation of flowering time and floral organ identity by a MicroRNA and its APETALA2-like target genes. *Plant Cell* 15, 2730–2741. doi: 10.1105/tpc.016238

Baucher, M., Moussawi, J., Vandeputte, O. M., Monteyne, D., and Mol, A. (2013). A role for the miR396/GRF network in specification of organ type during flower development, as supported by ectopic expression of Populus trichocarpa miR396c in transgenic tobacco. *Plant Biol.* 15, 892–898. doi: 10.1111/j.1438-8677.2012.00696.x

Baumann, K. (2013). Plant cell biology: Mobile miRNAs for stem cell maintenance. *Nat. Rev. Mol. Cell Biol.* 14:128. doi: 10.1038/nrm3529

Baumberger, N., and Baulcombe, D. C. (2005). Arabidopsis ARGONAUTE1 is an RNA slicer that selectively recruits microRNAs and short interfering RNAs. *Proc. Natl. Acad. Sci. U. S. A.* 102, 11928–11933. doi: 10.1073/pnas.0505461102

Bazin, J., Khan, G. A., Combier, J. P., Bustos-Sanmamed, P., and Debernardi, J. M. (2013). MiR396 affects mycorrhization and root meristem activity in the legume Medicago truncatula. *Plant J.* 74, 920–934. doi: 10.1111/tpj.12178

Bergmann, D. C., and Sack, F. D. (2007). Stomatal development. *Annu. Rev. Plant Biol.* 58, 163–181. doi: 10.1146/annurev.arplant.58.032806.104023

Blein, T., Pulido, A., Vialette-Guiraud, A., Nikovics, K., and Morin, H. (2008). A conserved molecular framework for compound leaf development. *Science* 322, 1835–1839. doi: 10.1126/science.1166168

Bologna, N. G., Iselin, R., Abriata, L. A., Sarazin, A., and Pumplin, N. (2018). Nucleo-cytosolic shuttling of ARGONAUTE1 prompts a revised model of the plant MicroRNA pathway. *Mol. Cell* 69, 709–719. doi: 10.1016/j.molcel.2018.01.007

Borges, F., and Martienssen, R. A. (2015). The expanding world of small RNAs in plants. *Nat. Rev. Mol. Cell Biol.* 16, 727–741. doi: 10.1038/nrm4085

Bresso, E. G., Chorostecki, U., Rodriguez, R. E., Palatnik, J. F., and Schommer, C. (2018). Spatial control of gene expression by miR319-regulated TCP transcription factors in leaf development. *Plant Physiol.* 176, 1694–1708. doi: 10.1104/pp.17.00823

Brioudes, F., Jay, F., Sarazin, A., Grentzinger, T., and Devers, E. A. (2021). HASTY, the Arabidopsis EXPORTIN5 ortholog, regulates cell-to-cell and vascular microRNA movement. *EMBO J.* 40:e107455. doi: 10.15252/embj.2020107455

Brodersen, P., Sakvarelidze-Achard, L., Bruun-Rasmussen, M., Dunoyer, P., and Yamamoto, Y. Y. (2008). Widespread translational inhibition by plant miRNAs and siRNAs. *Science* 320, 1185–1190. doi: 10.1126/science.1159151

Buhtz, A., Springer, F., Chappell, L., Baulcombe, D. C., and Kehr, J. (2008). Identification and characterization of small RNAs from the phloem of Brassica napus. *Plant J.* 53, 739–749. doi: 10.1111/j.1365-313X.2007.03368.x

Bustos-Sanmamed, P., Mao, G., Deng, Y., Elouet, M., and Khan, G. A. (2013). Overexpression of miR160 affects root growth and nitrogen-fixing nodule number in Medicago truncatula. *Funct. Plant Biol.* 40, 1208–1220. doi: 10.1071/FP13123

Cambiagno, D. A., Giudicatti, A. J., Arce, A. L., Gagliardi, D., and Li, L. (2021). HASTY modulates miRNA biogenesis by linking pri-miRNA transcription and processing. *Mol. Plant* 14, 426–439. doi: 10.1016/j.molp.2020.12.019

Carbonell, A., Fahlgren, N., Garcia-Ruiz, H., Gilbert, K. B., and Montgomery, T. A. (2012). Functional analysis of three Arabidopsis ARGONAUTES using slicer-defective mutants. *Plant Cell* 24, 3613–3629. doi: 10.1105/tpc.112.099945

Carlsbecker, A., Lee, J. Y., Roberts, C. J., Dettmer, J., and Lehesranta, S. (2010). Cell signalling by microRNA165/6 directs gene dose-dependent root cell fate. *Nature* 465, 316–321. doi: 10.1038/nature08977

Cartolano, M., Castillo, R., Efremova, N., Kuckenberg, M., and Zethof, J. (2007). A conserved microRNA module exerts homeotic control over Petunia hybrida and Antirrhinum majus floral organ identity. *Nat. Genet.* 39, 901–905. doi: 10.1038/ng2056

Caruana, J. C., Dhar, N., and Raina, R. (2020). Overexpression of Arabidopsis microRNA167 induces salicylic acid-dependent defense against pseudomonas syringae through the regulation of its targets ARF6 and ARF8. *Plant Direct* 4:e270. doi: 10.1002/pld3.270

Chandran, V., Wang, H., Gao, F., Cao, X. L., and Chen, Y. P. (2018). MiR396-OsGRFs module balances growth and rice blast disease-resistance. *Front. Plant Sci.* 9:1999. doi: 10.3389/fpls.2018.01999

Chapman, E. J., Prokhnevsky, A. I., Gopinath, K., Dolja, V. V., and Carrington, J. C. (2004). Viral RNA silencing suppressors inhibit the microRNA pathway at an intermediate step. *Genes Dev.* 18, 1179–1186. doi: 10.1101/gad.1201204

Chen, X. (2004). A microRNA as a translational repressor of APETALA2 in Arabidopsis flower development. *Science* 303, 2022–2025. doi: 10.1126/science.1088060

Chen, Z. H., Bao, M. L., Sun, Y. Z., Yang, Y. J., and Xu, X. H. (2011). Regulation of auxin response by miR393-targeted transport inhibitor response protein 1 is involved in normal development in Arabidopsis. *Plant Mol. Biol.* 77, 619–629. doi: 10.1007/s11103-011-9838-1

Chen, H. M., Chen, L. T., Patel, K., Li, Y. H., and Baulcombe, D. C. (2010). 22-nucleotide RNAs trigger secondary siRNA biogenesis in plants. *Proc. Natl. Acad. Sci. U. S. A.* 107, 15269–15274. doi: 10.1073/pnas.1001738107

Chen, X., and Rechavi, O. (2021). Plant and animal small RNA communications between cells and organisms. *Nat. Rev. Mol. Cell Biol.* doi: 10.1038/s41580-021-00425-y [Epub ahead of print].

Cheng, X., He, Q., Tang, S., Wang, H., and Zhang, X. (2021a). The miR172/IDS1 signaling module confers salt tolerance through maintaining ROS homeostasis in cereal crops. *New Phytol.* 230, 1017–1033. doi: 10.1111/nph.17211

Cheng, Y. J., Shang, G. D., Xu, Z. G., Yu, S., and Wu, L. Y. (2021b). Cell division in the shoot apical meristem is a trigger for miR156 decline and vegetative phase transition in Arabidopsis. *Proc. Natl. Acad. Sci. U. S. A.* 118:e2115667118. doi: 10.1073/pnas.2115667118

Chiou, T. J., Aung, K., Lin, S. I., Wu, C. C., and Chiang, S. F. (2006). Regulation of phosphate homeostasis by MicroRNA in Arabidopsis. *Plant Cell* 18, 412–421. doi: 10.1105/tpc.105.038943

Chitwood, D. H., Nogueira, F. T., Howell, M. D., and Montgomery, T. A. (2009). Pattern formation *via* small RNA mobility. *Genes Dev.* 23, 549–554. doi: 10.1101/gad.1770009

Chuck, G. S., Brown, P. J., Meeley, R., and Hake, S. (2014). Maize SBP-box transcription factors unbranched2 and unbranched3 affect yield traits by regulating the rate of lateral primordia initiation. *Proc. Natl. Acad. Sci. U. S. A.* 111, 18775–18780. doi: 10.1073/pnas.1407401112

Chuck, G., Cigan, A. M., Saeteurn, K., and Hake, S. (2007a). The heterochronic maize mutant Corngrass1 results from overexpression of a tandem microRNA. *Nat. Genet.* 39, 544–549. doi: 10.1038/ng2001

Chuck, G., Meeley, R., Irish, E., Sakai, H., and Hake, S. (2007b). The maize tasselseed4 microRNA controls sex determination and meristem cell fate by targeting Tasselseed6/indeterminate spikelet1. *Nat. Genet.* 39, 1517–1521. doi: 10.1038/ng.2007.20

Chuck, G., Whipple, C., Jackson, D., and Hake, S. (2010). The maize SBP-box transcription factor encoded by tasselsheath4 regulates bract development and the establishment of meristem boundaries. *Development* 137, 1243–1250. doi: 10.1242/dev.048348

Curaba, J., Talbot, M., Li, Z., and Helliwell, C. (2013). Over-expression of microRNA171 affects phase transitions and floral meristem determinancy in barley. *BMC Plant Biol.* 13:6. doi: 10.1186/1471-2229-13-6

D'Ario, M., Griffiths-Jones, S., and Kim, M. (2017). Small RNAs: big impact on plant development. *Trends Plant Sci.* 22, 1056–1068. doi: 10.1016/j.tplants.2017.09.009

Dai, X., Lu, Q., Wang, J., Wang, L., and Xiang, F. (2021). MiR160 and its target genes ARF10, ARF16 and ARF17 modulate hypocotyl elongation in a light, BRZ, or PAC-dependent manner in Arabidopsis: MiR160 promotes hypocotyl elongation. *Plant Sci.* 303:110686. doi: 10.1016/j.plantsci.2020.110686

Dai, Z., Wang, J., Yang, X., Lu, H., and Miao, X. (2018). Modulation of plant architecture by the miR156f-OsSPL7-OsGH3.8 pathway in rice. *J. Exp. Bot.* 69, 5117–5130. doi: 10.1093/jxb/ery273

Dastidar, M. G., Scarpa, A., Magele, I., Ruiz-Duarte, P., and von Born, P. (2019). ARF5/MONOPTEROS directly regulates miR390 expression in the *Arabidopsis thaliana* primary root meristem. *Plant Direct* 3:e116. doi: 10.1002/pld3.116

Debernardi, J. M., Mecchia, M. A., Vercruyssen, L., Smaczniak, C., and Kaufmann, K. (2014). Post-transcriptional control of GRF transcription factors by microRNA miR396 and GIF co-activator affects leaf size and longevity. *Plant J.* 79, 413–426. doi: 10.1111/tpj.12567

Debernardi, J. M., Rodriguez, R. E., Mecchia, M. A., and Palatnik, J. F. (2012). Functional specialization of the plant miR396 regulatory network through distinct microRNA-target interactions. *PLoS Genet.* 8:e1002419. doi: 10.1371/journal.pgen.1002419

Dello, I. R., Galinha, C., Fletcher, A. G., Grigg, S. P., and Molnar, A. (2012). A PHABULOSA/cytokinin feedback loop controls root growth in Arabidopsis. *Curr. Biol.* 22, 1699–1704. doi: 10.1016/j.cub.2012.07.005

Deng, P., Muhammad, S., Cao, M., and Wu, L. (2018). Biogenesis and regulatory hierarchy of phased small interfering RNAs in plants. *Plant Biotechnol. J.* 16, 965–975. doi: 10.1111/pbi.12882

Ding, Y., Tao, Y., and Zhu, C. (2013). Emerging roles of microRNAs in the mediation of drought stress response in plants. *J. Exp. Bot.* 64, 3077–3086. doi: 10.1093/jxb/ert164

Du, F., Gong, W., Bosca, S., Tucker, M., and Vaucheret, H. (2020). Dose-dependent AGO1-mediated inhibition of the miRNA165/166 pathway modulates stem cell maintenance in arabidopsis shoot apical meristem. *Plant Commun.* 1:100002. doi: 10.1016/j.xplc.2019.100002

Du, Q., and Wang, H. (2015). The role of HD-ZIP III transcription factors and miR165/166 in vascular development and secondary cell wall formation. *Plant Signal. Behav.* 10:e1078955. doi: 10.1080/15592324.2015.1078955

Duan, C. G., Zhang, H., Tang, K., Zhu, X., and Qian, W. (2015). Specific but interdependent functions for Arabidopsis AGO4 and AGO6 in RNA-directed DNA methylation. *EMBO J.* 34, 581–592. doi: 10.15252/embj.201489453

Elbashir, S. M., Harborth, J., Lendeckel, W., Yalcin, A., and Weber, K. (2001). Duplexes of 21-nucleotide RNAs mediate RNA interference in cultured mammalian cells. *Nature* 411, 494–498. doi: 10.1038/35078107

Endo, Y., Iwakawa, H. O., and Tomari, Y. (2013). Arabidopsis ARGONAUTE7 selects miR390 through multiple checkpoints during RISC assembly. *EMBO Rep.* 14, 652–658. doi: 10.1038/embor.2013.73

Fahlgren, N., Montgomery, T. A., Howell, M. D., Allen, E., and Dvorak, S. K. (2006). Regulation of AUXIN RESPONSE FACTOR3 by TAS3 ta-siRNA affects developmental timing and patterning in Arabidopsis. *Curr. Biol.* 16, 939–944. doi: 10.1016/j.cub.2006.03.065

Fan, S., Zhang, D., Gao, C., Wan, S., and Lei, C. (2018). Mediation of flower induction by gibberellin and its inhibitor paclobutrazol: MRNA and miRNA integration comprises complex regulatory cross-talk in apple. *Plant Cell Physiol.* 59, 2288–2307. doi: 10.1093/pcp/pcy154

Fang, X., and Qi, Y. (2016). RNAi in plants: an Argonaute-Centered view. *Plant Cell* 28, 272–285. doi: 10.1105/tpc.15.00920

Fire, A., Xu, S., Montgomery, M. K., Kostas, S. A., and Driver, S. E. (1998). Potent and specific genetic interference by double-stranded RNA in Caenorhabditis elegans. *Nature* 391, 806–811. doi: 10.1038/35888

Floyd, S. K., and Bowman, J. L. (2004). Gene regulation: ancient microRNA target sequences in plants. *Nature* 428, 485–486. doi: 10.1038/428485a

Fouracre, J. P., He, J., Chen, V. J., Sidoli, S., and Poethig, R. S. (2021). VAL genes regulate vegetative phase change *via* miR156-dependent and independent mechanisms. *PLoS Genet.* 17:e1009626. doi: 10.1371/journal.pgen.1009626

Gaillochet, C., and Lohmann, J. U. (2015). The never-ending story: From pluripotency to plant developmental plasticity. *Development* 142, 2237–2249. doi: 10.1242/dev.117614

Guan, X., Pang, M., Nah, G., Shi, X., and Ye, W. (2014). MiR828 and miR858 regulate homoeologous MYB2 gene functions in Arabidopsis trichome and cotton fibre development. *Nat. Commun.* 5:3050. doi: 10.1038/ncomms4050

Guo, C., Jiang, Y., Shi, M., Wu, X., and Wu, G. (2021). ABI5 acts downstream of miR159 to delay vegetative phase change in Arabidopsis. *New Phytol.* 231, 339–350. doi: 10.1111/nph.17371

Guo, H. S., Xie, Q., Fei, J. F., and Chua, N. H. (2005). MicroRNA directs mRNA cleavage of the transcription factor NAC1 to downregulate auxin signals for arabidopsis lateral root development. *Plant Cell* 17, 1376–1386. doi: 10.1105/tpc.105.030841

Guo, C., Xu, Y., Shi, M., Lai, Y., and Wu, X. (2017). Repression of miR156 by miR159 regulates the timing of the juvenile-to-adult transition in arabidopsis. *Plant Cell* 29, 1293–1304. doi: 10.1105/tpc.16.00975

Gutierrez, L., Bussell, J. D., Pacurar, D. I., Schwambach, J., and Pacurar, M. (2009). Phenotypic plasticity of adventitious rooting in Arabidopsis is controlled by complex regulation of AUXIN RESPONSE FACTOR transcripts and microRNA abundance. *Plant Cell* 21, 3119–3132. doi: 10.1105/tpc.108.064758

Ha, M., and Kim, V. N. (2014). Regulation of microRNA biogenesis. *Nat. Rev. Mol. Cell Biol.* 15, 509–524. doi: 10.1038/nrm3838

Hamilton, A. J., and Baulcombe, D. C. (1999). A species of small antisense RNA in posttranscriptional gene silencing in plants. *Science* 286, 950–952. doi: 10.1126/science.286.5441.950

Han, J., Fang, J., Wang, C., Yin, Y., and Sun, X. (2014). Grapevine microRNAs responsive to exogenous gibberellin. *BMC Genomics* 15:111. doi: 10.1186/1471-2164-15-111

Han, M. H., Goud, S., Song, L., and Fedoroff, N. (2004). The Arabidopsis double-stranded RNA-binding protein HYL1 plays a role in microRNA-mediated gene regulation. *Proc. Natl. Acad. Sci. U. S. A.* 101, 1093–1098. doi: 10.1073/pnas.0307969100

Hay, A., Craft, J., and Tsiantis, M. (2004). Plant hormones and homeoboxes: bridging the gap? *BioEssays* 26, 395–404. doi: 10.1002/bies.20016

He, J., Xu, M., Willmann, M. R., McCormick, K., and Hu, T. (2018). Threshold-dependent repression of SPL gene expression by miR156/miR157 controls vegetative phase change in *Arabidopsis thaliana*. *PLoS Genet.* 14:e1007337. doi: 10.1371/journal.pgen.1007337

Hibara, K., Karim, M. R., Takada, S., Taoka, K., and Furutani, M. (2006). Arabidopsis CUP-SHAPED COTYLEDON3 regulates postembryonic shoot meristem and organ boundary formation. *Plant Cell* 18, 2946–2957. doi: 10.1105/tpc.106.045716

Huen, A. K., Rodriguez-Medina, C., Ho, A., Atkins, C. A., and Smith, P. (2017). Long-distance movement of phosphate starvation-responsive microRNAs in Arabidopsis. *Plant Biol.* 19, 643–649. doi: 10.1111/plb.12568

Ji, L., Liu, X., Yan, J., Wang, W., and Yumul, R. E. (2011). ARGONAUTE10 and ARGONAUTE1 regulate the termination of floral stem cells through two microRNAs in Arabidopsis. *PLoS Genet.* 7:e1001358. doi: 10.1371/journal.pgen.1001358

Jia, X., Ding, N., Fan, W., Yan, J., and Gu, Y. (2015). Functional plasticity of miR165/166 in plant development revealed by small tandem target mimic. *Plant Sci.* 233, 11–21. doi: 10.1016/j.plantsci.2014.12.020

Jing, X., Rui, M., and Blake, C. (2017). The emergence, evolution, and diversification of the miR390-TAS3-ARF pathway in land plants. *Plant Cell* 29, 1232–1247. doi: 10.1105/tpc.17.00185

Jodder, J. (2020). MiRNA-mediated regulation of auxin signaling pathway during plant development and stress responses. *J. Biosci.* 45:91. doi: 10.1007/s12038-020-00062-1

Jones-Rhoades, M. W., and Bartel, D. P. (2004). Computational identification of plant microRNAs and their targets, including a stress-induced miRNA. *Mol. Cell* 14, 787–799. doi: 10.1016/j.molcel.2004.05.027

Jones-Rhoades, M. W., Bartel, D. P., and Bartel, B. (2006). MicroRNAS and their regulatory roles in plants. *Annu. Rev. Plant Biol.* 57, 19–53. doi: 10.1146/annurev.arplant.57.032905.105218

Jung, J. H., and Park, C. M. (2007). MIR166/165 genes exhibit dynamic expression patterns in regulating shoot apical meristem and floral development in Arabidopsis. *Planta* 225, 1327–1338. doi: 10.1007/s00425-006-0439-1

Jung, J. H., Seo, P. J., and Park, C. M. (2009). MicroRNA biogenesis and function in higher plants. *Plant Biotechnol. Rep.* 3, 111–126. doi: 10.1007/s11816-009-0085-8

Jung, J. H., Seo, Y. H., Seo, P. J., Reyes, J. L., and Yun, J. (2007). The GIGANTEA-regulated microRNA172 mediates photoperiodic flowering independent of CONSTANS in Arabidopsis. *Plant Cell* 19, 2736–2748. doi: 10.1105/tpc.107.054528

Kang, J., and Dengler, N. (2002). Cell cycling frequency and expression of the homeobox gene ATHB-8 during leaf vein development in Arabidopsis. *Planta* 216, 212–219. doi: 10.1007/s00425-002-0847-9

Kasschau, K. D., Xie, Z., Allen, E., Llave, C., and Chapman, E. J. (2003). P1/HC-pro, a viral suppressor of RNA silencing, interferes with Arabidopsis development and miRNA unction. *Dev. Cell* 4, 205–217. doi: 10.1016/S1534-5807(03)00025-X

Kidner, C. A., and Martienssen, R. A. (2004). Spatially restricted microRNA directs leaf polarity through ARGONAUTE1. *Nature* 428, 81–84. doi: 10.1038/nature02366

Kim, V. N. (2005). Small RNAs: classification, biogenesis, and function. *Mol. Cells* 19, 1–15.

Kim, J. H., Choi, D., and Kende, H. (2003). The AtGRF family of putative transcription factors is involved in leaf and cotyledon growth in Arabidopsis. *Plant J.* 36, 94–104. doi: 10.1046/j.1365-313X.2003.01862.x

Kim, J., Jung, J. H., Reyes, J. L., Kim, Y. S., and Kim, S. Y. (2005). MicroRNA-directed cleavage of ATHB15 mRNA regulates vascular development in Arabidopsis inflorescence stems. *Plant J.* 42, 84–94. doi: 10.1111/j.1365-313X.2005.02354.x

Kim, J. J., Lee, J. H., Kim, W., Jung, H. S., and Huijser, P. (2012). The microRNA156-SQUAMOSA PROMOTER BINDING PROTEIN-LIKE3 module regulates ambient temperature-responsive flowering *via* FLOWERING LOCUS T in Arabidopsis. *Plant Physiol.* 159, 461–478. doi: 10.1104/pp.111.192369

Kim, S., Yang, J. Y., Xu, J., Jang, I. C., and Prigge, M. J. (2008). Two cap-binding proteins CBP20 and CBP80 are involved in processing primary MicroRNAs. *Plant Cell Physiol.* 49, 1634–1644. doi: 10.1093/pcp/pcn146

Knauer, S., Holt, A. L., Rubio-Somoza, I., Tucker, E. J., and Hinze, A. (2013). A protodermal miR394 signal defines a region of stem cell competence in the Arabidopsis shoot meristem. *Dev. Cell* 24, 125–132. doi: 10.1016/j.devcel.2012.12.009

Koyama, T., Mitsuda, N., Seki, M., Shinozaki, K., and Ohme-Takagi, M. (2010). TCP transcription factors regulate the activities of ASYMMETRIC LEAVES1 and miR164, as well as the auxin response, during differentiation of LEAVES in Arabidopsis. *Plant Cell* 22, 3574–3588. doi: 10.1105/tpc.110.075598

Koyama, T., Sato, F., and Ohme-Takagi, M. (2017). Roles of miR319 and TCP transcription factors in leaf development. *Plant Physiol.* 175, 874–885. doi: 10.1104/pp.17.00732

Kumar, A., Gautam, V., Kumar, P., Mukherjee, S., and Verma, S. (2019). Identification and co-evolution pattern of stem cell regulator miR394s and their targets among diverse plant species. *BMC Evol. Biol.* 19:55. doi: 10.1186/s12862-019-1382-7

Kurihara, Y., and Watanabe, Y. (2004). Arabidopsis micro-RNA biogenesis through Dicer-like 1 protein functions. *Proc. Natl. Acad. Sci. U. S. A.* 101, 12753–12758. doi: 10.1073/pnas.0403115101

Kutter, C., Schob, H., Stadler, M., Meins, F. J., and Si-Ammour, A. (2007). MicroRNA-mediated regulation of stomatal development in Arabidopsis. *Plant Cell* 19, 2417–2429. doi: 10.1105/tpc.107.050377

Laufs, P., Peaucelle, A., Morin, H., and Traas, J. (2004). MicroRNA regulation of the CUC genes is required for boundary size control in Arabidopsis meristems. *Development* 131, 4311–4322. doi: 10.1242/dev.01320

Lauter, N., Kampani, A., Carlson, S., Goebel, M., and Moose, S. P. (2005). MicroRNA172 down-regulates glossy15 to promote vegetative phase change in maize. *Proc. Natl. Acad. Sci. U. S. A.* 102, 9412–9417. doi: 10.1073/pnas.0503927102

Lee, R. C., Feinbaum, R. L., and Ambros, V. (1993). The C. Elegans heterochronic gene lin-4 encodes small RNAs with antisense complementarity to lin-14. *Cell* 75, 843–854. doi: 10.1016/0092-8674(93)90529-Y

Lee, Y., Kim, M., Han, J., Yeom, K. H., and Lee, S. (2004). MicroRNA genes are transcribed by RNA polymerase II. *EMBO J.* 23, 4051–4060. doi: 10.1038/sj.emboj.7600385

Leng, X., Wang, P., Zhu, X., Li, X., and Zheng, T. (2017). Ectopic expression of CSD1 and CSD2 targeting genes of miR398 in grapevine is associated with oxidative stress tolerance. *Funct. Integr. Genomics* 17, 697–710. doi: 10.1007/s10142-017-0565-9

Li, W., Cui, X., Meng, Z., Huang, X., and Xie, Q. (2012). Transcriptional regulation of Arabidopsis MIR168a and argonaute1 homeostasis in abscisic acid and abiotic stress responses. *Plant Physiol.* 158, 1279–1292. doi: 10.1104/pp.111.188789

Li, T., Gonzalez, N., Inze, D., and Dubois, M. (2020). Emerging connections between small RNAs and Phytohormones. *Trends Plant Sci.* 25, 912–929. doi: 10.1016/j.tplants.2020.04.004

Li, W. X., Oono, Y., Zhu, J., He, X. J., and Wu, J. M. (2008). The Arabidopsis NFYA5 transcription factor is regulated transcriptionally and posttranscriptionally to promote drought resistance. *Plant Cell* 20, 2238–2251. doi: 10.1105/tpc.108.059444

Li, Z., Peng, J., Wen, X., and Guo, H. (2013). Ethylene-insensitive3 is a senescence-associated gene that accelerates age-dependent leaf senescence by directly repressing miR164 transcription in Arabidopsis. *Plant Cell* 25, 3311–3328. doi: 10.1105/tpc.113.113340

Li, X., Qian, Q., Fu, Z., Wang, Y., and Xiong, G. (2003). Control of tillering in rice. *Nature* 422, 618–621. doi: 10.1038/nature01518

Li, Y., Tong, Y., He, X., Zhu, Y., and Wang, W. (2021). The rice miR171b–SCL6-IIs module controls blast resistance, grain yield, and flowering. *Crop J.* doi: 10.1016/j.cj.2021.05.004, Epub ahead of print

Li, J., Yang, Z., Yu, B., Liu, J., and Chen, X. (2005). Methylation protects miRNAs and siRNAs from a 3′-end uridylation activity in Arabidopsis. *Curr. Biol.* 15, 1501–1507. doi: 10.1016/j.cub.2005.07.029

Lian, H., Wang, L., Ma, N., Zhou, C. M., and Han, L. (2021). Redundant and specific roles of individual MIR172 genes in plant development. *PLoS Biol.* 19:e3001044. doi: 10.1371/journal.pbio.3001044

Liebsch, D., and Palatnik, J. F. (2020). MicroRNA miR396, GRF transcription factors and GIF co-regulators: A conserved plant growth regulatory module with potential for breeding and biotechnology. *Curr. Opin. Plant Biol.* 53, 31–42. doi: 10.1016/j.pbi.2019.09.008

Lin, S. I., Chiang, S. F., Lin, W. Y., Chen, J. W., Tseng, C. Y., Wu, P. C., et al. (2008). Regulatory network of microRNA399 and PHO2 by systemic signaling. *Plant Physiol.* 147, 732–746. doi: 10.1104/pp.108.116269

Liu, H., Guo, S., Xu, Y., Li, C., and Zhang, Z. (2014a). OsmiR396d-regulated OsGRFs function in floral organogenesis in rice through binding to their targets OsJMJ706 and OsCR4. *Plant Physiol.* 165, 160–174. doi: 10.1104/pp.114.235564

Liu, H., Jia, S., Shen, D., Liu, J., and Li, J. (2012). Four AUXIN RESPONSE FACTOR genes downregulated by microRNA167 are associated with growth and development in Oryza sativa. *Funct. Plant Biol.* 39, 736–744. doi: 10.1071/FP12106

Liu, B., Li, J., Tsykin, A., Liu, L., and Gaur, A. B. (2009a). Exploring complex miRNA-mRNA interactions with Bayesian networks by splitting-averaging strategy. *BMC Bioinformatics* 10:408. doi: 10.1186/1471-2105-10-408

Liu, Z., Li, J., Wang, L., Li, Q., and Lu, Q. (2016). Repression of callus initiation by the miRNA-directed interaction of auxin-cytokinin in *Arabidopsis thaliana*. *Plant J.* 87, 391–402. doi: 10.1111/tpj.13211

Liu, P. P., Montgomery, T. A., Fahlgren, N., Kasschau, K. D., and Nonogaki, H. (2007). Repression of AUXIN RESPONSE FACTOR10 by microRNA160 is critical for seed germination and post-germination stages. *Plant J.* 52, 133–146. doi: 10.1111/j.1365-313X.2007.03218.x

Liu, D., Song, Y., Chen, Z., and Yu, D. (2009b). Ectopic expression of miR396 suppresses GRF target gene expression and alters leaf growth in Arabidopsis. *Physiol. Plant.* 136, 223–236. doi: 10.1111/j.1399-3054.2009.01229.x

Liu, N., Wu, S., Van Houten, J., Wang, Y., and Ding, B. (2014b). Down-regulation of AUXIN RESPONSE FACTORS 6 and 8 by microRNA 167 leads to floral development defects and female sterility in tomato. *J. Exp. Bot.* 65, 2507–2520. doi: 10.1093/jxb/eru141

Liu, Q., Yao, X., Pi, L., Wang, H., and Cui, X. (2009c). The ARGONAUTE10 gene modulates shoot apical meristem maintenance and establishment of leaf polarity by repressing miR165/166 in Arabidopsis. *Plant J.* 58, 27–40. doi: 10.1111/j.1365-313X.2008.03757.x

Llave, C., Xie, Z., Kasschau, K. D., and Carrington, J. C. (2002). Cleavage of scarecrow-like mRNA targets directed by a class of Arabidopsis miRNA. *Science* 297, 2053–2056. doi: 10.1126/science.1076311

Lopez-Ruiz, B. A., Juarez-Gonzalez, V. T., Sandoval-Zapotitla, E., and Dinkova, T. D. (2019). Development-related miRNA expression and target regulation during staggered *in vitro* plant regeneration of tuxpeno VS-535 maize cultivar. *Int. J. Mol. Sci.* 20:2079. doi: 10.3390/ijms20092079

Lu, Y., Feng, Z., Liu, X., Bian, L., and Xie, H. (2018). MiR393 and miR390 synergistically regulate lateral root growth in rice under different conditions. *BMC Plant Biol.* 18:261. doi: 10.1186/s12870-018-1488-x

Ma, Z., Hu, X., Cai, W., Huang, W., and Zhou, X. (2014). Arabidopsis miR171-targeted scarecrow-like proteins bind to GT cis-elements and mediate gibberellin-regulated chlorophyll biosynthesis under light conditions. *PLoS Genet.* 10:e1004519. doi: 10.1371/journal.pgen.1004519

Ma, J., Zhao, P., Liu, S., Yang, Q., and Guo, H. (2020). The control of developmental phase transitions by microRNAs and their targets in seed plants. *Int. J. Mol. Sci.* 21:1917. doi: 10.3390/ijms21061971

Mallory, A. C., Bartel, D. P., and Bartel, B. (2005). MicroRNA-directed regulation of Arabidopsis AUXIN RESPONSE FACTOR17 is essential for proper development and modulates expression of early auxin response genes. *Plant Cell* 17, 1360–1375. doi: 10.1105/tpc.105.031716

Manuela, D., and Xu, M. (2020). Patterning a leaf by establishing polarities. *Front. Plant Sci.* 11:568730. doi: 10.3389/fpls.2020.568730

Marin, E., Jouannet, V., Herz, A., Lokerse, A. S., and Weijers, D. (2010). MiR390, Arabidopsis TAS3 tasiRNAs, and their AUXIN RESPONSE FACTOR targets define an autoregulatory network quantitatively regulating lateral root growth. *Plant Cell* 22, 1104–1117. doi: 10.1105/tpc.109.072553

Martin, A., Adam, H., Diaz-Mendoza, M., Zurczak, M., and Gonzalez-Schain, N. D. (2009). Graft-transmissible induction of potato tuberization by the microRNA miR172. *Development* 136, 2873–2881. doi: 10.1242/dev.031658

Melnyk, C. W., Molnar, A., and Baulcombe, D. C. (2011). Intercellular and systemic movement of RNA silencing signals. *EMBO J.* 30, 3553–3563. doi: 10.1038/emboj.2011.274

Merelo, P., Ram, H., Pia, C. M., Ohno, C., and Ott, F. (2016). Regulation of MIR165/166 by class II and class III homeodomain leucine zipper proteins establishes leaf polarity. *Proc. Natl. Acad. Sci. U. S. A.* 113, 11973–11978. doi: 10.1073/pnas.1516110113

Millar, A. A., and Gubler, F. (2005). The Arabidopsis GAMYB-like genes, MYB33 and MYB65, are microRNA-regulated genes that redundantly facilitate anther development. *Plant Cell* 17, 705–721. doi: 10.1105/tpc.104.027920

Millar, A. A., Lohe, A., and Wong, G. (2019). Biology and function of miR159 in plants. *Plan. Theory* 8:255. doi: 10.3390/plants8080255

Montgomery, T. A., Howell, M. D., Cuperus, J. T., Li, D., and Hansen, J. E. (2008). Specificity of ARGONAUTE7-miR390 interaction and dual functionality in TAS3 trans-acting siRNA formation. *Cell* 133, 128–141. doi: 10.1016/j.cell.2008.02.033

Muller, C. J., Valdes, A. E., Wang, G., Ramachandran, P., and Beste, L. (2016). PHABULOSA mediates an auxin signaling loop to regulate vascular patterning in arabidopsis. *Plant Physiol.* 170, 956–970. doi: 10.1104/pp.15.01204

Muraro, D., Mellor, N., Pound, M. P., Help, H., and Lucas, M. (2014). Integration of hormonal signaling networks and mobile microRNAs is required for vascular patterning in Arabidopsis roots. *Proc. Natl. Acad. Sci. U. S. A.* 111, 857–862. doi: 10.1073/pnas.1221766111

Nair, S. K., Wang, N., Turuspekov, Y., Pourkheirandish, M., and Sinsuwongwat, S. (2010). Cleistogamous flowering in barley arises from the suppression of microRNA-guided HvAP2 mRNA cleavage. *Proc. Natl. Acad. Sci. U. S. A.* 107, 490–495. doi: 10.1073/pnas.0909097107

Naqvi, A. R., Sarwat, M., Hasan, S., and Roychodhury, N. (2012). Biogenesis, functions and fate of plant microRNAs. *J. Cell. Physiol.* 227, 3163–3168. doi: 10.1002/jcp.24052

O'Brien, J., Hayder, H., Zayed, Y., and Peng, C. (2018). Overview of MicroRNA biogenesis, mechanisms of actions, and circulation. *Front. Endocrinol.* 9:402. doi: 10.3389/fendo.2018.00402

Ori, N., Cohen, A. R., Etzioni, A., Brand, A., and Yanai, O. (2007). Regulation of LANCEOLATE by miR319 is required for compound-leaf development in tomato. *Nat. Genet.* 39, 787–791. doi: 10.1038/ng2036

Palatnik, J. F., Wollmann, H., Schommer, C., Schwab, R., and Boisbouvier, J. (2007). Sequence and expression differences underlie functional specialization of Arabidopsis microRNAs miR159 and miR319. *Dev. Cell* 13, 115–125. doi: 10.1016/j.devcel.2007.04.012

Pal-Bhadra, M., Bhadra, U., and Birchler, J. A. (2002). RNAi related mechanisms affect both transcriptional and posttranscriptional transgene silencing in drosophila. *Mol. Cell* 9, 315–327. doi: 10.1016/S1097-2765(02)00440-9

Pant, B. D, Buhtz, A., Kehr, J., and Scheible, W. R. (2008). MicroRNA399 is a long-distance signal for the regulation of plant phosphate homeostasis. *Plant J.* 53, 731–738. doi: 10.1111/j.1365-313X.2007.03363.x

Park, M. Y., Wu, G., Gonzalez-Sulser, A., Vaucheret, H., and Poethig, R. S. (2005). Nuclear processing and export of microRNAs in Arabidopsis. *Proc. Natl. Acad. Sci. U. S. A.* 102, 3691–3696. doi: 10.1073/pnas.0405570102

Parry, G., Calderon-Villalobos, L. I., Prigge, M., Peret, B., and Dharmasiri, S. (2009). Complex regulation of the TIR1/AFB family of auxin receptors. *Proc. Natl. Acad. Sci. U. S. A.* 106, 22540–22545. doi: 10.1073/pnas.0911967106

Piazza, P., Jasinski, S., and Tsiantis, M. (2005). Evolution of leaf developmental mechanisms. *New Phytol.* 167, 693–710. doi: 10.1111/j.1469-8137.2005.01466.x

Qi, Y., Denli, A. M., and Hannon, G. J. (2005). Biochemical specialization within Arabidopsis RNA silencing pathways. *Mol. Cell* 19, 421–428. doi: 10.1016/j.molcel.2005.06.014

Qi, Y., He, X., Wang, X. J., Kohany, O., and Jurka, J. (2006). Distinct catalytic and non-catalytic roles of ARGONAUTE4 in RNA-directed DNA methylation. *Nature* 443, 1008–1012. doi: 10.1038/nature05198

Qu, L., Lin, L. B., and Xue, H. W. (2019). Rice miR394 suppresses LEAF inclination through targeting an F-box gene, LEAF INCLINATION 4. *J. Integr. Plant Biol.* 61, 406–416. doi: 10.1111/jipb.12713

Ramachandran, P., Carlsbecker, A., and Etchells, J. P. (2017). Class III HD-ZIPs govern vascular cell fate: An HD view on patterning and differentiation. *J. Exp. Bot.* 68, 55–69. doi: 10.1093/jxb/erw370

Raman, S., Greb, T., Peaucelle, A., Blein, T., and Laufs, P. (2008). Interplay of miR164, CUP-SHAPED COTYLEDON genes and LATERAL SUPPRESSOR controls axillary meristem formation in *Arabidopsis thaliana*. *Plant J.* 55, 65–76. doi: 10.1111/j.1365-313X.2008.03483.x

Rodriguez, R. E., Mecchia, M. A., Debernardi, J. M., Schommer, C., and Weigel, D. (2010). Control of cell proliferation in *Arabidopsis thaliana* by microRNA miR396. *Development* 137, 103–112. doi: 10.1242/dev.043067

Ru, P., Xu, L., Ma, H., and Huang, H. (2006). Plant fertility defects induced by the enhanced expression of microRNA167. *Cell Res.* 16, 457–465. doi: 10.1038/sj.cr.7310057

Rubio-Somoza, I., and Weigel, D. (2013). Coordination of flower maturation by a regulatory circuit of three microRNAs. *PLoS Genet.* 9:e1003374. doi: 10.1371/journal.pgen.1003374

Salvi, S., Sponza, G., Morgante, M., Tomes, D., and Niu, X. (2007). Conserved noncoding genomic sequences associated with a flowering-time quantitative trait locus in maize. *Proc. Natl. Acad. Sci. U. S. A.* 104, 11376–11381. doi: 10.1073/pnas.0704145104

Schommer, C., Debernardi, J. M., Bresso, E. G., Rodriguez, R. E., and Palatnik, J. F. (2014). Repression of cell proliferation by miR319-regulated TCP4. *Mol. Plant* 7, 1533–1544. doi: 10.1093/mp/ssu084

Schoof, H., Lenhard, M., Haecker, A., Mayer, K. F., and Jurgens, G. (2000). The stem cell population of Arabidopsis shoot meristems in maintained by a regulatory loop between the CLAVATA and WUSCHEL genes. *Cell* 100, 635–644. doi: 10.1016/S0092-8674(00)80700-X

Schwab, R., Palatnik, J. F., Riester, M., Schommer, C., and Schmid, M. (2005). Specific effects of microRNAs on the plant transcriptome. *Dev. Cell* 8, 517–527. doi: 10.1016/j.devcel.2005.01.018

Scofield, S., Dewitte, W., and Murray, J. A. (2014). STM sustains stem cell function in the Arabidopsis shoot apical meristem and controls KNOX gene expression independently of the transcriptional repressor AS1. *Plant Signal. Behav.* 9:e28934. doi: 10.4161/psb.28934

Sijen, T., Vijn, I., Rebocho, A., van Blokland, R., and Roelofs, D. (2001). Transcriptional and posttranscriptional gene silencing are mechanistically related. *Curr. Biol.* 11, 436–440. doi: 10.1016/S0960-9822(01)00116-6

Singh, R. K., Gase, K., Baldwin, I. T., and Pandey, S. P. (2015). Molecular evolution and diversification of the Argonaute family of proteins in plants. *BMC Plant Biol.* 15:23. doi: 10.1186/s12870-014-0364-6

Skopelitis, D. S., Benkovics, A. H., Husbands, A. Y., and Timmermans, M. (2017). Boundary formation through a direct threshold-based readout of mobile small RNA gradients. *Dev. Cell* 43, 265–273. doi: 10.1016/j.devcel.2017.10.003

Skopelitis, D. S., Hill, K., Klesen, S., Marco, C. F., and von Born, P. (2018). Gating of miRNA movement at defined cell-cell interfaces governs their impact as positional signals. *Nat. Commun.* 9:3107. doi: 10.1038/s41467-018-05571-0

Somssich, M., Je, B. I., Simon, R., and Jackson, D. (2016). CLAVATA-WUSCHEL signaling in the shoot meristem. *Development* 143, 3238–3248. doi: 10.1242/dev.133645

Song, J. B., Huang, S. Q., Dalmay, T., and Yang, Z. M. (2012). Regulation of LEAF morphology by microRNA394 and its target LEAF CURLING RESPONSIVENESS. *Plant Cell Physiol.* 53, 1283–1294. doi: 10.1093/pcp/pcs080

Song, X., Li, Y., Cao, X., and Qi, Y. (2019). MicroRNAs and their regulatory roles in plant-environment interactions. *Annu. Rev. Plant Biol.* 70, 489–525. doi: 10.1146/annurev-arplant-050718-100334

Sorin, C., Declerck, M., Christ, A., Blein, T., and Ma, L. (2014). A miR169 isoform regulates specific NF-YA targets and root architecture in Arabidopsis. *New Phytol.* 202, 1197–1211. doi: 10.1111/nph.12735

Stricklin, S. L., Griffiths-Jones, S., and Eddy, S. R. (2005). C. Elegans noncoding RNA genes. *WormBook* 25, 1–7. doi: 10.1895/wormbook.1.1.1

Su, Z., Wang, N., Hou, Z., Li, B., and Li, D. (2020). Regulation of female germline specification *via* small RNA mobility in arabidopsis. *Plant Cell* 32, 2842–2854. doi: 10.1105/tpc.20.00126

Sun, Z., Li, M., Zhou, Y., Guo, T., and Liu, Y. (2018). Coordinated regulation of Arabidopsis microRNA biogenesis and red light signaling through Dicer-like 1 and phytochrome-interacting factor 4. *PLoS Genet.* 14:e1007247. doi: 10.1371/journal.pgen.1007247

Sun, X., Wang, C., Xiang, N., Li, X., and Yang, S. (2017). Activation of secondary cell wall biosynthesis by miR319-targeted TCP4 transcription factor. *Plant Biotechnol. J.* 15, 1284–1294. doi: 10.1111/pbi.12715

Sunkar, R., and Zhu, J. K. (2004). Novel and stress-regulated microRNAs and other small RNAs from Arabidopsis. *Plant Cell* 16, 2001–2019. doi: 10.1105/tpc.104.022830

Szczygiel-Sommer, A., and Gaj, M. D. (2019). The miR396-GRF regulatory module controls the embryogenic response in arabidopsis *via* an auxin-related pathway. *Int. J. Mol. Sci.* 20:5221. doi: 10.3390/ijms20205221

Tamiru, M., Hardcastle, T. J., and Lewsey, M. G. (2018). Regulation of genome-wide DNA methylation by mobile small RNAs. *New Phytol.* 217, 540–546. doi: 10.1111/nph.14874

Tang, G., Yan, J., Gu, Y., Qiao, M., and Fan, R. (2012). Construction of short tandem target mimic (STTM) to block the functions of plant and animal microRNAs. *Methods* 58, 118–125. doi: 10.1016/j.ymeth.2012.10.006

Tatematsu, K., Toyokura, K., and Okada, K. (2015). Requirement of MIR165A primary transcript sequence for its activity pattern in Arabidopsis leaf primordia. *Plant Signal. Behav.* 10:e1055432. doi: 10.1080/15592324.2015.1055432

Tirumalai, V., Swetha, C., Nair, A., Pandit, A., and Shivaprasad, P. V. (2019). MiR828 and miR858 regulate VvMYB114 to promote anthocyanin and flavonol accumulation in grapes. *J. Exp. Bot.* 70, 4775–4792. doi: 10.1093/jxb/erz264

Tsikou, D., Yan, Z., Holt, D. B., Abel, N. B., and Reid, D. E. (2018). Systemic control of legume susceptibility to rhizobial infection by a mobile microRNA. *Science* 362, 233–236. doi: 10.1126/science.aat6907

Tsuji, H., Aya, K., Ueguchi-Tanaka, M., Shimada, Y., and Nakazono, M. (2006). GAMYB controls different sets of genes and is differentially regulated by microRNA in aleurone cells and anthers. *Plant J.* 47, 427–444. doi: 10.1111/j.1365-313X.2006.02795.x

Vaten, A., Dettmer, J., Wu, S., Stierhof, Y. D., and Miyashima, S. (2011). Callose biosynthesis regulates symplastic trafficking during root development. *Dev. Cell* 21, 1144–1155. doi: 10.1016/j.devcel.2011.10.006

Vaucheret, H. (2008). Plant ARGONAUTES. *Trends Plant Sci.* 13, 350–358. doi: 10.1016/j.tplants.2008.04.007

Veit, B. (2009). Hormone mediated regulation of the shoot apical meristem. *Plant Mol. Biol.* 69, 397–408. doi: 10.1007/s11103-008-9396-3

Voinnet, O. (2009). Origin, biogenesis, and activity of plant microRNAs. *Cell* 136, 669–687. doi: 10.1016/j.cell.2009.01.046

Waheed, S., and Zeng, L. (2020). The critical role of miRNAs in regulation of flowering time and flower development. *Genes* 11:319. doi: 10.3390/genes11030319

Wang, J., Bao, J., Zhou, B., Li, M., and Li, X. (2021b). The Osa-miR164 target OsCUC1 functions redundantly with OsCUC3 in controlling rice meristem/organ boundary specification. *New Phytol.* 229, 1566–1581. doi: 10.1111/nph.16939

Wang, L., Gu, X., Xu, D., Wang, W., and Wang, H. (2011). MiR396-targeted AtGRF transcription factors are required for coordination of cell division and differentiation during leaf development in Arabidopsis. *J. Exp. Bot.* 62, 761–773. doi: 10.1093/jxb/erq307

Wang, J. J., and Guo, H. S. (2015). Cleavage of INDOLE-3-ACETIC ACID INDUCIBLE28 mRNA by microRNA847 upregulates auxin signaling to modulate cell proliferation and lateral organ growth in Arabidopsis. *Plant Cell* 27, 574–590. doi: 10.1105/tpc.15.00101

Wang, H., Li, Y., Chern, M., Zhu, Y., and Zhang, L. L. (2021a). Suppression of rice miR168 improves yield, flowering time and immunity. *Nat. Plants* 7, 129–136. doi: 10.1038/s41477-021-00852-x

Wang, L., Liu, Z., Qiao, M., and Xiang, F. (2018). MiR393 inhibits *in vitro* shoot regeneration in *Arabidopsis thaliana via* repressing TIR1. *Plant Sci.* 266, 1–8. doi: 10.1016/j.plantsci.2017.10.009

Wang, J. W., Schwab, R., Czech, B., Mica, E., and Weigel, D. (2008). Dual effects of miR156-targeted SPL genes and CYP78A5/KLUH on plastochron length and organ size in *Arabidopsis thaliana*. *Plant Cell* 20, 1231–1243. doi: 10.1105/tpc.108.058180

Wang, H., and Wang, H. (2015). The miR156/SPL module, a regulatory hub and versatile toolbox, gears up crops for enhanced agronomic traits. *Mol. Plant* 8, 677–688. doi: 10.1016/j.molp.2015.01.008

Wang, J. W., Wang, L. J., Mao, Y. B., Cai, W. J., and Xue, H. W. (2005). Control of root cap formation by MicroRNA-targeted auxin response factors in Arabidopsis. *Plant Cell* 17, 2204–2216. doi: 10.1105/tpc.105.033076

Wang, R., Yang, X., Guo, S., Wang, Z., and Zhang, Z. (2021c). MiR319-targeted OsTCP21 and OsGAmyb regulate tillering and grain yield in rice. *J. Integr. Plant Biol.* 63, 1260–1272. doi: 10.1111/jipb.13097

Wang, T., Zheng, Y., Tang, Q., Zhong, S., and Su, W. (2021d). Brassinosteroids inhibit miRNA-mediated translational repression by decreasing AGO1 on the endoplasmic reticulum. *J. Integr. Plant Biol.* 63, 1475–1490. doi: 10.1111/jipb.13139

Werner, S., Bartrina, I., and Schmulling, T. (2021). Cytokinin regulates vegetative phase change in *Arabidopsis thaliana* through the miR172/TOE1-TOE2 module. *Nat. Commun.* 12:5816. doi: 10.1038/s41467-021-26088-z

Wightman, B., Ha, I., and Ruvkun, G. (1993). Posttranscriptional regulation of the heterochronic gene lin-14 by lin-4 mediates temporal pattern formation in C Elegans. *Cell* 75, 855–862. doi: 10.1016/0092-8674(93)90530-4

Williams, L., Grigg, S. P., Xie, M., Christensen, S., and Fletcher, J. C. (2005). Regulation of Arabidopsis shoot apical meristem and lateral organ formation by microRNA miR166g and its AtHD-ZIP target genes. *Development* 132, 3657–3668. doi: 10.1242/dev.01942

Windels, D., and Vazquez, F. (2011). MiR393: integrator of environmental cues in auxin signaling? *Plant Signal. Behav.* 6, 1672–1675. doi: 10.4161/psb.6.11.17900

Wollmann, H., Mica, E., Todesco, M., Long, J. A., and Weigel, D. (2010). On reconciling the interactions between APETALA2, miR172 and AGAMOUS with the ABC model of flower development. *Development* 137, 3633–3642. doi: 10.1242/dev.036673

Wu, G., Park, M. Y., Conway, S. R., Wang, J. W., and Weigel, D. (2009). The sequential action of miR156 and miR172 regulates developmental timing in Arabidopsis. *Cell* 138, 750–759. doi: 10.1016/j.cell.2009.06.031

Wu, G., and Poethig, R. S. (2006). Temporal regulation of shoot development in *Arabidopsis thaliana* by miR156 and its target SPL3. *Development* 133, 3539–3547. doi: 10.1242/dev.02521

Wu, M. F., Tian, Q., and Reed, J. W. (2006). Arabidopsis microRNA167 controls patterns of ARF6 and ARF8 expression, and regulates both female and male reproduction. *Development* 133, 4211–4218. doi: 10.1242/dev.02602

Xia, R., Xu, J., and Meyers, B. C. (2017). The emergence, evolution, and diversification of the miR390-TAS3-ARF pathway in land plants. *Plant Cell* 29, 1232–1247. doi: 10.1105/tpc.17.00185

Xie, K., Wu, C., and Xiong, L. (2006). Genomic organization, differential expression, and interaction of SQUAMOSA promoter-binding-like transcription factors and microRNA156 in rice. *Plant Physiol.* 142, 280–293. doi: 10.1104/pp.106.084475

Xing, L., Zhu, M., Luan, M., Zhang, M., and Jin, L. (2021). MiR169q and NUCLEAR FACTOR YA8 enhance salt tolerance by activating PEROXIDASE1 expression in response to ROS. *Plant Physiol.* 188, 608–623. doi: 10.1093/plphys/kiab498

Xu, M., Hu, T., Smith, M. R., and Poethig, R. S. (2016a). Epigenetic regulation of vegetative phase change in arabidopsis. *Plant Cell* 28, 28–41. doi: 10.1105/tpc.15.00854

Xu, M., Hu, T., Zhao, J., Park, M. Y., and Earley, K. W. (2016b). Developmental functions of miR156-regulated SQUAMOSA PROMOTER BINDING PROTEIN-LIKE (SPL) genes in *Arabidopsis thaliana*. *PLoS Genet.* 12:e1006263. doi: 10.1371/journal.pgen.1006263

Xu, M. Y., Zhang, L., Li, W. W., Hu, X. L., and Wang, M. B. (2014). Stress-induced early flowering is mediated by miR169 in *Arabidopsis thaliana*. *J. Exp. Bot.* 65, 89–101. doi: 10.1093/jxb/ert353

Yadav, A., Kumar, S., Verma, R., Lata, C., and Sanyal, I. (2021). MicroRNA 166: An evolutionarily conserved stress biomarker in land plants targeting HD-ZIP family. *Physiol. Mol. Biol. Plants* 27, 2471–2485. doi: 10.1007/s12298-021-01096-x

Yan, J., Wang, P., Wang, B., Hsu, C. C., and Tang, K. (2017). The SnRK2 kinases modulate miRNA accumulation in Arabidopsis. *PLoS Genet.* 13:e1006753. doi: 10.1371/journal.pgen.1006753

Yan, J., Zhao, C., Zhou, J., Yang, Y., and Wang, P. (2016). The miR165/166 mediated regulatory module plays critical roles in ABA homeostasis and response in *Arabidopsis thaliana*. *PLoS Genet.* 12:e1006416. doi: 10.1371/journal.pgen.1006416

Yanai, O., Shani, E., Russ, D., and Ori, N. (2011). Gibberellin partly mediates LANCEOLATE activity in tomato. *Plant J.* 68, 571–582. doi: 10.1111/j.1365-313X.2011.04716.x

Yang, T., Wang, Y., Teotia, S., Wang, Z., and Shi, C. (2019). The interaction between miR160 and miR165/166 in the control of leaf development and drought tolerance in Arabidopsis. *Sci. Rep.* 9:2832. doi: 10.1038/s41598-019-39397-7

Yao, X., Chen, J., Zhou, J., Yu, H., and Ge, C. (2019). An essential role for miRNA167 in maternal control of embryonic and seed development. *Plant Physiol.* 180, 453–464. doi: 10.1104/pp.19.00127

Yokotani, N., Nakano, R., Imanishi, S., Nagata, M., and Inaba, A. (2009). Ripening-associated ethylene biosynthesis in tomato fruit is autocatalytically and developmentally regulated. *J. Exp. Bot.* 60, 3433–3442. doi: 10.1093/jxb/erp185

Yoon, E. K., Yang, J. H., Lim, J., Kim, S. H., and Kim, S. K. (2010). Auxin regulation of the microRNA390-dependent transacting small interfering RNA pathway in Arabidopsis lateral root development. *Nucleic Acids Res.* 38, 1382–1391. doi: 10.1093/nar/gkp1128

Yu, S., Galvao, V. C., Zhang, Y. C., Horrer, D., and Zhang, T. Q. (2012). Gibberellin regulates the Arabidopsis floral transition through miR156-targeted SQUAMOSA promoter binding-like transcription factors. *Plant Cell* 24, 3320–3332. doi: 10.1105/tpc.112.101014

Yu, Y., Jia, T., and Chen, X. (2017). The 'how' and 'where' of plant microRNAs. *New Phytol.* 216, 1002–1017. doi: 10.1111/nph.14834

Yu, S., and Wang, J. W. (2020). The crosstalk between MicroRNAs and gibberellin Signaling in plants. *Plant Cell Physiol.* 61, 1880–1890. doi: 10.1093/pcp/pcaa079

Yu, L., Yu, X., Shen, R., and He, Y. (2005). HYL1 gene maintains venation and polarity of leaves. *Planta* 221, 231–242. doi: 10.1007/s00425-004-1439-7

Zhai, J., Jeong, D. H., De Paoli, E., Park, S., and Rosen, B. D. (2011). MicroRNAs as master regulators of the plant NB-LRR defense gene family *via* the production of phased, trans-acting siRNAs. *Genes Dev.* 25, 2540–2553. doi: 10.1101/gad.177527.111

Zhang, X., Henderson, I. R., Lu, C., Green, P. J., and Jacobsen, S. E. (2007). Role of RNA polymerase IV in plant small RNA metabolism. *Proc. Natl. Acad. Sci. U. S. A.* 104, 4536–4541. doi: 10.1073/pnas.0611456104

Zhang, T. Q., Lian, H., Tang, H., Dolezal, K., and Zhou, C. M. (2015). An intrinsic microRNA timer regulates progressive decline in shoot regenerative capacity in plants. *Plant Cell* 27, 349–360. doi: 10.1105/tpc.114.135186

Zhang, B., Pan, X., and Stellwag, E. J. (2008). Identification of soybean microRNAs and their targets. *Planta* 229, 161–182. doi: 10.1007/s00425-008-0818-x

Zhang, F., Wang, L., Lim, J. Y., Kim, T., and Pyo, Y. (2016). Phosphorylation of CBP20 links MicroRNA to root growth in the ethylene response. *PLoS Genet.* 12:e1006437. doi: 10.1371/journal.pgen.1006437

Zhang, Y. C., Yu, Y., Wang, C. Y., Li, Z. Y., and Liu, Q. (2013). Overexpression of microRNA OsmiR397 improves rice yield by increasing grain size and promoting panicle branching. *Nat. Biotechnol.* 31, 848–852. doi: 10.1038/nbt.2646

Zhang, H., Zhang, L., Han, J., Qian, Z., and Zhou, B. (2019). The nuclear localization signal is required for the function of squamosa promoter binding protein-like gene 9 to promote vegetative phase change in Arabidopsis. *Plant Mol. Biol.* 100, 571–578. doi: 10.1007/s11103-019-00863-5

Zhang, J., Zhou, Z., Bai, J., Tao, X., and Wang, L. (2020). Disruption of MIR396e and MIR396f improves rice yield under nitrogen-deficient conditions. *Natl. Sci. Rev.* 7, 102–112. doi: 10.1093/nsr/nwz142

Zhao, B., Ge, L., Liang, R., Li, W., and Ruan, K. (2009). Members of miR-169 family are induced by high salinity and transiently inhibit the NF-YA transcription factor. *BMC Mol. Biol.* 10:29. doi: 10.1186/1471-2199-10-29

Zhao, Y., Lin, S., Qiu, Z., Cao, D., and Wen, J. (2015). MicroRNA857 is involved in the regulation of secondary growth of vascular tissues in arabidopsis. *Plant Physiol.* 169, 2539–2552. doi: 10.1104/pp.15.01011

Zhao, Y. F., Peng, T., Sun, H. Z., Teotia, S., and Wen, H. L. (2019). MiR1432-OsACOT (acyl-CoA thioesterase) module determines grain yield *via* enhancing grain filling rate in rice. *Plant Biotechnol. J.* 17, 712–723. doi: 10.1111/pbi.13009

Zheng, L., Zhang, X., Zhang, H., Gu, Y., and Huang, X. (2019). The miR164-dependent regulatory pathway in developing maize seed. *Mol. Gen. Genomics.* 294, 501–517. doi: 10.1007/s00438-018-1524-4

Zhong, R., and Ye, Z. H. (1999). IFL1, a gene regulating interfascicular fiber differentiation in Arabidopsis, encodes a homeodomain-leucine zipper protein. *Plant Cell* 11, 2139–2152. doi: 10.1105/tpc.11.11.2139

Zhong, R., and Ye, Z. H. (2004). Amphivasal vascular bundle 1, a gain-of-function mutation of the IFL1/REV gene, is associated with alterations in the polarity of leaves, stems and carpels. *Plant Cell Physiol.* 45, 369–385. doi: 10.1093/pcp/pch051

Zhou, G. K., Kubo, M., Zhong, R., Demura, T., and Ye, Z. H. (2007). Overexpression of miR165 affects apical meristem formation, organ polarity establishment and vascular development in Arabidopsis. *Plant Cell Physiol.* 48, 391–404. doi: 10.1093/pcp/pcm008

Zhou, X., Wang, G., Sutoh, K., Zhu, J. K., and Zhang, W. (2008). Identification of cold-inducible microRNAs in plants by transcriptome analysis. *Biochim. Biophys. Acta* 1779, 780–788. doi: 10.1016/j.bbagrm.2008.04.005

Zhu, Q. H., and Helliwell, C. A. (2011). Regulation of flowering time and floral patterning by miR172. *J. Exp. Bot.* 62, 487–495. doi: 10.1093/jxb/erq295

Zhu, H., Hu, F., Wang, R., Zhou, X., and Sze, S. H. (2011). Arabidopsis Argonaute10 specifically sequesters miR166/165 to regulate shoot apical meristem development. *Cell* 145, 242–256. doi: 10.1016/j.cell.2011.03.024

Zhu, Q. H., Upadhyaya, N. M., Gubler, F., and Helliwell, C. A. (2009). Over-expression of miR172 causes loss of spikelet determinacy and floral organ abnormalities in rice (Oryza sativa). *BMC Plant Biol.* 9:149. doi: 10.1186/1471-2229-9-149

Conflict of Interest: The authors declare that the research was conducted in the absence of any commercial or financial relationships that could be construed as a potential conflict of interest.

Publisher's Note: All claims expressed in this article are solely those of the authors and do not necessarily represent those of their affiliated organizations, or those of the publisher, the editors and the reviewers. Any product that may be evaluated in this article, or claim that may be made by its manufacturer, is not guaranteed or endorsed by the publisher.

frontiers in Plant Science

ORIGINAL RESEARCH
published: 24 February 2022
doi: 10.3389/fpls.2022.835437

Four-Year and Five-Developing-Stage Dynamic QTL Mapping for Tiller Number in the Hybrid Population of *Agropyron* Gaertn.

Yonghe Che[1,2], Yutong He[1,2], Nan Song[1,2], Yanping Yang[1,2], Lai Wei[1,2], Xinming Yang[3], Yan Zhang[3], Jinpeng Zhang[3], Haiming Han[3], Xiuquan Li[3], Shenghui Zhou[3], Weihua Liu[3] and Lihui Li[3]**

[1] Hebei Key Laboratory of Crop Stress Biology, Qinhuangdao, China, [2] College of Agronomy and Biotechnology, Hebei Normal University of Science and Technology, Qinhuangdao, China, [3] Institute of Crop Sciences, Chinese Academy of Agricultural Sciences, Beijing, China

OPEN ACCESS

Edited by:
Xigang Liu,
Hebei Normal University, China

Reviewed by:
Yonghong Wang,
Institute of Genetics and Developmental Biology (CAS), China
Longbiao Guo,
China National Rice Research Institute (CAAS), China

***Correspondence:**
Yonghe Che
13933502823@163.com
Lihui Li
lilihui@caas.cn

Specialty section:
This article was submitted to Crop and Product Physiology, a section of the journal Frontiers in Plant Science

Received: 14 December 2021
Accepted: 24 January 2022
Published: 24 February 2022

Citation:
Che Y, He Y, Song N, Yang Y, Wei L, Yang X, Zhang Y, Zhang J, Han H, Li X, Zhou S, Liu W and Li L (2022) Four-Year and Five-Developing-Stage Dynamic QTL Mapping for Tiller Number in the Hybrid Population of Agropyron Gaertn. Front. Plant Sci. 13:835437. doi: 10.3389/fpls.2022.835437

Tiller number (TN) is an important agronomic trait affecting gramineous crop yield. To understand the static and dynamic information of quantitative trait locus (QTLs) controlling TN of *Agropyron* Gaertn., both the unconditional and conditional quantitative trait loci (QTL) mapping of TN were conducted using a cross-pollinated (CP) hybrid population with a total of 113 plant lines from the cross between *Agropyron cristatum* (L.) Gaertn. Z1842 and *Allium mongolicum* Keng Z2098, based on the phenotypic data of TN at five developmental stages [i.e., recovering stage (RS), jointing stage (JS), heading stage (HS), flowering stage (FS), and maturity stage (MS)] in 4 years (i.e., 2017, 2018, 2020, and 2021) and the genetic map constructed of 1,023 single-nucleotide polymorphism (SNP) markers. Thirty-seven QTLs controlling TN were detected using two analysis methods in 4 years, which were distributed in six linkage groups. Each QTL explained 2.96–31.11% of the phenotypic variation, with a logarithum of odds (LOD) value of 2.51–13.95. Nine of these loci detected both unconditional and conditional QTLs. Twelve unconditional major QTLs and sixteen conditional major QTLs were detected. Three relatively major stable conditional QTLs, namely, *cQTN1-3*, *cQTN1-5*, and *cQTN4-1*, were expressed in 2020 and 2021. Meantime, two pairs of major QTLs *cQTN1-5* and *qTN1-4* and also *cQTN2-4* and *qTN2-3* were located at the same interval but in different years. Except for *qTN2-2* and *qTN3-5*/*cQTN3-5*, other thirty-four QTLs were first detected in this study. This study provides a better interpretation of genetic factors that selectively control tiller at different developmental stages and a reference for molecular marker-assisted selection in the related plant improvement.

Keywords: ***Agropyron*** **Gaertn., tiller number, unconditional QTL, conditional QTL, CP hybrid population**

INTRODUCTION

Agropyron Gaertn. is a perennial forage grass, which is a wild relative of wheat with a P genome, and has the characteristics of high yield, good quality, strong stress resistance, and wide adaptability (Dewey, 1984; Asay and Johnson, 1990; Li and Dong, 1991). They are mainly distributed in arid and semiarid areas, such as Eurasia sandy temperate grassland, and in the northeast, northwest, Inner Mongolia, and other arid regions of China (Dewey and Asay, 1982; Che et al., 2014). Due to the advantages of withering late and returning early of *A*. Gaertn., and the withered grass that can also be eaten by animals, it has high feeding value and economic value, and it has been valued by the United States, Canada, and other animal husbandry developed countries. The root system of *A*. Gaertn. is well developed, so it shows strong drought tolerance. At the same time, *A*. Gaertn. also has a certain resistance to wheat susceptible diseases, such as stripe rust and powdery mildew, which is a high-quality genetic resource of wheat. Over the years, people have been committed to wide hybridization between perennial grasses and wheat, introducing excellent genes of wheat perennial grasses into wheat crops, and have made some progress (Liu et al., 2010). The hybridization between *A*. Gaertn. and wheat has been successfully achieved (Li and Dong, 1991), and several wheat cultivars having elite genes of P genome have been released in northern China. To sum up, *A*. Gaertn. is not only an excellent forage variety but also an important valuable donor of stress resistance and agronomic traits for wheat improvement (Alejandro et al., 2021).

The construction of a genetic linkage map is the basis of quantitative trait loci (QTL) mapping and molecular marker-assisted breeding for important traits of crops. The first genetic linkage map of tetraploid hybrid crested wheatgrass was constructed by a chromosome-doubling population, which used colchicine to introduce hybrid F_1 seed (Jiang et al., 2015; Yu et al., 2015). Based on the map of tetraploid material, a total of 136 quantitative trait locus (QTLs) for 11 agronomy traits were detected (Yu et al., 2020). However, cross-pollinated (CP) plants, such as *A*. Gaertn., can only obtain heterozygous individuals caused by self-incompatible, and it is impossible to construct a population that can be inherited stably similar to the recombinant inbred line (RIL) or double haploid (DH) population of wheat (Ma et al., 2020; Jonathan et al., 2021). Thus, an alternative way was mentioned. Through the mapping method of "double pseudo-crossing," some effective QTLs have been found in lots of forages (Jensen et al., 2005; Herrmann et al., 2006; Hirata et al., 2006). A genetic map of *Lolium perenne* was constructed, and QTL for resistance to stem rust was also detected using the "pseudo-crossing" F_1 population (Pfender et al., 2011). Thus, we obtained the first high-density genetic linkage map of *A*. Gaertn. constructed using a CP population that contains 1,023 markers on seven linkage groups, with a total of 907.8 cm and an average distance of 1.5 cm between adjacent loci (Zhang et al., 2015). Based on this map, the major and stable QTL for plant height (PH; Che et al., 2020) and QTL for other characteristics of the spike (Che et al., 2018) in *A*. Gaertn. have been detected.

Tiller is the special branching method of gramineous plants and is closely related to yield. For example, the reduced-tillering wheat has yielded advantages when the water supply is less than 200 mm (Houshmandfar et al., 2019). The low expression of *TaPIN1* genes increases the tiller number (TN) as well as grain yield per plant of wheat (Yao et al., 2021). Thus, locating the gene that controlled TN will help improve the grain yield.

The TN is controlled by multiple genes (Haaning et al., 2020). At present, several candidate genes associated with TN have been reported in barley (Bai et al., 2021), and several single genes that control TN have been identified in wheat (Peng et al., 1998; Spielmeyer and Richards, 2004; Kuraparthy et al., 2007; Zhang et al., 2013; Wang et al., 2021). A validated, major QTL for effective tiller number (ETN) *Qetn-sau-1B.1* was located on chromosome 1BL of wheat, which could improve the ETN significantly, with the genetic map constructed of 55K array, simple sequence repeat (SSR), and kompetitive allele-specific PCR (KASP) markers (Liu et al., 2020). Another new, major, stably expressed QTL *Qetn-DW-4B.1* for ETN was identified on chromosome 4BL of tetraploid wheat (Chen et al., 2021). Moreover, the studies on TN were not only limited to the maturity stage, but also observed the growth stages of tillering dynamics that were dissected to find out the genetic information of dynamic expression of TN (Li et al., 2010). The dynamic QTL analysis of TN at four growth stages was conducted in wheat and predicted the candidate genes for TN (Ren et al., 2018). Although TN is important for yield and there are more studies on tillering dynamics, the understanding and investigation of the genetic basis of TN in *A*. Gaertn. are limited. Thus, the expression of QTL for TN at different developmental stages was investigated in this study combined with relevant phenotypic data and a genetic map. It could provide a foundation for TN genetic research of *A*. Gaertn. and related plant study.

MATERIALS AND METHODS

Plant Material

A total of 113 individuals of the CP hybrid population, obtained by crossing between *Allium mongolicum* Z2098 (female, $2n = 14$, PP) and *Agropyron cristatum* Z1842 (male, $2n = 14$, PP), and two parents were transplanted to the farm of Hebei Normal University of Science and Technology in April 2014 (Che et al., 2018), and then clonal propagated from tillers and transplanted 115 ideal seedlings (including two parents) in April 2017. For controlling the planting density, the materials were transplanted in March 2020 again. The geographic location of the test site is 119°15′ E, 39°72′ N, with an average annual precipitation of 638.33 mm; frost-free period lasts up to 186 days; the soil is cinnamon soil, light loam, deep soil layer, and good permeability; it belongs to warm temperate, semi-humid continental climate. The designed planting row spacing in the experimental plot was 0.6 m, and the planting spacing was 0.4 m. Each material was designed with three replications and managed conventionally. The experiment was conducted in 2017, 2018, 2020, and 2021.

Trait Phenotype and Data Analysis

The TN of the CP hybrid population and parents was investigated at each developmental stage in 2017, 2018, 2020, and 2021.

The developmental stages were investigated every 2 days from the date of transplantation, and TN was investigated at each developmental stage in 2017; the survey was conducted from RS, JS, HS, and FS to MS including five developmental stages in 2018, 2020, and 2021 according to the standard ways (Li and Li, 2006). The SPSS 20.0 (SPSS, Chicago, IL, United States) was used for data statistics and analyzing genetic variation.

Quantitative Trait Loci Mapping

Based on the CP hybrid population, the genetic map of the *Agropyron* whole genome was constructed using the specific-locus amplified fragment sequencing (SLAF-seq) to genotype single-nucleotide polymorphism (SNP) markers. The total length of the genetic map is 907.8 cm, including 1,023 SNP markers on seven linkage groups. JoinMap 4.0 (Stam, 1993) was used to construct the genetic linkage map (Zhang et al., 2015).

The QTL mapping was performed by GACD software (Li et al., 2008; Wang, 2009) with inclusive composite interval mapping. The walking speed for all QTL was set at 1.0 cM, $P < 0.001$, and logarithm of odds (LOD) > 2.5. When a chromosome interval met the above conditions, it was considered that there was a QTL affecting TN. When a QTL was detected with a contribution rate >10% in different environments, it was regarded as a major QTL, and the QTL that was detected in at least three different environments was defined as a stable QTL (Fan et al., 2015; Che et al., 2020). The name of the unconditional QTL is "q + TN + chromosome number + serial number" (Mccouch et al., 1997). The conditional QTL was named with "cQ + TN + chromosome number + serial number" to distinguish and describe. The QTL found in the same site in the chromosome was regarded as the same QTL in this study.

The conditional QTL analysis was according to the method described by Zhu (1995). The genetic effect of conditional QTL refers to the net genetic effect from one time to the other. For example, JS-RS was the net growth of TN phenotype value at RS-JS, and HS-JS was the net growth value at JS-HS. The genetic effect of unconditional QTL represents the total amount of genetic effect from sowing to the specified time.

RESULTS

Phenotype Analysis in *Agropyron* Gaertn.

The TN of the *Agropyron* CP hybrid population had been surveyed at RS-MS in 4 years. There were some differences in TN growth trends in 4 years, and TN also showed significant differences at each developmental stage of the year. TN increased slowly at the early growth stages and faster at the later growth stages in 2017 and 2018. TN experienced a gradual decrease and then a slow increase in 2020. Then, in 2021, TN increased at RS-JS started decreasing at JS-FS, and increased again at FS-MS. The stage of the most TN was MS in 2017, 2018, and 2020 but, in 2021, was JS due to special climate situations (warm winter in 2020 and summer waterlogging in 2021). In addition, there were great differences in TN among different individuals. The male parent had more TN than the female parent at the initial stage (JS), but the TN of the female parent was higher than that of the male parent at the later stage (FS and MS). The variation coefficient of TN in the CP hybrid population was 53.52–78.48, 77.48–98.42, 45.00–97.23, and 31.28–46.12% in 2017, 2018, 2020, and 2021, respectively (**Table 1**). TN in all 4 years showed a normal distribution, which was suitable for the QTL analysis (**Figure 1**).

Unconditional Dynamic Quantitative Trait Loci Analysis of Tiller Number

A total of seventeen QTLs controlling TN were discovered using unconditional QTL analysis in 4 years, which were located on six linkage groups except chromosome 7. There were four, four, five, one, one, and two QTLs from chromosome 1 to chromosome 6, respectively. The phenotypic variation explained (PVE) of a single QTL ranged from 2.96 to 31.11%, and the LOD value ranged from 2.51 to 13.95 (**Table 2** and **Figures 2**, **3**). Four, four, two, and seven QTLs were detected in 2017, 2018, 2020, and 2021, respectively. There were 70.59% (12/17) of the unconditional QTLs that were detected as major QTL (with PVE more than 10%).

Four TN QTLs (*qTN1-4, qTN2-2, qTN2-3,* and *qTN5-1*) expressed at RS with the LOD value of 2.51–2.85, of which *qTN1-4* and *qTN2-3* were the major QTLs with 29.76 and 22.53% PVE, respectively. Five QTLs (*qTN1-1, qTN1-4, qTN3-2, qTN5-1,* and *qTN6-2*) expressed at JS were mapped, of which *qTN1-4* and *qTN5-1* were detected for the second time with the LOD values of 13.93 and 2.92 and the PVE of 31.11 and 12.31%, respectively. Also, *qTN1-1* and *qTN3-2* explained 12.57 and 10.58% phenotypic variation. Three major QTLs (*qTN1-2, qTN1-3,* and *qTN5-1*) at HS were located with the LOD value from 2.78 to 8.88, of which the *qTN5-1* was detected for the third time with 11.79% PVE. Four QTLs (*qTN2-1, qTN3-4, qTN4-1,* and *qTN5-1*) at FS were detected with the LOD value of 3.23–4.05. All of them were the major QTLs with 12.68–23.14% PVE, of which *qTN5-1* was detected for the fourth time at this stage. Five QTLs (*qTN2-4, qTN3-1, qTN3-3, qTN3-5,* and *qTN6-1*) at MS were detected with the LOD value of 2.52–3.07, of which *qTN2-4* and *qTN3-3* were the major QTLs with 11.40 and 21.77% PVE, respectively. Among the seventeen QTLs, *qTN5-1* was detected at four developmental stages (and as a major QTL at JS-FS), major QTL *qTN1-4* at two stages (RS-JS), and others once.

Conditional Dynamic Quantitative Trait Loci Analysis for Tiller Number

In this study, we analyzed the expression of TN QTL at any two stages. No QTL was detected at RS-HS and RS-MS. A total of twenty conditional QTLs were detected by the conditional QTL analysis method, and a number of these QTLs distributed on chromosomes 1, 2, 3, 4, 5, and 6, were six, four, five, one, three, and one, respectively. Six QTLs were detected in each of the 4 years, respectively. There were 16 major QTLs and the single major QTL with PVE from 10.02 to 25.91%. Notably, three conditional major QTLs detected in 2020 (*cQTN1-3, cQTN1-5,* and *cQTN4-1*) were detected again in 2021 (**Table 3** and **Figures 2**, **3**).

TABLE 1 | Tiller number (TN) of F_1 population at different stages in *A.* Gaertn. under 4 years.

Year	Trait	Mean ± SD	Range	Coefficient of variation (%)	Skewness	Kurtosis	*W*-test
2017	TN at JS	11.63 ± 8.31	45	71.48	1.09	1.83	0.92
	TN at HS	21.86 ± 17.15	98	78.48	1.72	3.71	0.85
	TN at FS	36.46 ± 23.88	147	65.60	1.53	4.21	0.90
	TN at MS	71.29 ± 38.15	190	53.52	0.78	0.32	0.94
2018	TN at RS	15.13 ± 14.89	56	98.42	1.24	0.55	0.82
	TN at JS	39.82 ± 31.83	124	79.94	1.17	0.41	0.84
	TN at HS	76.59 ± 63.14	313	82.45	1.74	3.04	0.81
	TN at FS	121.82 ± 94.39	481	77.48	1.75	3.06	0.81
	TN at MS	148.66 ± 121.97	645	82.05	1.83	3.52	0.81
2020	TN at RS	23.11 ± 8.96	73	45.00	1.45	4.74	0.92
	TN at JS	13.95 ± 10.75	78	88.25	2.18	7.79	0.83
	TN at HS	11.87 ± 8.56	50	96.97	1.39	2.14	0.86
	TN at FS	27.87 ± 20.35	83	97.23	1.11	0.78	0.88
	TN at MS	64.58 ± 38.13	207	88.89	0.68	−0.23	0.92
2021	TN at RS	342.05 ± 135.90	632	42.12	0.18	−0.10	0.98
	TN at JS	352.38 ± 148.59	801	46.12	0.75	0.41	0.97
	TN at HS	237.51 ± 77.50	417	35.11	0.90	−0.68	0.96
	TN at FS	209.69 ± 68.50	432	36.43	1.57	0.26	0.96
	TN at MS	218.16 ± 54.07	311	31.28	0.41	0.52	0.98

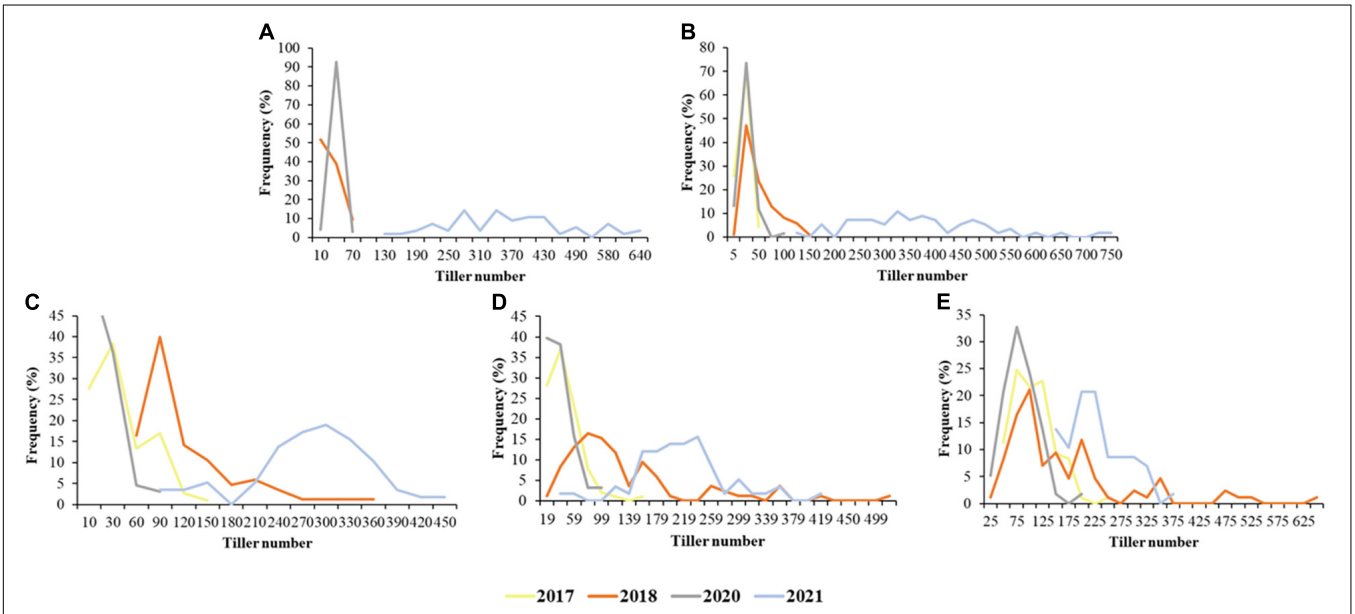

FIGURE 1 | Frequency of tiller number (TN) at different stages in the *Agropyron* cross-pollinated (CP) population in 4 years. **(A–E)** Were the frequency of TN at the recovering stage (RS), jointing stage (JS), heading stage (HS), flowering stage (FS), and maturity stage (MS), respectively; the different colors for the different years.

With a start of RS, a total of eight conditional QTLs were detected. The highest number of QTLs were detected at RS-JS, with six in total, distributed on chromosomes 1, 3, and 5. The LOD value ranged from 2.51 to 4.23, and the PVE ranged from 5.96 to 15.05%. Two (*cQTN3-2* and *cQTN5-2*) of them were the major QTLs. Two major conditional QTLs (*cQTN2-2* and *cQTN5-1*) controlled TN at RS-FS were detected with the LOD values of 3.41 and 3.84 and the PVE of 12.11 and 13.94%. Starting with JS, a total of nine conditional QTLs were detected. Two major conditional QTLs (*cQTN2-1* and *cQTN4-1*) were detected at JS-HS. Three major conditional QTLs (*cQTN1-5, cQTN2-3,* and *cQTN3-4*) were detected at JS-FS, of which *cQTN1-5* was detected for the second time, with a larger PVE value of 24.91%. Five QTLs (*cQTN1-2, cQTN1-5, cQTN2-4, cQTN3-5,* and *cQTN6-1*) were located at JS-MS, of which *cQTN1-2, cQTN1-5,* and *cQTN2-4* were major, and *cQTN1-5* was detected for the third time, with the PVE of 24.10%. One (*cQTN3-3*) and three major QTLs (*cQTN1-3, cQTN1-6, and*

TABLE 2 | Unconditional quantitative trait locus (QTL) positioning of TN at different stages in *A.* Gaertn.

QTL	Stage	Position	Marker interval	LOD	Phenotypic variation explained (%)	Additive effect (female)	Additive effect (male)
qTN1-1	TJ4	39	Marker16227-Marker6778	7.22	12.57	104.15	−2.69
qTN1-2	TH4	81	Marker3909-Marker15691	4.65	12.19	40.55	−10.63
qTN1-3	TH4	101	Marker31281-Marker14952	8.88	26.32	−60.08	−7.69
qTN1-4	TR4	173	Marker47658-Marker20270	2.82	29.76	−46.86	3.79
	TJ4	173	Marker47658-Marker20270	13.93	31.11	−162.91	−4.43
qTN2-1	TF2	47	Marker21073-Marker23241	3.31	12.68	−36.59	−16.40
qTN2-2	TR2	72	Marker11517-Marker14862	2.51	7.02	−4.68	−2.79
qTN2-3	TR3	98	Marker12103-Marker8035	2.85	22.53	−1.43	2.62
qTN2-4	TM4	176	Marker13951-Marker40608	2.52	11.40	−22.92	−8.57
qTN3-1	TM1	5	Marker11037-Marker10239	3.07	9.39	12.16	1.37
qTN3-2	TJ2	9	Marker11241-Marker10342	2.89	10.58	9.97	3.35
qTN3-3	TM3	25	Marker63663-Marker5155	2.99	21.77	−2.36	2.49
qTN3-4	TF1	51	Marker5431-Marker19138	4.05	18.87	8.91	0.94
qTN3-5	TM1	67	Marker10138-Marker53481	2.66	8.25	12.79	−2.05
qTN4-1	TF4	142	Marker7921-Marker28775	3.23	23.14	24.26	−15.27
qTN5-1	TR2	11	Marker17933-Marker18656	2.78	7.73	2.39	1.16
	TJ2	11	Marker17933-Marker18656	2.92	12.31	4.22	−0.45
	TH2	11	Marker17933-Marker18656	2.78	11.79	8.01	2.98
	TF2	11	Marker17933-Marker18656	3.87	15.22	5.10	4.81
qTN6-1	T M1	58	Marker7799-Marker12834	2.56	7.90	−4.67	2.40
qTN6-2	TJ4	65	Marker52861-Marker7985	2.70	2.96	−19.93	6.70

QTL named "q + trait + chromosome + number," such as qTN1-1 indicating that the first QTL controlling TN, was located on chromosome 1; The numbers after stages means the stage of which year, 1 for 2017, 2 for 2018, 3 for 2020, and 4 for 2021.

cQTN3-1) were detected at HS-FS, and HS-MS, respectively. The *cQTN1-3* was previously expressed at RS-JS with a lower PVE (6.02%) than HS-MS (10.59%). Two major QTLs (*cQTN1-1 and cQTN4-1*) were found at FS-MS, while the *cQTN4-1* was also detected at JS-HS.

Overlapping Unconditional and Conditional Quantitative Trait Locus

A total of nine intervals detected both conditional and unconditional QTLs. Seven pairs of conditional and unconditional QTLs with the same flanking markers were detected in the same year (**Figures 2**, **3**). Among them, the unconditional major QTL *qTN5-1* was located at 11 cM on chromosome 5 (Marker17933–Marker18656), expressed at RS-FS, with a gradually increased PVE (total of 47.06%). Meanwhile, *cQTN5-1* was located at the same interval, and controlled TN at RS-FS, with 13.37% PVE. Also, two intervals were detected major conditional and unconditional QTLs that were expressed in different years. QTLs *cQTN2-4* and *qTN2-3* were located at Marker12103–Marker8035 on chromosome 2, of which *cQTN2-4* regulated TN at JS-MS in 2017, and *qTN2-3* was detected at RS in 2020. Another pair of QTL was located at Marker47658–Marker20270 on chromosome 1. The unconditional major QTL *qTN1-4* was detected at the two developmental stages of RS and JS in 2021, and conditional major QTL *cQTN1-5* was at RS-JS in 2020. The conditional QTL *cQTN1-5* was also expressed in 2021, which started from JS to FS and MS, respectively.

DISCUSSION

Continuous Quantitative Trait Loci Associated With Tiller

A stable QTL for TN through the different environments is vital for marker-assisted selection in breeding varieties adapted to various ecological environments (Bilgrami et al., 2020). This study did not detect a stable QTL in more than three environments. This might cause by the difference of environments or climate in four different years (Campbell et al., 2003); or as a kind of perennial plant, the regrowth capacity of *A.* Gaertn. planted from 2014 to 2021 might be weakened year by year, and tiller ability has also declined. With the meta-analysis method, three stable marker-trait associations for maximum tiller in spring were detected on chromosomes 1B, 2B, and 6B of wheat in two different environments (Chen et al., 2017). Two stable QTLs for ratoon stunting disease resistance were detected in 2 years (You et al., 2021). The stable QTLs in the above mentioned studies were detected in 2 years or two environments. Similarly, the three major conditional QTLs, namely, *cQTN1-3, cQTN1-5,* and *cQTN4-1*, were detected in 2 years in this study, although the period they expressed was different in 2 years. Thus, these QTLs could be regarded as relatively stable QTL. Furthermore, conditional and unconditional QTLs detected in the same interval but in different years could also be considered as stable QTLs, such as *cQTN2-4* and *qTN2-3*. To sum up, a total of four stable QTLs were detected in this study.

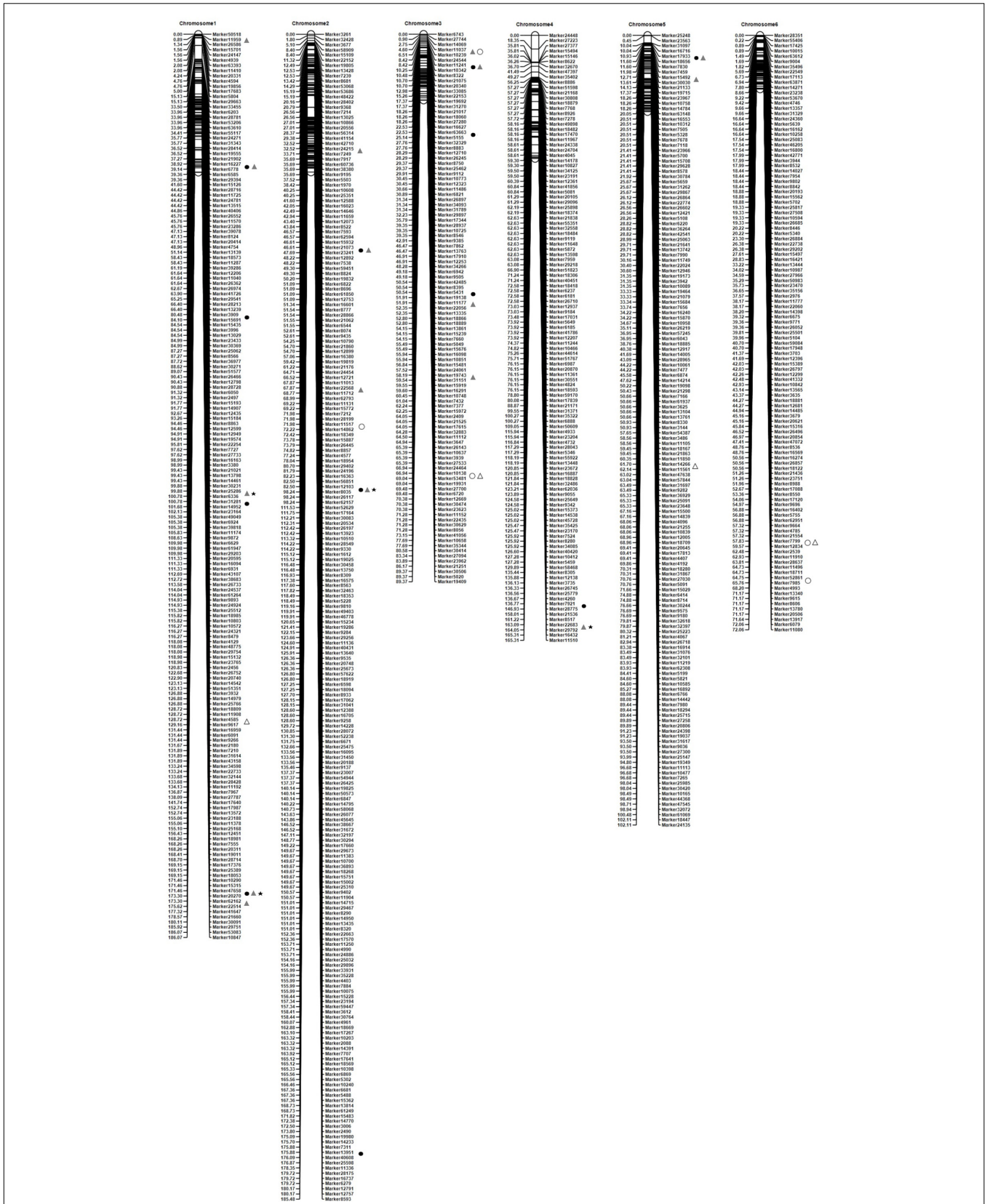

FIGURE 2 | Dynamic identifications of quantitative trait loci (QTLs) controlling TN in different periods in the *Agropyron* CP hybrid population. ●, major unconditional QTL; ○, no-major unconditional QTL; ▲, major conditional QTL; △, no-major conditional QTL; ★, QTL detected in 2 years.

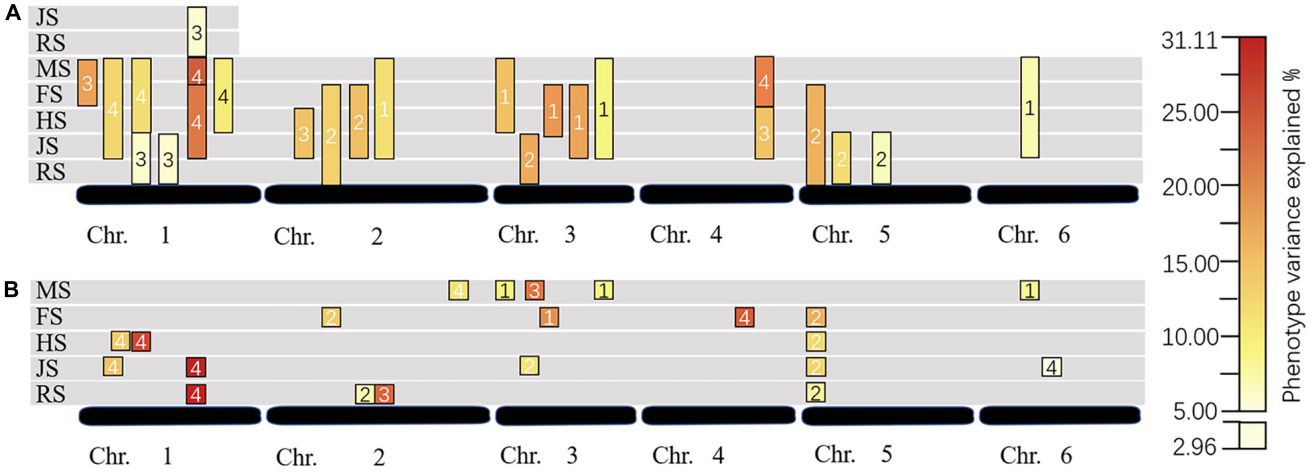

FIGURE 3 | Dynamic QTL changes in different stages and years. **(A)** For conditional QTL; **(B)** for unconditional QTL; RS, JS, HS, FS, and MS for recovering stage, jointing stage, heading stage, flowering stage, and maturity stage, respectively; the numbers in the box: 1 for 2017, 2 for 2018, 3 for 2020, and 4 for 2021.

TABLE 3 | Conditional QTL positioning of TN at different stages in *A.* Gaertn.

QTL	Stage	Position	Marker interval	LOD	Phenotypic variation explained (%)	Additive effect (female)	Additive effect (male)
cQTN1-1	TMTF3	1	Marker11959-Marker26586	2.72	16.80	−1.59	−7.85
cQTN1-2	TMTJ4	39	Marker16227-Marker6778	8.18	11.46	−110.47	−3.76
cQTN1-3	TJTR3	100	Marker25286-Marker6336	2.76	6.02	−2.50	0.78
	TMTH4	100	Marker25286-Marker6336	2.85	10.59	27.71	−4.84
cQTN1-4	TJTR3	129	Marker4585-Marker9617	2.73	5.96	−2.51	0.56
cQTN1-5	TJTR3	173	Marker47658-Marker20270	2.95	6.43	−2.37	0.65
	TFTJ4	173	Marker47658-Marker20270	2.99	24.91	49.59	−11.12
	TMTJ4	173	Marker47658-Marker20270	13.95	24.10	159.58	−2.09
cQTN1-6	TMTH4	175	Marker62162-Marker22514	2.67	10.02	27.55	−1.46
cQTN2-1	THTJ3	33	Marker24215-Marker7249	2.57	12.95	−0.10	−1.45
cQTN2-2	TFTR2	47	Marker21073-Marker23241	3.41	12.11	−32.15	−12.98
cQTN2-3	TFTJ2	68	Marker22568-Marker11712	2.57	13.33	−24.94	−9.65
cQTN2-4	TMTJ1	92	Marker12103-Marker8035	2.54	11.10	7.19	−6.42
cQTN3-1	TMTH1	5	Marker11037-Marker10239	2.77	13.85	9.18	2.68
cQTN3-2	TJTR2	10	Marker11241-Marker10342	4.23	15.05	7.17	2.38
cQTN3-3	TFTH1	52	Marker11177-Marker22056	5.04	16.73	6.41	2.46
cQTN3-4	TFTJ1	59	Marker19743-Marker31151	3.54	15.64	7.43	0.81
cQTN3-5	TMTJ1	67	Marker10138-Marker53481	2.65	8.89	11.64	−1.51
cQTN4-1	THTJ3	164	Marker22683-Marker29792	2.88	12.98	0.93	−2.04
	TMTF4	164	Marker22683-Marker29792	2.63	19.18	−19.01	20.17
cQTN5-1	TFTR2	11	Marker17933-Marker18656	3.84	13.94	3.25	3.83
cQTN5-2	TJTR2	13	Marker15492-Marker30030	2.99	10.74	0.52	−1.12
cQTN5-3	TJTR2	62	Marker14266-Marker11561	2.51	7.75	−4.91	−1.21
cQTN6-1	TMTJ1	58	Marker7799-Marker12834	2.51	7.41	−3.37	1.98

QTL named "cQ + trait + chromosome + number," such as cQTN3-1 indicating that the first QTL controlling tiller in a period, was located on chromosome 3; The numbers after stages means the stage of which year, 1 for 2017, 2 for 2018, 3 for 2020, and 4 for 2021.

In addition, a QTL had multiple effects that could improve the efficiency of assistant breeding (Wang et al., 2018). For example, the QTL controlling TN of rice also controls the number of leaves (Liu et al., 2009). Also, on the interval of Marker11517–Marker14862 of the QTL *qTN2-2* on chromosome 2 with a conditional QTL that controlled PH at several developmental stages in two environments, the high genetic variation of PH was explained (Che et al., 2020), as well as on the interval of Marker10138–Marker53481 of *qTN3-5*/*cQTN3-5* on chromosome 3 with a QTL affecting ear stem length (ESL) in different years and environments (Che et al., 2018). These regions may contain several QTLs

controlling TN, PH, and ESL, respectively, or one QTL affecting these traits meantime. Therefore, further studies on these regions can provide a reliable basis for improving the breeding efficiency of *A*. Gaertn. The continuous QTL in this study that affected TN at different stages could also be regarded as the multiple effects of QTL by temporal. Such multifunctional QTL needs to be finely mapped in future studies to provide a basis for assistant breeding of valuable traits and joint breeding of multiple excellent traits of the *Agropyron* plants.

The Temporal Expression Characteristics of Tiller Number

There was no QTL for TN that could be detected in every period, and some QTL was expressed in several periods (**Figure 3**), such as major QTLs *cQTN1-3, cQTN1-5, cQTN4-1, qTN1-4,* and *qTN5-1*, which were all detected more than once and controlled different stages of TN each time. This implies that the QTL expression selectively had different effects at different stages that showed the characteristics of time expression. In this study, the trend of TN development rate performed as increased rapidly at first stage then decreased slowly and increased gradually at last stage, which showed that the tiller of *A*. Gaertn. was more active at RS-JS than HS-MS. Meanwhile, the number of QTLs detected at RS-JS was greater than HS-MS. Thus, the number of QTLs may be related to the tiller rate. This may be because by the late stages of the *A*. Gaertn. growth, many nutrients were transported to the reproductive organs, caused the tiller bud no more born even the died of tillers, so the TN decreased gradually (Shang et al., 2021).

Comparative Conditional and Unconditional Analysis Methods

Compared to the two methods of QTL analysis, conditional analysis detected more QTLs than unconditional analysis, and eleven and eight QTLs were detected by conditional or unconditional analysis methods, respectively; other nine QTLs were identified by two analysis methods. This may be the effect of these conditional QTLs being faint that not reaching significant levels and could not be identified by unconditional analysis. Conversely, some QTLs may have been expressed with small effects being undetectable but accumulated to a certain period, of which they are sufficient to be identified as unconditional QTLs. The combination of conditional and unconditional methods can detect more QTLs than the unconditional method only, which means that more alternative loci can be provided for marker-assisted breeding.

Notably, located in the same interval, *cQTN3-1* (TMTH) and *qTN3-1* (TM) controlled TN in 2017, but the PVE of *cQTN3-1* (13.85%) was greater than that of *qTN3-1* (9.39%). A similar situation was found for *qTN3-2* and *cQTN3-2* and also for *qTN3-5* and *cQTN3-5*. Generally, the PVE of a certain QTL indicated the ratio between the variance induced by the QTL and the total phenotypic variance. This contradictory result may be caused by the large differences in the total variance of TN at different stages. Another possibility is that there are some negatively expressed QTLs before the HS with very weak undetectable effects and offset part of the effect of *cQTN3-1*, resulting in a reduced cumulative effect, so that the PVE of *qTN3-1* is larger than that of *qTN3-1* (Tian et al., 2011). This implies that TN is a continuous process, and the effects of the same QTL will change with time.

Relationship Between Quantitative Trait Locus of Tiller Number of *Agropyron* Gaertn. and the *Triticeae* Species

A new tillering regulation gene that inhibited the growth of tillering buds was fine mapping in 0.35 cM interval on chromosome 2DL of wheat (Wang et al., 2021). In this study, a stable major QTL *qTN2-3/cQTN2-4* was also detected on chromosome 2. In addition, since the *A*. Gaertn. is a homologous species of wheat, three QTLs were found at the collinearity intervals by comparing the maker sequences of seven linkage groups of *A*. Gaertn. with the genomic sequences of wheat. The unconditional QTL *qTN3-4* was detected at Marker53481 on chromosome 3, which corresponds to wheat 3DS_2575113. The unconditional QTL *qTN2-2* was detected at Marker11517 on chromosome 2, which corresponds to wheat 5DL_4543085. The conditional QTL *cQTN1-4* was located at Maker4585 on chromosome 1, corresponding to wheat 1DL_2269856 (Zhang et al., 2015).

Compared with the barley, two QTLs could have corresponded to the collinearity interval of barley; one conditional QTL *cQTN1-4* was located at Marker4585 on chromosome 1, which corresponding to barley morex_contig_1638559; and one unconditional QTL *qTN2-2* was detected at Marker11517 on chromosome 2, which corresponding to barley morex_contig_79233 (Zhang et al., 2015). Most of the loci had no corresponding relationship between wheat and barley, indicating that the genome of *A*. Gaertn. might be quite different from that of the *Triticeae* species, but these corresponding relationships may provide a basis for gene transfer in the future.

CONCLUSION

In total, 37 QTLs for TN were detected by unconditional and conditional QTL mapping method in 4 years. A total of 12 major unconditional QTLs and 16 major conditional QTLs for TN were located. Most of the QTLs expressed at one developmental stage, unconditional major QTLs *qTN1-4* and *qTN5-1*, conditional major QTLs *cQTN1-3*, *cQTN1-5*, and *cQTN4-1* were detected more than once. Four relatively major stable conditional QTLs were detected in 2 years. In this study, conditional and unconditional QTL methods were combined to describe the development of tillering of *A*. Gaetrn. more comprehensively, and the temporal expression of these TN-related QTLs was revealed. This study brings an in-depth perception of the genetic basis of TN, as well as helpful to the utilization of forage resources.

DATA AVAILABILITY STATEMENT

The original contributions presented in the study are included in the article/supplementary material, further inquiries can be directed to the corresponding author/s.

AUTHOR CONTRIBUTIONS

YC, WL, and LL designed the research. YC, YH, NS, and YY performed the research. YC, YH, and NS wrote the manuscript. LW, XY, YZ, JZ, HH, XL, and SZ participated in the preparation of the reagents and materials in this study. All authors contributed to the article and approved the submitted version.

FUNDING

This study was supported by the Key Research and Development Program in Hebei Province (Grant No. 19226350D) and the National Natural Science Foundation of China (Grant No. 31471493).

REFERENCES

Alejandro, C. P., Carmen, P., and Adoración, C. (2021). Development and characterization of wheat-*Agropyron cristatum* introgression lines induced by gametocidal genes and wheat ph1b mutant. *Agronomy (Basel, Switz.)* 11:277. doi: 10.3390/agronomy11020277

Asay, K. H., and Johnson, D. A. (1990). Genetic variances for forage yield in crested wheatgrass at six levels of irrigation. *Crop Sci.* 30, 79–82. doi: 10.2135/cropsci1990.0011183x003000010018x

Bai, Y. X., Zhao, X. H., Yao, X. H., Yao, Y. H., An, L. K., Li, X., et al. (2021). Genome wide association study of plant height and tiller number in hulless barley. *PLoS One* 16:12. doi: 10.1371/journal.pone.0260723

Bilgrami, S. S., Ramandi, H. D., Shariati, V., Razavi, K., Tavakol, E., Fakheri, B. A., et al. (2020). Detection of genomic regions associated with tiller number in Iranian bread wheat under different water regimes using genome-wide association study. *Sci. Rep.* 10:14034. doi: 10.1038/s41598-020-69442-9

Campbell, B. T., Baenziger, P. S., Gill, K. S., Eskridge, K. M., Budak, H., Erayman, M., et al. (2003). Identification of QTLs and environmental interactions associated with agronomic traits on chromosome 3A of wheat. *Crop Sci.* 43, 1493–1505. doi: 10.2135/cropsci2003.1493

Che, Y. H., Song, N., Yang, Y. P., Yang, X. M., Duan, Q. Q., Zhang, Y., et al. (2018). QTL mapping of six spike and stem traits in hybrid population of *Agropyron* Gaertn. in multiple environments. *Front. Plant Sci.* 9:1422. doi: 10.3389/fpls.2018.01422

Che, Y. H., Song, N., Yang, Y. P., Yang, X. M., Zhang, Y., Zhang, J. P., et al. (2020). Dynamic QTL mapping for plant height in the hybrid population of *Agropyron* Gaertn. *Plant Breed.* 139, 1016–1028. doi: 10.1111/pbr.12814

Che, Y. H., Yang, Y. P., Yang, X. M., Li, X. Q., and Li, L. H. (2014). Phylogenetic relationship and diversity among *Agropyron* Gaertn. germplasm using SSRs markers. *Plant Syst. Evol.* 301, 163–170. doi: 10.1007/s00606-014-1062-4

Chen, F. G., Wu, R. G., Li, D. M., Yu, H. X., Deng, Z. Y., and Tian, J. C. (2017). Genome wide association study for seeding emergence and tiller number using SNP markers in an elite winter wheat population. *J. Genet.* 96, 177–186. doi: 10.1007/s12041-016-0731-1

Chen, L., Li, H., Liu, Y. M., Yang, J., and Hou, Y. (2021). Genetic identification of a major, novel and stably expressed QTL for effective tiller number from tetraploid wheat. *Biotechnol. Biotechnol. Equip.* 35, 1538–1545. doi: 10.1080/13102818.2021.1996271

Dewey, D. R. (1984). "The genomic system of classifification as a guide to intergenetic hybridization with the perennial Triticeae," in *Gene Manipulation in Plant Improvement*, Vol. 35, ed. J. P. Gustafson (New York, NY: Plenum Publishing Corporation), 209–279. doi: 10.1007/978-1-4613-2429-4_9

Dewey, D. R., and Asay, K. H. (1982). Cytogenetic and taxonomic relationships among three diploid crested wheatgrasses. *Crop Sci.* 22, 645–650.

Fan, X. L., Cui, F., Zhao, C. H., Zhang, W., Yang, L. J., Zhao, X. Q., et al. (2015). QTLs for flag leaf size and their influence on yield-related traits in wheat (*Triticum aestivum* L.). *Mol. Breed.* 35:24. doi: 10.1007/s11032-015-0205-9

Haaning, A. M., Smith, K. P., Brown-Guedira, G. L., Chao, S., Tyagi, P., and Muehlbauer, G. J. (2020). Natural genetic variation underlying tiller development in barley (*Hordeum vulgare* L). *G3 Genes Genomes Genet.* 10, 1197–1212. doi: 10.1534/G3.119.400612

Herrmann, D., Boller, B., Studer, B., Widmer, F., and Kölliker, R. (2006). QTL analysis of seed yield components in red clover (*Trifolium pratense* L.). *Theor. Appl. Genet.* 112, 536–545. doi: 10.1007/s00122-005-0158-1

Hirata, M., Cai, H. W., Inoue, M., Yuyama, N., Miura, Y., Komatsu, T., et al. (2006). Development of simple sequence repeat (SSR) markers and construction of an SSR-based linkage map in Italian ryegrass (*Lolium multiflorum* Lam.). *Theor. Appl. Genet.* 113:270. doi: 10.1007/s00122-006-0292-4

Houshmandfar, A., Rebetzke, G. J., Lawes, R., and Tausz, M. (2019). Grain yield responsiveness to water supply in near-isogenic reduced-tillering wheat lines-an engineered crop trait near its upper limit. *Eur. J. Agron.* 102, 33–38. doi: 10.1016/j.eja.2018.11.003

Jensen, L. B., Andersen, J. R., Frei, U., Xing, Y. Z., Taylor, C., Holm, P. B., et al. (2005). QTL mapping of vernalization response in perennial ryegrass (*Lolium perenne* L.) reveals co-location with an orthologue of wheat VRN1. *Theor. Appl. Genet.* 110, 527–536. doi: 10.1007/s00122-004-1865-8

Jiang, Z. Y., Yu, X. X., Yu, Z., Liu, Z. H., Hao, Z. M., and Li, X. L. (2015). Construction of an AFLP-based genetic linkage map of tetraploid hybrid wheatgrass. *J. Triticeae Crops* 4, 457–463.

Jonathan, B., Quddoos, H. M., Jörg, P., Martin, W. G., and Marion, S. R. (2021). Linkage mapping identifies a non-synonymous mutation in FLOWERING LOCUS T (FT-B1) increasing spikelet number per spike. *Sci. Rep.* 11:1585. doi: 10.1038/s41598-020-80473-0

Kuraparthy, V., Sood, S., Dhaliwal, H. S., Chhuneja, P., and Gill, B. S. (2007). Identification and mapping of a tiller inhibition gene (tin3) in wheat. *Theor. Appl. Genet.* 114, 285–294. doi: 10.1007/s00122-006-0431-y

Li, H. H., Ribaut, J. M., Li, Z. L., and Wang, J. K. (2008). Inclusive composite interval mapping (ICIM) for digenic epistasis of quantitative traits in biparental populations. *Theor. Appl. Genet.* 116, 243–260. doi: 10.1007/S00122-007-0663-5

Li, L. H., and Dong, Y. S. (1991). Hybridization between *Triticum aestivum* L. and *Agropyron michnoi* Roshev. 1. Production and cytogenetic study of F1 hybrids. *Theor. Appl. Genet.* 81, 312–316. doi: 10.1007/BF00228669

Li, L. H., and Li, X. Q. (2006). *Standard of Description and Data in Wheat Germplasm Resources*. Beijing: China Agriculture Press.

Li, Z. K., Peng, T., Xie, Q. G., Han, S. X., and Tian, J. C. (2010). Mapping of QTL for tiller number at different stages of growth in wheat using double haploid and immortalized F2 populations. *J. Genet.* 89, 409–415. doi: 10.1007/s12041-010-0059-1

Liu, G. F., Zeng, R. Z., Zhu, H. T., Zhang, Z. M., Ding, X., Zhao, F. M., et al. (2009). Dynamic expression of nine QTLs for tiller number detected with single segment substitution lines in rice. *Theor. Appl. Genet.* 118, 443–453. doi: 10.1007/S00122-008-0911-3

Liu, J. J., Tang, H. P., Qu, X. R., Liu, H., and Li, C. (2020). A novel, major, and validated QTL for the effective tiller number located on chromosome arm 1BL in bread wheat. *Plant Mol. Biol.* 104, 173–185. doi: 10.1007/s11103-020-01035-6

Liu, W. H., Luan, Y., Wang, J. C., Wang, X. G., Su, J. J., Zhang, J. P., et al. (2010). Production and identification of wheat-*Agropyron cristatum* (1.4P) alien translocation lines. *Genome* 53, 472–481. doi: 10.1139/G10-023

Ma, J., Tu, Y., Zhu, J., Luo, W., Liu, H., Li, C., et al. (2020). Flag leaf size and posture of bread wheat: genetic dissection, QTL validation and their relationships with yield-related traits. *Theor. Appl. Genet.* 133, 297–315. doi: 10.1007/s00122-019-03458-2

Mccouch, S., Cho, Y., Yano, M., Paule, E., Blinstrue, M., Morishima, H. M., et al. (1997). Report on QTL nomenclature. *Rice Genet. Newsl.* 14, 11–13.

Peng, Z. S., Yen, C., and Yang, J. L. (1998). Genetic control of oligo-culms character in common wheat. *Wheat Inform. Serv.* 86, 19–24.

Pfender, W. F., Saha, M. C., Johnson, E. A., and Slabaugh, M. B. (2011). Mapping with RAD (restriction-site associated DNA) markers to rapidly identify QTL for stem rust resistance in *Lolium perenne*. *Theor. Appl. Genet.* 122, 1467–1480. doi: 10.1007/S00122-011-1546-3

Ren, T. H., Hu, Y. S., Tang, Y. Z., Li, C. S., Yan, B. J., Ren, Z. L., et al. (2018). Utilization of a wheat55K SNP array for mapping of major QTL for temporal expression of the tiller number. *Front. Plant Sci.* 9:333. doi: 10.3389/fpls.2018.00333

Shang, Q. S., Wang, Y. P., Tang, H., Sui, N., Zhang, X. S., and Wang, F. (2021). Genetic, hormonal, and environmental control of tillering in wheat. *Crop J.* 9, 986–991. doi: 10.1016/j.cj.2021.03.002

Spielmeyer, W., and Richards, R. A. (2004). Comparative mapping of wheat chromosome 1AS which contains the tiller inhibition gene (tin) with rice chromosome 5S. *Theor. Appl. Genet.* 109, 1303–1310. doi: 10.1007/s00122-004-1745-2

Stam, P. (1993). Construction of integrated genetic linkage maps by means of a new computer package: join Map. *Plant J.* 3, 739–744. doi: 10.1111/j.1365-313X.1993.00739.x

Tian, B., Liu, B., Zhu, Z. L., Xie, Q. G., and Tian, J. C. (2011). Conditional and unconditional QTL mapping of grain starch accumulation in wheat. *Sci. Agric. Sin.* 44, 4551–4559. doi: 10.3864/j.issn.0578-1752.2011.22.001

Wang, J. K. (2009). Inclusive composite interval mapping of quantitative trait genes. *Acta Agron. Sin.* 35, 239–245. doi: 10.3724/SP.J.1006.2009.00239

Wang, R., Liu, Y. X., Isham, K., Zhao, W. D., Wheeler, J., Klassen, N., et al. (2018). QTL identification and KASP marker development for productive tiller and fertile spikelet numbers in two high-yielding hard white spring wheat cultivars. *Mol. Breed.* 38:135. doi: 10.1007/s11032-018-0894-y

Wang, Z. Q., Wu, F. K., Chen, X. D., Zhou, W. L., Shi, H. R., Lin, Y., et al. (2021). Fine mapping of the tiller inhibition gene TIN4 contributing to ideal plant architecture in common wheat. *Theor. Appl. Genet.* doi: 10.1007/s00122-021-03981-1

Yao, F. Q., Li, X. H., Wang, H., Song, Y. N., and Li, Z. Q. (2021). Down-expression of TaPIN1s increases the tiller number and grain yield in wheat. *BMC Plant Biol.* 21:443. doi: 10.1186/s12870-021-03217-w

You, Q., Sood, S., Luo, Z. L., Liu, H. B., Islam Md, S., Zhang, M. Q., et al. (2021). Identifying genomic regions controlling ratoon stunting disease resistance in sugarcane (*Saccharum* spp.) clonal F1 population. *Crop J.* 9, 1070–1078. doi: 10.1016/j.cj.2020.10.010

Yu, X. X., Jiang, Z. Y., Yu, Z., Ma, Y. H., Yun, J. F., Su, H., et al. (2015). The new variety breeding of tetraploid hybrid wheatgrass—Mengza NO.1. *Pratecultural Sci.* 32, 94–100.

Yu, X. X., Ma, Y. H., Jiang, Z. Y., Shi, Y., Yang, D. S., and Yu, Z. (2020). Construction of a high–density genetic linkage map and identification of QTLs for main agronomic traits of tetraploid hybrid crested wheatgrass. *Grassl. Sci.* 66, 161–173. doi: 10.1111/grs.12265

Zhang, J., Wu, J., Liu, W., Lu, X., Yang, X., Gao, A., et al. (2013). Genetic mapping of a fertile tiller inhibition gene, ftin, in wheat. *Mol. Breed.* 31, 441–449. doi: 10.1007/s11032-012-9801-0

Zhang, Y., Zhang, J. P., Huang, L., Gao, A. N., Zhang, J., Yang, X. M., et al. (2015). A high-density genetic map for P genome of *Agropyron* Gaertn. based on specific-locus amplified fragment sequencing (SLAF-seq). *Planta* 242, 1335–1347. doi: 10.1007/s00425-015-2372-7

Zhu, J. (1995). Analysis of conditional genetic effects and variance components in developmental genetics. *Genetics* 141, 1633–1639. doi: 10.1093/genetics/141.4.1633

Conflict of Interest: The authors declare that the research was conducted in the absence of any commercial or financial relationships that could be construed as a potential conflict of interest.

Publisher's Note: All claims expressed in this article are solely those of the authors and do not necessarily represent those of their affiliated organizations, or those of the publisher, the editors and the reviewers. Any product that may be evaluated in this article, or claim that may be made by its manufacturer, is not guaranteed or endorsed by the publisher.

frontiers in Plant Science

ORIGINAL RESEARCH
published: 04 March 2022
doi: 10.3389/fpls.2022.850726

Regulation of *WOX11* Expression Represents the Difference Between Direct and Indirect Shoot Regeneration

Jiong Hui Liu[1†], Wan Chen Dong[1†], Fang Fang Fei[1], Xiao Tong Li[1], Xiao Hang Zhang[1], Yangyan Zhou[2], Xian Sheng Zhang[1], Ya Lin Sang[1] and Zhi Juan Cheng[1*]*

[1] State Key Laboratory of Crop Biology, State Forestry and Grassland Administration Key Laboratory of Silviculture in Downstream Areas of the Yellow River, College of Life Sciences, College of Forestry, Shandong Agricultural University, Taian, China, [2] Shandong Salver Group, Salver Academy of Botany, Rizhao, China

OPEN ACCESS

Edited by:
Xigang Liu,
Hebei Normal University, China

Reviewed by:
Lin Xu,
Center for Excellence in Molecular Plant Sciences (CAS), China
Hao Chen,
North Carolina State University, United States

****Correspondence:***
Zhi Juan Cheng
chengzj@sdau.edu.cn
Ya Lin Sang
sangyl@sdau.edu.cn

[†] These authors have contributed equally to this work

Specialty section:
This article was submitted to Crop and Product Physiology, a section of the journal Frontiers in Plant Science

Received: *08 January 2022*
Accepted: *27 January 2022*
Published: *04 March 2022*

Citation:
Liu JH, Dong WC, Fei FF, Li XT, Zhang XH, Zhou Y, Zhang XS, Sang YL and Cheng ZJ (2022) Regulation of WOX11 Expression Represents the Difference Between Direct and Indirect Shoot Regeneration. Front. Plant Sci. 13:850726. doi: 10.3389/fpls.2022.850726

Somatic cells of higher plants possess the remarkable ability to regenerate new individuals via reestablishing apical meristems. Reconstitution of shoot meristem is the vital process and is required for application of plant biotechnology. Under *in vitro* culture condition, shoot meristem can be formed directly or indirectly, depending on the absence or presence of callus as the intermediate status. However, the difference of regulatory mechanisms between the two regeneration types remains unknown. In this study, we established a bi-directional system in which shoots regenerated directly from lateral root primordia (LRP) and indirectly from hypocotyl-derived callus simultaneously. The results based on this system revealed that regulation of *WOX11* expression represents the difference between the two regeneration types in two aspects. Firstly, number of founder cells expressing *WOX11* is tightly associated with regeneration types. Relatively more founder cells gave rise to callus and produce larger meristem, whereas less founder cells produce LRP that regenerate smaller meristem. Secondly, non-CG DNA methylation specifically regulated *WOX11* transcription in LRP and promoted direct shoot regeneration, but had no influence on indirect regeneration. The results provide new insights for understanding the regulatory mechanisms of cell fate transition during *de novo* organogenesis.

Keywords: shoot regeneration, meristem, callus, lateral root primordial, *WOX11*, DNA methylation

INTRODUCTION

Plant somatic cells have a powerful capacity to generate whole individuals under *in vitro* conditions (Su et al., 2011). A normal process is *de novo* organogenesis, in which the explants give rise to ectopic meristems and subsequently shoots and roots. The balance of phytohormones auxin and cytokinin controls the developmental types of regenerating organs. High ratios of auxin to cytokinin induced root formation, whereas low ratios of auxin and cytokinin led to shoot regeneration (Skoog and Miller, 1957). *De novo* organogenesis is the prerequisite of micropropagation and genetic transformation, and provide an important system for studying fundamental biological questions (Sang et al., 2018a; Williams and Garza, 2021).

Shoots can be induced from the explants directly or indirectly, which relies on absence or presence of callus, a mass of proliferating cells, in the intermediate phase (Ikeuchi et al., 2019). The callus for shoot regeneration originates from perivascular cells which are similar to the founder cells of lateral roots (Zhai and Xu, 2021). Different lines of evidences have shown that the founder cells do not undergo dedifferentiation but give rise to callus via a procedure similar to lateral root formation (Atta et al., 2009; Sugimoto et al., 2010). The callus could eventually generate roots or shoots depending on the concentration of auxin and cytokinin of the medium (Che et al., 2007). The typical example of direct regeneration is the conversion of lateral root primordia (LRP) to shoot meristems. Under induction of exogenous cytokinin, LRPs can be converted to shoot meristems without forming callus (Atta et al., 2009; Chatfield et al., 2013; Kareem et al., 2015; Rosspopoff et al., 2017). The conversion from LRPs to shoot meristems occurs within a narrow developmental window and is defined to be a transdifferentiation process.

De novo organogenesis comprises three steps. During the first step, auxin induces the transcription of *WUSCHEL-RELATED HOMEOBOX11/12* (*WOX11/12*), which encode homeodomain transcription factors, and promote the transition of perivascular cells to founder cells (Liu et al., 2014). Subsequently, WOX11/12 activates *WOX5/7* expression and confers the acquisition of regeneration competency by establishing root meristem fate (Atta et al., 2009; Sugimoto et al., 2010; Hu and Xu, 2016; Rosspopoff et al., 2017). Finally, cytokinin signaling components type-B ARABIDOPSIS RESPONSE REGULATORs initiate the expression of *WUSCHEL* (*WUS*), the master regulator of shoot meristem maintenance, and thus generate the shoot meristem (Meng et al., 2017; Zhang et al., 2017; Zubo et al., 2017). The interaction of auxin and cytokinin plays critical roles in *de novo* organogenesis through altering epigenetic modifications and controlling expression of key transcription factors (Li et al., 2011; Cheng et al., 2013; Ikeuchi et al., 2019).

Recent studies provided substantial insights for understanding *de novo* organogenesis (Ikeuchi et al., 2019; Williams and Garza, 2021). However, the difference of regulatory mechanisms between direct and indirect shoot regeneration remains unknown. Distinct culture conditions of these two regeneration types make the comparison difficult. In this study, we established a bi-directional regeneration system, in which shoots regenerated directly and indirectly simultaneously. The results based on this system revealed that callus generated more founder cells which express *WOX11* and gave rise to lager converting organs and shoot meristems. Both *WOX11* transcription and direct shoot regeneration were regulated by non-CG DNA methylation. The results suggest that non-CG DNA methylation play different roles in direct and indirect regeneration via modulating *WOX11* transcription.

MATERIALS AND METHODS

Plant Materials and Growth Conditions

Arabidopsis thaliana ecotype Col-0 was used as the wild type in this study. The *gWUS-GFP3* reporter lines were kindly provided by Thomas Laux (University of Freiburg) (Tucker et al., 2008). The of *pARR1:ARR1-GFP* reporter lines have been described previously (Meng et al., 2017). The *WOX11pro:H2B-eGFP*reporter lines were kindly provided by Lin Xu (Chinese Academy of Sciences) (Zhai and Xu, 2021). The *drm1 drm2 cmt3-11* triple mutant was kindly provided by Xiaofeng Cao (Chinese Academy of Sciences) (Cao et al., 2003).

Seedlings were grown under sterile condition at 20–22°C, with 16 h of white light and 8 h of dark. Segments containing hypocotyl and root were used as explants, which were firstly germinated in GM medium containing 10 μM auxin transport inhibitors naphthylphthalamic acid (NPA), and then transferred onto the medium containing Gamborg's B5 medium with 2% glucose, 0.5 g/L MES, 10 μM 1-naphthaleneacetic acid (NAA), and 0.8% agar. After 2 days culture, explants were transferred onto SIM containing Gamborg's B5 medium with 2% glucose, 0.5 g/L MES, 9 μM 2-isopentenyladenine (2-iP) and 0.8% agar for shoot induction. Explants were cultured under full white light. For calculation of shoot regeneration frequency, regenerated tissues containing a meristem surrounded by three or more leaf primordia with a phyllotactic pattern were considered as a shoot.

Explant Imaging and Analysis

Olympus SZX-16 stereoscopic microscope (Olympus) was used to observe explants during regeneration procedures. The expression signals of reporter lines were observed using low melting point agarose embedding section. Confocal microscopy images were taken using a Zeiss LSM 880 NLO confocal microscope with a 20 × lens. Multitracking in line scanmode and a 488/561main dichroic filter were used to image GFP and dsRED together (Heisler et al., 2005). A 561-nm laser line and a 600–640-nm band-pass filter were used for dsRED. A 488-nm laser line and a 505–550-nm band-pass filter were used for GFP. Cell outline was stained with Fluorescent Brightener. A 405-nm laser line and a 425–475-nm band-pass filter was used for observation.

qRT-PCR

Total RNA was extracted using the TRIzol^{TM} Reagent (catalog no. 15596-026, Invitrogen). The full-length cDNA was generated with the RevertAid First-strand cDNA synthesis kit (Thermo). qRT-PCR was performed on a Chromo4 real-time PCR system (Bio-Rad) using SYBR Master mix (Vazyme) with gene-specific primers (**Supplementary Table 1**). Transcript levels of the examined genes were normalized to that of the housekeeping gene tubulin2. Values shown are the mean ± standard deviation (SD) of three biological replicates.

Bisulfite Sequencing Analysis

DNA was isolated using a cetyltrimethylammonium bromide method. DNA methylation assay was performed using DNA Bisulfite Conversion Kit (Tiangen). PCR products amplified with Methylation specific PCR kit (Tiangen) were cloned into Blunt3 vector (TransGen Biotech) and sequenced. Bisulfite sequencing data were analyzed by the CyMATE software. The results returned by CyMATE were put into GraphPad Prism 9.0 to illustrate DNA methylation frequency at CG, CHG and CHH

(where H = A, C or T), respectively. Primers were list in **Supplementary Table 1**.

RESULTS

Establishment of the Bi-Directional Regeneration System

In order to study the difference between regulatory mechanisms of direct and indirect shoot regeneration, we first tied to establish a bi-directional regeneration system in which shoots can be generated through the two pathways under the same culture condition. For this purpose, we used segments containing hypocotyl and root as explants, and modified a direct regeneration system reported previously by adjusting the hormone concentrations (Rosspopoff et al., 2017). The results show that when explants were treated with 10 μM NAA for 48 h and then cultured in shoot-inducing medium (SIM) containing 9μM 2-iP, shoots were regenerated from both the hypocotyl and the root (**Figure 1**). After 2 days incubation on SIM (SIM2), the hypocotyl produced callus while the root gave rise to protuberances. Subsequently, both callus and protuberance grew in size and produced shoot meristems at SIM6. At SIM8, leafy shoots were formed. Therefore, in this system, shoots were generated indirectly from hypocotyls and directly from roots simultaneously (**Figure 1**).

Callus Produced Larger Shoot Meristems Than That of Lateral Root Primordia

We next compared the cytological features of these two regeneration procedures by observing their histological structures. Consistent with previous studies, NAA treatment promoted the formation of LRPs (Chatfield et al., 2013; Rosspopoff et al., 2017). After transfer to SIM, the LRP gradually grew into roundish converting organ based on cell divisions at multiple orientations (**Figure 2A**). Leaf primordia initiated at SIM4 and the structure of shoot meristem was established in the following 1–2 days. In comparison, exogenous NAA induced callus formation in hypocotyls (**Figure 2B**). After 1 day culture in SIM, the callus grew into a flattened structure. Compared with that of LRP at the same stage, the basal part of callus was much wider, which gave rise to converting organs and shoot meristems with significantly larger size in the subsequent stages.

Callus Initiation Was Accompanied by More Founder Cells Expressing *WOX11* Than That of Lateral Root Primordia

To investigate the cause of the different meristem size that regenerated from the two regeneration types, we examined the transcriptional levels of genes involved in shoot regeneration. The selected genes encode transcriptional factors regulating

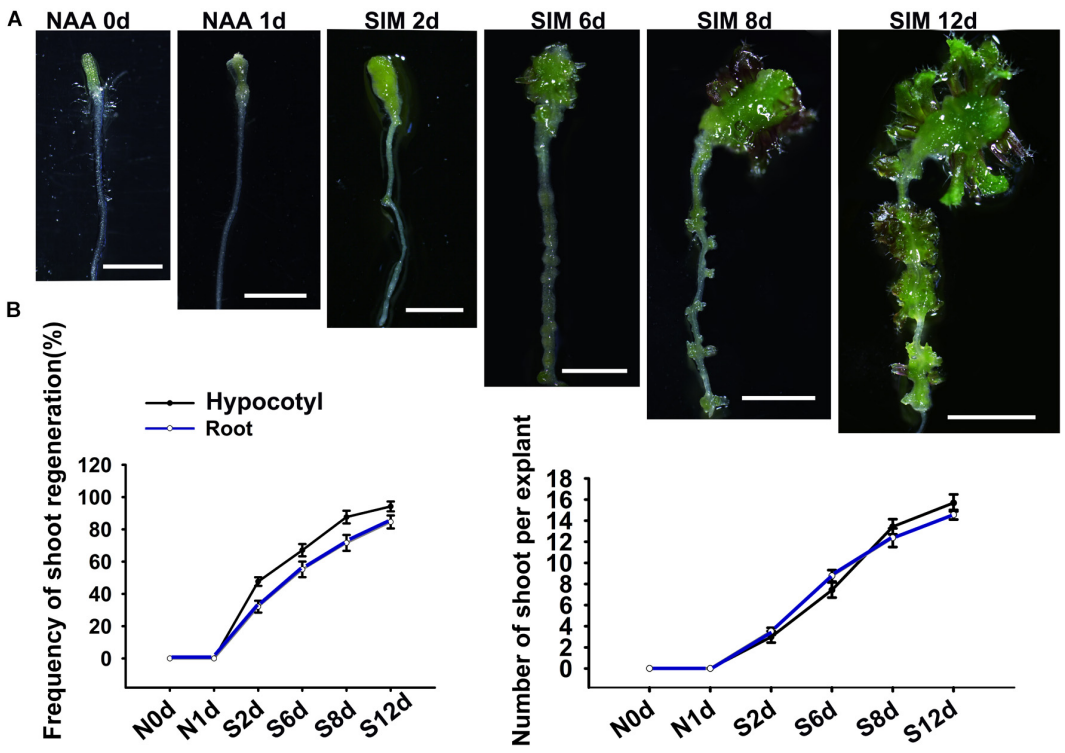

FIGURE 1 | The bi-directional shoot regeneration system. **(A)** Explants exposed to NAA treatment or incubated in SIM at different days. Scale bars represent 20 mm. **(B)** Frequency of shoot regeneration and regenerated shoot number per explant. Error bars represent the standard deviations of three biological replicates. For each replicate, more than 50 individual plants were used.

auxin/cytokinin signaling (*ARF5* and *ARR1*) or stem cell identity (*LBD16*, *PLT1*, *SCR*, *WOX5*, *WOX11,* and *WUS*). qRT-PCR revealed that transcriptional levels of *ARF5*, *ARR1*, *LBD16*, *PLT1,* and *SCR* exhibited similar dynamic patterns between direct and indirect regeneration procedures, suggesting their conserved roles in the two different regeneration pathways (**Figure 3**). Transcripts of *WUS* was not detectable during NAA-treatment stage. However, SIM-incubation caused obvious increase of *WUS* expression, which was more significant in the hypocotyl explants. Transcription of *WOX5* and *WOX11* was induced by exogenous NAA but decreased during SIM culture. The NAA-mediated alteration of *WOX11* and *WOX5* was more pronounced in hypocotyl explants than that in root. The results suggest that conversion of cell identity might be differently regulated between direct and indirect regeneration.

To get more insights into the cell fate transition process, we visualized the spatio-temporal expression signals of *WOX5*, *WUS,* and *WOX11*, respectively (**Figures 4**, **5**). The *pWOX5:RFP; gWUS-3GFP* double reporter lines revealed that *WOX5* and *WUS* were expressed in similar patterns in hypocotyl and root explants (**Figure 4**). After 48 h NAA-treatment, *WOX5* was expressed in the middle cell layers in both callus and LRP. At SIM1, the expression signal of *WOX5* vanished while that of *WUS* was initiated in a few cells. As the callus and LRP grow in size, *WUS* expression expanded into larger domains. When shoot meristem was formed, *WUS* expression was confined to the organizing center. The most obvious difference between the two types of explants is that the expression domain of *WOX5* at the end of NAA-treatment in callus was larger than that in LRP.

In the *pWOX11:H2B-eGFP* lines, GFP signals were first detected in pericycle cells at 6 h of NAA-treatment (**Figure 5**). Different from that of LRP, where *WOX11* was induced in about 8 cells before periclinal division at 12 h, expression signals were visible in more than 15 continuous cells in the initiating

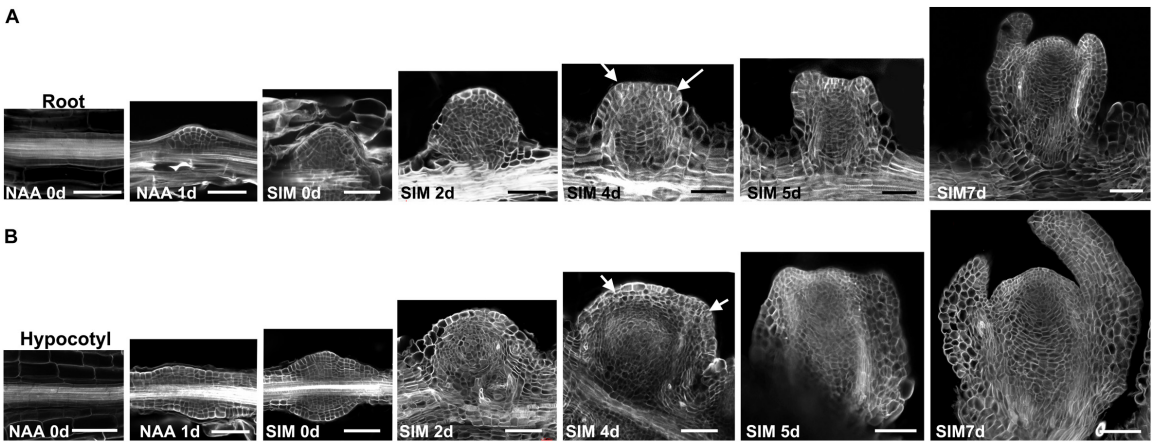

FIGURE 2 | Cytological features of shoot regeneration procedures of the bi-directional system. **(A)** Shoots were regenerated through direct conversion from LRP into shoot meristem. **(B)** Shoots were produced indirectly from the hypocotyl-derived callus. Days after NAA-treatment or SIM-culture are indicated in the bottom left corner of each panel. Arrows point to the position of leaf primordia. Scale bars represent 50 μm.

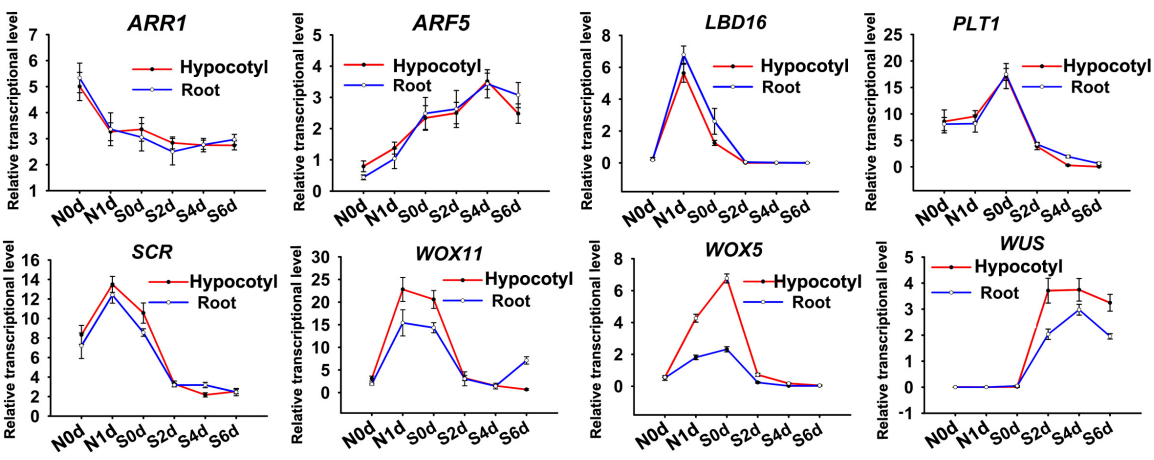

FIGURE 3 | qRT-PCR analysis of genes involved in shoot regeneration. N represents days after NAA treatment. S indicates days for SIM incubation. Error bars show standard deviations of three biological repeats.

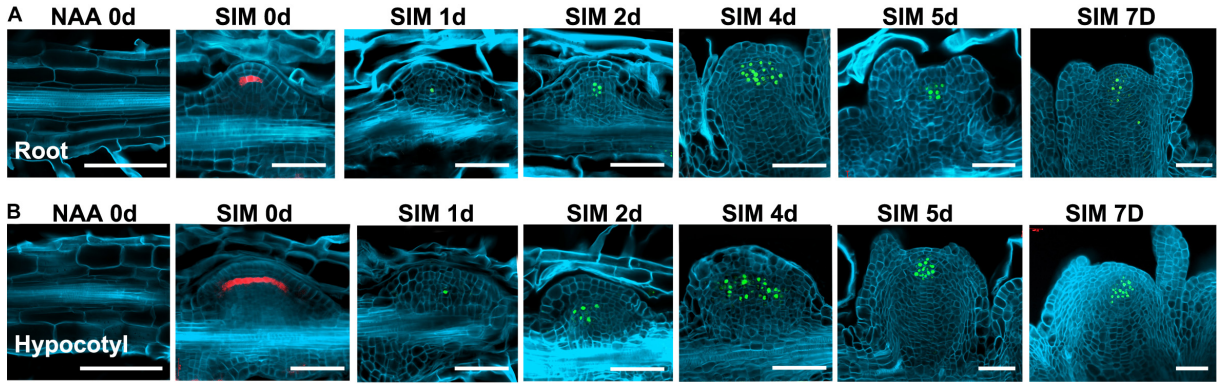

FIGURE 4 | Expression signals of the *pWOX5:RFP; gWUS-3GFP* double reporter lines during shoot regeneration. **(A)** Procedure of direct regeneration through conversion from LRP into shoot meristem. **(B)** Indirect regeneration from the hypocotyl-derived callus. Days after NAA-treatment or SIM-culture are indicated on top of each panel. Scale bars represent 50 μm.

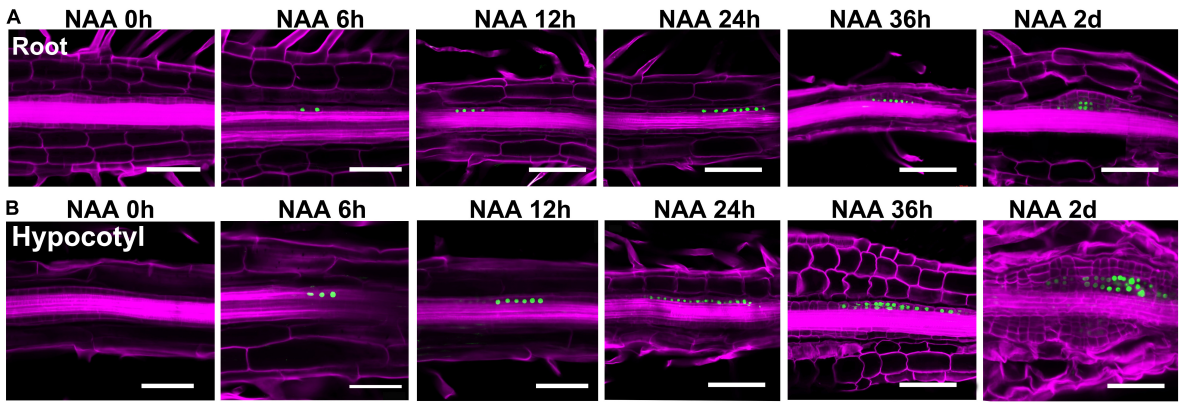

FIGURE 5 | Expression patterns of *WOX11* revealed by the *pWOX11:H2B-eGFP* lines during shoot regeneration. **(A,B)** Illustrate direct and indirect regeneration processes, respectively. Hours or days for NAA-treatment are indicated on top of each panel. Scale bars represent 50 μm.

callus. During the primary cell divisions, the signals were also observed in newly proliferated cells. When organized cell files were established, *WOX11* was expressed in the founder cells at basal part of the callus and LRP. Therefore, number of founder cells in the incipient stage was tightly associated with the regeneration types and the size of regenerated meristems. Relatively more *WOX11*-expressing founder cells gave rise to callus which produce larger meristem, whereas less founder cells led to the formation of LRP that regenerate smaller meristem.

Non-CG DNA Methylation Regulates Direct but Not Indirect Shoot Regeneration

We next intend to explore the factors regulate *WOX11* expression. Previous studies showed that non-CG methylation is involved in acquisition of pluripotency (Shemer et al., 2015). It has been shown that non-CG DNA methylation is almost completely lost in the triple mutant of DOMAINS REARRANGED METHYLTRANSFERASE1/2 CHROMOMETHYLASE3 (*drm1 drm2 cmt3*) (Cokus et al., 2008; Stroud et al., 2014). We thus examined the shoot regeneration capacity of the *drm1 drm2 cmt3* (*ddc*) triple mutant using the bi-directional system described above. As a result, both the frequency and the number of regenerated shoots per explant were significantly increased in root of the *ddc* triple mutant compared with those of wild type (**Figure 6**). However, the regeneration ability of hypocotyl did not show obvious changes between the mutant and the wild type. The results indicate that non-CG DNA methylation negatively regulates direct shoot regeneration but did not affect indirect regeneration. No obvious phenotype was observed in *drm1* and *cmt3* single mutants, as well as *drm1 drm2* double mutant, suggesting the functional redundancy among *DRM1*, *DRM2* and *CMT3*.

Non-CG DNA Methylation Mediated *WOX11* Expression and Lateral Root Primordia Formation

To determine whether the expression of *WOX11* is mediated by non-CG DNA methylation, bisulfite sequencing was performed to compare DNA methylation between the *ddc* triple mutant and

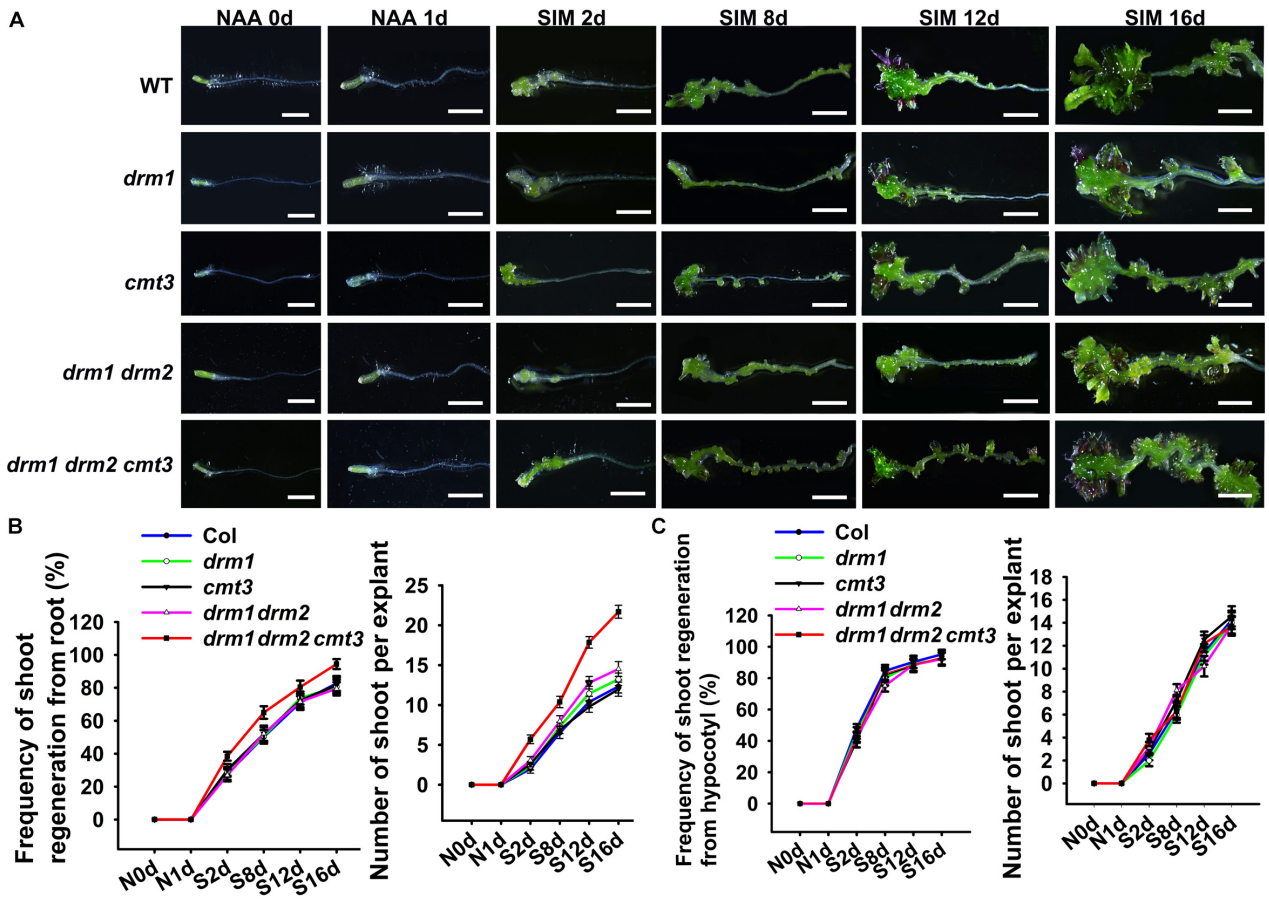

FIGURE 6 | Comparisons of shoot regeneration capacity between the *ddc* triple mutant and the wild type. **(A)** Shoot regeneration of *drm1*, *cmt3*, *drm1 drm2,* and *ddc* mutants. Days after NAA-treatment or SIM-culture are indicated in the bottom left corner of each panel. Frequency of shoot regeneration and number of regenerated shoots per explant are shown for direct **(B)** and indirect **(C)** regeneration systems. The frequency of direct regeneration was calculated as the shooted hypocotyl number/total hypocotyl number, while that of indirect regeneration was determined as the shooted root number/total root number. Error bars indicate the standard deviations of three biological replicates. For each replicate, more than 50 individual plants were used. Scale bars represent 10 μm.

the wild type. The results illustrate that after NAA-treatment for 1 day, 13 sites of the genomic fragments 1,036–1,529 bp and 2,635–3,044 bp upstream of the coding sequence were hypermethylated in wild type. However, the level of methylation in the same sites were substantially decreased in the *ddc* mutant (**Figure 7**). Correspondingly, compared with that of wild type, transcriptional level of *WOX11* was significantly higher in the *ddc* root during NAA-treatment (**Figure 8A**). On the contrary, in the hypocotyl explants at the same stages, both the methylation and the expression of *WOX11* did not show obvious difference between *ddc* and wild type (**Figure 8B** and **Supplementary Figure 1**). The results demonstrate that non-CG DNA methylation negatively regulate *WOX11* transcription during LRP formation but had no influence on callus.

De novo shoot regeneration comprises three steps, including the activation of initial cells, acquisition of regenerative competency and establishment of shoot meristem (Sang et al., 2018b). *WOX11* controls the former two steps by promoting the first cell fate transition and activating *WOX5* expression (Liu et al., 2014; Hu and Xu, 2016; Zhai and Xu, 2021). Subsequently, genes responsible for shoot meristem maintenance such as *WUS* regulate the third step. Therefore, if non-CG methylation regulate shoot regeneration via modulating *WOX11* expression, the *ddc* triple mutant would produce more LRP. To test this hypothesis, we examined lateral root number. The results show that the *ddc* triple mutant give rise to significantly more lateral roots than that of wild type, indicating an increase in LRP formation (**Figure 8C**).

Previous study showed that after transfer to hormone-free medium, auxin-induced callus which resembles LRP can be converted to roots (Atta et al., 2009). To analyze the difference of NAA-induced callus/LRP formation between the *ddc* triple mutant and wild type, we transferred explants after 48 h NAA-treatment to hormone-free medium. As a result, the *ddc* triple mutant generated significantly more lateral roots than wild type (**Figure 8D**). However, the number of adventitious roots derived from hypocotyls did not demonstrate obvious changes, suggesting that callus formation capacity was similar between the *ddc* triple mutant and wild type (**Figure 8E**). These results suggest that non-CG methylation is implicated in shoot regeneration through mediating *WOX11* expression.

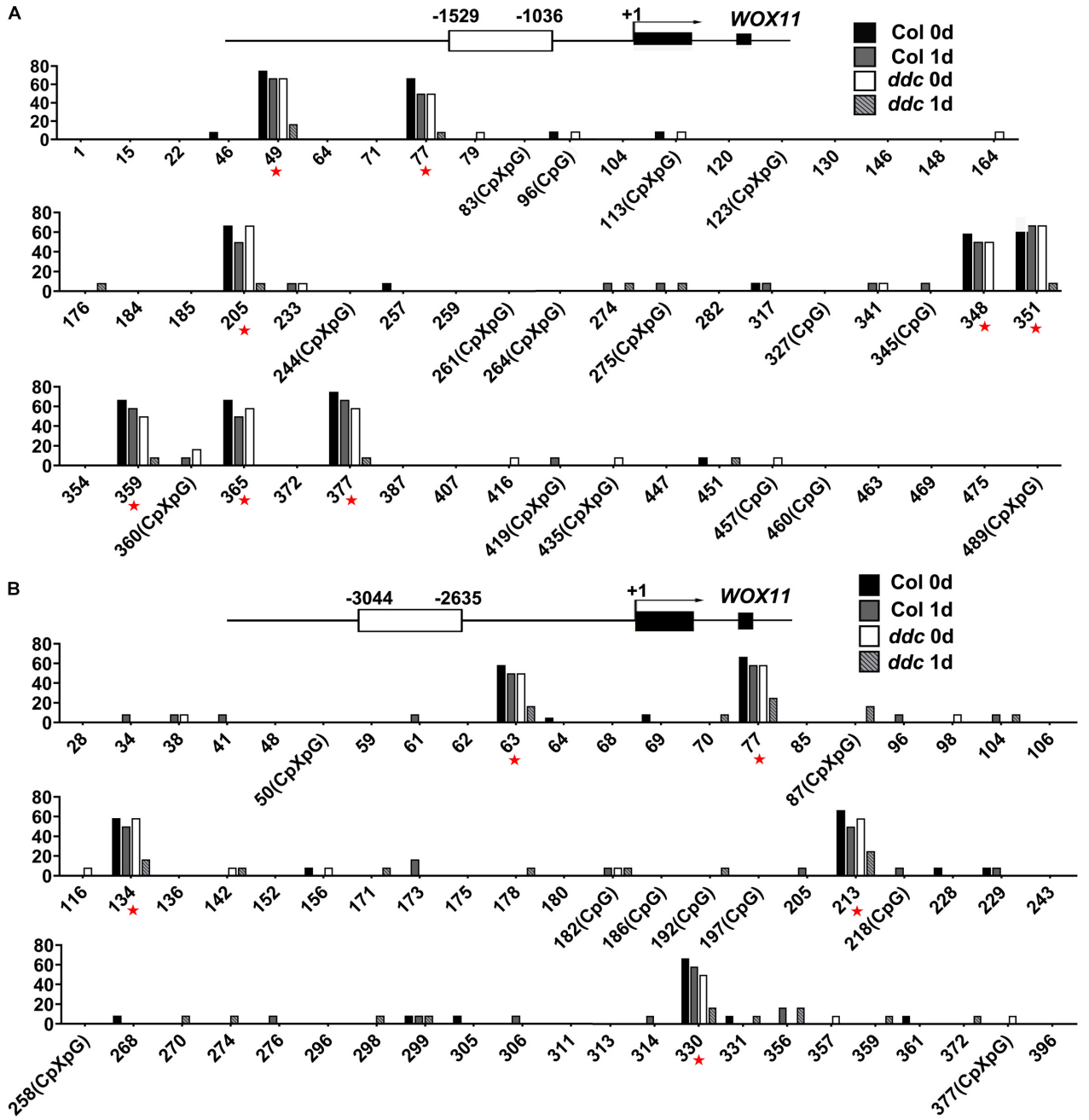

FIGURE 7 | Analysis of methylation level in the promoter region of *WOX11* via bisulfite sequencing. Levels of cytosine methylation in genomic fragments 1,036–1,529 bp **(A)** and 2,635–3,044 bp **(B)** upstream of the coding sequence were detected. Root explants incubated under NAA-treatment were used for analysis. Red asterisk.

DISCUSSION

Owing to its theoretical and practical importance, shoot regeneration have been substantially studied (Williams and Garza, 2021). It is well acknowledged that during culture in auxin-rich medium, explants from aerial or root organs give rise to callus, which subsequently generate shoots under cytokinin induction (Duclercq et al., 2011). Recent studies showed that exogenous cytokinin can directly convert LRP into shoot meristem (Atta et al., 2009; Chatfield et al., 2013; Kareem et al., 2015; Rosspopoff et al., 2017). Thus, the direct and indirect regeneration experienced distinct developmental programs, but the difference of their regulatory mechanisms remains elusive. Because the media formulations used in these two pathways are quite different, it is difficult to compare direct and indirect regeneration under the same condition. In the present study,

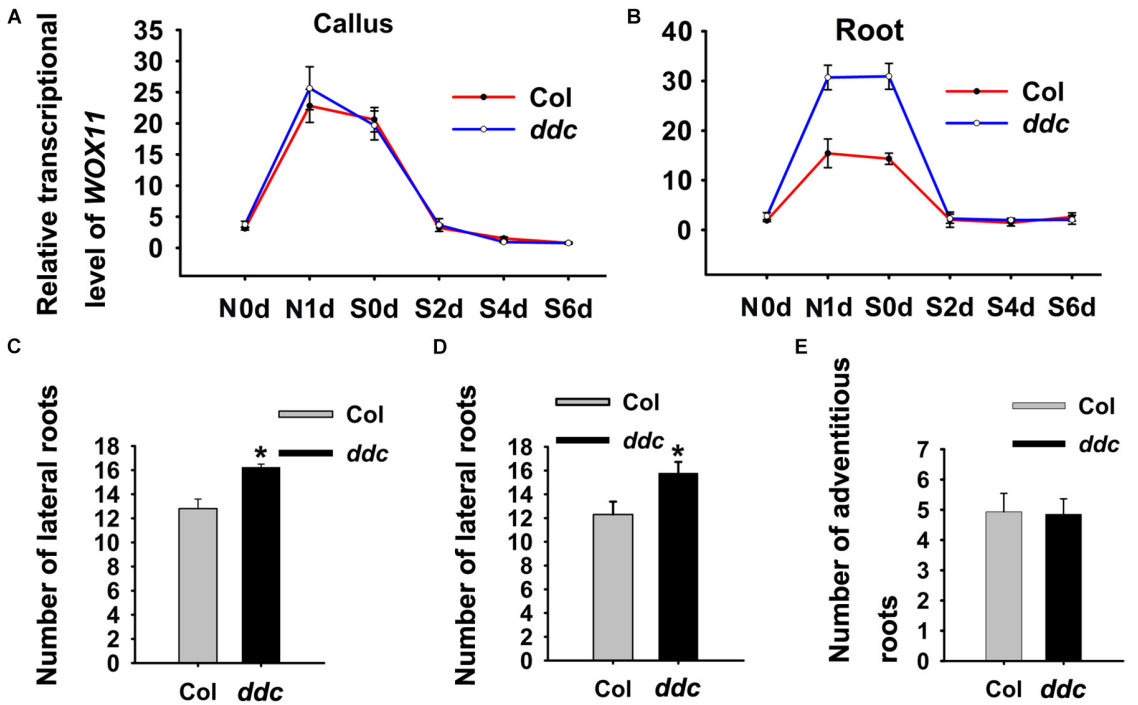

FIGURE 8 | Dynamics of *WOX11* transcript levels in hypocotyl **(A)** and root **(B)** explants derived from *ddc* and wild-type seedings. **(C)** Lateral root numbers derived from *ddc* and wild-type seedlings grown on hormone-free medium. **(D)** Lateral root numbers of *ddc* and wild-type explants after 48 h NAA-treatment. **(E)** Adventitious root number of *ddc* and wild-type hypocotyls which were cultured in hormone-free medium after 48 h NAA-treatment. Error bars show standard deviations of three biological repeats. *$0.001 < P < 0.01$ are determined by two-tailed Student's *t*-tests.

we established a bidirectional system, in which shoots were produced directly from root and indirectly from hypocotyl synchronously, and thus provided a system for comparing the different regeneration pathways (**Figure 1**).

Using the bi-directional regeneration system, we analyzed the expression of homeodomain family genes that mark cell fate transition. Of them, the expression patterns of *WOX5* and *WUS*, which represent the identity of stem cell niches, were similar between the procedures of direct and indirect regeneration (Aichinger et al., 2012). Consistent with previous findings, *WUS* expression signal was initiated in only a few cells at early stage of cytokinin-incubation, and expended into larger domain afterward, indicating that fate transition from root meristem to shoot meristem is a gradual process (**Figure 4**; Meng et al., 2017; Zhang et al., 2017). *WOX11* activates the initial step for regeneration by priming founder cells, and is continuously expressed in the founder cells during callus formation (Liu et al., 2014; Zhai and Xu, 2021). In this context, perivascular cells expressing *WOX11* can be reckoned as stem cells, which produce new cells through proliferation and maintain their identity at the same time. Our results show that at the early stages of regeneration, perivascular cells with *WOX11* expressional signal were much more in callus than those in LRP, indicating that the "initiating site" for callus formation was relatively larger (**Figure 5**). Consistently, in the following stages, callus formed wider structure and generated larger converting organs and shoot meristems than that of LRP. The results suggest that the number of founder cells determines the manner of regeneration and the size of regenerated organ.

It has been revealed previously that *WOX11* is not expressed and not involved in LRP initiation from seedlings grown vertically on hormone-free medium (Sheng et al., 2017). However, when the primary root is damaged, *WOX11* expression is induced at the wounding site and mediates lateral root formation. The wound-induced lateral roots are completely inhibited by excision of aerial part and can be recovered by application of auxin at the decapitated region. The results suggest that the basipetal auxin transport is required for lateral root formation upon wounding by inducing *WOX11* expression. Therefore, it is plausible to infer that in the present study, exogenous NAA in the early culturing stage initiated *WOX11* expression and subsequent LRP formation.

Non-CG DNA methylation provided a conjunction that connected *WOX11* expression to shoot regeneration. In the *ddc* triple mutant, where non-CG DNA methylation is almost completely lost, direct regeneration was significantly promoted while indirect regeneration was unaffected (**Figure 6**). Correspondingly, the transcriptional level of *WOX11* was increased in *ddc* root compared with that of wild type, but was unchanged between *ddc* and wild-type hypocotyl (**Figures 8A,B**). Therefore, it is reasonable to speculate that DNA methylation-mediated *WOX11* expression was specifically implicated in the regulation of direct shoot regeneration.

Callus formation resembles the root development pathway (Atta et al., 2009; Sugimoto et al., 2010). It is possible that callus derived from aerial organs was generated similar to adventitious root. Recent studies have revealed different regulatory mechanisms between the formation of adventitious and lateral roots (Bellini et al., 2014; Verstraeten et al., 2014). DNA methylation-mediated *WOX11* expression might be a specific factor for the latter.

Overall, our study compared direct and indirect shoot regeneration using the bi-directional system. The results revealed two lines of difference, both of which were mediated by *WOX11*. Firstly, number of founder cells that express *WOX11* determined the type of regeneration. Callus initiation was accompanied by more founder cells and regenerated larger organs, while less founder cells were established in LRP and gave rise to smaller meristems. Secondly, non-CG DNA Methylation specifically regulated *WOX11* expression and direct shoot regeneration, and had no influence on indirect regeneration.

DATA AVAILABILITY STATEMENT

The original contributions presented in the study are included in the article/**Supplementary Material**, further inquiries can be directed to the corresponding author/s.

AUTHOR CONTRIBUTIONS

ZC and YS conceived and designed the experiments. JL and WD performed the experiments and data analysis with the help of FF, XL, XHZ, and YZ. XSZ and YS wrote the manuscript. All authors contributed to the article and approved the submitted version.

FUNDING

This work was supported by the National Natural Sciences Foundation of China (31870178 and 31870292), the Shandong Province Natural Science Foundation of Major Basic Research Program (ZR2020ZD18), and the Introduction and Training Plan of Young Creative Talents in Universities of Shandong Province: "Research Group of Tree Biotechnology."

ACKNOWLEDGMENTS

We thank T. Laux (University of Freiburg), X. Cao, and L. Xu (University of California at San Diego) for providing materials.

SUPPLEMENTARY MATERIAL

The Supplementary Material for this article can be found online at: https://www.frontiersin.org/articles/10.3389/fpls.2022.850726/full#supplementary-material

Supplementary Figure 1 | Methylation level in the promoter region of *WOX11* via bisulfite sequencing. Cytosine methylation levels in genomic fragments 1,036–1,529 bp **(A)** and 2,635–3044 bp **(B)** upstream of the coding sequence were detected. Hypocotyl explants incubated under NAA-treatment were used for analysis.

REFERENCES

Aichinger, E., Kornet, N., Friedrich, T., and Laux, T. (2012). Plant stem cell niches. *Annu. Rev. Plant Biol.* 63, 615–636. doi: 10.1146/annurev-arplant-042811-105555

Atta, R., Laurens, L., Boucheron-Dubuisson, E., Guivarc'h, A., Carnero, E., Giraudat-Pautot, V., et al. (2009). Pluripotency of *Arabidopsis* xylem pericycle underlies shoot regeneration from root and hypocotyl explants grown in vitro. *Plant J.* 57, 626–644. doi: 10.1111/j.1365-313X.2008.03715.x

Bellini, C., Pacurar, D. I., and Perrone, I. (2014). Adventitious roots and lateral roots: similarities and differences. *Annu. Rev. Plant Biol.* 65, 639–666. doi: 10.1146/annurev-arplant-050213-035645

Cao, X., Aufsatz, W., Zilberman, D., Mette, M. F., Huang, M. S., Matzke, M., et al. (2003). Role of the *DRM* and *CMT3* methyltransferases in RNA-directed DNA methylation. *Curr. Biol.* 13, 2212–2217. doi: 10.1016/j.cub.2003.11.052

Chatfield, S. P., Capron, R., Severino, A., Penttila, P. A., Alfred, S., Nahal, H., et al. (2013). Incipient stem cell niche conversion in tissue culture: using a systems approach to probe early events in *WUSCHEL*-dependent conversion of lateral root primordia into shoot meristems. *Plant J.* 73, 798–813. doi: 10.1111/tpj.12085

Che, P., Lall, S., and Howell, S. H. (2007). Developmental steps in acquiring competence for shoot development in *Arabidopsis* tissue culture. *Planta* 226, 1183–1194. doi: 10.1007/s00425-007-0565-4

Cheng, Z. J., Wang, L., Sun, W., Zhang, Y., Zhou, C., Su, Y. H., et al. (2013). Pattern of auxin and cytokinin responses for shoot meristem induction results from the regulation of cytokinin biosynthesis by AUXIN RESPONSE FACTOR3. *Plant Physiol.* 161, 240–251. doi: 10.1104/pp.112.203166

Cokus, S. J., Feng, S., Zhang, X., Chen, Z., Merriman, B., Haudenschild, C. D., et al. (2008). Shotgun bisulphite sequencing of the *Arabidopsis* genome reveals DNA methylation patterning. *Nature* 452, 215–219. doi: 10.1038/nature06745

Duclercq, J., Sangwan-Norreel, B., Catterou, M., and Sangwan, R. S. (2011). De novo shoot organogenesis: from art to science. *Trends Plant Sci.* 16, 597–606. doi: 10.1016/j.tplants.2011.08.004

Heisler, M. G., Ohno, C., Das, P., Sieber, P., Reddy, G. V., Long, J. A., et al. (2005). Patterns of auxin transport and gene expression during primordium development revealed by live imaging of the *Arabidopsis* inflorescence meristem. *Curr. Biol.* 15, 1899–1911. doi: 10.1016/j.cub.2005.09.052

Hu, X., and Xu, L. (2016). Transcription Factors WOX11/12 Directly Activate *WOX5/7* to Promote Root Primordia Initiation and Organogenesis. *Plant Physiol.* 172, 2363–2373. doi: 10.1104/pp.16.01067

Ikeuchi, M., Favero, D. S., Sakamoto, Y., Iwase, A., Coleman, D., Rymen, B., et al. (2019). Molecular Mechanisms of Plant Regeneration. *Annu. Rev. Plant Biol.* 70, 377–406. doi: 10.1146/annurev-arplant-050718-100434

Kareem, A., Durgaprasad, K., Sugimoto, K., Du, Y., Pulianmackal, A. J., Trivedi, Z. B., et al. (2015). *PLETHORA* Genes Control Regeneration by a Two-Step Mechanism. *Curr. Biol.* 25, 1017–1030. doi: 10.1016/j.cub.2015.02.022

Li, W., Liu, H., Cheng, Z. J., Su, Y. H., Han, H. N., Zhang, Y., et al. (2011). DNA methylation and histone modifications regulate de novo shoot regeneration in *Arabidopsis* by modulating *WUSCHEL* expression and auxin signaling. *PLoS Genet.* 7:e1002243. doi: 10.1371/journal.pgen.1002243

Liu, J., Sheng, L., Xu, Y., Li, J., Yang, Z., Huang, H., et al. (2014). WOX11 and *12* are involved in the first-step cell fate transition during de novo root organogenesis in *Arabidopsis*. *Plant Cell* 26, 1081–1093. doi: 10.1105/tpc.114.122887

Meng, W. J., Cheng, Z. J., Sang, Y. L., Zhang, M. M., Rong, X. F., Wang, Z. W., et al. (2017). Type-B ARABIDOPSIS RESPONSE REGULATORs Specify the Shoot Stem Cell Niche by Dual Regulation of *WUSCHEL*. *Plant Cell* 29, 1357–1372. doi: 10.1105/tpc.16.00640

Rosspopoff, O., Chelysheva, L., Saffar, J., Lecorgne, L., Gey, D., Caillieux, E., et al. (2017). Direct conversion of root primordium into shoot meristem relies on

timing of stem cell niche development. *Development* 144, 1187–1200. doi: 10.1242/dev.142570

Sang, Y. L., Cheng, Z. J., and Zhang, X. S. (2018a). iPSCs a comparison between animals and plants. *Trends Plant Sci.* 23, 660–666. doi: 10.1016/j.tplants.2018.05.008

Sang, Y. L., Cheng, Z. J., and Zhang, X. S. (2018b). Plant stem cells and de novo organogenesis. *New Phytol.* 218, 1334–1339. doi: 10.1111/nph.15106

Shemer, O., Landau, U., Candela, H., Zemach, A., and Eshed Williams, L. (2015). Competency for shoot regeneration from *Arabidopsis* root explants is regulated by DNA methylation. *Plant Sci.* 238, 251–261. doi: 10.1016/j.plantsci.2015.06.015

Sheng, L., Hu, X., Du, Y., Zhang, G., Huang, H., et al. (2017). Non-canonical *WOX11*-mediated root branching contributes to plasticity in Arabidopsis root system architecture. *Development* 144, 3126–3133. doi: 10.1242/dev.152132

Skoog, F., and Miller, C. O. (1957). Chemical regulation of growth and organ formation in plant tissues cultured in vitro. *Symp. Soc. Exp. Biol.* 11, 118–130.

Stroud, H., Do, T., Du, J., Zhong, X., Feng, S., Johnson, L., et al. (2014). Non-CG methylation patterns shape the epigenetic landscape in *Arabidopsis*. *Nat. Struct. Mol. Biol.* 21, 64–72. doi: 10.1038/nsmb.2735

Su, Y. H., Liu, Y. B., and Zhang, X. S. (2011). Auxin-cytokinin interaction regulates meristem development. *Mol. Plant* 4, 616–625. doi: 10.1093/mp/ssr007

Sugimoto, K., Jiao, Y., and Meyerowitz, E. M. (2010). *Arabidopsis* regeneration from multiple tissues occurs via a root development pathway. *Dev. Cell* 18, 463–471. doi: 10.1016/j.devcel.2010.02.004

Tucker, M. R., Hinze, A., Tucker, E. J., Takada, S., Jurgens, G., and Laux, T. (2008). Vascular signalling mediated by ZWILLE potentiates WUSCHEL function during shoot meristem stem cell development in the *Arabidopsis* embryo. *Development* 135, 2839–2843. doi: 10.1242/dev.023648

Verstraeten, I., Schotte, S., and Geelen, D. (2014). Hypocotyl adventitious root organogenesis differs from lateral root development. *Front. Plant Sci.* 5:495. doi: 10.3389/fpls.2014.00495

Williams, K. L., and Garza, L. A. (2021). Diverse cellular players orchestrate regeneration after wounding. *Exp. Dermatol.* 30, 605–612. doi: 10.1111/exd.14248

Zhai, N., and Xu, L. (2021). Pluripotency acquisition in the middle cell layer of callus is required for organ regeneration. *Nat. Plants* 7, 1453–1460. doi: 10.1038/s41477-021-01015-8

Zhang, F., May, A., and Irish, V. F. (2017). Type-B *ARABIDOPSIS* RESPONSE REGULATORs Directly Activate *WUSCHEL*. *Trends Plant Sci.* 22, 815–817. doi: 10.1016/j.tplants.2017.08.007

Zubo, Y. O., Blakley, I. C., Yamburenko, M. V., Worthen, J. M., Street, I. H., Franco-Zorrilla, J. M., et al. (2017). Cytokinin induces genome-wide binding of the type-B response regulator ARR10 to regulate growth and development in *Arabidopsis*. *Proc. Natl. Acad. Sci. U S A.* 114, E5995–E6004. doi: 10.1073/pnas.1620749114

Conflict of Interest: The authors declare that the research was conducted in the absence of any commercial or financial relationships that could be construed as a potential conflict of interest.

Publisher's Note: All claims expressed in this article are solely those of the authors and do not necessarily represent those of their affiliated organizations, or those of the publisher, the editors and the reviewers. Any product that may be evaluated in this article, or claim that may be made by its manufacturer, is not guaranteed or endorsed by the publisher.

Advantages of publishing in Frontiers

OPEN ACCESS
Articles are free to read for greatest visibility and readership

FAST PUBLICATION
Around 90 days from submission to decision

HIGH QUALITY PEER-REVIEW
Rigorous, collaborative, and constructive peer-review

TRANSPARENT PEER-REVIEW
Editors and reviewers acknowledged by name on published articles

Frontiers
Avenue du Tribunal-Fédéral 34
1005 Lausanne | Switzerland

Visit us: www.frontiersin.org
Contact us: frontiersin.org/about/contact

REPRODUCIBILITY OF RESEARCH
Support open data and methods to enhance research reproducibility

DIGITAL PUBLISHING
Articles designed for optimal readership across devices

FOLLOW US
@frontiersin

IMPACT METRICS
Advanced article metrics track visibility across digital media

EXTENSIVE PROMOTION
Marketing and promotion of impactful research

LOOP RESEARCH NETWORK
Our network increases your article's readership